Development of the high throughput mammalian PIG-A gene mutation assay in vitro.

Rees, Benjamin James

Development of the High Throughput Mammalian *PIG-A* Gene Mutation Assay in vitro.

Volume 1 of 2

Benjamin James Rees Bsc (Hons)

A thesis submitted to Swansea University in fulfilment of the requirements for the Degree of Doctor of Philosophy in the College of Medicine

Swansea University

2015

Summary

The field of genetic toxicology has recently undergone reform which has limited or banned the use of animal models within a number of different industries (cosmetics). Consequently, greater emphasis has been placed on developing novel, highly sensitive, in vitro test systems which can generate robust data to aid regulatory hazard and risk assessment.

The main aims of this project were i) to develop a highly sensitive and specific, high throughput mammalian in vitro *PIG-A* gene mutation assay to enable quantitative dose response modelling and further investigate the potential use of in vitro data within human health assessment. ii) Investigate the genotype to phenotype relationship, a potentially delaying step within future OECD guideline drafting for the current in-vivo *Pig-a* mutation assay and iii) help develop and optimise a preliminary comprehensive human *PIG-A* bio-monitoring platform.

During in-vitro and ex-vivo *PIG-A* assay development, flow cytometry was the fundamental technique utilised. Multiple additional laser excitation platforms were evaluated for use, including Amnis ImageStream ™ and laser scanning confocal. Proteomic as well as genomic techniques were used during the supplementary investigations surrounding assay development, with microbiological groundings throughout.

The finalised in-vitro assay protocol was established within human, metabolically active, MCL-5 cells. Using the refined assay design, proof of principle experimentations were able to show the potential for future quantitative work and the general promise with this novel approach. The genotype to phenotype relationship validation is currently still on-going following the preliminary work described herein and recent publications. The ex-vivo human *PIG-A* assay platforms were shown to require further optimisation in terms of sensitivity, excluding red blood cells, but showed good aptitude for future use.

Currently it looks promising that further refinement could lead to a comprehensive high content, high-throughput assay system with the potential to be used within future hazard and risk assessment.

Declaration

This work has not previously been accepted in substance for any degree and is not being concurrently submitted in candidature for any degree.

Signed ..... (candidate)

Date ...25/02/2016.....

STATEMENT 1

This thesis is the result of my own investigations, except where otherwise stated. Where correction services have been used, the extent and nature of the correction is clearly marked in a footnote(s).

Other sources are acknowledged by footnotes giving explicit references. A bibliography is appended.

Signed ... _ _ ..... (candidate)

Date .....25/02/2016.....

STATEMENT 2

I hereby give consent for my thesis, if accepted, to be available for photocopying and for inter-library loan, and for the title and summary to be made available to outside organisations.

Signed .... (candidate)

Date .....25/02/2016.....

Acknowledgements

Undertaking a Ph.D. project was a much greater task than I had first anticipated, and I would like to say a personal thank you to all of those people who have played their respective parts in the completion of the thesis. Sadly, I will not be able to name all of those who contributed, but I am sincerely grateful for your time and effort.

Firstly I would like to thank Prof. Cathy Thornton for her initial help and the use of her Flow Cytometer, without which none of this project would have been completed. Dr Graham Botley for his ear and dependable flow cytometry related advice and Dr John Wills for his continued friendship, and technical imaging support.

I would also like to mention Dr Matt Hitching and Dr Sion Bayliss for their guidance and subsequent work towards the later part of the project. The GSK Stevenage staff for their respective help with next generation sequencing work and the group at Gentronix ltd. for their contributions towards the in vitro *PIG-A* project.

Additionally, I would like to acknowledge Prof. Richard Walmsley and Prof. Anthony Lynch for their considerable guidance throughout this thesis and Dr Hasan Haboubi for his companionship in the labs and contributions towards the human *PIG-A* development project.

My supervisor, Associate Prof George Johnson, provided me with the opportunities to not only complete my thesis but experience so much in such a short period of time. Without his support, as well as the financial aid I was able to obtain, I would not have been able to travel across the world either collaborating or presenting my work at scientific conferences - thank you for the help.

Finally, I would like to say thank you to my family and girlfriend for their constant support and use of the conservatory for the final few months of writing up. My eyes aren't thankful, but I am truly grateful for your constant support.

List of Figures/Tables

Definitions/Abbreviations

2,4 DNP	2,4 Dinitrophenol
6-TG	6-Thioguanine
7-AAD	7-Aminoactinomycin D
AA	Acrylamide
ACDU	Automated Cell Deposition Unit
ADME	Absorption, Distribution, Metabolism and Excretion
AHH-1	Human B-Lymphoblastoid Cells – High level of Oxidative Activity
APC	Allophycocyanin
AT	Adenine-Thymine
ATCC	American Type Culture Collection
BD	Becton, Dickinson and Company
BE	Barrett's Oesophagus
BER	Base Excision Repair
BMD	Bench Mark Dose
BPF	Band Pass Filter
BSA	Bovine Serum Albumin
BVDV	Bovine Viral Diarrhoea Virus
BWA	Burrows-Wheeler Aligner
CA	California
CCD	Charge Coupled Device
CD	Cluster Differentiation
CD15	3-Fucosyl-N-Acetyl-Lactosamine
CD24	Heat Stable Antigen
CD48	B-lymphocyte Activation Marker (Blast-1)
CDK	Cyclin Dependent Kinase
CED	Critical Effect Dose
CEDL	Lower Confidence Interval
CEDU	Higher Confidence Interval

CH	Constant Heavy
CHO	Chinese Hamster Ovary Cell Line
CL	Constant Light
COMET	Genetox Assay - Measures DNA strand breaks
CROM	Cromer Blood Group System
CT	Computerised Tomography
DAF	Decay Accelerating Factor
DIVA™	Becton Dickinson Flow Cytometry Software
DMEM	Dulbecco's Modified Eagles Medium
DMSO	Dimethyl Sulfoxide
DNA	Deoxyribonucleic Acid
DSB-X	Biotin Technology
ECL	Enhanced Chemiluminescence
EDF	Extended Depth of Focus
EDTA	Ethylenediaminetetraacetic Acid
EEA	European Economic Area
EGT	Estimated Generation Time
EMA	European Medicines Agency
EMGT	Estimated Mean Generation Time
EMS	Ethyl-Methane Sulfonate
ENU	Ethyl Nitrosourea
EPA	Environmental Protection Agency
ER	Endoplasmic Reticulum
EURl-EVCA	European Private Equity and Venture Capital Association
FACS	Fluorescence-Activated Cell Sorting
FBS	Foetal Bovine Serum
FCM	Flow Cytometry
FDA	Food and Drug Administration
FITC	Fluorescein Isothiocyanate
FL	Fluorescence
FL-A	Fluorescence Area

FLAER	Fluorescent Aerolysin
FL-H	Fluorescence Height
FL-W	Fluorescence Width
FSC	Forward Scatter
FTH	First Time in Human
GA (adduct)	Glycidamide
GC	Guanine-Adenosine
GERD/GORD	Gastroesophageal Reflux Disease
GI	Gastrointestinal
GLP	Good Laboratory Practice
GPI – AP	Glycophosphatidylinositol Anchor Proteins
GPT	DNA Repair Deficient Rodent (Mouse) Model
GUI	Graphical User Interface
HAT	Aminopterin
HBM	Human Bio-monitoring
HepG2	Human Liver Cancer Epithelial Cell Line
HiS	Heat Inactivated Serum
HLA-DR	Human Leukocyte Antigen - DR
HO-1	Haemeoxygenase 1
HPRT	Hypoxanthine-guanine phosphoribosyltransferase
HRP	Horse Radish Peroxidase
HS	Heat Serum
IARC	The International Agency for Research on Cancer
ICH	International Conference on Harmonisation
ICS	Instrument Calibration Standard
ID	Identification
IHC	Immunohistochemistry
ILSI-HESI	International Life Sciences Institute Health and Environmental Sciences Institute
IWGT	International Workshop of Genotoxicity Testing
LGC	British Independent Science Based Service Company

LOAEL	Lowest Observed Adverse Effect Level
LOAEL	Lowest Observed Adverse Effect Level
LOH	Loss of Heterozygosity
LPF	Long Pass Filter
MAC	Membrane Attack Complex
MCL-5	Human B-Lymphoblastoid Cells Expressing Five Cytochrome p450s
MGMT	Methyl Guanine Methyl Transferase
MHC	Major Histocompatibility Complex
MLA	Mouse Lymphoma Assay
MMC	Mitomycin C
MMS	Methyl-Methane Sulfonate
MN	Micronucleus
MNC	Mononuclear Cell
MNT	Micronucleus
MNU	Methyl Nitrosourea
MPG	N-Methylpurine-DNA Glycosylase
MS	Mechanosensitive
MSDS	Material Safety Data Sheet
ND	Nanodrop
NDMA	Nitrosodimethylamine
NER	Nucleotide Excision Repair
NGS	Next Generation Sequencing
NHS	National Health Service
NIH	National Institute of Health
NME	New Molecular Entity
NOAEL	No Observed Adverse Effect Level
OECD	Organisation for Economic Co-operation and Development
OEL	Occupational Exposure Limits
ORF	Open Reading Frame
p16(INK4a)	Tumour Suppressor Gene

P19(ARF)	Tumour Suppressor Gene
PBS	Phosphate Buffered Saline
PCR	Polymerase Chain Reaction
PE	Phycoerythrin
PE-cy5	Phycoerythrin-Cyanide 5
Pe-cy7	Phycoerythrin-Cyanide 7 Conjugate
PerCP	Peridinin Chlorophyll
PerCP-cy5.5	Peridinin Chlorophyll-Cyanide 5 Conjugate
PFA	Paraformaldehyde
PIG-Genes	Phosphatidylinositol Glycan Biosynthesis Genes
PMT	Photomultiplier Tube
PNC	Polynuclear Cell
PNH	Paraoxysmal Nocturnal Haemoglobinuria
PPE	Personal Protective Equipment
PS	Phosphatidyl Serine
PVDF	Polyvinylidene Difluoride Membranes
QA	Quality Assurance
qRT	Quantitative Real Time
QSARS	Quantitative Structure Activity Relationship
RAS	Guanosine-Nucleotide Binding Protein
RBC	Red Blood Cells
RCC	Relative Cell Counts
REACH	Registration, Evaluation, Authorisation & restriction of Chemicals
RET	Reticulocyte
RETIC	Reticulocyte
RICC	Relative Increase in Cell Counts
RIPA	Radioimmunoprecipitation Assay Buffer
RLP-19	Receptor Like Protein
RNA	Ribonucleic Acid
ROS	Reactive Oxygen Species
RPD	Relative Population Doubling

RPMI	Rosemary Park Memorial Institute
RT	Real-time
RT	Room Temperature
SAM	Sequence Alignment /Map
SAV	Sequence Analysis Viewer
SD	Standard Deviation
SDS-PAGE	Sodium Dodecyl Sulphate – Polyacrylamide Gel Electrophoresis
SEM	Standard Error of the Mean
SNP	Single Nucleotide Polymorphism
SOP	Standard Operating Procedure
SSC	Side Scatter
STD	Slope Transition Dose
SYBR®	Asymmetrical Cyanide Dye
TDI-CCD	Time Delay and Integration Charge Coupled Device
TEMED	Tetramethylethylenediamine
TFT	Trifluorothymidine
TIFF	Tagged Image File Format
TK	Thymidine Kinase
TK6	Human B-Lymphoblastoid Cells
ToxCast™	Toxicity Forecasting Software
UK	United Kingdom
USA	United States of America
UV	Ultraviolet
V79	Chinese Hamster Lung Cell Line
VH	Variable Heavy
VL	Variable Light
WBC	White Blood Cell
WIL-2	Human B-Lymphoblastoid Cell Line
WOE	Weight of Evidence
WT	Wild Type
ZEN	Imaging Software

Contents Page

Chapter 1: General Introduction

1.1 Genetic Toxicology

Genetic Toxicology is the study of the interaction, direct or indirect, mechanism and subsequent damage to the genetic material, located within the cell [1]. DNA consists of four nucleotide bases, the purines; adenosine and guanine as well as the pyrimidines; thymine and cytosine, each attached to a sugar (deoxyribose) phosphate backbone. Following enzymatic assembly, via the DNA polymerase family of enzymes, a comprehensive, intricate, polymer of multiple nucleotides are joined following linear covalent phosphodiester bond formation (condensation reaction) (Figure 1.1). Due to the conformed, highly regulated structure of double stranded DNA, a direct consequence of the specificity of base-to-base interactions, minute alterations to the overall structure of DNA can result in irreversible catastrophic damage. Such damage can threaten the viability of the host organism, not solely that specific somatic or germ-line cell [2] or result in deleterious disease phenotypes such as cancer.

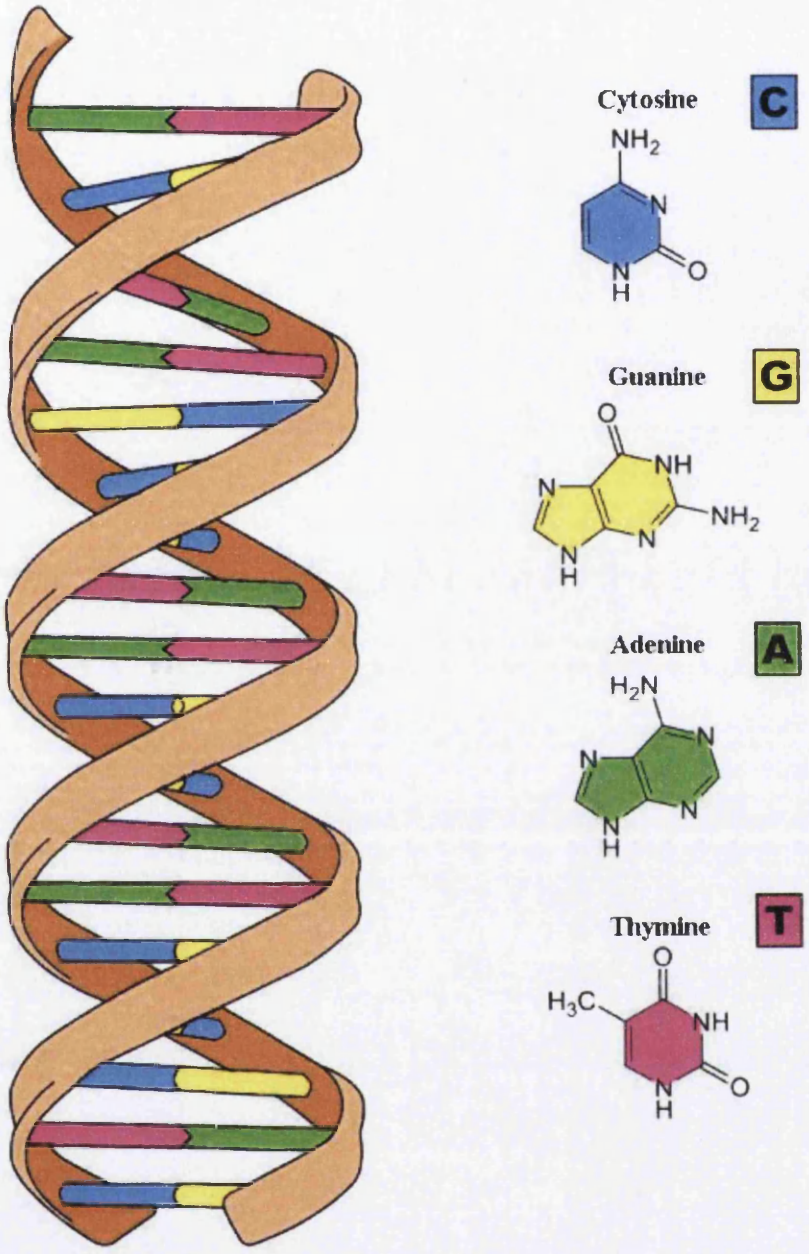

Figure 1.1. The DNA molecule and its respective nitrogenous base building blocks, adenine, thymine, guanine and cytosine - adapted from [3].

1.1.1 Mechanisms of DNA Damage

DNA damaging agents are often grouped into two main categories, i) DNA reactive; chemicals which physically orientate, associate and/or interact with the central DNA double helix (direct gene expression regulation) at specific base related locations. [4]. II) Non-DNA reactive; agents which often are associated to DNA replication machinery and/ or other mechanisms related to gene expression and maintenance. Irrespective of the nature of the DNA damage mechanism, each specific category of DNA damaging agent for example, Reactive Oxygen Species (ROS) [5] has the ability to induce a wide plethora of results. Such results vary in terms of acuteness as well as longevity, and have effects ranging from mildly aberrant to catastrophic on the phenotype. Phenotypic alterations are based on i) the nature of exposure, in terms of length and severity ii) oncogenes or tumour suppressor gene expression alterations, leading to long term carcinogenesis [6] and a whole abundance of genetic diseases (e.g. Deletion Syndrome [7]) and iii) irreversible genomic instability, leading to apoptosis and non-transmission of hereditary material (cell death) [8]. Accumulated DNA damage can be considered a direct contributor to some of the features of aging, single strand breaks have been identified as such a feature within the brain [9]. DNA damaging agents originating from within the human body are referred to as endogenous sources of damage; these include ROS, and often are generated as bi-products of routine biochemical synthesis or biological pathways. Such pathways include the electron transport chain within the mitochondria [10]. However, the body can also be exposed to deleterious sources of DNA damage which originate from the environment; these are referred to as exogenous agents and include such well known human carcinogens as Benzo(a)pyrene (B[a]P) [11], and cyclophosphamide [12, 13]. Deleterious pathology, cancer, aging, cell death, are often observed when the homeostatic DNA repair mechanisms become saturated and are no longer capable of efficient repair (Figure 1.2), hence why repair rate is a direct determinant of cell pathology [14].

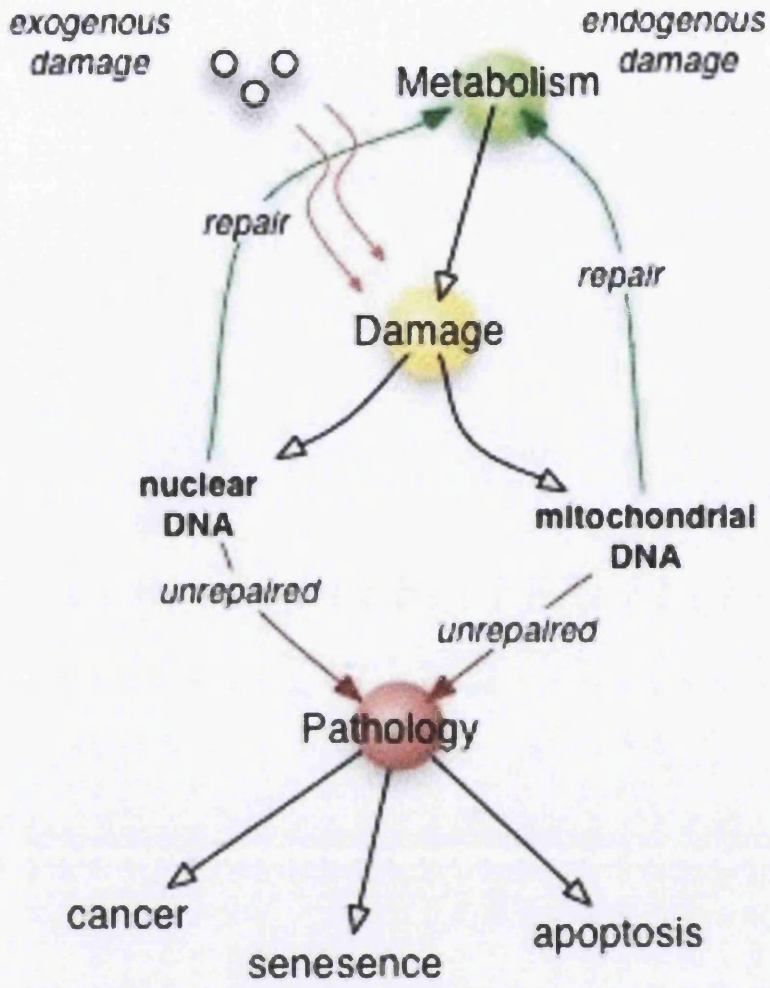

Figure 1.2. General overview of the complex relationship between endogenous and exogenous sources of DNA damage and their respective repair mechanisms. Adapted from an image generated by Harold Brenner.

1.1.1.1 DNA Reactive Compounds

Alkylating agents are a subgroup of DNA reactive compounds that physically interact with the DNA double helix through either a single (mono) or bi-functional mechanism. The reactivity and specificity of such compounds are graded by the Swain Scott constant value (S) [15]; the higher the value, the less reactive and more specific the nature of potential base adduct formation occurs.

The mono-functional alkane sulfonates, such as methyl and/or ethyl methane sulfonate (MMS and EMS respectfully), tend to be more highly selective than the nitrosamines, and primarily react with N7G, N3A and O6 guanine (3 common adducts to both alkylating agents) at a rate 4-5 x fold higher [16]. Nitrogen based alkylation is associated with chromosome aberrations such as single and double strand DNA breakage. Whereas, oxygen based alkylation has been demonstrated to be the only lesion induced by EMS which leads to direct mutagenic events (Figure 1.3); miscoding of thymine opposite of the adducted guanine base resulting in DNA sequence alterations GC -> AT transitions [17].

Bi-functional alkylating agents such as nitrogen mustards (mustard gases) have multiple functional/active groups able to facilitate multiple points of contact/interactions being same strand or adjacent DNA strands and often result in DNA adduct formation or inter-strand cross-linking [18]. The results of exposure often highly affect DNA replication, as a result wound healing is heavily inhibited and hence severe cytotoxicity is often observed [19]. The specificity of the alkylating patterns induces unique DNA adduct formation and hence, subsequent mutation spectra revealing hot spots upon miss-regulation [20].

Nitrosamines such as ethyl-nitrosourea (ENU) or methyl-nitrosourea (MNU) have a much lower Swain Scott constant and are deemed more reactive substances [21], for example, they do not distinguish between areas of high or low nucleophilicity (i.e. areas abundant with electrons) and therefore, often do not distinguish between oxygen or nitrogen atoms as their specific target atoms for alkylation within the DNA double helix [22]. As a result of this, they are often associated with a plethora

or alkylated base effects including the most common N7G, N3A and O^6mG (repaired by methyl guanine – DNA methyl transferase (MGMT)).

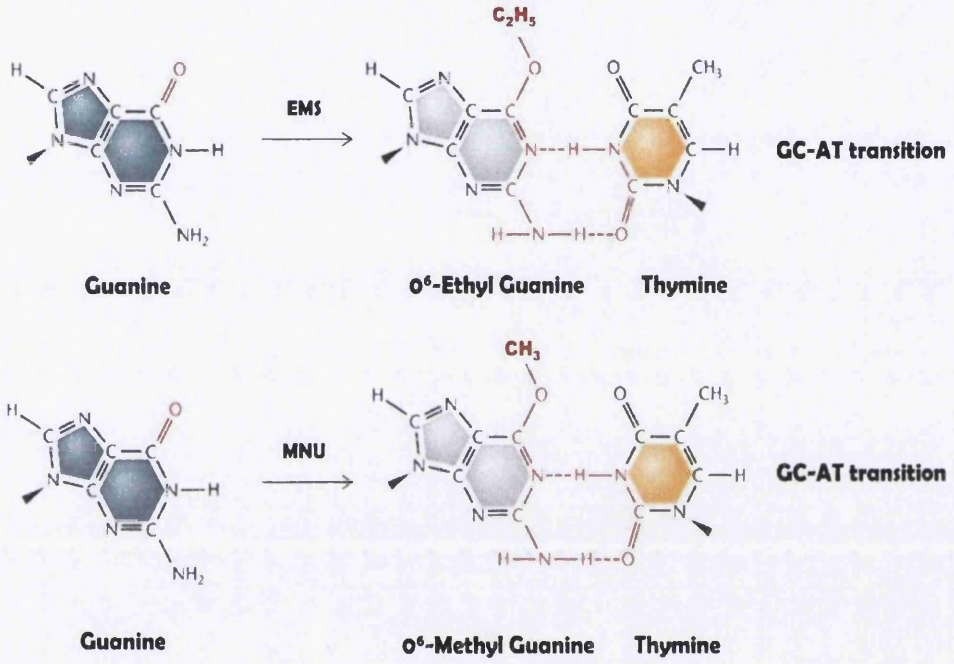

Figure 1.3. Formation of O^6 methyl/ethyl-guanine mutagenic lesions following, EMS and MNU, model alkylating exposure. Homeostatic DNA repair mechanisms, including MGMT, have been omitted to enable simplistic clarity of mutagenesis within the DNA molecule. Adapted from [23]

1.1.1.2 Non-DNA Reactive Compounds

Not all compounds that result in potential genotoxicity directly react with DNA, non-DNA reactive genotoxicants are a category of compounds which can be just as potent as DNA reactive compounds at inducing carcinogenesis or related deleterious end points/mechanisms of damage [24].

Common targets appear within this category of compounds, which often relate to DNA replication machinery and/or DNA re-arrangement, epigenetic. A good example of such a compound is Vincristine which is a vinca alkyloid (similar to Vinblastine) originally isolated from the *Catharanthus roseus (Periwinkle Plant)*, which specifically targets and inhibits tubulin production and hence, correct micro-tubulin attachment and DNA replication, potentially resulting in un-even DNA distribution to daughter cells through mitosis [25] or even cell death. The end result of this can be loss of genetic material, entire chromosome loss [26], and can result in genetic disease within somatic cells, i.e. carcinogenesis and other disease related phenotypes. Non-direct DNA reactive agents, due to not directly altering base chemistry, cannot directly impact on the germ-line cells; failure to under mitosis and subsequent cell division does not facilitate propagation of genetic damage through this mechanism. However, un-even distribution of genetic material, non-disjunction, leading to such conditions including Klinefelter syndrome (XXY) can be observed [27].

1.1.2 Mutagens, Aneugens and Clastogens

As mentioned above, there are two main categories that can be used to separate or identify any genotoxic chemical/compound (DNA reactive, or non-DNA reactive damaging agents). However, additional to this level of classification, there is an additional level of identification; which makes a commentary of the detailed mechanism of DNA damage as a result of such chemical exposure. Within the DNA reactive compounds, one can further sub-categories compounds based on their actual method of DNA damage; mutagens, which alter the sequence of nucleotides within

the nuclear DNA and clastogens, which cause chromosome breaks and often result in dose dependent micronuclei formation [28].

Mutagens are compounds or high energy electromagnetic waves, such as radiation, as mentioned above, which physically interact with the DNA molecule and result in an alteration to the linear DNA sequence, mutagenesis. The consequences of this can be silent, i.e. there are no alterations in the amino acids sequence, due to the degenerate nature of the genetic code, within all regions of the specified gene and hence, the protein product remains unchanged. Alternatively, the alteration or numerous alterations can result in protein truncation, via premature stop codon transcription, or on the other hand a completely different polypeptide sequence via alternate splicing, exon exclusion [29]. This can result in progressive loss of protein functionality, due to the nature of the codon change or polypeptide structure, or in the case of an acute change; with regards to hydrophobicity and stoichiometric differences between the reference and novel amino acid, total loss of protein functionality [30].

As mentioned above, any chemical which interacts directly with the DNA molecule and alters the nucleotide sequence can be termed a mutagen; typical examples of such mutagens are the alkylating agents. Following alkylating agent exposure, depending upon the functionality of the alkylating agent and specificity, a number of mutagenic lesions can form. In the example of ethyl methanesulfonate (EMS), a typical mono-functional alkylating agent, the ethyl group from the hydrocarbon is highly electron deficient, electrophile, and actively associates to the electron rich moieties, nucleophiles, within the DNA structure [31]. Due to EMS being a relatively strong alkylating agent, via Swain-Scott constant grading, it is able to undergo both a Sn1 and Sn2 nucleophilic substitution reactions [32]; Sn2 mechanisms promote the specific targeting of strong polarised nucleophiles (Nitrogen) within the DNA double helix which have at least a single lone pair of valence electrons. However, in this case, due to additional Sn1 mechanistic capability of EMS, the oxygen atom at the 6^{th} position within guanine is also able to be targeted and subsequently results in the main mutagenic lesion following exposure (0^6-ethyl-guanine) [33].

Clastogens, as the name suggests, operate under a clastogenic mechanism, which alludes to their nature of DNA damage. Clastogens act via physical alterations to the DNA molecule [34] which result in chromosome aberrations, often attributed to disease phenotype and progression. Clastogenic lesions are able to be repaired, at a fidelity dependent upon the repair mechanism and therefore, are not solely restricted to deleterious cellular pathology, however, any DNA lesions which become fixed within the DNA molecule are highly associated to deleterious effects including cell death and DNA damage. The reason for this is that even though abasic sites and other structural abnormalities resulting from clastogenic lesions are typically not heritable and hence, do not confer any genetic consequence, close proximity of such DNA structural damage can induce a hypermobility and hence, induce DNA strand breakage [35].

There are a plethora of mechanisms in which clastogens can induce DNA damage; Acrylamide is an example of a clastogen [36] which generations chromosome aberrations via such a mechanism. Acrylamide exposure induces an increased frequency of adducted nitrogen based alkylations within the nitrogenous base guanine. As a direct result of this, DNA repair mechanisms such as the nucleoside excision repair (NER) and base excision repair (BER) are often self-sufficient in order to remove such adduct formation and aid the re-synthesis of the corresponding nucleotide base within the adjacent strand in order to further chromosome aberration events [37].

Finally, aneugens are in-direct acting compounds which have been demonstrated to increase the frequency of specific DNA damaging events which alter the total number of chromosomes. The resultant conditions are referred to as aneuploidy; a deviation from the correct number of species specific chromosomes. Aneuploidy can be caused by such events as non-disjunction, errorous sister chromatid exchange and mitotic spindle apparatus inhibition. As well as aneugens generating daughter cells with chromosome number abnormalities, they often increase the frequency of micronuclei formation. Micronuclei generating as a result of an aneugenic mechanism, commonly as a result of chromosome lag during mitosis, are centromere positive and often contain the whole chromosome [12].

1.1.2.1 Genotoxicity: Mutagenic Lesions

0^6eG adducts have been demonstrated repeatedly to be the most prominent cause of mutagenesis during in-vivo studies at various gene loci [17]. Since the 1980s increasing evidence has been put forward to support that GC-TA transitions form as a direct result of EMS exposure [38], with a positive correlation between the levels of ethylation at the O^6 guanine base and mutation frequency has been reported within standard genotoxic test systems [17]. Following the addition of the ethyl group to the guanine base at the 0^6 position, the base takes on a new structural/stoichiometric identity which mimics that of the purine base, adenine. As ensuing and direct results of this adduct formation, a miss alignment occurs during DNA replication and an adenine base is incorporated mistakenly into the non-template strand. At this moment in time, there is potential repair via a miss-match repair (MMR) mechanism, however, saturation of such mechanisms will consequently lead to a mutagenic event occurring (Figure 1.4). Following subsequent synthesis a transition mutation occurs in-which the initial GC base coupling is replaced with an AT within one of the subsequent daughter cells [39].

1.1.2.2 Genotoxicity: Clastogenic Lesions

Following ingestion of acrylamide (formed during the heating of certain foods), metabolic activity via P450 enzymes converts AA into the genotoxic epoxide metabolite, glycidamide (GA). GA forms DNA adducts, primarily at N7 of guanine (N7-GA-Gua) [40]. An additional example which follows a similar path as described above is the clastogenic lesions following EMS treatment. During alkylation of specific base moieties within the DNA double helix, most prominently nitrogen atoms, the base under goes a structural change which results in a potential clastogenic event [41]. N7 Guanine lesions, induced at relatively high frequency following EMS exposure, are deemed innocuous; there is no immediate deleterious affect post alkylation. Yet due to their novel chemical instability which often leads to such downstream processes as de-protonation, decomposition, depurination and C-8-

Guanine adduct formation, leading to potential DNA strand breakage [42]. However, such lesions can be initially identified and repaired by N-methylpurine DNA glycosylase (MPG) [43], an initiator of the base excision repair pathway (BER). MPG directly binds to the DNA lesion and removes the adduct forming an abasic site (potential for strand breakage due to proximity to additional abasic sites). Obviously if BER saturation occurs (Figure 1.4), abasic site formation can lead to primarily DNA strand breakages and chromosomal aberrations [44] however, mutagenic events can also occur at a much lower frequency.

The distribution and potency, in respect to carcinogenesis, of an adduct spectra following chemical exposure is highly variable; this is highly dependent upon the specific types of end point, i.e. mutagenic or clastogenic as well as the efficiency and saturation limit of the homeostatic repair mechanism. DNA reactive chemicals more often than not do not operate by a single mechanism of DNA damage, due to the heterogeneity of target moieties within the DNA molecule.

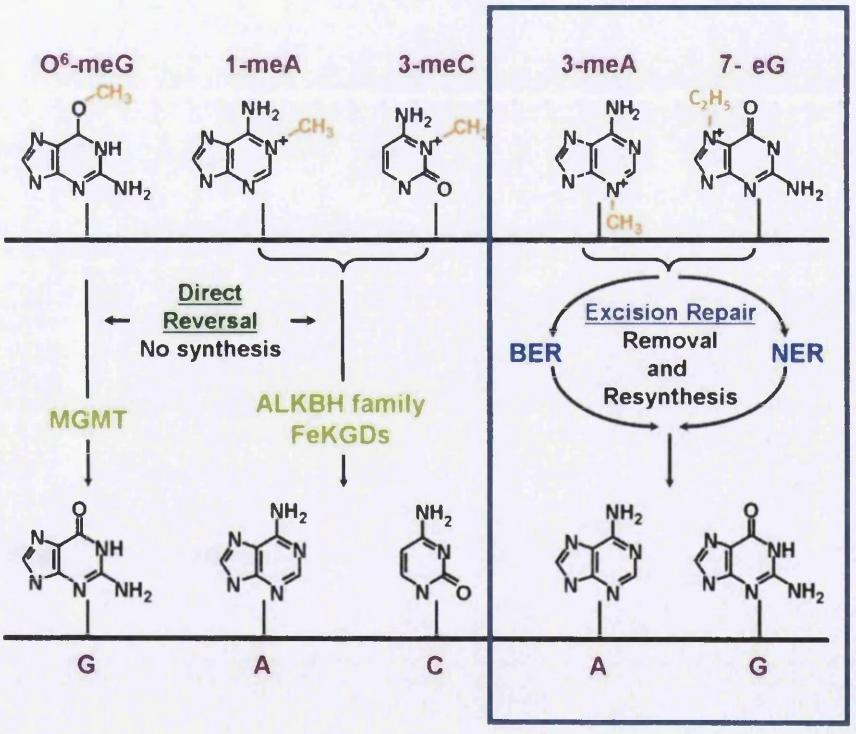

Figure 1.4. Mammalian cell – DNA repair mechanisms; inclusive of direct reversal MGMT activity, scavenger enzyme, targeting mutagenic oxygen lesions (0^6 methyl/ethyl guanine) as well as glycosylase induced BER for non-mutagenic nitrogen lesions (N3-Methyl Adenine and N7-ethyl guanine) – Use of box to highlight the potential clastogenic lesions – Adapted from [45].

1.1.2.3 Genotoxicity: Aneugenic Mechanisms

Following acute aneugenic chemical exposure, cells have a much greater probability of undergoing an errorous mitosis as a direct consequence of potential mitotic machinery inhibition (Figure 1.5); daughter cells have a greater frequency of an aneuploidy phenotype [46]. Aneugenic alterations in the total number of chromosomes have been associated with a great number of genetic diseases, such conditions include Trisomy 21 (Down syndrome), caused primarily by incorrect separation, non-disjunction, of chromosome 21 during early development [47]. Aneugenic chemical treatment and hence, micronucleus frequency are directly proportional due to the mechanism of DNA damage i.e. specific inaccuracies during mitosis generating micronuclei. However, as micronuclei have two distinct mechanisms of formation; one being clastogenic in origin and the other aneugenic, it is a necessity to utilise centromere specific fluorescence probes to provide evidence of the mechanism of formation (Figure 1.5).

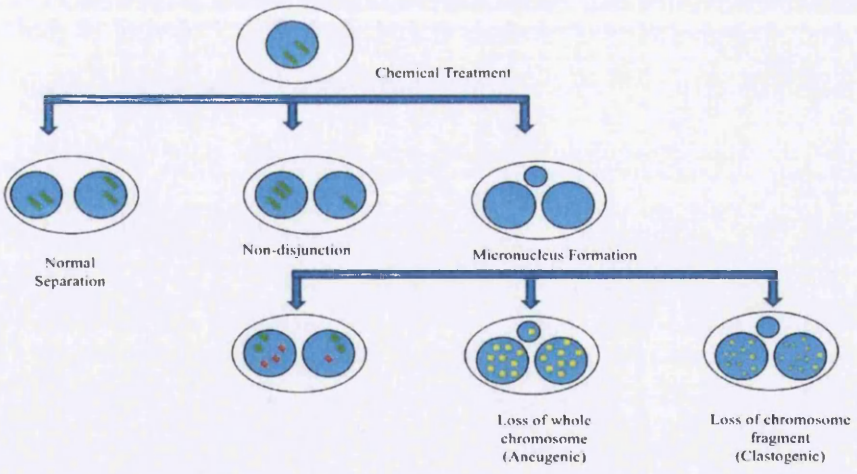

Figure 1.5. Micronucleus formation as well as observed errors during mitosis following acute chemical treatment. For illustration purposes multiple colours have been included to aid explanation; yellow – centromere structures associated to whole chromosomes, green – correctly separated and orientated chromosomes and red – inaccuracies in chromosome orientation and/or separation during mitosis - Adapted from [46].

There are many additional forms of DNA damage, modes of action as well as DNA repair mechanisms which have not been included within this brief commentary [48], as they fall outside of the primary focus of this specific research project. Examples of these include; DNA cross linkers/ intercalating agents, a large number of nucleotide specific fluorescence molecules used to measure DNA content and/or cellular viability operate under this mechanism, which will be discussed in greater detail within the flow cytometry application constraints. Pyrimidine dimers, induced following UV radiation [49], double strand breakages [50], homologous recombination [51] as well as specific detailed examples of endogenous sources of DNA damage, including the generation of ROS, oxidative stress and aging [52].

1.2 Hazard and Risk Assessment: Regulatory Guidance for Safe Operating Exposure Limits (OELs)

Toxicology as a field of research is utilised extensively in defining safety assessed, biologically insignificant, operating levels following prolonged or acute exposure to chemical substances, xenobiotic or foreign antigens. Routes of exposure can include respiratory inhalation, intra-venous/muscular/peritoneal injection, topical application and physical ingestion.

Exposure in itself is interesting and complex; exposure duration, route of exposure and the substance of exposure each are critical in collecting enough biologically significant data to ensure an acceptably low risk of hazard is defined complying to the REACH obligations [53].

Hazard and risk are intimately intertwined in one and another, hazard is a commentary or definition of the deleterious mechanism or result which can result post exposure. Risk on the other hand, is the likelihood or frequency of that hazard actually being exposed to a biological system and hence, causing such biologically deleterious effects [54]. Without one and another, each definition is biologically insignificant without the content the conjunctive commentary provides, similar to the idea of antagonistic muscles. In the example of the typical research laboratory,

known genotoxic chemicals or bacterial toxins, which has an acutely high hazard potential and a human lethal dose 50% (LD50) value within the micro or nanogram scale, for example Abrin [55]; implying that minute amounts of such compound are fatal in humans. However, as the toxin is in-frequently used and is freely soluble in water, non-volatile, exposure is limited to a single route (ingestion); the risk associated with use is particularly low. Correct personal protective equipment (PPE), such as a laboratory coat and nitryl gloves are sufficient to reduce the potential exposure to minimal risk – highlighting the necessity for context.

Prior to routine exposure, either acutely or over an extended period of time, the initial experimental work is carried out extensively within rodent models, primarily rat and mouse. However, one must always consider the caveat that rodent models are a satisfactory model of human exposure; although, humans have a different genome and hence, have subsequent different gene expression and protein presence within somatic and germ line cells. In order to associate said sources of limited and potentially human irrelevant data the use of correlation factors and extrapolation calculations are implemented to artificially create a buffering affect to limit further risk. Historically some of the safety (correlation factors) included were i) a factor from 1 to 10 for animal to human extrapolation (if NOEL is based on animal data), ii) a factor from 1-10 for human to human intra-species variability and iii) a factor from 1-10 to consider study duration [56-58] in order to generate a conservative human OEL, airing on the side of caution. The field still relies on this traditional dogma to create safe exposure limits, however, due to the advancements within genetic toxicology, a potential paradigm shift could be seen in the near future through the inclusion of qualitative dose response data within OEL definition.

1.3 Safety Assessment and Drug Development

Each and every drug which progresses from theoretical compound, through manufacturing and eventually into the domestic or global market has to undergo a strict and thorough hazard and safety assessment to ensure safety following regulated progress. The global pharmaceutical market was estimated to be worth approximately 170-180 billion US dollars in 2012 [59], with an estimated peak of 880 billion US dollars by 2014 [60]. The surge in the global market over recent years is primarily down to a massive increase in the third world markets; Chinese market contributed an additional 50 billion dollars, 25% of the entire global market and secondly due to increased spending on nationalised healthcare in the developed market [59]. However, the United Kingdom, an example of a typical western market, has been steadily falling down the global rankings, in terms of market size, of the pharmaceutical industry since 2007 (Table 1.1).

Table 1.1. Statistical summary of the global pharmaceutical market for 2010 and 2012 respectively, highlighting observed trends – adapted from [61]

	2010			2012		
Country	**World Ranking**	**Size of Market (Mill $)**	**Growth (%)**	**World Ranking**	**Size of Market (Mill $)**	**Growth (%)**
USA	1	319,552	6	1	326,892	-1
Japan	2	96,355	7	2	112,067	0
China	3	54,865	21	3	81,698	22
Germany	4	42,181	2	4	42,333	-6
France	5	38,529	-5	5	36,674	-8
Brazil	7	26,259	38	6	29,112	-6
Italy	6	26,639	-2	7	26,231	-8
Canada	9	21,655	13	8	21,877	-2
UK	10	20,297	2	9	21,635	0
Spain	8	22,220	-2	10	19,935	-12

1.3.1 Safety Assessment and Drug Development: Standard Battery of Genetic Toxicology Tests

New molecular entities (NMEs) is the term given to novel drugs as they leave the drug discovery phase, a novel compound that has been shown generally to be highly promising as a potential therapeutic target to a disease, the initial judgment often occurs within in-silico methods, such as Quantitative Structure-Activity Relationships (QSARS) for example, Derek-Nexus[62]. However, the strengths associated with in-silico approaches are often limited to the database which the software sources it's information, often resulting in much lower specificity and sensitivity when applied to novel classes of compounds [63]. NMEs are coming to market at a consistent rate each year, a direct result of numerous independent private bio-technology companies; often graduate spin out companies, however, at the drug discovery phase little is known about the toxicity, pharmacodynamics and kinetics of the compound. Within the field of genetic toxicology, a standard tiered test system of genotoxic assays is utilized extensively in order to cover the wide variety of potential genotoxic end points; mutagenicity, chromosome aberrations etc. enabling the investigator or regulatory committee to generate sufficient data in order to construct a complex, in context, overview of the ensuing hazards following environmental exposure [64, 65].

The above assessment programme is often referred to as the Genotoxicity Test - Battery and consists of the following; i) "Crude" bacterial reverse gene mutation assay; the Ames test [66] – in which Salmonella histidine mutants, often combined with human or rodent S9, are utilised to detect mutagenic carcinogens. The resultant Ames test is highly sensitive, ideal for hazard identification, however, is often criticised for being overly sensitive; due to some bacterial tester strains harbouring additional mutations other than the histidine synthesis genes. These include lipopolysaccharide synthesis, resulting in the cell membrane becoming more permeable [67], and excision repair pathways common to Eukaryotes [68].

ii) Mammalian in-vitro genotoxicity; either the a) in-vitro micronucleus test (mono and bi-nucleus with or without recovery) [69]or the b) thymidine kinase (*TK*) – MLA [70]/ hypoxanthine phosphoribosyl transferase (*HPRT*) gene mutation assays [71].

iia) The micronucleus test is a highly validated chromosome aberration assay in which chemicals operating under a clastogenic and aneugenic mode of action can be detected and identified via the sequential use of centromeric stains, post micronuclei induction [72].

iib) The *HPRT* gene is located on the X-chromosome of mammalian cells, and subsequently used as a model gene to investigate gene mutation. The test follows a very similar methodology to the thymidine kinase (*TK*) – mouse lymphoma assay (MLA), with the additional of aminopterin to promote the purine DNA salvage pathway and both are included in the guidelines for mammalian gene mutation tests (OECD (1997) [73]. The *MLA* methodology is such that mutations which destroy the functionality of the *TK* gene and or/protein are detected by positive selection using a toxic analogue (6-thioguanine), and TK^- mutants are seen as viable colonies. Unlike bacterial reverse mutation assays, mammalian gene mutation assays respond to a broad spectrum of mutagens, since any mutation resulting in the ablation of gene expression/function produces a TK^- mutant [74]; common mammalian cells routinely used: L5178Y – Mouse lymphoma [70], TK6 and AHH-1 – Human B-lymphoblastoid immortalised cell lines [71, 75].

Finally iii) Mammalian in-vivo test for genotoxicity; either micronuclei (peripheral blood and bone marrow) [76], chromosomal aberrations, or gene mutation; either in vivo *Pig-a* [77] or transgenic: GPT MutaMouse of BigBlue ™ [78] or finally, the COMET assay (all tissues) [79]. Rodent transgenic mutation assays are well-established assays that utilise transgenic rats and mice which contain multiple copies of chromosomally integrated plasmid or phage DNA. Concealed within the DNA molecules are reporter genes for the detection of mutation. Mutations occurring within such a rodent are subsequently scored by recovering the vector and analysing the phenotype of the reporter gene in a bacterial host [80]. DNA extraction from any tissue type therefore, circumvents many of the existing limitations associated with the study of in-vivo gene mutation.

The test battery is currently outlined by the Food and Drug Administration (FDA) [81], presented at the International Committee for Harmonization (ICH) [82], summarising OECD guidelines in order to facilitate a global template for assay protocol; enabling homogeneity within test protocols and subsequent comparable

data acquisition [65]. The reason for such a document is due to the nature of global genotoxicity testing, as each country or continent is often regulated by a different committee or governing body; for example Europe: European Environmental Agency (EEA) [83], now formally known as the European Medicines Agency (EMA), and the United States of America: Food and Drug Administration (FDA) [81], the subsequent data generated by individual regions often cannot be compared against like data sets from a different continent. Assay protocol varies heavily depending upon the governing body which quality assures the data; standard recovery time, dosing regime and cell type may be very different. The ICH's goal is to promote communication between global pharmaceutical industry figureheads to facilitate the standardisation of genetox testing; reducing heterogeneity within the resultant data [82].

In the past 10-20 years the field of genotoxicity as well as other scientific disciplines has been steadily re-structuring in order to fit current governmental demands, as well as a direct reflection of the global economy. The National Institute of Health (NIH) had to cut their 2013 budget by 5% in March as a direct sequestration legislation brought in by the president [84]. Increasing numbers of governmental based legislations as well as initiatives have been founded in order to address budget cuts as well as to appease the global position on animal testing, especially within the cosmetic industry (Europe). Two specific examples of this would be the 3Rs initiative [85] and the Cosmetics directive [86]. The 3Rs initiative is a worldwide enterprise with the overall goals to replace, reduce and refine the use of animal models within drug testing. The goal of the 3R's is more drastically reflected by the cosmetics directive, a legalisation which has banned the use of animal model within cosmetics testing.

1.4 Governmental Reforms within Genetic Toxicology Testing: New Direction

Due to the pressure applied by the introduction of this paradigm shift within government legislation concerning animal testing, within genetic toxicity and related health sciences, a consequential move in the currently implemented approaches to

drug testing is inevitable. Increased resources are being allotted into the field of novel in vitro assays, not solely limited to genetic toxicology endpoints (Skin sensitisation [87]) as well as of quantitative in-vitro-in-vivo dose extrapolation [88]. Restrictions within in vivo testing has not only affected the cosmetic field, but increasing government driven cut backs and limitations has resulted in many animal-model based assays losing favour due to the associated pressure of animal usage as well as shear difficulty to acquire ethical approval [89].

As a direct consequence of these reforms, increasing focus is being placed upon alternative novel approaches to toxicology animal testing, i.e. in silico and in vitro based test systems [90] as well as integrating multi-end-point analysis, comet (all tissues) and erythrocyte *Pig-a*, within current 28-day toxicology studies [91]. For the scope of this project in vitro test system will be discussed at length; in vitro systems do not simply infer 2-dimensional traditional immortalised cell line assays, *TK* and MLA for example. Modern, novel 3-dimensional tissue constructs, originally sourced from primary tissue samples, can be used to accurately represent the cell types as well as growth dynamics of combinations of cells making up specific tissue and even minor organ systems [92]. Currently favoured assays include the 3D skin tissue model [93] as well as numerous bronchial epithelial lung models [94] in which many preliminary toxicology publications have demonstrated initial robustness within primarily the micronucleus endpoint [95]. However, even though preliminary data looks promising, there are currently no consensus OECD guidelines published and further validation is required.

1.4.1 Advantages and Disadvantages of Novel Reforms

Drug delivery is not a fixed mono-direction interaction, it is not a simple easy to model system in which a potential therapeutic solely identifies and conjugates to its own highly specific target (pharmacodynamics). During drug exposure, the body in-directly acts upon the drug simultaneously (pharmacokinetics) and therefore, constructs a much more complex interaction system with multiple high variable factors. Utilising mammalian models, during safety assessment, allows the

investigator to explore the multifaceted relationship between the ability of a drug to act upon its target and the corresponding response the body has on said drug. The pharmacokinetic aspect of drug interactions can be categorised as follows; absorptions, distribution, metabolism and excretion (ADME) [96]. Take an orally administered antibiotic for example, initially the drug coating must first be considered in order to enable the drug to reach the target organ and extend the half-life to enable efficient distribution around the body. Failure to meet these requirements will decrease the likelihood of drug–target interactions, reduce the concentration of said drug at the target (increased cytotoxicity is often seen following increased therapeutic dose to counter this) and increase the chance of bacterial resistance [97]. Point of initial drug contact and routes of admission are contributing factors in modifying the dose of the therapeutic, higher doses applied topically can be better tolerated when compared to an intra-venous injection, for example (generally due to distribution and actual penetrable dose). Drug compounds once exposed to the human proteome can often become unstable, due to enzymatic degradation of the therapeutic compound, generally this aids elimination, however, in certain circumstances, for example paracetamol; the metabolites are extremely toxic, localised within the liver and can result in acute hepatoxicity [98]. Certain drug compounds, due to inefficient methods of elimination, have been reported to accumulate, bioaccumulation, within specific tissues or organ systems within the body. Reports suggest that human adipose tissue is a source of a whole host of lipid soluble compounds, for example pesticides [99], which are notoriously difficult to remove from the body.

Currently, this complex state is most viably modelled within animal exposure; interspecies variability is a known caveat associated with rodent to human extrapolation. The human genome and subsequent proteome, is highly conserved within other mammalian species, however, is larger and more complex than the rodent. The paradigm shift within toxicology away from in-vivo testing has led to increasing focus on novel predictive in silico and in vitro approaches [90], as previously mentioned. However, the pharmaceutical industry stands to lose a large amount of supplementary biologically relevant rodent data during safety assessment, and gain an abundant amount of in vitro safety data. Controversially, this will appear to have a detrimental effect on the overall drug development system, due to the

caveats associated with in-vitro to in-vivo extrapolation as well as increasing limitations beings placed on animal pharmacodynamics and kinetic studies. However, recent studies have shown increased potential within in-vitro to human dose extrapolation; in vitro generated quantitative dose response data will be used more extensively in the future of drug development [100], as well as the in vitro genetic toxicology assays proving to be extremely sensitive to genotoxins and provide a cost effective approach to screening of large numbers of environmental xenobiotics [101].

1.5 Gaining Favour – In vitro Test Systems

3-dimensional tissue models may be the distant future of genotoxicity testing, however, the mammalian cell in vitro immortalised cell lines host a wide variety of routinely used and OECD certified genetox assays, such as *TK*–MLA (L5871Y)[70], *HPRT* (AHH-1/*TK*6) [74] as well as the more traditional ,controversial, HGPRT (CHO/V79) [102]. Following decades of routine use within the tiered genetox test battery, historically in-vitro (cell line based) genetox assays have proven their requirement and practicality, and have the reputation and historical data to facilitate inclusion in future amendments to the ICH guidelines (S2B). However, as in the case of any genetox assay, specific forewarnings are applied directly to the in vitro assays, these include; sensitivity, crudeness to model human exposure and hence, biological relevance. Such resultant data should be used cautiously for anything greater than hazard identification and information on potency and modes of action [103].

1.5.1 In vitro Testing: The Future of Drug Development?

The majority of disadvantages associated with in vitro testing are directly consequential of comparing the test systems with in vivo animal models with analogous end points. As stated in the ICH guidelines [64] there is still a present need for in-vitro gene mutation and chromosome aberration assays; coupling this with the restrictions applied by recent governmental legislations, as mentioned

previously, animal models could in the future play a much less prominent role within the standard genetox battery. Therefore, priority has been put into developing novel in vitro test systems which are in-expensive, high throughput, highly sensitive and able to generate stand-alone useable data. However, the following section will endeavour to provide a balanced overview of their potential advantageous and deleterious characteristics; improvements can be made in a number of areas.

Sensitivity, within this particular topic, refers directly to an assays ability to differentiate between spontaneous background and an induced increase in the measurable endpoint, when compared to negative controls. For example, within an in-vitro micronucleus assay [69], sensitivity refers to the assays ability to detect a compound induced statistically, biologically, significant increase in the frequency of micronuclei when compared to a con-current vehicle control. In-vitro test systems historically have been criticized for being overly sensitive, i.e. a number of in-vivo negative compounds have generated positive results within the in-vitro assay protocol [104]. Consequentially the in-vitro systems tend to generate lower PoD potency metrics when likened to the same chemical within in-vivo rodent models, as expected, due to crudeness of chemical delivery. However, due to this relationship, preliminary investigations into in-vitro to in-vivo dose extrapolation (Carcinogenicity PoD) look promising [28].

This elevated false positive rate when compared to in-vivo assays has led to criticism, within the pharmaceutical industry, and has potentially large implications; Ames positive potential therapeutic compounds can be abandoned due to their high likelihood of a corresponding positive result in subsequent in-vivo genetox assays. However, the relevance of the data as well as the test conditions utilised to generate the data have come under reproach; with suggestions of exaggerated dosing regimens at biologically irrelevant concentrations that can often cause such false positive results [105]. In-vitro test systems if suitably designed are cost effective and can be used as the first stage in pre-clinical safety assessment. Their often over sensitive and easily modified/manipulated experimental design [106] is highly beneficial for early stage drug attrition. Consequently, novel mammalian cell in-vitro genetox assays are being assessed for their use in follow up testing as more accurate predictive tools for genotoxic carcinogenicity [107] taking into account biologically relevant maximum test concentrations.

The route of drug administration within basic in-vitro test system is often criticized, the fundamental approach within in vitro 2D mono-culture based test systems, direct exposure, does not take into account or facilitate the modelling and impact that route of admission (absorption), point of contact, drug half-life, distribution, metabolism (not true in all cases) and elimination have on dose response metrics following compound exposure [108]; often resulting in elevated maximum dose concentrations and false positives. Therefore, in order to generate an environment more analogous to that of human exposure, 3D-tissue constructs provide an in-vivo mimicking microenvironment encompassing a number of pharmacokinetic physiognomies, for example, within the 3D-skin constructs (Figure 1.6), the point of contact, drug penetrance, reactivity of drug following penetrance (half-life) as well as distribution are all modelled [93].

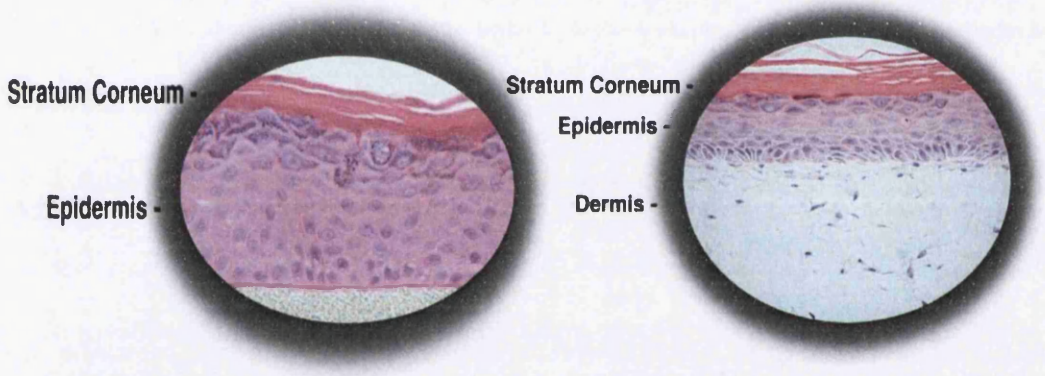

Figure 1.6. Two commercially available MatTek 3-D epidermis models, EpiDERM and the EpidermFT. The EpiDERM model (pictured left) consists of normal, human-derived epidermal keratinocytes, whereas the EpiDERMFT (pictured right) additionally consists of human-derived dermal fibroblasts. Note the supplementary presence of the Dermis as a direct result of fibroblast co-culture - Taken from [109].

However, the relative crudeness of an in vitro system actually radically increases the number of downstream applications said cells can be used within. Most cell/tissue types within in-vitro test systems can be processed on numerous downstream appliances, plate reader, flow cytometer, in-cell analyser etc. with minimal processing and hence, low levels of cellular attrition. At this point fixing the cells, a technique utilised to preserve the finer structure of the cell through the induction of protein polymerisation; cross linking between adjacent free functional groups resulting in a matrix like insoluble lattice [110], for long term storage or microscopy

applications generates high quality end results. However, processing in-vivo/ex-vivo samples often requires more extensive protocol design; intense often deleterious homogenisation and high speed centrifugation [111] result in heterogeneity within the subsequent population decreasing assay reproducibility and robustness, tissue location depended.

Traditionally, mammalian cell (non-human) cell lineages, for example Chinese Hamster Ovary (CHO) cells as well as Chinese Hamster Lung V79 [102] were routinely used within genetox testing. In recent years criticism has been attributed to these rodent cell lines; unacceptable levels of genomic instability as well as questionable or no functional TP53 status, leading to progressive disuse [112]. Human biological relevance, especially in the context of in-vitro to human extrapolation, has gained significant aptitude and resultantly has advanced the field into using human-p53 competent cell lines (*TK*6) [113-115] instead of the traditional commercially available rodent alternatives.

TP53 is a tumour suppressor gene which has been reported to be mutated in the region of 10-99% (depending upon metastatic potential and aggression) of all cancer types [116]. The TP53 gene encodes a 53 kDa nuclear transcription factor - in its in-active form, MDM2 associates to the protein (increasing the likelihood of degradation) and subsequently the protein complex is shuttled into the cytoplasm distal to any potential nuclear target genes [117]. In response to oxidative stress, DNA damage, hypoxia and osmotic shock p53 becomes active (Figure 1.7); conformational activation via a phosphorylation at the N-terminus domain (serine 15) and is shuttled back into the nucleus (dramatic associated half-life increase) [118]. P53 has subsequent roles in apoptosis and cell cycle regulation, via the modulation of nuclear proteins such as p21 (WAF1-CIP1) [119], and following Cyclin dependent Kinase 2 inhibition (CDK2) causes arrest within the G1/2 regulation checkpoint, the cell is either able to facilitate p53 dependent DNA repair and fix said DNA damage or alternatively, the cell can begin to facilitate the initial stages of apoptosis, programmed cell death [120].

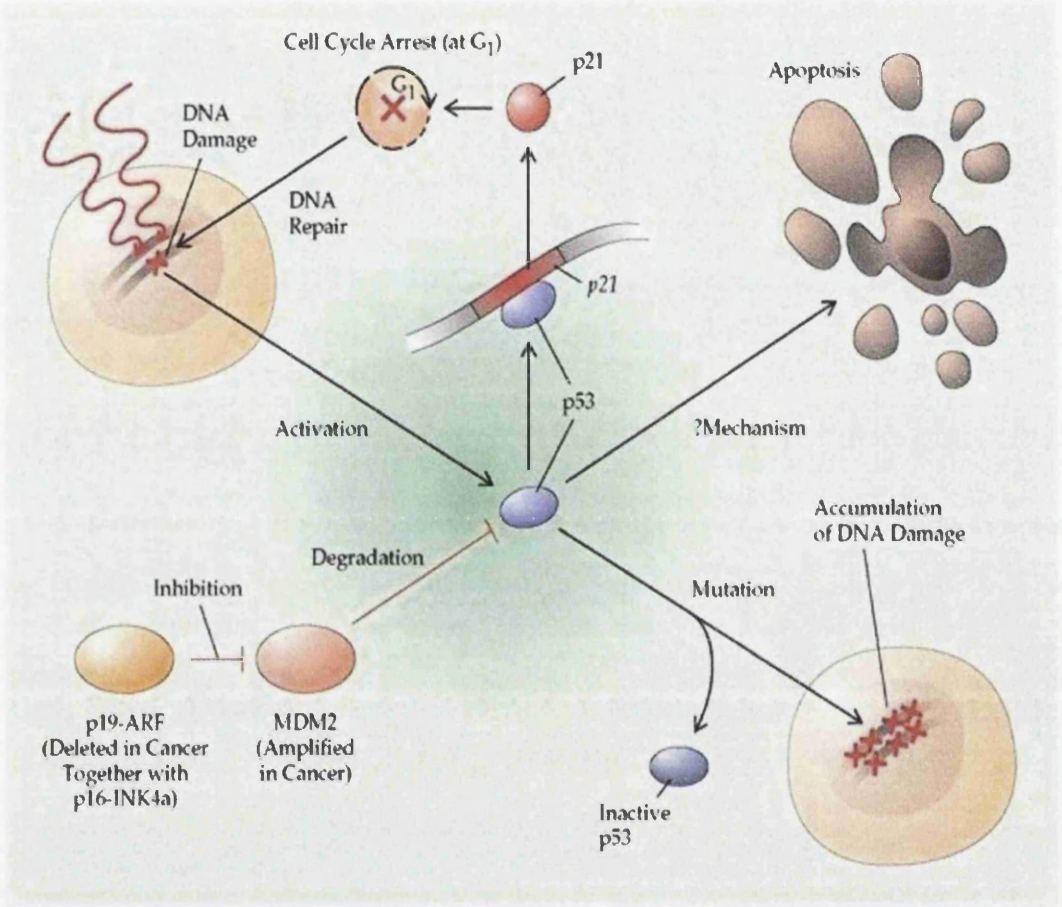

Figure 1.7. The p53-DNA damage response pathway. p53 is activated after DNA damage (cytoplasm) and shuttled to the nucleus, resulting in either of two cellular responses: induction of the CDK inhibitor p21, which leads to a G1/2-phase cell cycle arrest, allowing time to repair DNA damage before cellular division; and programmed cell death (apoptosis).MDM2 induces the normal degradation of p53 protein, and amplification of MDM2 in some tumours results in loss of p53 function. p19-ARF inhibits the effects of MDM2 and contributes to the activation of p53 in response to DNA damage. p19-ARF is commonly deleted in human cancers, along with its neighbouring gene, p16-INK4a - Taken from [121].

Somatic human cells are primarily homozygous p53 wild type (wt), however, heterogeneity at the p53 locus greatly increases the frequency of carcinogenesis [122]. The reasons for this are; firstly, there is only a single functional copy (allele) of the p53 gene within each cell and secondly, the probability of formation of the p53 protein is highly reduced, due to the homo-tetramer tertiary structure of the p53 protein [123]. P53 competency is of major importance within genetic toxicology, not only for biological relevance; point of departure matrices are significantly dependent upon the functional p53 status, within the test system assayed. Within heterogeneous and homogeneous mutant genotype cultures, mutant p53 phenotypes such as the loss of the G1 checkpoint and delayed apoptotic cell death are readily reported; characteristics which have been consistently observed in the AHH-1 *TK*+/- cell line following exposure to DNA-damaging agents [124]. P53 competency provides cellular cultures with a biologially insignifcant level of mutation, a buffer zone, which is not strictly deleterious in nature due to the fact that the mutation has not become fixed and is able to be potentially repaired and hence, the fate of the cell is not static.

For example, following MMS exposure, a typical somatic cell acquires a O^6methylguanine adducted base, which we know to be mutagenic in nature [16]. Functional p53 competency, if such DNA damage is identified, can result in p21-mediated checkpoint arrest and subsequently facilitates the cell to actively remove such a lesion via MGMT activity or alternativey subject the cell to programmed cell death; both mechanisms prevent the mutation from becoming fixed within the genome and preventing harm. Deleterious effects will only become significant, when either MMS concentrations saturate DNA repair mechanisms or cytotoxicity raises to a level which does not facilitate cell viability. However, when directly comparing this to dis-functional P53 cell line (heterzygous or more dramtically homozygous p53 mutant). Due to either limited p53 protein or dis-functional TP53 expression the subsequent somatic cells lack the ability to deviate the cell's fate (apoptosis) or induce a checkpoint arrest to help enable DNA reapir of mutagenic or clastogenic lesions. As a result of this, p53 incomptency results in a cell being overly sensitive to compound exposure and hence, has a much lower point of departure metric. Subsequent highly conserved point of departure metrics have little biological

significance in the context of human exposure. "Rigorous quantitative studies of p53 dynamics in the context of differential activation of DNA repair, cell cycle arrest, and apoptosis pathways are urgently required. To determine the low–dose- response behaviour for mutation and the point of departure to adversity" [125]

P53 status within cell lines routinely used for genetox assays ,TK6, AHH-1, MCL-5 etc. have been debated consistently over the past 20 years [126]. Typical mutation hot spots, Codon 282 - exon 8 , have been assessed and analysed (restriction analysis) within the p53 genes; inconsistencies related to derivation of cell line and maintenace of cell stock have led to contradictory publications [124, 126].

Discrepancies observed during direct inter-laboratory trial data, mainly as a result of genetic drift post undocumented distribution, has resulted in numerous journals requiring supplementary certification other than the original purchase order prior to publication. This can partly be attributed to the lack of global harmonisation of assay protocol [82]; elevated genomic instability (e.g. loss of gain of whole chromosomes), hyper variable spontaneous mutant frequency (within the same or common ancestral cell lines [127]), lack of good clinical practice (GCP) and raised inconsistency within experimental repeats suggests a more fundamental problem.

The introduction of nanoparticle research within the field of genetic toxicology generated a substantial problem for traditional in-vitro assays. The reasons for this are extensive [128], nevertheless in brief; nano particles often are small enough to enter the nucleus and hence, theoretically can interact directly with the DNA molecules [129] potentially resulting in replication error (aneugenic) and potential DNA damage lesions (mutagenic/clastogenic). However, in practice due to the heterogeneity of nano particles; surface charge, surface structure/coating, agglomeration status, loading capability and numerous other factors, typically standard in-vitro test systems are unable to accurately model such elements; often resulting in insignificant false negatives [130]. Taking agglomeration status as an example, nanoparticles have a tendency to associate and hence form agglomerates of varying shapes and sizes often due to surface charge or protein coating as a result of serum containing media dispersion [131]. This subsequent net increase in size and charge frequently fundamentally alters the physical characteristics of the nanoparticle and for this specific example, lowers nanoparticle penetrance into the

nuclear envelope and hence prevents direct DNA interaction, thus generating no significant positive result [132]. However, bio-accumulation of such foreign nanoparticles within the intracellular endosomal compartments is a potential source of oxidative stress, which can lead to the induction of reactive oxygen species (ROS), the up-regulation of Haemeoxygenase 1 (HO-1) expression, apoptosis and autophagy [133]. The net result is that nano particles can also induce secondary toxicity in macrophage lineages, due to their role in phagocytosis and subsequent clearance of damaged cells [134]. Current in vitro test systems require substantial modification in order to try and address some of these issues; co-culture assay design, utilising human macrophage cell lines could be one potential adaptation to more accurately model secondary toxicity.

However, regardless of the potential caveats associate to the use of in-vitro test systems they maintain a distinctive role and facilitate a need for inclusion within future safety assessment. In vitro systems can offer high throughput, high precision and high content analysis which enable such applications as ToxCast™ to provide a chemical evaluation of a compound. A most important part of EPA's Computation Toxicology research is the Toxicity Forecaster (ToxCast™). ToxCast™ uses automated chemical screening technologies, high-throughput screening assays, to expose living cells or isolated proteins to chemicals. The cells or proteins are then subsequently assessed for variations in biological activity that may suggest potential toxicity [135].

Therefore, in conclusion in vitro test systems are relatively inexpensive, quick, high content and sensitive, however, there is a real need to develop more modern, equivalent assays to which take into account the limitations listed formerly and thus, can enable the generation and compiling of significantly more biologically relevant 21st century genetox data. An example of such an initiative is the federal agency collaboration called Toxicity Testing in the 21st Century (Tox21), which pools such chemical research data and has successfully compiled high-throughput screening data on nearly ten thousand chemicals [136].

1.6 Phosphatidyl Inositol Glycan Biosynthesis Class A Gene (*PIG-A*)

Paroxysomal Nocturnal Haemoglobinuria (PNH) is a clonally non-malignant acquired haematological disorder, which has been reproducibly shown to result from a somatic gene mutation within a bone marrow stem cell or early progenitor cell [137]. Bone marrow stem cells are the precursors for the entire haematopoietic system and thus, this specific gene mutation within such a fundamental cell type can effect numerous cell lineages; pluripotent characteristics demonstrated by the bone marrow stem cells facilitate a number of different genotoxicity assays being directed at tissues of haemopoetic origin [138]. Symptoms of PNH include the consequences of complement-mediated haemolysis, venous thrombosis and bone marrow failure; anaemia, discolouration of urine (especially prominent within the first urination of the day), exhaustion and abridged patient life span [139]. PNH is easily diagnosed via immunocytochemistry staining, coupled with subsequent flow cytometry analysis, of a minute volume of peripheral blood; requiring no highly invasive investigatory techniques such as a colonoscopy. PNH effects approximately 1-2 persons per million of the general population [140], however, the symptoms are severe enough to warrant investigation. Following the identification of the mutational event inducing the disease phenotype, primarily a silencing event within the *Pig-A* gene [141]; deriving the biological implications this genotype has on functionality was the next logical goal of research.

The phosphatidylinositol glycan complementation group Class A (*PIG-A*) gene is located on the X-chromosome, X. p22.1 (Molecular Location on the X chromosome: base pairs 15,319,450 to 15,335,553) [142] and due to its X-linked location (heterozygous), makes it highly sensitive to mutational inactivation. The *Pig-A* gene encodes a protein critical for the synthesis for a catalytic subunit of the N-acetyl-glucosamine transferase complex which is required for the first step of glycosylphosphatidylinositol (GPI) anchor biosynthesis [143]. GPI anchors are small membrane tethers which attached a whole plethora of surface antigens which make up the complement of GPI-linked cellular surface markers; each cell type has lineage specific GPI-linked proteins facilitating characteristic surface membrane trafficking and cellular function. The process of GPI anchor biosynthesis requires at least 12

genes and, theoretically, silencing events of any of these would lead to GPI anchor deficiency [137]. However, the *Pig-A* gene is the only gene involved in this process which is not autosomal, x-linked, thus requiring only a single silencing event to cause GPI anchor deficiency, and making it a potential candidate to act as a reporter gene within a gene mutation assay [144]. For autosomal genes critical within the GPI-anchor synthesis pathway, mutations on both active alleles must occur prior to an observed null phenotype, insensitivity of a homozygous reporter gene, and hence the probability of such a linked event is low ($1x10^{-20}$ – 2 x (Overall error of DNA polymerase ($1x10^{-8}$) multiplied by the fidelity of repair ($1x10^{-2}$)) [145]. This double mutational event is extremely rare and it is therefore, perceived that the inability to anchor GPI-linked proteins to the cell membrane is equivalent to a *Pig-A* mutation [137]. To further cement this idea, continued research into the origins of the acquired genetic disease involving GPI anchor deficiency, known as (PNH), indicates that cells lacking GPI anchors or GPI-anchored cell surface proteins is almost always caused by a somatic mutation in the *PIG-A* gene [143], however, *PIG-T* mutations recently have been shown to induce the GPI-AP deficient phenotype [146].

PNH presents itself as a highly variable, heterogeneous, disorder which has recently adopted the term "PNH syndrome" in order to encapsulate additional disease phenotypes [141]. Due to the variability of the original silencing event, both in terms of cell lineage (clonal origin and expansion) and time of development (congenital or acquired) manifestations and subsequent prognosis is also highly variable [147]. Classical congenital PNH (silencing affect within the *PIG-A* gene locus) results in patients lacking the full complement of cellular surface antigens on the extracellular surface of the cellular membrane due to an inhibition of GPI anchor biosynthesis. Antigens on the cell membrane have numerous roles within signal transduction [148], receptor ligand binding, immunology (complement system regulation), cell trafficking, cellular uptake, cell signalling and identification [149]. Therefore, when a cell presents with such a phenotype, autoimmune response is common due to severe loss of cell functionality. Human erythrocytes (red blood cells) are initially differentiated from hematopoietic stem cells located within the bone marrow (Erythropoiesis) [150], with the ability to self-renew indefinitely in culture while also maintaining the aptitude to become almost any cell type in the human body [151].

Somatic mutational silencing occurring within the *PIG-A* gene of a bone marrow stem cell, or early progenitor cell, can potentially result in the clonal expansion of said PNH phenotype; systemic distribution of GPI-linked surface antigen deficient haemopoetic cells (erythrocytes and leukocytes). In the case of human erythrocytes; there are a number of vital GPI-linked surface antigens, complement regulatory proteins, which are critical in homeostatic regulation of haemopoetic tissue [152]. CD59, also referred to as protectin, encodes a cell surface glycoprotein that regulates complement-mediated cell lysis, and it is involved in lymphocyte signal transduction. This protein is a potent inhibitor of the complement membrane attack complex (MAC), whereby it binds complement C8 and/or C9 during the assembly of this complex, thus preventing the incorporation of multiple copies of C9 into the complex which is thought to be necessary for osmolytic pore formation. Mutations in this gene, as well as GPI-anchor biosynthesis genes, cause CD59 deficiency; a disease phenotype exhibiting haemolytic anaemia and thrombosis symptoms, which can potentially cause cerebral infarction (stroke), due to licentious MAC mediated haematocyte lysis [153]. CD55 encodes a protein involved in the regulation of the complement cascade. The encoded glycoprotein is also known as the decay-accelerating factor (DAF); binding of DAF to complement proteins accelerates their decay, disrupting the cascade and preventing damage to host cells (mainly through lysis). Antigens present on the DAF glycoprotein constitute the Cromer blood group system (CROM) [154]. The combined action of CD55 and CD59 regulates homeostatic haemolysis within the peripheral circulatory system; this is critical due to the nature of erythrocytic maturation. Erythrocytes pass through an immature precursor stage in which they have an active RNA reticule, providing them with their classification – Reticulocytes. Once matured, red blood cell (RBC) remain within the circulatory system for an estimated 100-120 days [155]. Remnants of mRNA remain at this point (post nucleus expulsion at earlier stages) and therefore, if the RBC takes sufficient damage whilst within the periphery, functionality is comprised requiring; accumulation of damaged erythrocytes could increase risk of blood clotting, (stroke and myocardia infraction) and anaemia.

Compliment system mediated haemolysis of GPI-AP defective RBCs is an example of the auto-immune response within humans; attacking erythrocytes deficient with regulatory proteins (CD59/CD55). This phenomenon is not only observed within

humans, mice express two analogous genes to human CD59 (hCD59) mCD59a and mCD59b and rats express a single analogous gene rCD59, both have been experimentally proven to induce protection from complement mediated lysis (haemolytic anaemia) [156, 157]. Therefore, when designing a rodent/human genetic toxicology assay based around GPI-AP deficiency (CD55/CD59 presence), one must take into account the caveat of potential GPI-AP mutant clearance via autoimmune complement mediated responses; theoretically making the task of estimating subsequent DNA damage post exposure very problematic within the haematocyte cell lineage.

1.6.1 Development of the Rodent *Pig-a* Gene Mutation Assay

In the early 21st century Litron ™ began to file patents for the design of a commercial kit, with the sole intent to in-directly measure the *Pig-a* gene mutation frequency within rodent erythrocyte models [158-160]. The patents describe the detailed use of immunohistochemical staining (fluorescence polyclonal antibody conjugates) against GPI-linked cellular surface antigens (CD59, CD24 etc.) coupled to high throughput flow cytometric analysis [143, 161]. Wild type, presumed *Pig-a* gene proficient cells, retain intact functional GPI-anchor moiety biosynthesis; the anchor structure, comprising of three mannose, a glucose and a inositol sub unit, as well as the required extracellular proteins (CD24, CD59 etc.) are coupled together, within the endoplasmic reticulum, and transported to the cellular membrane [162]. At this point in the mechanism, the anchored proteins are attached to the membrane via fatty acid tail hydrolysis [163] and can be subjected to fluorescence antibody conjugation as a form of detection and qualitative assessment [143]. Therefore, the mutation rate at the *Pig-a* gene locus is in-directly measured by the direct quantitation of the absence or presence of GPI – associated surface antigens, species specific (Figure 1.8).

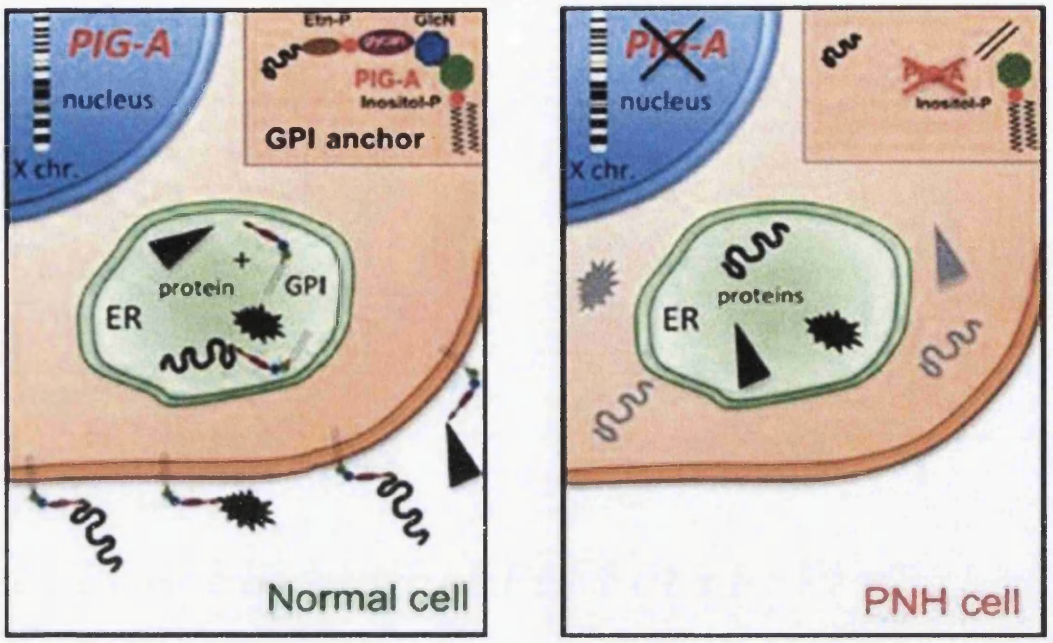

Figure 1.8. The molecular basis of PNH; biosynthetic machinery produces the GPI molecule within the Endoplasmic Reticulum (ER) of a normal cell (left). An early step in this pathway is catalysed by an acetylglucosaminyl transferase: one of the subunits of this enzyme is encoded by the gene PIG-A. A number of cellular proteins become covalently linked to the GPI molecule that serves for conveying and anchoring them on the surface of the cell membrane. The PNH cell (right) has a mutation in the PIG-A gene that impairs acetylglucosaminyl transferase activity and causes a total (or partial) block in the synthesis of the GPI molecule. As a result, the proteins requiring a GPI anchor are unable to bind to the membrane and will be lacking on the cell surface - Taken from [164].

Continued development provided an initial in vivo rat *Pig-a* gene mutation assay protocol, employing both mature erythrocytes (RBCs) and the immature fraction, reticulocytes (RETs). Dual end point analysis was performed in order to assess the growth dynamic, i.e. do Pig-a deficient clones have a growth positive or negative bias [165], and relationship between mutational event and clonal origin within the haemopoetic tissue, during an extended international *Pig-a* cross laboratory trial [166, 167]. Initial results of such trial demonstrated an inadequacy in sample collection; limited number of RET events were able to be captured during analysis and therefore, sample sizes were required to be increased in order to provide more statistical robustness [143]. In order to address this problem, due to the time contstraints working with haemopoietic tissue provides, a novel approach utilising

magnetic beads to enrich for *Pig-a* mutants was implemented [168]. Enriched mutant data was directly compared against con-current total events, counting bead derived, in order to provide a more robust sample size and mutant frequency data. The subsequent modernised experimental design was able to capture enriched RET and RBC fractions, and provide adequate outcomes to warrant increased momentum from regulatory with the overall achievable aim of an OECD guideline [13, 91, 169, 170]. Observations were made throughout the data acquisition stage; RETs expectedly were demonstrated to present induced mutant frequencies at an earlier time points (day 15) then their RBC counterparts [171] and the *Pig-a* assay was confirmed to be able to be incorporated into a routine 28-day tox study without compromising dose response metrics [91].

However, the erythrocyte-based analyses also highlighted a disadvantage; mature erythrocytes or reticulocytes do not contain a viable nucleus and therefore, definitive proof of genotype-phenotype relationship cannot be demonstrated via standard (Sanger) or novel (Next Generation) sequencing approaches. This postulation was deemed acceptable due to the sheer amount of published literature confirming the common *PIG-A* mutation exhibited within PNH patients [172, 173]. However, purists still remained sceptical about the origins of the presumed *Pig-a* mutants, GPI-AP deficient cells, any number of PIG genes (twenty-two) involved in either the GPI-AP biosynthesis pathway [174] as well as structural/transport or the individual surface antigen marker could be the cause of the observed phenotype [146], even though statistically unlikely. Measuring GPI-AP deficiency was not cell type reliant, but more GPI-AP dependent. Thus, assay portability into different haemopoetic cell lineages as well as transferability was something of great interest [144, 175].

Accordingly, analogous preliminary studies, utilising cells of haemopoetic lineage (erythroid and T-lymphocyte respectively), to the rodent *Pig-a* in-vivo assay have provided increasing evidence that mutational events within the *PIG-A* gene are the fundamental cause of the GPI-AP deficient phenotype [77, 161]. Significant investment into a complimentary rodent leukocyte (nucleated) *PIG-A* assay has been undertaken in order to facilitate, at least initially, parallel experiments to provide further classification of the GPI-AP deficiency mechanism [77, 144, 169, 175, 176].

As stated above the *Pig-a* gene mutation assay has demonstrated great transferability within haemopoetic tissue; the highly conserved nature of GPI-anchor synthesis, there is a great degree of interspecies conservation of the *PIG-A* genes structure, function and locus and should facilitate the application of this basic methodology across any species of toxicological interest [177] – recently, a study describing the development of an in-vitro *PIG-O* assay in DT40 chicken cells was published, further emphasizing assay transferability [178].

The in vivo *Pig-a* assay still requires additional information to fully satisfy the regulatory community, subsequently leading to OECD guideline sanction. Single cell sequence and dose response data validating more ambiguous chemicals, historically proving the bane of number other test systems [179], will still need to be generated , however, the assay appears to be highly promising. One potential method of strengthening the mechanistic exploration of the assay, as well as to modernise the current mammalian in-vitro gene mutation test assays, would be with the development of an in vitro *PIG-A* correlate assay; utilising the equivalent high throughput flow cytometry based system of analysis (lineage specific GPI-anchor deficiency). Providing an in-vitro correlate assay could initially deliver a platform in order to produce additional evidence validating the true identity of presumptive *Pig-a* mutants [180] and hence, increasing the likelihood full assay acceptance. Utilising a biologically relevant human haemopoetic cell lineage, equivalent to *Pig-a* analysis of T-lymphocytes isolated from the spleens of rodents [144] – B-Lymphocyte (*TK*6), and analogous immuno-cytological staining procedure, endeavours have been made to provide a suitable test system to generate in-expensive large quantities of quantitative dose response data and detailed mechanistic evaluation [181].

1.7 Current Regulatory Mammalian in vitro Gene Mutation Assays: Do They Require Modernising?

The ICH, FDA, OECD and IWGT expert guidance and subsequent individual guidelines, still state the required need for in-vitro, mammalian cell, gene mutation assays within the early stages of pre-clinical drug development [65]. Historically, this niche has often been filled by either the *HPRT* (academia) or *TK – MLA* (industry) assays [70, 71]; both assays are fully validated and are outlined in detailed within the published OECD protocol [73] and have been used routinely for decades generating reproducible genetic toxicology data following assay evolution.

However, both assays are known to have specific constraints and disadvantages within the scope of a quantitative genetox testing, initially let us consider the *HPRT* assay. Clonal expansion/growth in order to assess cytotoxicity, post mutation fixing, requires the assay to take place over a number of weeks, depending upon the specific method and/or cell type used. Allowing immortalised cells to achieve high passage increases the likelihood of genetic drift and subsequent genomic instability; these factors could elevate mutant frequencies (spontaneous and induced) and thus affect subsequent dose response data. The *HPRT* assay has high transferability between in-vitro cell lines and in-vivo somatic cells, due to the conserved nature of the X-linked gene. However, the choice of cell line should demonstrate competent DNA repair and homozygous p53 status, a feature which has been debated within the AHH-1 cell line commonly chosen for the assay [182]. The *HPRT* can be described as a highly laborious 96 well plate assay requiring manual microscopic scoring and a high level of expertise in order to generate robust, reproducible data. Cost and time investments can rapidly multiply when utilising the assay for dose response investigations [39].

The (*TK*) Mouse Lymphoma Assay (*MLA*) operates under a similar principle to the *HPRT* assay, however, due to subtle differences has dissimilar disadvantageous associated to the design. The use of a rodent immortalised cell line, L5178Y cells, with demonstrated dysfunctional p53 status [183] has led to the assay previously being described as overly sensitive and thus, generating false positive results [184]. The MLA assay shares an analogous design in terms of plating and cloning

efficiency to the *HPRT* assay and therefore, also shares the laborious manual 96 well plate scoring. The assay was first described in the 1970's by Clive et al., [185, 186] and subsequently could benefit from utilising more modern technology in order to increase throughput and reduce subjectivity.

Therefore, providing an in-vitro correlate to the in vivo *Pig-a* assay in order to more fully investigate mechanistic studies could also have a larger impact on genetic toxicology testing. An in vitro *PIG-A* gene mutation assay could also reform the more traditional manually scored genetox assays (*TK/MLA* and/or the *HPRT*); conforming to current regulatory pressure and utilising 21st century technology to increase assay content, sensitivity, biological relevance (human cell p53 functional cell lines) and throughput [187].

1.7.1 21st Century Technology: Novel Genetic Toxicology Testing

In order to transport genetic toxicology testing into the 21st century, there is a potential need to utilise contemporary technological advances within the immediate field, as well as adjacent related fields, to facilitate this modernisation. Application of computational toxicology, more specifically in-silico QSAR packages [63], as well as the expanded use of toxicogenomics to illuminate mechanisms within safety testing are possible means for reducing the requirement for extensive animal testing and human clinical trials [187]. However, for the scope of this project we will focus upon the development of novel 21st century technology to facilitate the establishment of a potential highly sensitive, high content, high throughput, high precision, biologically relevant in vitro gene mutation assay which hopefully will coincide with other additional developing assays such as Ames 2 [188], H2AX [189, 190] and Bluescreen™ [191]. Generating such data through the ToxCast™ strategy, as well as compiling the data through such initiatives as Tox21, will provide increasing novel chemical evaluations [135, 136].

Flow cytometry is a technology which simultaneously measures and then records numerous physical characteristics of single particles within a fluid stream as they pass through a high energy beam of light (Figure 1.9). Routinely used within

biological sciences, the particle is often a single whole cell or a small agglomerates of cells. The recorded properties include relative size of cell – forward scatter (FSC), relative granularity/complexity, side scatter (SSC) and relative fluorescent intensity. As well as these three typical measure, most commercial flow cytometers now have to option to provide additional information about the actual properties of the detected resultant fluorescence light beam, these include a time of flight measurement (fluorescence width), the maximum intensity of the light (fluorescence height) and the total fluorescence measured during the analysis period (fluorescence area). Commonly these parameters are measured via an optical (high energy laser) to electron (photocathode within a photon multiplier tube) capturing system which record how the subject element scatters the incident high energy laser light and emits and subsequent fluorescence [192].

Coupling this system with the use of immunohistochemical staining and the user is able to generate accurate data based on biological markers of interest including; cellular surface antigens, cell cycle, cellular viability, cellular proliferation etc., for each event within the population often greater than $1x10^6$ total cells. This capability of high content/ high throughout analysis has radically enabled genetic toxicology to exponentially increase the sample size and number of measurable end points within the specific assay able to be recorded, when compared to traditional manually scored genetox assays [69]. Increasing the biological relevance as well as the sheer total number of events recorded has the effect of greatly increasing biological significance, statistical power and confidence within subsequently generated data sets.

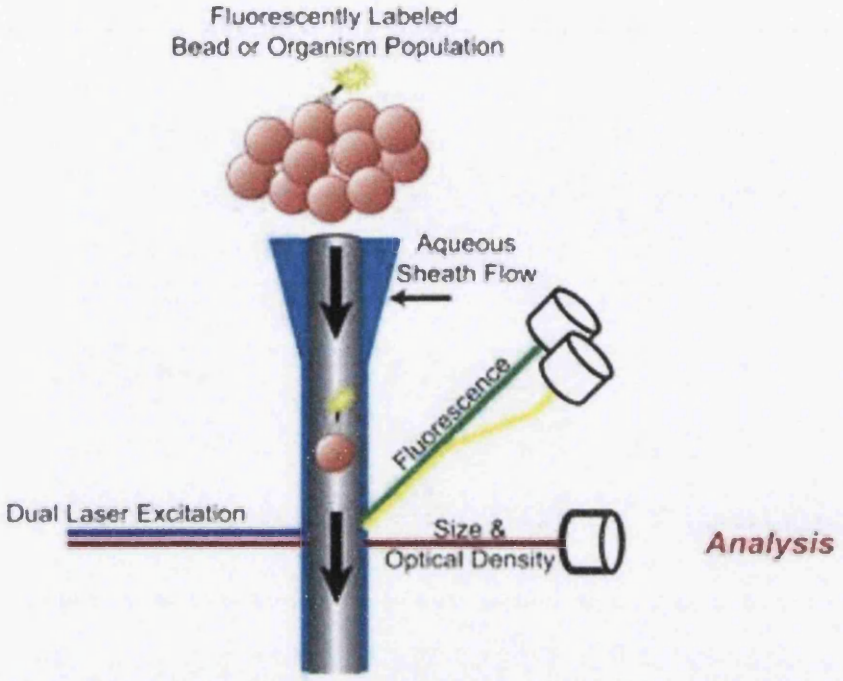

Figure 1.9. Flow cytometry basics: Particles or cells are subjected to high energy laser illumination in order to capture detailed information based on scattering of resultant light. Cell or particle size, complexity/granularity as well as emitted fluorescence profile, when utilised in conjunction with fluorophores, can be directed onto detectors and displayed in an electrical format via coupled computational software. Adapted from an image produced by Union Biometrica.

Traditionally, fluorescence microscopy and like techniques are highly labour intensive in terms of preparations as well as data interpretation, often conveying a sense of subjectivity especially during the latter stage of image interpretation and analysis. However, the modernisation of such techniques with the development of stage scanning microscopy [193] and more recently, ImageStream ™ [194] analysis has enabled the labour intensive preparation to be fully exploited to enable high content, multi-end point mutual analysis with fixed scoring criteria and objective results.

In terms of the ImageStream ™ system, relatively high resolution microscopy (Figure 1.10) has been combined with simple flow cytometry to produce a system able to generate either 2-D or extended 3-D renders of each event as it passes through the point of laser interrogation.

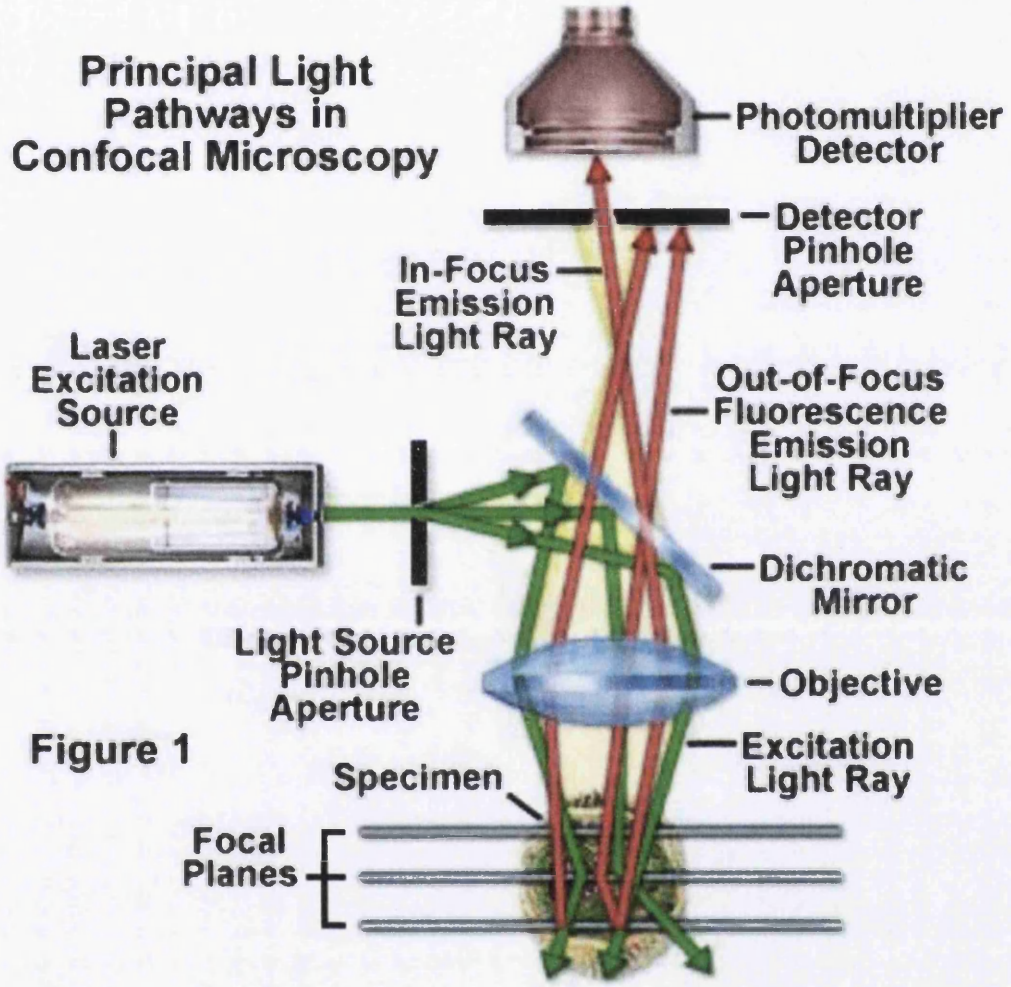

Figure 1.10. Confocal Microscopy Principles: Specimens are exposed to light, in this case high energy laser, and the resultant emitted light is re-focussed within a pin hole aperture. Confocal imaging approach provides a marginal improvement in both axial and lateral resolution, but it is the ability of the instrument to exclude from the image the "out of focus" flare that occurs in thick fluorescently labelled specimens, which has caused the recent explosion in popularity of the technique - Taken from [195].

This technology enables the user to benefit from most of the advantageous associated with flow cytometry, high content, high through put etc., without the associated disadvantage of not being able to see a render of the actual event to further increase

confidence of the recorded data. Laser scanning confocal microscopy enables the user to prepare a sample in the traditional procedure however, allows the user to benefit from the scanning feature which progressively moves along the prepared slide capturing in excess of thousands of tiled images which can be re-constructed together retrospectively to generate image data for sample sizes comparable of flow cytometry workloads. This exponential increase in sample size, with minimal tweaks to methodology, has propelled somewhat of an advanced sample specific technique to a more general, easily accessible common laboratory technique whilst maintaining high integrity detailed image data.

In order to help modernise such a field as genetic toxicology into the 21st century, and potentially update the previous routinely used current assay the implementation of such novel techniques/developments are essential. With the incorporation of novel technologies within genetox assays, a resultant positive feedback loop of technique incorporation, leading to technique interrogation and technical improvement should be observed further increasing assay transferability, sensitivity, robustness and usage within daily safety assessment and genetic toxicology applications.

1.8 Development of an in vitro *PIG-A* Gene Mutation Assay: 21st Century Genetox?

If applying a blue sky thinking approach to 21st century genetic toxicology one could come to the following conclusions; the field requires a high content - providing high levels of statistical power and multiplex analysis to facilitate adequate content and depth of data, human - enabling more adequate pharmacokinetic and dynamic modelling, in-vitro - to coincide with recent governmental reforms, high throughput - facilitating greater sample sizes, highly transferable - cross-platform validation, and highly sensitive - to enable low dose quantitative response modelling, genetic toxicology assay as mirrored by the ICH guidelines [64].

Within this project of work, the development of an in vitro *PIG-A* gene mutation assay is described. The assay was established with all of the potential advantages, as listed above, taken into account to attempt to provide a novel genetox assay which

will facilitate the modernisation of the current field. The assay is based on an analogous design to the current in vivo *Pig-a* gene mutation assay [196], i.e. immunohistochemical antibody staining and subsequent flow cytometric analysis of GPI-anchored cellular surface markers. Flow cytometry provides the assay with a high content/throughput system enabling exaggerated sample size as well as significantly more contextual information than comparable current in-vitro assays [185]. The assay will utilise p53 competent B-lymphoblastoid human cell lines, in order to firstly, increase biological relevance within the data set, as well as allow a downstream sequencing approach to assay validation and avoid further animal usage within the industry. The conserved nature of the GPI-AP allows the approach to be mirrored into other species as well as primary human samples, highlighting assay transferability.

Chapter 2: General Materials and Method

All work carried out in preparation and during the biological experiments which make up the body of this thesis project were carried out in an aseptic manor and hence, unless otherwise stated all consumables and apparatus can be assumed to be sterile, or sterilised prior to usage.

2.1 Human Cell Lines

All human cell lines used within this project, unless otherwise stated were purchased from American Type Culture Collection (ATCC) in partnership with LGC standards, Middlesex UK. Cell culturing conditions were undertaken as specified by the supplied information following original purchase of the cell line.

2.1.1 TK6 Cell Culture

Epstein-Barr viral transformed TK6 human B lymphoblastoid cells were isolated from the HH4 lymphoblastoid line [197] which in turn originated from the WIL-2 cell line. TK6 cells express wild-type P53 and are heterozygous at the thymidine kinase locus [198]. The cell line was shown to test negative for Bovine Viral Diarrhoea Virus (BVDV).

2.1.2 "Low Passage" TK6 Cell Culture

Epstein-Barr viral transformed TK6 human B lymphoblastoid cells originally isolated from the WIL-2 cell line, maintained at a much lower passage number and supplied by Masa Honma, National Institute of Health Sciences (NIHS).

2.1.3 AHH-1 Cell Culture

AHH-1 human B-lymphoblastoid cells were derived from a culture of lymphoblasts supplied originally by Roswell Park Memorial Institute (RPMI), referred to as RPMI-1788 cells, for their high levels of mixed function oxidative activity; the cells were demonstrated to be highly sensitive to BaP exposure related cytotoxicity and hence, were selected for their basal and inducible oxidative activity. The cell line was shown to test negative for mycoplasma [199].

2.1.4 MCL-5 Cell Culture

MCL-5 cells were derived from a parental culture of AHH-1 B-lymphoblastoid cells, constitutively expressing human cytochrome P-450 CYP1A1 and also expressing five transfected human cDNAs encoding drug-metabolizing enzymes; cDNAs encoding CYP1A2, CYP2A6, and microsomal epoxide hydrolase (mEH) were introduced by using a vector conferring hygromycin B resistance, and cDNAs encoding CYP2E1 and CYP3A4 were introduced by using a vector conferring resistance to 1-histidinol [200]. The established MCL-5 cell line was demonstrated TK+/-, homologous to the parental AHH-1 cell line.

2.1.5 HepG2 Cell Culture

The Human hepatocellular HepG2 cell line was originally derived from a 15 year old male Caucasian presenting with a liver carcinoma. Epithelial in nature, the cell line demonstrates a large portion of cellular functions such as, expression of hepatocyte-specific cell surface receptors and synthesis and secretion of plasma proteins [201].

2.2 Cell Culture Procedure

Cell culture was under taken within a temperature controlled micro-environment, aseptic conditions were established within a Scanlaf Mars Pro (LaboGene, Lynge, Denmark) class two safety cabinet. Daily the cabinet was pre-cleaned with 70% ethanol following a pro-longed UV sterilisation. Greiner Bio-One (Gloucestershire, UK) supplied the majority of sterile culture apparatus including, Pasteur pipettes as well as a wide variety of different sized culture flasks. Cellular cultures were incubated and maintained under an artificial humidified atmosphere of 37°C, 5% CO_2 inside a NU-5510 DHD Autoflow incubator (The Nuaire Group, Caerphilly, UK). Centrifugation was undertaken using a temperature-controlled Eppendorf 5810R centrifuge with a 180 mm radius (Eppendorf, Hamburg Germany). Culture medium was specific for each cell line utilised as well as each constituent pre-warmed to 37°C; Normal TK6 and AHH-1 growth medium consisted of 89% (RPMI) 1640, 1% L-glutamine (Gibco®, Paisley, UK) and 10% horse serum (BioSer, Sussex, UK). Low Passage TK6 growth medium consisted of 89% RPMI 1640, 1% Penicillin-Streptomycin (Sku, 1514012210,000 U/mL, Gibco®, Paisley, UK) and 10% heat-inactivated horse serum (Cat No. 26050-088, Gibco ®, Paisley, UK). MCL-5 growth medium consisted of 89% RPMI 1640, 1% L-glutamine and 10% horse serum supplemented with additional Hygromycin B (Lot. No D00151132, 50 mg/mL, Merck, Hoddesdon, UK). HepG2 growth medium consisted of 90% Dulbecco's Modified Eagle Medium (DMEM) (Gibco®, Paisley, UK) and 10% Foetal Bovine Serum (FBS) (Cat No. 10091-148, Gibco®, Paisley, UK). Stock cell cultures were critically maintained between 1 x 10^5 and 1 x 10^6 cells/mL in 75

cm^2 culture flasks by routine sub-culturing, with exception of the normal TK6 cell line which was able to grow consistently from a 4 x 10^5 seeding concentration.

2.2.1 Cell Counting

All cell cultures were counted on either a Z1 Coulter Counter (Beckman Coulter, High Wycombe, UK); 100 µL aliquot of cellular suspension was diluted within 10 mL of Isoton (Beckman Coulter, High Wycombe UK) and cells counted using cell line specific optimised classifiers based on the cell size (TK6, AHH-1 10-17 µm, MCL-5 5-17 µm and HepG2 10-20 µm); or alternatively a glass Haemocytometer (Hawksley-Improved Neubauer, Depth 0.1 mm, 1/400 mm^2, Sussex, UK) and cover slip (Hawksley, 0.13-0.17 mm, Sussex, UK) was used in conjunction with an Axiovert 25 light microscope (Carl Zeiss, Cambridge, UK); low resolution optics were utilised in order to count the average distribution of cells via capillary action under the glass cover slip, all concentrations generated were regarded as estimates and repeated for concordance.

2.2.2 Dilution Equations

Equation 1 was initially used in order to generate a preliminary result, which was later cross referenced and checked against the result produced when using equation 2.

Equation 1

$$V_1 * C_1 = A$$
$$A/C_2 = B$$
$$V_1 - B = C$$

Equation 2

$$V_2 = (C_1/C_2) * V_1$$

Where,

A = Total number of cells required for seeding of new culture flask at desired concentration

B = Volume of suspension required to be aliquotted from the parental culture flask

C = Volume of fresh growth medium required to be added to volume B in order to construct the new culture flask at the desired seeding concentration.

V_1, C_1 = The respective volume and seeding concentration of the new culture flask

V_2, C_2 = The respective volume and cell concentration of the parental culture flask.

2.2.3 Cell Line Sub-Culturing

Prior to any laboratory cell culture, all cultures were examined under an Axiovert 25 light microscope (Carl Zeiss, Cambridge, UK) for obvious signs of contamination and general cellular viability; routine testing for Mycoplasma using MycoAlert® mycoplasma detection kit (Cat no: LT07-318, Lonza, Slough, UK) and corresponding controls (Cat no: LT07-518, Lonza, Slough, UK), was also under taken.

2.2.3.1 Suspension Cell Lines

Cell cultures were removed from incubation, moderately shaken and counted prior to a volume of cell suspension, corresponding to the desired reseeding concentration, being aliquotted into a sterile 50 mL centrifuge tube, centrifuged and supernatant aspirated. The cellular pellet was agitated utilising a large bore pipette in a minimal volume of new growth medium, preceding transfer to a new sterile 75 cm^2 culture flask. New growth medium was added to the culture flask to a final volume of 50 mL in order to reach the desired concentration and cultures returned back to incubation; sub culturing in this manner was repeated every 2-3 days. Wash steps entailed of 10 mL of pre-warmed Ca^{2+}, Mg^{2+} ion free phosphate buffered saline (PBS) (Gibco®, Paisley, UK) being added to the cellular pellets, inverted 2-3 times, followed by centrifugation and removal of supernatant.

2.2.3.2 Adherent Cell Lines

Cell cultures were removed from incubation, the existing growth medium discarded and the cells washed in excess pre-warmed pH 7.4 PBS, addition of the PBS was administered to the adjacent side of the culture flask to the adhered cells. 2-3mL of pre-warmed dissociating trypsin solution (Cat No. 25300-054, Gibco®, Paisley, UK) was added to the cells, dispersed evenly across the monolayer of adherent cells, the flasks rotated and then returned to incubate for a further 2-5 mins. When >90% of

cells were deemed to be detached, excess pre-warmed PBS or growth medium was added, pipetted across the base of the flask. Flask contents were then transferred into a 50 mL centrifuge tube, centrifuged and the supernatant aspirated. Prior to cell counting, minimal volumes of growth medium was added to the cell pellets, and the required volume of cells for re-seeding was initially removed and then diluted to the desired seeding concentration with new growth medium before being aliquotted into a new sterile 25-75 cm^2 culture flask. Cells were returned back to incubation and monitored every 48 hr for growth and sub-cultured 1-2 weekly in this manner.

2.3 Long Term Cellular Storage

Approximately 50 mL volume of confluent ($1x10^6$ cells mL^{-1}) cell culture was centrifuged at 800-1100 rpm (cell line dependent), within conical bottomed 50 mL centrifuge tubes (CellStar® Tubes, Greiner-Bio, Gloucestershire, UK), the supernatant aspirated and discarded. Cell cultures were re-suspended in 25 mL storage solution consisting of 1:9 volume ratio of dimethyl Sulfoxide (DMSO) (Sigma Aldrich, Gillingham, UK) to horse serum (Gibco ®, Paisley, UK) and carefully aliquotted into labelled (Cell line, Passage, Date and Operators initials) cryovials (Elkay Laboratory Products, Basingstoke, UK). Each cryovial was placed within an iso-propanol containing Nunclon (Thermo Scientific, Hampshire, UK), facilitating cooling at a 1°C/min rate, and housed within a -80°C freezer (Innova U725, New Brunswick Scientific, Hamburg, Germany) for 24 hr. Cryovials were independently removed from within the Nunclon and placed within liquid nitrogen (Locator SR Plus, Thermo Scientific, Hampshire, UK), primarily -196 °C liquid phase, for long term storage. Cryovial resurrection was undertaken at the start of each new experiment and involved a rapid thawing of the preserved culture at 37 °C, within a temperature controlled water bath (Sub Aqua 18, Grant, Cambridge, UK), immediately post thawing the culture was transferred to 49 mL of fresh culture medium within a 75 cm^2 culture flask.

2.4 General Handling and Preparation of Chemicals

Genotoxic chemicals as well as general laboratory solutions were handled within a controlled environment, either aseptically inside a Scanlaf Mars Pro class 2 safety cabinet or alternatively for volatile chemicals a AFA1000 (Clean Air Ltd, Bolton, UK) fume cupboard. All necessary personal protective equipment (PPE) were used according to the material safety and data sheet (MSDS) supplied on purchase of such chemical under assay, including arm length soft latex gloves (Cat No. 260685, KRUTEX, KRUUSE, Langeskov, Denmark), laboratory coat (65% Polyester, 35% Cotton), suitable protective eye wear and face mask (Disposable Respirator, 3M ™, Bracknell, UK).

All substances on arrival were assessed for correct storage conditions, optimum short term storage conditions were identified; light sensitive substances were wrapped in aluminium foil and the use of a temperature controlled (2-4 °C) cold room, -20 °C (Liebherr, Bulle, Switzerland) or -80 °C freezer where appropriate. For solutions requiring dilution with sterile water an autoclave (Prior Clave, London, UK) was utilised, alternatively filter-distilled water was prepared using a Milli-Q water system (Merck Millipore, Nottingham, UK). Where necessary, weighing out of chemicals was completed using a Sartorius LA120S Analytical Balance (Sartorius Group, Surrey, UK) coupled with weighing boats and pH value measured by way of a Jenway 3510 pH meter (Bibby Scientific Ltd, Staffordshire, UK). Stock solutions were prepared in varied sized glass ware, generally 0.25L-1L, bottles (Sigma Aldrich Gillingham, UK), suitably buffered and stored at appropriate temperature as necessary to enable optimum usage conditions. All items regardless of preparation required were stored at optimum conditions, double contained to prevent accidental leakages and labelled; name, date on arrival, expiration date, storage conditions and initials.

2.4.1 General Preparation of Hazardous Genotoxic Chemicals (G4 compounds)

Table 2.1 – Properties of G4 compounds

Trade Name/Abbreviation	Physical form (22°C)	Density (g/mL 20°C)	Boiling Point (°C)	Solvents (vehicles)	Container Description	Solvent Administration Method
Ethyl methanesulfonate (EMS)	Liquid	1.206g	85-86	H_20/DMSO	Glass Vial	Pipette
Methyl methanesulfonate (MMS)	Liquid	1.3	202-203	H_20/DMSO	Glass Vial	Pipette
1.1 N-Nitroso-N-ethylurea (ENU)	Solid (powder)	-	-	H_20	ISOPAC (pressurized container)	Large Bore needle and syringe
N-nitroso-n-methylurea (MNU)	Solid (powder)	-	-	H_20	ISOPAC (pressurized container)	Large Bore needle and syringe

2.4.2 General Dosing Regime of Hazardous Genotoxic Chemicals

Cultures were established as described in (Section 2.2.), cell counts were initially recorded prior to culture seeding, 10 mL total volume at 1 x 10^5 cells/mL. At this point, additional precautions were under taken to ensure personal safety; long arm latex gloves, polycarbonate clear safety spectacles (Safety4eyes, Dorset, UK) and a supplementary outer layer of latex free nitrile gloves (Samper Guard, Semperit Technische Produkte , Vienna, Austria) were worn. The hazardous chemicals were then removed from storage, doubly contained, and placed within the class two biosafety cabinet and serial diluted within a suitable solvent in order to construct smaller quantities of known concentration stock solutions. The required doses were assembled from the stock solutions, with the addition of further solvent, and aliquotted from either glass or plastic "Biju" or McCartney bottles (Greiner-Bio-One, Gloucestershire, UK). 100 µL aliquots of the chemical were then administered to the cultures, solvent dependent; via a 20-200 µL pipette, ensuring an even distribution and incubated for 24 hr. All cellular culture flasks post treatment, were placed within a cuboid Perspex box during initial incubation. Ensuing incubation, cultures were microscopically assessed and washed as outlined in (Section 2.2.3.1). All cellular pellets were manually dislodged prior to re-suspension in excess new growth medium and counted as described in (Section 2.2.1). Sterile, labelled, 25 cm^2 culture flasks were then established, seeding the flasks at a concentration suitable to maintain optimal growth, and replaced back into incubation for future use within a conjunctive downstream application, including RPD or mammalian cell in vitro *PIG-A* gene mutation assay.

2.5 Preparation of Cellular Cultures Prior to Experimentation

At least 72 hr prior to experimentation start date, generally 96 hr, a fresh cryopreserved vial of stock cell culture was removed from liquid nitrogen long term storage and immediately placed within a temperature controlled water bath set to 37 °C (Section 2.2). Once thawed, the contents of the vial were transferred into a new

sterile culture flask (75 cm^2), using a sterile Pasteur pipette, and pre-warmed cell line specific culture medium was added to the flask to a total volume of 50 mL. The culture flask was then labelled accordingly and placed within a humidity controlled environment for a minimum of 48 hr with routine (24 hr) microscopy based assessment. Once 72 hr incubation had completed the cell culture was removed from the incubator, counted (Section 2.2.1) and sub-cultured (Section 2.2.3); re-seeing the culture to a concentration suitable to test exponential growth phase. The culture was incubated for an additional 24 hr and re-counted to ensure exponential growth phase was achieved. At this point, the cultures were deemed suitable for usage within biological experimentation or alternatively exposed to Virkon® (Potassium monopersulphate (49.8% wt/wt) Anachem Ltd., Bedfordshire, UK) for 20 min - 24 hr prior to disposal, adhering to University policy on disposal of genetically modified biological material.

2.6 Assessment of Chemical Genotoxicity – Dose Range Finding Studies

2.6.1 Controls for Relative Population Doubling (RPD) and in vitro Mammalian cell *PIG-A* Gene Mutation Assay

Within the RPD and *PIG-A* studies the use of a known genotoxin in order to induce a significant decrease in cellular viability, was deemed not to be necessary due to the nature of the chemicals being used within the assays. The use of "G4" chemicals as validatory compounds within the assay design pre-disposes the subsequent generated data and hence, removes ambiguity. Negative control cultures were dosed with 100 µL of solvent controls (vehicle controls) and/or filter prepared water, mimicking the growth conditions of the assessed cultures.

2.6.2 Relative Population Doubling

Cultures were constructed as described in the (Section 2.2), and subsequently exposed to model genotoxins for 24 hr according to (Section 2.4), washed and allowed an additional 24 hr recovery period (1-1.5 cell cycles). Cellular counts were initially recorded at the time of seeding/exposure, post 24 hr (recovery), 48 and 72 hr post exposure. Relative Population doubling, Relative Cell Counts (RCC) and Estimated Mean Generation Time (EMGT) were all calculated according to the equations 3, 4 and 5 outlined below.

2.6.2.1 RPD, RCC and EGT Equations

Equation 3

$$\textbf{Relative Population Doubling} = \frac{\text{(No. of Population doublings in treated cultures)}}{\text{(No. of Population doublings in control cultures)}} \times 100$$

Where:

$$\textbf{Population Doubling} = \frac{[\log_{10}(\text{Post-treatment cell number} \div \text{Initial cell number})]}{\log_2}$$

Equation 4

$$\textbf{Relative Cell Counts} = \frac{\text{(Cell number of Treated Flask)}}{\text{(Cell number of Control Flask)}} \times 100$$

Where:

All cell counts are expressed as vales with a common 10 to the power function.

Equation 5

$$\text{Estimated Mean Generation Time} = \frac{(0.301*(\text{Experimental Length}))}{(\text{Log}_{10}(\text{Post-treatment cell number})-\text{Log}_{10}(\text{Initial Cell Number}))}$$

Where:

0.301 is the conversation factor for using Log_{10} instead of $\log_2$

2.7 Preparation of Fixatives for the use of Flow Cytometry and Microscopy Applications

Fixative formulation required the use of an AFA1000 fume cupboard, due to the reactivity and volatile nature of the chemicals used, additional PPE including eye protection and long arm gloves were also worn. Accurately measuring the mass out such chemicals was achieve via the use of an external balance and sealed glass McCartney bottles, pre weighed empty, to adhere to health and safety regulations.

2.7.1 4% Paraformaldehyde (4% PFA)

4g of 95-105% paraformaldehyde powder (Cat No. 158127-500G, Sigma Aldrich, Gillingham, UK), weighed in a sealed glass McCartney bottle, was transferred into a 250 mL conical flask and temporarily sealed using parafilm (SPI, West Chester, USA). 100 mL of PBS was added to the powder within the conical flask, shaken thoroughly and magnetic flea added. The conical flask was then transferred onto a HC1202 Ceramic Hot Plate/ Magnetic Stirrer (Bibby Scientific, Staffordshire, UK), moderately heated and mixed until an observed colour change was apparent (~10-30 min). Once the solution had changed from turbid white to a clear colourless solution, heat was removed, cooled and aliquotted into pre labelled plastic biju bottles. Fixative was stored at 4°C, if intended for long term storage the use of glass apparatus is required.

2.7.2 BD Cell Fix

1 mL of 10X BD Cell Fix (BD CytoFix™, BD Biosciences, Oxford, UK) was diluted 1:9 with pre-filtered dH_20 within glass McCartney bottles, constructing a final working solution of 1 X BD Cell Fix. BD Cell Fix is light sensitive; all work was carried out in the absence of direct light and stored at 2-4°C for immediate short term storage.

2.7.3 Dulbecco's 4% Paraformaldehyde (4-Para 4)

4g of 95-105% paraformaldehyde powder (Cat No. 158127-500G, Sigma Aldrich, Gillingham, UK), weighed in a sealed glass McCartney bottle, was transferred into a 250 mL conical flask, repeated and both flasks temporarily sealed using parafilm (SPI, West Chester, USA). Either 100 mL of Dulbecco's PBS $Ca2^+$ and $Mg2^+$ ion free (21600044, Gibco®, Paisley, UK) or alternatively Dulbecco's PBS Ca^{2+} and Mg^{2+} ion present (14040133, Gibco®, Paisley, UK) was added to the powder within the conical flasks, shaken thoroughly and magnetic flea added. The conical flask was then transferred onto a HC1202 Ceramic Hot Plate/ Magnetic Stirrer, moderately heated and mixed until an observed colour change was apparent (~10-30 min). Once the solution had changed from turbid white to a clear colourless solution, heat was removed, pH measured and adjusted to ~7.2, cooled and aliquotted into pre labelled plastic biju bottles. Fixative was stored at 4°C, if intended for long term storage the use of glass apparatus is required.

2.8 Flow Cytometry

All flow cytometry, unless stated differently, within this project was carried out using a BD Biosciences FACS Aria I flow (BD Biosciences, Oxford, UK) cytometer utilising FACS DIVA™ (BD Biosciences, Oxford, UK) software versions for subsequent analysis. Prior to flow cytometric analysis, the cytometer was initially run through the start-up process consisting of the following; lasers were switched on and allowed to warm to a consistent temperature, PC was switched on and all necessary passwords entered, fluidics were primed, the nozzle was microscopically assessed and often sonicated to remove blockages, the inlet system and stream were decontaminated using a combination treatment of FACS Clean, FACS RINSE (BD Biosciences, Oxford, UK) and filter prepared dH_20 and finally calibration was passed using the BD Biosciences supplied multicolour fluorescent calibration beads (Cat No. 642412, BD Cytometer Setup and tracking bead, Cat No. 340486, CaliBRITE™ 3 BD Biosciences, Oxford, UK). Additionally, manual assessment of stream alignment, O-ring integrity, detector sensitivity and voltage requirement was carried out daily when running the instrument calibration standard (ICS) sample (Figure 2.1). Cell cultures were loaded onto the machine within either 5 mL flow cytometry tubes (BD Falcon ™ round bottom tubes, BD Biosciences, Oxford, UK) or alternatively 15 mL BD Falcon ™ tubes were also used in conjunction with a small adapter applied to the sample carrier. Unless otherwise stated, all fluorescence analysis was carried out utilising a 70 µm nozzle with corresponding 70 pounds per square inch (PSI) sheath pressure, excited with either a 405 (UV/Blue), 488 (Blue) and/or 605/635 (Red) nm laser and subjected to a standard threshold applied to the forward side scatter (1,000) in order to ensure debris was removed from data acquisition and ensuing analysis. A minimum of 10,000 cellular events were recorded for each sample, with each dose being conducted in triplicate where possible from independent cryopreserved cell cultures.

The use of an instrument calibration sample was required for every experiment as well as single stained fluorescence controls, when multiple fluorophores were to be used, to facilitate the correct calibration of the flow cytometer prior to analysis, in terms of gating and compensation accuracy.

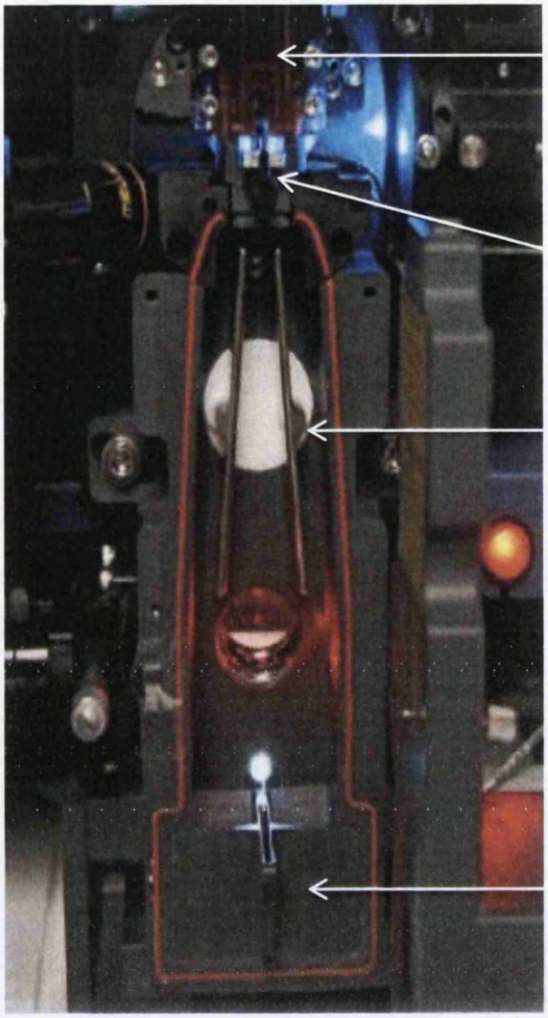

Figure 2.1. Overview of the internal components of the BD FACS Aria Flow Sorter, excluding the optics system. Critical elements within the generalised running and upkeep of the machine are highlighted.

2.8.1 Suspension and Adherent Cellular Cultures Fluorescent Antibody/Fluorophore Treatment

All fluoresce associated work was carried out under the assumption of light sensitivity and therefore, in the absence of direct light. Aluminium foil was used in order to maintain these conditions where appropriate. Cell cultures were established as outlined in (Section 2.2) and counted (Section 2.2.1). The equivalent volume of culture to 1 x 10^6 single cells was removed, using a 100 µL – 1000 µL pipette (Finnpipette®, Thermo Scientific, Hampshire, UK) and corresponding pipette tip, aliquotted into a sterile 15 mL centrifuge tube (BD Falcon ™, BD Biosciences, Oxford, UK), centrifuged and supernatant carefully aspirated. The cellular pellet was

re-suspended in 50 μL of new culture medium and treated with the desired amount of the fluorescence conjugated antibody. Treatment consisted of the initial depositing pipette followed by a minimum of five re-suspensions in order to achieve maximum distribution. The culture sample was incubated for 30 min in a temperature controlled (2-4 °C) cold room, protected from direct light, transferred into a centrifuge, spun down, supernatant removed and washed (Section 2.2.3) a minimum of twice. The cultures were re-suspended in a final volume of 1 mL pH 7.4 PBS, ensuring a suitable concentration for flow cytometry applications, and stored on ice for a maximum of 1 hr prior to flow cytometric analysis.

2.8.2 Assessing Fluorescence Properties using Flow Cytometry

Cell cultures were prepared as outlined by (Section 2.2) and treated with fluorescence conjugated antibodies or directly fluorescent chemicals, such as DNA targeting intercalating agents, in an analogous manner to (Section 2.8.1). Following treatment, cells were washed twice with pre-warmed PBS and then re-suspended in a minimal volume of PBS/Medium at a suitable concentration for flow cytometric analysis.

2.8.2.1 Flow Cytometry Compensation Analysis

Single stained samples for each fluorophore utilised within the experiment were constructed (Section 2.8.1) loaded (Section 2.8) and analysed on the flow cytometer. Fluorophores with known similar or overlapping emission spectra were of particular interest; once a single stained sample was loaded into the flow cytometer the corresponding pre-selected specific detector as well as the neighbouring detectors were assessed for any potential signal pick up. A histogram/dot plot was drawn for each detector and individually assessed for a positive signal as defined by instrument calibration standard (ICS). If a positive signal was detected within a neighbouring detector the PMT voltage corresponding to the excitatory channel was reduced until the positive nature was deemed negligible (Figure 2.2).

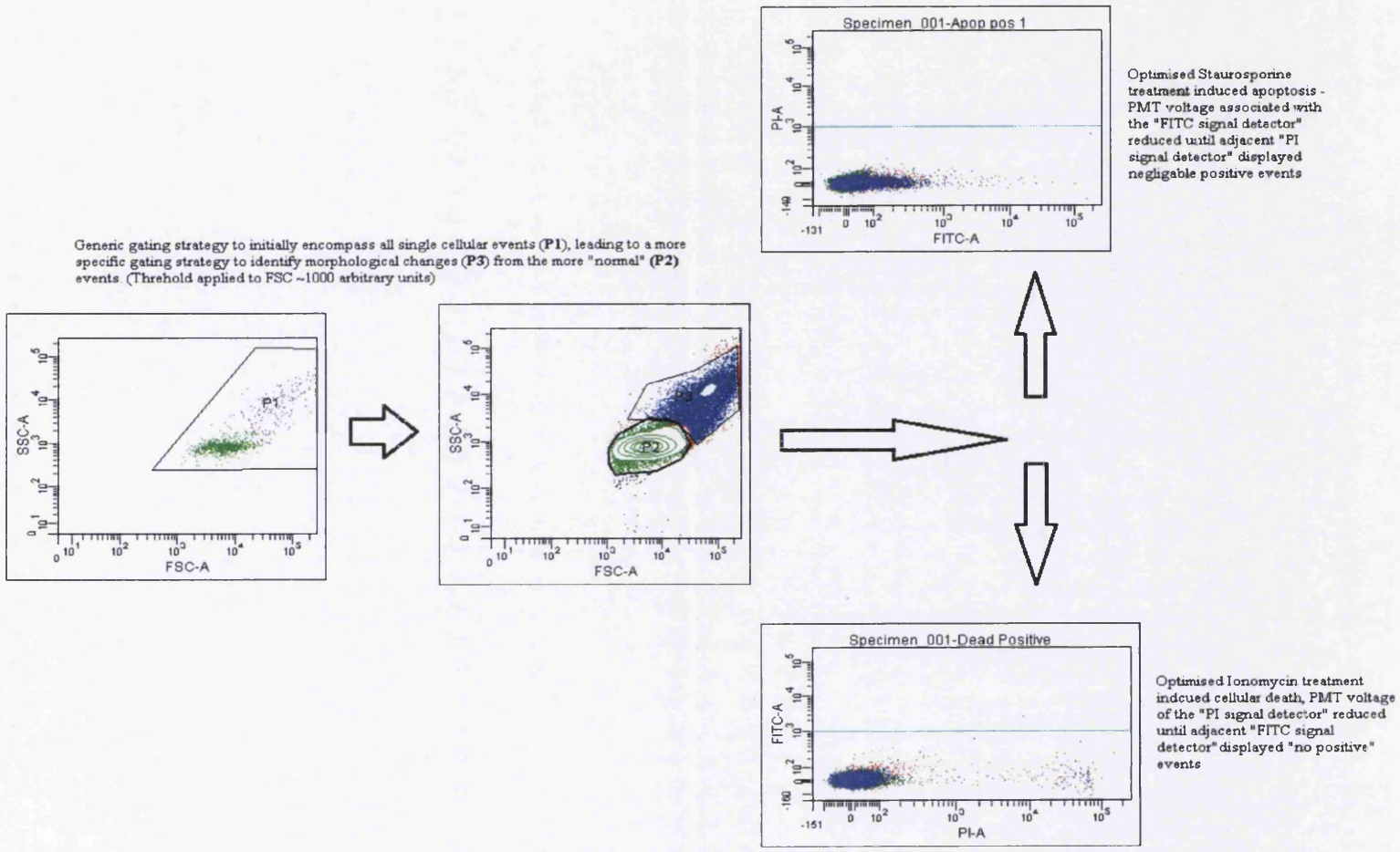

Figure 2.2. Compensation procedure outlined within sequential flow cytograms; Ionomycin and Staurosporine optimised treatment employed to induce sufficient levels of cellular death and apoptosis respectively to provide confidence in compensatory data. Note, samples treated independently of one and another in the first instance as outlined above.

However, if the reduction within that specific detector was greater than 30%, the combination of fluorophores were assessed for "goodness of fit" within that specific experimental design to prevent insensitivity to actual positive signals. This process was repeated for each fluorophore within the experimental design until adjacent detectors displayed negligible traces of positive signals; at this point detectors were assessed for positivity for their own specific fluorophore to maintain detection integrity and then dual stained standards were often utilised for further confidence.

2.8.2.2 Flow Cytometric Data Analysis

Data analysis was carried out using the supplied BD Biosciences approved FACS DIVA™ software, initially a sequential template of a combination of 2-D histograms, 3-D density plots and scatter plots (Figure 2.3) for a variety of variables were constructed in order to facilitate the accurate identification, separation and analysis of subpopulations within the cellular cultures.

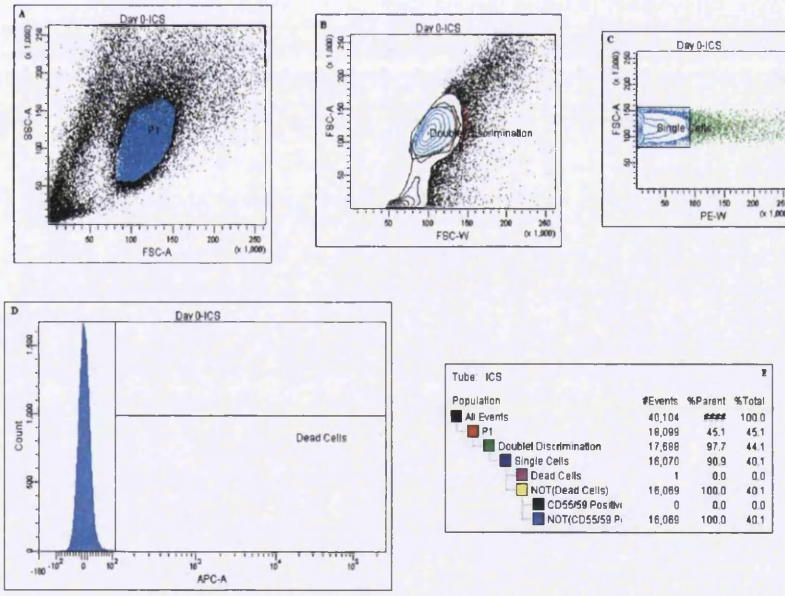

Figure 2.3. Generic process of cell type classification and subpopulation distribution for an unstained instrument control sample. The order in which each stain is retrospectively analysed provides a greater level of depth and biological content to the analysis; A) Generalised gate for all potential single cellular events conforming to a normal morphology. B) Localised gate excluding cells which could potentially be debris or doublets. C) Specific gate categorising cells based on their time of flight measurement for the cellular surface antigen. D) Gate to exclude cells positive for loss of membrane integrity.

Cellular events, which were deemed single cell in nature (Figure 2.3 A and B) not including debris or aggregates, were then defined to be viable (Figure 2.3 D) and then assessed for their respective GPI-AP status (Figure 2.3 E). Flow cytometry gating was based on the data acquired from the use of an ICS, un-stained mimicking sample, and prior to every experiment in order to obtain accurate and reproducible data (Figure 2.4).

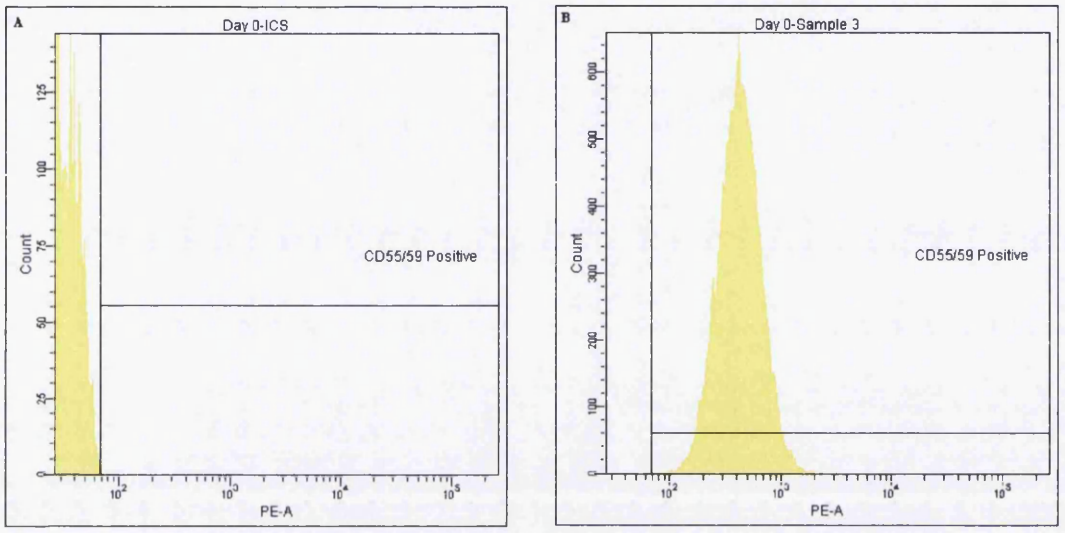

Figure 2.4. 2D histograms displaying the distribution of cells following anti-CD55/59 PE antibody treatment; A) An instrument calibration standard and B) A wild type untreated cellular population.

2.8.3 Fluorescence Activated Cell Sorting (FACS)

Cellular samples were treated with anti-GPI-AP specific fluorescently labelled antibodies (Section 2.8.1) and analysed on the flow cytometer (Section 2.8.2).

The BD FACS ARIA flow cytometer was set up (Section 2.8), once completed an additional sterilization process consisting of a "long clean" ~ 20 min clean using 70% ethanol, was undertaken. The fluidics start up procedure was repeated, and all internal surfaces cleaned with bleach (10% Virkon solution) and dried thoroughly, removing any salt build up. At this point the standard sheath pressure and nozzle were adjusted to fit the application needs. Generally, a larger nozzle and lower pressure (100 µm and 20 psi respectively) were selected; the nozzles were sonicated prior to the O-ring fitment.

The nozzle was inserted within the quartz block, at the base of the flow cell, and the stream was established (Figure 2.1). The intercepting diode laser, used primarily for drop delay calibration, was attuned and the sorting related parameters adjusted; "Gap", "Amplitude" and "Frequency". For stability reasons, 20-30 mins probationary period was deemed necessary to account for temperature and voltage variations associated with the flow cytometry laboratory (Figure 2.5). During the probation period, the "Sweet Spot" function was utilised, flow alignment and critically the sorting voltages were adjusted to enable side stream formation. Side stream adjustment continued until the point of contact with the collection tube was directly in the centre of the vessel. Prior to running the Accudrop ™ flow cytometry beads a test sort was under taken to check all the parameters were correct, a sorting template loaded onto the software, *automated cell deposition unit* (ACDU) adapter (96 well plates) or collection tube holder loaded and manually the drop delay was calculated.

Once satisfied with the prerequisite system calibrations, sorting was commenced and the recovered cellular population/s were collected within 5 mL polystyrene (12 x 75mm) sorting tubes (BD. Biosciences, Hertfordshire, UK) within fresh cell line specific growth medium (1 mL) or 15 mL BD Falcon Tubes. Consecutively cells were sub-cultured (Section 2.2.3) within 25 cm^2 culture flasks prior to long term

cryopreservation (Section 2.3). Quality assurance (QA) FCM based *PIG-A* phenotype assessment was carried out prior to and 72-96 hr. following enrichment.

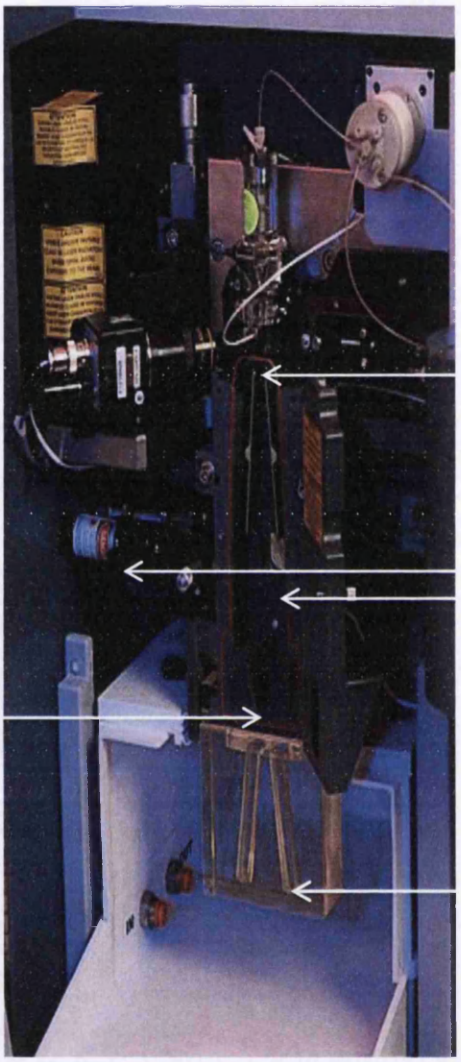

Figure 2.5. The internal components of the BD FACS Aria sorter continued; a more detailed look at the internal components which are essential for optimum FACS

2.9 Amnis ImageStream ™ Flow Cytometry

All ImageStream flow cytometry during this project was undertaken on an Amnis IS100 imaging flow cytometer in conjunction with Amnis INSPIRE® software versions 4 and 5 (Merck Millipore, Nottingham, UK). The cytometer was switched on, software loaded and calibrated. 100 µL aliquots of cell suspension at the correct concentration to facilitate analysis ($1x10^7$ cells/mL) were transferred into 0.5 mL eppendorf allowing direct loading onto the sample uptake tube. A minimum of 10,000 cells were assessed for each experimental sample.

The use of an instrument calibration sample was required a necessity for every experiment as well as single stained fluorescence controls, when multiple fluorophores were to be used, to facilitate the correct calibration of the flow cytometer prior to analysis.

2.9.1 ImageStream™ Data Analysis

Following image collection, all ImageStream data analysis started initially with a sequential template of a combination of 2-D histograms and scatter plots (Figure 2.6) for a variety of variables were constructed in order to facilitate the accurate identification, separation and analysis of sub-populations within the cellular cultures.

Cellular events, which were deemed single cell in nature (Figure 2.6 A) not including debris or aggregates, were then defined to be focussed (Figure 2.6 B) and then assessed for their respective GPI-AP status (Figure 2.6 C). Flow cytometry gating was based on the data acquired from the use of an ICS, un-stained mimicking sample, and prior to every experiment in order to obtain accurate and reproducible data. The finalised output was broken down into the large scale statistical analysis as well as the visualisation of the individual events as demonstrated above; this feature is unique to the ImageStream™ platform.

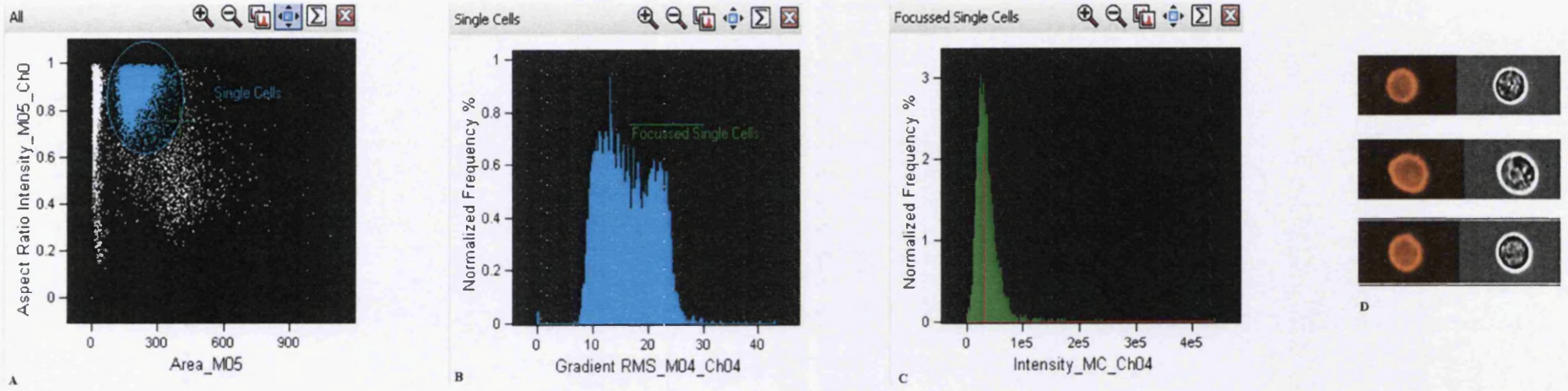

Figure 2.6. The progressive design of an experimental work flow on the Amnis ImageStream™ platform; A) The initial gating system in which the aspect ratio and area of the cells are analysed in order to estimate the single cell population, B) the focus gating to exclude smearing effects from biasing the subsequent data, C) the relative intensity of the fluorescence emission post antibody treatment for each cellular event and D) the finalised output of events meeting the stringent criteria.

2.10 Generic, 5-Day, in vitro *PIG-A* Gene Mutation Assay Protocol

All data generated following daily *PIG-A* mutation assessment were evaluated for normality and variance (P value $\geq$0.05) using the Shapiro-Wilk and Bartlett's Test respectively, carried out within DrSmooth through the R-Software Package (R-3.0.2, Free Software Foundation's GNU project). Following assessment, data was either defined as normally distributed or non-normal and subsequently, parametric (Dunnett's Two-Tailed T-Test) or non-parametric (Dunn's Two-Tailed T-Test) statistical analysis was undertaken within an extension of the R-software. The use of two-sided analysis was to facilitate the detection of both increases and decreases within the number of *PIG-A* phenotypic mutants as well as to prevent disputed results. Statistical analysis was implemented to state at what dose, if any, rejection of the Null hypothesis was to be assumed (P-value $\leq$0.05). At such a dose, variation of the *PIG-A* mutant frequency was a direct result of a noteworthy factor and not as a result of chance.

2.10.1 Background Analysis

Cell cultures were established and maintained as outlined in (Section 2.2), the parental cell culture was counted and subsequently 25 cm^2 culture flasks were constructed at a concentration of 4 x 10^5 cells/mL in accordance to the number of doses within the assay design. Established 25 cm^2 flasks were successively exposed to acute chemical treatment, under the standard genotoxic chemical treatment protocol (Section 2.4.2), and placed within a temperature and humidly controlled environment for the 24 hr incubation. At this point, PPE associated with toxic chemical usage as well as the initial toxic vials was disposed of safely and correctly according to health and safety protocol. Simultaneously, three 1 x 10^6 cellular samples were extracted from the un-treated parental culture, transferred into sterile 15 mL BD Falcon centrifuge tubes, centrifuged (250 x g for 7 min) and supernatant aspirated and discarded. Excess 1 x PBS solution was added to each tube in order to wash the cellular pellets. The samples were then centrifuged (250 x g for 7 min),

supernatant aspirated and discarded and the cellular pellets re-suspended in 100 µL of pre-warmed (37 °C) culture media. 20 µL of anti-human CD55 R-PE antibody was added to each sample excluding the ICS, and incubated at 2-4°C for 30 min protected from light.

Following the incubation, cultures were centrifuged (250 x g for 7 min), supernatant removed and re-suspended in 10 mL of 1 X PBS solution. Samples were centrifuged for an additional time, forming sufficient pellets, supernatant carefully aspirated, removing any residual excess antibodies, and re-suspended within 5 mL of 1 X annexin binding buffer (made freshly that day to prevent deterioration). Samples were centrifuged, supernatant aspirated and re-suspended in an additional 100 µL of 1 X annexin binding buffer. 5 µL of Alexa Fluor® 488 annexin V was added to each sample, excluding the ICS and incubated for 15 min at room temperature, protected from light. Post incubation, excess 1 X annexin binding buffer was added, cultures centrifuged, supernatant aspirated and re-suspended in 200 µL of annexin binding buffer. 5 µL (0.25 µg) per test (per million cells) of 7-AAD was added, mixed thoroughly and incubated for 20 minutes, protected from light, on ice. Samples were maintained on ice protected from light for a maximum of 4 hr prior to analysis.

2.10.2 Day 1 Analysis

Post 24 hr chemical exposure within a temperature controlled incubator (Section 2.4), whilst wearing the correct PPE and suitable disposal methods ready, cultures were transferred directly into 15 mL Falcon tubes and centrifuged (250 x g for 7 min). Carefully, presumed toxic supernatants were aspirated and discarded safely. 10 mL of 1 x PBS solution was added to each tube, in order to wash potential residual chemical treatment out of the cellular pellets, centrifuged (250 x g for 7 min), toxic supernatant aspirated and re-suspended in 10 mL of fresh culture medium. At this point PPE associated with toxic chemical usage as well as the collected toxic supernatants and culture flasks were disposed of safely and correctly according to health and safety protocols. Cells were counted as described in (Section 2.2.1) and volumes containing 1 x 10^6 cells per culture were transferred into sterile 15 mL BD

Falcon tubes and set aside. Sterile corresponding 25 cm^2 culture flasks were labelled correctly and constructed from the parental cultures to a concentration of 1 x 10^5 cells/mL within a final 10 mL volume of supplemented culture media. Culture flasks were placed within the incubator for 24 hr ready for the ensuing following day's *PIG-A* mutant assessment.

The set aside cellular samples were centrifuged (250 x g for 7 min) and supernatant aspirated and discarded. Excess 1 x PBS solution (10 mL) was added to each tube in order to wash the cellular pellets. The cultures were centrifuged (250 x g for 7 min); supernatant aspirated and re-suspended in 100 µL of pre-warmed (37 °C) culture media. 20 µL of anti-human CD55 R-PE antibody was added to each sample excluding the ICS, and incubated at 2 - 4°C for 30 min protected from light.

Following the incubation, cultures were centrifuged (250 x g for 7 min), supernatant removed and re-suspended in 10 mL of 1 X PBS solution. Samples were centrifuged for an additional time, forming sufficient pellets, supernatant carefully aspirated, removing any residual excess antibodies, and re-suspended within 5 mL of 1 X annexin binding buffer (made freshly that day to prevent deterioration). Samples were centrifuged, supernatant aspirated and re-suspended in an additional 100 µL of 1 X annexin binding buffer. 5 µL of Alexa Fluor® 488 annexin V was added to each sample, excluding the ICS and incubated for 15 min at room temperature, protected from light. Post incubation, excess 1 X annexin binding buffer was added, cultures centrifuged, supernatant aspirated and re-suspended in 200 µL of annexin binding buffer. 5 µl (0.25 µg) per test (per million cells) of 7-AAD was added, mixed thoroughly and incubated for 20 minutes, protected from light, on ice. Samples were maintained on ice protected from light for a maximum of 4 hr prior to analysis.

2.10.3 Days 2-5 *PIG-A* Analysis

Post 24 hr incubation (Section 2.2), cultures were counted as described in (Section 2.2.1) and volumes containing 1 x 10^6 cells per culture were transferred into sterile 15 mL BD Falcon tubes and set aside. Sterile corresponding 25 cm^2 culture flasks were labelled correctly and constructed from the parental cultures to a concentration

of 1 x 10^5 cells/mL within a final 10 mL volume of supplemented culture media. Culture flasks were placed within the incubator for 24 hr ready for the ensuing following day's *PIG-A* mutant assessment.

The set aside cellular samples were centrifuged (250 x g rpm for 7 min) and supernatant aspirated and discarded. Excess 1 x PBS solution (10 mL) was added to each tube in order to wash the cellular pellets. The cultures were centrifuged (250 x g for 7 min); supernatant aspirated and re-suspended in 50 µL of pre-warmed (37 °C) culture media. 20 µL of anti-human CD55 R-PE antibody was added to each sample excluding the ICS, and incubated at 2-4°C for 30 min protected from light.

Following the incubation, cultures were centrifuged (250 x g for 7 min), supernatant removed and re-suspended in 10 mL of 1 X PBS solution. Samples were centrifuged for an additional time, forming sufficient pellets, supernatant carefully aspirated, removing any residual excess antibodies, and re-suspended within 5 mL of 1 X annexin binding buffer (made freshly that day to prevent deterioration). Samples were centrifuged, supernatant aspirated and re-suspended in an additional 100 µL of 1 X annexin binding buffer. 5 µL of Alexa Fluor® 488 annexin V was added to each sample, excluding the ICS and incubated for 15 min at room temperature, protected from light. Post incubation, excess 1 X annexin binding buffer was added, cultures centrifuged, supernatant aspirated and re-suspended in 200 µL of annexin binding buffer. 5 µl (0.25 µg) per test (per million cells) of 7-AAD was added, mixed thoroughly and incubated for 5 minutes, protected from light, on ice. Samples were maintained on ice protected from light for a maximum of 4 hr prior to analysis.

This process occurred every 24 hr for 5 days in order to generate daily *PIG-A* mutant frequency data to facilitate dose response modelling.

Chapter 3: The Concept and Development of an Early Stage in vitro *PIG-A* Gene Mutation Assay

3.1 Introduction

The work presented within this chapter was carried out in order to develop a rudimental mammalian cell in vitro *PIG-A* gene mutation assay, analogous to the in vivo *Pig-a* gene mutation assay developed by Litron ™ Laboratories [196]. Once the conceptual idea was established, and shaped into a qualitative assay, much effort was put into investigating the additional features of the assay to establish robustness and reproducibility. Critical validation of the assay at each point of development was the driving feature which enabled the assay evolution and subsequent increments in content and complexity.

3.1.1 X-linked Gene Mutation Assays and their Role in Safety Assessment

Gene mutation assays, both in vitro and in vivo, are utilised as fundamental features of drug development; their respective assay sensitivity is the vital pre-requisite characteristic which ensures their necessity and future inclusion. Gene mutation has been identified as the current most relevant end point for assessing carcinogenicity [202] when likened to dissimilar DNA damage end points, including chromosome aberrations [103]. Thus, DNA damage can be detected at lower doses utilising a gene mutation end point and therefore, more precisely predicting potential hazard and risk assessments. However, due to the diversity of the endpoints, it is clear that potential genotoxicity and/or mutagenicity of a compound cannot be assessed by a single assay system [203], a battery tier system is required.

X-linked gene loci have been routinely utilised as highly sensitive reporters for gene mutation within the field of genetic toxicology for a number of decades; the HPRT assay [204] being such an example. X-linked reporters benefit from the heterozygous

nature of gene expression of the target gene, resulting in "one hit" sensitivity; based on Knudson's "Two hit" hypothesis for early onset retinoblastoma [205]. A single functional copy of the gene is present on the X-chromosome and hence, a single deactivating DNA damaging event can result in loss of genotype, a paradigm of "single genetic hit" inactivation-mediated carcinogenesis [206]. However, biological context, sensitivity and specificity (especially relevant with the use of rodent cell lines [113]), human relevance as well as the laborious manual scoring techniques adopted by the subsequently designed assays has proven to restrict their use within a safety assessment environment [105], with the exception of MLA. Such assays lend themselves well for routine qualitative/quantitative dose response modelling, often carried out within academic institutes, but are not favoured when compared to pre-existing validated standard test battery assays. Pre-clinical pharmaceutical safety assessment requires cost effective, reproducible assays which often have debatable human relevance [184] but uncompromising sensitivity in order to maintain an optimum detection of genotoxic characteristics within drug compounds. During safety assessment a compound progresses through in vitro assessment in parallel to more thorough and costly in vivo and long term carcinogenicity assessments with the aim of subsequent first time in human (FTH) exposure and the pharmaceutical market.

Current in vitro gene mutation assays presently within the standard test battery [65], during early drug development, have uncompromising assay sensitivity which often triumphs over other features such as biological relevance, specificity and p53 status [113-115]. This situation has recently become more apparent, with increasing critical review, as the subsequent data generated has potentially limited usage within the wider context of safety assessment and human health risk assessment [207-209] [210]. However, high sensitivity does facilitate quantitative dose response modelling and lends itself well to traditional methods of qualitative hazard and risk assessment [211]. An established maximum no adverse observed effect level (NOAEL) following dose response analysis, typically in vivo, ensued by a variety of safety factors in order to extrapolate a figure deemed applicable to human exposure [212]. This assessment traditionally assumed a linear dose response for genotoxicity for direct acting DNA-reactive compounds, including alkylating agents such as Ethyl-

methanesulfonate; resulting in a correctly conservative hazard and risk assessment for calculated exposure levels.

There has been a recent move in the field away from the assumption of linearity for specific cases depending upon mechanistic data, and dichotomous qualitative evaluations may be superseded by a more system based derivation of PoD based on non-linear models [211, 212] Point of departure metric calculation using novel software packages, PROAST, Bench Mark Dose Software [213] and DrSmooth [214] including the BMD, BMDS and Slope transition dose (STD) are currently being evaluated for their inclusion within quantitative evaluations of hazards [28, 100, 213]. Although, pre-existing assay platforms are able to generate the quality of data required for comprehensive dose response modelling [215], they appear overly sensitive [210] and lack the refinement and biological contextual data which can be generated using novel high content, high through put methodologies [113-115]. Combining the use of novel high content assays, to generate human pertinent quantitative dose response data, with highly composite data modelling packages, to derive more precise and relevant point of departure metrics, in an analogous fashion to supplementary fields of toxicology could hypothetically advance the field of genetic toxicology [100, 216].

3.1.2 Drug Attrition within the Pharmaceutical Industry

Within pharmaceutical safety assessment, drug attrition is a major factor on the overall financial health of the company. Early stage drug attrition of potentially "misleading" compounds is critical to prevent over spending and loss of potential profit [217]; enabling the company to continue long term therapeutic drug development and therefore, maintaining their service to public health and shareholders. The Ames test, a historically modest bacterial reverse mutation assay designed in the early 1970s is still the prominent early stage core genetic toxicity test in which all drug compounds are assessed. The assay is extremely sensitive [218], as mentioned previously, inexpensive and throughout its development and validation has been modified to incorporate minor pharmacodynamics features such as human

or rat S9 presence [66] to mimic phase 1 (cytochrome p450s) and 2 metabolism (transferase). The Ames test does not detect all carcinogens and hence, the development of the extensive mammalian cell in vitro assay systems [73] was commenced to identify the hazard of human specific carcinogens [105].

The Ames tests ability to detect the majority of carcinogenic risk within pre-clinical assessment validates its continued inclusion decades after first implementation within the standard test battery. A positive outcome within the Ames test is almost certain to halt the development of a NME [105], even though the test system is prokaryotic based and very limited biological data is known at the time of assessment. Therefore, there is a potential niche within the pharmaceutical industry which is yet to be fulfilled; no single genetic toxicology test system encompasses all features required to provide a quantitative risk assessment approach and not just hazard identification within pre-clinical safety assessment. A statement backed by the continued reform of current test systems [130] as well as the re-direction [128] and advances within alternative pre-clinical assessment tools [100, 125] such as in-silico approaches [90], even though they still provide cost effective, highly sensitive hazard assessment. This niche could be filled by a supplementary novel in vitro assay which meets the criteria pre-defined by the current historically used in vitro assays [219], however, also include such benefits as high throughput, high content (multiplexing), high precision and a greater amount of human relevance, facilitating a higher specificity of carcinogen detection and potential in vitro to human extrapolation, to supersede the data generated by the currently favoured assays.

3.1.3 The Introduction of the Rodent Pig-a Gene Mutation Assay.

The introduction and early stage validation of the in vivo rodent Pig-a gene mutation assay has demonstrated its potential to be incorporated within the core standard battery of early stage drug development assays [167]. The assay design lends itself very well to full integration within safety assessment [180]; a combination of un-invasive sample harvesting, facilitating routine incorporating within 28 day toxicology studies [91], highly sensitive and vital reporter partnership, within the

erythrocyte and the cellular surface marker [141], as well high content flow cytometric analysis and quantitative dose response modelling [160]. However, the assay utilises only rodent haemopoetic tissue, primarily the erythrocyte sub population and therefore, the pre-existing question about direct human relevance and limitations induced via in vivo rodent to human extrapolation [220] still remain.

The major advantage of the rodent in vivo Pig-a gene mutation assay which aren't shared by analogous transgenic gene mutation assays, BigBlue™ or MutaMouse™ [80], is the highly conserved nature of the reporter system, i.e. the GPI-anchor moieties themselves are highly conserved amongst most mammalian species [162] as well as the ease of modification to the flow cytometric analysis. This feature provides potential transferability of assay design throughout mammalian species, retaining the current associated benefits as well as potentially significantly increasing data integrity and human relevance. Therefore, as well as having a cost effective in-vivo assay which can be integrated into current 28 day tox studies with no additional cost [91], an in vitro or ex vivo equivalent assay within human tissue can also be utilised; extensive low dose quantitative dose response modelling, academic setting, as well as a future potential novel test battery assay, pharmaceutical pre-clinical safety assessment.

3.1.4 *PIG-A* Assay Development and Compatibility to the Current State of Affairs

When designing novel test systems or bio-monitoring tools one must always take into account the running costs and autonomy of such a system. Current in-vitro gene mutation assays such as the *MLA* (*TK*) are perfect examples of systems which have uncompromising high sensitivity to detect rodent carcinogens but also limited have specificity, increasing the likelihood of false positive results [210]. In addition to this, debatable human biological bearing [113] also limits use, but due to the minimal expense of the test as well as robust historical data the test system still remains in use within the core standard test battery [65].

Designing such a novel test system is therefore, not purely a combination of favourable, beneficial characteristics and features all bundled into a test system but an elaborate balancing act in which one must adhere to achieve as many of the beneficiary features within a system whilst always complying to the limitations and restrictions placed upon the system by the current environment [85]. The subsequent development of a mammalian cell in vitro *PIG-A* gene mutation assay is no different to previously stated; the assay endeavours to achieve high content and high sensitivity to enable robust, stand alone, cost effective data. Providing such an assay, once validated, could potentially alleviate the need for drug compound attrition based purely on positive Ames test data [112], and provide an alternative to pre-existing rodent and clonal expansion based in vitro gene mutation assays [72].

The in vivo and in vitro *PIG-A* gene mutations assay currently share a homologous in-direct reporter system for mutagenesis [77] and therefore, there is no direct method of assessing the certainty of the stated results. An assumption is made about the *PIG-A* genotype based on physical observation, presence or absence of the specific cellular surface marker acting as the reporter [221] and due to the likelihood of such an observation as well as the supporting published literature, weight is credited [77, 141, 143, 144, 173, 175]. However, the in-direct nature of measurement can always be scrutinised especially from a regulatory point of view due to the lack of definitive evidence validating the mechanism; extensive validation is ongoing in order to assess the likelihood of implementation within 28 day repeat tox studies [91], particularly appropriate within the in vivo assay, and broad mechanistic investigation [146, 172, 222], heavily focussing on *Pig-a* sequence data, to evaluate the identity of putative mutant events in alternative haemopoetic tissue.

Immunofluorescence labelling is a technique, used in conjunction with flow cytometry , in which antibody molecules are conjugated to a specific fluorophore for the purpose of antigen detection and quantification [223]. In brief, antibody molecules (circulatory immunoglobulin), in this particular case IgG, are proteins which are produced in response to the introduction of a specific pathogen into the body, and due to their unique structure can bind in a highly specific manor to their triggering antigen. All antibodies share a consensus structure, and in the most basic terms are "Y" shaped; two hyper variable regions at the upper extremity comprised of an interlocking light and heavy chain (VH and VL regions) constituting the

antigen binding site [224], with a further constant region (CH and CL) held together by di-sulphide bonds.

The *Pig-a* assay hinges on assumption that X-linked characteristics provides both adequate sensitivity as well as fundamental biological reasoning to why a mutational event within the *Pig-a* gene is equivalent to the absence of GPI-AP markers on the cellular surface [141]. However, unlike currently validated mutagenicity assays, presumed mutants are unable to be directly sequenced due to the limited amount of mRNA and no nuclear DNA present within either reticulocyte or mature red blood cell populations. Therefore, is no definitive proof, in-vivo, the actual measurable mechanism within the *Pig-a* gene mutation assay is mutagenesis; however, sequencing data is beginning to emerge within other haemopoetic lineages validating the reporter mechanism [144, 173, 178, 222, 225]. Although, within published data, experimental design and use of mutant enrichment methodologies can equally be criticised for potential induced bias. Therefore, until further fundamental sequence data is derived, or the mechanism disproved, mutagenesis is the presumed measurable end point.

Pre-clinical drug development is not the only target area for the assay, providing an assay system able to generate reproducible dose response data facilitates the further investigation into the possibility of in-vitro-in-vivo dose extrapolation [28] and correlation. This would further increase the alignment of future drug development with novel governmental reforms to reduce animal usage within pharmaceutical testing [85, 86]. Also, increasing support is being generated for in-depth research into mutagenesis as a potential apical end point for carcinogenesis; based on quantitative low dose response modelling, Point of Departure (PoD) [212]. PoDs are calculated threshold-like-doses which can be extrapolated to human risk assessment utilising specific uncertainty factors [226]. Mutation has long been thought of as a highly sensitive end point for carcinogenesis, preceding chromosome aberrations [202], however, novel research has demonstrated potential correlation between in vivo mutagenesis (tissue independent) and genetic toxicology cancer metrics [227]. Therefore, the in vitro *PIG-A* gene mutation assay could provide a test system able to further research within this novel area, evaluating the potential of in vitro to in vivo extrapolation for the use of human carcinogenicity prediction.

Typically, cryopreservation is utilised to enable long term genotoxicity testing; the cell stock to be stored in a stable manner to prevent the continuous culture of all cell lines, at all times. Without the method of stock preservation, continual culturing would dramatically increase the passage number and increase the likelihood of genetic variation across laboratory stocks. A long term preservative/storage method should reduce the risk of contamination, enable consistent passage number, adhering to good cell banking practices and reduces costly overheads. However, there are potential deleterious disadvantages associated with the technique which include cytotoxicity as a result of solute concentration post freezing [228], which are significantly outnumbered by the advantages

3.1.5 Heterogeneity of GPI-Anchored Cellular Surface Antigens

Within the scope of designing a novel mutation assay, there is often a lot of focus attributed to the criteria required for success; high sensitivity and specificity appear to feature heavily. Aspiring to meet these criteria as well as learning from the restrictions of analogous assays within the literature [210] can potentially secure the assay regulatory acceptance and eventual OECD guideline drafting. Therefore, failing to recognise potential flaws in early stage assay development can be a critical oversight which will fundamentally weaken the developmental process.

Within all gene mutation assays, sensitivity, the assay's ability to classify a compound as hazardous, is often quoted as the most desirable feature. All current assays are aspiring to reach a level of sensitivity in line with the mutation rate observed at a random nucleotide within humans (2.5×10^{-8}) [145]. The early concept of the in vitro *PIG-A* gene mutation assay was no different. Spontaneous background mutant frequency, the number of observed putative *PIG-A* mutants within an un-treated parental test population, governs the overall sensitivity of the assay system and was predicted to be a known issue. Heterogeneity of the candidate GPI-APs for analogous cell lines had previously been reported [229].

The human Lymphoblastoid cell line, TK6, was the initial candidate following praises within recent publications as being a prominent proficient cell line within

genetic toxicology [113-115]. In short, TK6 cells have been shown to demonstrate a stable genotype, intact DNA repair, active p53 status and favourable generation time and culture conditions. However, one consideration be aware of is the non-crucial nature of the specific GPI-anchored proteins chosen to report mutation at the *PIG-A* gene locus within human leukocytes. Within the erythrocytic rodent Pig-a assay, the cellular surface antigens chosen as reporters for mutation are vital antigens to prevent haemolysis [141]; naturally, homologous cellular surface antigens are present on the surface of leukocytes however, the presence of absence in this case does not trigger a complement protein response. Lymphoblasts are renowned for their variable cellular surface expression, especially prominent within auto-immune disease phenotypes [230-232] as well as physiological disease states such as cardio vascular disease [233] and antigen presenting mechanisms within the immune response [149, 234].

Therefore, following highly varied and often lower than predicted, ~75% GPI-AP wild type, expression of homologous GPI-AP to the rodent in vivo Pig-a assay [229]. Investigations were initiated into the integration of a mutant depletion step, analogous to the HAT (Aminopterin) treatment within the HPRT or TK assays [75], within the assay design.

3.1.6 Considerations and Limitations of Flow Cytometry

Flow cytometry has been demonstrated in recent years to be a fundamental technique used throughout biological research [235]. The nature of the high content analysis allows a holistic approach facilitating the development of exciting new research fields including systems biology [236], which deviate from the reductionism norm. However, as often is the case with the introduction of high through-put new technology, the quality of data analysis methodologies often lags behind the developmental approaches [237]. This observation is often exaggerated by subjectivity existing within data acquisition; the user is often forced to make assumptions based on the limited contextual data available at the time [238]. In the context of the in vitro *PIG-A* gene mutation assay, flow cytometry is the backbone of

data capture as well as both real time and retrospective analysis. Therefore, sufficient understanding of the major considerations and limitation associated with the technology as well as the sample is needed to ensure optimum use of the novel technique and high quality data generation.

The BD FACS Aria Flow sorter was the major platform on-which the in vitro *PIG-A* assay was developed and it has its own unique specifications [239]. The sorter utilises a complex "detector wheel" configuration, comprising of sequential long pass filters (LPF) as well as corresponding band pass filters (BPF) enabling emitted light to strike a detector suitable to measure a photo event, and hence convert such event into an electrical signal able to be intensified, manipulated and analysed with the respective flow cytometry software. The detector wheel set up is laser specific and is exposed to all emitted light post illumination; light travels through the fibre optic bundle and passes through the initial LPF, this enables light of specific wave lengths to travel towards a corresponding BPF and then onto a PMT to record the signal [192]. Any light not able to pass the LPF is deflected towards the next LPF and BPF set up with a wave length lower than the previous, this system continues until a minimum wavelength is reached. The minimum wave length for each laser specific detector wheel directly corresponds to the excitation frequency (wave length) of the source laser.

However, due to the nature of fluorophore fluorescence emission, i.e. a gradual slopped curve with an exaggerated range of wavelength, when compared to synthetic quantum dots; multiple fluorophores used within a specific experiment can have partial emission within a single detector, causing signal overlap and ambiguous results (Figure 3.1). This occurrence can be detected, analysed and compensated against; however, diminishing returns are associated.

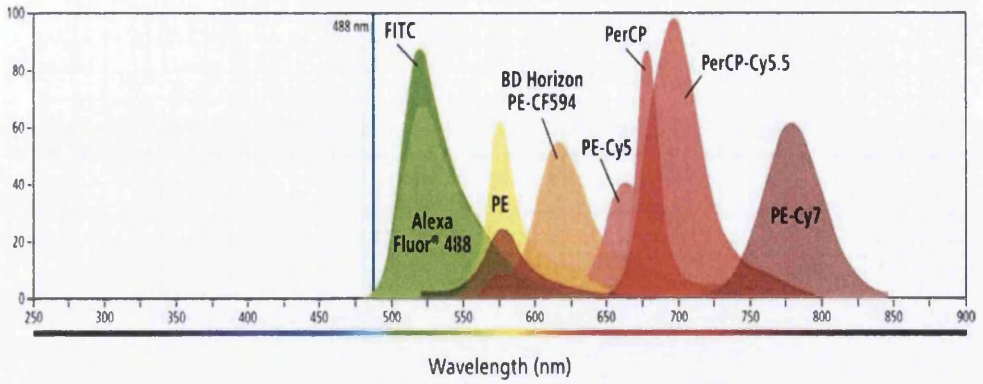

Figure 3.1. The nature of fluorescence emission spectra following 488 nm laser light excitation. Overlapping fluorescence spectra is a potential source of ambiguity or false positivity within flow cytometric analysis, the schematic highlights the minimum wavelength required for detection. Fluorescein isothiocyanate (FITC), Phycoerythrin (PE), Peridinin chlorophyll (PerCP), Phycoerythrin-cyanide 5 (PE-Cy5), Peridinin Chlorophyll – cyanide 5 conjugate (PerCP-Cy5.5) and Phycoerythrin Cyanide 7 conjugate (PE-Cy7).

Fluorescence compensation is the term given to this process; single stained flow cytometry samples are analysed within adjacent detectors of similar wavelengths ranged to identify signals of a positive nature. Subsequently, if a signal is detected, the voltage of the perpetrating fluorophore is reduced until the signal loses its positive characteristics.

Fluorescence emission overlap is not just observed within high-end flow cytometers, the problem is often more acute within lower specification systems or equally more complex systems. The ImageStream ™ system, even though hailed as a multicolour cytometer has no band pass filters or specific detectors. Therefore, the need for highly sophisticated masks as well as user defined features is required in order to, post capture, remove said overlap from adjacent channels and provide fluorophore specific data [240].

Additional technical limitations are also present within flow cytometry in terms of electrical noise and signal identification; however, for the scope of this thesis the only other major limitation which is significant is the lack of actual visualisation of cellular events, which is enabled when using ImageStream™ Technology.

3.2 Materials and Methods

3.2.1 Antibody Optimisation in Conjunction with Cellular Surface Expression Analysis - Fluorescein Isothiocyanate vs. Phycoerythrin

TK6 cell cultures were established, counted (Section 2.2) and the equivalent volume of medium containing 1 x 10^6 cells removed and transferred into sterile 15 mL BD Falcon ™ centrifuge tubes. The parental cellular cultures were placed back within the incubator for future use; passage number was critically monitored to prevent clonal deviation from the phenotype (signs of cellular clumping). Cellular samples were centrifuged (~ 250-300 x g for 7 min), and the supernatant was aspirated. 50 µL of fresh pre-warmed media was added and the cell pellets thoroughly re-suspended via pipetting. 5 µL of Human purified Fragment crystallisable (Fc) block (Cat No. 564220, BD Biosciences, Hertfordshire, UK) was added to 50% of the samples and all samples were incubated for 20 min, protected from light, on ice.

Post Fc block incubation, samples were stained with 20 µL of their respective anti-CD59 fluorophore conjugate solutions; human anti-CD59 PE (Cat No. 555764, BD Biosciences, Hertfordshire, UK), human anti-CD59 FITC (Cat No. 555763, BD Biosciences, Hertfordshire, UK) or alternatively their isotype control antibodies; PE Mouse IgG2a, κ Isotype Control (Cat No. 555574, BD Biosciences, Hertfordshire, UK), FITC Mouse IgG2a, κ Isotype Control (Cat No. 555573, BD Biosciences, Hertfordshire, UK) and incubated for 20 min, protected from light, at 2-4 °C. Post antibody incubation, samples were centrifuged (~300 x g for 7 min), supernatants carefully aspirated and washed twice via the addition of 10mL 1 x PBS solution. Following the wash steps the samples were centrifuged, as above, and re-suspended in 1 mL of 1 x PBS in order to construct viable concentrations of cellular solutions to be analysed optimally on the flow cytometer.

FITC and R-PE fluorophores were both excited using the 488nm laser line and assessed within the pre-specified "FITC" and "PE"" detectors; FITC, 502LP combined with a 530/30 band pass filter and PE, 556 LP combined with a 585/42 band pass filter.

3.2.2 Enrichment Strategies to Optimise CD59 Expression with the Human Lymphoblastoid TK6 Cell Line

3.2.2.1 Dynabead ® Enrichment and Subsequent Magnetic Bead Retrieval of the TK6 cells expressing the CD59 Cellular Surface Antigen

DSB-X™ Biotin Protein Labelling Kit (Cat No. D-20655, Molecular Probes, Life™ Technologies, Paisley, UK) was utilised in order to fully biotinylate an anti-human anti-GPI-AP antibody. Prior to biotinylation, kit contents were stored at 2-4 °C as well as fresh PBS pH 7.2 and 1M sodium bicarbonate was prepared. The biotinylation of the anti-human purified CD59, clone P282 (H19) Mouse IgG2a $_{k}$ antibodies purchased from BD Biosciences (Cat No. 555761, BD Pharmingen™, San Jose CA, USA) was undertaken as outlined within the accompanying protocol (Appendix Section 3.3.2.1). In brief, activated DSB-X biotin ester was conjugated to the purified anti-CD59 antibody, spin column purified and isolated. Bovine serum albumin (BSA) was added to a concentration of 1-10 mg/mL, the conjugate was stored at 2-4 °C for future usage.

Following preparation of the biotinylated antibody conjugate, Dynabeads ® Flow Comp™ Flexi Kit (Cat No. 11061D, Molecular Probes, Life™ Technologies, Paisley, UK) was used to positively select the phenotypic *PIG-A* wild type cells (Appendix Section 3.3.2.1). In brief, cells were washed in pre-cooled isolation buffer, DSB-X conjugate antibody added and subsequently treated with Flow Comp™ Dynabeads. Post conjugation, Dynabead® bound cells were magnetically isolated and subsequently beads removed via the addition of release buffer. Putative bead free wild type cells were re-cultured and QA FCM assessed for *PIG-A* phenotype. Recovered cells were cryo-preserved for future use.

3.2.2.2 Clonal Expansion Enrichment of the TK6 cells expressing the CD59 Cellular Surface Antigen

Cellular samples were treated with anti-GPI-AP specific fluorescently labelled antibodies (Section 2.8.1) and analysed on the flow cytometer (Section 2.8) in order to assess their phenotypic *PIG-A* status. Once the population selected met the desired characteristics, the parental cellular culture was removed from incubation and counting was repeated (Section 2.2)). A volume of culture was removed, centrifuged and the supernatant aspirated prior to being diluted with fresh growth medium in order to construct a final concentration of 200 cells/mL. 100 µL aliquots of the culture were transferred into each well of a sterile 96 well plate (Ref 655090, Greiner –Bio-One, Gloucestershire, UK) using a multichannel pipette (Finnipipette®, Thermo Scientific, Hampshire, UK) and repeated in order to generate six identical plates. The plates were labelled accordingly and placed within a Perspex box and incubated for 72 hr. Post incubation, each plate was removed and microscopically each well was assessed for colony presence and their respective efficiency of growth. 144 colonies deemed to be well established, exhibiting optimum growth, were selected and transferred into 6 x 24 well plates using a 100 µL pipette set to a total volume of 20 µL. 280 µL of fresh growth medium was added to each well in order standardise the final volume and each plate was incubated for a further 72 hr. Post incubation, each well was thoroughly examined and the ten largest colonies were identified and marked. Each marked colony (excess of ~1000 cells) were transferred into separate sterile 25 cm^2 culture flasks, excess growth medium to a total volume of 10 mL was added, and incubated for 48 hr. Post incubation, the cultures were deemed to be confluent (~ 1-7 x 10^5 cells/mL) and were flow cytometry assessed for analogous cellular surface protein expression (Section 2.8). Post analysis selected 25 cm^2 flasks were centrifuged, supernatant aspirated and prepared for long term cryopreservation.

3.2.2.3 Fluorescence Activated Cell Sorting (FACS) Enrichment of the TK6 Cells expressing the CD59 Cellular Surface Antigen

Cellular samples were treated with anti-GPI-AP specific fluorescently labelled antibodies (Section 2.8.1) and subsequently analysed on the flow cytometer (Section 2.8.2) and FACS sorted (Section 2.8.3). A larger nozzle and lower pressure (100 µm and 20 psi respectively) were utilised for the sensitive TK6 cells.

Post sorting, the recovered cells, pooled presumed homogeneous, population were collected within 5 mL polystyrene (12 x 75 mm) sorting tubes (BD. Biosciences, Hertfordshire, UK) with fresh cell line specific growth medium (1 mL) and consecutively sub-cultured (Section 2.2.3) within 25 cm^2 culture flasks prior to long term cryopreservation (Section 2.3). Quality assurance (QA) FCM based *PIG-A* phenotype assessment was carried out prior to and 72 - 96 hr. following enrichment.

3.2.3 Proof of Principle Evaluation Utilising CD59 as a Phenotypic Reporter for Mutation at the *PIG-A* Locus within the TK6 Cell Line Following EMS Exposure

A clonally expanded, pre-enriched for the CD59 cellular surface antigen, TK6 cell culture was thawed and maintained as outlined in (Section 2.2.) and exposed to EMS for 24 hr under standard chemical treatment as described within (Section 2.4.2). Post chemical exposure, cultures were washed, counted and seeded ready for initial flow cytometric analysis using anti-human CD59 PE conjugate (Cat No. 555764, BD Pharmingen ™, San Jose CA, USA). Flow cytometric analysis as defined in (Section 2.8.2) was undertaken within an hour of sample preparation, samples were stored on ice, protect from direct light, until analysis.

After gating for single cells on a SSC/FSC dot plot and/or counter map, a minimum of 10,000 events were analysed for the surface expression of the CD59 surface antigen (Section 2.8.2). *PIG-A* phenotype was assessed utilising an instrument

calibration standard (ICS), an unstained sample used to set voltages and mutant gating. During ICS analysis, the mutant mimicking sample is utilised to detect auto fluorescence within the channel of collection in order to distinguish between a positive event and background noise at the channel's photon multiplier tube (PMT).

All analyses within this section of work were performed using a standard 70 µm nozzle at the manufactures suggested 70 psi pressure. FACS Diva 6.0 software (BD Biosciences) was used for operating the cytometer and for data analysis. All fluorescence measurements on the FACSAria were recorded using the "area" parameter coupled with band pass emission filter of 585+/- 21 in the "PE" channel; excitation of PE fluorophore was achieved by the 488 nm argon laser. Following flow cytometric analysis, parental cell cultures were removed from incubation every 24 hr for repeated *PIG-A* mutagenesis assessment as described at length in (Section 2.10).

3.2.4 Long-term Cryo-preservation Assessment on CD59 Phenotype Stability

A clonally expanded, pre-enriched for the CD59 cellular surface antigen, TK6 cell culture was thawed and maintained as outlined in (Section 2.2.). The surface expression of the specific cryo-vial chosen was previously flow cytometry defined as 99.8% CD59 positive, this analysis was repeated and confirmed following the construction of the to be assessed specific candidate preservation media.

Approximately 250 mL of confluent pre-enriched TK6 cells were counted; 81 million cells were required for the experiment, as outlined in the table below, as well as an additional 1 x 10^6 cellular sample to confirm initial CD59 presence on the cellular surface of the heterogeneous population.

The 1 x 10^6 cellular samples were centrifuged, washed and stained as outlined in detail within (Section 2.8.1) and subsequently flow cytometrically analysed (Section 2.8.2), enabling detection of potential degradation of the surface expression due to the initial freeze thaw process, to act as a reference for the ensuing experiment.

All potential candidate media were made with the constituents as described in Table 3.1, however, the sucrose was bought in as a powder and required reconstituting into a solution prior to usage. 10 g of sucrose powder was weighed out accurately, and transferred into a 250 mL glass McCartney bottle. 60 mL of dH_20 was added to the sucrose powder and mixed thoroughly until the powder had dissolved, the final volume of the solution was adjusted to 100 mL via the addition of dH_20 constructing a 10% (w/v) solution.

Table 3.1. Description of the constituting elements within each candidate preservation media.

Sample Identifier	Major Constituent (90% total volume)	Minor Constituent (10% total volume)
Sample 1	Serum	DMSO
Sample 2	Serum	Sucrose
Sample 3	Serum	Glycerol
Sample 4	Heat Inactivated Serum	DMSO
Sample 5	Heat Inactivated Serum	Sucrose
Sample 6	Heat Inactivated Serum	Glycerol
Sample 7	Media	DMSO
Sample 8	Media	Sucrose
Sample 9	Media	Glycerol

Each candidate media was made up of two parts; a major constituent (90%) and a corresponding minor constituent (10%) to assess practicality of long term cryo-preservation of pre-enriched cultures. Media (Serum free RPMI 1640), Heat inactivated Horse Serum, Serum (Horse), Dimethyl Sulfoxide (DMSO) (Cat No. D8418, Sigma Aldrich, Hertfordshire, UK), Sucrose (Cat No. S0389, Sigma Aldrich, Gillingham, UK) and Glycerol (Cat No. G5516, Sigma Aldrich, Gillingham, UK).

Each sample was constructed in triplicate, and made up in a sterile 15 mL BD Falcon ™ centrifuge tube; the equivalent volume of medium containing 3 x 10^6 cells was transferred into each centrifuge tube, centrifuged (~250 x g for 7 min) and supernatant aspirated. Each vial was reconstituted constructed at a final

concentration of 2 x 10^6 per mL, requiring a total volume of 1.5 mL of preservation media. Each sample received 0.15 mL of the minor constituent (DMSO, Sucrose or Glycerol) and 1.35 mL of the major constituent (Serum, Heat-inactivated Serum and Serum free media) as outlined in Table 3.1.

The contents of each centrifuge tube were transferred into pre-labelled 2 mL cryovials, resulting in the construction of 21 samples in total, and placed within an iso-propanol housed Nunclon container to facilitate progressive 1°C/min temperature decrease. Following initial 24 hr incubation within the - 80°C freezer, the individual cryovials were transferred into the liquid nitrogen dewer for long term storage, as described in (Section 2.3).

Following one, three and 6 month incubation periods within liquid nitrogen cryo-preservation a single sample from each batch, as outlined in Table 3.1 were removed, thawed quickly as outlined in (Section 2.2) and the contents transferred into a sterile 25 cm^2 culture flask. 8.5 mL of fresh, pre-warmed growth media (RPMI 1640 supplemented with 10% HS and 1% L-Glut) was added, via pipette and pipette controller, and the flasks placed into an incubator and monitored every 24 hrs, until normal growth dynamics were achieved.

Once log phase and subsequent revival was established, a 1 x 10^6 cellular sample was removed from each flask and transferred into a sterile 15 mL BD Falcon ™ centrifuge tube. Each sample was centrifuged (250 x g for 7 min), supernatant aspirated and re-suspended in 50 µL of fresh pre-warmed growth medium. 20 µL of human anti-CD59 R-PE conjugate antibody was added to each solution and incubated for 20 min, protected from light, at 2-4°C. A single ICS was also constructed, acting as a mutant mimicking control to enable flow cytometric calibration.

Post incubation the tubes were centrifuged (~250 x g for 7 min), supernatant aspirated and re-suspend in 2 mL of 1 x PBS solution. Samples were centrifuged, as above, supernatant aspirated and again re-suspended in excess 1 x PBS solution. This step was repeated in total twice to ensure removal of excess antibody titre. Post washing, the cellular pellets were re-suspended in 1 mL PBS and the contents of each centrifuge transferred into a separate 5 mL Flow tube (BD Biosciences, Hertfordshire, UK). Samples were stored on ice, protected from light, for a

maximum of one hr prior to flow cytometric analysis, a brief re-suspension was required pre-analysis.

R-PE was assessed within the pre-specified "PE" detector; PE, 556 LP combined with a 585/42 band pass filter and analysed utilising the FACS DIVA® software..

3.2.5 Introductory Investigations into Potential Non-viable, *PIG-A* Mutant Mimicking Events

A fresh vial of TK6 cells pre-enriched for the CD59 cellular surface antigen were removed from cryopreservation and established as outlined within (Section 2.2). An expression level greater than 95%, CD59, was utilised within this experiment. Once the cellular culture had re-established itself, samples were prepared for each fluorophore, in an analogous fashion to the generalised multi-stained sample outlined below, and stored on ice, protected from light, until ready for compensation analysis. Also a single instrument calibration standard was prepared, facilitating auto-fluorescence detection within the relevant detectors.

Cellular samples, post re-suspension, were treated with 20 µL of the anti-CD59 PE antibody solution and incubated for 20 min at 2-4°C, protected from light. Post incubation, samples were centrifuged (250 x g for 7 min), supernatant aspirated and washed twice with excess 1 x PBS solution. Simultaneously to the washing steps, Annexin V-binding buffer 10X (Cat No. 14084, Abcam, Cambridge, UK) was diluted 1:9 parts respectively with dH_20 and placed on ice to cool rapidly. Following washing, the cellular pellets were re-suspended in 1 mL of 1X constructed Annexin V-binding buffer, centrifuged (as above) and re-suspended in 100 µL of the 1 x Annexin V-binding buffer.

5 µL of Alexa Fluor® 488 Annexin V conjugate (Cat No. A13201, Life Technologies ™, Paisley, UK) was added to the 100 µL cell suspension and incubated at room temperature for 15 mins, protected from light. Post incubation, excess 1 x Annexin-binding buffer (~1 mL) was added to each culture and centrifuged (250 x g for 7 mins). The resultant supernatant was aspirated, and the

cell pellet re-suspended in 200 µL of 1X Annexin V-binding buffer. 5 µL (0.25 µg) of 7-Aminoactinomycin D (7-AAD) (Cat No. A1310, Life Technologies ™, Paisley, UK) was added to each sample, incubated for a minimal of 5 mins on ice, protected from light and flow cytometrically analysed within 4 hr of initial antibody treatment.

Annexin V, Alexa Fluor® 488, R-PE and 7-AAD were assessed within the pre-specified "FITC" , "PE" and "APC" detectors; FITC, 502LP combined with a 530/30 band pass filter. PE, 556 LP combined with a 585/42 band pass filter and APC, No LP combined with a 660/20 band pass filter. Alexa Fluor 488® and PE were excited off the 488nm laser line, and the 7-ADD off the 633 nm laser line, best matching their excitation maxima's.

3.3 Results

The aim of the following section was to experimentally fully characterise the potential antibody candidates available for phenotypic CD59 *PIG-A* mutant reporting. In an endeavour to reduce further subjectivity within FCM analysis, extensive antibody optimisation was undertaken.

3.3.1 Antibody Optimization in Conjunction with Cellular Surface Expression Analysis

- Fluorescein Isothiocyanate vs. Phycoerythrin

Initially focussing on the FITC data (Table 3.2), the results appeared to be fairly similar; average fluorescence intensity, 3688 and 3500, the number of events defined positive, 7884 and 7440 and the percentage of the parental population, 73.4 and 71.7% in the presence and absence of Fc Blocker respectively. However, in the absence of Fc block reagent; a 5.1% decrease in intensity, 5.6% decrease in the number of events defined positive and a 1.7% reduction in the parental population was observed when compared when compared to the Fc block reagent present samples.

Phycoerythrin demonstrated an analogous relationship when comparing the impact Fc block reagent had on the subsequent sample statistics; average fluorescence intensity was shown to be 6497 and 5761 arbitrary units, a decrease of 11% in the absence of Fc block reagent. The number of events attributed positive for a PE signal was again analogous within the inter-fluorophore comparison, 7068 to 7047 events presence to absence respectively. Finally the population statistics generated within this sample were highly reproducible, 70.7 to 70.5% identification post antibody treatment.

Comparing FITC against PE directly, summarising both Fc blocker positive and negative samples, the data demonstrates little differences with respect to the subsequent population sizes, in terms of number as well as the percentage of the parental un-refined population, following either antibody treatment. However, there is a more obvious difference in their respective fluorescence intensity following antibody treatment; the PE treated samples demonstrated an implicitly higher fluorescence intensity value, in regards to arbitrary units, when compared to the corresponding comparable FITC treated samples, 6129 to 3594 respectively.

Table 3.2. Description of the characteristics observed following human TK6 lymphoblastoid cells treated with undiluted (1X) quantities of the two assayed fluorescent conjugated antibodies (FITC and PE) in the presence and absence of Fc Block reagent. Events were deemed positive based on a homologous instrument calibration standard (ICS) which was utilised to gauge auto-fluorescence within the specific detector channel utilised. Quoted "Fluorescence intensity" refers to the "Area" measurement , taking into account the entire signal and not just the maxima (height) or time of flight measurement (width) and measured in arbitrary units. N=1, 10,000 events captured per sample.

	Fluorescein Isothiocyanate (FITC)		**Phycoerythrin (PE)**	
	Fc Block Positive	**Fc Block Negative**	**Fc Block Positive**	**Fc Block Negative**
Average Fluorescence Intensity (Area)	3688	3500	6497	5761
Number of Events Deemed Positive	7884	7440	7068	7047
Percentage of Parental Population (%)	73.4	71.7	70.7	70.5

Considering the FITC isotype treated samples; in the absence of Fc block reagent 19 cellular events were deemed positive, constituting 0.2% of the parental population with an average fluorescence intensity of 697 (Figure 3.2 A). In the presence of Fc block reagent (Figure 3.2 B) 7 events were considered positive, constituting 0.1% of the parental population with an average fluorescence intensity of 2489. Both samples were demonstrated to produce comparable data with an estimated binding efficiency of 0.06% in the presence of Fc block and 0.18% in the absence of Fc block reagent respectively.

The PE isotype treated samples generated equivalent results; 36 and 38 cellular events were defined as positive, constituting 0.4 and 0.3% of the parental population and with an average fluorescence intensity of 8942 and 3790 arbitrary units in the absence and presence of Fc block reagent respectively (Figures 3.2 C and D). Binding efficiencies were estimated at 0.35% in the presence of Fc block and 0.36% in the absence of Fc block respectively.

Comparing the FITC and PE isotype data, an analogous trend was observed as previously demonstrated in (Table 3.2); little difference was seen between the two samples. The PE isotype data was consistently demonstrated to produce marginally larger population statistics than the comparable FITC data. However, all increments were negligible and therefore, not statistically significant in the overall context of the experiment. Average binding efficiencies, incorporating both Fc block present and absent samples, of the PE isotype control were again shown to be marginally higher than comparable FITC statistics, 0.355 to 0.12% respectively.

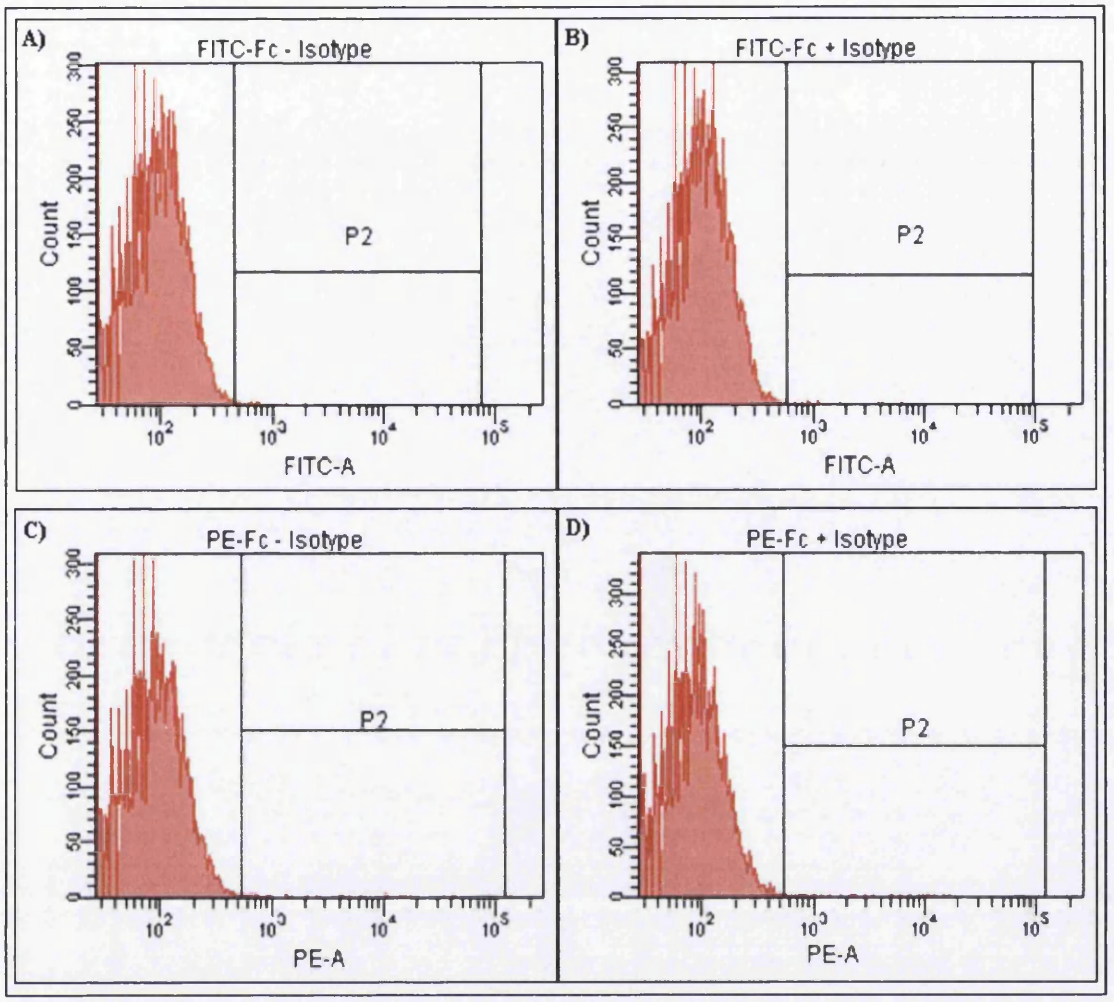

Figure 3.2. Average fluorescence intensity values for Human TK6 lymphoblastoid cells following isotype control fluorophore-conjugate antibody treatment in the absence and presence of Fc block reagent. Antibody Specificity Assessment following (1X) isotype control treatment for the two assayed fluorescent conjugated antibodies (FITC and PE). Direct visual comparison can be drawn between samples of like fluorophore; A) anti-CD59 FITC treated, Fc Block negative and B) anti-CD59 FITC treated Fc Block Positive or alternatively C) anti-CD59 PE treated, Fc Block negative and D) anti-CD59 PE treated, Fc Block positive. N=1, >10,000 events captured per sample. The "P2" region is the defined positive signal region following ICS auto-fluorescence assessment.

The FITC conjugate antibody data, in the presence of Fc block, exhibited a positive correlation between antibody concentration and the resultant average fluorescence intensity (Table 3.3). This correlation, although not directly proportional, was echoed within the FITC Fc block absence data (Table 3.3). A linear trend line was fitted to the Fc block negative data, and the resultant equation was $y = 29.5x + 926.4$ (Figure 3.3 A). The resultant gradient of the slope (29.5) and the intercept (926.4) highlighted the non-linear characteristics of the data.

The PE-conjugate antibody data, similar to the FITC data, equally shares and displays an analogous positive correlation observed between antibody concentration and subsequent fluorescence intensity within both Fc block present and absent samples (Table 3.3). Again, a linear trend line was fitted to the Fc block negative sample ($y = 57.6x + 67.2$) and was demonstrated equally not to be linear (Figure 3.3 B). However, the PE antibody was shown to be more representative of a directly proportional relationship than the comparable FITC data, with "goodness of fit" R^2 values of 0.999 and 0.879 respectively.

When discussing the data as a whole, irrespective of Fc block presence, the top two antibody concentrations (0.5 and 1X) resultant in comparable fluorescent intensity data, all lesser concentrations demonstrated significant diminishing returns in respect to relative fluorescent intensity (Table 3.3).

In addition, PE data consistently had higher associated fluorescence area intensity values, at equivalent antibody concentrations, than the FITC data. However, this relationship is reversed as the concentration of the antibody decreases below 0.5X for all ensuing antibody concentrations, as shown in Table 3.3.

Table 3.3. Antibody titration analysis following human TK6 lymphoblastoid treatment of the two assayed fluorescent conjugated antibodies (FITC and PE) in the presence and absence of Fc Block reagent. Events were deemed positive based on a homologous instrument calibration standard (ICS); direct comparison can be made between like fluorophores. N=1, >10,000 events captured per sample.

	Average Fluorophore Staining Intensity - Area (Arbitrary Units)			
	Fc Blocker +ve		**Fc Blocker-ve**	
Antibody Concentration	**Fluorescein Isothiocyanate (FITC)**	**Phycoerythrin (PE)**	**Fluorescein Isothiocyanate (FITC)**	**Phycoerythrin (PE)**
1 X	3688	6497	3500	5761
0.5 X	3140	4043	2942	3076
0.25 X	2258	1776	2218	1553
0.125 X	1249	870	1418	751
0.0625 X	717	380	262	356
Average Fluorescence (Area) over Concentration Range	**2210.4**	**2713.2**	**2068**	**2299.4**

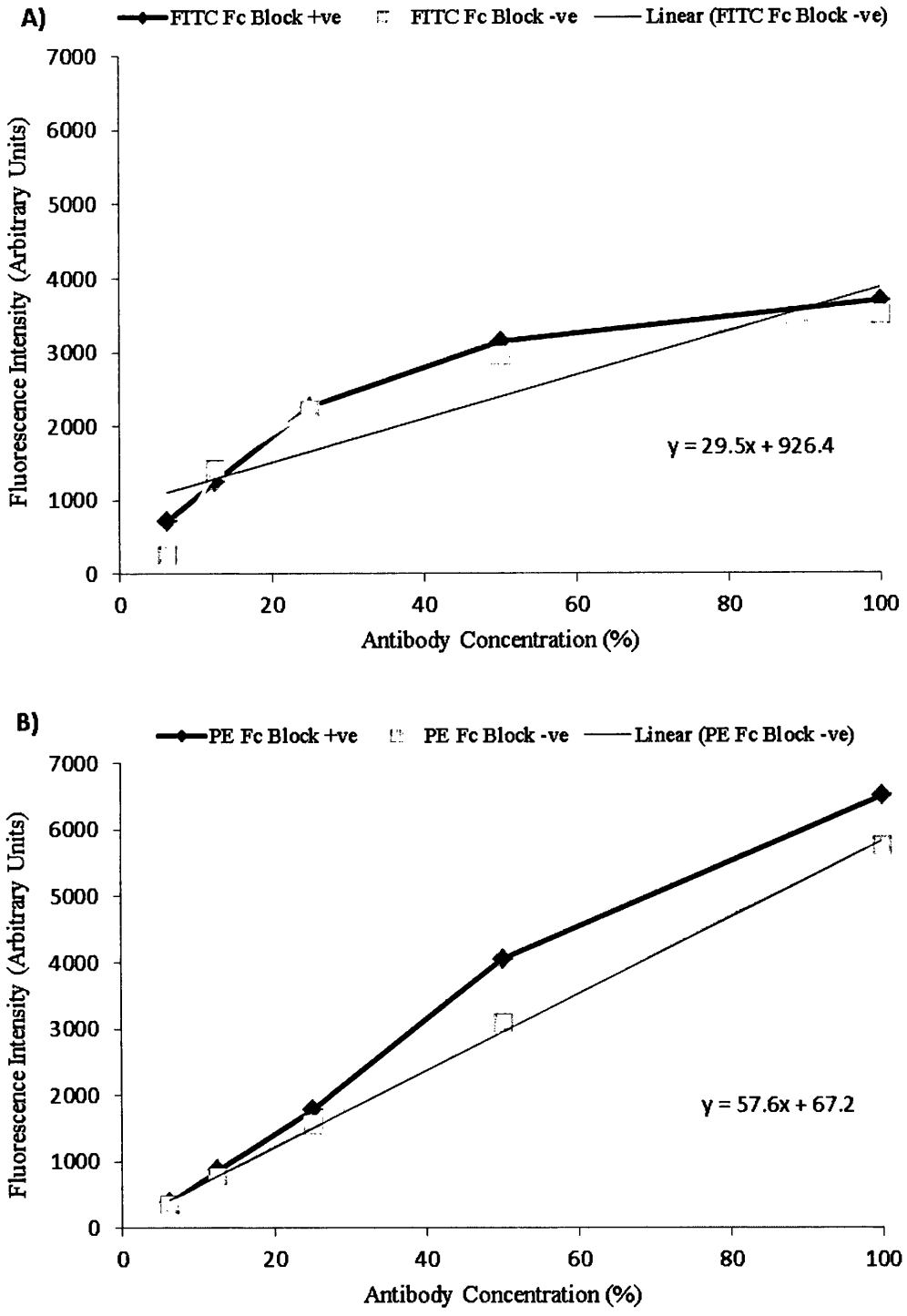

Figure 3.3. Antibody Titration Analysis values following human TK6 lymphoblastoid treatment with fluorophore-conjugate antibodies (A) FITC and B) PE. Average Fluorescence intensity values following FITC or PE conjugate antibody treatment, in the presence or absence of Fc block reagent. Linear trend line drawn for Fc block negative sample, with equation displayed on graph. N=1, >10,000 events captured per sample.

3.3.2 Enrichment Strategies to Optimise CD59 Expression with the Human Lymphoblastoid TK6 Cell Line

Within the cryo-preserved TK6 stock cultures, used within this body of work, the CD59 cellular surface expression was routinely determined to be heterogeneous, approximately 3:1 in favour of CD59 presence. Therefore, ~ 25% of all cells analysed displayed limited or complete absence of the CD59 cellular surface antigen. The aim of the subsequent result section was to identify potential pre-enrichment strategies and compare their efficiency in order to deplete heterogeneous stock TK6 solutions of phenotypic *PIG-A* mutants, in this case cells staining negative for CD59 surface antigen presence.

3.3.2.1 Dynabead ® Enrichment and Subsequent Magnetic Bead Retrieval of the TK6 Cells Expressing the CD59 Cellular Surface Antigen

Initially, focussing on the Dynabead ™ paramagnetic enrichment data, Sample 1 was demonstrated to have an average CD59-PE expression frequency of 84.3% (Table 3.4). 83.7% of the sample was demonstrated to be single cell in nature and therefore, applicable for subsequent flow cytometry based analysis. Sample 2 and 3 were shown to achieve moderately higher enrichment yields; with corresponding CD59 expression frequencies of 96.5 and 95.9% respectively (Table 3.4). Both samples 2 and 3 generated analogous heterogeneous populations in terms of basic cellular morphology and aggregation status as the initial sample, 82.2 and 83.5% single cell morphology respectively. The maximum enrichment, in terms of CD59 cellular surface antigen expression, was 96.5%.

Table 3.4. Summary of the R-PE CD59 cellular surface expression within Human B-Lymphoblastoid TK6 Cells following DSB-X biotinylation and subsequent paramagnetic Dynabead ™ enrichment. Positivity was attributed to a cellular event exhibiting an arbitrary fluorescence value in excess of the maxima determined for an un-stained calibration samples within the same detector; a fixed gating strategy was applied for all samples. Standard Deviation value = 0.19, for percentage "CD59 Positive Events". Individual ICS samples were run for each sample derived from a different purchased kit. Sample 1 was derived from the originally purchased DSB-X Biotinylation kit; subsequent samples (2 and 3) were generated using an additional purchased kit.

Cellular Culture ID.	Number of Events	Percentage of Total Captured Events	Number of cells determined CD59 Positive	CD59 Positive Events (Percentage of Total applicable Events)	Number of cells determined CD59 Negative	CD59 Negative Events (Percentage of Total applicable Events)
ICS1	8325	83.2	0	0	8325	100
ICS2	8305	83.0	0	0	8305	100
Sample 1A	8216	82.8	6909	84.1	1307	15.9
Sample 1B	8461	84.6	7136	84.3	1325	15.7
Sample 1C	8379	83.8	7077	84.5	1302	15.5
S1 Average	**8352**	**83.7**	**7041**	**84.3**	**1311**	**15.7**
Sample 2	**11388**	**82.2**	**10985**	**96.5**	**403**	**3.5**
Sample 3	**10000**	**83.5**	**9588**	**95.9**	**412**	**4.1**

3.3.2.2 Clonal Expansion Enrichment of the TK6 Cells Expressing the CD59 Cellular Surface Antigen

Following clonal expansion enrichment, subsequent flow cytometric analysis resulted in varied heterogeneous yields in terms of CD59 cellular surface expression, ranging from 28-99.8% (Figure 3.4); reflecting the heterogeneity of the specific GPI-AP surface marker within the parental un-enriched populations. The majority of samples analysed constituted mainly of defined CD59 positive events for example, sample 1B was the exception. The maximum observed enrichment, in terms of CD59 cellular surface antigen expression was 99.8%.

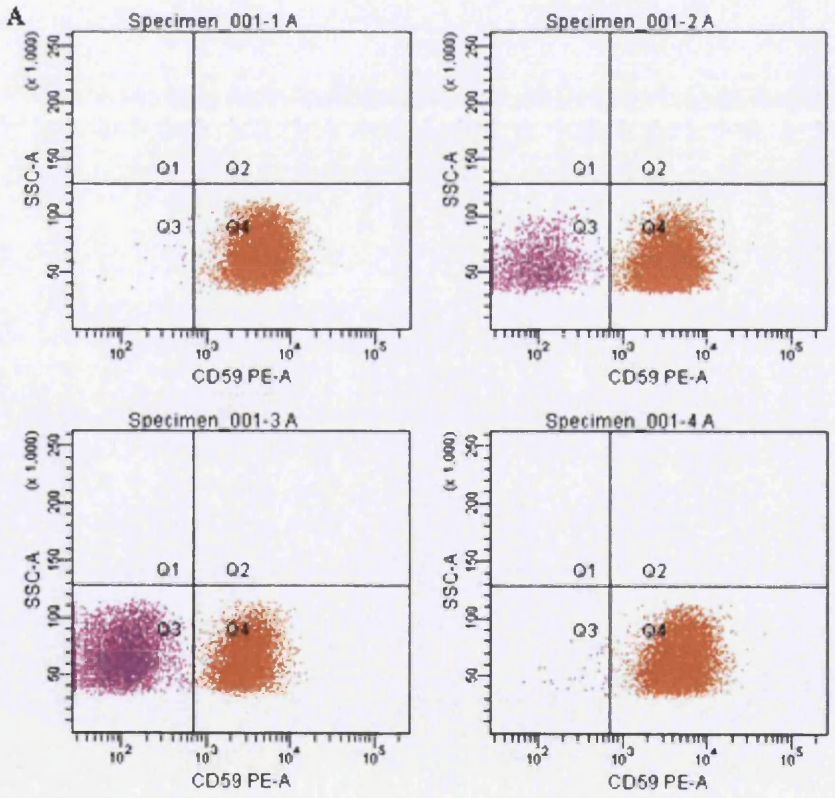

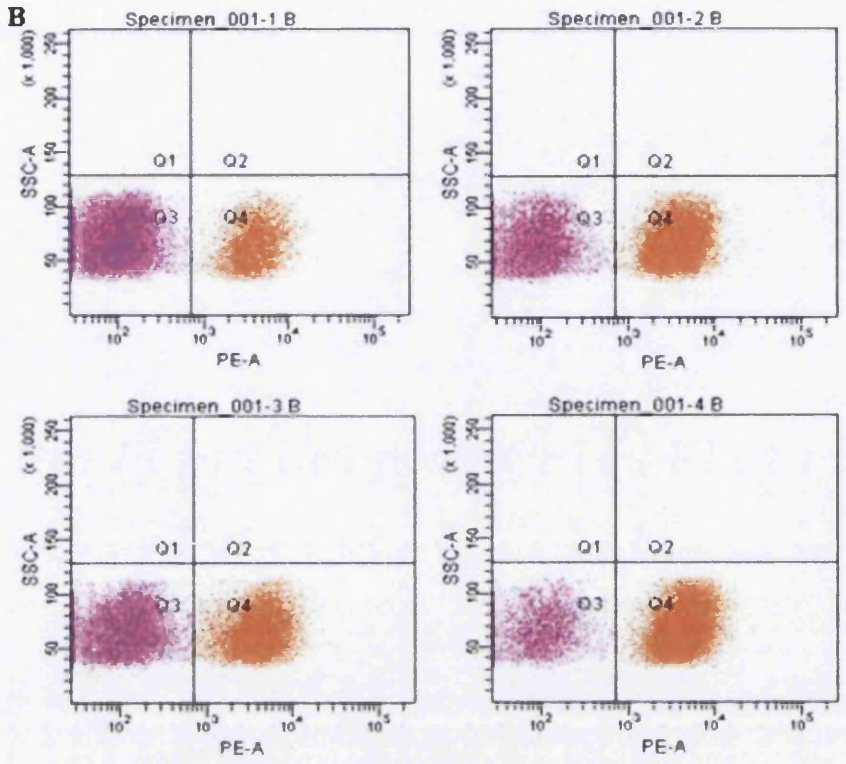

Figure 3.4. Flow Cytometric Analysis of Human Lymphoblastoid TK6 cells following anti-CD59 R-PE conjugate antibody treatment post Clonal Expansion. Cells were clonally expanded (Section 3.2.2.2) and flow cytometry used to assess for CD59 cellular surface antigen expression following anti-CD59 R-PE treatment. Initially, an instrument calibration sample (ICS) was analysed in order to define the single cell population, based on forward and side scatter profiles, and positivity within the relevant fluorophore detector. The intersect between Q3 and Q4 was the resulting boundary of positivity, hence, events falling within Q4 were deemed positive for the CD59 surface antigen, and subsequently Q3 events were deemed negative. 10,000 presumptive single cell events were recorded for each sample; 1A 99.8%, 2A 84.5%, 3A 54.7%, 4A 99.7%, 1B 28%, 2 B 61.8%, 3B 54.4% and 4B 83.8% relative CD59 positive presence.PE-A and CD59 PE-A - Phycoerythrin Area; SSC-A - Side Scatter Area.

3.3.2.3 Fluorescence Activated Cell Sorting (FACS) Enrichment of the Human Lymphoblastoid TK6 Cells Expressing the CD59 Cellular Surface Antigen

Finally, following FACS (Section 2.8.3) and the allotted subsequent recovery period, 72-96 hr to enable re-establishment of "normal" growth dynamics, flow cytometric analysis of three triplicate samples were shown to record an average CD59 expression of 95.3% (Table 3.5). All three samples were analogous in terms of morphology and aggregation status prior to flow cytometric analysis and generated consistent expression/presence data. The maximum average recovered CD59 cellular surface expression using this technique was demonstrated to be 96.48%.

With the exception of clonal expansion, the two additional enrichment methodologies were demonstrated to generate highly reproducible results in terms of relative CD59 antigen presence. However, clonal expansion generated the highest mutant depletion efficiency as observed within sample 1 A within Figure 3.4.

Table 3.5. Summary of the CD59 antigen expression status on the surface of recovered, 72-96 hr, human lymphoblastoid TK6 cells following FACS. Samples denoted by the identical sample number were extracted from the same homogeneous parental culture, different sample number represents a completely different parental sample; ~10,000 single cellular events were scored and each sample was analysed in triplicate.

	Total Number of Single Cell Events	Number of Events Defined CD59 Negative	Number of Events Defined CD59 Positive	Number of Cells Defined CD59 Positive (Percentage of Total Single Cell Events)	Standard Deviation of the Mean
Sample ID.	**FLASK 1**				
1a.	9480	427	9053	95.50	
1b.	9467	358	9109	96.22	
1c.	9337	410	8927	95.61	
1. Average	**9428**	**398**	**9030**	**96**	**0.39**
	FLASK 2				
2a.	9867	259	9638	97.68	
2b.	10179	451	9762	95.90	
2c.	10194	410	8927	87.57	
2. Average	**10080**	**373**	**9442**	**94**	**5.40**
	FLASK 3				
3a.	10900	425	10475	96.10	
3b.	9919	349	9570	96.48	
3c.	9787	359	9428	96.33	
3. Average	**10202**	**378**	**9824**	**96**	**0.19**

3.3.3 Proof of Principle Evaluation Utilising CD59 as a Phenotypic Reporter for Mutation at the *PIG-A* Locus within the TK6 cell line following EMS Exposure

Initial proof of principle experiments were carried out in order to assess the feasibility of qualitative or quantitative dose response modelling following acute model mutagen exposure within the in vitro *PIG-A* gene mutation assay (Section 2.10). The chemical selected for this initial experiment is a model mutagen, an alkylating chemotherapeutic agent, Ethyl Methane Sulfonate (EMS), with comprehensive pre-existing dose response modelling reported in literature [39, 91, 211, 241-243]. All "*PIG-A* mutants" are events phenotypic of CD59 absence (relative fluorescence negative) and therefore, presumptive genotypic *PIG-A* mutants. Identification of presumptive mutant events is highly dependent upon the specific gating strategy used.

Low dose EMS treatment of TK6 cells, clonally enriched for the presence of the CD59 cellular surface antigen, resulted in an apparent sub-linear dose response or no dose response for all days of *PIG-A* analysis, i.e. a number of test concentrations were observed not to significantly increase the respective *PIG-A* mutant frequency (Figure 3.5) when compared to concurrent controls.

Initially, all data was tested for normality and only Day 3 was demonstrated to be normally distributed, $p = 0.67$, and thus was the sole day requiring parametric statistical analysis (Dunnett's 2-sided t-test).

In terms of cytotoxicity, doses greater than and including 5 µg/mL demonstrated a significant toxic effect with resulting RPD values below 50%.; RPD values as low as 21.7% were observed on Day 2 for the top dose (10 µg/mL) tested. However, it appears that at least 24 hrs are required to pass following EMS treatment, prior to any observed toxic effects (Figure 3.5 B).

Day 4 was the only day which demonstrated a significant increase or decrease in the average number of putative *PIG-A* mutants and hence, the resultant average *PIG-A* mutant frequency was observed to rise (Figure 3.5 D). The top dose on Day 4 induced a significant increase in the *PIG-A* mutant frequency ($P<0.01$, Dunn's Two-Tailed T-Test) ($P=0.0003$ and 0.73% respectively) with respect to con-current

negative control values. Cytotoxicity was shown to be marginal at the top dose (10 µg/mL) with an average RPD value of 78.6%.

A) Day 1

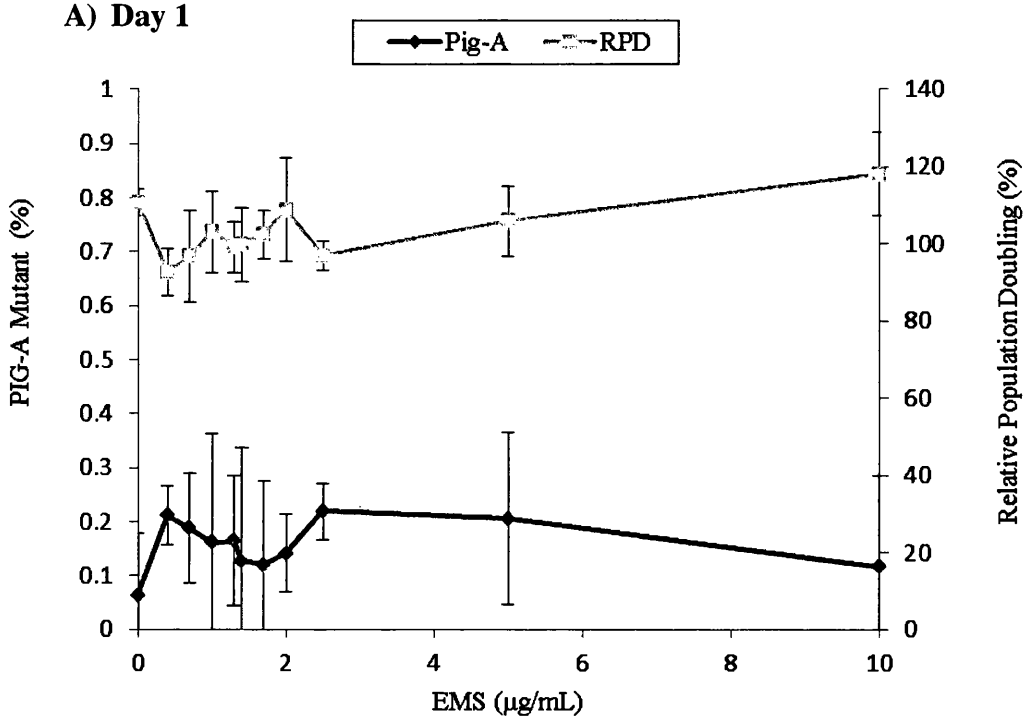

B) Day 2

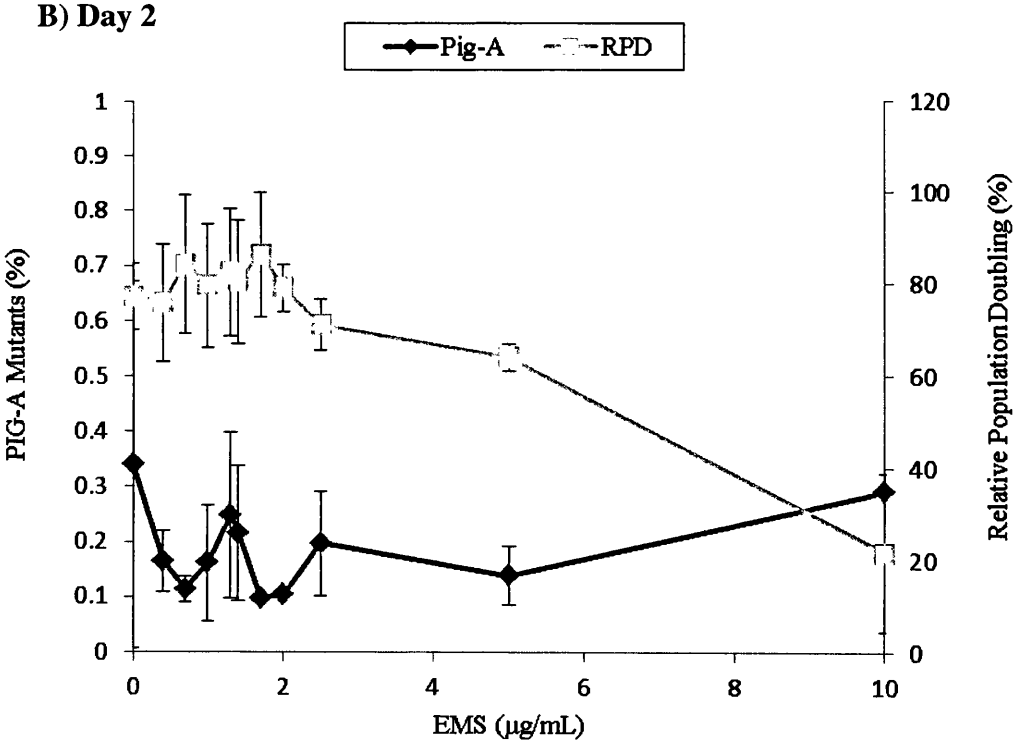

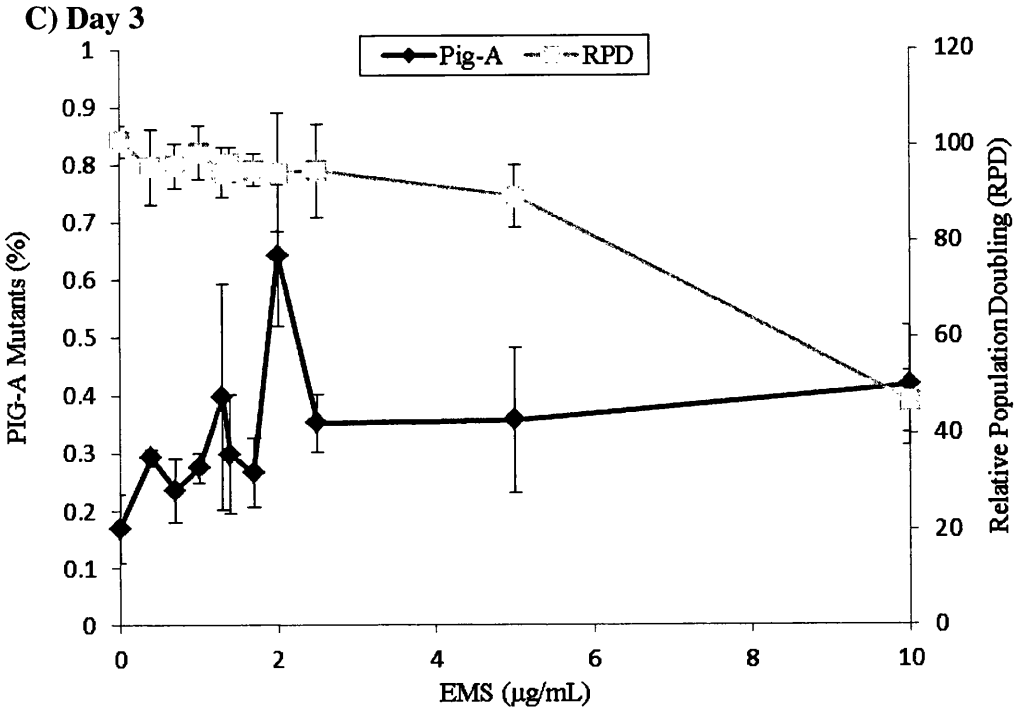

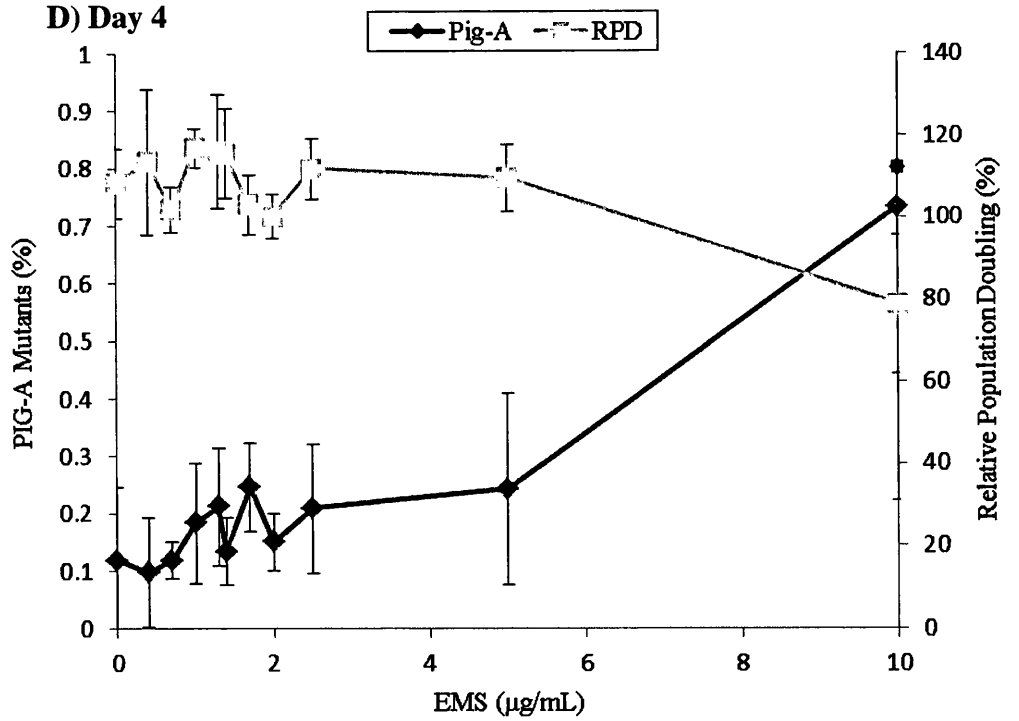

Figure 3.5. Human lymphoblastoid cells (TK6) *PIG-A* mutant frequency following 24 hr low dose EMS exposure, Day 1 – 4 (A-D) respectively, CD59 antigen utilised. Frequencies of *PIG-A* mutant TK6 cells (Clonally selected) following 24 hr low dose EMS exposure (N=3, Error Bars ±1SD) *PIG-A* mutants displayed as percentage of total single cellular events (0.1% *PIG-A* Mutants = 1 mutant x 10^{-3} cells). Vehicle control data displayed within each graph. Statistical Analysis was undertaken following normality testing (Dunn's or Dunnett's Test ($p < 0.05$*)(N=10,000 cells). A single replicate for Day 4 top dose (10 µg/mL) removed due to spurious nature, error bars omitted.

Day 4 data was further analysed utilising the PROAST package (Proast 38.9, National Institute for Public Health, Netherlands) to derive a Bench mark dose (BMD) point of departure (PoD) metric [212]. The BMD is derived from the complete data set by fitting a variety of dose response models, assurance is presented as the ratio between the confident intervals around the BMD_{10} (Figure 3.6), with a lower ratio presenting greater confidence in the BMD value. The BMD_{10} or CED and corresponding $CEDL_{10}$ and $CEDU_{10}$ values were derived as 0.587, 0.439 and 0.881 respectively (Figure 3.6). The "Nested" set of models, utilised to derive the BMD_{10}, as well as the log likelihood function, utilised to calculate the upper and lower confidence limits, are more fully detailed in the appendix (Appendix Section 3.3.3).

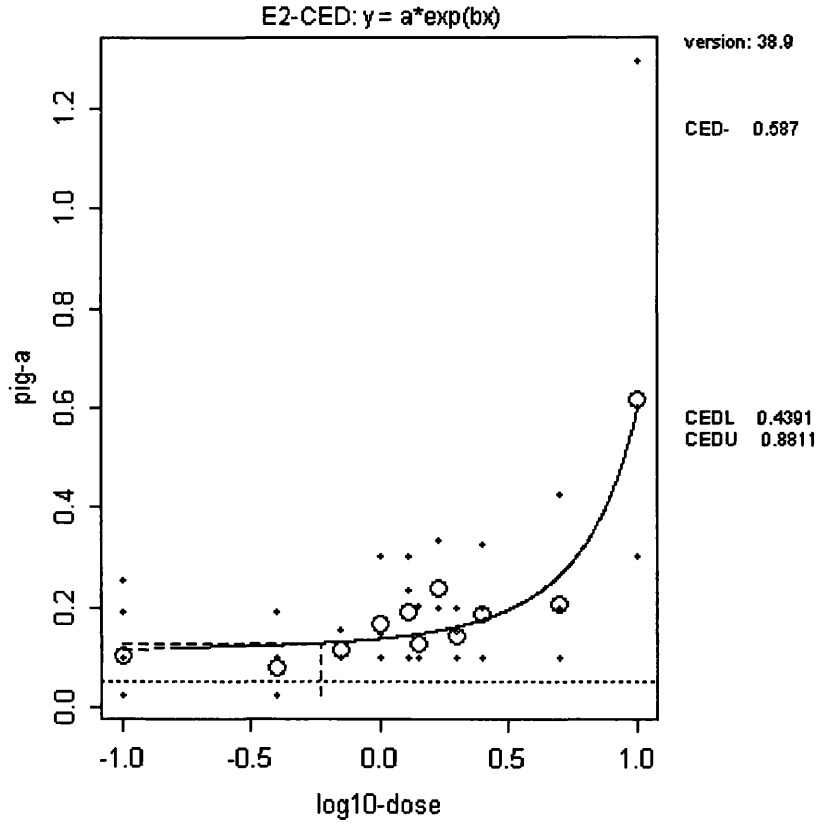

Figure 3.6. Human lymphoblastoid cells (TK6) Day 4 *PIG-A* mutation frequency data following 24 hr. low dose EMS exposure, CD59 antigen utilised. Day 4 frequencies of *PIG-A* mutant TK6 cells (Clonally selected) following 24 hr low dose EMS exposure (Dose - µg/mL). (N=3) "pig-a" mutants displayed as percentage of total single cellular events (0.1% *PIG-A* Mutants = 1 mutant x 10^{-3} cells). PROAST 38.9 modelling; CED, CEDL and CEDU represent the BMD_{10}, $BMDL_{10}$ (Lower confidence limit) and $BMDU_{10}$ (Upper Confidence Limit). Mean *PIG-A* mutant frequencies represented by (o).

3.3.4 Long-term Cryo-preservation Assessment on CD59 Phenotype Stability

Designing a highly sensitive novel gene mutation assay system is not solely adequate; the test system needs to be robust and reproducible to enable inter-laboratory validation and routine use within industrial settings. The following section of data investigates the feasibility to store the pre-enriched, or mutant depleted TK6 populations over an extended period of time, 6 months, and retaining their characteristic growth dynamics and phenotypic cellular surface antigen expression. All *PIG-A* mutant events are phenotypic of CD59 absence, no current genotypic assessment available and therefore, are defined as presumptive *PIG-A* mutants.

Prior to cryopreservation, clonally expanded enriched TK6 cells, for the CD59 surface antigen, were demonstrated to have an average CD59 expression of 99.85% and hence, a spontaneous background *PIG-A* mutant frequency of 0.15% (Appendix Section 3.3.4). All data within this section was defined not normally distributed, Shapiro Wilks $p<0.05$) and therefore, the Dunn's non-parametric T-tests (1 and 2-sided) were utilised for statistical analysis post phenotypic *PIG-A* mutant frequency assessment to state at what dose, if any, rejection of the Null hypothesis was to be assumed (P-value ≤ 0.05).

Following liquid nitrogen storage (liquid phase), across the entire 6 month period, all samples' *PIG-A* mutant frequency rose in comparison to the con-current negative control values; DMSO as a major constituent was demonstrated to have a non-statistically significant effect on phenotypic *PIG-A* mutant frequency, across all time points, when compared to the control sample. However, Glycerol based samples generated statistically significant increases in phenotypic *PIG-A* mutant frequency at each time point (Figure 3.7).

Over the entire 6 month cryopreservation period, DMSO was demonstrated to be the most consistent major constituent in respect to CD59 surface antigen presence stability. DMSO M was the sample which over all three analysis time points demonstrated the smallest increase in phenotypic *PIG-A* mutant frequency with an average of 0.27%, when compared to the negative con-current control value of 0.15%. Glycerol S was observed to be the sample which generated the highest increments in *PIG-A* mutant frequency, 10.62% - 3 month, this was further apparent

as the 6 month sample deteriorated and consequently prevented flow cytometric analysis (Figure 3.7).

10% sucrose was the additional major constituent assessed, however, was shown to be highly detrimental to the TK6 cell cultures and no ensuing analysis was able to be undertaken (Appendix Section 3.3.4). Regardless of storage cocktail utilised, *PIG-A* mutant frequencies did appear to increase proportionally with time, however, increments were deemed not statistically significant with DMSO based samples.

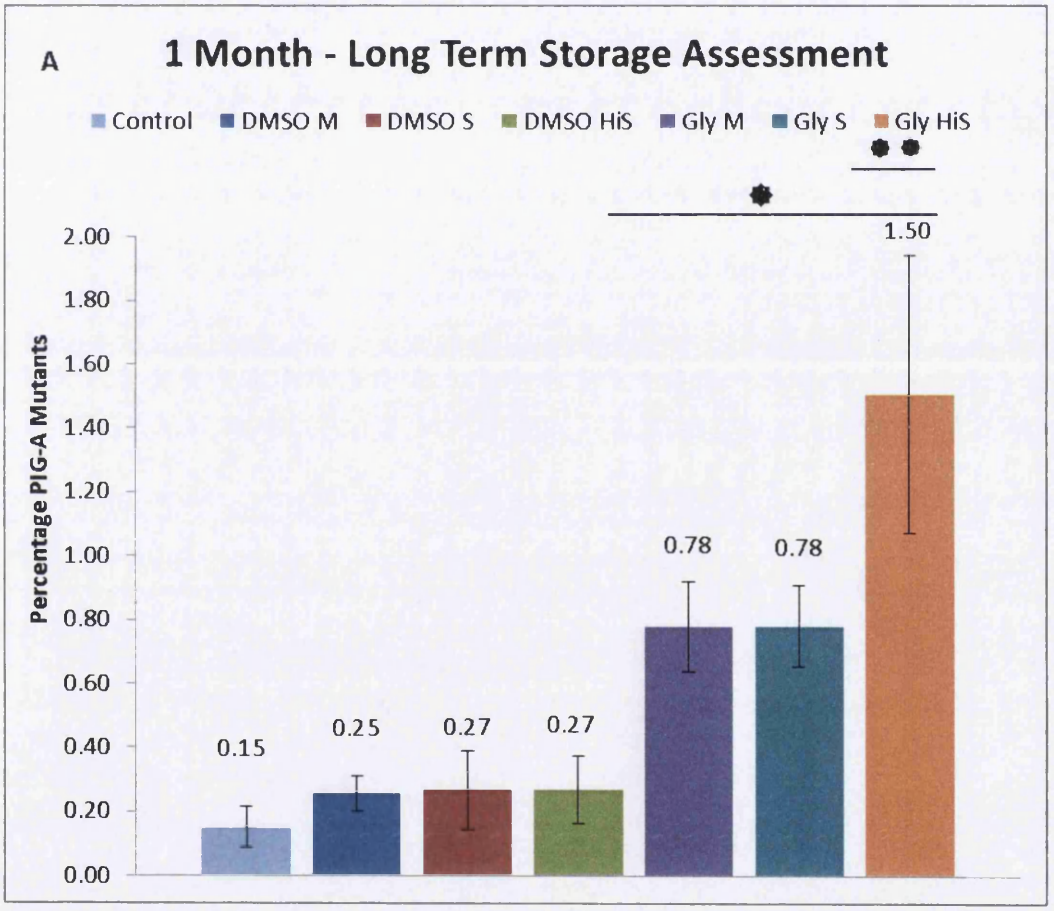

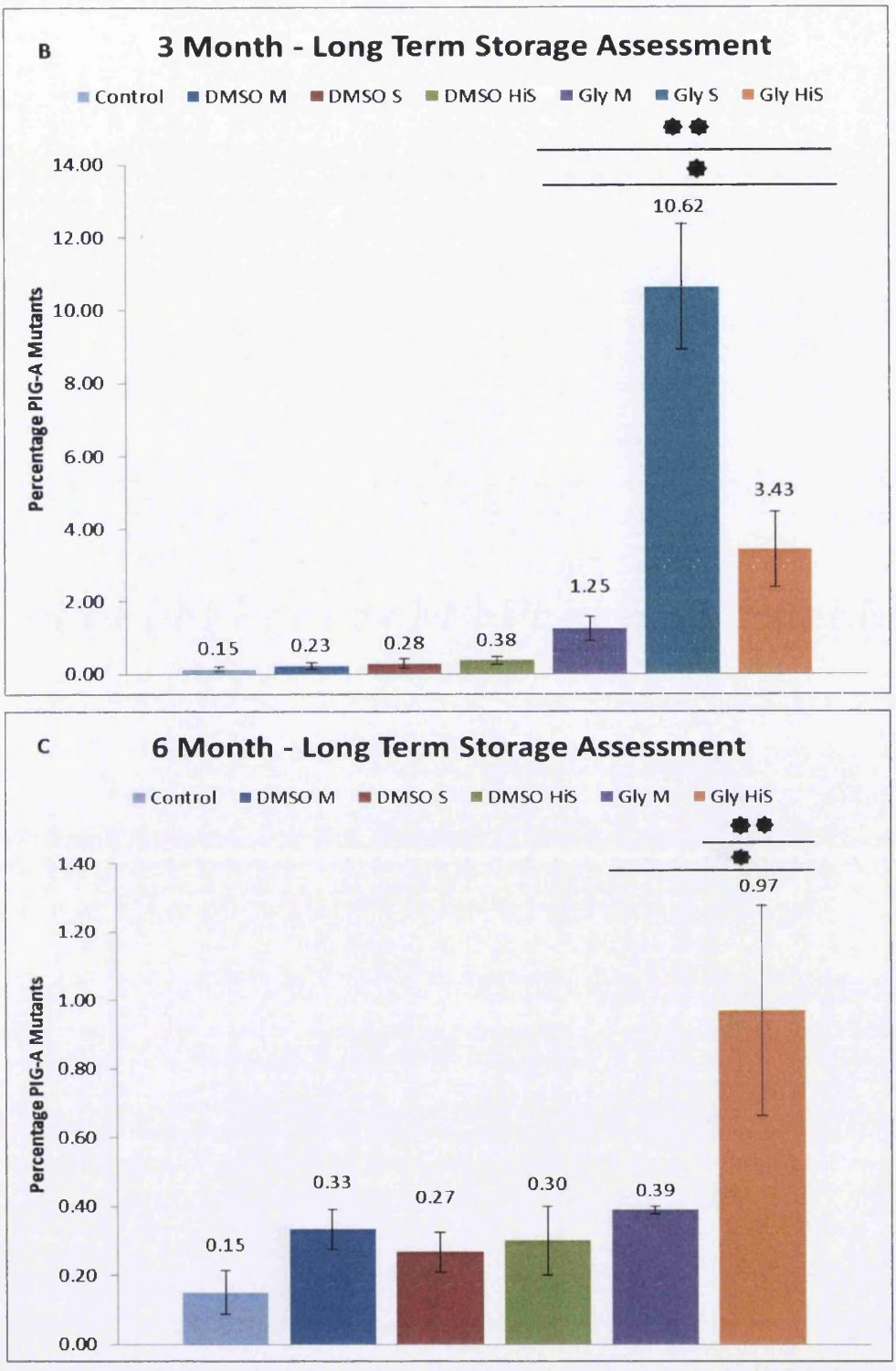

Figure 3.7. 1, 3 and 6 Month flow cytometric analysis of TK6 populations post cryopreservation. Average phenotypic *PIG-A* mutant frequency analysed through the use of the CD59 cellular surface antigen reporter. (Dunn's One-Tailed T-Test ($p < 0.05$*), Dunn's Two-Tailed T-Test ($P < 0.05$**)) (N=3, Error Bars ±1SD) *PIG-A* mutants displayed as percentage of total Single cellular events (0.1% *PIG-A* Mutants = 1 mutant x 10^{-3} cells). DMSO, Dimethyl Sulfoxide; Gly, Glycerol; M, Serum Free Media; S, Serum; HiS, Heat In-activated Serum. Gly-S Data omitted from the 6 Month data set due to poor recovery (Control – unfrozen clonally expanded cells).

3.3.5 Introductory Investigations into Potential Non-viable, *PIG-A* Mutant Mimicking Events

In the endeavour to more accurately define putative phenotypic *PIG-A* mutant events, the following section of work describes advanced FACS Aria I analysis of spontaneous presumptive genotypic *PIG-A* mutant events within un-treated human lymphoblastoid TK6 culture. The inclusion of viability dyes, 7-Aminoactinomycin-D (7-AAD) and Annexin V Alexa Fluor 488 were investigated for their ability to more accurately define the *PIG-A* mutant phenotype during analysis of dose response data. Presumptive phenotypic *PIG-A* mutant events shown to be non-viable will be excluded from future analysis and the effect of this will be evaluated in the context of assay sensitivity.

The use of an instrument calibration standard (ICS) was implicitly required for auto-florescence assessment detection and signal positivity definition across all relevant detectors (Figure 3.8); the resultant regions Q4-4 (*PIG-A* wild type), P2/P4 (apoptosis positive), Q2-2/Q2-3 (necrotic positive) and P3/P5 (loss of membrane integrity) were established. In the context of the *PIG-A* phenotype assessment, the precision of the PE-A gating is critical to accurately defining putative mutant and wild type events; the threshold of positivity is set at the auto-florescence maxima as outlined in (Section 2.8.2).

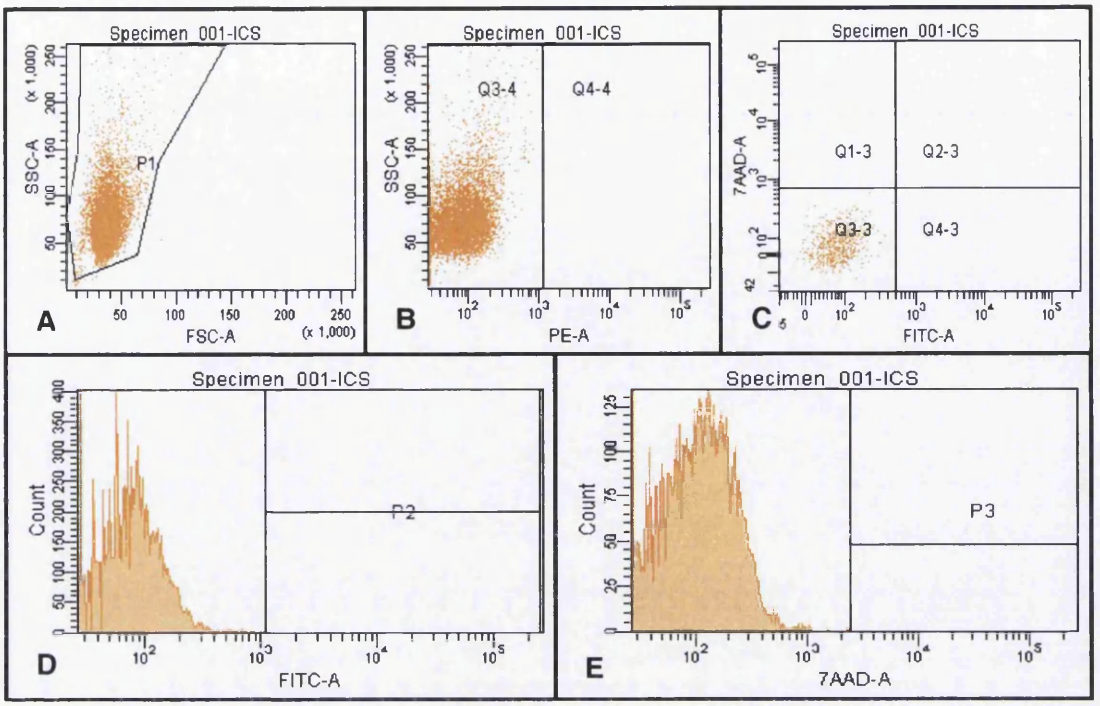

Figure 3.8. Viability Assessment gating strategy for un-stained human TK6 cells (Clonally selected) cultures. A) Initial Crude Single Cell Gate B) *PIG-A* Mutant phenotype Assessment C) Viability Dot Plot D) FITC – channel fluorescence histogram measuring Apoptosis E) 7-AAD – channel fluorescence histogram measuring Loss of Membrane Integrity (Cell Death) (~10,000 Single cellular events).

Following anti-CD59 R-PE antibody treatment, the phenotypic *PIG-A* wild type sub-population was the majority population within the heterogeneous parental population (97.6% cells). This was demonstrated to be viable, with only 10.4 and 2.1% of the population in apoptosis and losing cellular membrane integrity respectively (Figure 3.9).

The phenotypic *PIG-A* mutant defined sub population was much smaller (~2%) when compared to the defined *PIG-A* wild type population and displayed a significant decrease in cellular viability. The frequency of non-viable cells defined positive for both apoptosis and loss of cellular membrane integrity was significantly higher than the comparable wt statistics at 36.4 and 39.2% respectively.

During the extended analysis period, >500,000 single cellular events were collected to investigate potential analysis bias induced with regards to defined putative *PIG-A* mutant phenotype as well as viability (Figure 3.10).

Dramatically increasing the size of the captured TK6 parental population (50 x fold increase) had minimal effects on the population statistics in terms of sub-population composition; phenotypic *PIG-A* mutant frequencies, viability and single cell nature. Defined phenotypic *PIG-A* wild type cells constituted 96.5% of total single cells and displayed respective apoptosis and loss of membrane integrity values of 8.3 and 4.3% respectively, comparable to the equivalent population figures collected within the limited sample size (Figure 3.10). Presumed *PIG-A* phenotypic mutant events displayed 32.9 and 49.5% values for apoptosis and loss of cellular membrane integrity respectively, again mimicking the previous relationship observed within the comparable limited sample size figures (Figure 3.9).

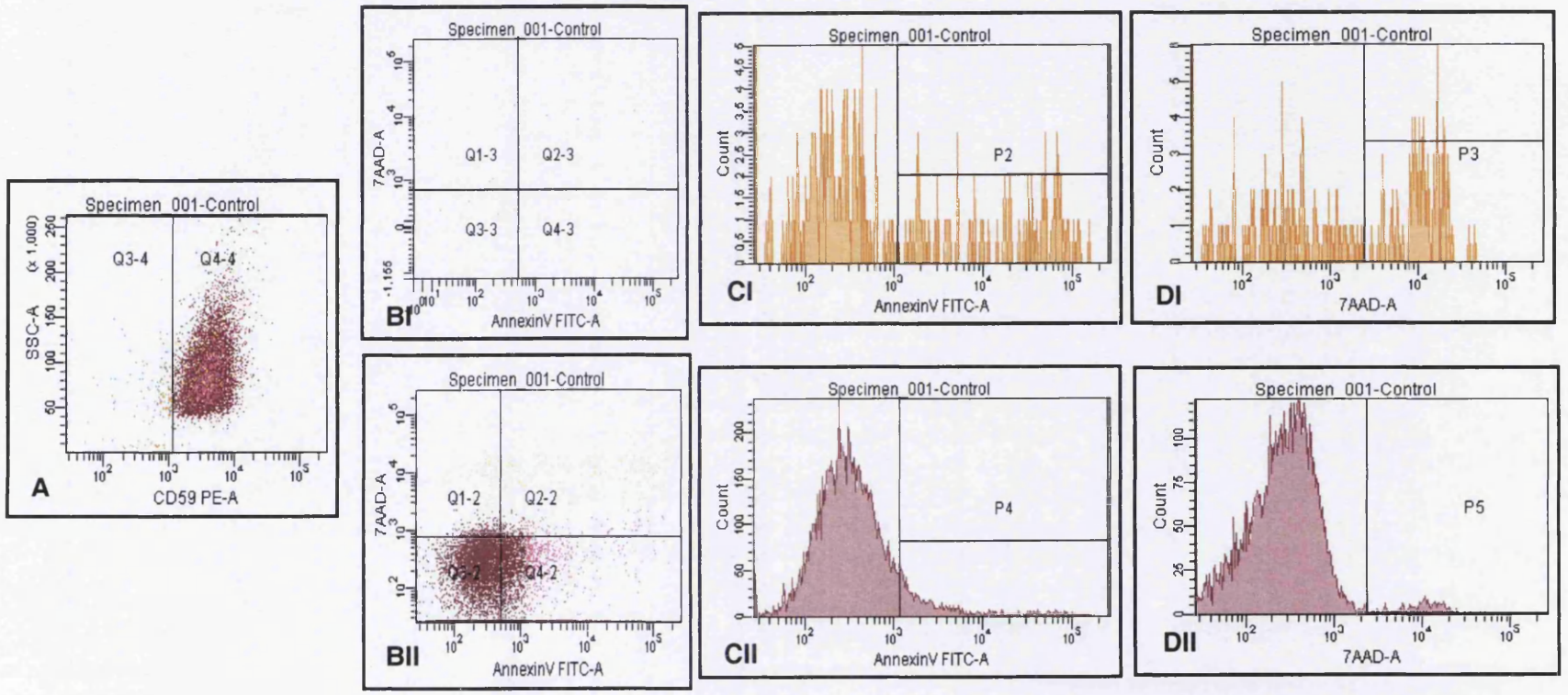

Figure 3.9. Viability Assessment gating strategy for anti-CD59 R-PE stained TK6 cells (Clonally selected) cultures. A) *PIG-A* Mutant phenotype Assessment, BI,II) Viability Dot Plot, CI,II) FITC – channel fluorescence histogram measuring Apoptosis and DI,II) 7-AAD – channel fluorescence histogram measuring Loss of Membrane Integrity (Cell Death) (~10,000 Single cellular events), *PIG-A* mutant phenotype and *PIG-A* wild type cytograms denoted by I and II respectively. P gates defined from maximum auto fluorescence observed following ICS analysis within the respective channel.

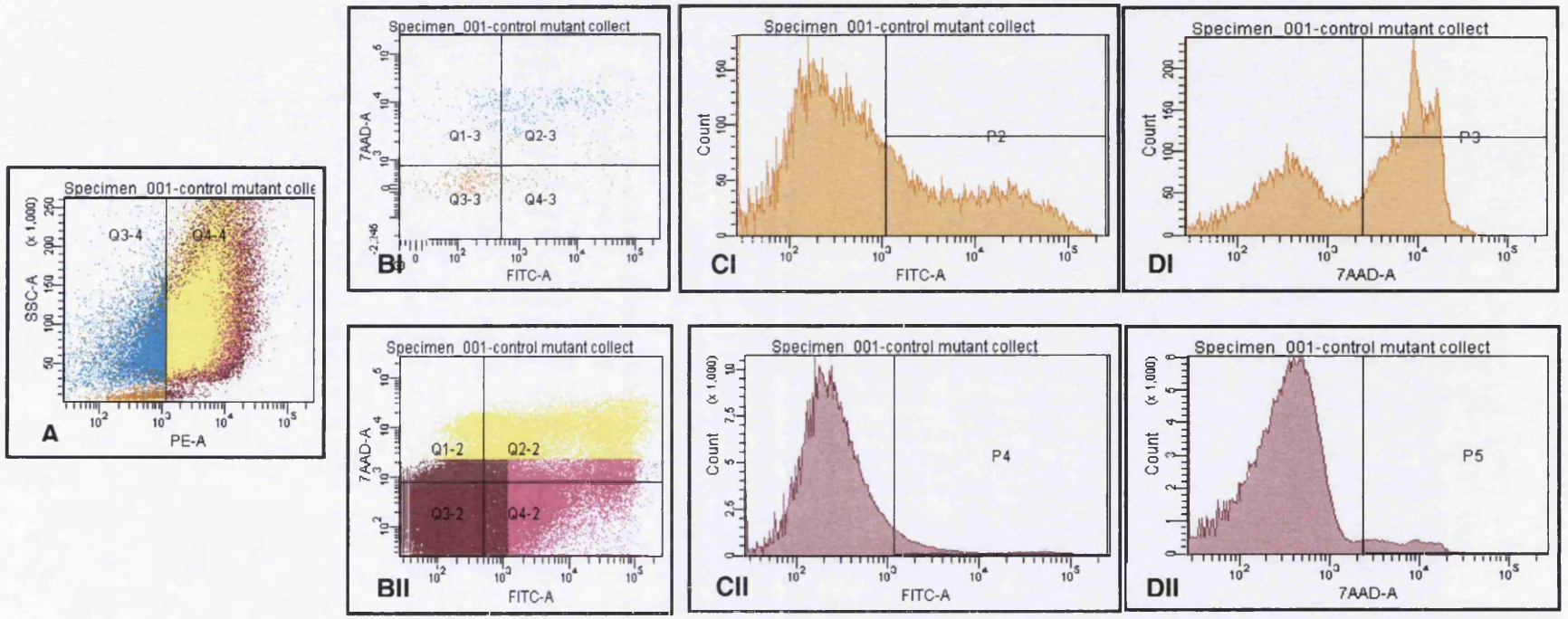

Figure 3.10. Extended Viability Assessment Gating strategy for anti-CD59 R-PE TK6 cells (Clonally selected) cultures. A) *PIG-A* Mutant phenotype Assessment BI,II) Viability Dot Plot CI,II) FITC – channel fluorescence histogram measuring Apoptosis DI,II) 7-AAD – channel fluorescence histogram measuring Loss of Membrane Integrity (Cell Death) (~500,000 Single cellular events), *PIG-A* mutant phenotype and *PIG-A* wild type cytograms denoted by I and II respectively. P gates defined from maximum auto fluorescence observed following ICS analysis within the respective channel.

3.4 Discussions and Conclusions

3.4.1 Antibody Optimisation in Conjunction with Cellular Surface Expression Analysis - Fluorescein Isothiocyanate vs. Phycoerythrin

Flow cytometry is a high throughput, high precision method for mass data acquisition [192]. However, as often is the case with incorporation of modern technology, advancements within technology specific to scientific fields often lead to a lack of standardisation amongst studies [244]. This observation inclines to lead to lack of reproducibility and lowers the integrity of standalone data, until thorough validation and subsequent standardisation of data handling has occurred, due to increasing subjectivity unknowingly introduced through uneducated novel data handling. Recent incorporations of more standardised analysis approaches within flow cytometry, as well as genetic toxicology in general, has led to the quality of publication being increased [245, 246] However, remnants of the subjectivity, even potential bias, within data gating strategies does still remain and can have negative implications, especially when developing a desired reproducible assay. Therefore, in an endeavour to establish a highly reproducible platform, many assay features were investigated with the aim of coordinating an approach to negligate potential sources of subjectivity.

Fluorescence staining of this nature is the fundamental technique that was used within the in vitro *PIG-A* gene mutation assay design, to define and characterise sub-populations within the heterogeneous population; therefore, antibody-antigen binding efficiency is by proxy an essential technique to maintain sensitivity and accuracy within subsequent flow cytometric applications.

Flow cytometers much like antibodies often appear generic and therefore, can be mistakenly utilised within specific application needs. However, numerous explicit features, unique to both flow cytometers (equipment and analysis software) as well as antibodies (specificity and sensitivity) highly influence the sensitivity and utility of the subsequently generated data. The initial antibody-fluorophore trials consisted of two main candidates, an IgG k FITC-conjugated anti-CD59 antibody and an analogous PE-conjugated antibody, their respective intensity post illumination and

specificity when coupled to FACS Aria I analysis were unknown. The preliminary experimental results, following undiluted antibody treatment (Section 3.3.1) to controlled sample sized cultures of TK6 cells, implied there were little differences between the two candidates. However, it was noted that the phycoethryin conjugate antibody was on average much more intense post illumination, within its specific detector, and therefore, was initially favoured for assay incorporation.

Antibody specificity was the next feature under direct investigation, due to the potential confounding factor that non-specific antibody binding could have on the mutation frequency at the *PIG-A* gene locus. Events positive for CD59 antigen status, could in fact be putative *PIG-A* mutant events which have a fluorophore-conjugate antibody attached via an unspecific mechanism. Immune cells, very commonly B-lymphoblast cells, have been demonstrated to have a high number of fragment crystallisable (Fc) receptors on their cell surface [247] which are able to directly interact and hence bind to Fc regions on the IgG molecule thus, inducing a potential for false positivity within the assay design. Additional to this, hydrophobic interactions have also been identified as a potential mechanism for un-specific interaction and an additional potential confounding factor [248]. Both of these characteristics of antibodies have recently been extensively reviewed and demonstrated to be resolved via the use of routine fixation, approaches heavily utilised within immunohistochemistry applications [249]. However, in order to enable live cell analysis, a technique vital to maintain the cells in a state best representative of their natural conditions, the ability of endogenous Fc receptors to bind in an unspecific manor was assessed with the use of isotype controls in the absence and presence of Fc block reagent. Fc block reagent is designed specifically to block the non-specific FcR-mediated Ig-Fc binding in human samples during flow cytometric analysis [250].

When compared to isotype controls, both antibodies again produce highly comparable data in terms of un-specific binding; the FITC-conjugate isotype antibody demonstrated a lower percentage of total non-specific binding when compared to the PE-conjugate isotype control. The data suggests that the FITC antibody is more specific than the comparable PE antibody (Section 3.3.1), however, the PE antibody has lower FcR mediated interactions. The lymphoblastoid nature of

the cell line, as well as human primary samples, intended on being used within the assay biases the decision of antibody candidate towards the PE antibody.

Antibody conjugates destined for research based immunofluorescence applications are more expensive than their un-conjugated, purified counterparts [221] and therefore, when designing a novel high content assay system, assay practically and costly overheads must be taken into account. In an attempt to minimise costs, each antibody candidate was investigated for potential antibody titration whilst retaining assay sensitivity and integrity. The resultant data suggests that a single dilution (0.5X) for both antibody candidates did not significantly decreases the average antibody intensity observed. However, additional dilutions resulted in diminishing returns in sensitivity as well as signal resolution and subsequent population identification. Therefore, to maintain the optimum sensitivity undiluted antibody was favoured for assay design.

The undiluted Phycoerythrin conjugated antibody solution was chosen as the working concentration of antibody to be incorporated into the in vitro *PIG-A* assay system. Predominantly, both antibody candidates were very comparable, however, even though the FITC conjugate antibody demonstrated to be marginally more specific, in the context of the lymphoblastoid based *PIG-A* assay, this was deemed insignificant. The major advantage of the PE-conjugate was the significant increase in average fluorescence intensity, as well as the more directly proportional nature of the antibody binding metrics (Section 3.3.1). The reason for the increase in fluorescence when directly comparing the two antibodies is the actual structure of the antibody-conjugate molecules. Fluorescein isothiocyanate (FITC) has a high quantum yield, efficiency of energy transfer from absorption to emission fluorescence, however only 3-5 molecules on average are present following conjugation. When comparing this to R-phyocoerythrin (PE), a photosynthetic pigment found in red alga, 34 phycoerythrobilin fluorochromes are present per molecule, making it a brighter, ideal pigment for flow cytometric applications [251].

Providing a tool to remove ambiguity within sub-population definition was believed to be more important in the context of the sensitivity of the mutagenicity assay, this can be easily seen within (Section 3.3.1), than a negligible potential increase in false negativity within subsequent data analysis. Due to the minimal level of un-specific

antibody binding observed with BD-Bioscience manufactured primary antibodies, the use of isotype controls was believed to be un-necessary for future analogous applications.

3.4.2 Enrichment Strategies to Optimise CD59 Expression with the Human Lymphoblastoid TK6 Cell Line

Spontaneous background mutant frequency is the occurrence of pre-existing mutant events, within a gene mutation assay system, prior to chemical exposure. Assay sensitivity is inversely proportional to the spontaneous background mutant frequency [252], therefore, the inclusion of a pre-enrichment or comparable mutant depletion step is often observed within most validated in vitro gene mutation assays [71, 75]. The spontaneous background mutant frequency in-directly defines the number of induced mutational events required in order for a chemical dose to be classified as statistically mutagenic; therefore, utilising such media as HAT, for the *HPRT/TK* assays, actively removes pre-existing mutants and increases sensitivity.

With the potential change in dogma with regards to data analysis, in vivo restrictions and modelling, even greater pressure is placed upon the sensitivity of an assay system [28, 85, 212]. Programmes such as PROAST calculate their dose response matrices with greater emphasis on assay sensitivity, moving away from the more traditional NOGEL approach [213]. Therefore, the following section endeavours to compare and contrast mutant depletion methodology for inclusion within this preliminary in vitro *PIG-A* assay design

Dynabead ™ enrichment was shown to generate variable capture efficiency between homologous samples and hence the resultant CD59 enrichment showed approximately a 10% yield difference (Figure 3.4). The maximum TK6 CD59 enrichment achieved was in the region of 95% and therefore, an estimated spontaneous background mutant frequency of 50,000 x 10^{-6} cells scored was calculated. Paramagnetic positive cell enrichment is a fundamental method used within many aspects of cell biology [168, 253, 254], however, even though the

principles may be rudimentary the actual DSB-X - Dynabead ™ concept relies on a number of cellular interactions, antibody conjugations and magnetic enrichment steps (diminishing returns) which are potential sources of error and hence, reduce the overall process efficiency when compared to the other two methodologies. Dynabead ™ kits are developed with intended use of proteins with relatively large molecular weights and therefore, the limited size, ~20 kDa of the CD59 protein maybe retarding the enrichment process. Based on the current efficiency of enrichment and no additional immediate methods for optimisation, Dynabead™ enrichment was deemed inappropriate for this assay design, however, would be highly cost effective.

FACS is a routinely utilised technique within microbiological research as well as clinical medicine [255, 256]. FACS theoretically has the accuracy to isolate and capture a single cellular event identified during real-time sample analysis. In order to avoid the potential limitations induced following clonal growth expansion, a pooled sample approach was initially accepted in which thousands of CD59 defined positive homogenous cellular events were collected within a single sample tube and subsequently assessed for overall CD59 surface expression. FACS yielded highly consistent results, with a comparable maximum enrichment of 96% recorded (Table 3.5). However, the CD59 expression of recovered samples was directly proportional to the viability of the cells post sorting. Operator ability and experience in ensuring optimal cellular viability played a critical role in the effectiveness of this technique. Due to the relative high operator skill required, potentially FACS would only have limited usage within such an assay design; more modern FACS machines are more user friendly and stable, generating a more suitable platform and increasing reproducibility and robustness.

Clonal expansion methodologies are prevalent within current in vitro gene mutation assays, as seen previously within HPRT/TK (MLA) colony scoring [70, 186], however, as a method for wild type enrichment/mutant depletion this would appear to be novel within the field. Again, this method resulted in a high degree of variation between colonies, an approximate 70% difference in surface antigen expression. Nevertheless, the technique generated highly effective enrichment for the CD59 antigen with recorded maxima of 99.8% (Figure 3.4), greater than the comparable Dynabead ® and FACS methods, establishing an estimated spontaneous mutant frequency of 2,000 $x10^{-6}$ cells scored. TK6 cells lend themselves well to clonal

expansion as a method for mutant depletion due to the primarily CD59 positive subpopulation within the heterogeneous parental stock culture. However, as this technique requires growth from a single cell into a large enough colony to facilitate flow analysis and subsequent cryo-preservation, the additional elongated growth period can induce phenotypes characteristic of cellular distress [257]. Induced deleterious increases in genomic instability as a direct result of cellular distress and aging have the effect of increasing mutant frequency and hence, indirectly decreasing assay sensitivity and robustness.

The enrichment technique which offers most of the beneficial features required within a modern in vitro gene mutation assay would be FACS; high throughput, high precision and extensive reproducibility without additional overhead expenses [235, 255]. However, FACS is a highly skill dependent technique requiring experience, as well as significant knowledge in sample preparation pre and post sorting [237]. Insufficient maintenance, leading to vastly variable performance, limits usage within the current assay design (Figure 3.5). However, the selected method for future assay design will be clonal expansion, based on the optimal CD59 surface antigen enrichment, 99.8 % (Figure 3.4) being significantly greater than the achieved FACS yields. Additional investigations into alternative methods for mutant depletion will continue, specifically FACS optimisation, to achieve higher assay sensitivity and consequently moving away from the known limitations associated with clonal expansion and extended cell culture.

3.4.3 Proof of Principle *PIG-A* Assessment of TK6 cells Following 24 hr low dose Ethyl-methanesulfonate (EMS) Exposure

Following the establishment of a basic in vitro assay design within a human lymphoblastoid cellular platform (Section 2.10), coupled with a clonal expansion mutant depletion step (Section 3.2.2.2) the assay required initial validation in order to assess the direction of further progress and to critically analyse current performance to aid future assay refinement. Ethyl Methane Sulfonate was chosen for

the initial assay due to the wealth of dose response data utilising validated comparable in vitro gene mutation assays [31, 33, 211].

The first three days of analysis generated largely expected data (Section 3.3..3); relative cellular viability of the population dramatically decreased at the higher doses, following model mutagen exposure, allowing for cytostasis and recovery post-treatment. However, no significant change in *PIG-A* mutant frequency was detected (Figure 3.5), when compared to control values. The proposed reason for the initial decrease in viability is that following high dose exposure, a large proportion of the cells begin to undergo DNA damage and therefore, depending upon a number of biological factors, p53 status etc., are halted within the cell cycle and subsequently either begin to undergo recovery or alternatively controlled cellular death (apoptosis) [258]. Both mechanisms have a common lag period, comparable to cytostasis, in which no extracellular phenotypic variation occurs [259]. When measuring population cell number, techniques solely utilising cellular size descriptors, such as the Coulter Principle [260], can be misleading as their data is strictly limited to counting particle size. Such measures are unable to correctly identify intracellular or surface membrane alterations indicating loss of viability and therefore, can be miss-representative of the overall condition of the population. More advanced methodologies such as Vi Cell Series ™ (Beckman Coulter, High Wycombe, UK) as well as integrated flow cytometric viability dye assessment, coupled with counting beads [261], could generate much more accurate cellular viability data which more accurately describes the population.

The proposed reason for the lack of observed variation in *PIG-A* mutant frequency is based on the idea of mutation fixing as well as phenotypic lag. Assay platform, choice of cell line etc., defines a unique time period in which mutagenesis is unrepresented and therefore, extended assessment of mutagenesis is required prior to standard operating procedure (SOP) drafting. Mutation fixing is generally referred to as the amount of time or number of DNA replications in order to facilitate a mutational event, for example, the incorporation of the mismatched base within the corresponding DNA strand following an adduct induced point mutation; until DNA replication occurs the adducted base has no influence [30]. Phenotypic lag, in the context of the *PIG-A* assay, is the period of time in which no measurable phenotypic change will occur following a fundamental genotypic alteration. This is best

illustrated by the following example, suppose that a frame shift mutation within the promoter of a constituently expressed gene prevents transcription. However, prior to mutation, that specific gene product is present in abundance within the cytoplasm, as well as residual functional mRNA available for limited translation. Therefore, for a finite number of generations the cells would continue to have functional proteins within the cytoplasm in sufficient quantities to preclude loss of function [262]. Assessing both the mutation fixing period as well as the phenotypic lag, the in vitro *PIG-A* assay appears to be insensitive to mutation until 72 hr post mutagenic exposure (Figure 3.5), inclusion of more accurate viability measure or cell cycle analysis may give an indication of DNA damage at an earlier time point [189].

For the purpose of initially assessing mutagenesis, four consecutive *PIG-A* daily analyses were undertaken to account for potential mutant lag as well as wild type phenotype stability evaluation. 96 hr post mutagenic exposure, EMS generated a significant increase in the *PIG-A* mutant frequency (Figure 3.5) and the BMD_{10} metric was comparable to that modelled at the *HPRT* endpoint in lymphoblastoid cell line following EMS exposure [39, 263]. The day 4 *PIG-A* data, as well as day 1, were not normally distributed, however, a LOAEL was defined using Dunn's but this was nearly 10 fold higher than the comparable statistic defined within AHH-1 cells with the *HPRT* endpoint [39]. Limitations within the dosing regimen must be taken into account and a more accurate statement would be the LOAEL was >5 µg/mL. The assay appears to lack sensitivity at the lower doses, even though additional investigation will be required due to discrepancies between the cell lines, a critical flaw when considering the strengths of the comparable currently validated assays [87, 202, 218].

The current assay background, i.e. spontaneous mutant frequency at the *PIG-A* gene locus, was 0.117% on Day 4 (Figure 3.5) which extrapolates into the detection of approximately 1,170 mutagenic events per 1 x 10^6 events scored (only 10,000 events captured within analysis). Current validated mutation assays, *HPRT* for comparison, have an average background of 1-50 mutational events per 1 x 10^6 events scored [264] and as such are greatly more sensitive as X-linked reporter systems due to requiring lower increments in mutant induction to define statistical significance [75]. Therefore, assuming all X-linked genes have an approximate homogenous spontaneous mutant frequency, disregarding minor variation due to location and

length, there is potential for subpopulations of events within the assay being incorrectly labelled as *PIG-A* mutants which do not actually contain a genotypic alteration within the *PIG-A* gene. The human GPI synthesis pathway consists of upwards of 20 human genes [265] and therefore, even though unlikely, due to the autosomal nature of the genes involved, excluding *PIG-A*, potentially any of these genes could induce a mutant mimicking event if down regulated. This phenomenon was demonstrated recently with a *PIG-T* mutation inducing the human PNH disease phenotype [146]. Alternatively, there are a number of additional potential causes of an observed elevated spontaneous mutant frequency; ineffective mutant purging within the wild type enrichment methodology, non-viable cells mimicking *PIG-A* mutant events, antibody marker binding efficiency or loss of marker conjugation and clonal expansion of pre-existing *PIG-A* mutants. Each of the listed potential sources of error will be investigated in more detail within subsequent sections.

3.4.4 Long-Term Cryo-preservation Assessment on CD59 Phenotype Stability

In order to facilitate potential validation of the proposed in vitro *PIG-A* gene mutation assay design, the assay platform in this case pre-enriched TK6 cell culture, will need to be distributed amongst a number of genetic toxicology laboratories [166, 167, 176]. Therefore, due to the variance observed within the yields of CD59 antigen expressing TK6 cells, following mutant depletion (Appendix Section 3.3.4, Table 3.1), one potential solution would be the distribution of a pre-enriched cell line as the supplied platform. To enable the established distribution of the bespoke cell line, cryopreservation will need to be applied; however, initial investigations into the effect said cryopreservation has on the *PIG-A* phenotype will need to be evaluated prior to distribution. For this to be an appropriate solution, the preservation and subsequent awakening process cannot be demonstrated to increase the spontaneous background mutant frequency, to a point which would facilitate the need for an additional mutant depletion step. Additional preparative stages would increase the likelihood of genetic variation amongst testing populations as well as introducing a key element of variance within ensuing data analysis.

The results of the long term storage assessment revealed that the routinely used cryopreservant DMSO generated the most reproducible results in terms of *PIG-A* mutant frequencies, with respect to stability over time, when compared to glycerol as well as 10% sucrose (Section 3.3.4). Glycerol another well-known cryopreservant [266] was shown not be a viable candidate when used in conjunction with TK6 cell lines; *PIG-A* mutant frequencies were observed to rise significantly as well as distinct decrease in cellular viability over time. Sucrose, often a key constituent when freeze drying bacterial cell cultures to preserve extracellular function [266], was observed to induce unprecedented levels of cytotoxicity (Appendix Section 3.3.4, Table 3.2). This strictly deleterious effect was thought to be a direct result of the change in osmotic potential and the consequential decrease in turgor within the system [267]. Bacterial cells, either gram positive or gram-negative, have distinct cell wall structures governed by their peptidoglycan constitution which enables cellular resilience to changes in osmotic potential due to the exerted constraining force. Cellular integrity is further maintained through the interplay between the peptidoglycan cell wall and mechanosensitive (MS) channels that modulate turgor [268]. Animal cells, dissimilar from bacterial or plant cells, lack a cell wall structure surrounding the cellular membrane and therefore, are less able to tolerate hypertonic conditions; specific intracellular solute concentrations rise following an efflux of water from the cell via osmosis resulting in plasmolysis, cell shrinkage and eventual cell death [269]. Both increases and decreases within osmotic potential can exert fatal effects on animal cells, often associated with the movement of K^+ ions triggering apoptosis [270]. However, even minor alterations within the microenvironment can induce cellular stress resulting in reduced viability within the cellular population following recovery after cryopreservation [271]; this can potentially result in an increased presence of *PIG-A* mutant mimicking events and hence, decrease assay sensitivity.

The results of this investigation into cellular storage show that long term liquid nitrogen preservation of pre-enriched TK6 cultures is a viable mechanism for mass distribution of cell stocks. However, one caveat which must be considered is the minor increase in putative *PIG-A* mutant frequencies (Figure 3.7) following reawakening, as well as the corresponding decrease in cellular viability (recovery) (Appendix Section 3.3.4, Table 3.2) following the period of storage. Liquid nitrogen

cryopreservation, if undertaken correctly, is known to have limited deleterious effects on viability, nevertheless still potentially inducing minor increments in spontaneous *PIG-A* mutant frequency and hence desensitising the assay. Further investigation into the mechanisms of presumptive mutant generation will need to be assessed to more accurately define the potential sensitivity issues as well as solutions to exclude such a putative population from subsequent analysis.

3.4.5 Introductory Investigations into Potential Non-viable, *PIG-A* Mutant Mimicking Events

Previous sections within this chapter, have described a number of possible problems attributed to the preliminary assay design which could be responsible for the lack of observed sensitivity (Sections 3.3.1 – 3.3.4). Features included; potential inaccuracies within the reporter mechanism, immunofluorescence staining inefficiencies, caveats associated with use of immortalised cell lines, questionable viability correlation, robustness and variation concerns. Initial investigations have suggested that the frequencies of observed GPI-AP negative events do not correspond to the estimated biologically defined spontaneous mutant frequency values within human granulocytes [175] and hence, the observed induction of *PIG-A* mutant post mutagenic treatment does not liken to currently validated assays [75]; even though the data is not directly comparable, similarities would be expected to be observed.

Currently, as there is no evidence, in vivo, to suggest either a positive or negative growth bias within the *Pig-a* mutant sub-population [147]. The current assay design would be expected to capture a proportional representation of the clonally expanding induced mutant sub-population. The clonal characteristic of the assay post mutagenic treatment, offers the beneficial advantage of modest detection of mutants at low levels following induced mutagenesis. However, the limited experimental period in combination with assay design was implemented to prevent bias during scoring of putative *PIG-A* mutant events. Therefore, the validity of the early onset presence of

un-expected high numbers of observed putative mutant events is further questioned (Section 3.3.3).

Viability of presumptive mutants was assessed utilising two commercial methods; 7-aminoactinomycin-D, a fluorescent intercalating agent which under goes a spectral, stokes, shift following association with DNA. 7-AAD is excluded from live cells, and therefore, can be utilised as an indicator of cellular membrane integrity as well as having limited application as a cell cycle indicating tool [272]. Annexin V Alexa Fluor 488, a calcium (Ca^{2+}) dependent phospholipid-binding protein that has high affinity for phosphatidyl serine (PS) and therefore, once conjugated to a fluorophore, in this case an Alexa Fluor 488 ™ is a sensitive tool for apoptosis detection and quantification [273]. Apoptosis is distinguishable by a number of characteristic morphological changes, including compaction and fragmentation of the nuclear chromatin, shrinkage of the cytoplasm and loss of membrane asymmetry [274]. In living cells, phosphatidyl serine (PS) is located on the inner surface of the plasma membrane and therefore, cannot be targeting by annexin V molecules. However, during apoptosis, PS is trans-located onto the outer surface of the cellular membrane, via micro-membrane inversions, thus exposing the PS to the external environment. Within leukocyte populations, PS is a recognised marker of apoptosis and is associated to phagocytosis inducing by macrophage molecules [275].

The results demonstrated that the levels of non-viable cells within the two isolated sub populations were fundamentally different. Apoptosis as well as cell death, loss of membrane integrity, were significantly higher within the assumed *PIG-A* mutant population than the equivalent wild type populations. During apoptosis the cell membrane has been observed to lose symmetry [276] and therefore, during this disorganised fluid-like phase potentially the lipid raft rich areas of GPI-associated proteins may lose their position upon the outer cellular membrane, causing in-effective antibody association and hence, false *PIG-A* mutant status. Therefore, due to the observed increase in cytotoxicity within the presumed *PIG-A* mutant subpopulation, when compared to the homologous wild type population, both apoptosis as well as loss of cellular membrane integrity cannot be disregarded as potential mechanisms for the generation of subsequent false positive mutant event identification. Apoptosis levels still remained elevated for significant periods of time

following the typical 30 minute window of identification utilising cell lines of this type.

With the intention of removing such ambiguity, within the resultant *PIG-A* mutation data, viability dye inclusion will be an additional feature in future versions of the in vitro *PIG-A* mutation assay. This development within the assay design potentially could increase assay sensitivity significantly, via the removal of ~ 20-50% of non-viable presumed *PIG-A* mutant events, and subsequently greatly decreasing the spontaneous background mutant frequency.

The aim of this chapter was to endeavour to draft a preliminary standard operating procedure (SOP), following the identification of a realistic dose response, for a quantitative in vitro *PIG-A* gene mutation assay, comparable to currently validated mammalian cell genetic toxicology assays [75, 127, 200]. Initially, human lymphoblastoid TK6 cells were chosen as the cellular platform for the *PIG-A* assay, coupling this with phycoerythrin-conjugate CD59 antibodies, demonstrated to generate the most specific (non-Fc mediated interaction) and bright fluorescence signal post treatment, established a rudimental assay design (Section 2.10). With the intention of decreasing spontaneous mutant frequency, in line with comparable mammalian cell mutation assays, clonal expansion was deemed the most appropriate method for wild type enrichment (Section 3.3.2.2). This basic assay design was initially tested against acute 24 hr model mutagenic exposure in which EMS was demonstrated to induce a significant ($P<0.05$) increase in putative *PIG-A* mutant events on day 4 (96 hr) of analysis (Section 3.3.3). However, the assay was observed to be less sensitive than previously predicted and additional techniques (Amnis Image Stream ™) were investigated in order to validate current findings, review potential limitations as well as potential assay transferability away from strict flow cytometric analysis (Appendix Sections 3.5.3.1 – 3.5.3.3). Further investigations into the presumptive *PIG-A* mutant events alluded to poor viability within the subpopulation and additional phenotypic markers were introduced into the assay design, facilitating high content analysis (Section 3.3.4). Following implementation of enhancements to the assay design, the latest version of this in vitro *PIG-A* gene mutation assay was ready to undergo further investigations into potential quantitative dose response modelling.

Table 3.6. Summary of the data described within the chapter contents, the results and the conclusions drawn in relation to the advance of the in vitro PIG-A gene mutation assay standard operating procedure (SOP)

Theoretical in vitro *PIG-A* assay design		
Detailed Literature Review	Preliminary Investigative Experiments	→ **Initial SOP drafting (TK6)**
BD FACS Aria 1 – Flow Cytometry Assessment		
Antibody Assessment	Specificity	↓
	Molecular Fluorescent Intensity	
	Emission Signal Resolution	→ **Anti CD59 PE candidate Antibody Selected**
Enrichment Strategy Optimisation	DSB-X Biotinylation and Dynabead®	↓
	Clonal Expansion	
	FACS	→ **Clonal Expansion Selected**
Proof of Principle Evaluation	TK6, CD59, Acute 24 hr EMS	→ **Qualitative Dose Response (LOAEL 10µg/mL)**
Long Term Cryopreservation Study	DMSO, Glycerol, Sucrose	↓
	1, 3 and 6 month assessment	→ **DMSO cocktail proven most stable with regards to phenotypic *PIG-A* status over extended periods of cryopreservation**
Preliminary Viability Assessment	7-AAD and Annexin V	↓
	Apoptosis, Necrosis and Membrane Integrity	→ **Significant presence of non-viable cells within presumptive phenotypic mutant *PIG-A* cells**

Table 3.7. Summary of the additional supplementary data for this chapter, contained within the appendix, which details the validation and additional investigative experimentation surrounding the assay development.

Amnis Image Stream ™ – Cytometry Assessment – Supplementary Data

Image Stream ™ Investigation	Evaluation of technology as *PIG-A* assay platform	**Platform lacked sensitivity, validated phenotype**
Antigen Conjugate Integrity Assessment	Effects Fixation had on antibody conjugate strength	**Fixation improved assay robustness, prevented the loss of phenotypic markers during preparation**
Cellular Morphology Analysis	Fixations effects on cellular area and imaging	**Specific fixation demonstrated to standardise cell shape/size and increased image resolution**

Chapter 4: Consideration of Cell Lines in the Further Development of an in vitro *PIG-A* Gene Mutation Assay

4.1 Introduction

In the previous chapter, the preliminary experimentation established a basic in vitro *PIG-A* gene mutation assay design. The human lymphoblastoid TK6 cell line was used in combination with the reporting CD59 cellular surface marker, analogous to the in vivo *Pig-a* gene mutation assay, followed by flow cytometric high content, high-throughput and high-precision analysis. However, due to the varied level of CD59 expression within the parental TK6 cultures, a physical mutant depletion or wild type enrichment strategy was shown to be essential. In order to reduce pre-existing spontaneous background phenotypic mutant frequencies at the *PIG-A* gene locus enrichment optimisation was undertaken, and the resultant data demonstrated a sensitivity level suitable for qualitative dose response assessment (Section 3.3.2). However, further development and refinement is required prior to quantitative assessment, as initially predicted.

The initial proof of principle experiments demonstrated an increase in *PIG-A* mutant frequency in TK6 cells, following model mutagen exposure (Section 3.3.3). However, assay sensitivity was shown to be lacking as indicated by the dose response metrics, NOGEL (5µg/mL) and LOGEL (10µg/mL), being significantly higher than comparable data generated using a currently validated in vitro gene mutation assay [39]. The finalised background at the *PIG-A* gene locus was established in the region of 0.1-0.2% presumptive phenotypic mutants, which was significantly higher (10-20 fold) than the *TK* and/or *HPRT* gene mutation assays [39, 75, 264].

Continued review of the preliminary proof of principle experiments lead to further investigation into the identity and origins of presumptive *PIG-A* mutant events. In addition to the potential limitations associated with inefficient mutant purging, within the enrichment methodology, potential alternative mechanisms other than mutagenesis were identified (Section 3.3.5). Flow cytometric investigation,

following immunofluorescence staining, for characteristic markers of apoptosis, necrosis and loss of membrane integrity demonstrated a significant sub-population of non-viable cells within the presumptive *PIG-A* mutant population (Section 3.3.5). Therefore, the aim of the following results chapter is to i) further explore assay sensitivity issues, ii) provide initial validation of cell line selection, iii) further mechanistic evaluation and iv) exploration into high content screening.

4.1.1 Selecting a Cell Line for use in Genetic Toxicology Applications

Genetic toxicology data are routinely used worldwide in regulatory decision making [220], such decision making is often undertaken by large agencies such as the Food and Drug Administration (FDA) or Environmental Protect Agency (EPA) and can be subdivided into two main categories i) the approval and restrictions of pharmaceuticals medical devices and medical use products (including cosmetics) and ii) the setting of standards for acceptable exposure levels in water, air and food (including pesticides etc.) [277]. Genetic toxicology data are used extensively in the hazard identification stage for both of these regulatory decisions and therefore, have a pronounced bearing on the outcome of said decisions.

However, advancements within understanding as well as modernisations within the field of genetic toxicology [212, 219, 263, 278] have begun to reform the methods in which genetic toxicology data are collected. As a direct result of these changes, regulatory guidance, which is utilised to provide direction and standardisation within the field, is also implementing reform to address how much confidence can be attributed to this data. For example, a modern weight of evidence (WOE) approach is currently being implemented within regulatory decision making to optimise usage of genetic toxicology data within risk assessment decision making and potential human health risk assessment [263, 277]. As a direct result of advancements within the field, increasing pressure is now being attributed to gene tox assay design to ensure that the resultant data is not only complete, but offers extensive contextual depth and biological relevance [100, 187, 278]. Novel reforms are becoming more apparent with increasing amount of publications critically reviewing current gene tox data

[112] and providing advice on limitations as well as re-direction within the field away from certain assay types [210]. A specific example of this would be recent publications summarising the currently available cell lines for use within genetic toxicology testing and their respective beneficial characteristics and/or limitations [113, 114, 210].

Genetic toxicology testing, in the context of safety assessment, is limited by the cell type (platform) in which the test is under taken. The platform in which the system operates provides the specific characteristics which the test system utilises in order to define risk and hazard; as a direct result of this many criticisms of test systems fall under the initial choice of tissue, cell line or host [208].Traditionally a substantial amount of genetic toxicology data was generated using validated relatively high throughput, in vivo rodent gene tox assays often supplemented by inexpensive, often based on prokaryotic or rodent platforms, in vitro assays [67, 75, 102, 186, 202]. More recently, the latter test systems have been reviewed and shown to demonstrate high levels of false positivity and questionable human relevance within subsequent generated data [105, 112, 210]. Therefore, individually systems offer limited benefits outside of uncompromising sensitivity when reviewed in the context of regulatory decision based on a weight of evidence approach; however, still effective at hazard identification. As a consequence of this, certain assays have faded out of routine use and replaced by more appropriate, high throughput analogous human assay systems [279].

Even though the shift away from rodent based to standardised human cell line assay systems has removed specificity issues [115], the sheer genotypic variance demonstrated within the cell lines, even directly related cell lines, is somewhat imposing [75, 124, 127, 201]. However, governmental reforms and initiatives to further reduce animal testing within the pharmaceutical industry [85, 86, 203], as well as the potential insensitivity to detect genotoxic human carcinogens (~60% of total carcinogens) within pre-existing assay systems, has led to further refinement of supplementary testing; in vitro human as well as novel alternative test systems have received increasing weight [87, 90, 94, 208]. Human immortalised cell lines as an assay platform have a number of caveats associated with routine use [105, 112, 210], however, when used in tandem or as part of a hierarchy or test barrage [72, 73] the

resulting conclusions are effective and are an attractive test barrage representative of risk [112, 184].

Variance is an essential characteristic within cell lines routinely utilised in genetic toxicology due to the sheer diversity of applications which are explored within the field. No single cell line best represents the complexity and diversity observed within the human body. Therefore, to account for such natural variety as well as exposure mechanisms, a great assortment of representative cell lines, each with specific characteristics and traits, must be assayed [34, 73, 87, 89, 93, 94, 104, 108, 150] in order to identify those fit for purpose for use within a plethora of varying end point assay systems. However, this observation makes assessing data much more complex as regulators strive to quantify potential risk based on data collected from a plethora of assay systems.

Entirely preventing human exposure to harmful chemicals as well as having a single test system defining said risk is un-realistic. Therefore, in order to help facilitate a weight of evidence approach to regulatory decision making, increasing attention is being placed on explaining statistical analysis that enables derivation of comparable PoD metrics [100, 216]. Combining a potential quantitative metric for risk with more accuracy and confidence in in-vitro to in vivo data extrapolation, could provide the frame work for reformed human health risk assessment [88, 226].

4.1.2 Routinely used Human Lymphoblastoid Cell Lines within Genetic Toxicology

Human lymphoblastoid cell lines feature heavily within many validated genetic toxicology test systems [124, 126] and often share a number of perceived favourable characteristics; short cell cycle times, suspension growth dynamics and well-representative of human tissue [113] However, even though morphologically similar, some sharing common ancestral derivation [200], many subtle variations are present which are often overlooked. For example, TP53 status, cell cycle regulation, sensitivity to induced apoptosis and DNA repair are a number of features which are

well categorised, nevertheless, vary substantially between routinely used cell lines [124, 126, 127, 182, 200]. These disparities between analogous cell lines, for example p53 status, also appear to be diverse between different sources and hence, discrete laboratory assessment is required for individual assessment of practise [124, 126]. Additional features such as metabolism, cellular receptor expression and internalisation, immune cell activation status etc. all contribute as selection criteria when deciding upon a cell line for use in human health risk assessment.

Within the human lymphoblastoid cell line category there are three cell lines which are utilised extensively within the field of genetic toxicology research, TK6, AHH-1 and MCL-5 cells. TK6 are human B-lymphoblastoid cells, originally derived from the WIL-2 cell line, isolated from a 5 year old male suffering from hereditary spherocytosis [197]. AHH-1 cells are again human B-lymphoblastoid in nature, display high oxidative properties and were isolated from a 33 year old male [199] and finally, MCL-5 cells were reportedly derived directly from the AHH-1 cell lineage [200]. Collectively, these cell lines constitute the majority of currently available in vitro human genetic toxicology data generated in Swansea University and will no doubt have continued usage within safety assessment for the near future.

Indistinguishable usage of the fore mentioned human lymphoblastoid cell lines within a number of different gene tox end points, for example gene mutation or micronucleus assessment, can lead to potential misuse. Each cell line has comparable however, unique characteristics which promote optimum use within a specific application. The following example illustrates the need for holistic profiling of cell lines prior to use in order to provide accurate quantitative assessment. Firstly, TK6 are heterozygous at the *TK* and hemizygous at the *HPRT* loci and are sensitive to trifluorothymidine (TFT) and 6-thioguanine (6-TG) making them a useful cell line for quantitatively detecting mutation as either *HPRT* or *TK* gene loci [73]. AHH-1 cells equally are heterozygous at the TK and hemizygous at the *HPRT* gene loci and therefore, can also be implemented in either the *HPRT* or *TK* assays. However, what distinguishes the two cell lines is AHH-1's increased oxidative activity, primary metabolism (primarily CYP1A1), and can be used within mutagenesis assays for substances requiring basic metabolism; AHH-1 are more sensitive to B[a]P exposure and other metabolically activated substances [28]. Therefore, when selecting a cell line for usage within a particular application, not only are the physical properties

such as morphology etc. required to be considered, more in-depth analysis of the intrinsic properties of the cell line is also required; accurate, precise safety assessment is entirely dependent upon the appropriateness and exactness of the genetox data. S9 can also be utilised in combination with non-metabolically active cell lines to provide some level of metabolism in vitro.

4.1.3 Complexity of Human Cell Lines and their Applications in Genetic Toxicology

Within the design of this in vitro *PIG-A* assay, human lymphoblastoid cell lines were chosen as the most appropriate cell type for many of the same reasons why they feature so heavily within the genetic toxicology field [113], as outlined above. However, there are a number of specific features which led to the selection over analogous lung epithelial (point of contact) [132] as well as metabolically active liver cell lines, such as HepG2 [201]. One of the beneficial features within the in vivo Pig-a assay which provides a distinctive edge over comparable end points would be the un-invasive sample harvesting [77, 166]; similar genetic damage end points such as comet [91, 104] require termination in order for tissue harvesting. Retaining the origins of the cell line within haemopoetic tissue, maintains the advantageous feature, and potentially enables the direct transfer of the assay design into primary human samples [143, 280]. The suspension nature of the cell line facilitates more favourable sample processing with regards to centrifugation and predicted trypsin sensitivity of the GPI-AP surface markers [281]. Additionally, the human origins and nucleated status of the cell line provides both a method for mechanistic validation and successive human relevant gene tox data [115, 144, 173, 222]. Despite the fact that the selection of the parental cell lineage was decisive, the specific cell line chosen for the assay had to conform to a number of more particular features which were not so absolute.

DNA repair and p53 functionality are two of the features which have larger implications on the downstream generated data [22, 39, 45, 48, 51, 118, 264, 282].

The results of the initial EMS exposure demonstrated insensitivity and hence a consequential inability for quantitative dose response analysis and therefore, highlighted the necessity of further in-depth investigation; not only to assay design, but also to the cellular platform chosen for the assay. DNA can be thought of as a substance which is constantly being subjected to assault and sequential repair, and thus if damage is not adequately repaired deleterious consequences in the form of mutations and chromosome aberrations can occur often leading to disease phenotypes [14]. DNA repair is therefore, a fundamental mechanism which maintains a homeostatic control over genomic stability [51]; at times of excess environmental exposure, DNA repair mechanisms are believed to become saturated and the rate of DNA damage increases [283]. Organisms have therefore, evolved a complex system of DNA damage repair mechanisms, some associated to p53 status, able to firstly detect as well as either repair or remove such lesions [32, 37, 44, 45, 51, 284, 285]. DNA repair deficient cell lines have been demonstrated to be selectively sensitive to specific compound exposures; sensitivity is heavily dependent upon the mechanism of action (MOA) and corresponding deficient DNA repair mechanism [286]. Subsequently, DNA repair deficient cell types generate dose responses with more linear characteristics and subsequently defined PoD dose metrics are observed to be more conservative in nature [264]. If a cell line is deficient in p53, either heterozygous or homozygous loss-of-function mutations in the p53 tumour suppressor gene, an altered response to DNA-damaging agents is observed when compared to wild type cells. Included in the mutant p53 phenotype are the loss of the G_1/S checkpoint, due to a lack of p21 up-regulation, subsequent delayed apoptotic cell death and over sensitivity to genotoxic exposure due to the lack of p53 mediated repair; characteristics which have been consistently observed in the AHH-1 and $TK^{+/-}$ cell line following exposure to DNA damaging agents [124, 126].

Human B-lymphoblastoid cell lines have been repeatedly demonstrated to be variable at the p53 locus in terms of activity as well as functionality [124, 126, 182]. Therefore, prior to preparation of an advanced in vitro standard operating procedure (SOP), attaining to quantitative dose response modelling, further consideration of the implications such specific features brought was required to be assessed. To further emphasise the complexities associated with human cell line usage, the following

example describes the differences in resultant sensitivity to mutation at specific gene loci between two closely related cell lines. MCL-5 cells which were established from human lymphoblastoid (AHH-1) $TK^{+/-}$ cells, expressing human cytochrome p450 CYP1A1 and transfected with two additional separate plasmids containing cDNAs of human cytochrome P450s (CYP1A2, CYP2A6, CYP2E1, and CYP3A4) and microsomal epoxide hydrolase [200], and therefore, should be more sensitive as reporters for mutation for compounds requiring metabolic activation than comparable cell lines demonstrating limited metabolism. However, the AHH-1 cell line has been demonstrated to exhibit increased sensitivity at the *TK* gene loci to mutagenic exposure, when directly compared to the daughter MCL-5 cell line. Following N-nitrosodimethylamine (NDMA) exposure, the induced mutant frequency at the *TK* gene loci was shown to be 5 x fold higher in AHH-1 cells than MCL-5[127]. This result would appear to contradict the reasons for the derivation of the MCL-5 cell line; providing a superior metabolically active cell line for the use of genetox testing applications [200]. This observation was defined to be the result of AHH-1's insensitivity to apoptosis when compared to MCL-5 cells; AHH-1 are heterozygous p53 mutants, whereas MCL-5 are homozygous p53 wild type [126, 127, 182]. Thus the functionality defined by the wild type p53 gene status, facilitates a higher frequency of apoptosis in MCL-5 cells post loss of heterozygosity (LOH) mutations at the *TK* gene loci. AHH-1 cells have a lower frequency of DNA damage induced apoptosis and therefore, have a higher recovery of $TK^{-/-}$ mutants post LOH mutation [127, 182]. Specific features such as metabolic activity, p53 status, morphology and DNA repair individually define the application in which a cell line can be utilised.

P53 status is a known factor which must be considered when discussing the strength of gene-tox data. p53 deficient cell lines have been showed to have an increased sensitivity in MN induction and less of an active G1/S phase checkpoint following genotoxic exposure. Thus impaired p53 functionality is believed to sensitise cells to genotoxicants due to its essential role in the DNA damage response [287]. This understanding has clear importance for safety assessment of genotoxicity and further demonstrates how crucial p53 functionality is [117, 119, 120, 123, 124]. However, these features which truly defines the precision and subsequently the usefulness of the generated data [210].

4.1.4 Genetic Profiling of the Cell Lines and the Assessment of the Applied Molecular Techniques

Protein quantification via western blotting analysis is a fundamental technique extensively utilised in molecular biology; by using western blot the relative presence of an unknown quantity of target protein macromolecules can be identified from within a heterogeneous mixture [288]. In brief, the entire nuclear or cytoplasmic protein fraction, or both, is extracted from the cell or tissue of interest. Following extraction, the protein mixture is denatured and separated by size via the use of a resolving gel, often acrylamide based gels are utilised. Transfer onto a solid support is implemented to facilitate stable immunocytochemical staining for the target protein; primary antibody raised against the protein of interest, coupled with a reporter secondary antibody matching the species of host organism in which the primary was raised. If the protein of interest is present, depending upon the detection method, often horse radish peroxidase (HRP) or fluorophore conjugated based systems are used as a detection method; a notable emission will be detected.

However, there are a number of limitations to the subsequent data; initially protein quantification is generally considered semi-quantitative at best, and not an absolute measure of quantity [288]. Variations in loading and transfer rates between the samples in separate lanes, as well as separate blots, prevent direct comparison of data. These differences are corrected for via the standardization of assay protocol; however, the current technique lacks absolute reproducibility even though it is sufficiently robust. Additionally, the signal generated by detection is not linear across the concentration range of samples. Advancements within the technique have seen the incorporation of fluorophore conjugate secondary antibodies coupled with laser excitation and subsequent emission detection. This more modern approach to western blotting still utilises the analogous preparation steps in which certainty of transfer bias cannot be assured and therefore, offers marginal improvements in the relationship between detection and quantitation; however, additional spectrophotometry or colorimetric methods are available [289].

Real Time - Quantitative Polymerase Chain Reaction (qRT-PCR) measures PCR product accumulation over excess cycles through quantifiable increments within fluorescence emission. This method provides precise and reproducible quantitation of gene copies and does not require post-PCR sample handling, preventing PCR product contamination and results in a much faster and higher throughput assay [290]. There are two frequently reference methodologies which are commercially available; TaqMan ™ and SYBR® Green, each operating via comparable yet unique methods (Figure 4.1).

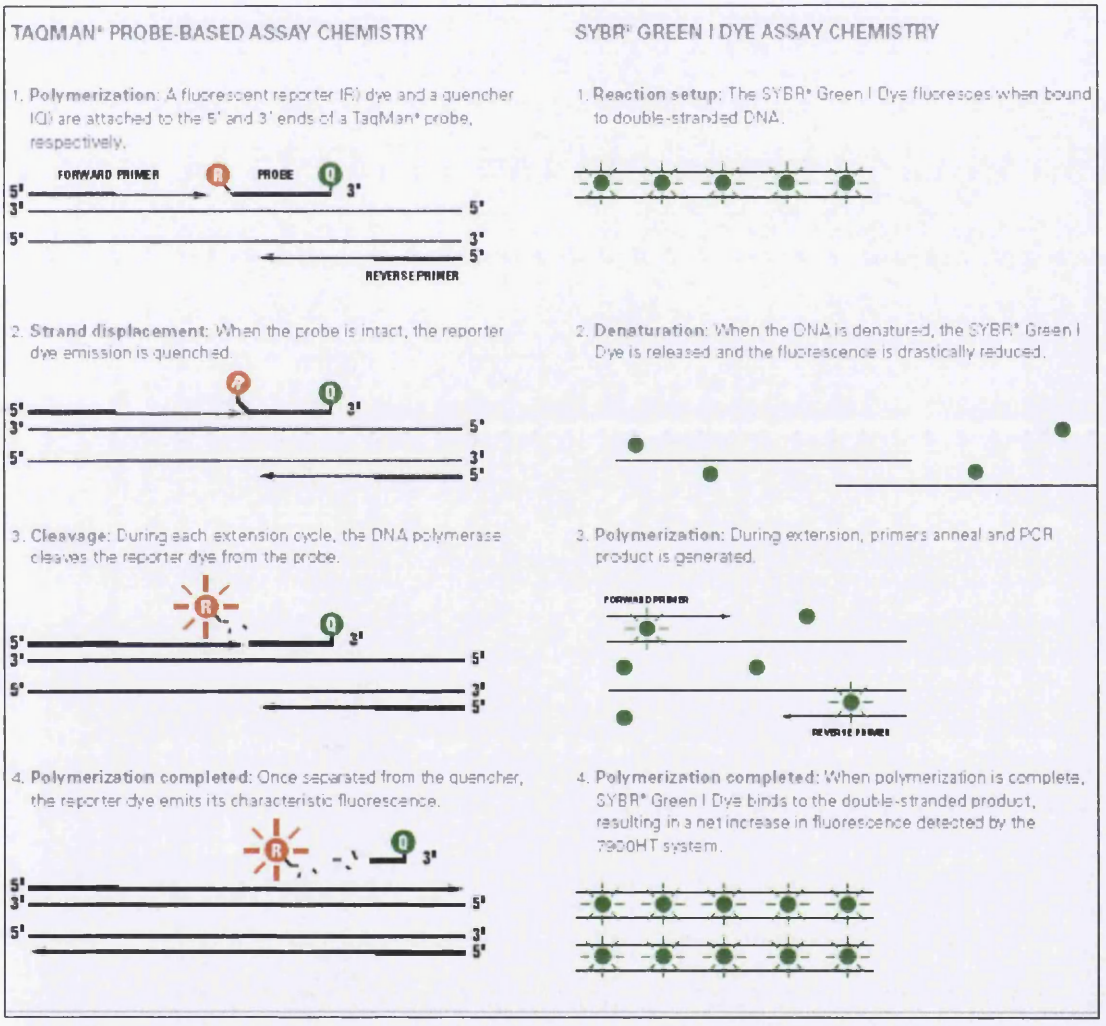

Figure 4.1. Representative methodologies for quantitative real time PCR assessment utilising both the TaqMan Probe ™ and SYBR® Green nucleic acid dye systems. Both methods share equivalent analysis equipment and are distinguished by the use of a fluorogenic TaqMan probe ™ providing assay refinement [291].

The science behind the reporter system distinguishes the two methodologies; SYBR® Green nucleic acid dye is an intercalating agent which binds dsDNA and subsequently fluoresces in response to a net increase in PCR product. Whereas, the use of a fluorogenic TaqMan probe ™ provides reproducible increased assay sensitivity, lower detection limits, multiplexing opportunities and a greater number of applicable downstream applications [291]. Real time detection systems were seen to improve following the introduction of fluorogenic-labelled probes that use the 5' nuclease activity of *Taq* DNA polymerase. The availability of these probes, such as Taqman, enabled the development of a real-time method for detecting only specific amplification products, however, the limited supply dramatically increase the costs and limits the number of applications which can benefit without the initial capital.

Within this chapter of work the quantitative PCR analysis was carried out utilising the SYBR® Green system, as described in Figure 4.1. However, the SYBR® detection system is known to generate potential false positive signals [291]; SYBR® dyes binds to any double-stranded DNA, therefore, they are able to bind to nonspecific double-stranded DNA sequences. As a result of this, it is imperative to have well-designed primers that do not amplify non-target sequences, and that melt curve analysis is performed within each run. An additional aspect of using DNA binding dyes is that multiple dye molecules can potentially bind to a single amplified DNA molecule; multiple dye binding defines the signal strength to be dependent upon the mass of double-stranded DNA produced in the reaction. Thus, if the amplification efficiencies are the same, amplification of an elongated product will generate a greater signal than a diminutive one. This is in contrast to the use of a fluorogenic probe, in which a single fluorophore is released from quenching for each amplified molecule synthesized, regardless of its length and hence has increased quantitative properties.

4.2 Material and Methods

Within the following chapter, two different TK6 cellular cultures were utilised; the higher passage referred throughout as "Normal" and the lower referred to as "Low Passage", their unique derivation and origins can be found within (Section 2.1.2). Initially, the Low Passage TK6 cells were assessed for their ability to be incorporated into the in vitro *PIG-A* assay design along with a corresponding change in phenotypic mutant frequency reporting GPI-AP. General cell line viability was investigated as well as FACS optimised to produce sufficiently wild type enriched, CD55 positive, Low Passage TK6 populations. Assay sensitivity was subsequently assessed, following model mutagen exposure, and resultantly additional lymphoblastoid cell line and reporting GPI-AP combinations were investigated. Validation of selected lymphoblastoid cell lines, focusing on p-53, p-p53 and p21 status as well as their functional induction following genotoxin exposure followed to further develop the assay design.

4.2.1 GPI-AP Expression Assessment within "Low Passage" TK6 Cells

A vial of "Low Passage" TK6 cells were established and maintained as outlined within (Section 2.2). Each experimental sample (1 x 10^6 cells), CD59 (Protectin) followed by CD55 (Decay Accelerating Factor), was run in triplicate in conjugation with a homologous instrument calibration standard (ICS); cellular cultures were treated with either anti-CD59 R-PE antibody or anti-CD55 R-PE (Cat No. 555694, BD Biosciences, Hertfordshire, UK) in a comparable manner as outlined (Section 2.8.1). Post incubation, samples were washed, and re-suspended in 1 mL of 1x PBS solution, maintained on ice and protected from light, prior to flow cytometric analysis.

4.2.2 CD55 Antigen Optimisation using Fluorescence Activated Cell Sorting (FACS)

4.2.2.1 Initial Aseptic Sort Evaluation

"Low Passage" TK6 cell cultures were established as outlined in (Section 2.2), counted and aliquots equivalent to $1x10^6$ cells were transferred into fresh 15 mL centrifuge tubes, the parental culture were placed back into incubation. Cellular samples were treated with anti-CD55-PE fluorescently labelled antibodies (Section 2.8.1) and analysed on the flow cytometer (Section 2.8.2).

The BD FACS Aria flow cytometer was started up following the procedure outlined (Section 2.8), once satisfied with the prerequisite system calibrations, sorting was commenced and the recovered presumed homogeneous cells pooled and collected within 5 mL polystyrene (12 x 75mm) sorting tubes (BD. Biosciences, Hertfordshire, UK) with fresh cell line specific growth medium (1 mL) and consecutively sub-cultured (Section 2.2.3) within 25 cm^2 culture flasks prior to potential long term cryopreservation (Section 2.3). Quality assurance (QA) FCM based *PIG-A* phenotype assessment was carried out prior to and 72-96 hr. following enrichment.

4.2.2.2 Preliminary FACS Sample Collection and Volume Asessment

"Low Passage" TK6 cell cultures were established as outlined in (Section 2.2), cellular samples, except the ICS, were treated with anti-CD55-PE fluorescently labelled antibodies (Section 2.8.1), washed and re-suspended in 1 mL of pre-cooled culture media prior to storage on ice, and protected from light. Samples were stored for a maximum of 1 hr prior to analysis on the flow cytometer (Section 2.8.2). The FACS Aria I was set up and operated in a homologous method to the one outlined in the previous optimisation experiment, however, within this experiment the drop distance as well as sample collection volume and viscosity were assessed for their individual effects on cellular viability post sorting. Eight unique collection tubes

were prepared for the experiment; a variety of collection media volume (drop distance) and constituents (viscosity and protein content) were assessed.

1) 15 mL BD Falcon tube – containing 10 mL of Heat inactivated serum (HiS)
2) 15 mL BD Falcon tube – containing 5 mL of HIS
3) 15 mL BD Falcon tube – containing 5 mL of RPMI 1640 culture media
4) 5 mL Flow tube – 3 mL HiS
5) 5 mL Flow tube – 3 mL Culture media
6) 5 mL Flow tube – 1 mL Culture media
7) 5 mL Flow tube - 0.5 mL HiS)

10-20,000 events (time dependent) were collected within each tube and immediately the recovery was assessed for CD55 antigen presence. Post sorting elongated recovery and subsequent extended viability was not directly assessed.

4.2.2.3 FACS, Refinement for Optimum Cellular Recovery

"Low Passage" TK6 cell cultures were established, as well as the BD FACS Aria I started up, and stained in an analogous method to the previous experiment outlined in (Section 4.2.2.2), however, within this experiment the finer refinements made to the collection volume were assessed for their individual effects on cellular viability post sorting. Nine unique collection tubes were prepared for the experiment; three separate collection media volumes were assessed in triplicate for potential subtle effects associated with marginally different drop distances.

1) 3 x 5 mL Flow tubes – containing 3 mL of RPMI 1640 media
2) 3 x 5 mL Flow tubes – containing 1 mL of RPMI 1640 media
3) 3 x 5 mL Flow tubes – containing 0.2 mL of RPMI 1640 media

Each initial experimental sample will be analysed in triplicate to generate some indication of intra-sample variance within the FACS Aria I platform.

4.2.3 "Low Passage" TK6 Viability

4.2.3.1 Viability Data for "Low Passage" CD55 enriched TK6 cells

A vial of CD55 enriched "Low Passage" TK6 cells were established and maintained as outlined within (Section 2.2). Three tubes were utilised for sample viability assessment, the fourth was an ICS used to set detector voltages and initial population gating. Cultures were treated with anti-CD55 PE antibody, in an analogous manner to the protocols defined in (Section 4.2.2.2 – 4.2.2.3). Post incubation, cultures were washed and re-suspended in 5 mL of 1 X annexin-binding buffer. Binding buffer was supplied at 10X concentration and therefore, required a 1 in 10 dilution in dH_20 prior to usage. Cultures were centrifuged (250 x g for 7 min), supernatant aspirated and re-suspended in an additional 100 µL of 1 X annexin binding buffer. 5 µL of Alexa Fluor® 488 annexin V was added to each culture, excluding the ICS and incubated for 20 mins. Post incubation, excess 1 X annexin binding buffer was added, cultures centrifuged, supernatant aspirated and re-suspended in 200 µL of annexin binding buffer. 5 µl (0.25 µg) per test (per million cells) of 7-AAD was added, mixed thoroughly and incubated for 5 minutes, protected from light, on ice. Samples were maintained on ice protected from light for a maximum of 4 hr prior to analysis. The pre-defined compensation matrix (Section 2.8.2.1) was entered into the flow cytometry template to prevent potential signal overlap, especially between the Alexa Fluor 488® and PE conjugated antibodies; due to the relative proximity of the "FITC" and "PE" detectors on the electromagnetic spectrum.

4.2.4 "Low Passage" TK6 preliminary *PIG-A* Assessment Utilising the CD55 Surface Antigen following Exposure to a Model Mutagen

"Low Passage" TK6 cell cultures were established and maintained as outlined in (Section 2.2) and exposed to EMS for 24 hr under standard chemical treatment as described within (Section 2.4.2). Post chemical exposure, cultures were washed,

counted and seeded ready for initial flow cytometric analysis using anti-human CD55 PE conjugate, Alexa Fluor 488® Annexin V and 7-AAD (Section 4.2.3.1). Flow cytometric analysis as defined in (Section 2.8) was undertaken within an hour of sample preparation, samples were stored on ice, protected from direct light, until analysed.

After gating for single cells on a SSC/FSC dot plot and/or counter map, a minimum of 10,000 events were analysed for the surface expression of the CD55 surface antigen. *PIG-A* phenotype was assessed utilising an instrument calibration standard (ICS), an unstained sample used to set voltages and mutant gating. During ICS analysis, the mutant mimicking sample is utilised to detect auto fluorescence within the channel of collection in order to distinguish between a positive event and background noise at the channel's photon multiplier tube (PMT).

EMS dose response data were produced using a FACSAria I cell-sorter (Section 2.8), all fluorescence measurements on the FACSAria were recorded using the "area" parameter; annexin V, Alexa Fluor® 488, R-PE and 7-AAD were assessed within the pre-specified "FITC", "PE" and "APC" detectors. FITC, 502LP combined with a 530/30 band pass filter, PE, 556 LP combined with a 585/42 band pass filter and APC, no LP combined with a 660/20 band pass filter. Alexa Fluor 488® and PE were excited off the 488nm laser line, and the 7-ADD off the 635 nm laser line, best matching their excitation maxima's.
Following flow cytometric analysis, parental cell cultures were removed from incubation every 24 hr for repeated *PIG-A* mutagenesis assessment as described in an analogous method (Section 2.10).

4.2.5 Normal TK6, AHH-1 and MCL-5 Cell Line Characterisation

Fresh vials of low passage number human lymphoblastoid TK6, "Low Passage" TK6, MCL-5 and AHH-1 cells were removed from cryopreservation, thawed quickly and cultured under standard conditions (Section 2.2). HepG2 required a longer growth establishment period and were more sensitive to physical agitation and therefore, approximately a week prior to experimentation a fresh vial of HepG2 cells were thawed (Section 2.1.5). Samples were prepared and stained in a homologous

manner to (Appendix Section 4.2.5) in order to generate comparable metrics for FLAER, CD48 and CD55/59 tandem treatment for their relative receptor presence. However, due to the adherent nature of the liver immortalised cell line (HepG2), different cell line maintenance as well as harvesting protocols were utilised, prior to staining, as outlined below.

A fresh vial of HepG2 was removed from liquid nitrogen storage and placed within a pre-warmed 37 °C water bath. Once thawed, the contents of the vial were transferred to a sterile 25 cm^2 culture flask and minimal culture media (Section 2.2) added in order to cover the base of the flask and placed within the temperature controlled incubator. Routinely, every 12-24 hr the flask was carefully removed, to prevent cessation of growth, and microscopically examined for growth. HepG2 cells should grow to a uniform monolayer of cells, cells should be passaged to prevent over confluency as well as culture medium replaced regularly to aid optimum growth dynamic and prevent disruption of the monolayer.

The cells were maintained and sub-cultured as outlined in (Section 2.2.3.2), following this, the cells were centrifuged, supernatant aspirated and re-suspended in 10 mL of fresh culture medium before being counted (Section 2.2.1) and treated with the allotted florescence dyes prior to flow cytometric analysis.

All cell lines were monitored regularly, assessed microscopically for signs of infection or morphological abnormalities, and sub-cultured once prior to the experimental start date to ensure correct growth dynamics.

4.2.5.1 Western Blotting –-Sodium Dodecyl Sulphate – Poly-Acrylamide Gel Electrophoresis (SDS-PAGE)

4.2.5.1.1 Total Protein Extraction

Total protein extractions were undertaken within a class 2 safety cabinet, in a temperature controlled environment 2-4 °C, in order to prevent high levels of protease enzymatic activity. All centrifugation steps were carried out at 2-4 °C

within a temperature-controlled Eppendorf 5810R centrifuge. Cell cultures were established as described in (Section 2.2), washed and counted in preparation for the protein extraction protocol. The equivalent volume of culture medium to 4-8 x 10^6 cells was transferred into a 50 mL centrifuge tube, spun down (~250 x g for 7 min) and supernatant aspirated. 5 mL of pre-cooled, 2-4°C, cold pH 7.4 PBS was added to the cell pellets, pellets were re-suspended thoroughly, centrifuged and the resultant supernatant was discarded. This step was repeated an additional time to ensure absence of growth medium. Cellular pellets were re-suspended in 200 µL Radio-Immunoprecipitation Assay (RIPA buffer) (R0278, Sigma Aldrich, Gillingham, UK) supplemented with 2.5 µL of (500x) protease inhibitor cocktail (Cat No. ab65621, Abcam, Cambridge, UK) and transferred into pre-cooled 1.5 mL micro-centrifuge Eppendorf tubes. Post transfer, each culture was incubated for 5 min at 4 °C prior to high speed vortexing, confirming cellular lysis. The lysate was centrifuged (10,000 x g for 10 min), and the supernatant transferred into new sterile 2 mL Eppendorf tubes. The contents of each tube, a mixture of both cytoplasmic and nuclear protein, was labelled accordingly , three 5 µL aliquots were removed for protein quantification and stored at -80 °C until future use.

4.2.5.1.2 Activ Motif Nuclear and Cytoplasmic Protein Extraction

Refined protein extraction was undertaken with the use of the Active Motif Nuclear Extract Kit (Cat. No. 40010, Active Motif, La Hulpe, Belgium) all kit components were stored at 2-4 °C upon arrival and protected from direct light. Cell cultures were establish as outlined in (Section 2.2), counted and washed (Section 2.2.3.1) prior to protein extraction protocol, which can be found in (Appendix Section 4.2.5.1.2). In brief; firstly, a number of additional solutions were also required to be constructed prior to lysis, following this, cellular cultures were treated with phosphatase inhibitors, hypotonically lysed and then exposed to detergent. Following incubation, cytoplasmic fraction was collected prior to an additional lysis stage, vortexing and the collection of the nuclear fraction. All fractions were aliquotted to enable protein quantification and stored at -80 °C for long term use.

4.2.5.1.3 Protein Quantification

All protein quantification within this body of work was carried out using the DC ™ Protein Assay Kit 1 (Cat No. 500-01111, Bio-Rad, Hertfordshire, UK) and followed as outlined within the supplied manufactures protocol (Appendix Section 4.2.5.1.3). In brief, bovine serum albumin (BSA) standards were constructed, and with the experimental samples loaded in triplicate to the designated 96 well plate (Appendix Section 4.2.5.1.3.2). Reagent A and S were mixed and subsequently pipetted onto the samples within the plate, followed by the addition of reagent B, and left to incubate. Post incubation, protein quantification was undertaken on the FLUOstar Omega spectrophotometer (BMG Labtech, Ortenberg, Germany) at 750 nm (Appendix Section 4.2.5.1.3.3)

4.2.5.1.4 Western Blotting Buffer Solution Preparations

Prior to the undertaking of any Western Blott analysis, a combination of long term (up to one month storage) and short term buffer solutions (maximum of one week storage) were required to be constructed (Appendix Section 4.2.5.1.4.1). Short term buffer solutions were made up fresh on the day of experimentation, and used immediately (Appendix Section 4.2.5.1.4.2).

4.2.5.1.5 Polyacrylamide Gel Preparation

All western blot analysis was carried out following the procedures outlined in (Appendix Section 4.2.5.1), the gels constructed for this body of work were polyacrylamide based and the constituent components of each gel were purchased and stored according to manufactures guidance (Appendix Section 4.2.5.1.5). The addition of TEMED in combination with Polyacrylamide forms a gel matrix suitable for the resolution of macromolecules; percentage composition polyacrylamide governs the lattice structure, in conjunction with detergent treatment facilitates a 2-dimensional linear separation of proteins. The percentage composition of resolving

gel was based directly upon the molecular weight of the protein under assay; large proteins required lower acrylamide composition. Preparation of gels was undertaken in an AFA1000 fume hood due to the hazardous nature of the chemicals used.

4.2.5.1.6 Gel Casting and Electrode Assembly

All western blott apparatus used within this project was purchased from Bio-Rad, prior to casting, all plates, spacers, combs and casting stands were washed thoroughly allowed to air dry, facilitating correct set up alignment (Appendix Section 4.2.5.1.6). In brief; the desired resolving gel was prepared and then applied directly to the apparatus, isopropanol, (Cat No. 190764, Sigma Aldrich, Gillingham, UK) was applied across the top of the gel and incubated. Post hardening, isopropanol was discarded and the stacking gel was applied directly onto of the resolving gel, in an analogous method. Following a final assessment for alignment and potential retarding bubble formation, the set up was further incubated (Appendix Section 4.2.5.1.6).

Post hardening and gel melding the plate assembly was removed from the casting stand, and transferred into a vertical electrophoresis system (Appendix Section 4.2.5.1.6). Protein samples were denatured, loaded along with protein standards and the apparatus filled with buffer to enable running. The lid of the electrophoresis system was placed onto the chamber, connected and ran. When the dye front had migrated to within an inch of the base of the gel, the power pack was disconnected and the running buffer removed and discarded.

4.2.5.1.7 Protein Transfer

Protein transfer during this thesis project was carried out using the Mini Trans-Blot® Electrophoretic Transfer Cell kit contents (Cat. No. 170-3930, Bi-Rad, Hertfordshire, UK), operated according to manufacturer's supplied guidance (Appendix Section 4.2.5.1.7) Unless otherwise stated, all apparatus was supplied within the kit and used in conjunction with buffers prepared according to (Appendix Section 4.2.5.1.4).

In brief; immuno-Blot PVDF membranes (Bio-Rad, Hertfordshire, UK) were temporarily dehydrated in 100% methanol, and re-hydrated along with fibre pads and thick blott papers in pre-cooled 4 °C transfer buffer (Appendix Section 4.2.5.1.7). Post hydration, transfer cassettes were constructed and placed within a Transfer cell, cooling unit added and filled with cold transfer buffer. The whole apparatus was placed within a polystyrene container filled with ice and moved into the cold room to maintain a constant 2-4°C environment. A power pack was attached to the transfer cell and ran. Post transfer, the cassette was removed from the transfer cell and the membrane was submerged in pre-cooled (2-4 °C) wash buffer (Appendix Section 4.2.5.1.4.2), agitated and cut to correct size.

4.2.5.1.8 Membrane Blocking and Antibody Incubation

Membrane/s were blocked overnight (approximately 8-12 hr) in BSA to prevent non-specific antibody binding, washed and exposed to primary antibodies within blocking buffer. Post treatment, membrane/s were washed several times and sequentially incubated in corresponding horse radish peroxidase (HRP)-conjugated secondary antibody solution. Post incubation, membranes were washed and analysed on the ChemiDoc ™ XRS (Bio-Rad, Hertfordshire, UK), Quantity One (Bio-Rad, Hertfordshire, UK) software. Full details described within (Appendix Section 4.2.5.1.8).

4.2.5.1.9 Protein Detection – ChemiDoc ™ XRS

4.2.5.1.9.1 Protein of Interest Detection

Protein detection was under taken using the Clarity Western ECL substrate (Cat No. 170-5060, Bio-Rad, Hertfordshire, UK) chemilluminescence kit, stored and operated as per manufacturers supplied instructions (Appendix Section 4.2.5.1.9.1). Post washing, the membrane/s were removed and placed onto the pre-cleaned

ChemiDoc™ surface, and positioned correctly. The visualising agent was applied liberally and visualised according (Appendix Section 4.2.1.5.10). Post probing for the protein of interest, the membranes were washed, stripped and treated with the anti-house keeper antibody (Appendix Section 4.2.5.1.9.2). The visualisation procedure was repeated and data analysed (Appendix Section 4.2.1.5.10).

4.2.5.1.10 Protein Quantification – Quantity One Software

All protein band detection and estimated quantification were retrospectively undertaken using the Quantity One – Advanced software purchased from Bio-Rad, Hertfordshire, UK. Briefly; the relative band intensities were initially standardised against the background, following this, each sample band was normalised against the corresponding house keeper band, averaged against experimental replicates and divided against the con-current negative control generating the average relative fold increase in band intensity when compared to un-treated controls (Appendix Section 4.2.5.1.10).

4.2.5.2 Qualitative Real Time – Polymerase Chain Reaction Protocol

4.2.5.2.1 Ribonucleic Acid (RNA) Extraction

Total RNA was extracted from the human lymphoblastoid cell lines using the Qiagen RNeasy Mini Kit (Qiagen, Sussex, UK) and followed according to the manufacturers` instructions (Appendix Section 4.2.5.2.1). Concisely, cell cultures were established as outlined in (Section 2.2) and lysed with buffer, precipitated in 70% ethanol and passed through a centrifugation column. Intracellular contents was DNase digested, extensively isolated and washed and finally, the subsequent RNA was collected (Appendix Section 4.2.5.2.1) and placed within a -80 °C freezer for short term storage.

4.2.5.2.2 RNA purity Assessment - Nanodrop

Following the RNA extraction (Section 4.2.5.2.1) the RNA yield was measured and the purity assessed (260:280 ratio) using a NanoDrop ND-1000 Spectrophotometer (Labtech International, Uckfield, UK). Full details of the protocol can be found within the (Appendix Section 4.2.5.2.2).

4.2.5.2.3 Double Stranded Complementary DNA (cDNA) Synthesis

Double stranded cDNA synthesis was carried out for all the human lymphoblastoid cell lines using the QuantiTect Reverse Transcriptase Kit (Cat No. 2053111, Qiagen, Sussex, UK) and followed according to the manufacturers` instructions. The full protocol for use is detailed (Appendix Section 4.2.5.2.3), however, In brief; thawed RNA was treated with Quantiscript reverse transcriptase, RT primer Mix (Oligo DT), gDNA Wipe-out buffer, Quantiscript RT buffer and nuclease-free H_20 and placed within a T100 PCR Thermal Cycler (BioRad, Hertfordshire, UK) for 2 min at 42°C. Following complementary strand synthesis, Quantiscript Reverse Transcriptase, RT Primer mix and Quantiscript RT buffer were all added to the template cDNA. Each sample was transferred back into the heating block and cycled for 15 min. Post incubation, each sample was in-activated for 3 min at 95°C, short term stored within a -80 °C freezer.

4.2.5.2.4 Quantitative Real-Time Polymerase Chain Reaction (qRT-PCR)

Real-time PCR experiments were undertaken using the QuantiFast™ SYBR® Green PCR Kit (Qiagen, Sussex, UK) in combination with synthesised cDNA, full details can be found (Appendix Section 4.2.5.2.4). In essence, template cDNA was treated with QuantiFast SYBR® Green PCR Mast Mix, forward and reverse primers and RNase-free water. All solutions were made in excess and run in triplicate within sterile 96-well 0.2 mL PCR plates (Sarstedt, Nuembrecht, Germany). Experimental samples, standard serial dilutions as well as non-template negative controls were also

included for each primer pair. Within the negative controls, cDNA was replaced with RNase-free water and the inclusion of standard wells allowed post analysis PCR efficiency to be calculated. Post plating, each individual 96 well-plate was sealed with an Absolute QPCR Seal sheet (Thermo Scientific, Surrey, UK), centrifuged briefly before being transferred into the iCycler iQ5 thermal Cycler (BioRad, Hertfordshire, UK). The thermal cycler was then programmed and run (Appendix Section 4.2.5.2.4.1), following completion the plates were kept for future molecular analysis. All retrospective analysis was carried out using the manufacturer supplied iCycler iQ5 software version 2.1 (BioRad, Hertfordshire, UK), which full details can be found within (Appendix Section 4.2.5.2.4.2 – 4.2.5.2.4.3).

4.2.5.3 P53 Functionality Assessment Following MMC Treatment

4.2.5.3.1 MMC induced p21 qRT-PCR Assessment

Following establishment of human lymphoblastoid cell lines (Section 2.2), cells were sub-passaged twice before the start of this experiment in order to assess rate of cell division, via RPD assessment. Prior to culture flask preparation, PPE was collected and worn in conjunction with collection of suitable vessels for toxic chemical disposal. Sterile 25 cm^2 culture flasks, four for each cell line, were seeded at 8 x 10^5 cells/mL and received a 100 µL dose of varying Mitomycin C (Table 4.1).

Table 4.1. MMC preparations, following establishment of stocks "A – 0.05mg/mL" and "B – 0.005mg/mL", prior to dosing of human lymphoblastoid cell lines, TK6, AHH-1 and MCL-5.

Dose (µg/mL)	Stock Solution	MMC (µL)	dH_20 (µL)
0	N/A	0	100
0.02	"B"	40	60.0
0.08	"A"	16	84.0
0.15	"A"	30	70.0

Following acute dosing, in which each culture flask was incubated at 37°C for 4 hr, the cultures were transferred into 15 mL sterile BD Falcon tubes and centrifuged (250 x g for 7 min). The presumed toxic supernatant was discarded, according to local health and safety protocols (Section 2.8.4), and cell pellets washed twice with 10 mL of 1x PBS. Following extensive washes, the supernatant was aspirated and discarded and re-suspended in 10 mL of fresh culture medium; at this point all toxic waste and toxic components were stored or discarded as per health and safety regime. The cultures were then processed in a homogenous manner to (Section 4.2.5.2) in which qRT-PCR analysis was undertaken to investigate p21 induction following genotoxin exposure.

4.2.5.3.2 p-p53 and p21 Western Blot Assessment following MMC treatment

Following establishment of human lymphoblastoid cell lines (Section 2.2); cells were sub-passaged twice before the start of this experiment and their growth recorded in order to assess rate of cell division to ensure that log phase growth dynamics were being exhibited by the cultures. Cultures were prepared and dosed with MMC as outlined in (Section 4.2.5.3.1) and subsequently processed as described in (Section 4.2.5.1) in order to facilitate p-p53 and p21 protein quantification via Western Blott analysis.

4.3 Results

4.3.1 GPI-AP Expression Assessment within "Low Passage" TK6 Cells

"Low Passage" Epstein-Barr viral transformed TK6 human B-lymphoblastoid cells, originally isolated from the WIL-2 cell line supplied by Masa Honma, National Institute of Health Sciences (NIHS); were believed to provide a potential benefit to the in vitro *PIG-A* assay platform through their assumed increased phenotypic stability, lower sensitivity to apoptosis and general increased genomic integrity when compared to the normal TK6 cells currently utilised within Swansea University. Initially their CD59 GPI-AP surface marker was immuno-fluorescently assessed for presence and potential usage, as in-direct reports for mutation at the *PIG-A* gene locus, within the proposed in vitro assay design.

"Low Passage" TK6 cells were demonstrated to exhibit minor protectin presence/expression on the cellular surface (0.17-0.58%); the resultant expression data, i.e. the positive signal detected within the relevant detector, was even observed to be lower than the un-stained instrument calibration standard in two of the three experimental samples (Figure 4.2). This experiment was repeated within an additional "Low Passage" TK6 population derived from a different cryo-preserved culture and the resultant data mimicked the original findings. The "Low Passage" TK6 cell line was demonstrated to be homogenous negative for the CD59 cellular surface antigen.

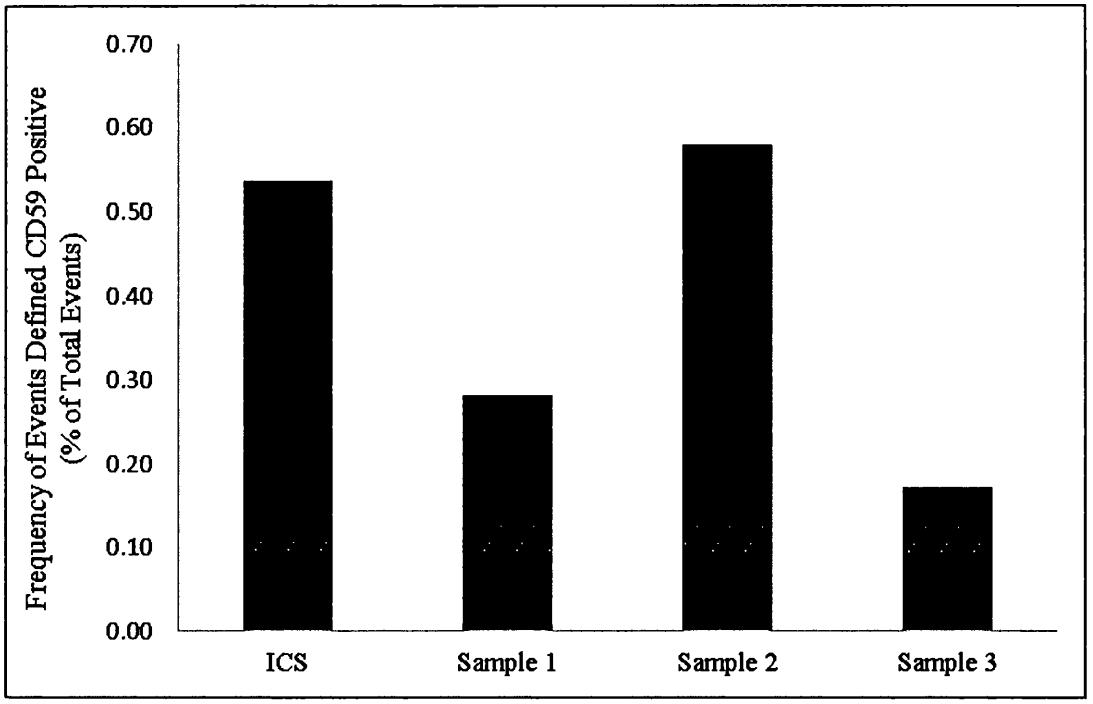

Figure 4.2. Relative positive expression of the pre-enriched CD59 surface antigen, within "Low passage" TK6 cultures following mouse-anti-human anti-CD59 R-PE treatment. Specific single cell gating strategies were omitted to provide an unbiased assessment on total recorded events, however, FSC-A threshold value was set to remove debris. Detector sensitivity was established following instrument calibration standard analysis (N =1)

Utilising the unchanged antibody solution, cellular samples of TK6 cells were exposed in a homologous manner to primarily provide further functional data for the antibody and secondly, provide a direct comparison between the two cell lines. The TK6 cells, previously utilised within the first results chapter (Section 3.3), were demonstrated to exhibit an approximately 70% distribution of CD59 positive cells within the heterogenous parental population (Figure 4.3).

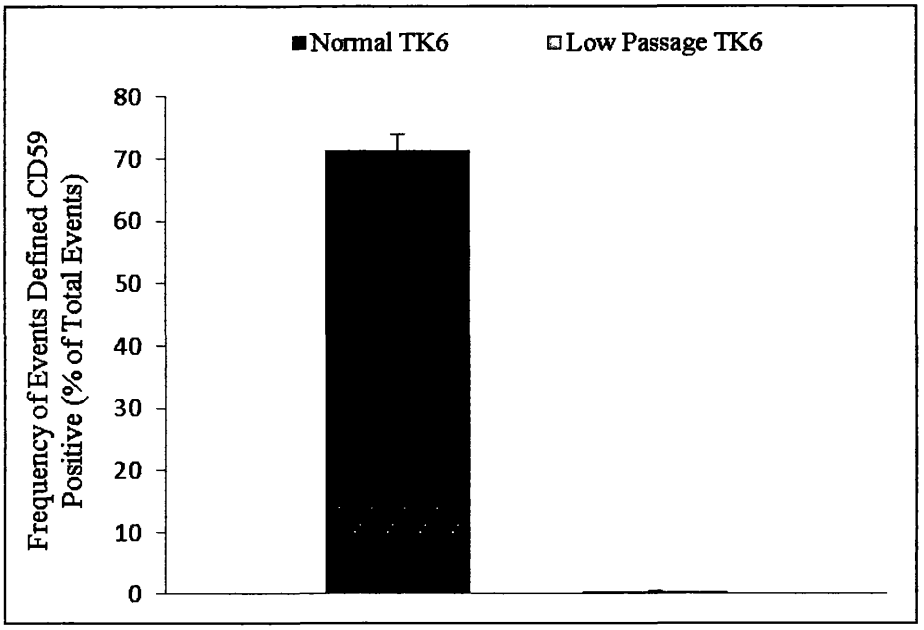

Figure 4.3. Relative expression of the pre-enriched CD59 surface antigen , within "Low passage" and normal TK6 cultures following mouse-anti-human anti-CD59 R-PE treatment. Specific single cell gating strategies were omitted to provide an unbiased assessment on total recorded events, however, FSC-A threshold value was set to remove debris. Detector sensitivity was established following ICS analysis (N=3, Error Bars ±1SD)

Cellular GPI-AP assessment continued with the subsequent analysis of the CD55 (DAF) antigen surface presence assessment. The "Low Passage" TK6 cell line was demonstrated to have highly comprehensive CD55 surface antigen presence over the majority of the defined cellular events within the heterogeneous population (Figure 4.4). An average of 97.3% of cells within the parental culture were demonstrated to display a positive signal in the relevant detector channel following antibody treatment. Even though the origins and functions of the two cellular surface antigen candidates is highly comparable, the resultant expression data was distinctly different and demonstrates no apparent correlation between GPI-AP expression and functionality within lymphoblastoid cell lines. Use of the CD59 surface antigen as a phenotypic marker for mutation at the *PIG-A* gene locus was discontinued within further applications utilising the "Low Passage" TK6 cellular populations.

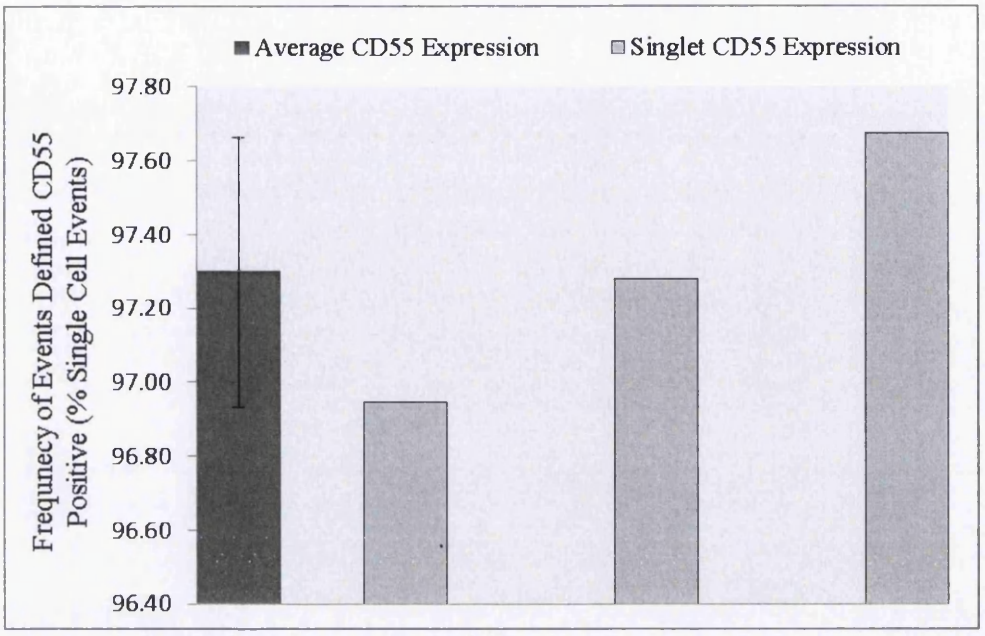

Figure 4.4. Relative expression of the pre-enriched CD55 surface antigen within "Low passage" TK6 cultures following mouse-anti-human anti-CD55 R-PE treatment. Specific single cell gating strategies were included; based on FSC-A vs SSC-A profile as well as a FSC-A threshold value was set to remove debris. Detector sensitivity was established following ICS analysis (N=3, Error Bars ±1SD)

4.3.2 CD55 Antigen Optimisation using Fluorescence Activated Cell Sorting (FACS)

From the conclusions drawn from the previous results chapter (Section 3.4), FACS was considered to be the enrichment methodology with the most future promise (Section 3.4.2). FACS potentially delivers the complete mutant depletion without the associated limitations associated to prolonged cell cultures, as observed within clonal expansion (Section 3.3.2.2), as well as antigen robustness, heavily featured in para-magnetic bead enrichment techniques (Section 3.3.2.1). Therefore, in order to fully evaluate the technique for incorporation into the assay design, a number of stepwise experimental protocols were established, each addressing a slightly different potential influencing factor with regards to sort efficiency and cellular viability. The data included within this section endeavours to create a finalised protocol, taking on board the caveats associated with the technology available and the circumstances of use, in which an optimum mutant depletion methodology was established.

4.3.2.1 Initial Aseptic Sort Evaluation

Considering the initial FACS data, utilising the CD55 antigen as the identification parameter in which the upper 50 percentile of subsequent cells expressing CD55 were captured; the initial GPI-AP expression was conservatively estimated at 80.36% (P2 - Figure 4.5C). The morphology of the cells as well as distribution and constitution of debris within the post sort parental sample was distinctly different from the ICS as well as pre-sort homologous stained sample. Figure 4.5 A (ICS) and B (Pre-sort stained sample) showed distinctly similar parental populations in terms of debris quantity and distribution, their markedly different fluorescence emission histograms were attributed to the un-stained nature of the ICS. However, Figure 4.5 C (post-sort analysis sample) demonstrated increased cellular debris and a resultant erratic single cell population following sorting. The partnering histogram for the post sort sample (Figure 4.5 C) alluded to a bimodal distribution between CD55 negative cells (presumed debris/apoptotic positive) and CD55 positive (presumed viable) cell type.

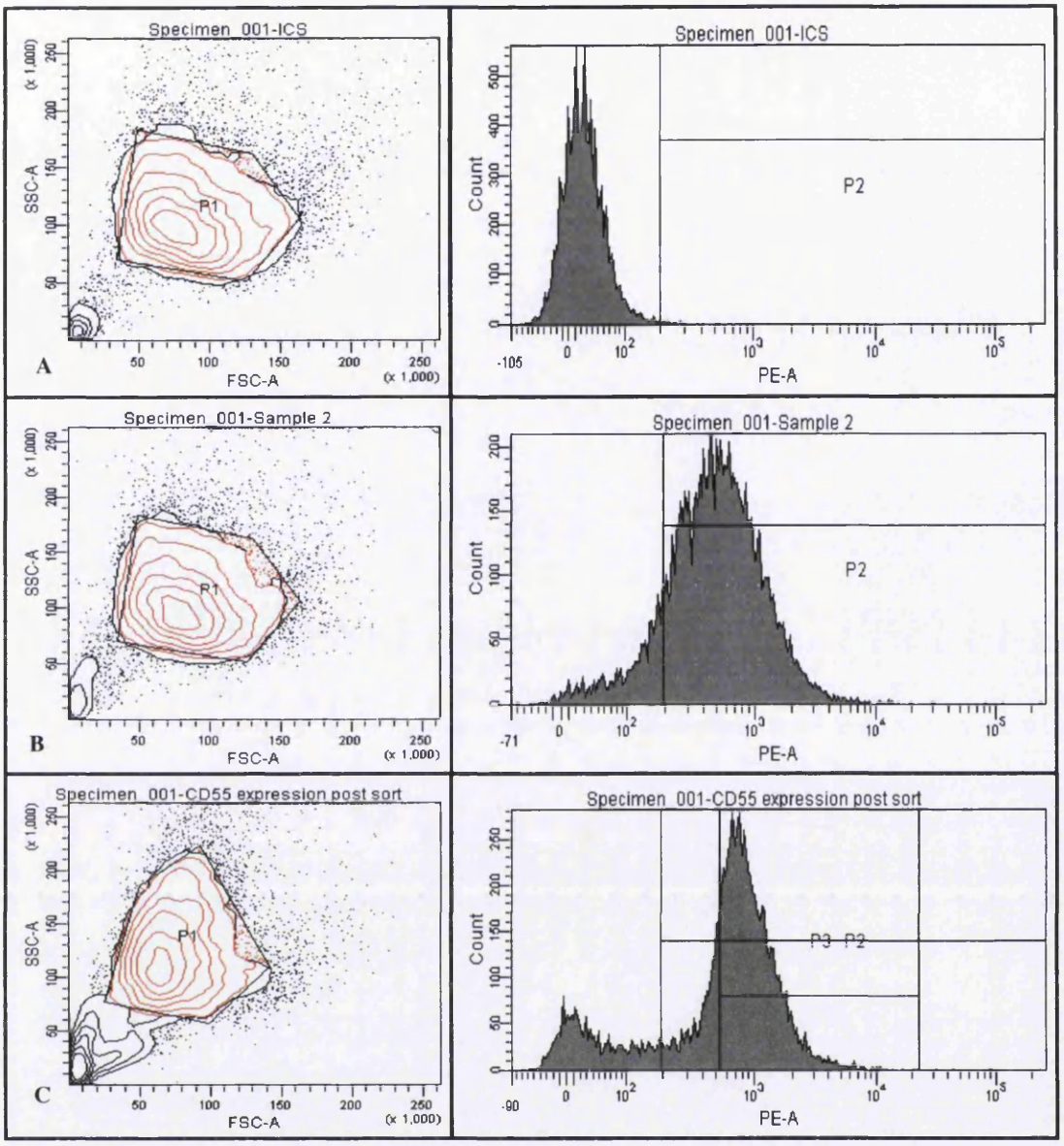

Figure 4.5. Immediate CD55 (DAF) surface antigen expression within "Low Passage" TK6 cells following initial Fluorescence Activated Cell Sorting (FACS) optmisation. Single cell gating strategy "P1" omitted within the histograms to appreciate the potential detremental effect within GPI-AP expression within the parental population following sorting. "P2" the threshold for positivity and "P3" visual indication of presumed significantly positve signals. A) Instrument Calibration Standard utilised to define positivity within the "PE-A" detector, B) Un-sorted control sample utilised to establish the basal CD55 expression and C) post-FACS enriched sample (N=1).

4.3.2.2 Preliminery FACS Sample Collection Volume Asessment

The 72 hr recovery optimised FACS data (Table 4.2) demonstrated recovered yields of $\geq$ 97% of the total population expressing the CD55 antigen; an increase of ~17% from previous initial FACS methodologies (Figure 4.5). Subtle variances appeared within the recovered yields for the different collection tube set ups, indicating that viscosity as well as drop distance both influenced cellular viability post sort and subsequent antigen recovery (these trends were seen repeatedly throughout sort optimisation). Some evidence for an inversely proportional relationship between drop distance and sort purity or yield was observed within the data (Table 4.2), i.e. as one decreases the volume of collection medium within the collection vessel the respective sort purity post recovery increases. This relationship was particularly apparent within the 15 mL BD Falcon tubes (Table 4.2) with the largest volume (10 mL) and the smallest volume (1 mL) resulting in a 97.4% and 98.3% yield respectively.

An additional inversely proportional relationship was also observed when evaluating the effect sample viscosity had on sort purity. Medium (RPMI 10% HIS and 1% Penstrep) was directly compared to pure heat inactivated serum as a collection media, utilising equivalent collection volume and vessel type. Medium demonstrated increased CD55 purity post recovery; both 3 mL collection volume within a 5 mL vessel and 5 mL collection volume within a 15 mL collection vessel were shown to have an increased CD55 expression, post recovery, when utilising medium as the collection solution (Table 4.2).

Table 4.2. Summary of the CD55 DAF surface antigen expression 72 hr following refined FACS within "Low Passage" TK6 cells. Single Cellular gating was used (P1) to enable a more accurate definition of surface expression within the context of presumptive PIG-A mutation analysis. Varied collection media constituency (viscosity) as well as size of collection vessle (drop distance) were assessed for ther impact on cellular viability and respective CD55 expression post sorting; HIS – Heat Inactivated Serum (N=1).

Sample ID	**Number of Single Cell Events (P1)**	**P1 as % of Total Events**	**Number of Cells Defined CD55 Positive**	**CD55 Positive (% of P1)**	**Number of Cells Defined CD55 Negative**	**CD55 Negative (% of P1)**
Instrument Calibration Standard	5255	52.6	23	0.44	5232	99.56
0.5 mL HIS (5 mL)	7699	77.0	7570	98.32	129	1.68
3 mL HIS (5 mL)	7343	73.4	7182	97.81	161	2.19
3 mL Media (5 mL)	7475	74.8	7350	98.33	125	1.67
Avg. 5 mL FACS Collection tube				**98.15**		**1.85**
10 mL HIS (15 mL)	6660	66.6	6488	97.42	172	2.58
5 mL HIS (15 mL)	7341	73.4	7160	97.53	181	2.47
5 mL Media (15 mL)	7535	75.4	7360	97.68	175	2.32
1 mL Media (15 mL)	7199	72.0	7075	98.28	124	1.72
Avg. 15 mL BD Falcon Collection Tube				**97.73**		**2.27**

The data displayed within (Table 4.2) as well as (Figure 4.6) also indicated that the collection vessel set up, i.e. either within 15 mL hard plastic tubes or smaller 5 mL softer plastic tubes played a role in cellular viability and hence sort purity. The 15 mL BD Falcon tubes were demonstrated to produce a slightly poorer purity (avg. ~97%) following recovery when directly compared to their 5 mL counterparts (avg. 98%). The optimum cellular viability, sort purity and a corresponding distribution analogous to the parental un-sorted cells was observed within the 5 mL collection tube containing 3 mL of medium (Figure 4.6). However, 0.5 mL of collection medium within the same vessel equally gave comparable sort purity post recovery.

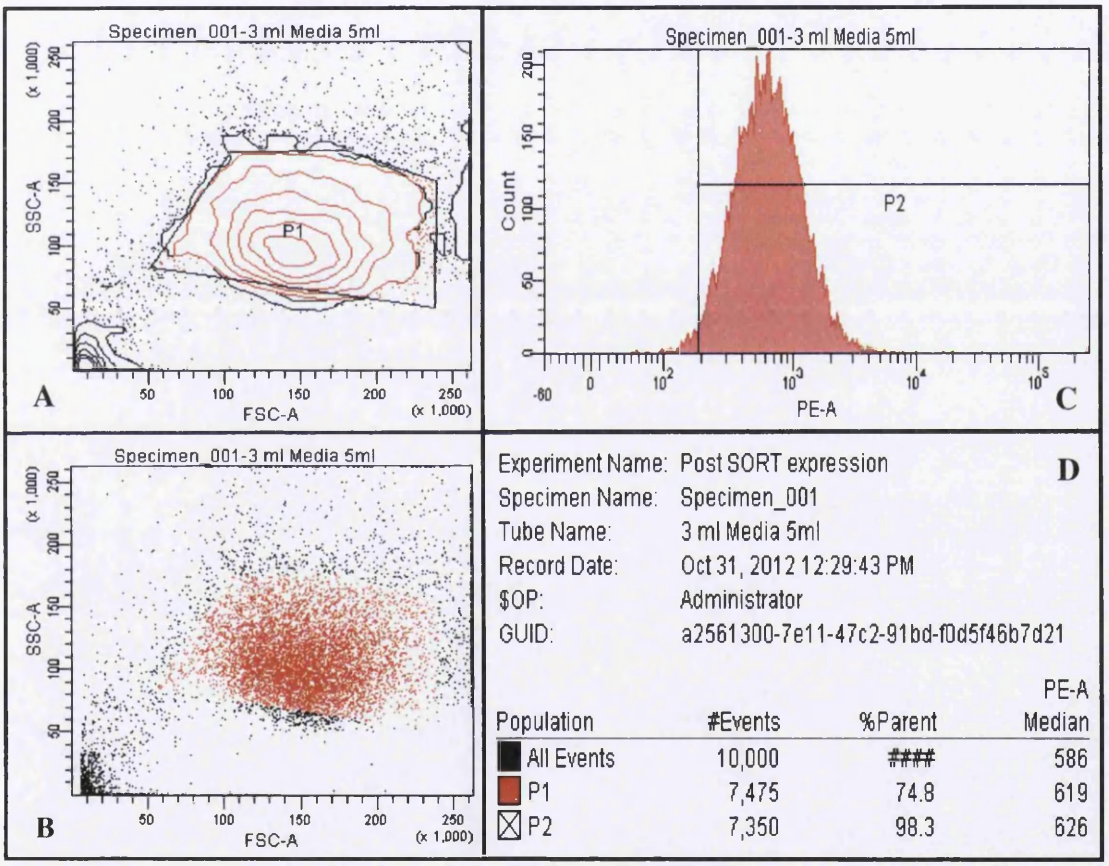

Figure 4.6. CD55 (DAF) surface antigen expression within "Low Passage" TK6 cells following Fluorescence Activated Cell Sorting (FACS) into a 5 mL FACS tubes containing 3 mL of RPMI 1640 culture medium. Single cell gating strategy "P1" included to best reflect CD55 expressioin within the context of subsequent *PIG-A* mutant analysis. "P2" is the threshold of presumed positivity. A) FSC-A vs SSC-A contour plot, B) FSC-A vs SSC-A dot plot C) CD55 signal within the "PE-A" detector and D) Statistics Summary table (N=1).

4.3.2.3 FACS Further Refinement for Optimum CD55 +ve Cellular Recovery

The data obtained following the final refinement of the FACS recovery method reinforced the subtle differences minor alterations within the set-up have on the resultant purity or sort efficiency of the overall process. Based on the previous findings, utilising 5 mL collection vessels in combination with varying volumes of culture medium as the collection solution generated highly comparable data without any specific sample generating profoundly unique results. FACS was observed to generate approximately 99% CD55 positive "Low Passage" TK6 cultures following 72 hr recovery (Figure 4.7). The effect sorting was exerting on the cell cultures in terms of cellular viability was deemed tolerable following the refinements to the protocol; cellular surface antigen assessment, to calculate sort purity, generated population scatter plots which conformed to previously observed untreated cultures. The recovered populations displayed minimal debris or cellular abnormalities when directly compared to un-treated control samples.

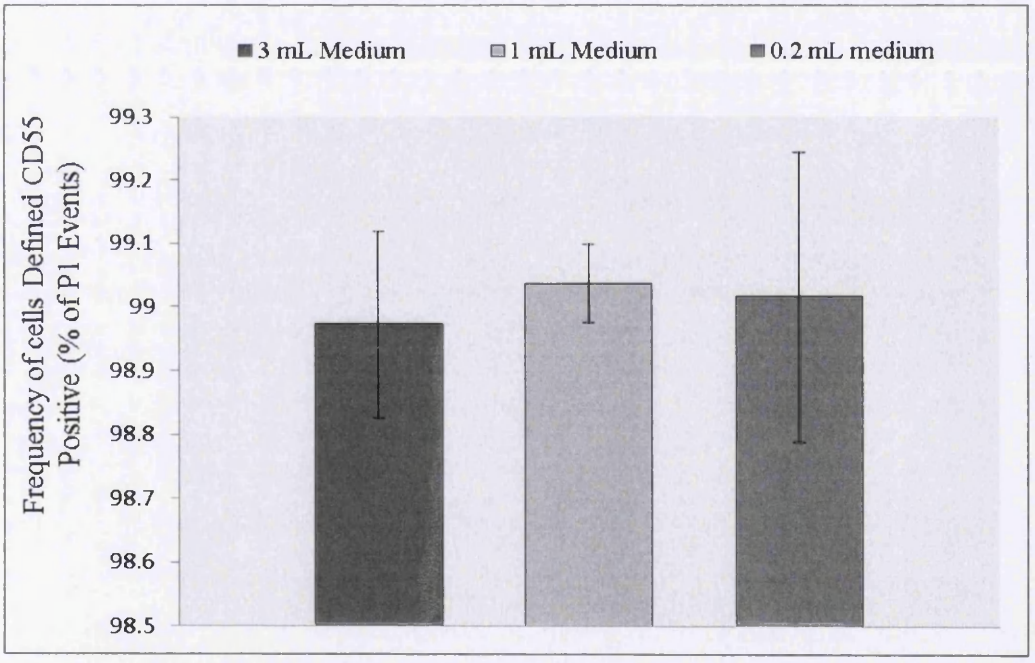

Figure 4.7. Relative expression of the CD55 (DAF) surface antigen, post 72 hr FACS enrichment and varying recovery methods, within "Low Passage" TK6 cultures following mouse-anti-human anti-CD55 R-PE treatment. Specific single cell gating strategies were included; based on FSC-A vs SSC-A profile as well as a FSC-A threshold value was set to remove debris. Detector sensitivity was established following ICS analysis (N=3, Error Bars ±1SD)

4.3.3 "Low Passage" TK6 Viability

4.3.3.1 Viability Data for "Low Passage" CD55 enriched TK6 cells

In order to assess the relative stability of untreated "Low Passage" TK6 cells, following compensation matrix establishment (Section 2.8.2), viability dyes were utilised to evaluate the basal levels of cytotoxicity within the populations. A direct comparison between unstained and viability dye stained "Low Passage" TK6 cells was utilised for investigation.

The results described a generally highly viable population with little evidence for elevated cytotoxicity. Subtle differences between the control ICS sample (unstained) and the three experimental samples were apparent; apoptosis (0.2%) and necrosis (0.113%) remained consistent across the samples, reflecting little cytotoxity. However, the percentage of dead cells was estimated at 4.5% within the experimental samples, a 9 fold increase over the untreated control. The experimental samples had an approximate 95.187% viable population, with no obvious signs of elevated levels of basal cytotoxicity, as to be observed within cultures experiencing adverse environmental stimuli (Figure 4.8). The described results reflect lower than expected levels of cytotoxicity, which were mimicked when microscopically assessed for phenotypic signs of damage, cells were demonstrated to be highly viable and appeared phenotypic indicator free, i.e. large cell clumps or loss of aspect ratio.

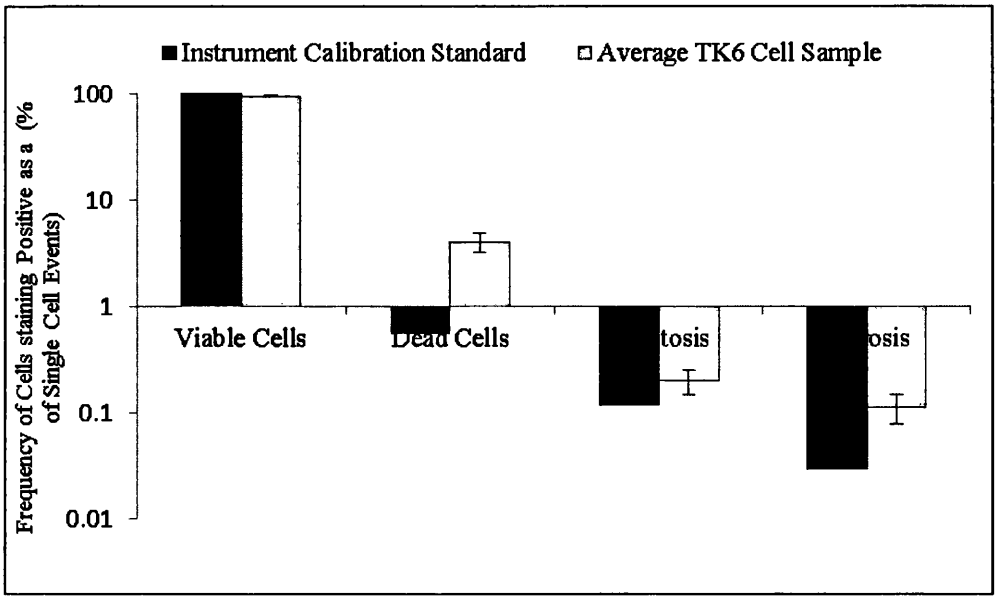

Figure 4.8. Viability assessment on "Low Passage", CD55 FACS enriched TK6 cells. Dead Cells; cellular events which stain positive for 7-AAD, Apoptotic Cells events which stain positive for Alexa Fluor 488™ Annexin V, Necrotic Cells; events which stain positive for both Annexin V and 7-AAD and finally, Viable Cells; are events which are not stained for any of the incorporated viability dyes (N=3, Error Bars ±1SD) ICS was utilised form the same homogenous "Low Passage" TK6 sample - Log y-axis utilised.

4.3.4 "Low Passage" TK6 preliminery *PIG-A* Assessment Utilising the CD55 Surface Antigen following Model Mutagen Exposure

Preliminary dose response experiments were carried out in order to assess the potential benefits associated with the refined assay design; novel "Low Passage" TK6 cells combined with FACS wild type enrichment, viability dye incorporation and CD55 utilised as the in-direct reporter for mutation phenotype. EMS was again chosen as the chemical for exposure, for the same reasons as stated previously (Section 3.4.3); all "*PIG-A* mutants" are events phenotypic of CD55 absence and therefore, are presumptive *PIG-A* mutants. Experimental design permitted the initial capture of 10,000 cellular events, which were then gated for single cell nature which restricted sample numbers to ~8,000 events.

All data generated following daily *PIG-A* mutation assessment were evaluated for normality and variance (P value $\geq$0.05) using the Shapiro-Wilk and Bartlett's Test respectively, carried out with DrSmooth within the R-Software Package (R-3.0.2, Free Software Foundation's GNU project). Following assessment, distribution and variance were defined in order to facilitate the correct statistical analysis; unique assumptions are made about the data within individual parametric and non-parametric statistical models, therefore, predisposing specific tests to specific data types. Subsequently, data was PROAST 38.9 modelled in order to define BMD_{10} and BMD_{L10} values and ensuing statistical analysis was undertaken within the R-software. Statistical analysis was implemented to state at what dose, if any, rejection of the Null hypothesis was to be assumed (P-value $\leq$0.05). At such a dose, variation of the viable phenotypic *PIG-A* mutant frequency was defined as a direct result of a significant factor and not as a result of chance.

Low dose EMS treatment of "Low Passage" TK6 cells, FACS enriched for the presence of the CD55 (DAF) cellular surface antigen, resulted in a sub-linear dose response for all days of phenotypic *PIG-A* analysis (Figure 4.9 A-D); Day 1 demonstrated no significant increases or decreases in average viable phenotypic *PIG-A* mutant frequency across the entire dose range, with an comparable relationship observed within the cytotoxicity measure (RPD) (Figure 4.9 A), data confirmed to be non-normally distributed (P value = 0.025). Day 2 data demonstrated that doses greater than and including the 5 µg/mL resulted in a noteworthy increase in the average cytotoxicity, with subsequent RPD values at 64.3 and 42.3 percent respectively. Variation was observed within the average phenotypic *PIG-A* mutant frequency across the dose range, however, significance was not achieved when compared to con-current negative control values (Figure 4.9 B). Data demonstrated to be normal (P = 0.83), with respect to distribution. Day 3 data mirrored the relationship observed within the previous daily analysis, with regards to average viable phenotypic *PIG-A* mutants, however, the cytotoxicity at the 5 µg/mL dose appeared to be negligible, with 62.7% RPD at 10 µg/mL (Figure 4.9 C); data shown to be non-normally distributed ($P = 3.4510^{-5}$)

Day 4 analysis showed that the top dose (10 µg/mL) appeared to induced an increase in the average number of viable putative *PIG-A* with respect to con-current negative control values, however, was proven to be insignificant (P>0.05). All doses tested

failed to induce statistically significant increases in the average number of CD55-deficient cells, similar to the previous three days of flow cytometry analysis. Cytotoxicity was shown to be similar to what was observed on day 2 with both 5 and 10 µg/mL doses eliciting substantial increases in cytotoxicity, 69.1 and 21.9% respectively. Data shown to be not normally distributed ($P = 3.51x10^{-7}$) and excessive intra dose variability was also observed, especially at the top dose (Figure 4.9 D), due to limited sample size.

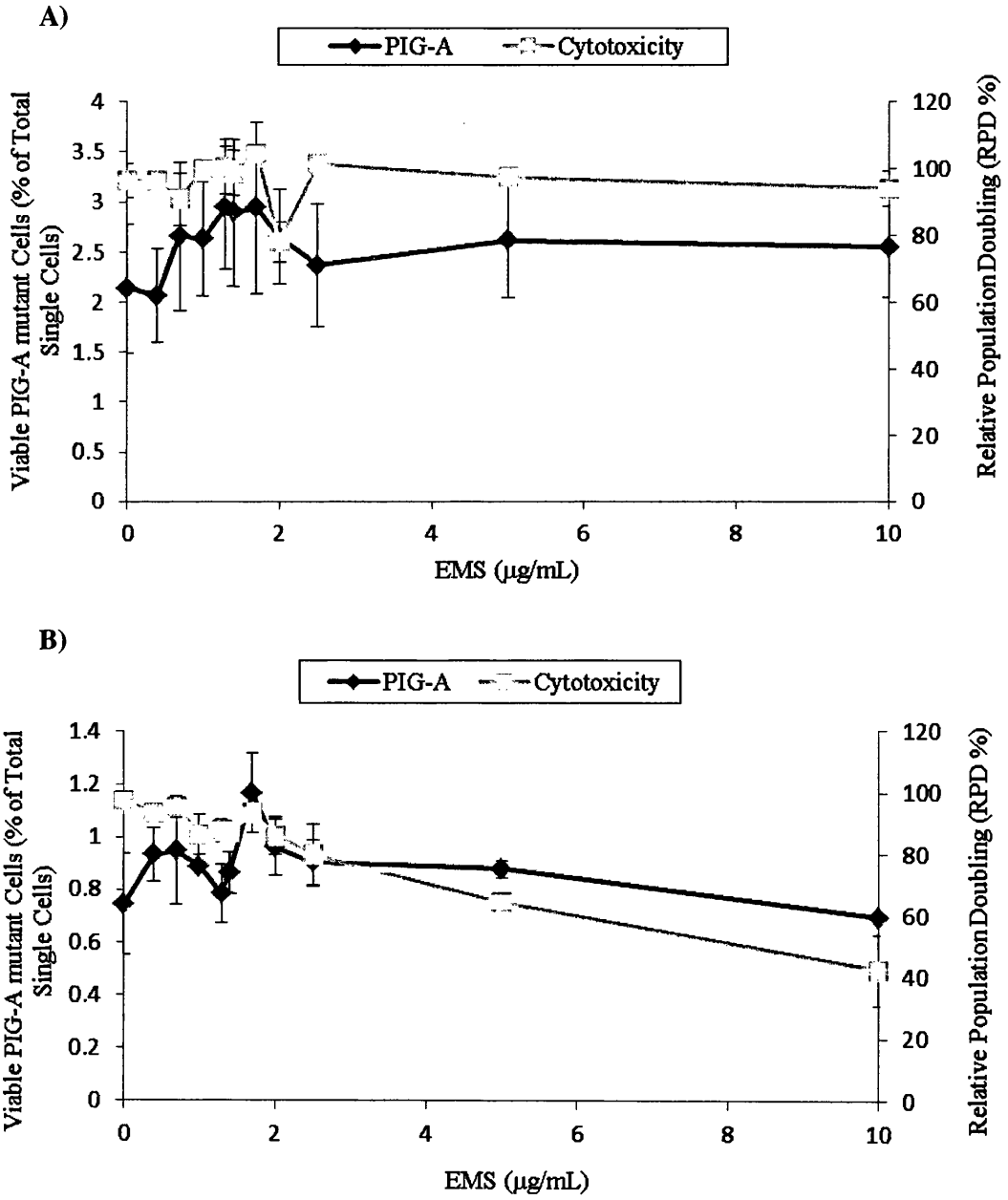

C)

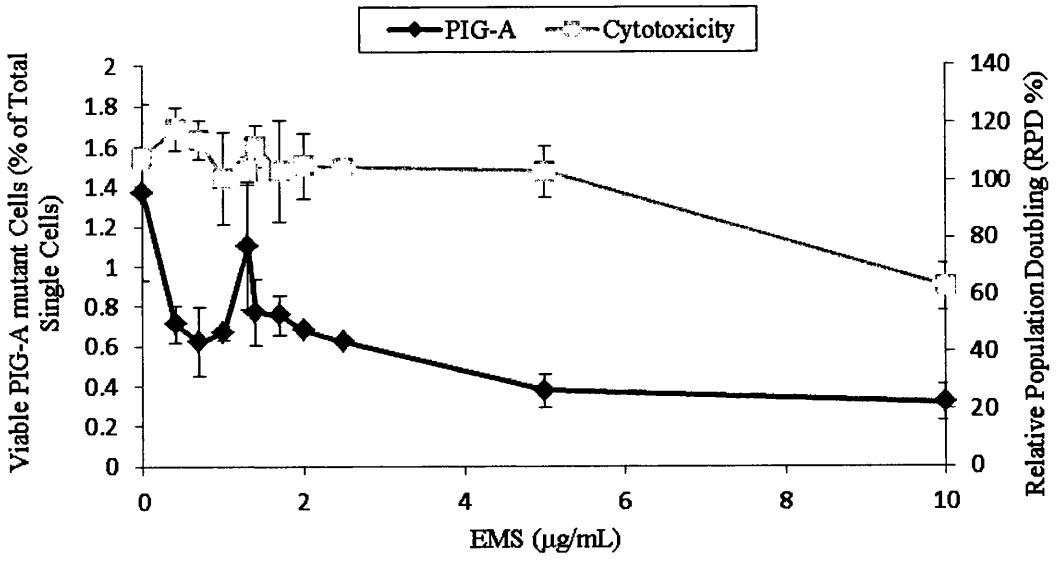

D)

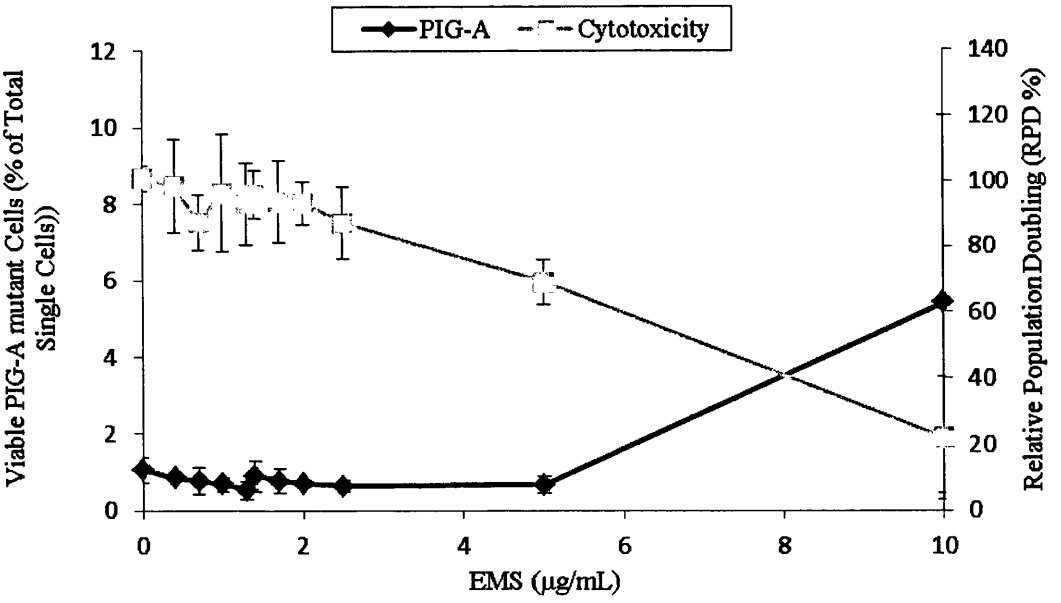

Figure 4.9 A,B,C and D - Days 1-4 frequencies of phenotypic *PIG-A* mutant "Low Passage" TK6 cells (FACS enriched) following 24 hr low dose EMS exposure, CD55 antigen utilised as reporter of mutation (Dunn's Test ($p < 0.05$*)((N=2, Error Bars ±SEM)) *PIG-A* mutants displayed as percentage of total single cellular events (0.1% *PIG-A* Mutants = 1 mutant x 10^{-3} cells) – A single replicate collected ~500 single cell events – Day 4 at the top dose.

4.3.5 Normal TK6, AHH-1 and MCL-5 Cell Line Characterisation

Initially, in order to evaluate the potential variability between the different selected human B-lymphoblastoid cell lines, terms of surface antigen expression, immunofluorescence staining was employed to assess the expression of well characterised cellular surface antigens on the extracellular surface. Fluorescence Aerolysin (FLAER), B-lymphocyte activation marker ((BLAST-1)/(CD48)) and Protectin (CD59) as well as Decay Accelerating Factor (DAF/CD55) were all assessed, due to their potential as potential future candidates for in-direct reporters of phenotypic *PIG-A* mutation.

Primarily, "Low Passage" and normal TK6 cell's surface antigen expression was directly compared to generate a baseline for further surface antigen expression investigations as well as potentially identify additional GPI-AP candidates. Briefly, "Low Passage" cells were demonstrated to generate very poor staining efficiency within all candidates, post antibody exposure, and discontinued from use. Whereas, normal TK6 cells exhibited comprehensive average surface staining following FLAER ~75%, CD48 ~73% and CD55/59 ~ 78% exposure (Appendix Section 4.3.5).

The comparable AHH-1 cell line was demonstrated to have more comprehensive FLAER staining (75.2%), at the top concentration tested (2.5 µg/mL), significant CD48 staining (83.45%) and extensive CD55/59 expression (99.2%) (Figure 4.10). Minimal variation was observed within the culture and cells were microscopically assessed for signs of distress prior to assessment. The cells demonstrated no signs of adverse health, in terms of aspect ratio and agglomeration status and lent themselves well to the preparative stages required for staining.

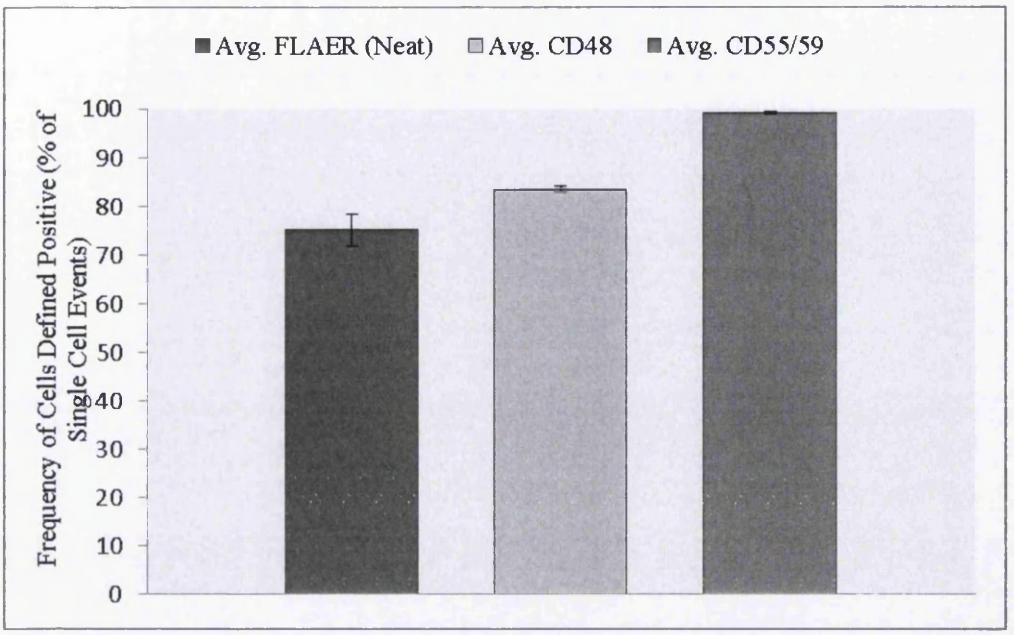

Figure 4.10. Average cell surface marker expression of the parental control AHH-1 cell population. FLAER (stock conc) Alexa Fluor 488 ™ conjugate, CD48 phycoerythrin conjugate and CD55/59 phycoerythrin conjugate fluorescent dyes utilised and data captured within their respective detectors. (~10,000 single cellular events) (N=3, Error Bars ±1SD).

However, the MCL-5 cells demonstrated the most extensive comprehensive staining, approximately 93.5% for FLAER, which facilitated the investigation of a 1:1 dilution (52.2%). CD48 was shown to be highly promising with an average expression of 92.15% and finally, when utilised in tandem CD55/59 were demonstrated to show 99.8% surface antigen expression within the cell line (Figure 4.11).

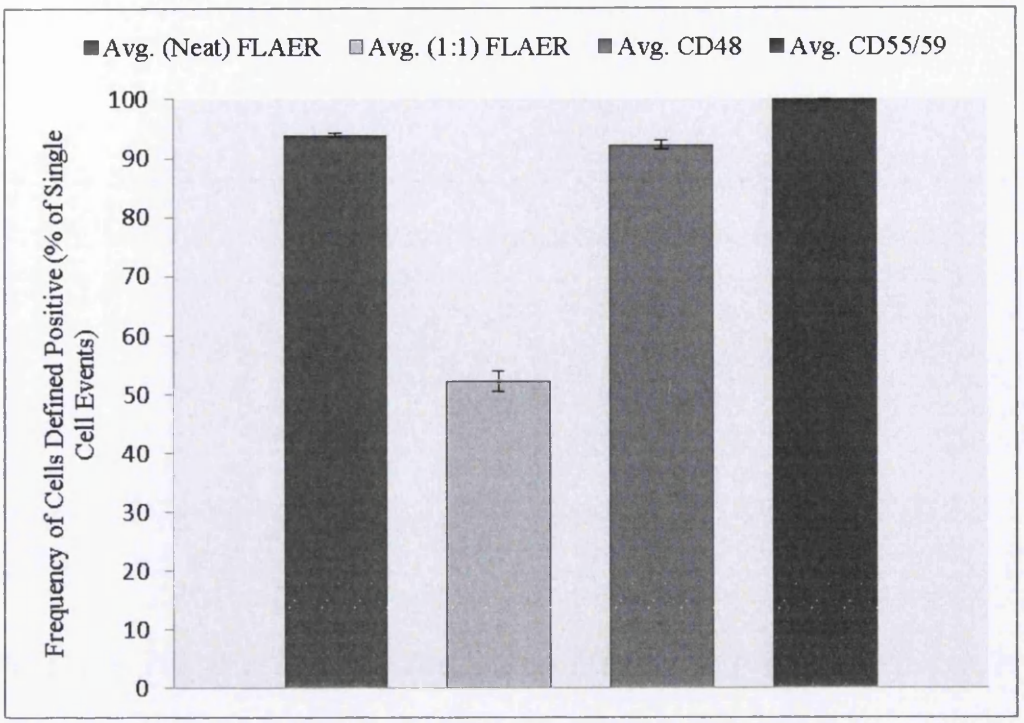

Figure 4.11. Average cell surface marker expression of the parental control MCL-5 parental population. FLAER (stock conc) and FLAER (1:1); Alexa Fluor 488 ™ conjugate, CD48; phycoerythrin conjugate and CD55/59; phycoerythrin conjugate fluorescent dyes utilised and data captured within their respective detectors. (~10,000 single cellular events) (N=3, Error Bars ±1SD).

4.3.5.1 Western Blotting –-Sodium Dodecyl Sulphate – Poly-Acrylamide Gel Electrophoresis (SDS-PAGE)

Prior to Western blot analysis and subsequent Chemidoc™ visualisation of the protein of interests, specific relevant house keeper proteins were initially screened for relevance and suitable localisation and elevated abundance within all cell lines tested. Human B-actin, one of six isomers for the constituently expressed protein molecules integral in cellular mobility and structural integrity, and Histone H3, one of five protein molecules associated with the structure of chromatin molecules, were selected as the cytoplasmic and nuclear house keeper proteins respectively, due to their abundant and comprehensive expression. B-Actin and Histone H3 were therefore, utilised within the subsequent experiments, to maintain data integrity.

Initially, P21 was demonstrated to be located in both the cytoplasmic and nuclear fraction of the protein extracted from each of the cell lines assessed, and deemed to be present at suitable quantities to facilitate future detection within any of the potential in vitro *PIG-A* assay cell line platforms (Figure 4.12). However, the relative band densities were significantly varied between cell lines, with little intra sample variance; AHH-1 demonstrating comprehensive p21 presence, noticeably greater than both MCL-5 and TK6 cells (Figure 4.12). TK6 were shown to exhibit the smallest amount of the p21 protein constitutively expressed within untreated cells, in either cytoplasmic or nuclear fraction, when directly compared to the other cell lines. Housekeepers B-actin (cytoplasmic) and Histone H3 (nuclear) were found to be extensively abundant across all cell lines, regardless of protein localisation, during western blott analysis.

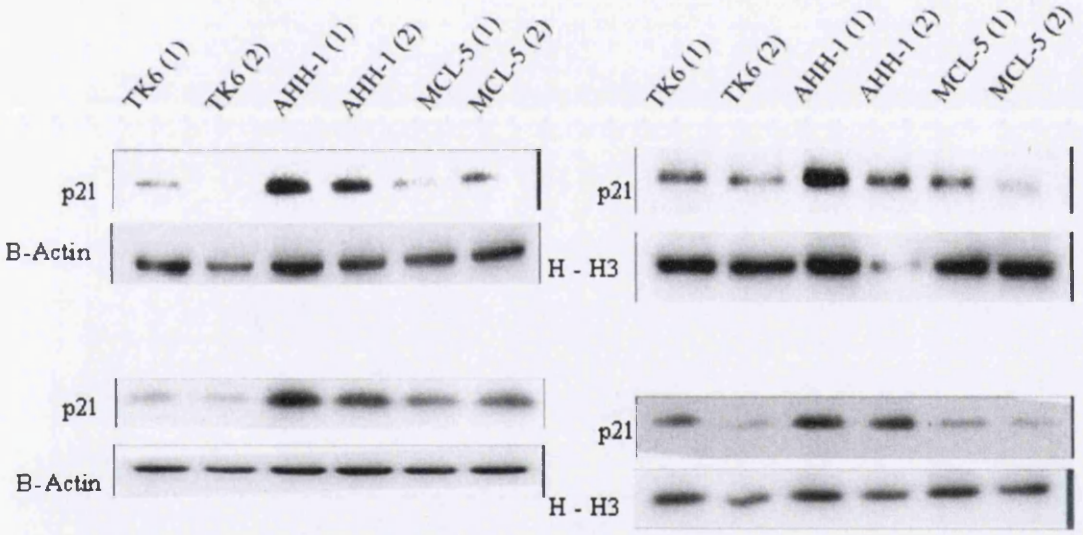

Figure 4.12. Relative protein band densities following primary anti-p21 and secondary-HRP conjugate antibody probing and subsequent UV exposure within Chemidoc™ imaging; A) Nuclear protein and B) cytoplasmic protein extracted from untreated control human lymphoblastoid cell lines. B-Actin (cytoplasmic) and Histone H3 (H-H3 (nuclear)) were utilised as housekeeper proteins.

P53 protein was shown to be present in both cytoplasmic and nuclear MCL-5 protein fractions following extraction, however, at noticeably different quantities. Protein band density within the nuclear fraction was far greater than the comparable cytoplasmic fraction (Figure 4.13), as to be expected with a nuclear transcription factor; little variance was apparent between analogous samples.

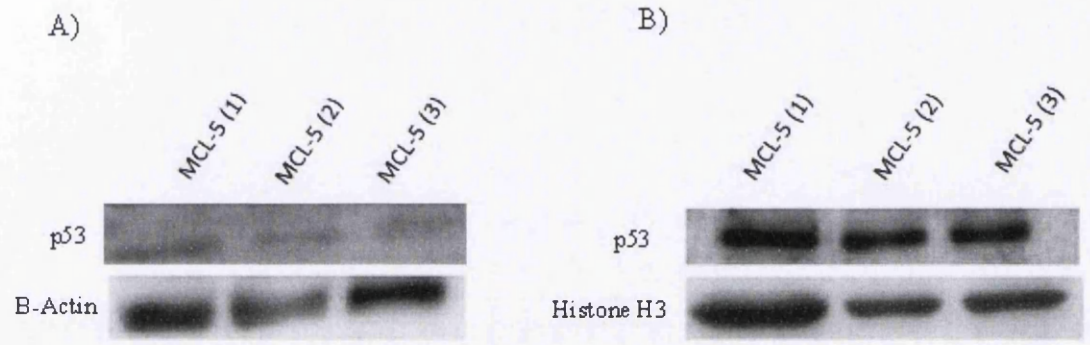

Figure 4.13. Relative protein band densities following primary anti-p53 and secondary-HRP conjugate antibody probing and subsequent UV exposure within Chemidoc™ imaging; A) Cytoplasmic protein and B) Nuclear protein extracted from untreated control MCL-5 cells. B-Actin (cytoplasmic) and Histone H3 (nuclear) were utilised as housekeeper proteins.

Following the initial investigation into p21 and p53 localisation, both proteins were evaluated across all three potential future cell lines for their respective constitutive expression and hence, protein band densities following western blot analysis; data was normalised against B-actin and histone H3 respectively for cytoplasmic and nuclear fraction derived proteins and displayed relative to the MCL-5 cell line protein densities (Figure 4.14). Cytoplasmic p21 expression was demonstrated to be present and comparable across the cell lines assessed, however, nuclear p21 expression was demonstrated to be significantly higher within the AHH-1 cell line, exceeding 2 x fold higher than comparable MCL-5 values. P53 protein levels were assessed and shown to be highly similar across all three cell lines, however, p-p53 levels for both TK6 and AHH-1 cells were greater than 2 x fold higher than the comparable MCL-5 cells.

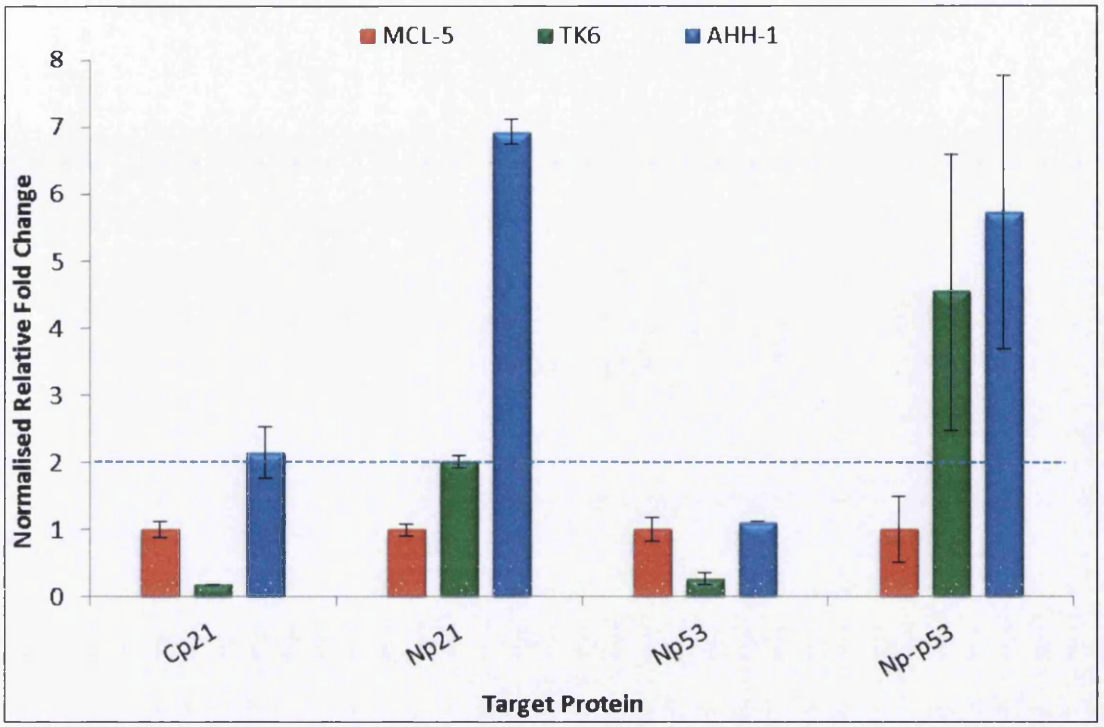

Figure 4.14. Average relative protein band densities, normalised against con-current house keeper data, following primary p21, p53 and p-p53 and secondary HRP-conjugate antibody probing and subsequent UV exposure and Chemidoc™ imaging. Cytoplasmic and nuclear protein extractions are represented by "C" and "N" respectively (N=2, Error Bars ±SEM).

In order to better evaluate the assessed cell line's p53 functionality and hence ability to react to genotoxin exposure, acute mitomycin C treatment was implemented and the normalised as well as relative protein quantities of p21 and p-p53 were detected within total protein extracts. TK6 cells demonstrated insignificant variations in the relative p-p53 abundancy with respect to MMC dose, however, a significant dose dependent relationship was apparent with p21 protein levels (Figure 4.15). AHH-1 cells demonstrated comprehensive dose dependent correlations for both p-p53 and p21 protein levels over the MMC dose range (Figure 4.15), and finally, MCL-5 cells displayed an analogous response to that described within the AHH-1 cell line, with a slight difference in regards to truncated dose response for the p21 expression at the top dose tested, 0.15 µg MMC. In respect to the band densities following normalisation, each cell line had comparable amounts of house keeper expression; the MCL-5 cell line displayed significantly lower quantities of proteins within the extract when compared to both TK6 and AHH-1 cells.

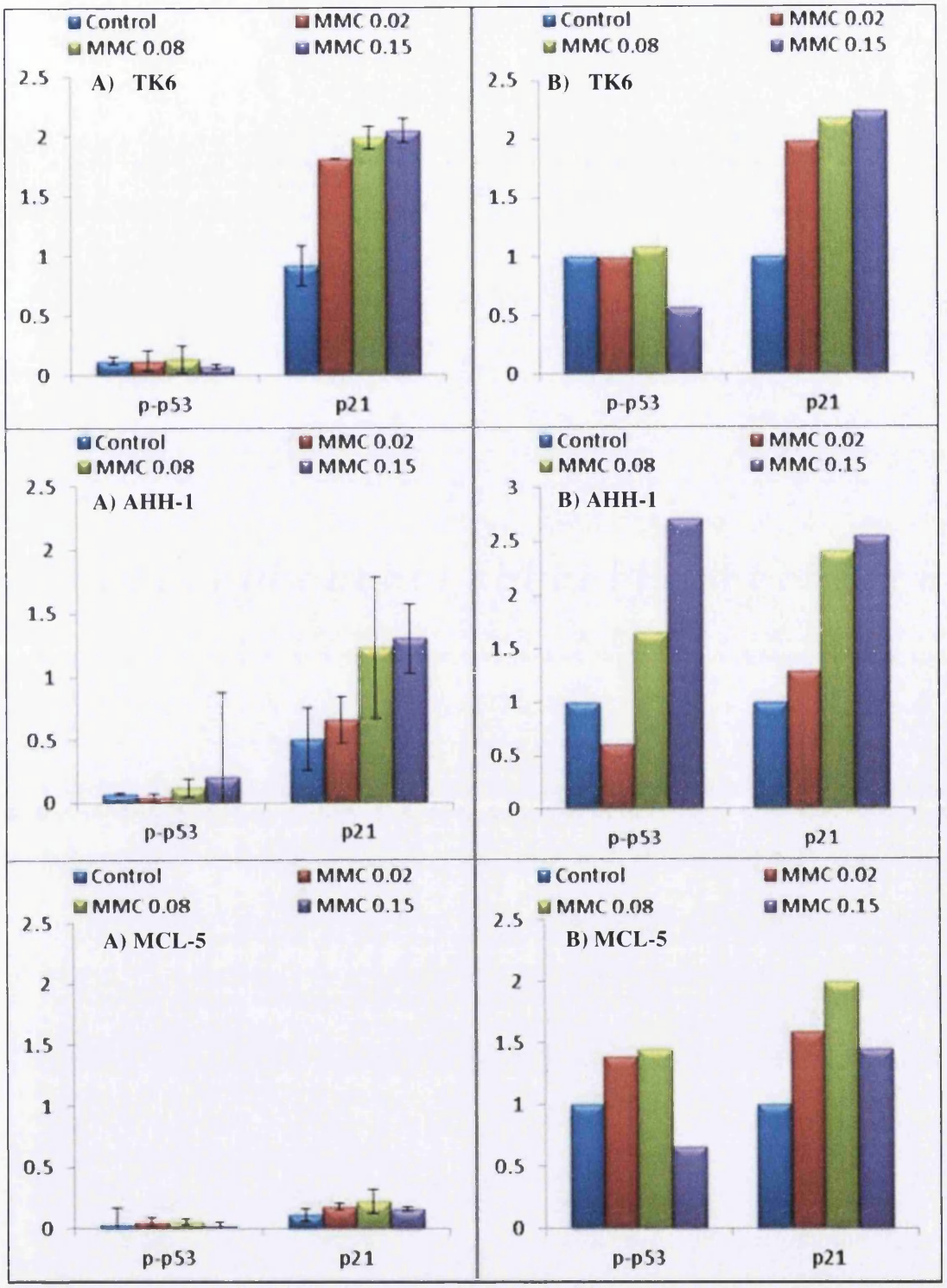

Figure 4.15. Average relative protein band densities following acute 4hr MMC exposure, total protein extraction, and subsequent imaging on the ChemiDoc™ platform. p21 and p-p53 proteins were assessed via the use of primary antibodies in conjunction with secondary HRP-conjugate and UV exposure; A) data was initially normalised against house keeper band densities (H-H3 and B-actin respectively) (Error Bars ±SEM) and B) presented as average relative fold change with respect to the untreated control for the respective human lymphoblastoid TK6, AHH-1 and MCL-5 cell lines.

4.3.5.2 Quantitative Real-Time Polymerase Chain Reaction (qRT-PCR)

Prior to quantitative real time PCR assessment of the target gene, specific relevant house keeper genes; comparable constituently expressed genes displaying elevated transcription rates, were optimised to ensure their comprehensive expression within all cell lines tested. Human receptor like protein-19 (RLP-19) and hypoxanthine phosphoribosyltransferase (HPRT) demonstrated the most consistent expression across all the cell lines, when compared to common housekeepers B-Actin and Histone H3, and therefore, we utilised within the subsequent experiments to ensure integrity

Quantitative real time PCR assessment, SYBR® green, was carried out on all three cell lines to more accurately determine the relative quantity of p21 constitutive and induced gene expression in response to MMC treatment. P21 was shown to constituently be transcribed within all three cell lines assessed (Figure 4.16 A), however, TK6 was determined to approximately express greater than 3 x fold more p21 than the comparable MCL-5 or AHH-1 cell types (Figure 4.16 B).

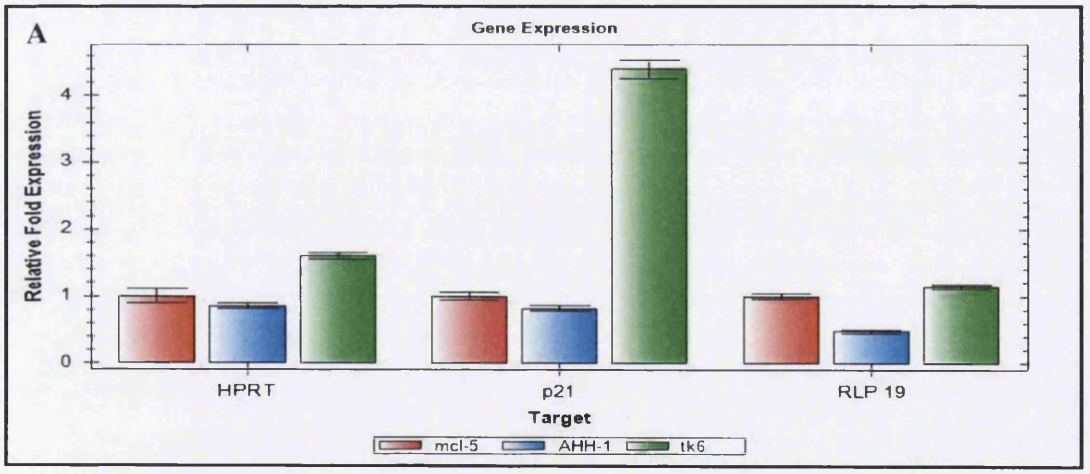

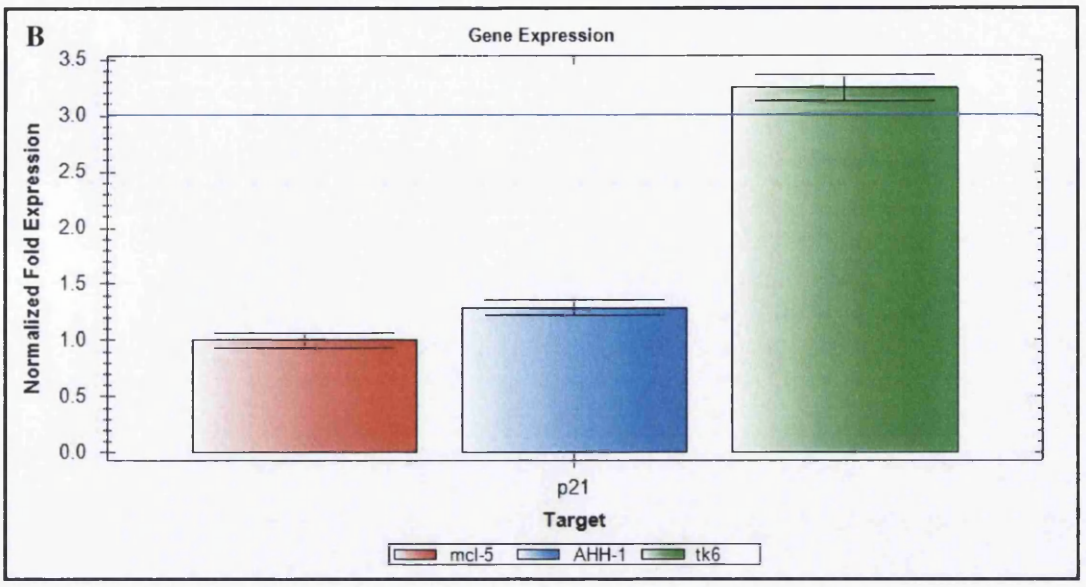

Figure 4.16. The relative expression of the (CIP1/WAF1) p21 gene across the human lymphoblastoid AHH-1, TK6 and MCL-5 cell lines; A) Expression data normalised against HPRT and RLP19 house keeper genes and B) Displayed as relative fold change when compared against the MCL-5 expression data (N=3 technical replicates, Error bars ±SD)

Following acute 4 hr MMC exposure, the TK6 cell line was shown to exhibit a typically dose dependent relationship, with dose being significantly positively correlated to amount of induced p21 expression (Figure 4.17); each increase in MMC dose resulted in a corresponding increase in p21 transcription. Both MCL-5 and AHH-1 were also shown to produce a similar relationship, with a strong correlation to dose increment and p21 induction, however, the top dose within AHH-1 and the top two doses within the MCL-5 data demonstrated shortened p21 expression; therefore, the dose responses appeared truncated at the higher doses (Figure 4.17).

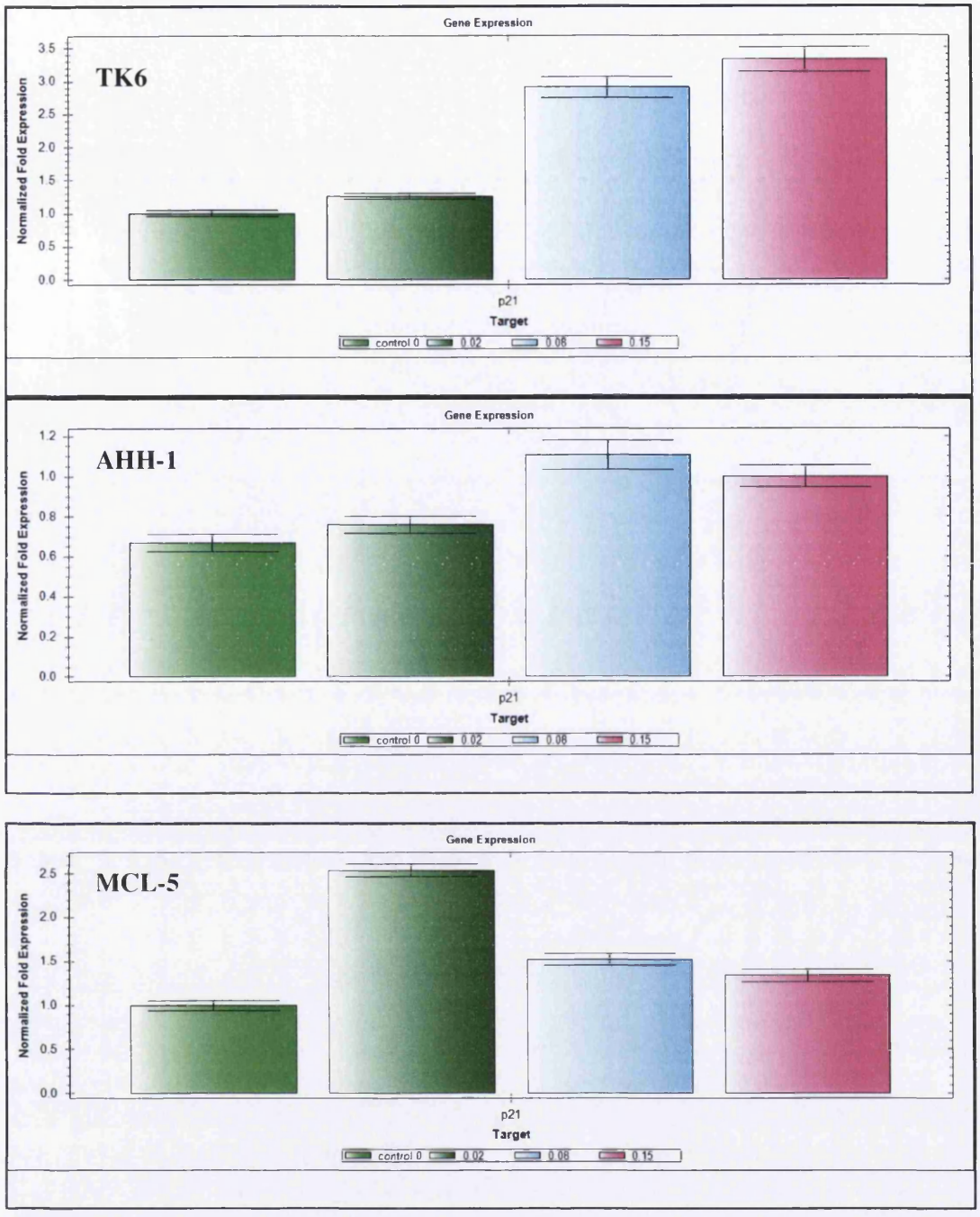

Figure 4.17. The normalised and comparable relative expression of the (CIP1/WAF1) p21 gene across the human lymphoblastoid AHH-1, TK6 cell lines and MCL-5 cell lines following acute 4hr MMC exposure (N=3, technical replicates)(Error bars ±SD).

4.4 Discussions and Conclusions

Human B-lymphoblastoid cell lines feature heavily within in vitro genetic toxicology assays; they provide sensitivity, apoptosis compatibility, p53 functionality, suspension growth characteristics and a variety of additional benefits [75, 113-115]. However, due to the nature of cell line distribution and increased risk of genomic instability associated to immortalised cell line usage [292], more prominent in academic institutes. The lack of standardisation has led to increasing variation, especially prominent within variable genetic toxicology end-point backgrounds, observed within comparable data sets [293]. To combat this, regulators have put forward the proposed use of specific cell lineages in tandem with specific genetic toxicology end points [113-115] and tentatively a homogenous cell sample for testing has been distributed to ensure inter-laboratory compatibility.

4.4.1 GPI-AP Expression Assessment within "Low Passage" TK6 Cells

"Low Passage" Epstein-Barr virally transformed human B-lymphoblastoid TK6 cells, originally isolated from the WIL-2 cell line supplied by Masa Honma, National Institute of Health Sciences (NIHS); were believed to provide more stable growth dynamics, a characterised reference karyotype and standardisation through trialled mass distribution to participating laboratories. Combining genomic stability with predicted assumed increased phenotypic stability, lower sensitivity to apoptosis and hence, reduced frequency of putative false positive events was believe to increase assay predictive ability and sensitivity to detect mutagens. Initially, GPI-AP surface markers were immuno-fluorescently assessed for presence and potential usage, as in-direct reports for mutation at the *PIG-A* gene locus, within the proposed in vitro assay design.

The resultant immuno-fluorescence flow cytometry data showed negligible CD59 expression on the surface of the "Low Passage" TK6 cells, grown under recommended culture conditions (Figure 4.2 – 4.3). In order to validate the functionality of the utilised antibody, the conventionally used normal TK6 cell line was assessed in a homogenous manner to estimate CD59 expression on the cell

surface; significant presence of the CD59 antigen was observed (Figure 4.3). In an attempt to identify a suitable GPI-AP candidate for the trial usage of the "Low Passage" TK6 cell line within the assay design, an additional marker CD55, currently implemented in clinical screening for the human condition PNH [294], was utilised and found to be highly expressed within the low passage TK6 population (Figure 4.4).

CD55 (Decay Accelerating Factor (DAF)) and CD59 (Protectin) are complement regulatory proteins which provide a vital function within mammalian species [294]; in brief, CD55 increases the decay rate of complement proteins and inhibits the formation of the C3 convertases which initiates and propagate autolysis of haemopoetic tissue [152]. CD59 prevents the terminal polymerization of the membrane attack complex (MAC) which facilitates haemolysis and thus, prevents uncontrollable autolysis [294]. Therefore, due to their interrelated roles and apparent analogous function there is no obvious reason why there should be a significant difference in the presence of either solely GPI anchored protein on the surface of a specific cell line. To make the situation more complex, the unexpectedly low surface antigen presence was observed within the proposed stable "Low Passage" TK6 cells and not the presumed high passage TK6 cell stock (Figures 4.2 - 4.4).

Human lymphoblastoid cells are not implicitly involved in the transport of oxygen around the body and have a much shorter life cycle than erythrocytes [295]. Therefore, they do not require the critical presence of either CD55 or CD59 on their respective cell surfaces to prevent complement mediated haemolysis [141]. However, this data suggests that each cellular antigen potentially has additional roles outside of complement mediation and thus, one antigen is more essential than the other, reflected in the apparent discrepancies between CD55 and CD59 expression. Recent literature has described a novel role for CD55 in granulocyte homeostasis and anti-bacterial host defence [296], providing an additional necessity for this specific maintained comprehensive surface expression.

Lack of CD59 presence within the "Low Passage" TK6 cells is very confounding, as a higher passage of the identical sample cell type apparently displays the antigen at a comprehensive rate within the population (Section 4.3.1). Initially, this data was considered erroneous; however, was un-officially re-enforced through the apparent

lack of expression demonstrated by an additional research laboratory. If the results were inverted, i.e. the high passage displayed lack of expression, the most likely potential causes of this would be an acquired mutation as a result from prolonged culture time [297], reflecting generalised genomic instability within the cell line. However, as it is the "Low Passage" showing minimal expression, the potential origin of the two cell stocks are questionable, or alternatively the higher passage have acquired an up-regulating mutational event within the CD59 gene, quite unlikely. The lack of expression does however, fit a lymphoblastoid model due to the redundancy of this specific complement mediating surface antigen; further investigation into analogous cell lineages and surface antigen expression is required to provide a more adequate conclusion about CD59 surface antigen discrepancies from the data.

The primary conclusion drawn from this section is that the CD55 antigen demonstrated sufficient surface antigen expression to warrant trial with the in vitro *PIG-A* assay design; the expression was borderline to require mutant depletion, however, deemed to be satisfactory for preliminary assessment due to the intended modifications to the design.

4.4.2 CD55 Antigen Optimisation using Fluorescence Activated Cell Sorting (FACS)

Following on from the initial work completed in the first results chapter (Section 3.3.2), it was clear that FACS had the potential of delivering a mutant depletion method with limited disadvantages. However, when initially optimised, the standard able to be obtained wasn't sufficient in terms of mutant depletion (Section 3.4.2), i.e. the remaining number of presumptive spontaneous phenotypic *PIG-A* mutants was too large. Estimated spontaneous background mutant frequency at the *PIG-A* locus was therefore, perceived to be much greater than comparable analogous X-linked gene loci [75], due to the presence of this substantial GPI-AP negative subpopulation. Consequently, the initial preliminary dose response experimentation was undertaken utilising clonal expansion as the foundation for enrichment and

resulted in qualitative dose response modelling (Section 3.3.3). However, the scope of further in-depth investigation was realised and FACS was temporarily suspended for evaluation in latter experiments.

FACS in brief, utilises an induced charge on a particle to deflect the trajectory of said particle, post analysis, to facilitate isolation and capture (Section 2.8.3). FACS, similar to all techniques, is limited to some extent by a number of equipment related factors, for example, voltage regulation and systematic pressurisation. As a direct result of this, inter-sample variability can be problematic, however, this can be minimised with regular maintenance and routine servicing. Additional to these flow cytometry specific issues, the perpetual problem associated with FACS is that the experimental conditions required for sample processing are unique to that specific sample, and are highly changeable [298]. Consequently, the user must be proficient in designing a robust protocol taking into account the specific needs of said sample type. Primary samples, even though highly inconstant in terms of behaviour, are often robust and are able to tolerate inconsistencies within the sorting procedure. However, sensitive immortalised human cell lines are much more problematic and require much greater attention to detail in order to maintain a high standard of sorting efficiency.

The resulting initial optimisation data demonstrated that using a larger drop distance within a smaller collection tube, i.e. minimising the collection liquid volume and utilising a collection medium with a minimal viscosity i.e. pure RPMI 1640 (negligible serum proteins) generated the optimum sort purity following recovery (>90%). However, in terms of a mutation assay this level of enrichment was still significantly sub-standard and therefore, further optimisation and/or protocol tweaking was needed. After an additional round of protocol modification, the results for the experiment demonstrated that there appears to be no further significant increase in FACS efficiency based on the drop, distance, collection medium viscosity and/or collection vessel (Section 4.3.2). In brief, increasing the drop distance provides additional buffering time for the velocity of the particle to slow, due to air resistance, prior to contact the with collection vessel and/or collection medium. In addition to this, decreasing surface tension via limiting the serum composition of the medium, contrary to published literature [299], as well as the density of the plastic polymer comprising the collection vessel, have similar positive

effects on viability. However, what appeared to increase the efficiency to >99% was the combination of numerous other additional factors, i.e. the period of time which the cells remain in solution, the rate of respiration occurring and hence the apoptosis status of the population.

The conclusions able to taken from this section of work are that there is no single or small sub group of factors which influence the efficiency of sorting, but a much more complex holistic approach is required in order to facilitate the predicted optimum yields in terms of mutant depletion/wild type enrichment [300]. However, additional factors, which aren't as apparent as their physical counter parts, which appear to maintain and regulate the high end efficiency attained are highly crucial and can be thought of as two separate sub groups; i) flow cytometry related, focussed on the software and hardware abort rates and ii) tissue type related and reflects directly on the sample to be processed, for example pH imbalances inducing apoptosis sensitivity (Appendix Section 4.4.2).

Further optimisation is required in order to assess the finalised degree of mutant depletion within parental populations. Irrespective of how problematic this appears, especially considering the sensitivity of the cell line to apoptosis, the use of conditioned medium, medium extracted from a well-established homologous cell culture, keeping the pre-sorted cell on ice and maintaining the collected populations at 37°C as well as adjusting the collection volume are potential further modification which may improve yield further. However, when compared to a chemically driven mutant depletion [75] it is unlikely that complete depletion will be obtained, however, reducing the pre-existing mutant numbers to a range to facilitate quantitative dose response modelling and hence compound screening may be applicable. Therefore, currently FACS is able to enrich a population for preliminary qualitative dose response modelling; however, low dose quantitative remodelling within the current assay design requires a level of sensitivity currently un-obtainable.

4.4.3 "Low Passage" TK6 Viability

4.4.3.1 Viability Data for "Low Passage" CD55 enriched TK6 cells

Prior to preliminary *PIG-A* dose response analysis, the "Low Passage" TK6 cells were assessed for viability following cytometer preparations. The reason for this was to look for a robust cell line, not overly sensitive to both intrinsic and extrinsic apoptotic induction [8, 276], which could be a potential future platform for an in vitro *PIG-A* mutation assay. The data displayed that the "Low Passage" TK6 cells had minor levels of cytotoxicity, typically lower than comparable cell lines, and thus generally were presumed very "healthy", in terms of numbers of cells displaying positivity for apoptosis, necrosis or cell death (Section 4.3.3). The number of cells displaying positive signals for 7-AAD uptake and hence a direct reflection of loss of cellular membrane integrity were the only sub category of non-viable cells to increase when compared to an unstained control samples (Section 4.3.3). Due to the absence of neighbouring fluorophore usage, a compensation matrix was deemed unnecessary for use, as well as a comprehensive single stained positive control assessment, there was little evidence to suggest that the viability was underestimated. Therefore, "Low Passage" TK6 cells appear to be highly stable pre-treatment, in terms of viability and phenotype, as well as consistent in their dose depended increase in cytotoxicity when exposed to chemical exposure (Appendix Section 4.5.3.1). Due to the above observations the cell line was deemed appropriate for use in conjunction with the CD55 cellular surface antigen within the current in vitro *PIG-A* assay design.

4.4.4 "Low Passage" TK6 preliminery *PIG-A* Assessment Utilising the CD55 Surface Antigen following Model Mutagen Exposure

"Low Passsage" TK6 cells were demonstated to be highly sensitive and stable (Section 4.3.3), via the generation of robust and reproducible dose responses

following cytotoxic exposure (Appdendix 4.5.3.1). In addition, when assessed for GPI-AP expression, the CD55 (DAF) cellular surface antigen was defined to have significant conserved expression across the cellular membrane of the parental cultures (Figure 4.4). Combining both the relative genomic stability and broad expression of a potential in-direct reporter candidate for *PIG-A* mutation status, as well as the incorporation of preliminery viability dyes, this particular combination was assessed for refinement of assay design.

The results were comparable, as observed when using the previous assay design, with the CD59 antigen as the reporter for mutagenesis. A superficial increase in cytotoxicty was observed at the top dose daily following the initial 24 hr recovery post treatment (Figure 4.9 A-D). On the final day of analyisis, Day 4, the number of viable presumptive *PIG-A* mutants at the top dose tested (10 µg/mL) was shown to marginally increase, however, due to the limited sample size and excessive variability observed between replicates it was deemed not significant ($P>0.05$)(Dunn's T-Test). Therefore, no doses across the concentraton range tested were demonstrated to significantly increase the number of viable presumed *PIG-A* mutants, as defined by CD55 absence (Figure 4.9 A-D). The background spontaneous mutant frequency, or pre-existing number of phenotypic mutant cells, was shown to be signficiantly higher utilising this reporter for mutation; as high at 2% on specific days of analysis, when compared to the CD59 antigen. Even following the addition of preliminary viability dyes, the resulant sensitivity was considered unacceptible when compared to validated comparable in vitro mammalian cell assays (200 x fold higher). Thus returning to the predicament of utilsing an alternative enrichment methodology within the assay design to deplete pre-existing phenotypic *PIG-A* mutants prior to assessment, to enable both spontanoeus mutation and induced mutant frequency estimation [301].

The descrepency between the analagous CD55 and CD59 data sets can be attributed to a number of different factors and hence, limited conclusions can be taken from this preliminery data. However, that being said it does raise the question of the origins or identities of the orignal mutants as defined by the CD59 dose response data. Following the incorporation of the viability dyes, into the assay design, the number of viable presumed *PIG-A* mutant events did not increase over the dose range tested (Section 4.3.3 – 4.3.4); understandably, the CD55 antigen may be

defective within this cell line as a reporter, due to the presence of a potential single pass membrane isomer [154], as well as the cell line inself not being appropriate for assessment, but there is potential for intial miss-classification of presumed mutant events within the CD59 assessment (Section 3.4.5). This potential miss-classification is re-infored by the intial viability assessment of the presumptive *PIG-A* mutant population (Section 3.3.5). Further clarification of presumed *PIG-A* mutant event will be required prior to further conclusive remarks made, however, the data generated does allude towards investigating alternative cell lines and reporter combinations in the aid of finding a logical combination, homologous to the CD59 and erythrocyte combinaiton observed within the in vivo rodent Pig-a assay [91, 161, 180, 302].

4.4.5 Normal TK6, AHH-1 and MCL-5 Cell Line Characterisation

Dose response data thus far has highlighted the critical need for mutant depletion prior to *PIG-A* assessment; lowering the number of pre-existing spontaneous mutants, prior to chemical exposure, facilitates a higher sensitivity to smaller fold increments in mutant induction [71]. However, due to the limitations currently observed when utilising "Low Passage" TK6 cells, alternative human cell lines were assessed for GPI-AP marker expression, and hence in-direct reporters for mutation. The aim of this section of work was to identify a potential cell line which had a sufficiently low pre-existing number of phenotypic *PIG-A* mutants and hence, spontaneous mutant frequency to enable dose response investigation without the required need for mutant depletion; as well as robust qualities lending it well to flow cytometry applications.

All cell lines investigated generated appealing results in terms of generalised GPI-AP expression (Section 4.3.5), apart from the HepG2 human hepatocellular carcinoma cell line which was demonstrated to be unsuitable for this specific application [113, 201], due to problems associated with cell growth and cellular adhesion, requiring trypsinisation, prior to flow cytometry analysis. The AHH-1 cell line was demonstrated to have comprehensive (FLAER), significant CD48 and

extensive CD55/59 expression (Figure 4.10). Minimal intra-sample variation was observed within the culture and cells microscopically showed little signs of distress prior to assessment. The MCL-5 cells, derived from the AHH-1 cell stock [126, 200], demonstrated even more extensive comprehensive staining, and when tandem surface marker expression was investigated demonstrated 99.8% surface antigen expression within the cell line (Figure 4.11).

FLAER as a marker was expected to generate the most comprehensive expression within all cell line assessed; due to its highly unambiguous nature of binding to GPI-AP moieties on the cellular surface [303]. FLAER, is the inactivated fluorescence form of aerolysin, a cytolytic pore-forming toxin exported by Aeromonas hydrophila, a gram-negative bacterium associated with diarrhoeal diseases [304]. Consequently, due to its GPI moiety targeting toxicity, it is considered a generic selective marker for GPI-AP presence [305]. However, it did not perform to the expected levels, as theoretically, unlike monoclonal antibodies which each bind to a single GPI anchor protein, FLAER should be sensitive to any single GPI-AP at high affinity; enabling subsequent binding and hence, a positive signal. Theoretically GPI-APs play a much less critical role within lymphoblastoid cell lines, when compared to primary erythrocytes, however, the idea of lymphoblastoid cell not having a single GPI-AP on the membrane to be highly improbable, regardless of low levels of expression. The most likely reason for this would be protocol limitations, GPI-AP shearing and loss of cellular membrane integrity and hence, inaccuracies within conditions to allow optimum usage.

Publications outlining the potential short falls of in vitro genetic toxicology test systems have been prevalent within the literature for decades [78, 184, 210, 279], however, more recently, a number of publications reporting more specific limitations regarding the use of rodent and human immortalised cell lines within in vitro genetic toxicology testing [113-115], especially focussing upon the biological features of the cell lines and the subsequent effect their respective features have on the integrity of the generated data. In brief, p53 competency, false positivity, sensitivity to apoptosis and a number of additional features were discussed in the context of highlighting current limitations, the extent to which such data can attribute weight of evidence within regulatory decision making, or alternatively, advising definite cell lines for future use in conjunction with specific genetic toxicology end points.

The definitive p53 status of a number of routinely used cell lines within genetic toxicology testing, including MCL-5, AHH-1 and TK6, are unknown due to the publication of contracting evidence as well as the lack of standardisation within cell line distribution [124, 126]. Typical mutational hot spots, codon 282 exon 8, have been assessed and analysed within these cell lines often resulting in contradicting opinion over the true p53 status and therefore, questing the potential accuracies associated to routine usage of said cell line within future testing [124, 126] (Appendix Section 4.4.5).

Due to the nature of the limitations associated with the techniques (Section 4.3.5) utilised within the experiments carried out in order to assess the p53 status of the TK6, MCL-5 and AHH-1 cell lines, no absolute comments on p53 status can be made from the preliminary data generated. Limited quantity of p53 protein was isolated from cytoplasmic protein fractions, and comprehensive p53 and p-p53 presence was demonstrated within the nucleus of all cell lines tested. AHH-1 and TK6 cells were demonstrated to have constitutively more p21 protein (Section 4.3.5.1) as well as p21 gene expression (Section 4.3.5.2) and nuclear p-p53 than the MCL-5 cells, indicating the potential homozygous wild type status of the p53 gene.

Following acute MMC exposure, the western blott analysis generally resulted in a dose dependent increase in p-p53 as well as p21 protein across all cell lines assessed, thus reflecting upon the p53 functionality within the cell lines. However, even though all cell lines appear to be p53 functional, MCL-5 again was shown to produce much lower quantities of p21 and p-p53 protein when compared to the other cell lines following MMC induction; again a potential additional factor eluding at MCL-5 cells having reduced p53 activity (less protein does not necessary mean less functionality). Finally, acute MMC exposure was once again utilised to assess the relative p21 gene expression following MMC induction, as a supplementary experiment to generate additional data to come to a conclusion about cell line specific p53 status. The results displayed a positive correlation between relative p21 expression and MMC dose, however, AHH-1 and MCL-5 displayed truncated dose responses, in which the top dose or doses were induced a significantly lower than expected for induction of p21 expression when compared to untreated controls.

The reason for this is most likely due to the uniqueness within the lymphoblastoid cell lines. As discussed previously, (Section 4.1), even though the cell lines chosen are highly similar in derivation, with MCL-5 and AHH-1 sharing a common ancestor [126, 200, 306], their unique levels of oxidation and/or metabolism have distinct impact on their response to specific compounds. When a compound which requires metabolism is assessed, for example, MMC, subtle pre-existing variations within dose response data are magnified. The truncation in the dose response is directly proportional to the metabolism status of the cell line; AHH-1 have exceptionally high oxidative ability when compared to TK6 cells which lack any extensive metabolism, and MCL-5 cells have additional plasmid derived CYP1A1 p450 cytochrome metabolism [200]. However, as MMC does not require a CYP-mediated metabolism to become active, MCL-5 cells should not receive any more potent dose of the chemical for an extended period of time and subsequently are exposed to a similar levels of chemical induced cytotoxicity (Section 4.3.5.2). However, the same effect is apparent within protein extraction yields at the higher doses, where increased cytotoxicity negatively affects the protein received yields (Section 4.3.5.1) alluding to an additional feature present within the MCL-5 and AHH-1 cells but not the TK6 cell line.

Tentatively, the conclusions which can be drawn from this section are that each cell line demonstrates some level of p53 activity and hence, functionality via the measurement of p21 induction, however, currently, no definitive conclusion can be made on the actual TP53 mutational status of the cell lines assessed.

Following sufficient experimentation, the MCL-5 cell line was chosen for on-going assessment and further development within the in vitro *PIG-A* assay design due to its extensive cellular surface marker expression, regardless of enrichment status and therefore, has subsequent potential as a reporter for mutation at the *PIG-A* locus. Tandem reporter marker usage was demonstrated to produce the most comprehensive surface antigen expression within the human B-lymphoblastoid cell lines, as well as p53 proficiency and functionality. However, TP53 status will be required to be more fully validated via sequencing prior to supplement the pre-existing karyotype before regulatory acceptance.

Table 4.3. Summary of the data described within the chapter contents, the results and the conclusions drawn in relation to the advance of the in vitro PIG-A gene mutation assay standard operating procedure (SOP)

BD FACS Aria 1 – Flow Cytometry Assessment

"Low Passage" TK6 Assessment

GPI-AP Candidate	"Low Passage" vs normal TK6	**Low Passage – unexpectedly low CD59 and comprehensive CD55 expression**
Enrichment Strategy Optimisation - FACS	Drop Distance Collection Media Viscosity Collection Tube Constituency	**Maximum drop distance, softer plastic collection tube and less viscous collection medium provided most promising FACS.**
Viability	Apoptosis (Annexin V) Necrosis Cell Membrane Integrity	**Immuno-fluorescent and microscopically defined to have high viability with little evidence for cellular stress.**
Phenotypic *PIG-A* Assessment	"Low Passage" TK6, CD55, Acute 24 hr EMS	**Qualitative Dose Response - some evidence of LOAEL (10µg/mL). Poor Assay sensitivity even with viability dyes.**

GPI-AP and Novel Cell Line Candidate Assessment

Normal TK6, AHH-1, HepG2 and MCL-5

Protein Quantity Assessment (p21, p-p53)

Gene Expression (p21)

All Cell Lines showed evidence for p53 functionality. HepG2 deemed inappropriate for flow cytometry assessment. MCL-5 potentially heterogeneous p53 wild type when compared to presumed homogeneous TK6 and AHH-1.

MCL-5 Cell line Chosen for further in vitro *PIG-A* Assay development.

Table 4.4 Summary of the additional supplementary data for this chapter, contained within the appendix, which details the validation and additional investigative experimentation surrounding the assay development.

BD FACS Aria 1 – Flow Cytometry Assessment

"Low Passage Stability Post Genotoxic Exposure	Relative Cell Counts (RCC)	
	Relative Population Doubling (RPD)	
	Estimated Average Generation Time (EGT)	➡ **Dissimilar to normal TK6 cells in terms of physiology, comparable dose response metrics and displayed a greater level of robustness post exposure.**
Preliminary Alternative Descriptor Assessment	FL-A vs FL-H	➡ **FL-H proven to be highly dependent upon the shape of particle and therefore, highly sporadic in terms of phenotypic *PIG-A* mutant calling.**
FCM Gating Strategy Evaluation	Mean + 2 SD	
	Outlier Exclusion	
	Upper Quartile	➡ **Statistical approaches demonstrated to generate robust comparable threshold values. Intra-sample variation demonstrated; protocol adjusted to account. Scripted FCM analyses able to be generated post finalisation of *PIG-A* assay design.**

Chapter 5: MCL-5 Optimisation, Preliminary Next Generation Sequencing and Continued Investigation into the in vitro *PIG-A* Gene Mutation Assay Platform

5.1 Introduction

Experimentation reported so far has described the progressive optimisation of a basic in vitro *PIG-A* assay design; commenting on limitations and their potential solutions with respect to enabling progressive development. A human lymphoblastoid derived cell line was identified with minimal numbers of pre-existing phenotypic *PIG-A* mutant events and was evaluated in terms of p53 functionality in response to cytotoxic exposure (Section 4.3). The metabolically active MCL-5 cell line provided data alluding to its potential as a novel platform for mutagenicity assessment. MCL-5 cells, chosen for further studies, were established from a male donor thus harbouring only one X-chromosome and therefore, only one copy of the *PIG-A* gene. This cell line, similar to the previous described TK6 and AHH-1 cell stocks, grows in suspension which is an important prerequisite to conduct the assay; preventing potential limitations associated with trypsinisation or like treatments.

MCL-5 cells constitutively express human cytochrome P-450 CYP1A1 and due to two unique transfected plasmids, also expresses five transfected human cDNAs encoding drug-metabolizing enzymes. cDNAs encoding CYP1A2, CYP2A6, and microsomal epoxide hydrolase (mEH) were introduced by using a vector conferring hygromycin B resistance, and cDNAs encoding CYP2E1 and CYP3A4 were introduced by using a second vector conferring resistance to 1-histidinol [200, 306]. As a direct result of this, MCL-5 cells, without incorporated add-ons, have the proficiency to accurately assess the mutagenic potential of a greater proportion of compounds listed within the EURL-ECVA [307] or IARC [308] lists than comparable routinely used genetox cell lines. Promutagens and/or procarcinogens, such as Benzo-(a)-Pyrene (B[a]P) which require both phase 1 and phase 2 metabolism, in order for the production of mutagenic and/or carcinogenic metabolites, could potentially be falsely defined as negative within analogous in vitro gene mutation assays with limited metabolism [67, 70, 75]. B[a]P once

metabolised forms the highly mutagenic, benzo[a]pyrene-diol epoxide. This large bulky adduct molecule intercalates within the DNA, primarily covalently binding to the nucleophilic guanine base at the N2 [11, 309]. Consequentially, the DNA becomes perturbed and the double-helical DNA structure is disrupted; these discrepancies induce errors within DNA replication and hence, result in mutagenic events. Human or rodent S9 can be utilised in tandem with pre-existing gene mutation assays which lack metabolism [310], in order to mimic in vivo metabolism. However, an all-inclusive, highly sensitive, human representative, test system would be favourable.

5.1.1 Fluorescence Based Platforms, Signal Capture and Review

Focussing on the fluorescence platforms utilised within this body of work, analogous to both flow cytometry and laser scanning confocal imaging is the use of photomultiplier tubes (PMT) to convert photons of light (emitted electromagnetic radiation with a discrete wavelength) to an electrical digital signal. PMTs allow even the signal from a single photon to be captured and up scaled without excessive electrical noise. Alternatively the image stream ™ platform utilises a more conventional approach with regards to the field of photography, in which a charge-coupled-device (CCD) is utilised to fulfil the same function.

Photomultiplier tubes are small glass envelopes, containing a vacuum inside, which houses a photocathode, several dynodes, and a corresponding anode. Event photons contact the photocathode metallic material, which is present as a thin deposit on the entry window of the device, and subsequently electrons are produced as a consequence of the photoelectric effect. These electrons are directed towards the consecutive dynodes constituting the electron multiplier, where electrons are multiplied by the process of secondary emission; upon striking the first dynode, more low energy electrons are emitted, and these electrons in turn are accelerated toward the second dynode. The dynode is configured geometrically to facilitate a chain cascade with an ever-increasing number of electrons being produced at each

stage. The resultant large number of electrons finally strike the anode and result in a detectable current pulse [311].

Confocal microscopy differentiates itself from typical light microscopy through the ability to acquire in-focus images from selected depths, a process known as optical sectioning. Images are acquired, through a progressive scanning method; the detected light within the specimen represents one pixel in the consequential image. As the laser scans over the specimen within the plane of interest, an image is obtained pixel-by-pixel, in which the brightness of the resulting image pixel corresponds to the relative intensity of detected light. This subsequent image is reconstructed within the computer, through the interpreted PMT signal; facilitating three-dimensional reconstructions of topologically complex objects (z-stacking). For samples in which light cannot penetrate easily (opaque specimens), this is useful for surface profiling, while for non-opaque specimens, interior structures can be clearly imaged at high resolution [312]. The confocal system therefore, confirms itself as a stand out piece of equipment for initial immuno-fluorescence cellular membrane surface evaluation and hence, surface reporter marker validation; illuminating the underlying mechanisms of the in vitro assay design.

Alternatively, Charge-coupled devices (CCDs) are devices which move electrical charges to an area where the charge can be manipulated. One of the most common examples of this is the conversion from light into a digital value. The process in which the electrical charge is transferred is known as shifting, in which the signal is relocated between different stages within the device. CCDs move charge between selective bins (capacitors) in the device, with the shifting terminating at the point of signal conversion (The last capacitor in the array dumps its charge into a charge amplifier, which converts the charge into a voltage.). When image acquisition begins, the image is projected onto a capacitor array and the incoming photons are converted into electron charges at the semiconductor interface; shifting occurs and the CCD is utilised to read out the initial charges, the charge being proportion to the original intensity of the captured image [313].

The Amnis Image Stream ™ system incorporates the use of CCDs to generate the 16-bit TIFF images associated with the platform; however, utilising a digital camera has some limitations, as well as some great associated advantages when compared to

similar platforms. Focus, or focal planning issues, is one of the main recognised limitations when imaging "in flow", attempting to maintain focus within a single plane of capture and translate said data to a crisp finalised image is highly complex. However, the Amnis Image Stream ™ does have some novel technology to implement this, including TDI-CCD facilitating 1000x faster image detection and capture than similar equipment [194, 314]. The benefits associated with this novel flow capture system are the high content, sensitivity as well as depth of field assessment unique to this platform. The image stream cements itself as a useful tool to investigate population distributions, in terms of cell cycle analysis, with respect to additional multiplexing fluorescence data capture, i.e. immuno-fluorescence cell surface marker status.

5.1.2 Fluorescence Signal Properties and their potential Relationships

Following the initial illumination of the incident particle, the emitted fluorescence light under goes pre-amplification, typically facilitated through the PMT, more specifically the dynode array, and the subsequent signal generates an electrical pulse [192]. This electrical signal (voltage) is processed and responded to if it passes the additional tertiary levels of analysis, i.e. the voltage intensity much exceed the threshold level to distinguish itself from debris and electrical noise and be subsequently sent to the computer. When the particle of interest, enters the illuminating laser beam and begins to scatter light (FSC or SSC) and/or fluoresce, a voltage pulse is created (Figure 5.1). Theoretically, when a particle is bisected centrally by the illuminating light, the maximum amount of scatter is achieved, and the highest amplitude of the pulse is recorded. However, fluorescence signal, unique across all detectors, can be more diverse due to the localisation of the probe and hence, is independent of the excitation plane of the laser, i.e. the fluorescence signal is dependent upon the localisation of the fluorescence probe and hence, is not necessarily optimal at the centre of the event (Figure 5.2). As the event exits the beam the signal voltage, or amplitude, reduces and the pulse returns to base line.

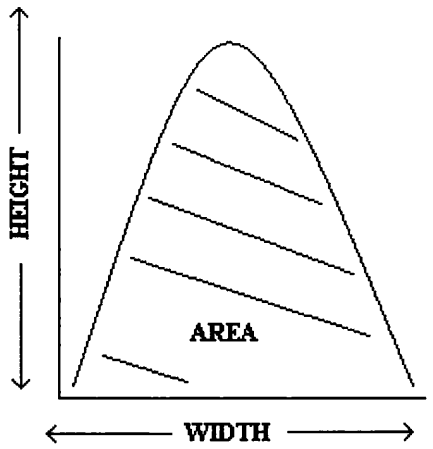

Figure 5.1 Representation of a typical fluorescence generated electrical pulse signal following PMT stimulation and subsequent electron amplification. The maximal amplitude achieved for the electrical signal (voltage) is the descriptor for the pulse height (FL-H), the corresponding descriptor for the pulse duration is pulse width (FL-W) and the total area or integral of the electrical signal is the referred to as the fluorescence area (FL-A).

Pulse shape analysis is based on particle speed, size, and width of the illumination beam. When referring to fluorescence single generation, distribution of the fluorophores within the particle or cell plays a critical role in influencing the resultant shape. Different measurements can be taken from the same signal, as outlined in the Figure 5.1 above, height, area and width, however, each variable gives unique information and characteristics of the cell or population under investigation [315].

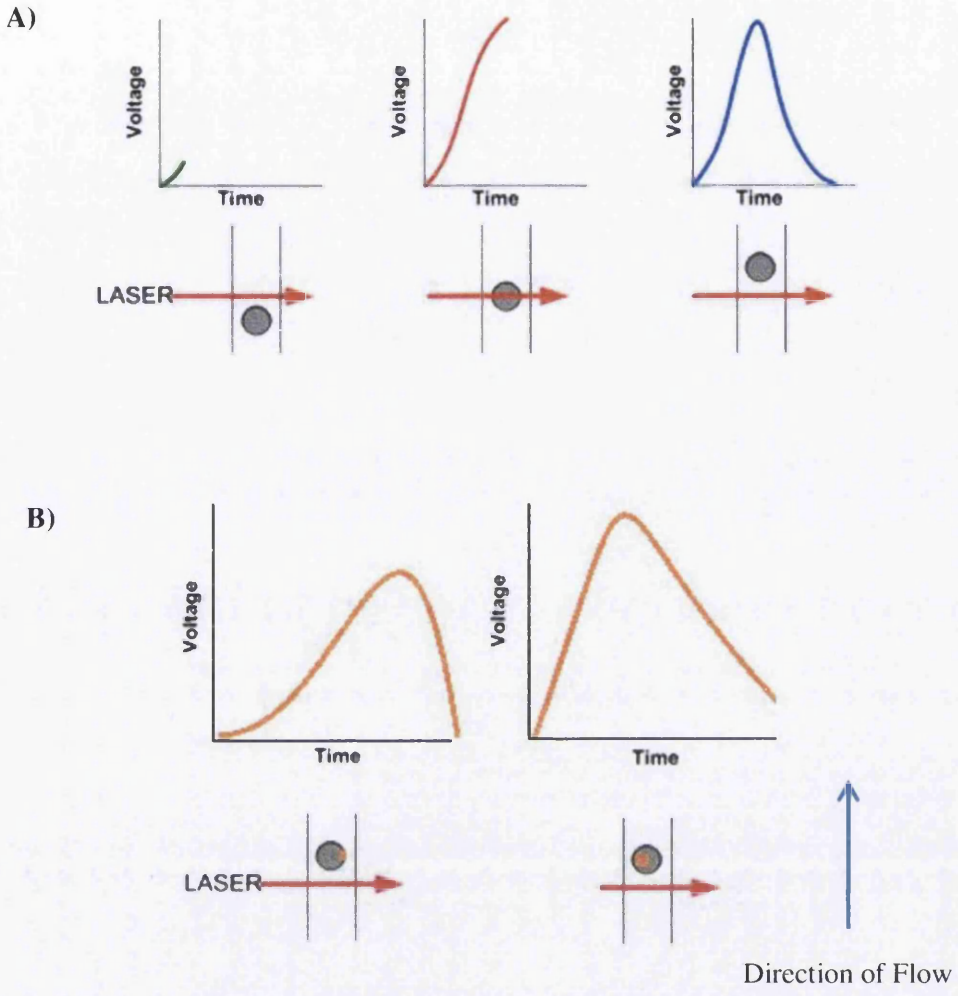

Figure 5.2 Fluorescence signal properties and their respective influencing factors. A) The generation of a fluorescence electrical signal following laser excitation of a free flowing particle and B) the influence fluorophore localisation as well as intensity has on electrical signals following PMT amplification. Note the counterintuitive flow of the sheath fluid and hence particles, typical of modern flow cytometers. Figure adapted from [315].

Typically within flow cytometry the use of scatter plots to display population or event data is common, and generally, the initial data analysis starts with the use of a FSC-A vs SSC-A dot scatter plot to differentiate debris from the population of interest. This principle relies on the FSC-A being a relative measure of particle size and SSC-A representing relative complexity, therefore, small, un-granulated particles are subjectively removed. However, due to the diverse nature of biological

sample, there would be relatively large diversity within cell size, as well as complexity, and therefore, gating can be misleading. In order to facilitate more accurate gating, the inclusion of additional gating strategies is now common practice, including the use of a doublet discrimination scatter plot, FSC-A vs FSC-W [316]. Fluorescence-W, a measure of the time taken for said particle to pass through the illumination beam, is independent of area and height and therefore, an additional measurement of relative cell size (Figure 5.2). Utilising this allows the user to exclude particles which do not conform to the average size of the particles defined as single cell in nature, removing both debris as well as cellular agglomerates.

However, utilising additional properties of the signal as specific variables to manipulate the data during analysis has specific limitations. One should be aware of the relationship of said variable and effects the manipulation could have on the subsequent data [317, 318]. For example, when utilising FL-W measurements as an additional gating strategy to remove non-conforming outlier events, the corresponding variable must be independent of fluorescence voltage or intensity not to bias the data. I.e. if using a FL1-W measure for a fluorophore under assay, utilising this in combination with a FL1-A or FL1-H measure, would significantly increase the risk of data bias due to the additional descriptors being influenced by the intensity of the attached fluorophore [318]. Figure 5.2 represents the relationship between FL-A and FL-H with respect to fluorophore localisation and intensity; width measurements are independent of intensity and therefore, can be used relatively freely to add additional levels of outlier exclusion. Overly complex and subsequently misleading flow cytometry gating can be as detrimental as no cytometry gating if the prejudice within the analysis impacts the finalised data, this is highly problematic within the in vitro assay design, in regard to the enumeration of presumptive mutant events.

5.1.3 Potential biasing within *PIG-A* data analysis – Does membrane integrity negatively bias data during analysis

Cellular viability has been commented on extensively with in the first two results chapters (Sections 3.3 and 4.3); however, limited actual conclusive remarks have been made in regards to the physical difference in *PIG-A* fluorescent intensity with respect to viability status. Currently, it is unknown whether or not cells undergoing apoptosis or early stage necrosis actually do present a true biasing effect within the subsequent in vitro data analysis, as a lack of membrane asymmetry and potential lack of membrane integrity [114, 274, 276] could induce inaccuracies in phenotypic definition. The initial data generated, demonstrated an extremely apparent correlation between phenotypic *PIG-A* mutant phenotype and loss of membrane integrity (Section 3.3.5), however, little could be taken with regards to progressive loss of membrane integrity sequentially affecting *PIG-A* mutant data. Due to this, apoptosis, necrosis and complete lack of membrane integrity have all be associated with the potential of eliciting false positive results (Section 3.3.5); however, further investigation is required to assess the likelihood of phenotypic mutant enumeration bias. Within the second results chapter's supplementary work, we demonstrated that FL-H, as a measure of phenotypic *PIG-A* mutant events, was highly variable due to its direct correlation to fluorescence intensity and particle shape, and therefore, was shown to be sub-optimal as a robust form of measurement (Appendix Section 4.5.3.2). In order to assess the likelihood of additional assay bias, alternative features of the cellular population, momentarily disregarding fluorescence staining, were considered for their impact on subsequent analysis.

Apoptosis has been thoroughly researched and well characterised during the latter stages of the 20th century [120, 124, 274], and due to this pioneering research the field now is better able to understand the triggers, these include; nutrient deprivation, infection (viral), hypoxia and increased cellular ion content [319] etc. Intrinsic or extrinsic apoptosis terminates with a highly organised mechanism of programmed cell death [275], however, even though apoptosis results in the eventual fragmentation of the cell, few if any morphological traits are apparent during the early stages. Condensation of the chromatin, loss of nuclear membrane integrity,

cellular membrane budding and the eventual formation of pyknotic bodies, which are engulfed via phagocytosis by circulating macrophages, are all characteristic of the latter stages which are easily morphologically identified within heterogenous populations [274, 276]. Apart from nuclear DNA laddering within gel electrophoresis, which is not practical single cell basis, only subtle changes within the structure of the lipid bi-layer are apparent within the early stages. Loss of membrane asymmetry, the migration of negatively charged phospholipids to the extracellular surface, is the characteristic which we chose to exploit to enable early stage apoptosis detection; the newly acquired negative charge on the cell membrane permits Ca^{2+} mediated fluorophore-conjugated annexin V binding [273, 274]. After detecting an un-even distribution of non-viable, annexin V positive, cells within the presumptive *PIG-A* mutant population when compared to the corresponding wild type phenotype (Section 3.3.5); tentatively apoptosis was concluded to appear to induce an effect which resulted in characteristic loss of GPI-AP binding. However, little is known about the extent in which apoptosis, as well as necrosis, have an effect on GPI-AP binding, which is a topic which will be assessed within this results chapter. Although, GPI-AP deficiency has been alluded to increasing resistance against apoptosis and hence, is a potential mechanism describing the expansion in numbers of *PIG-A* mutants within patients suffering from PNH [320]; this mechanistic data conflicts with the data within chapter 2 and further increases the need for more detail investigation into the mutant mimicking identity of non-viable cells. Theoretically, as cells progress through apoptosis, they accumulate significantly more severe membrane alterations, inversions, budding and eventual rupture, and therefore, GPI-AP expression or presence may have a negative correlation with apoptosis progression, a useful dynamic to correct against during subsequent *PIG-A* analysis.

This progressive loss of membrane integrity, experienced within apoptosis, is required to be studied in order to assess the additional requirement of integral transmembrane protein immuno-fluorescence labelling inclusion within the assay design. If GPI-AP binding is negatively biased by apoptosis progression, then a point in which alterations in membrane structure, preventing GPI-AP presence, should be identified via the loss of supplementary lipid raft associated membrane proteins [321]. HLA-DR or Human Leukocyte Antigen - DR is a specific subtype of a MHC

class II cell surface receptor, encoded by the HLA complex on chromosome 6 [322]. HLA were originally defined as cell surface antigens with a critical role in mediation between "graft versus host disease" and therefore, play a vital role in rejection or acceptance of tissue transplantation [323]. Due to the complex nature of MHC class receptors, there are three specific HLA-complexes each with a number of isoforms, miss-match can result in fatal rejection of tissue transplantation in HLA-mismatched donors. HLA-DR is also involved in several autoimmune conditions, disease susceptibility and disease resistance and therefore, is a vital cellular antigen which is constituently expressed at high density within the cellular membrane of most leukocyte cell lineages [321, 323-325].

Utilising HLA-DR as a sole progressive marker for membrane integrity loss, or in combination with pre-existing measurements as well as maintaining apoptosis evaluation should improve assay sensitivity as well as provide more of an identity to the resultant flow cytometry data. An additional feature which HLA-DR staining provides, unable to be obtained by live or dead cell staining, is the conformation of membrane integrity and a generic expression of surface antigens, which is useful when commenting on general cellular health and defining the normal phenotype.

5.1.4 Next Generation Sequencing and its Necessity to Validate the Presumptive *PIG-A* Mutant Status to offer Validity within the Test System

The present in vivo Pig-a mutation assay is currently within an extensive validation in order to assess its likelihood of OECD guidelines drafting and finalised acceptance within the tiered genetic toxicology standard test battery [77, 143, 166, 169, 176, 196]. The sheer extent of published data supporting the mechanism and broad steering committee guidance has provided the assay with the best chance of integration within 28-day tox studies and inclusion within safety assessment [13, 91, 144, 170, 172, 173, 178, 222, 280]. However, due to the nature of erythrocytes, the true identity of the presumptive mutant events will never be fully validated as they lack an intact nucleus, and therefore, cannot be sequenced to validate the *Pig-a* mechanism. The ideology of the mechanism has been investigated in a number of

additional haemopoetic tissues and has been reproducibly determined to demonstrate extensive *PIG-A* mutation as the critical mutational event determining lack of phenotype [172, 173]. However, more recent publication has demonstrated the presumed *PIG-A* deficient phenotype to be a result of an autosomal double knock out mutational event within the *PIG-T* gene, re-enforcing the counter argument that even though statistically insignificant, additional silencing effects other than the *PIG-A* gene can result in a GPI-AP negative phenotype [146].

Additional to the extensive primary leukocyte sequencing, generally splenocytes collected from rodent models, in which the origins of the loss of phenotype were investigated [169, 176]. Very little is known about how these outliers could potentially impact the assay mechanics, especially due to the extensive sample size and subjectivity within flow cytometry gating. Therefore, there is much use in producing a flow based assay within equivalent haemopoetic tissue, utilising an analogous reporter system in order to in-directly validate the reporter as well as evaluate the presence of such non-*PIG-A* mediated mutant events within the total population of phenotypic *PIG-A* mutants [181]. Traditionally, sanger sequencing utilising chain termination dideoxynucleotides, has been the primary method of genomic sequencing [326], however, due to the highly limited read sizes (300-500 base pairs), as well as other limitations, additional methods based on sequencing through synthesis were developed. Pyrosequencing, in which cycled nucleotide exposure is correlated to light output, based approaches were developed which enable multiplexing sequence analysis, but however, limit reads to 25-100 bp in length [326]. Nonetheless, recently, the world of genomics has grown exponentially with the invention of the next generation sequencing approaches in which solid state sequencing, in combination with Pyrosequencing approaches are miniaturised within a single platform to facilitate the sequencing of thousands of DNA molecules at once, allowing whole genomes to be sequenced within minutes at an affordable cost [327, 328].

The advancements of Next generation sequencing (NGS) techniques had enabled the rapid sequencing of whole genomes at relatively low costs [329]; this feat has brought about numerous benefits to scientific research as well as a number of novel challenges to the biomedical research field [330]. With costs rapidly falling (the first

human genome cost $3 billion dollars), the challenge now has evolved from physically sequencing the genome (currently ~$1-5,000), a feat unable to be achieved financially using older sanger methodology [326], but to handle and confidently interpret the shear amount of raw data generated during sequencing. As the field of NGS rapidly grows and the applications in which NGS can be implemented expands due to the removal of financial constraints, the software available to be implemented into the analysis pipeline is also rapidly escalating [327, 328, 330, 331], each version of the software becoming more advanced and containing additional algorithms for novel problem solving [332-334]. However, due to a lack of a single standardised approach [335], and the emergence of individual fields of research within NGS data analysis, for example metagenomics [336]; increasing numbers of possible software packages to complete the same or an analogous analysis task are becoming publically available [330, 337, 338]. As a direct result of this, leading sequencing institutes can therefore, generating sequence data and interpret such data using a unique analysis pipeline constructed by themselves, without publishing said pipeline competitive institutes are unable to reproduce their data as well as potential critique their analysis flaws, therefore, each data analysis has its own unique caveats established through the construction of their analysis pipeline.

Metagenomics analysis has begun to make good advancements towards the establishment of a single standardised pipeline [327, 336], however due to the complexity, sheer volume and plethora of applications for human genome NGS analysis, a single pipeline would be too crude for each individual application. Therefore, when assessing or interpreting NGS data a very thorough understanding of the specific pipeline and individual caveats and variation between the separate elements within a pipeline is advised.

Utilising next generation sequencing approaches, in combination with a hetero or homogenous population of flow cytometry defined *PIG-A* mutant phenotype cells, could provide data on the error rate within detection, the origins of the mutation events, the type of mutation occurring, the synonymy of the mutation and hence, functionality of the cell in terms of *PIG-A* protein as well as parallel investigation into a number of additional genetic causes of the presumed *Pig-a* deficient

phenotypic (multiplexing). Obtaining such data could provide supplementary information to validate the accuracy of the currently proposed in vivo *Pig-a* mechanism and enable the further optimisation of assay design, including gating strategies, to facilitate a more accurate prediction of hazard and risk assessment.

The next generation sequencing (NGS) experiment carried out within the following chapter utilised an Illumina™ MiSeq in combination with a heterogenous pooled DNA sample, in order to assess the phenotype-genotype relationship within the in vitro *PIG-A* assay design. Genomic DNA extracted from EMS treated MCL-5 cells were FACS, prior to sequencing, to obtain a heterogenous phenotypic *PIG-A* mutant population, as identified by a characteristic lack of CD55/59-RPE related fluorescence signal. Once isolated, the genomic DNA was amplified, adapter ligated and sequenced at a >90% coverage and >3,000 average depth across all genes of interest. Four genes were selected for sequencing variant analysis, *PIG-A*, *PIG-T*, *CD55* and *CD59*; intrinsic and exonic sequences as well as sizable 5' and 3' regulatory regions were assessed.

5.2 Materials and Method

5.2.1 Trialled usage of HLA-DR Staining to Validate Single Marker *PIG-A* Dose Response Data within MCL-5 Cells

Low passage (p4) MCL-5 cell cultures were established and maintained as outlined in (Section 2.2) and exposed to MNU, ENU, EMS and 2,4 DNP for 24 hr under standard chemical treatment as described within (Section 2.4) at Gentronix Ltd. Post chemical exposure, cultures were washed, counted and seeded ready for initial flow cytometric analysis; 10 µL anti-human anti-CD59 R-PE, 40 µL HLA-DR FITC (Cat No. 555871, BD Biosciences, Hertfordshire, UK) and 10 µL 7-AAD (Section 4.2.4) were used. Flow cytometric analysis as defined in (Section 2.8.2) was undertaken within an hour of sample preparation, samples were stored on ice, protect from direct light, until analysed. Work undertaken by Matthew Tate, Jodie Allsop and Sabrina Khaliq under the guidance of Prof. Richard Walmsley.

5.2.2 Confocal microscopy GPI-AP expression analysis

5.2.2.1 GPI-AP Expression Analysis on the Surface of 4% PFA fixed MCL-5 Cells

MCL-5 cells were established as outlined in (Section 2.2) and treated with anti-human anti-CD55 and/or CD59 R-PE antibodies for 30 min according to (Section 2.8.1) before being washed twice in pre-warmed, 37 °C PBS. Briefly, cells were re-suspended and fixed using 1 mL of 4% PBS buffered paraformaldehyde (Section 2.7) and incubated for 15 min at 37°C, within the temperature controlled NU-5510 DHD Auto flow incubator, before being washed twice with excess 1 x PBS. Coverslips, Precision 0.17 mm thickness, (Cat No. 474030-9000, Carl-Zeiss,

Hertfordshire, UK) were then prepared for cellular adhesion on one side; this was achieved by placing the attachment side down in a 0.1 mL aliquot of 1mg / mL aqueous poly-L-lysine (Sigma-Aldrich, Gillingham, UK) on Parafilm. The cover slips were allowed to incubate for 10 min at room temperature, within a class 2 safety cabinets, and then washed thoroughly using dH_20 and left to air dry. Coverslips were then incubated in 1% PBS bovine serum albumin (Sigma-Aldrich, Gillingham, UK) for at least 1 hour to prevent subsequent fluorophore conjugates binding the cationic poly-L-lysine and causing excessive background fluorescence. The fixed cells were centrifuged (~350 x g for 7 min), washed, re-suspended in 3 mL of PBS and then aliquotted into 6-well plates (Greiner Bio-One, Hertfordshire, UK) at a suitable concentration to provide sufficient coverage ~1 x 10^5 - 10^6 cells/mL. Each well received a poly-L-lysine coated cover slip using forceps, adhesion surface facing upwards, and was incubated for 10 mins at room temperature. Post incubation, the cells were analysed under a light microscope to ensure that attachment was successful before begin retrieved and washed thoroughly in a fresh 6-well plate containing PBS. Post incubation, cover slips were washed in PBS and dried via the touching of filter paper to the outer edge of the cover slip, to prevent damage to the cell surface. Cover slips were then mounted within a medium designed to minimise the change in refractive index and limit excessive bleaching - 1,4-diazabicyclo[2,2,2]octane (DABCO) (Cat No. D27802, Sigma Aldrich, Gillingham, UK). The mountant was constructed as follows; 45 mL glycerol (G55-16 100 mL, Sigma Aldrich, Gillingham, UK), 2.5 mL Tris-HCL buffer (pH 8) and 2.5 mL dH_20. Polished glass slides (Cat No. 11562203, Fisher Scientific, Loughborough, UK) were used in conjunction with autoclave tape in order to construct two "mounts" or "posts", preventing the weight of the cover slips crushing the attached cells. Loaded cover slips were laid attached side down onto 50 µL mountant, central between the two posts, within the centre of the supported glass slide. Due to the addition of posts, cells remained in their 3-D conformation and due to fixation were stable to be stored protected from light at 2-4 °C for a number of days prior to analysis.

5.2.2.2 Confocal Microscopy Image Analysis

Confocal microscopy was carried out using a LSM-710 laser scanning confocal microscope and supplied ZEN software version 2009 in conjunction with either a 40x or 63x oil immersion DIC objective (Carl Zeiss, Cambridge, UK). All fluorochromes/fluorophores were excited using the 405, 488, 594 or 633 nm lines. During analysis artifactual data was always referenced against unstained or single stain negative controls to ensure consistency, as well as objectives, laser excitation intensity and laser gain settings remained consistent to provide comparable data sets. For proof of principle experiments, all necessary information was saved associated to the file in order to replicate the sample of interest. Retrospective image analysis was carried out using the ZEN software, as described within the manufacturers supplied information.

5.2.3 Preliminary MCL-5 *PIG-A* Assessment; Tandem CD55/CD59 Surface Antigens utilised as reporter following MNU Exposure

Low passage MCL-5 cell cultures were established and maintained as outlined in (Section 2.2) and exposed to MNU for 24 hr under standard chemical treatment as described within (Section 2.4). Post chemical exposure, cultures were washed, counted and seeded ready for initial flow cytometric analysis using anti-human anti-CD55 R-PE in tandem with anti-CD59 R-PE conjugate antibodies and 7-AAD (Section 2.8.1)). Flow cytometric analysis as defined in (Section 2.8.2) was undertaken within an hour of sample preparation, samples were stored on ice, protected from direct light, until analysed.

Two different gating strategies were implemented to enable a direct comparison in method; after gating for single cells on a SSC/FSC dot plot and/or counter map, an additional doublet discrimination (FSC-A vs FSC-W) as well as novel FL-2-W vs FSC-A scatter pot were implemented to exclude non-single cell events. A minimum of 10,000 single cell events were analysed for the surface expression of the CD55/CD59 surface antigen. *PIG-A* phenotype was assessed utilising an instrument

calibration standard (ICS), an unstained sample used to set voltages and mutant gating. During ICS analysis, the mutant mimicking sample is utilised to detect auto fluorescence within the channel of collection in order to distinguish between a positive event and background noise at the channel's photon multiplier tube (PMT).

MNU dose response data were produced using a FACSAria I cell-sorter ™ (BD Biosciences, Hertfordshire, UK), analogous to the previous work utilising EMS induction (Section 3.3.3 and 4.3.4). All fluorescence measurements on the FACSAria were recorded using the "area" parameter; R-PE and 7-AAD were assessed within the pre-specified "PE" and "APC" detectors. PE, 556 LP combined with a 585/42 band pass filter and APC, no LP combined with a 660/20 band pass filter. PE was excited off the 488nm laser line, and the 7-ADD off the 633 nm laser line, best matching their excitation maxima's.

Following flow cytometric analysis, parental cell cultures were removed from incubation every 24 hr for repeated *PIG-A* mutagenesis assessment as described at length in (Section 2.10).

5.2.4 Assay Refinement - Gating Strategy Comparison and Apoptotic Morphology Investigation

5.2.4.1 Gating Strategy Direct Comparison

Low passage MCL-5 cell cultures were established and maintained as outlined in (Section 2.2) and counted. In an analogous method to previous sections, cells were treated with anti-CD55 R-PE antibody and washed prior to being run on the flow cytometer (Section 2.8). Within the FACS Diva ™ 6 software, samples were run in triplicate utilising different gating strategies, 2-D histograms and 2D-density scatter plots, and were assessed utilising the FL-W measure of the fluorophore channel as well as the FSC-W. Gates were drawn subject to ~90% of parental population and output was commented in terms of numbers/percentage phenotypic *PIG-A* mutant single cell events.

5.2.4.2 Apoptotic Morphology Investigation

Low passage MCL-5 cell cultures were established and maintained as outlined in (Section 2.2) and counted (Section 2.2.1). The equivalent volume containing 4 x 10^6 cells was transferred into six fresh 15 mL centrifuge tubes, and the total volume adjusted to 10 mL via the additional of culture media. 100 µL aliquots of 1 µM doses of Staurosporine solution were added to five of the culture flasks for the following exposure lengths; 30 min, 1 hr, 2 hr, 3 hr , 4 hr and 8 hr. Following Staurosporine exposure, all flask contents were transferred into sterile 15 mL falcon tubes, centrifuged (~250 x g for 7 mins) and the toxic supernatant carefully discarded. 10 mL of 1 x PBS was added to re-suspend the cell pellets and remove any excess residual chemical (Section 2.4). Samples were centrifuged, supernatant aspirated (presumed toxic) and re-suspended in 10 mL of fresh medium. Each sample was counted (Section 2.2.1) and three subsequent samples were constructed, each sample containing 1 x 10^6 cells. Subsequently, samples were centrifuged (250 x g for 7 min), supernatant aspirated, and re-suspended in 100 µL of pre-warmed media. Each sample, excluding the ICS, was treated with 20 µL of anti-human anti-CD55 PE antibody in combination with 20 µL of anti CD59 R-PE and incubated at room temperature for 30 min, protected from light (Section 2.8.1). Following incubation, samples were centrifuged, supernatant aspirated and re-suspended in 5 mL of 1 X PBS solution. Samples were re-centrifuged, supernatants discarded, and re-suspended within 1 mL of 1 X Annexin binding buffer, this step was repeated three times. Samples were re-suspended within 100 µL of annexin binding buffer and treated with 5 µL of Alexa Fluor 488 nm Annexin V, excluding the ICS sample. All samples were incubated for 15 min at room temperature, protected from light. Excess 1 X Annexin binding buffer was added to each sample, prior to centrifugation, supernatant aspiration and re-suspension within 200 µL of 1 X Annexin binding buffer. 5 µL of 7-AAD was added, excluding the ICS and incubated for 15 min prior to flow cytometry analysis; samples were stored on ice protected from light (Section 4.2.3 – 4.2.4).

5.2.5 Next Generation Sequencing

Next generation sequencing performed within this body of work was carried out within the Glaxo SmithKline Research and Development centre at Stevenage, UK. The sequencing was physically undertaken by Miss Lucy Field, under the supervision of Dr Nalini Mehta and group leader David Dow respectively, on an Illumina MiSeq platform (San Diego, California, USA) in conjugation with SureSelectXT Reagent Kit (Cat No. G9611A, Agilent Technologies, Wokingham, UK). All work was carried out according to GLP, regularly inspected, and when applicable carried out within class 2 safety cabinets to prevent contamination (thorough ethanol cleaning as well as UV sterilisation was undertaken regularly).

Details of the full methodology used can be found at (Appendix Section 5.2.5), however, in brief initially the "Genes of Interest" target sequences were identified (*PIG-A*,*PIG-T*, *CD55* and *CD59*), and cross validated across a number of different software packages: Berkley Drosophila Genome Project – Neural Network Promoter Prediction [339], Promoter 2.0 Prediction Server [340] and SoftBerry – FPROM [341] (Appendix 5.2.5.1). Following this, SureSelect oligonucleotide primers [342] were designed to span across each amplicon (inclusive of the entire coding region as well as an additional 1,000 bp 5' and 3' buffer zone) with sufficient coverage to provide confidence and integrity with subsequent next generation sequencing results (Appendix Section 5.2.5.2).

Following FACS (Section 2.8.3) phenotypic *PIG-A* mutant cellular events had their DNA extracted and cleaned up using the QIAamp DNA Micro Kit (50) (Cat No. 56304, Qiagen, Manchester, UK), the resultant isolated DNA was quantified using the NanoDrop ND-1000 Spectrophotometer (Appendix Section 5.2.5.3) and Qubit ® 2.0 Fluorometer (Life ™ Technologies, Paisley, UK) apparatus (Appendix Section 5.2.5.4).

Following DNA extraction, the genomic DNA was sheared, using the covaris sonication method (Covaris M220 Focused-ultrasonicator ™ (Covaris, Massachusetts, USA)) (Appendix Section 5.2.5.6), and quality assured for complete degradation on a 2100 Bioanalyzer (Agilent Technologies, Wokingham, UK).

Sequentially, the single stranded DNA (ssDNA) was converted into blunt ended double stranded DNA (dsDNA) (Appendix Section 5.2.5.7), additional 5' adenine overhangs constructed (Appendix Section 5.2.5.8) and adapter oligonucleotides were ligated onto the template DNA sequences (Appendix Section 5.2.5.9) utilising components from the SureSelect Library Prep Kit (ILM), SureSelect Target Enrichment Kit (ILM) indexing Hyb Module Box #2 and Herculase II Fusion DNA Polymerase (Agilent Technologies, Wokingham, UK). The entire library at this point was amplified through thermal cycler exposure (T100 thermal cycler (Bio-Rad, Hertfordshire, UK)) (Appendix Section 5.2.5.10). Following amplification, Agencourt AMPure XP (Cat No. A63882, Beckman Coulter, High Wycombe, UK) beads were added to the amplified library in order to wash (ethanol), purify and isolate the freshly constructed dsDNA (Appendix Section 5.2.5.11). At this point another additional quality assurance (2100 Bioanalyzer) step was utilised to ensure that the size of the dsDNA molecules constructed was in the range of 225-250 bp in length.

Following on from purification, the dsDNA underwent hybridisation (utilising components from the SureSelect^{XT} Reagent Kit)(Appendix 5.2.5.12) prior to magnetic bead identification (using Dynabead MyOne Streptavidin T1 and corresponding Dynabeads®) and isolation of Target Sequence dsDNA (Appendix Section 5.2.5.13). Index tags were now added (Appendix Section 5.2.5.14) following hybridisation (SureSelect^{XT} Reagent Kit) and isolation prior to additional rounds of speciifc library amplification (Appendix Section 5.2.5.15). Again the dsDNA under went purification using magnetic beads and isolation using analgous Agencourt magnetic beads (AMPure XP beads)(Appendix Section 5.2.5.16). Measures were taken to assess the homogenous nature of the molecules, ensuring that the dsDNA lenghts were in the range of 250-325 bps (2100 Bioanalyzer). Following this, the Index Tagged Amplified library was quantiativiely assessed using a SYBR® Green QPCR method (QPCR NGS Library Quantification Kit (Illumina) (Cat No. G4880A, Agilent Technologies, Wokingham, UK)) - at this point the Illumina adaptor speciifc PCR primers were also added to the template dsDNA(Appendix Section 5.2.5.17).

Post quantification and subsequent sample concentration ammendments (Appendix 5.2.5.18), the Illumina flow cell and MiSeq™ platform were thawed and calibrated

prior to use. The amplfied illumina adaptor ligated index library was denatured into ssDNA, diluted appropraitly and loaded into the MiSeq™ reagent cartridge, analgous controls were also constructed at this point. The Illumina MiSeq® was loaded, cleaned according to the Illumina MiSeq® system user guide, and the ssDNA sequenced (Appendix Section 5.2.5.19). Real time analysis of run efficiency and progress was carried out on an adjacent computer running Sequence Analysis Viewer software ((SAV) software (Illumina, San Diego, UK)).

5.3 Results

5.3.1 Trialled usage of HLA-DR Staining to Validate Single Marker *PIG-A* Dose Response Data within MCL-5 Cells

Dose response experiments were carried out in order to assess the potential benefits associated with the refined assay design; low passage MCL-5 cells combined with HLA-DR (membrane integrity) staining, limited viability dye incorporation and CD59 utilised as the in-direct reporter for mutation phenotype. EMS was continuously chosen as one of the chemicals for assay, along with MNU and ENU, additional members of the G4 compounds. 2,4 Dinitrophenol (2,4 DNP), a precursor to sulphur dyes extensively used in the manufacturing of cotton products, was also selected for its dissimilar properties and mechanism. All events labelled as *PIG-A* mutants are events, phenotypic viable single cells with an apparent absence or reduction of CD59 presence on the extracellular surface membrane, and therefore, are presumptive *PIG-A* mutants. Experimental design, undertaken at Gentronix Ltd., permitted the capture of ~50,000 defined viable single cell events

All data generated following 4 day *PIG-A* mutation assessment were evaluated for normality and variance (P value $\geq$0.05) using the Shapiro-Wilk and Bartlett's Test respectively, carried out within DrSmooth in the R-Software environment (R-3.0.2, Free Software Foundation's GNU project). Following assessment, data was either defined as normally distributed (ENU and 2,4 DNP) or non-normal (MNU and EMS) and subsequently, PROAST38.9 modelled in order to define BMD_{10} and BMD_{L10} values (Appendix Section 5.3.1). Statistical analysis, Dunns' or Dunnett's' t-tests was implemented to state at what dose, if any, rejection of the Null hypothesis was to be assumed (P-value $\leq$0.05). At such a dose, variation of the viable phenotypic *PIG-A* mutant frequency was a direct result of a significant factor and not as a result of chance.

Acute MNU exposure resulted in an apparent sub linear day 4 dose response within viable MCL-5 cells (Figure 5.3.A). Doses less than 20 μM appeared to illicit no

effect on the relative percentage of phenotypic mutant, when compared to concurrent negative control data. However, as doses increased, a strong positive correlation between dose, toxicity and phenotypic *PIG-A* mutant number was observed, but no doses were demonstrated to be statistically significant ($P>0.05$). Variance was apparent, specifically significant at the higher doses, with much greater deviation around the mean displayed; this can highly influence statistical analysis and therefore, prevent significance from being derived. BMD_{10} and $BMDL_{10}$ values of 4.51 and 3.17 μM were derived respectively using PROAST 38.9 (Appendix Section 5.3.1). Cell viability was demonstrated to be dose dependent, with doses greater than 5 μM resulting in excess of 20% cytotoxicity (Figure 5.3.A). RICC was shown to decrease to 20% viability by 40 μM; larger doses demonstrated an analogous result.

Acute 2,4 DNP exposure resulted in a sub linear day 4 dose response within viable MCL-5 cells (Figure 5.3.B). All doses tested within the concentration range failed to statistically increase the relative average phenotypic mutant frequency, and had very little effect on the resultant dose response ($P>0.05$). Due to the apparent innate activity of the chemical as a genotoxicant, and hence, lack of dose response of the PROAST modelled data; BMD_{10} and therefore, $BMDL_{10}$ values were unable to be derived (Appendix Section 5.3.1). Cytotoxicity again was demonstrated to be highly dose dependent, with a generalised decrease apparent over the entire dose range. Doses exceeding ~125 μM resulted in an approximate 50% decrease in viability (Figure 5.3.B) with greater doses resulting in even more severe cytotoxic effects. Little variance in terms of both viability and relative phenotypic *PIG-A* frequency was demonstrated within the data.

Acute 24 hr EMS exposure resulted in a seeming sub linear day 4 dose response within viable MCL-5 cells (Figure 5.3.C). There was an apparent dose dependent increase in the relative phenotypic *PIG-A* mutant frequency, when compared to concurrent negative control data, at the top dose of ~160 μM (equivalent to 20 μg/mL) eliciting a statistically significant increase ($P<0.05$). Limited variance was shown, excluding 5 and 120 μM, throughout the dose range with respect to both cytotoxicity and *PIG-A* mutant frequency. Succeeding PROAST modelling, BMD_{10} and $BMDL_{10}$ values of 11.5 and 8.8 μM were derived respectively (Appendix Section 5.3.1). Cell

viability was demonstrated to be dose dependent, with doses greater than 40 μM (5 μg/mL) resulting in excess of 40% cytotoxicity (Figure 5.3.C). RICC was shown to decrease to 20% viability by 100 μM (12.5μg/ml); larger doses demonstrated an analogous result.

Acute ENU exposure resulted in a sub-linear day 4 dose response within viable MCL-5 cells (Figure 5.3.D). All doses tested within the concentration range failed to statistically increase the relative average phenotypic mutant frequency, and had very little effect on the resultant dose response ($P>0.05$). Due to this, and the lack of positive gradient attributed to the data following PROAST modelling, BMD_{10} and $BMDL_{10}$ values were subsequently unable to be derived (Appendix Section 5.3.1). Cytotoxicity again appeared to decrease in a dose dependent manner, with a generalised decrease apparent over the entire dose range. Doses exceeding 200 μM resulted in an approximate 40% decrease in viability (Figure 5.3.D) with greater doses resulting in even more severe cytotoxic effects. Significant variance in terms of both viability and relative phenotypic *PIG-A* frequency was demonstrated throughout the entire dose range, and hence, extensive deviation from the mean was apparent (Figure 5.3.D).

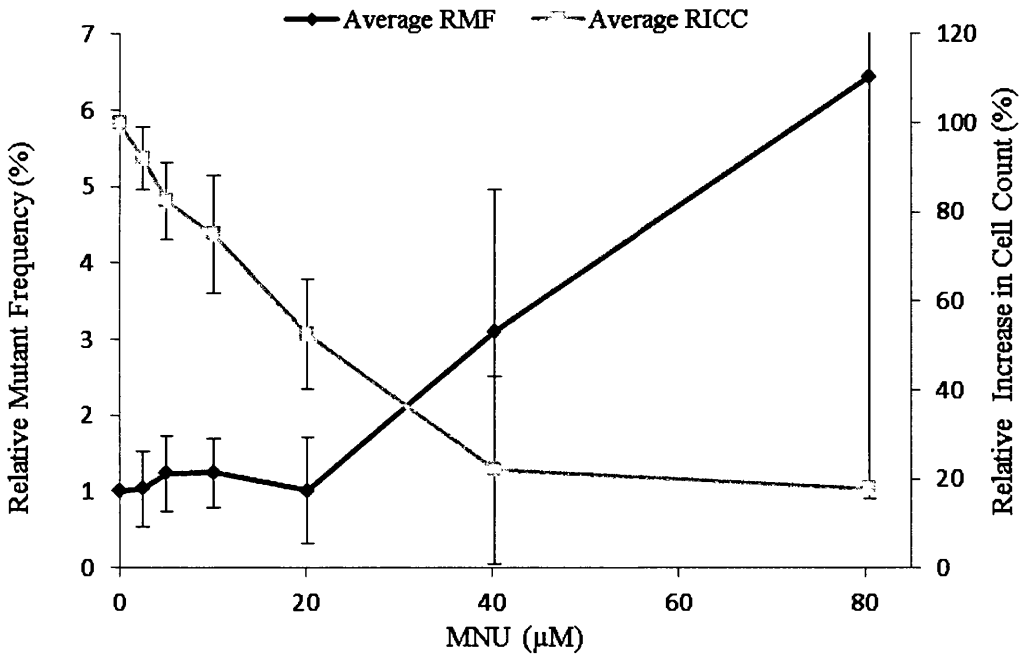

Figure 5.3.A Day 4, low passage human lymphoblastoid cells (MCL-5) average relative phenotypic *PIG-A* mutant frequency following 24 hr MNU exposure, CD59 antigen utilised as reporter for mutation, inclusion of HLD-DR and 7-AAD staining to ensure cellular membrane integrity. (Dunn's Test ($p < 0.05$*)(N=4)(Error Bars ±1SD) *PIG-A* mutant data relative to the percentage of phenotypic *PIG-A* mutants observed within the con-current control (top dose *PIG-A* data, two replicates omitted, N=2).

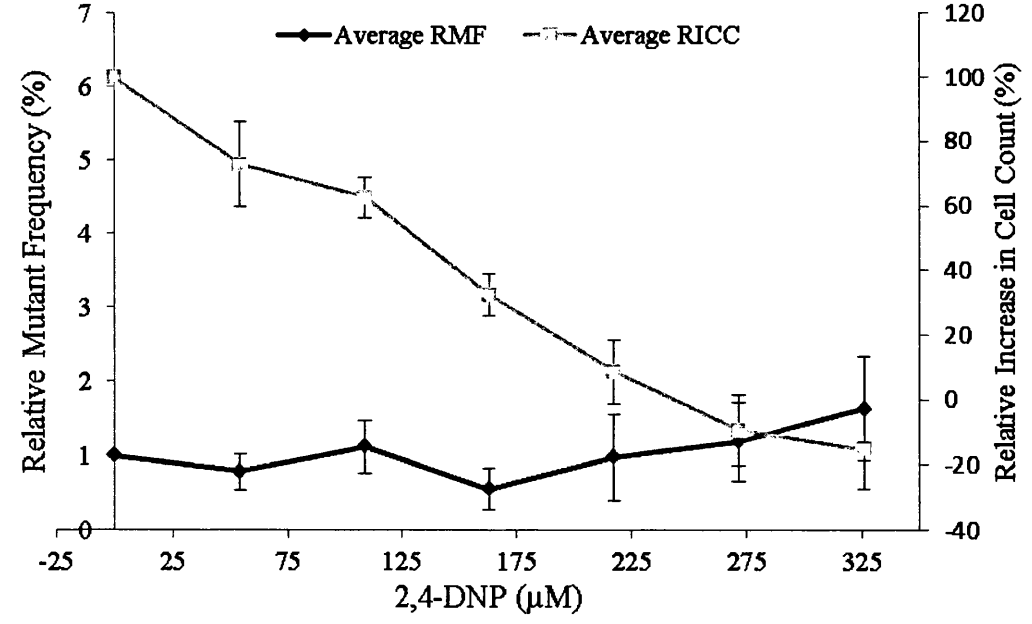

Figure 5.3.B Day 4, low passage human lymphoblastoid cells (MCL-5) average relative phenotypic *PIG-A* mutant frequency following 24 hr 2,4-DNP exposure, CD59 antigen utilised as reporter for mutation, inclusion of HLD-DR and 7-AAD staining to ensure cellular membrane integrity. (Dunnett's Test ($p < 0.05$*)(N=3)(Error Bars ±1SD)) *PIG-A* mutant data relative to the percentage of phenotypic *PIG-A* mutants observed within the con-current control.

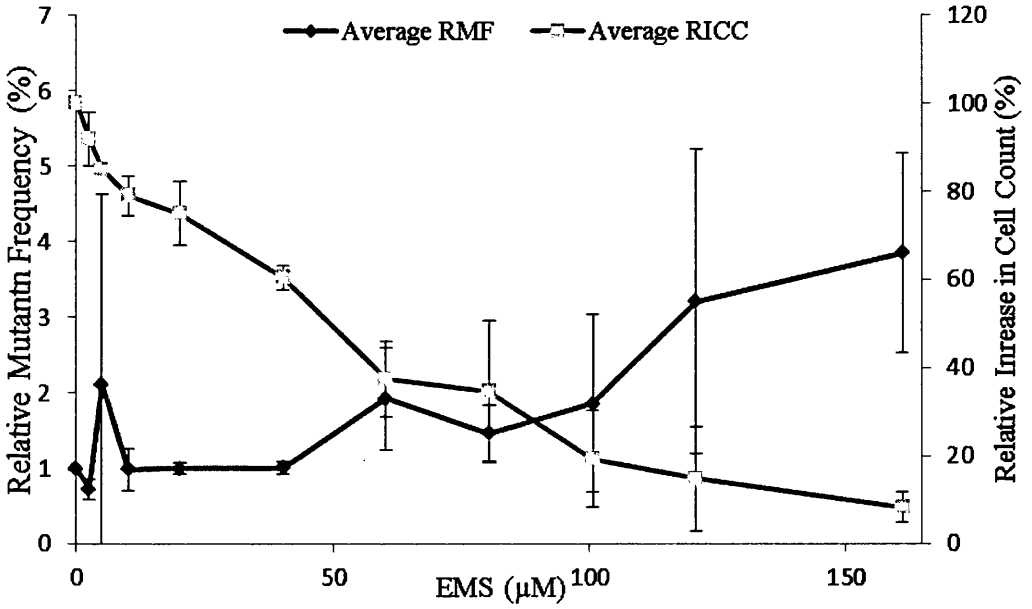

Figure 5.3.C Day 4, low passage human lymphoblastoid cells (MCL-5) average relative phenotypic *PIG-A* mutant frequency following 24 hr EMS exposure, CD59 antigen utilised as reporter for mutation, inclusion of HLD-DR and 7-AAD staining to ensure cellular membrane integrity. (Dunn's Test ($p < 0.05$*)(N=3)(Error Bars ±1SD)) *PIG-A* mutant data relative to the percentage of phenotypic *PIG-A* mutants observed within the con-current control.

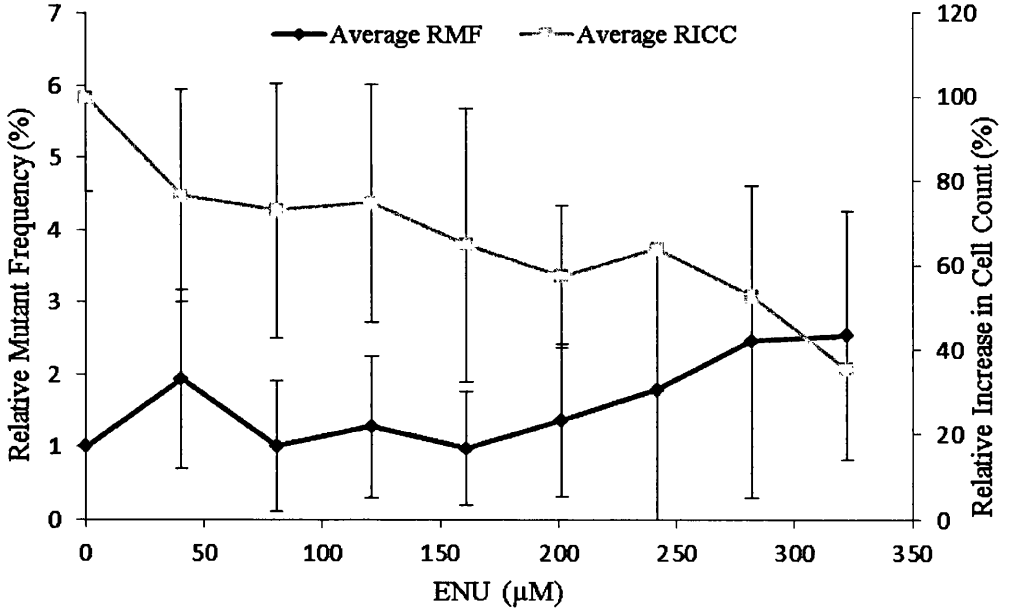

Figure 5.3.D Day 4, low passage human lymphoblastoid cells (MCL-5) average relative phenotypic *PIG-A* mutant frequency following 24 hr ENU exposure, CD59 antigen utilised as reporter for mutation, inclusion of HLD-DR and 7-AAD staining to ensure cellular membrane integrity. (Dunnett's Test ($p < 0.05$*)(N=3)(Error Bars ±1SD) *PIG-A* mutant data relative to the percentage of phenotypic *PIG-A* mutants observed within the con-current control.

5.3.2 Confocal Microscopy GPI-AP Expression Analysis

Within published in vivo rodent *Pig-a* and human *PIG-A* data, the focus is very much directed towards the quantitative dose response analysis following chemical exposures. This data serves a vital role within the future of safety assessment, and should enable the more apt hazard and risk assessment utilising the assay platform, however, little is known in terms of the biological mechanics of the reporter system. Due to the highly limited amount of mechanistic data, excluding sequencing of additional primary haemopoetic tissues, the purpose of this section was to assess the reproducibility of the biology behind the in-direct reporter system and come to a preliminary conclusion about the potential limitations associated with such a reporter and therefore, the most appropriate method for integration within the assay platform.

In an attempt to better characterise the reporter system utilsed within the *PIG-A* established mutation assays, laser scanning confocal microscopy imaging was implemented to more throroughly investigate the surface expression of the selected GPI-AP reporter marker as well as potentially evaluate future caveats associated to in-direct mutagenesis reporting and subsequent flow cytometry assessment.

The intial CD55 data conveyed that when assessed under a x 40 (Figure 5.4 A) or x 63 oil (Figure 5.4 B) objective the resultant antibody conjugation was comprehensively associated with the extracellular membrane; a distinctive halo was apparent within the images reflecting on the presence of preiphery staining. The antibody staining appeared to be relatively inclusive in nature, but was not entirely surface spanning and appeared to be heavily linked to specific regions along the membrane. When visualised within a 3D reconstructed image, based on ~ 0.1 μm z-stacked focussed images, the GPI-AP expression was more clearly defined as spartial in nature and consisted mainly of smaller dense pockets of expression, consistent with the current literature (Figure 5.5). However, an additonal minor internal CD55 signal was also detected within a central location within a subsection of MCL-5 cells.

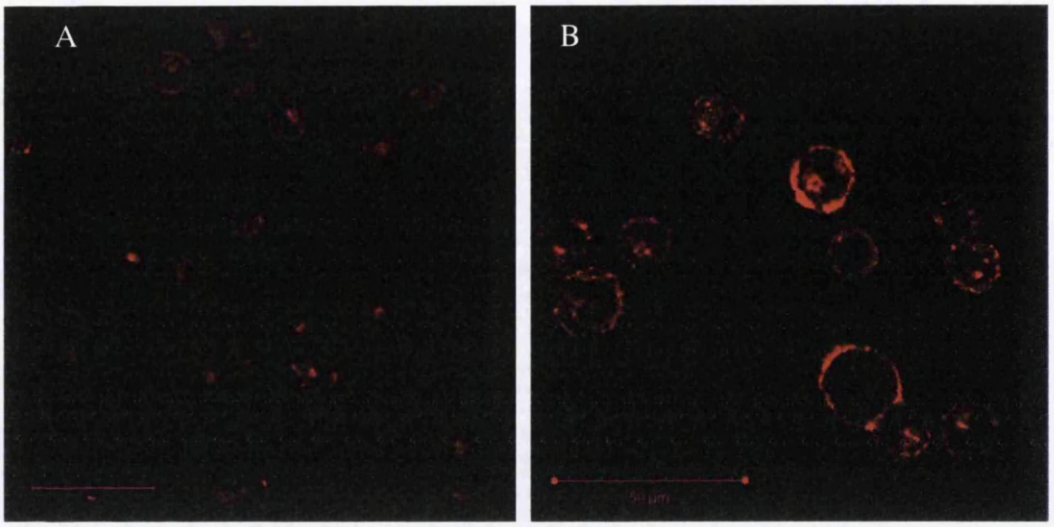

Figure 5.4. Anti-CD55 R-PE treated 4% PFA fixed MCL-5 cells imaged under A) x 40 and B) x 63 oil immersion objective utilising the laser scanning confocal microscope. Detected, R-PE signal was retrospectively artificially coloured red for image clarity and cohesion (Scale bar 50µM).

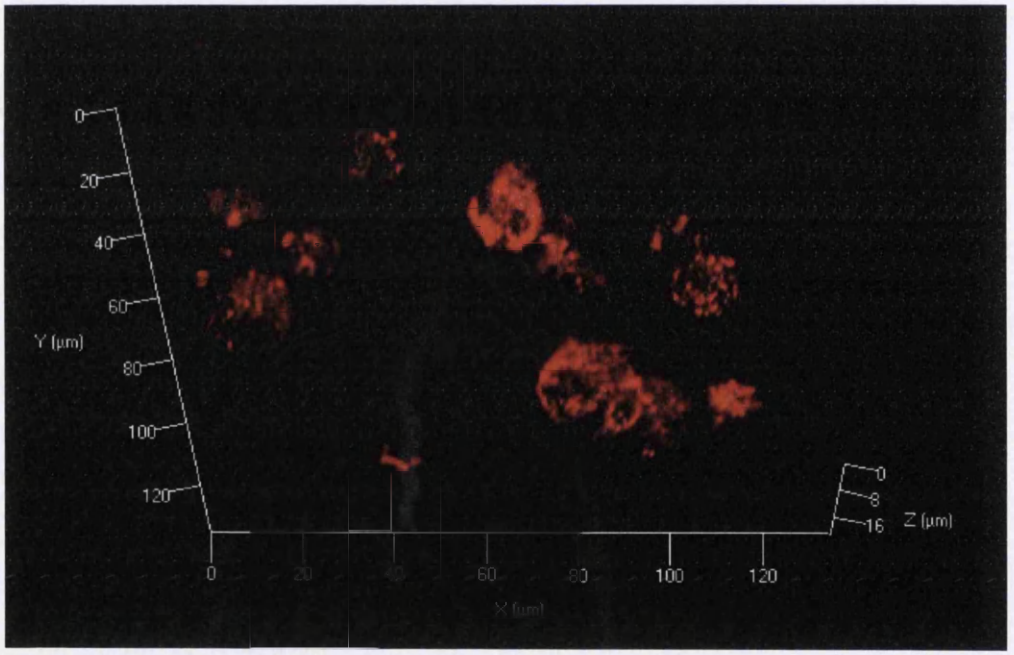

Figure 5.5. Anti-CD55 R-PE treated 4% PFA fixed MCL-5 cells, displayed within a 3D reconstruction following x 63 oil immersion, 1024 x 1024, z-stack capture utilising the laser scanning confocal microscope. Detected, R-PE signal was retrospectively artificially coloured red for image clarity and cohesion (Scale bar 50µM).

The subsequent CD59 data again demonstrated an analagous relationship in terms of the density of surface antigen staining with respect to localisation on the cellular membrane (Figure 5.6 A and B); CD59 surface antigen expression was estimated to be less comprehensive than the comparable CD55 data, in agreeance with previously reported data (Section 4.3.1), but again was localised within distinct pockets of expression (Figure 5.6 A and B). When 3D assessed, the density of expression was more apparent and the highly sporadic natrure of expression was also more prominent, CD55 resulted in a far more encompasing surface expression. The presence of intracellular stainng was not detected within the CD59 data, all signals were localised to the periphery of the cell.

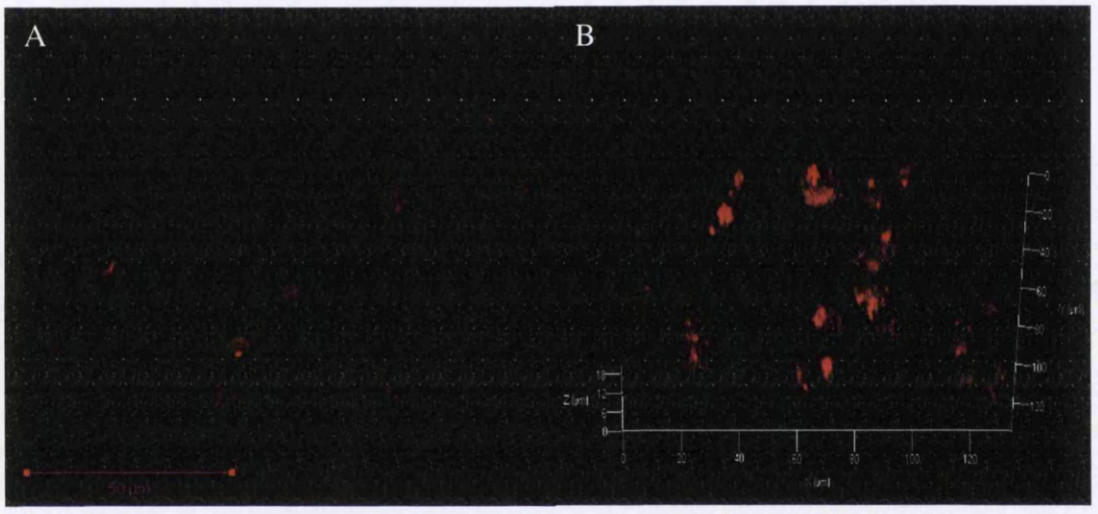

Figure 5.6. Anti-CD59 R-PE treated 4% PFA fixed MCL-5 cells captured under the x 63 oil immersion objective (A) and displayed within a 3D reconstruction following 1024 x 1024, z-stack capture (B) utilising the laser scanning confocal microscope. Detected, R-PE signal was retrospectively artificially coloured red for image clarity and cohesion (Scale bar 50µM).

When assessed following tandem exposure, the CD55/59 data generated significantly more comprehensive surface expression coverage, as expected, than either single stained antigen (Figure 5.7). Regardless of image manipulation, the most stringent optical settings resulted in well stained samples, with distinctive surface expression (Figure 5.7 A and B). However, even though the extracellualr surface was highly dense with CD55 or CD59 antigen presence, the sporadic nature of binding, reflected

the uniqueness of each cell within the population and this in it-self was highlighted as a potential limitation when utilised in conjuction with laser light excitation platforms.

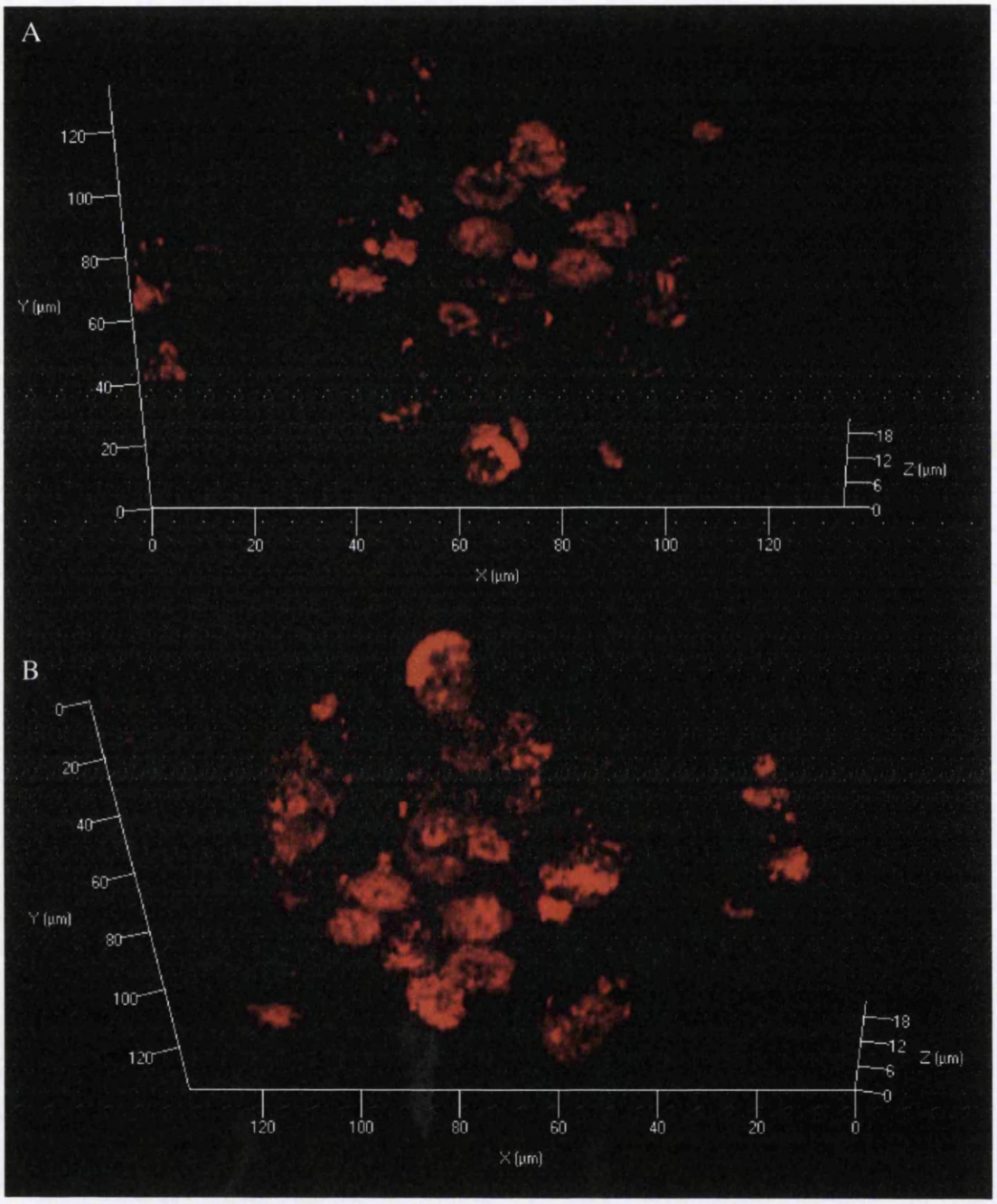

Figure 5.7. Anti-CD59/55 R-PE treated 4% PFA fixed MCL-5 cells captured under the x 63 oil immersion objective and displayed within a 3D reconstruction following 1024 x 1024, z-stack capture utilising the laser scanning confocal microscope. Conservative estimation of surface GPI-AP expression (A) and maximal estimation of surface expression (B). Detected, R-PE signal was retrospectively artificially coloured red for image clarity and cohesion.

Tandem marker coverage (Figure 5.7 and 5.8) was far superior to either of the single marker surface expression assessed (Figures 5.4 – 5.6). In an attempt to potentially relate the nature of surface marker expression with potential physical or morphological features on the extracellular membrane the use of transmitted light was implemented in conjunction with the detected emitted fluorescence signals. The resultant data, clearly showed the diverse variation within surface staining between homogeneous cells; no clear association of marker density or expresion was linked to any particular morphological feature of the membrane. However, a noteworthy correlation between antigen expression and dense localisation within the membrane was apparent due to the discrete nature of binding.

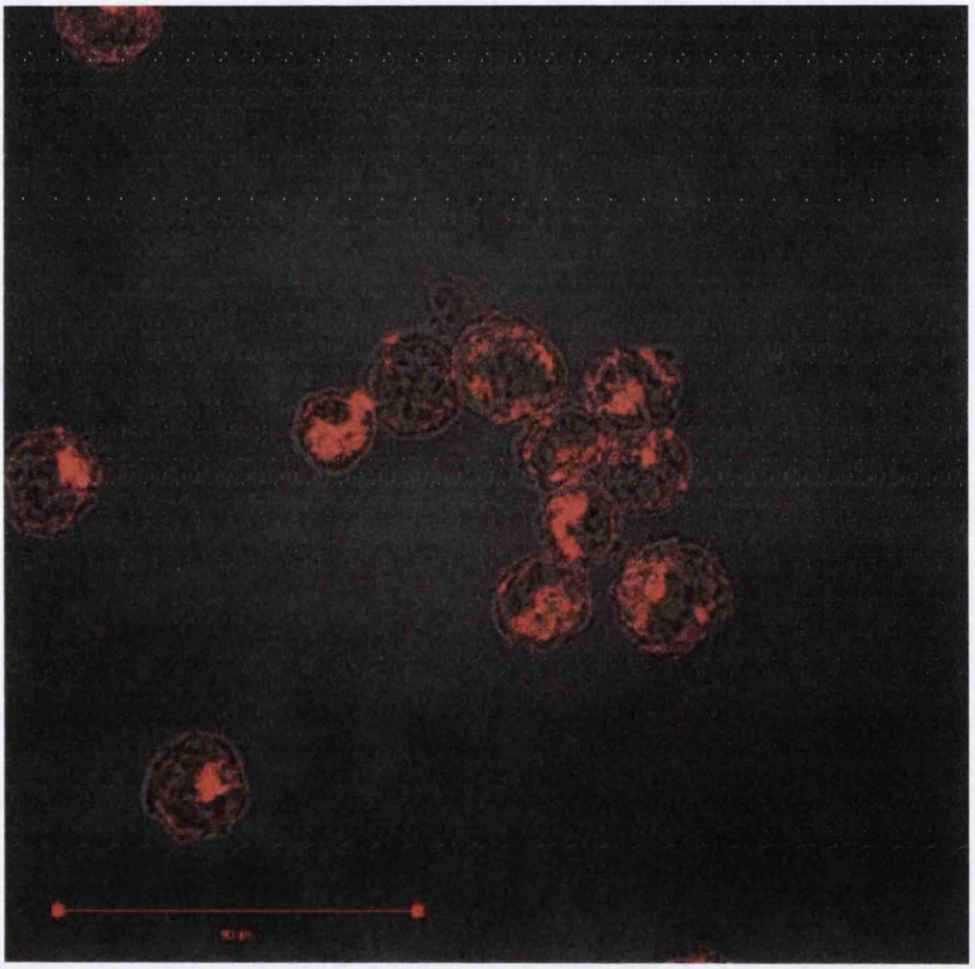

Figure 5.8. Anti-CD59/55 R-PE treated 4% PFA fixed MCL-5 cells captured under the x 63 oil immersion objective and displayed layer onto a transmitted light image (tPMT) utilising the laser scanning confocal microscope. GPI-AP surface expression defined clearly too specific regions of the surface membrane, GPI-AP do not entirely cover the extra-cellular surface of the cellular membrane. Detected, R-PE signal was retrospectively artificially coloured red for image clarity and cohesion (Scale bar 50μM).

Finally, the ability of 4% paraformaldehyde to act as a permeabilising agent within MCL-5 cell line usage was assessed via the inclusion of a counter stained analagous triton-x sample. In the presence of detergent, minor intra-cellular nucleic acid signal was identified (Figure 5.9), however, an analagous, but reduced signal was detected within the untreated sample, reflecting upon either the limited effectiveness of formaldehyde based fixatives on lymphblastoid membrane permeability.

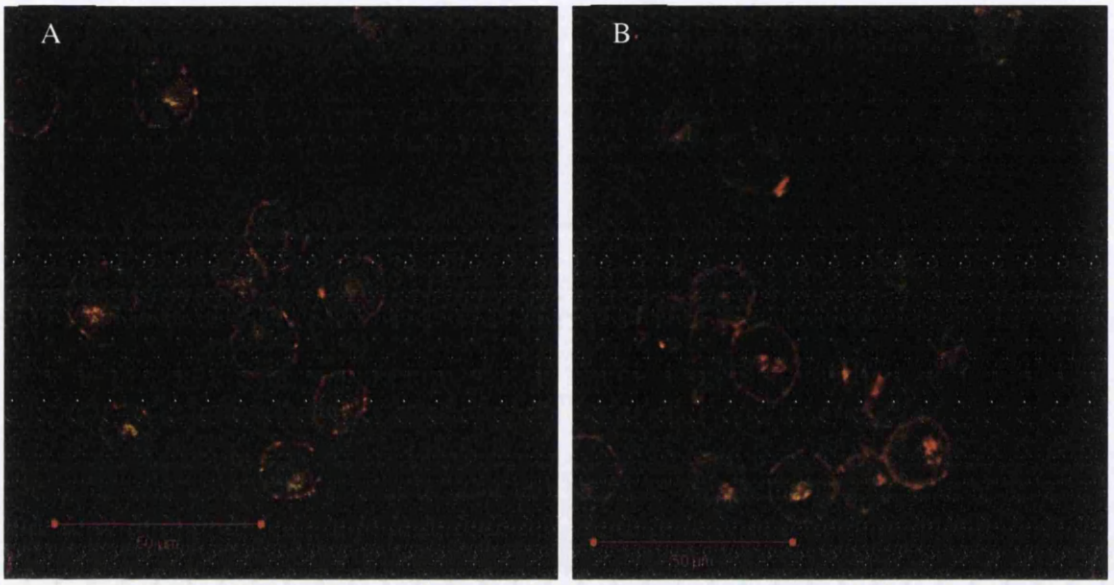

Figure 5.9. Anti-CD55/59 R-PE and 7-AAD treated 4% PFA fixed MCL-5 cells captured under the x 63 oil immersion objective (A) in the presence of Triton X and B) in the absence of Triton X utilising the laser scanning confocal microscope. Detected, R-PE signal was retrospectively artificially coloured red and the 7-AAD signal coloured green for image clarity and cohesion (Scale bar 50μM).

5.3.3 Preliminary MCL-5 *PIG-A* Assessment; Tandem CD55/CD59 Surface Antigens utilised as reporter following MNU Exposure

Following the dose finding experiments in which a suitable dose range of both EMS and MNU were obtained, MNU was chosen as the initial compound to be assessed within the revised in vitro *PIG-A* assay design. MNU is a highly potent alkylating agent and induces a well characterised mutagenic lesion, 0^6 methyl-guanine, resulting in GC -> AT transition mutations [264]. Due to the sheer potency of the compound, an estimated increase in presumptive phenotypic *PIG-A* mutant numbers is predicted. The use of tandem GPI-associated anchor proteins in order to reduce false positivity, as well as reduce the resting background mutant numbers in conjunction with a novel gating system approach, was trialled to evaluate potential sensitivity within the low dose region.

All data generated following daily *PIG-A* mutation assessment were evaluated for normality and variance (P value ≥ 0.05) using the Shapiro-Wilk and Bartlett's Test respectively, carried out within the DrSmooth add-on R-Software Package (R-3.0.2, Free Software Foundation's GNU project). The daily *PIG-A* data acquire following acute 24 hr MNU exposure was statistically determined to be non-normally distributed ($p<0.05$).

Based on the preliminary MNU dose finding study (Appendix Section 5.5.3.2) the final *PIG-A* analysis was scheduled for 72 hr post treatment (Day 3). The Day 3 data was retrospectively assessed following acquisition utilising two distinctly different gating strategies i) the original unrefined gating system and ii) novel exclusive method. When applying the original gating strategy, the background *PIG-A* mutant frequency was estimated as high as 80% of the total population, within the control samples (77.08%). The number of presumptive *PIG-A* phenotypic cells did not display any definite correlation to the applied dose of genotoxicant; however, the percentage *PIG-A* phenotypic viable mutants did appear to reduce as the doses increased, 46.6% observed at the top dose (Figure 5.10 A). Cytotoxicity was demonstrated to increase in a dose dependent manner, with a maximum 28% RPD value obtained at the top dose of MNU tested, 0.1 µg/mL. Even though the data was limited to a single biological replicate, the relationships observed were inconsistent

with those previously defined utilising an analogous reporter and cell line (Section 5.3.1).

However, when utilising the novel reformed gating strategy, the same experimental data collect at the day 3 analysis showed that the top dose (1 µg/mL) appeared to induce an increase in the percentage of viable putative *PIG-A* phenotype cells (0.2%) with respect to con-current negative control values (0.01%). An approximate 20-fold increase over the lowest observed control frequency was observed, however, due to replication limitations, i.e. data was a single replicate, cannot be assessed for statistical significance (Figure 5.10 B). The data appeared to show a dose dependent increase in percentage viable *PIG-A* mutants, especially prominent at the top dose, with little affect observed at the lower doses; defining a seeming sub linear dose response. Doses greater than 0.05 µg/mL seemed to demonstrate a noteworthy decrease in cytotox, with the top dose resulting in a 72% decrease in RCC values.

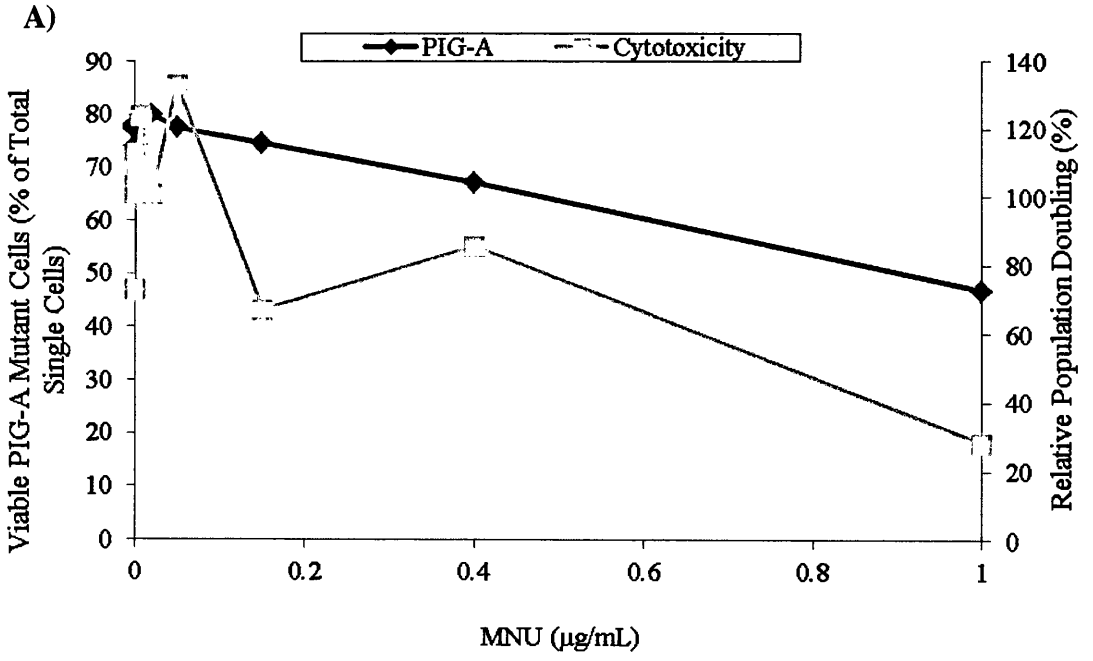

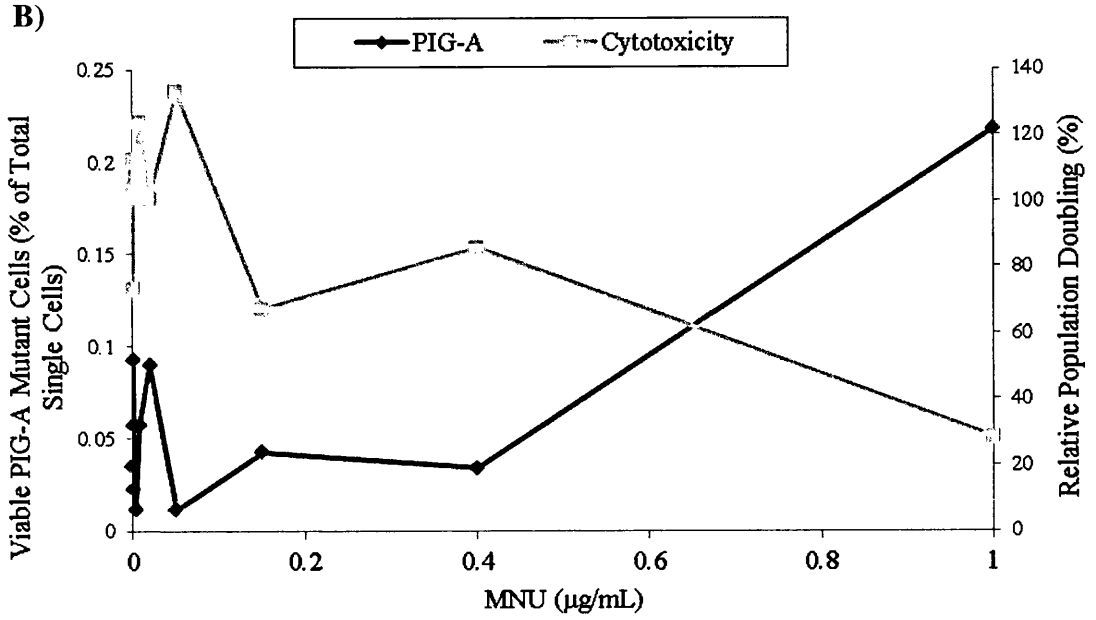

Figure 5.10. Dose response Day 3 *PIG-A* data for MCL-5 cellular cultures exposed to acute 24 hr MNU treatment. Tandem anti-CD55/CD59 R-PE conjugate antibodies utilised as reporters for loss of phenotype assessment and membrane integrity dye (7-AAD) incorporated. Original Gating System (A) and novel FL-W based gating system (B) (N=1) (>10,000 Single Cell Events acquired).

5.3.4 Assay Refinement - Gating Strategy Comparison and Apoptotic Morphology Investigation

Within the flow cytometry gating strategy, utilised to assess the cellular populations for phenotypic *PIG-A* mutant status, there are multiple stages which can be manipulated and hence, are subjective to the operator. Additional to the threshold value, as currently determined by the operator following ICS analysis, the mechanism of event exclusion was also investigated to detect potential bias within the subsequent data. Within all subsequent data displayed within this section, only a FSC-A threshold was applied, the newly incorporated FSC-A vs FSC-W doublet discriminating gate was removed as well as the use of viability dyes, to increase the effect the trialled supplementary gating strategies would have on the subsequent data. Utilising tandem CD55/59 markers, the original, novel (FSC-A vs PE-W) and future proposed (PE-A vs PE-W) additional discriminating gates were evaluated for their direct effect on *PIG-A* reporting.

5.3.4.1 Gating Strategy Direct Comparison

Utilising the original gating system, with no discriminating gates to exclude apoptotic cells, doublets or debris ~85% of MCL-5 cells stained positive for CD55/59 presence and hence, were defined phenotypic *PIG-A* wild type. When the novel gating system was assessed, the pre-existing number of phenotypic *PIG-A* mutants was reduced significantly, from ~15% to ~0.005% (Table 5.1), and subsequently increased assay sensitivity considerably. However, when the potential future additional gating strategy was assessed, the number of pre-existing phenotypic *PIG-A* mutants was shown to be completely eliminated from all samples analysed and hence, the gating strategy was shown to demonstrate a significant bias on the subsequent *PIG-A* mutant data (Table 5.1).

Table 5.1. Summary of the relative presumed phenotypic PIG-A wild type data, within control untreated MCL-5 cells, evaluating the potential bias within the gating strategies trialled. Tandem surface antigen markers CD55 and CD59 were utilised as in-direct reporters of PIG-A mutation. (>20,000 defined single cellular events were assessed).

Sample Identification	Total Number of Recorded Events	Number of Events Defined "Single Cell"	Trialled Gating Strategy Descriptor	Number of Viable Cells	Number of Cells Defined CD55/59 Positive	Percentage CD55/59 Positive of Viable Cells
ICS	43856.0	20575.0	17574.0	17573.0	0.0	0.00
Original Gating	48629.0	20569.0		17577.0	17577.0	85.45
FSC-A vs PE-W 1	48629.0	20391.0	18056.0	17874.0	17873.0	99.99
FSC-A vs PE-W 2	59135.0	20495.0	17983.0	17750.0	17748.0	99.99
FSC-A vs PE-W 3	48190.0	20418.0	18171.0	18019.0	18019.0	100.00
Average	51984.7	20434.7	18070.0	17881.0	17880.0	99.99
PE-A vs PE-W 1	48629.0	20841.0	18584.0	18407.0	18407.0	100.0
PE-A vs PE-W 2	59135.0	20882.0	18384.0	18140.0	18140.0	100.00
PE-A vs PE-W 3	48190.0	20748.0	18431.0	18245.0	18245.0	100.00
Average	51984.7	20823.7	18466.3	18264.0	18264.0	100.00

Within the novel gating strategy, in which doublets are more accurately removed by the inclusion of a supplementary doublet and debris discriminator to the pre-existing FSC-A vs FSC-W measure, FSC-A vs PE-W, was accepted as the proposed analysis method to continue assay development. Utilising the novel gating strategy, in the absence of a typical doublet discriminating plot, the background spontaneous mutants/resting mutant frequency was estimated to be 0.005% or 50 phenotypic *PIG-A* mutant cells $x10^{-6}$ events scored (Figure 5.11), analogous to validated genetic toxicology mammalian in vitro gene mutation assays as well as recent published literature.

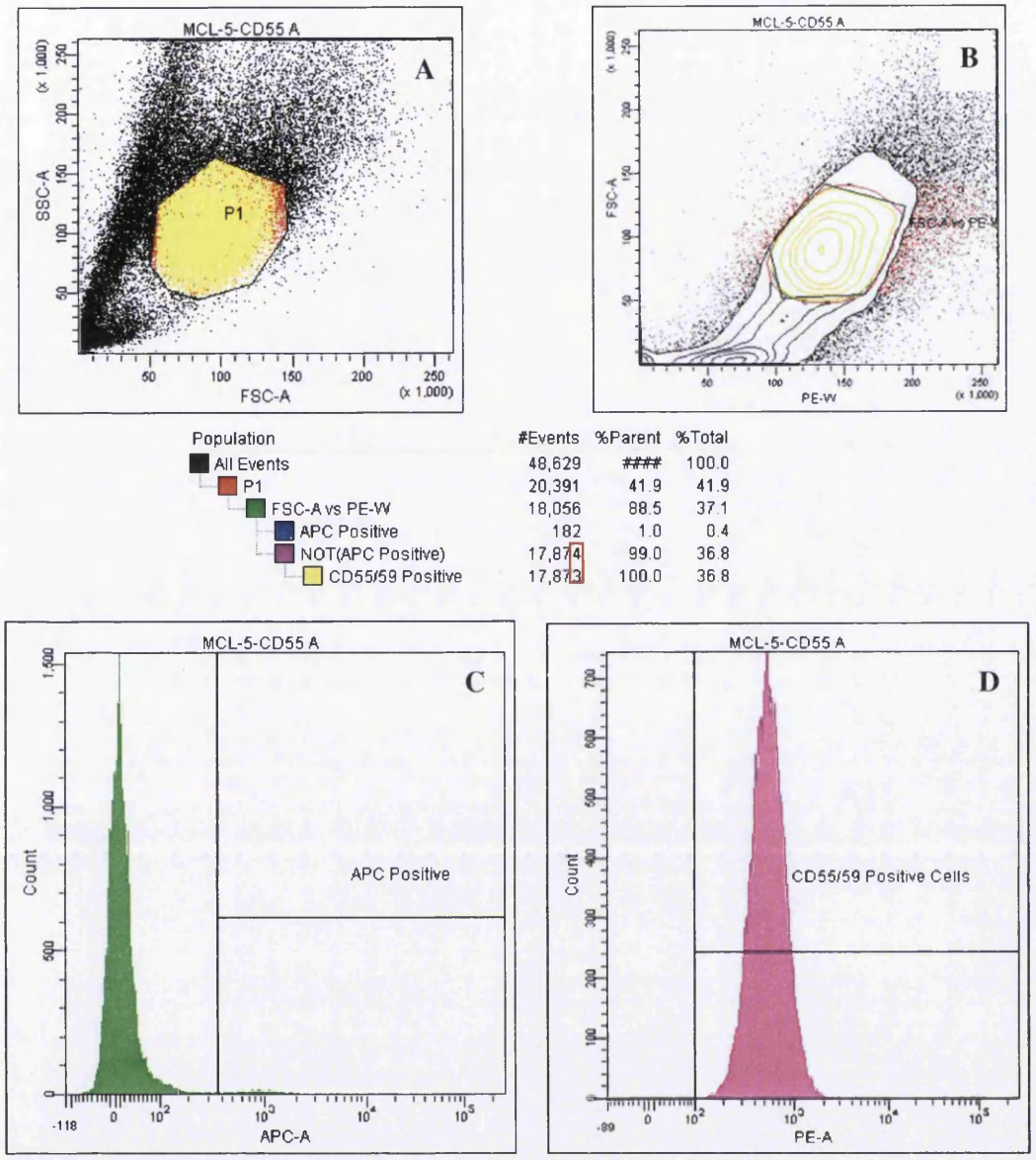

Figure 5.11. A representation of the current optimal gating strategy, excluding the usage of an apoptotic marker, within untreated MCL-5 cells; A) initially an estimated single cell population (FSC-A vs SSC-A), followed by the use of B) fluorophore specific pulse width measure (PE-W) to remove agglomerates and debris prior to C) loss of membrane integrity exclusion (7-AAD) and D) *PIG-A* phenotype assessment (anti-CD55/59 R-PE). (~50,000 Cells were scored for *PIG-A* phenotype, 0.005% pre-existing phenotypic *PIG-A* mutants estimated (~50 x 10^{-6}).

5.3.4.2 Apoptotic Morphology Investigation

Apoptosis is a highly characterised event in terms of the biological processes occurring within the cell, reflecting in the sheer number of publications available reviewing the mechanistic aspects driving initiation and propagating the removal of cells. However, even though microscopy derived images, IHC, and flow based platform data are available, very little is published on the ability to track apoptosis without the use of fluorescence conjugated dyes. Therefore, in an attempt to better characterise apoptotic cells within parental populations, in order to more accurately exclude this potential *PIG-A* mutant phenotype mimicking event, as well as assess its impact on the fidelity of the reporter system the following experiments were undertaken.

Within previous chapters, the data has suggested that the populations of presumed *PIG-A* deficient phenotypic cells, either untreated or following chemical exposure, constitutes of a higher proportion of cells which are non-viable when compared directly against the phenotypic wild type cells. Therefore, because of this, there is reason to believe that biological pathways shared by non-viable cells, i.e. apoptosis or necrosis could be inducing a *PIG-A* mutant phenotype, during flow cytometry analysis, when there is a lack of mutation at the *PIG-A* gene locus. In order to investigate this phenomenon and theoretically identify novel methods of excluding such mutant mimicking events from subsequent flow cytometry analysis, the morphology of apoptosis and necrosis, and their effects on cellular surface antigen expression were assessed.

Initially, MCL-5 cells undergoing loss of cellular membrane integrity and apoptosis, as a result of 8 hr acute toxic Staurosporine exposure, were assessed in terms of their respective light scatter properties. Utilising FSC-A (size) and FSC-W (time of flight) measures, both dead and dying (apoptosis) cells were retrospectively artificially coloured, and visualised in terms of the general single cell population. Dead and dying (apoptosis) cells did not appear to significantly change in morphology, with respect to cellular size, when compared to the general population of viable cells (Figure 5.12). However, dead cells did appear to be marginally smaller, as described by a lower average FSC-A value. This relationship was again re-enforced by the

results obtained when FSC-A was compared against PE-W, in which cells which lack membrane integrity easily visualised as "smaller" events, especially when directly compared to apoptotic cells, with regards to the viable population (Figure 5.12). The distribution of the dead cell population was distinctly lower within the doublet discriminating gate, than the comparable apoptotic data.

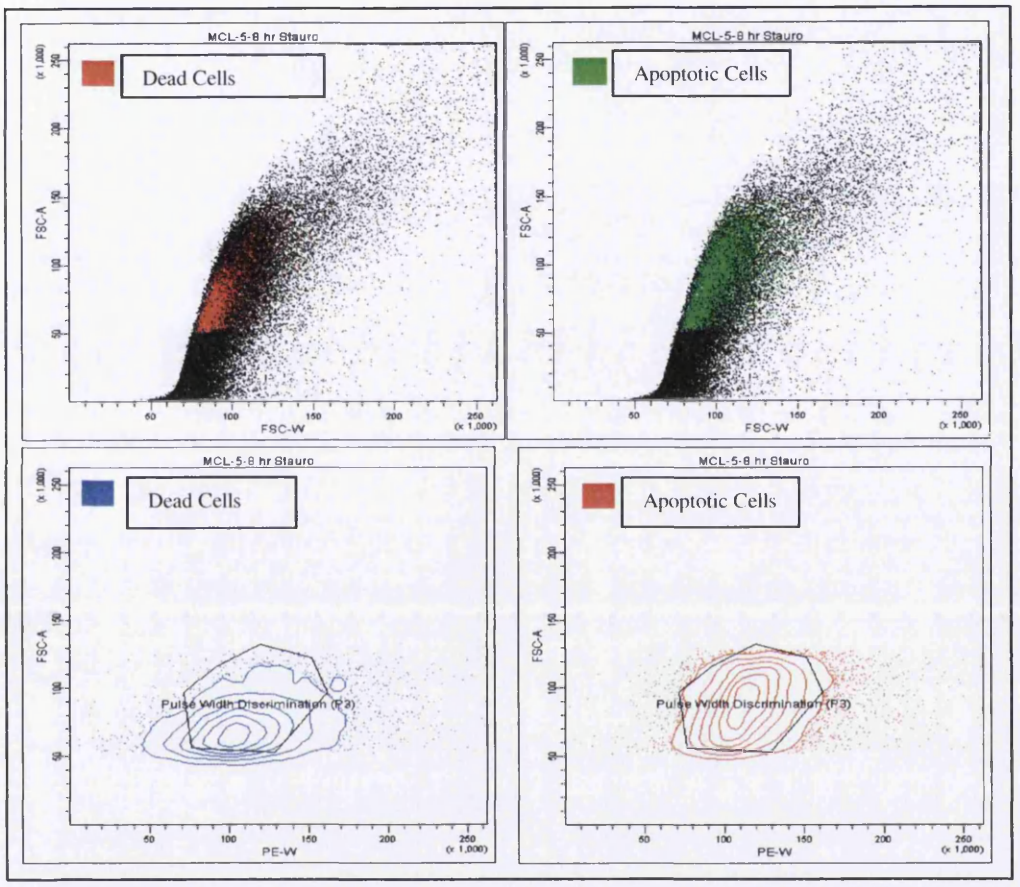

Figure 5.12. Tracking apoptotic and complete loss of membrane integrity within phenotypic *PIG-A* wild type MCL-5 cells; in terms of their physical light scatter properties within the context of typical *PIG-A* gating strategy following acute 8 h 1 µM Staurosporine exposure (>20,000 acquired and subsequently analysed).

Following Staurosporine (1 µM) time course exposure, relative percentages of apoptosis and necrosis cells; categorised by complete loss of membrane integrity as well as annexin V sensitivity, were demonstrated to increase in a dose dependent manner, excluding "60 min" necrosis data (Table 5.2). Apoptosis and necrosis were demonstrated to rise from 2.3 and 27.8 to 46.7 and 76% respectively as the Staurosporine exposure duration increased from 30 to 480 min (Table 5.2). When the

data was graphically plotted to establish the nature of the relationship, an ostensibly linear correlation was observed; both apoptosis and necrosis revealed a highly comparable linear correlation with analogous equation for the line of best fit, the comparable R^2 values for the slope reflects the positive nature of the correlation (Figure 5.13).

It was also apparent that as the exposure time of Staurosporine increased, and therefore, the cells were further progressed along their respective death pathways, the numbers of cells scoring as phenotypic *PIG-A* mutants also increased (Table 5.2). At the lower exposure times, and hence, early stages of either apoptosis or necrosis, no cells were scored as phenotypic mutants. However, as the exposure time increased and the cells were much further established within their respective pathways, the number of potential phenotypic *PIG-A* mutants was also demonstrated to increase (Table 5.2).

Table 5.2. 1μM Staurosporine summary MCL-5 data following a time course exposure (0-480 min). Apoptosis was determined by events defined positive for Annexin V sensitivity , necrosis was defined by events defining positive for both complete loss of cellular membrane integrity (7-AAD) as well as being apoptotic (Annexin V); relative PIG-A data assessed following anti-CD55/59 R-PE tandem exposure (>3,000 events captured for each time period).

Sample Identification	Dead Cells Defined Necrotic (%)	PIG-A WT (%)	PIG-A Mutant (%)	Viable Cells Defined Apoptotic (%)	Pig-A WT (%)	PIG-A Mutant (%)
30 min	27.8	100	0	2.3	100	0
60 min	43	100	0	4.4	100	0
120 min	24.9	100	0	5.2	100	0
240 min	61.8	100	0	44.2	99.9	0.061
480 min	76	98.7	1.3	46.7	99.9	0.108

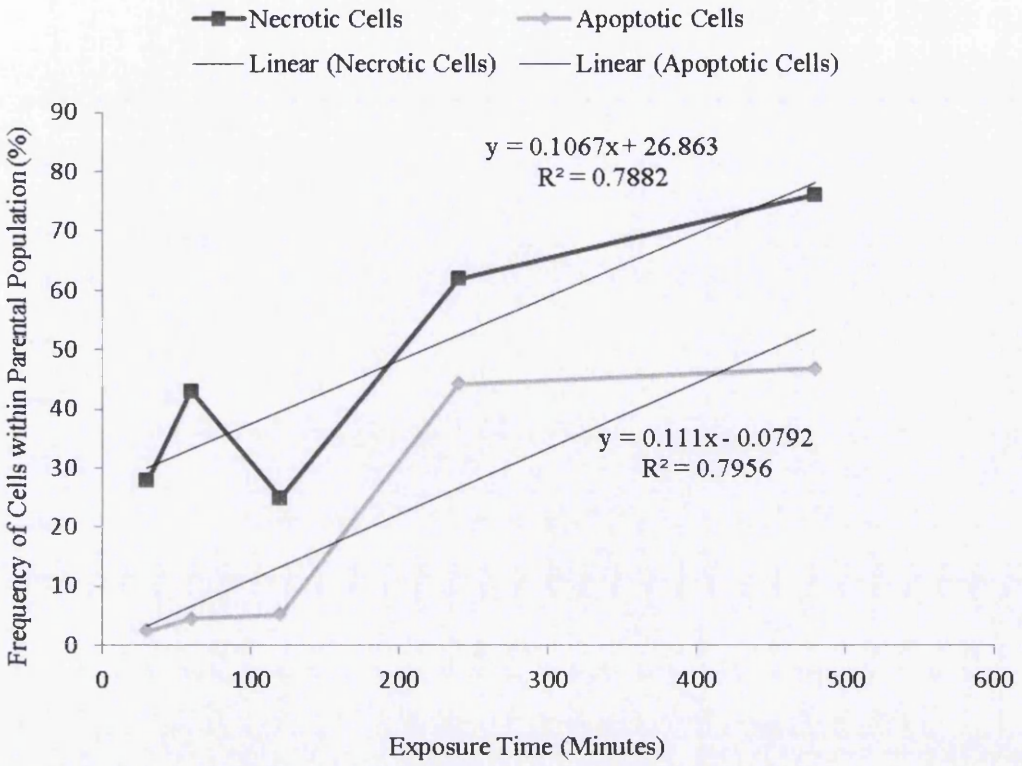

Figure 5.13. Relative percentage of Necrotic and Apoptotic cells in relation to 1µM Staurosporine exposure time, within MCL-5 cell cultures. Linear Trend lines calculated and R^2 values for both data sets to reflect the correlation within the cellular viability and duration of genotoxin exposure (>6,000 events scored for each time period).

This observation was more thoroughly investigated through the sequential flow cytometry histograms tracking the respective fluorescence intensity signal data emitted from specific anti-CD55/59 mediated GPI-AP binding (Figure 5.14). The data visually displays the observation that as the length of Staurosporine exposure increases, and hence, the progression through the death pathway develops; the average fluorescence intensity values corresponding to GPI-AP expression decreases. For prolonged exposure, 4 hr or greater, the average fluorescence intensity values begin to pass the threshold value, as pre-defined by the ICS, and hence, can be classified as phenotypic *PIG-A* mutant events – their integrity as mutants is highly sceptical as phenotypic expression of GPI-AP loss is estimated as 3-4 days.

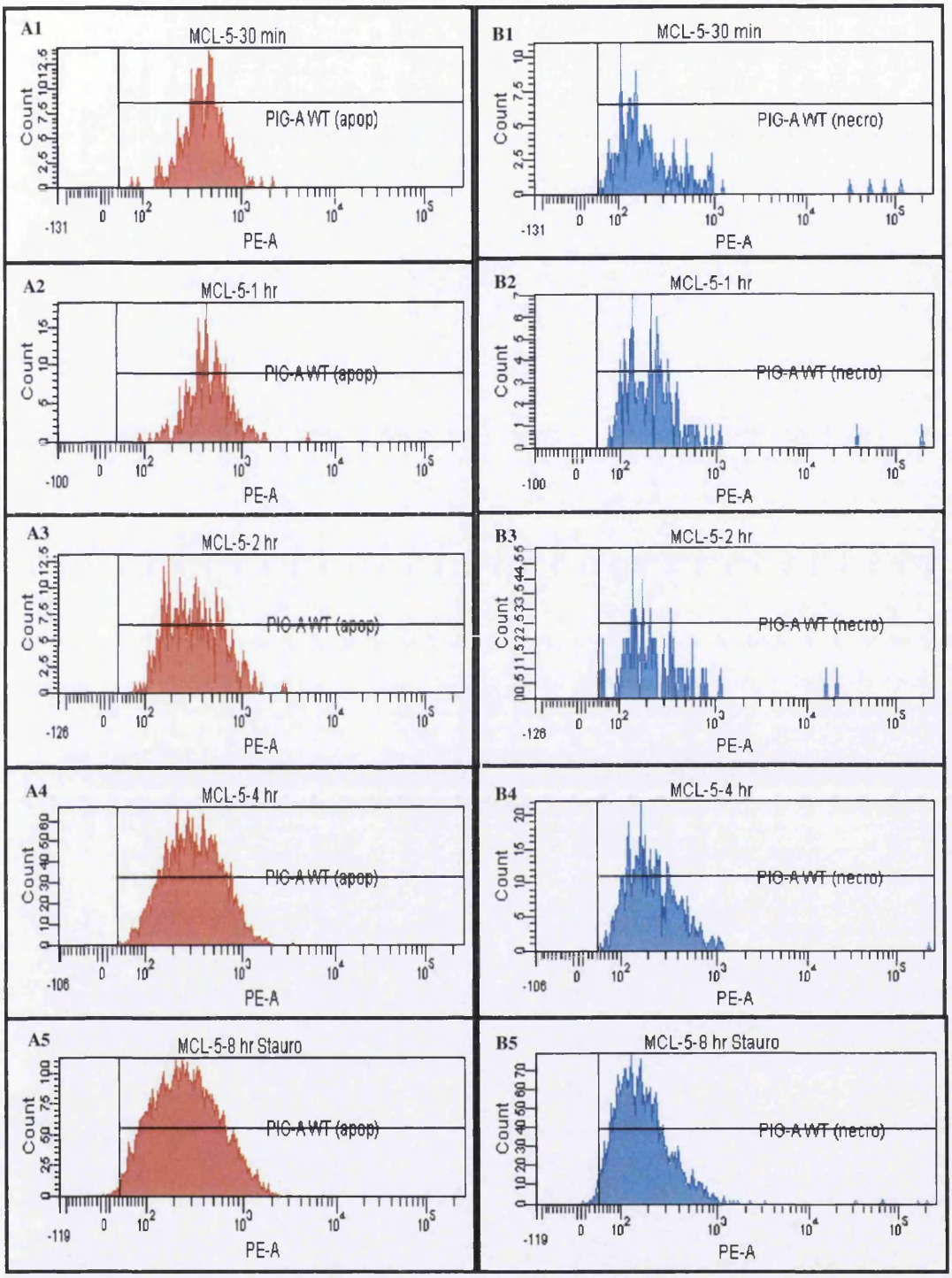

Figure 5.14. Relative phenotypic *PIG-A* mutant frequency data for MCL-5 cells undergoing A) Apoptosis and B) Necrosis following a time course acute 1 µM Staurosporine Exposure. 1) 30 min, 2) 60 min, 3) 120 min, 4) 240 min and 5) 480 min. Relative PE detector signals utilised as the measure for surface GPI-AP expression (>3,000 Events analysed in each sample)."*PIG-A* WT" gate present defines threshold for phenotypic *PIG-A* mutant status.

5.3.5 Next Generation Sequencing

Using each gene as a reference sequentially, the pooled paired-end reads were aligned to the reference using the "mem" command within Burrowers Wheeler Alignment (BWA) [343], formatted "mpileup", SAM tools [344], and variants called, VarScan [345]. The parameters required for a variant to be called were as follows, read length - >80 bp, minimum coverage - >8 reads, minimum variant frequency - 1%, minimum average quality score - Q30. In addition, reads were removed from analysis if the average quality of a 4 base "window" or section dropped below a score of Q20. Following variant calling, sequential graphical outputs were generated describing the relationship between depth and variance, the localisation of variants, including insertions or deletions (indels), in regards to the coding regions as well as the nature of variants with respect to the open reading frame (ORF). Data alignment and variant calling pipeline was constructed under guidance and run by Dr. Matt Hitchings, and subsequent re-formatting and graphical output construction was implemented by Dr. Sion Bayliss.

Unfortunately, the control spontaneously induced phenotypic *PIG-A* mutant cell population failed during sample preparation and therefore, with no control data set in order to validate the effects of the chemical, subsequently the integrity of the EMS induced data is highly affected. As a direct consequence of this, the conclusions able to be taken from this data are speculative and offer little confidence and therefore, are available within the Appendix only (Appendix Section 5.3.5).

5.4 Discussions and Conclusions

5.4.1 Trialled usage of HLA-DR Staining to Validate Single Marker PIG-A Dose Response Data within MCL-5 Cells

To date within in vitro *PIG-A* assay development, an unceasing point of discussion is the impact which cellular viability, cytotoxicity, has on the flow cytometry based phenotypic *PIG-A* mutant scoring. Previously, comments have been made on the required need for inclusion of viability dye incorporation within the assay design; due to apparent un-equal distribution of non-viable events between phenotypic wild-type and mutant *PIG-A* populations. Therefore, viability dyes not only appear to be needed to be incorporated indefinitely into the assay design, but additional early stage detection of such cellular pathways need to be investigated to ensure optimum assay sensitivity within the context of false positivity scoring.

Utilising HLA-DR molecules as direct reporters of membrane integrity may offer an initial replacement for the inclusion of highly sensitive, possibly overly sensitive, live or dead DNA intercalating fluorescence molecules such as propidium iodide or 7-AAD [346], as well as provide a more descriptive phenotype of the cellular event. The current use of such dyes provides limited biological contextual information, an event is simply defined as membrane integrity intact or membrane integrity loss, and therefore, there is potential for cells prior to complete loss of membrane integrity to suffer from GPI-AP inversion and other such processes which could induce a false negative signal.

Following the modified assay design, four chemicals were selected to be assessed for in-direct *PIG-A* mutant frequency, through the use of anti-CD59 staining in conjunction with HLA-DR; these were EMS and MNU for consistency, along with ENU and 2,4 Dinitrophenol (2,4 DNP). All compounds were to be assessed to concentrations greater than the corresponding LD_{50} dose. As previously described, EMS, MNU along with ENU are highly mutagenic alkylating agents, which operate under both Sn1 and Sn2 mechanisms [16, 41, 264] which have found limited use as chemotherapeutic agents [347]. 2,4 DNP however, was selected not for its mutagenic

ability, but more to evaluate the assay design to assess a more complex compound (Appendix Section 5.4.1). 2,4 DNP has an essential function as a proton ionophore, it therefore, defeats the proton gradient and reduces the efficiency of the electron transport chain. For this purpose 2,4 DNP was extensively used in diet pills within the 20th century until recalled due to onset of dangerous side effects, however, found continued use especially prominent within substance abuse within bodybuilders. 2,4 DNP is a well-known environmental contaminant, however, has no direct mechanism for genotoxicity and offers an interesting case study within the context of the in vitro *PIG-A* assay development. 2,4-DP has been demonstrated to be highly toxic but not genotoxic [348, 349].

Initially reflecting on the EMS and MNU dose response data; previously, EMS chemicals had been shown to elicit a sub linear dose response with elevated doses displaying statistically significant increments within the frequency of phenotypic *PIG-A* mutant events. Utilising the modified assay design, following HLA-DR inclusion, both chemicals demonstrated a comparable sub-linear dose response, with the EMS top dose (160 µM) inducing a statically significant increase in phenotypic *PIG-A* mutants. A LOAEL was observed approximately at 20 µg/mL, comparable to the previous TK6 data (Sections 3.3.3 and 4.3.4). MNU treatment was not shown to generate a statistically significant increase, due to the observed variance between replicates, however, was observed to induce a larger relative fold increase in phenotypic *PIG-A* mutant frequency (data mirrored by PROAST38.9 modelling (Appendix Section 5.3.1). These data comply with currently published literature describing alkylating ability and potency [39, 167, 264, 350] and offers preliminary validation for the sensitivity of the assay design. However, increases in phenotypic *PIG-A* mutants were potentially associated to increased cytotoxicity, but not within the ENU and 2,4 DNP data – alluding that the method for toxicity measurement especially when using highly genotoxic chemicals may be inappropriately over estimating toxicity.

However, the resultant data following ENU treatment was not as expected; no doses (including the LD_{50}) induced an apparent increase in phenotypic *PIG-A* mutant frequency for this known alkylating agent (Figure 5.3 D). ENU, like MNU, is another potent mutagenic compound which should have been defined positive within this assay design and has been demonstrated to be significantly positive within the

analogous in vivo Pig-a assay [166, 176, 196, 350]. A reason for the lack of apparent dose response would be due to the diverse variation observed within dose response replicates, due to this, the statistically derived metrics for determining significance, which take into account the variance, could be underestimating the response. This is more apparent when looking at the PROAST modelled data (Appendix Section 5.3.1), as the individual replicates are apparent, and the sheer variance can be appreciated. 2,4 DNP, the compound believed to be non-genotoxic was demonstrated to be negative within the assay design; no significant increments in phenotypic *PIG-A* mutant frequency were observed across the entire tested dose range.

The data collected from this limited validation ranked the compounds in terms of potency, with the exception of ENU, in line with that historically described within the literature [39, 350], and the unknown, presumed genotoxic negative compound, generated no obvious increase in phenotypic *PIG-A* mutant frequency at doses which displayed significant toxicity.

Previously, the dose response data could be scrutinised heavily for the apparent correlation between increased recorded phenotypic *PIG-A* mutant frequency and cytotoxicity, especially prominent at doses approaching the LD_{50} value (Section 3.3.3 and 4.3.4). However, following the implementation of the novel membrane integrity marker, the apparent relationship was significantly reduced if not removed; 2,4 DNP and to some extent the ENU data at doses higher than and including the corresponding dose equivalent to the LD_{50}, no significant variation in mutant frequency was detected. This demonstrates a perceived greater level of accuracy when reporting the presumptive phenotypic *PIG-A* mutant frequency utilising this design when compared to previous versions.

Incorporating HLA-DR staining, in tandem with anti-CD59 PE in-direct phenotype reporting, appears to be an additional viable methodology for assessing, at least qualitatively, compounds for mutagenicity. Although due to micro-invaginations or inversions of the membrane prior to integrity loss, additional apoptotic marker incorporation would also be advised to prevent potential *PIG-A* reporting bias. In conclusion the MCL-5 cells without enrichment appear to be as sensitive as the previous TK6 platform (dose spacing reliant) for the future development of the in vitro *PIG-A* gene mutation assay. In order to assess quantitative dose response

modelling, the potential use of tandem marker assessment in conjunction with HLA-DR, apoptotic markers and the proposed novel gating systems would be required. This planned combination of factors gave the impression to be able to deliver a level of sensitivity unobtainable with the use of TK6 cells, which have recently been shown to be acceptable under specific technical circumstances [301] or different cells.

5.4.2 Confocal Microscopy GPI-AP Expression Analysis

Both the in vitro and in vivo Pig-a gene mutation assay designs rely on the accurate reporting of GPI-AP presence as the in-direct reporter for mutational events at the *PIG-A* gene locus [166, 301, 351]. The in vivo assay is currently a significant way through the progressive validatory stage to facilitate OECD guideline drafting [166, 180]; however, there is a lack of morphological data attributed to both the mutant and wild type phenotype. Due to this, the well documented reporter system is still un-validated on a biological level and has received criticism due to the lack of definitive mechanistic proof. GPI-AP distribution, on the extracellular cell surface, has been reported to be highly conserved in nature as well as distinctly localised in discrete areas of high lipid density [352]. These areas are termed lipid rafts and have an accumulated protein rich density, believed to be the primary binding sight for antibodies raised against GPI-AP antigens. Minimalistic distribution on the cell membrane actually hinders the reporter system for use in conjunction with laser excitation platforms, especially those which favour transverse image capture [240, 314]. The reason for is the planar bias which corresponds to the distribution of lipid rafts across the membrane, each cell may provide a distinctly positive average signal, with 95% of said signal originating from 5% of the surface area. In order to investigate the GPI-AP distribution of the selected reporter antigens and their subsequent effect on the potential laser excitation platforms within the in vitro design, high resolution confocal imaging was utilised in conjunction with immunofluorescence staining.

Single stained anti-CD55 and CD59 R-PE PFA 4% fixed MCL-5 cellular samples displayed typically comprehensive surface emission profiles when visualised under

high resolution 1024 x 1024 confocal imaging. Both examples of a transverse section demonstrated a distinctly halo like effect, with a comprehensive distribution on the extracellular surface of the cellular membrane (Figures 5.4 - 5.6). However, this apparent extensive expression was demonstrated to be highly orientation plane specific, distinctly sporadic in nature and relatively sparse across the entire surface area of the membrane following 3D reconstructive z-stack imaging. The images outlined in Section 5.3.2, reported in detail the limited surface expression and the highly restricted distribution, seemingly associated to specific areas of high density on the membrane, as outlined by transmitted light composite images (Figure 5.8). This lack of true surface abundancy potentially limits the use of such a reporter with laser scanning or laser penetrance platforms. The Amnis image stream ™ system, in which fluorescence data is displayed within images analogous to transverse light microscopy, could falsely report GPI-AP status; an observation which is seen due to the focus and plane sensitivity which is apparent within the consequential image stream generated Ideas® 5 data (Appendix Sections 3.5 and 5.5). 3-dimensional extended depth of field (3D-EDF) imaging is available on the image stream ™ to account for this however; it has little impact on the overall relationships displayed.

However, tandem GPI-AP staining was shown to produce a more favourable staining efficiency within the parental lymphoblastoid cell lines (Figure 5.7 and 5.8), the results appear to further highlight the potential risk of false positivity within single reporting antigen samples. In addition to this, the CD55 antibody reported intracellular staining within the z-stacked confocal images collected; a result of potential internalisation following limited PFA induced permeability. Triton-X treatment appeared to have little effect on membrane permeability and if the use of intracellular markers were to be investigated, then in future more optimisation would be required.

The confocal imagery within this section provides solid evidence to support a biological mechanism of GPI-AP association and density profiling on the extracellular surface of human immortalised cell lines. In conjunction with flow cytometry and similar platforms, in which the diameter of the excitatory laser is greater than the diameter of the cellular event, there is little evidence to suggest potential plane issues. Tandem phenotypic marker staining resulted in a more

comprehensive surface expression profile, as expected, and would remain the advised procedure to limit the risk of plane biasing or false positivity reporting.

5.4.3 Preliminary MCL-5 *PIG-A* Assessment; Tandem CD55/CD59 Surface Antigens utilised as reporter following MNU Exposure

Prior to any physical or chemical mutant depletion methodology, MCL-5 cells were demonstrated to exhibit an optimal comprehensive surface coverage of tandem GPI-APs, CD55 and CD59 (99.8%). Following biological assessment, the need for tandem antigen reporting was concluded. Therefore, in an attempt to quantify the increase in base line increase in assay sensitivity following the incorporation of tandem reporting antibody inclusion, HLA-DR staining was omitted. Therefore, the proposed in vitro *PIG-A* assay protocol was assessed for phenotypic *PIG-A* mutant frequency following acute MNU treatment. However, in addition to assessing the chemicals ability to induce genotoxicity, the assay design itself was further tested by the trial of a novel gating strategy aimed to further remove ambiguity within flow cytometry data. As previously discussed, misinterpretations of cells based on crude light scatter profiles can potentially dramatically increase the number of events scoring as presumptive phenotypic *PIG-A* mutants [318]; therefore, the trialled incorporation of pulse width measures to exclude debris and doublets to improve assay sensitivity was also assessed.

The MCL-5 cells demonstrated a significant lag period in which limited growth was observed, highly similar to that observed within the previously reported dose finding study (Appendix Section 5.5.3.2). 24 hr post treatment, a large proportion of the cell populations went into apparent cytostasis, but appeared to improve following 1-2 cell cycles recovery period; some evidence suggesting the immediate cytostatic effect of the genotoxin exposure [353]. Following 72 hr post treatment, phenotypic *PIG-A* mutation data was collected and retrospectively assessed utilising the "original" and "novel" gating strategies. In brief, the original strategy purely relied on limited viability dye exclusion of non-viable cells and basic FSC vs. SSC scatter plots for single cell morphology, whereas the novel strategy utilised a modified

doublet discrimination plot requiring the pulse width measure of the anti-CD55/59 fluorophore to define event morphology.

The subsequent MCL-5 *PIG-A* data generated was significantly different; 72 hr post exposure the original gating strategy reported no obvious increase in phenotypic *PIG-A* mutant frequency across the trialled dose range (Figure 5.10 A), with a distinctly unsatisfactory background number of pre-existing phenotypic mutants. However, the novel system appeared to substantially increase assay sensitivity, background mutant frequency defined as 0.01% with a resultant sub linear dose response in which the top dose appeared to increase the relative number of phenotypic *PIG-A* mutants 8-fold (Figure 5.10 B).

Even with the newly modified increase in assay sensitivity, only the top dose of 1 μg/mL elicited a significant effect on the phenotypic *PIG-A* mutant frequency. This LOAEL appears to be significantly higher when compared to analogous data within equivalent cell lines [264]. Also, following the omission of HLA-DR staining, the continuous association between elevated phenotypic *PIG-A* mutant frequency and increased low level cytotoxicity re-appeared, emphasising the additional measurable mechanisms supplementary to mutagenesis within the assay design.

However, utilising the novel gating strategy within the modified pre-existing assay design appeared to greatly increase assay sensitivity, and should facilitate the generation of further validatory quantitative dose response data. Assessing the novel gating strategy for bias potential will need to be completed prior to more definite conclusive remarks, however, elongating the experimental time period, including HLA-DR or similar staining as well as comprehensive viability dye assessment should facilitate actual quantitative dose response modelling.

5.4.4 Assay Refinement - Gating Strategy Comparison and Apoptotic Morphology Investigation

5.4.4.1 Gating Strategy Direct Comparison

Currently, FSC and SSC measurements within flow cytometry analysis are the most commonly observed variables in which population statistics are derived [13, 192, 235, 299, 302, 318, 354, 355]. However, recent reports of inaccuracies as a result of over dependence on such crude measures are emerging; FSC values in particular have been focussed for their potential misuse due to being particularly sensitive to surface area and orientation of the cellular event. Proboscis, micro extensions from a cells surface, have been shown to greatly increase a cell's FSC value; therefore, a small dying cell with such proboscis could have a corresponding FSC value of a normally distributed single viable cell [356]. The original in vitro gating strategy relied solely upon FSC and SSC measures to exclude cellular debris and doublets and therefore, could be a significant source of error [318]. In order to investigate this more thoroughly, a retrospective parallel analysis was carried out on a shared data set, in which the currently trialled novel gating system was directly compared against the original strategy and a heavily biasing comparable pulse width measure (Section 5.3.4); any pre-existing doublet discrimination based on FSC-W was removed for experimental purposes [316, 317].

The results of this experiment demonstrated that the original gating strategy was establishing a threshold which resulted in an unacceptable number of defined pre-existing phenotypic mutants (Section 5.3.3), primarily as a consequence of poor classifier identification. The known biasing strategy, in which the fluorescence area of the anti-CD55/59 R-PE fluorophore was included as a variable, reported a 0% phenotypic *PIG-A* mutant frequency as expected (Appendix Section 5.4.4.1). However, interesting, the novel gating strategy facilitated the detection of phenotypic *PIG-A* mutants at a frequency comparable to currently validated analogous gene mutation assays, providing some confidence in the novel strategy.

In brief, the inclusion of a variable directly associated to the definition of phenotypic *PIG-A* mutant status, induces a significant bias towards underestimating the number of phenotypic mutants (Section 5.3.4). In conclusion, the inclusion of this un-biased novel gating system, with a comparable high sensitivity, appears to facilitate the assay system to undertake quantitative dose response modelling and allow further mechanistic validation.

5.4.4.2 Apoptotic Morphology Investigation

Within the first results chapter, it was demonstrated that cellular viability was not equally distributed between flow cytometry defined phenotypic *PIG-A* mutant and wild type populations (Section 3.3.5). Theoretically, this suggested that phenotypic *PIG-A* mutants/GPI-AP deficient cells have a positive association to apoptosis and/or necrosis, directly conflicting against recent published in vivo evidence which describes the accumulation of such a phenotype, within the bone marrow and subsequent peripheral circulation, as a result of resistance to apoptosis [320]. It is actually more likely for phenotypic *PIG-A* mutants, in vitro and in vivo, to be highly sensitive to apoptosis, which is currently described within this and the previous chapter's observed results (Sections 4.3.3, 4.3.4 and 5.3.4.2).

Therefore, evaluation whether non-viable cells present a phenotype equivalent to a presumptive *PIG-A* mutant event is required, as the integrity of the in vitro reporter system is determined by this; currently unobtainable within in vivo erythrocytic assay designs, due to their inability to undergo apoptosis [351]. If such an occurrence does transpire within the in vitro assay mechanism, p53 dependent (Appendix Section 5.4.4.2), a consequential masking effect, high background of pre-existing phenotypic *PIG-A* mutant events, would dramatically decrease assay sensitivity and therefore, could be the current inhibition of quantitative usage [181].

Relying solely on molecular evaluation of non-viable events may limit the detection of the entire non-viable population. Therefore, investigating additional characteristic morphological features of apoptosis could provide a supplementary system for exclusion of non-viable events. The results demonstrated that apoptotic and dead cells were equally distributed across the defined single cell population of MCL-5

cells, however, when assessed through a doublet discrimination gate, dead cells did appear to have a lower average FSC value than comparable apoptotic cells. Although, morphological differences were detected, the variation was not solely large enough to build a gating strategy around as without molecular viability tagging, discrimination from the viable population is impossible. Consequently, the use of comprehensive viability dyes is recommended within this lymphoblastoid based assay design.

In order to investigate for additional biasing effects apoptotic cells could be inducing upon the reporter system, the GPI-AP expression of non-viable cells was tracked through apoptosis (PS sensitivity) and necrosis (PS sensitivity combined with lack of membrane integrity) respectively. In theory, as cells progress through apoptosis they accumulate increased risk of progressive lack of membrane integrity. Subsequently, lipid raft GPI-AP distribution is disrupted and the consequential emission profile of bound anti-GPI-AP antibody conjugated fluorophores is inhibited. The results demonstrated a positive correlation between Staurosporine exposure duration and the number of non-viable cells scored, with evidence suggesting that progression through apoptosis into necrosis was also exposure correlated, as expected (Section 5.3.4.2). Staurosporine is a known apoptosis inducing chemical and is frequently used as a positive control within scientific experimentation [357]. More interestingly, GPI-AP fluorescence emission signal was shown to progressively decrease over the exposure duration, with the threshold of signal positivity, defied by the ICS, being crossed at the 8hr exposure. Consequently, events would be defined as presumptive phenotypic *PIG-A* mutants with little evidence for a mutational origin. Even though as cells progress through the death pathways, their genomic instability subsequently rises and therefore, they are more likely to undergo greater levels of genomic mutational activity, however, as they are no longer dividing the mutational event isn't fixed and therefore, would not result in mutational silencing events at the *PIG-A* gene. However, the observed progressive diminishing of GPI-AP signal over the exposure time provides evidence towards a biasing effect elicited upon FCM phenotypic *PIG-A* scoring.

In conclusion, apoptosis and cellular death are unable to be excluded purely based on a forward or side scatter morphological measure and hence, must be detected

through molecular probes [273]. There is preliminary evidence within the section for the generation of mutant mimicking events as a result of loss of membrane integrity through death pathway progression; however, this can be neutralised by the extensive use of viability dyes. Therefore, the continued uses of such dyes are highly recommended within any in-direct extracellular protein reporting based within an apoptosis sensitive cell platform.

5.4.5 Next Generation Sequencing

Due to the failure of the control sample during the DNA extraction stage, the subsequent purity/integrity of the DNA was not sufficient to enable sequencing, the EMS induced results were analysed without the con-current control data; as a direct result of this, the proportion of SNPs as a result of the treatment, as opposed to the generic background SNPs, cannot be estimated.

Therefore, due to the lack of integrity within the subsequently analysed data (Appendix Section 5.3.5), no conclusions can be drawn; however, the experimental design along with the complexities of this project offer insight into how to undertake such a novel task and are to be discussed.

The goal of the sequencing data was to investigate the genotypic nature of presumptive phenotypic *PIG-A* mutant events; in addition, known chemical treatment was to be utilised to further explore the relationship between mutational induction, mutation spectra and genotype. Following FCM, approximately 100,000 phenotypic *PIG-A* mutant cells were FACS. The data generated was based on a pooled heterogenous population of phenotypic *PIG-A* mutant events (CD55 and CD59 deficient viable cells), which had been acutely treated with a sufficient dose of EMS to expectantly induce enough additional mutants to significantly alter the mutational finger print when compared to spontaneous phenotypic *PIG-A* mutants. However, as the fold increase following EMS treatment within phenotypic *PIG-A* mutants is approximately 2-fold, therefore, only 50% of the population is likely to be a result of EMS exposure. In additional, the primary mutagenic lesion

(0^6ethylguanine) approximately constitutes 2% of the total adducts formed following treatment [22]. Consequently, observing a visible shift within the adduct spectra of the control and EMS induced samples may prove problematic; however the mutation spectra should prove more favourable.

Hypothetically, all putative phenotypic *PIG-A* mutant events should be statistically genotype *PIG-A* deficient, due to the x-linked nature of the reporter gene [144, 358]. Any number of mutational events, point mutations, frameshifts etc. within either the coding or non-coding region could induce such a deficient phenotype. Therefore, during analysis all mutational events, including insertions and deletions were investigated across the entire coding and non-coding regions of the gene of interest. The specific amplicons chosen comprised of an approximate basal read depth or coverage of 1-2,000 reads across each nucleotide within the gene of interest sequence, with an additional 5' and 3' buffer zone to look for promoter mutations. Within the current *pig-a* sequence literature, assay designs typically utilised mRNA and cDNA synthesis approaches, focus was placed on SNPs within the coding region of the *pig-a* gene; little or no focus was placed on alternative SNP locations which we now know can be as detrimental to phenotype as their coding region counterparts [359].

The reference sequence used to call SNPs (hg19_DNA [360]), utilised within the UCSC genome browser [361] and the NCBI library environments, potentially is not an exact reflection of the nuclear DNA sequence within the immortalised MCL-5 cell lines used. Therefore, there may be some variation which could confound SNP variant calling, however, to rationally ensure against this, any SNP variant with a corresponding frequency >99% of the pooled read population was excluded from analysis. Additionally, one is able to retrospectively construct their own reference genome following the sequencing, at sufficient depth and coverage, of control samples.

As there is no standard pipeline for a "metagenomics" approach to human amplicon NGS data analysis, each programme used within this pipeline has unique caveats and restrictions which can be more fully described at their respective developer's websites [344, 345, 362].

Due to the experimental design, there is no finite way to trace the origins of the SNP variant to any particular cell. Unique oligonucleotides or similar high throughput tracking methods can be added to the primers during amplification [363], this enables ancestral analysis to be undertaken; in which specific reads can be traced back to their parental DNA molecules. This technique provides significantly more confidence in the SNP call, however, utilising a heterogenous assay design with approximately 100,000 starting DNA molecules did not facilitate much benefit from this method, with approximately 1,000 modified primer pairs per experiment adding to the cost. In addition to this, as is the nature of amplicon sequencing, primer efficiency variation can lead to PCR duplicates; currently there is no standardised method to remove primer duplication from amplicon sequencing data, due to the common amplification start and stop sites [331]. The SNP variant frequencies can therefore, be debated, capping primer duplicate numbers can be a method of standardisation; however, often very little difference is apparent within the finalised statistics data.

Finally, the hemizygotic properties of the *PIG-A* gene mutation facilitate a single mutational deactivation to result in a null phenotype; however, the homozygous natures of the additional genes of interest still require a double in-activating event within both parental alleles to result in a null phenotype. This observation must be taken into account when comparing the four genes of interest, an additional level of DNA molecular tracking may have been important for increased ancestral clarity, however, highly difficult experimentally to implement utilising the pool extraction method. Assuming all these known limiting factors, and what would have been the ideal experimental design (homogenous clone approach) the data was collected and analysed to the best of the experimental ability.

Table 5.3 Summary of the data described within the chapter contents, the results and the conclusions drawn in relation to the advance of the in vitro PIG-A gene mutation assay standard operating procedure (SOP)

BD FACS Aria 1 – Flow Cytometry Assessment

MCL-5 Assay Development

Trialled usage of HLA-DR staining to validate single marker *PIG-A* dose response data within MCL-5 cells

ENU, MNU, EMS and 2-4,DNP → **Establishment of a more quantitative assay platform**

Assay able to rank compounds in regards to published potency – 2,4 DNP demonstrated not to be positive within assay system

Limited evidence for correlation between genotoxicity and cytotoxicity.

Confocal microscopy GPI-AP expression analysis

CD55, CD59 and Tandem CD55/CD59 → **Sporadic and clustered expression (lipid raft associated)**

Highly limited surface expression for both CD55 (possible intracellular presence) and CD59

Combined usage of CD55/59 antibodies resulted in comprehensive surface coverage, increasing reporting accuracy.

Preliminary MCL-5 *PIG-A* Assessment; Tandem CD55/CD59

Acute MNU Exposure, 3 Day analysis → **Orignal gating resulted in lingering cytotoxicity correlation**

Novel gating system appeared to result in sub-linear dose response, estimated LOAEL 1µg/mL ~ 9.7µM

Assay approx 4 fold more sensitive than previous HLA data

Assay Refinement - Gating Strategy Comparison and Apoptotic Morphology Investigation.

Gating Strategy Direct Comparison

Apoptotic Morphology Investigation → **Phenotypic background *PIG-A* mutant frequency of $50x10^{-6}$**

Background in-line with published data; facilitates future quantitative analysis

Apoptosis progression appeared to correlate with loss of GPI-AP presence, comprehensive viability dye incorporation

Illumina MiSeq™ Next Generation Sequencing Assessment

↓

Next Generation Sequencing

EMS Induced apparent mutant phenotype

PIG-A, PIG-T, CD55 and CD59 → **Failings of the control data prevented any conclusions being taken from the obtained data set (See Appendix).**

Table 5.4 Summary of the additional supplementary data for this chapter, contained within the appendix, which details the validation and additional investigative experimentation surrounding the assay development.

Supplementary Data

FD FACS Aria 1 Assessment

Antibody Specificity

CD55 Monoclonal Antibody → **0.006% of binding as a result of Fc mediated interactions**

0.003% additional non-specific interactions

CD55 antibody gained approval for use within assay system

Dose Finding Study, EMS and MNU Exposure

Acute EMS and MNU Exposure → **EMS Doses >2.5µg/mL appeared to be cytotoxic**

MNU Doses >1µg/mL appeared to be cytotoxic

Preliminary Investigations into Cell Cycle and GPI-AP Expression Correlation

BD FACS Aria 1 Investigation → **No significant correlation observed between GPI-AP presence and cell cycle progression**

Amnis Image Stream ™ – Cytometry Assessment

Preliminary Investigations into Cell Cycle and GPI-AP Expression Correlation

Amnis Image Stream ™ Investigation → **No significant correlation observed between GPI-AP presence and cell cycle progression**

Proteomics and Fluorescence Microscope Assessment

Preliminary Intracellular *PIG-A* Protein Investigation

BD FACS Aria 1 Investigation

Fix and Perm ™ Reagent → **Fix and Perm ™ reagent demonstrated not to be viable with this specific cell lineage**

Preliminary Intracellular *PIG-A* Protein Investigation

Fix and Perm ™ Reagent

Methanol Fixation and Permeabilisation

PIG-A Trial and Histone H3 Housekeeper →

Fix and Perm ™ reagent confirmed not to be viable with this specific cell lineage

Optimised Methanol fixation permitted intracellular staining and minimal deleterious morphological affects

PIG-A protein identified abundantly within the nucleus with evidence for limited cytoplasmic localisation

Histone H3 protein heavily localised within the nucleus.

Illumina MiSeq™ Next Generation Sequencing Assessment

Next Generation Sequencing

EMS Induced apparent mutant phenotype

PIG-A, PIG-T, CD55 and CD59 ➡ **Presumptive mutational events identified within all genes, probable mutational activity highly correlated to Exonic regions. *PIG-A* gene observed to have the highest activity (Exon 6), EMS mutational spectra apparent across all genes.**

Chapter 6: Human *PIG-A* – A Potential Biomarker Tool for Epidemiology Bio-Monitoring Studies

6.1 Introduction

The previous chapters have described the progress and advancement of a potential in vitro gene mutation assay, which if fully validated could be implemented within future tiered genetic toxicology test batteries to improve hazard identification and categorization. The assay design fulfils a current niche within safety assessment, assessing environmental pollutants or therapeutic drug candidates for potency and has limited use within current human health assessment. However, in vitro data is currently being assessed for future inclusion within human health risk assessment through the ongoing work of the ILSI-HESI joint committee. Due to the highly conserved nature of the GPI-anchor structure, in combination with an un-invasive harvesting method, the fundamentals of the assay system can be exploited within humans to enable a potential bio-monitoring tool for epidemiology studies.

Regardless of where we live and to some extent how we live, environmental chemicals completely surround us; they are present within the water we drink, air we breathe and food we eat. However, most of these substances occur naturally, are well categorised, and at low levels of exposure pose little risk. Nevertheless, there are others, natural or man-made, which are less well categorised and little is known about their presence within the human population (animal populations in general), their chemical reactivity and hence, the subsequent interactions they create following exposure. This is where human bio monitoring (HBM) as a scientific discipline allows access to the data whether or not such chemicals have entered the body and to what extent this exposure can harm and how it may change over time [364]. In a general sense HBM studies measure the concentration of such natural and synthetic compounds in body fluids, and provide the data necessary to contextualise environmental exposures and help identify potential health risks [365]. The major strength of HBM is that it provides data, generally highly detailed, on the internal

exposure of an individual at a precise time, which in combination with a number of other methods can be utilised to evaluate a potential health risk [209].

HBM is more than just a potential quantitative measure of an environmental chemical; it can provide route of entry (administration) data and capture key insights into the deleterious side effects or consequences of such exposure. Often such a study is undertaken in parallel to interview or detailed questionnaires to facilitate more specific evaluation of data and interpretation to minimise potential future risk [364]. HBM can be thought of as a pipeline to provide additional data to aid regulatory decision making, not for NMEs (new molecular entities); the initial frame work of planning, budgeting and ethical approving is followed by sampling, analysis and interpretation [53, 366]. This stimulates communication, further research and additional training, which in turn eventually lead to policy drafting, coordination and implementation of decisions [367].

In the case of a specific chemical exposure, HBM can identify trends within the population, investigate potential cultural and life style contributing factors and isolate groups at increased risk of incident. Two specific examples of HBM studies in which the investigations lead to policy changes at a national level were; in Germany risk of amalgam fillings, especially within children was identified, and the decline of metal contamination via drinking water revision (German Drinking Water Ordinance) and in Belgium (the Flanders bio monitoring programme) the collection of pesticide waste was improved, following observed elevated levels of banned pesticides in the blood of rural populations [209, 364].

HBM falls into a larger category of epidemiology, the study of patterns, causes and effects of health and disease conditions in defined populations [368]. Both HBM and epidemiology studies rely on other scientific disciplines in order to better understand the disease processes, a biologist is often consultant in parallel with a statistician and physical engineer to make a more effective use of the data and draw more accurate conclusions. An example of a famous case study was preliminary reported in 1954 [369] and latter in 1956 [370] in which the published results of a British Doctors Study (1951-2001), led by Richard Doll and Austin Hill, provided strong statistical support to the suspicion that tobacco smoking was linked to lung cancer, a modern relationship which is fundamentally implied. This work was later followed by the

DNA adduct and mutation spectrum of lung cancers being linked to cigarette smoke [371, 372].

6.1.1 Genetic Toxicology's Impact within Human Bio-Monitoring Studies

Genetic toxicology, as a field is directly involved in the future prevention of human risk through rigorous safety assessment within the tier standard battery during novel drug formulation/development [373]. However, aside from the potential of drug impurities or contamination within drug development, which would stimulate a genetic toxicology based assessment within the population affected, there is little cross over into potential large scale epidemiology studies. Nevertheless, with increased risk associated to naturally occurring environmental compounds, more accurately described by their potential exposure within the population, genetic toxicology end points are often considered when constructing a decision in order to reform, or provide policy on a current issue.

Genetic toxicology data is becoming more prevalent within decision making, undertaken by regulatory agencies for risk assessment purposes, especially in regards to the backlog of known man-made compounds with the potential to cause risk following exposure, for example smoking [370-372] and Asbestos [374]. A highly relevant example was in 2007 when Roche, the Swizz Pharmaceutical Company, recalled the antiviral Viracept (nelfinavir) following identification of contamination at the manufacturing stage by ethyl methane sulfonate (EMS) [242, 243]. This lead to one of the first example of a known genotoxic compound, previously believed to be linear, having a non-linear dose response defined following exposure [241, 350], the no-longer currently used Lutz and Lutz hockey stick model [375], showed a clear sub-linear response. As well as man-made exposures, natural environmental compounds have also been demonstrated, following novel research, to have potential deleterious bioaccumulation or damaging mechanisms. These such compounds termed persistent, bio accumulative and toxic chemicals (PBTs) are often highly lipid soluble [376].

6.1.1.1 The Micronucleus Assay as a Bio-Monitoring Tool

Micronucleus testing is a well-established assay within the genetic toxicology field and is a frequent method utilised within human bio monitoring studies [69, 377, 378]. The micronucleus assay is thoroughly validated, providing both OECD guideline publications for use within in genetic toxicology testing and recommendations for its use in HBM [379]. The formation and frequencies of micronuclei do not necessarily reflect a consistent mode of action within all the various test protocols, biological basis of the formation is dependent upon the context of chemical exposure [34, 69, 95]. Mutation can be thought of a potential superior endpoint, due to its recent classification as an apical endpoint, or key event within carcinogenesis [380]. The adapted MNT protocol is frequently used for monitoring genetic damage in humans; MNT frequencies are monitored across a variety of cell types these include, peripheral leukocytes, erythrocytes and epithelial cells [381]. Specific sub-protocols such as the MNT with exfoliated epithelial cells (buccal cavity) are used as a minimalistic invasive method for monitoring genotoxic damage at the point of contact [382]. However, a more standardised approach is the MNT frequency assessment within human cultured leukocytes from human patients following exposure or suspected exposure [383]. An additional particular method which is gaining favour is the flow cytometry assay, in which the MNT frequency is quantified within the RET population of peripheral erythrocytes [383]. MN are assessed within the most immature fraction of transferrin receptor positive reticulocytes (CD71-positive); cells released by the bone marrow are immuno-magnetically isolated before they are removed from circulation by the spleen [384]. Therefore, this method fundamentally requires a bone marrow exposure to induce a relevant MN response. Chemotherapy and radiotherapy have both been demonstrated to induce a statistically significant increase in MN ret formation when compared to un-treated control patients [385]. The limited lifespan of reticulocytes along with the limitation in which exposure most occur still limit this method of HBM for the detection of damage after low-level chronic exposure. Different methods must be investigated to ensure a more accurate description of exposure related induction [379].

6.1.1.2 The Human *PIG-A* Assay as a Potential Bio-Monitoring Tool

Potentially there is a niche for a genetic toxicology end point which is easy accessible, un-invasive, able to be high throughput and a general description of genetic damage following either acute or long term chronic exposure. This method of measuring somatic mutation rate is an important biological parameter, as it may influence the development and/or the risk of acquiring genetic diseases, particularly cancer [386]. The somatic mutation rate can be indicative of the environmental stresses, and hence exposures exhibited onto the general population. The X-linked basis of the *PIG-A* gene makes it a prominent candidate for a quantitative somatic mutation rate reporter [387] and facilitates the assay design to be able to be undertaken within a large plethora of different tissues in theory. However, initially focussing on human erythrocytic *PIG-A* [351], utilising the rodent *Pig-a* as a basis for finalised design, human peripheral blood erythrocytes can be assessed for genetic damage. Again much like the MNT assay, in vivo, the exposure would be required to be chronic, and of a highly deleterious nature to induce a significant measurable long term end point.

Initial pilot studies exploiting the *PIG-A* gene loci have been carried out within the FDA, further eluding more data in terms of mechanistic studies as well as potential deviation within sexes, species and cell lineages. Initially, the spontaneous somatic mutation frequency was calculated within a "normal", healthy population (average of $5.1 \pm 4.9 \times 10^{-6}$; median of 3.8×10^{-6} and mutant frequency less than 8×10^{-6} for 75% of subjects). However, a statistically significant difference in median mutant frequencies between males and females was detected as well as *PIG-A* RBC mutant frequency displayed poor correlation with the age and no correlation with the smoking status of the subjects. Limited evidence was collected to suggest robustness following an additional project failing to measure significant increases in mutant frequency following patient exposure to chemotherapeutic treatments [280]. Much like peripheral blood reticulocytes being removed via the action of the spleen, mature RBC will actively be removed via complement protein mediated haemolysis and hence, could result in an underestimation of genetic damage, especially if the exposure was acute in nature [152, 153]. The rodent in vivo Pig-a assay is relatively

unaffected due to the lack of complement system complexity within the species [388].

Therefore, not only investigating erythrocytic lineages as a potential bio monitoring tool for systemic exposure, human leukocyte *PIG-A* offers a more favourable assay design to facilitate more accurate risk assessment. Leukocytes, both granulocytes and lymphocytes are nucleated and therefore, permit downstream direct sequencing to validate the identity of the FCM defined event as well as provide further mechanistic evaluation of the nature of exposure. Even though Leukocytes undergo an analogous sequential maturation within the bone marrow, their general fixed distribution (granulocytes) as well as active gene expression and ability to divide (lymphocytes) facilitate accurate reporting of systemic genetic damage [389]. Harvesting leukocytes from specific organs or locations around the body would better reflect the microenvironment from which they were taken, allowing a more point of contact and distribution approach to the exposure to be assessed. However, lymphocytes are highly prone to surface antigen expression alterations, especially following activation when called into action by the immune system or following the onset of disease phenotype [390]. Therefore, utilising an analogous cell type, with a homogenous microenvironment, which are less susceptible to activation would greatly benefit the bio-monitoring platform. Therefore, monitoring human granulocytes, more specifically activated neutrophils, could provide an effective platform for the collected of spontaneous, as well as specific chemical exposure induced, *PIG-A* mutant frequency data within localised and peripheral blood of donors (see Figure 6.1 for details).

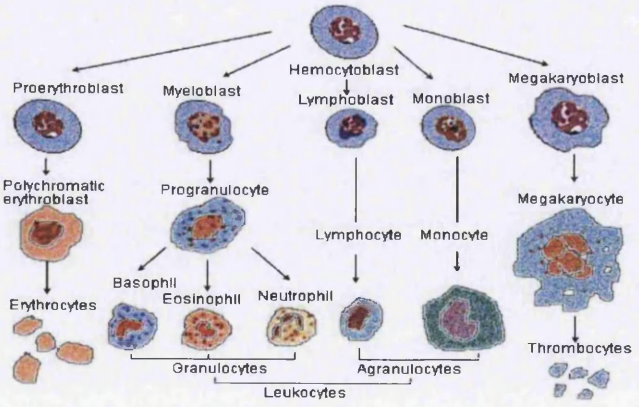

Figure 6.1. Overview of the differentiation lineages within haemopoetic tissue of the bone marrow. Image taken from [391]

Rondelli et al., 2013 published data showing a diverse range of spontaneous phenotypic *PIG-A* mutant granulocytes within a normal population. Further development from the same group showed robustness within the approach and defined a "normal" range of mutant granulocytes (1×10^{-6} - 37.5×10^{-6}, with a median of 4.9×10^{-6}) [175]. Unlike other techniques commonly employed in population studies, such as comet assay, this method can detect any kind of mutation, as long as the *PIG-A* gene is functionally inactivated [79, 392]. At the end of 2014, Litron ™ published a development paper on human erythrocytic *PIG-A*, analogous to the paper presented by the FDA a few years earlier, with the extension of mutant RET measurement [351]. The spontaneous mutant frequency was estimated from the analysis from 52 – non-smoking self-reported healthy normal volunteers (mean frequency of $RET^{CD59-/CD55-}$ and $RBC^{CD59-/CD55-}$ were 6.0×10^{-6} and 2.9×10^{-6}, respectively). The difference, demonstrates the "modest selective pressure against mutant phenotype mature erythrocytes in the circulation", and suggests the major advantage of reticulocyte measurement utilising the modernised methodology, immuno-paramagnetic mutant enrichment. Thus this publication demonstrated the ability to feasibly collect *PIG-A* mutant data, utilising a highly un-invasive sample harvesting method, which could be utilised as a potential HBM assay.

6.1.1.3 Genetic Data: The Future of Toxic Tort Legislation

Currently one of the biggest obstacles to overcome during toxic tort cases is establishing, with adequate proof that exposure to a potential toxin resulted in the proposed injury. Currently, in a general sense causation is determined through a complex overview based on multiple witnesses, each putting forward an expert opinion either for or against the proposed mechanism of injury. However, through recent advances in gene sequencing, biomarker identification and generalised more comprehensive understanding of pathogenesis markers some plaintiffs have begun to use genetic information in order to more solidly put forward the case of exposure related toxicity, which more likely than not induced damage [393]. Biomarkers in this case can be used as directly measurable molecular changes in the blood, sometimes even unique moieties directly related to a specific compound interaction,

which can indicate abnormalities or disease. Currently, the most important biomarkers in terms of damage estimates are those which demonstrate chromosomal rearrangements (both aberrations as well as aneuploidy) or specific gene mutations. These genetic biomarkers in combination with sufficiently high sensitivity assessment are beginning to more accurately estimate duration and potency of exposure. Equally, genetic information can also be used by a defendant providing a case for pre-disposition to a genetic condition or disease phenotype; a gene expression which is atypically of exposure can provide strong evidence to disregard a proposed exposure related illness. Ideally, utilising more genetic information and providing a sufficiently details comprehensive assessment should enable a more objective, pure approach to these cases, minimalising the need for personal opinions from experts in the field [394].

Even though in principle the ideology of utilising extensive genetic information regarding gene expression and biomarker study provides a more objective view point to a decision making process. The complexities and understanding in order to come to an objective opinion following data interpretation in my opinion is still fundamentally lacking. The sheer complexity of human biological nature requires extensive validation and the presence of anomalies or spurious data cannot be disregarding as within this specific context could immensely damage a company's reputation or individuals life style. Additionally, high expense and time consuming protocols are associated with genetic testing. However, advances in modern technology and medicine especially in the fields of biomarker or bio-monitoring, which in essence should provide more holistic objective data, can provide data in less than a few days at a relatively low cost [393].

6.1.2 Cancers and additional Genetic Diseases

The *PIG-A* mechanism in-directly reports the mutation frequency observed at the *PIG-A* gene locus [387], and therefore, is fundamentally a non-specific measure of mutation; although potential assay revisions into more specific tissue types has endeavoured to provide localisation data for mutation frequency (Appendix Section

5.5.3.4). Mutation has recently been elevated as a genetic toxicology end point, defined as an apical end point of carcinogenesis, and therefore, is increasingly a critical measure for the detection of genetic damage and potential carcinogenesis [380]. Cancer appears to be the most topical genetic disease which affects humans, of which there a numerous unique sub-types. Research has shown the progressive stages in which a tissue generally undergoes prior to the adoption of the cancer phenotype; these include, alterations in gene expression (down regulation of tumour suppressor genes (p53), up regulation of pro-oncogenic genes (RAS), over expression of growth factors, resistance to hypoxia through the recruitment of angiogenesis regulators and increased genomic instability [395]. These so called hall marks of cancer are commonly found within the vast majority of cancer phenotypes; there are also additional unique features which further categorise the cancer phenotype and often provide identity and localisation to the cancer. Tissues, therefore, in some respect undergo a progressive cancer development, which if identified at an early stage can be effectively treated with therapeutic agents, however, as the cancer develops the amount of genomic instability increases which facilitates the further development of the phenotype. As the phenotype reaches its latter stages, often the condition is untreatable, due to the systemic affect the cancer has on the patient following node penetration, i.e. metastatic expansion often associated with very poor prognosis [396].

However, mutational events are either directly present or as of a consequence of a number of further disease phenotypes. For example, inflammation is common to rheumatoid arthritis [397] and is highly associated to reactive oxygen species (ROS) activity [398], which in turn have been demonstrated to induce mutational damage [399]. Therefore, via localised *PIG-A* mutation frequency assessment, tissues potentially affected by ROS activity and therefore, a potential risk of disease development could be detected. However, without a viable physical phenotype alluding to preliminary ROS mediated damage, it is highly difficult to detect the onset of the disease phenotype prior to initial symptoms.

6.1.3 Additional Purposes of Developing a Human *PIG-A* Bio-Monitoring Tool

The aim of this chapter was to develop a suitable human *PIG-A* bio-monitoring platform, able to sensitivity measure mutation. As previously mentioned, there is a number of pre-existing published studies which were undertaken with this common aim [175, 351, 358, 387]. Utilising such models as smoking exposure, limited convincing data has been generated demonstrating any correlation [351] to date. However, the lack of obvious correlation may be as a result of limited assay protocol, focussing heavily on RET and/or RBC data potentially could limit the observed response due to the required chronic systemic nature of exposure. Therefore, more recent analogous studies were published focussing more heavily on the establishment of a robust WBC (granulocyte) assay platform to enable more localised *PIG-A* assessment [175].

Developing a Human Granulocyte assay platform in combination with the more traditional erythrocytic versions of the *PIG-A* assay, offers additional benefits specifically poignant within the current in vivo *Pig-a* validation. Each cell type offers a particular advantage in the context of data acquisition; periphery erythrocytes would have limited sensitivity to tissue specific exposure, due to their limited gene expression. However, any potential accumulation of damage whilst within the bone marrow is easily detected due to the ~100 day maturation within the circulatory system. Alternatively, white blood cells, even though less prevalent in terms of numbers, are more robust, sensitive to environmental stimuli and are sensitive to DNA damage, as well as are nucleated to permit direct sequencing. Direct sequencing validation of the presumed phenotypic *PIG-A* mutant events would, in a homologous manner to the in vitro *PIG-A* assay, enable some level of validation to the putative *PIG-A* deficient phenotype, as observed within the erythrocytic assay designs. Lacking complete validation of the presumptive mutant phenotype is still a retarding data gap potentially preventing OECD guideline drafting. Therefore, granulocytes could provide a generic biomarker for chronic exposures, including such disease phenotypes as smoking, obesity and aging, as well as a potential platform to validate the assay set up in regards to direct sequencing.

6.2 Materials and Method

6.2.1 Human Haematocyte *PIG-A* Exposure Assay

This body of work was constantly progressing to improve three separate *PIG-A* exposure assays. In order to achieve this, numerous progressive developmental stages were undertaken often assessing similar reagents for performance. Throughout this section, unless otherwise stated, human blood was collected directly into a heparin coated vaccutainer succeeding venipuncture within the median cubital vein, following verbal consent. All blood was stored blind within a biohazard cool bag within a 2-4 ℃ temperature controlled environment, protected from light. All human blood work was carried out within Scan Lab class 2 safety cabinets, with extensive 70% ethanol cleaning and additional use of detergents to prevent contamination or biohazard. Sample often were "racked" which is a process similar to vortexing which breaks down agglomerates without the excessive shear forces associated.

6.2.1.1 Human Erythrocyte (RBC) *PIG-A* Exposure Assay

4 mL of venous blood was removed via venipuncture, most commonly bled from the Median Cubital Vein located on the ventral surface of the forearm; into 4 mL heparin (60 USP) coated vaccutainers (Cat No. 367 884, BD Biosciences, Oxford, UK). Vaccutainers were stored protected from light at room temperature to prevent photo-degradation. Vaccutainers were de-capped, 5 µL of heparinised whole blood removed and aliquotted directly into the base of a 1.5 mL eppendorf tube containing 95 µL of filter (0.2 µM) sterilised PBS supplemented with 0.2% BSA (1:20 dilution). The diluted blood was pipetted up and down a number of times to prevent undesirable agglomerates and aid clotting cessation. The entire contents of the eppendorf tube were transferred into a sterile 15 mL falcon tube, taking additional care to prevent any blood from touching the side of the tubes, this step ensures against artifactual *PIG-A* mutants during analysis. 20 µL of human anti-CD55 R-PE

antibody (IgG 2_{ak}) (Cat. No. 555694, BD Biosciences, Oxford, UK), 20 µL of human anti-CD59 R-PE (IgG 2_{ak}) (Cat No. 555764, BD Biosciences, Oxford, UK) as well as 5 µL of human anti-CD235a APC (IgG 2_{bk}) (Cat No. 551336, BD Biosciences, Oxford, UK) (1:10 dilution within 0.1 % BSA/ 0.05% NaN_3/PBS) antibody were added in unison to the 15 mL falcon tube, pipetted a minimum of 5 times and incubated at room temperature (22 °C ± 2 °C), protected from light for 30 min. Post incubation, the samples were centrifuged (500 x g for 5 min), supernatant aspirated and discarded. 5 mL of 1 x PBS was added re-suspending the cellular pellets, centrifuged at 500 x g for 5 minutes. The supernatant was aspirated and discarded. An additional 5 mL volume of 1 x PBS was added, centrifuged (500 x g for 5 min) and supernatant discarded. Cellular pellets were re-suspended in 1 mL 1 X PBS solution, racked extensively and stored up to an hour on ice protect from light prior to flow cytometric analysis. Instrument calibration standards (unstained) as well as single stained sample controls were also prepared for calibration and compensation respectively.

6.2.1.2 Human Reticulocyte (RET) *PIG-A* Exposure Assay

6.2.1.2.1 Erythrocytic Depletion: Haemolysis Variant

Versalyse (Cat No. 41116015, Beckman Coulter, High Wycombe, UK) was stored as outlined within the manufacturer's guidelines at 18 – 25 °C and was used within a 90 day period starting the day of first use. Blood was collected from a healthy control donor as outlined in (Section 6.2.1.1); 100 µL of heparinised un-diluted whole blood was transferred into a fresh 15 mL falcon tube, taking great care to expel the contents of the pipette directly into the base of the tube. The whole blood was treated with erythrocyte specific antibodies as outlined in (Section 6.2.1.1) and incubated at room temperature, protected from light for 30 min. Following incubation, 1 mL of VersaLyse solution (1X) was added, vortexed immediately (1 sec) and allowed to incubate at room temperature, protected from light, for 10 min. Immediately following incubation, the lysed sample was centrifuged (150 x g for 5 min), supernatant aspirated and re-suspended in 3 mL of 1 X PBS solution. Due to mass

lysis, take great care when discarding supernatant not to remove cells of interest. The sample was centrifuged, supernatant aspirated, treated with 1 mL of 0.1 % Retic Count diluted within PBS/BSA (2%) and allowed to incubate at room temperature for 1 hr protected from light. Post incubation, the sample was gently mixed, racked extensively and stored on ice for up to an hour prior to flow cytometric analysis. Instrument calibration standards (unstained) as well as single stained sample controls were also prepared for calibration and compensation respectively.

6.2.1.2.2 Erythrocytic Depletion: Concentration Gradient Variant

Versalyse was stored as outlined within the manufacturer's guidelines at 18 – 25 °C and was used within a 90 day period starting the day of first use. Blood was collected from a healthy control donor as outlined in (Section 6.2.1.1). However, 10 mL heparin coated vaccutainers (Cat No. 367 980, BD Biosciences, Oxford, UK) were used and loaded with 9 mL of venous blood. 5 mL of heparinised blood was transferred using a sterile 10 mL pipette in conjunction with a pipette controller onto 5 mL of histopaque ® 1077 (Cat No. 1077-100mL, Sigma Aldrich, Gillingham, UK) within a 15 mL Falcon tube. Samples were centrifuged (~300 x g for 30 min) at room temperature, forming a distinctly reproducible layered blood sample. Starting with the least dense, the plasma layer was removed, "buffy white coat" presumed lymphocytes, followed by the histopaque ® 1077, and very carefully the layer of reticulocytes/polymorphonuclear white blood cells removed and aliquotted into a fresh 15 mL centrifuge tube (~100 µL volume). The erythrocyte dominated cellular pellet as well as the additional layers, excluding the reticulocyte layer were discarded and disposed of according to health and safety protocol. Excess (~10 mL) of pre-warmed RPMI 1640 medium was added to the minimal volume of suspected reticulocytes and centrifuged at (~280 x g for 10 min) room temperature. Post centrifugation, supernatant was aspirated and the cell pellets initially re-suspended in a minimal volume of RPMI 1640 medium, before additional excess was added. Cellular sample was centrifuged (~280 x g for 7 min), supernatant aspirated and discarded, and washed with excess RPMI medium – this step was repeated an additional two times. Cell pellets were re-suspended in 0.5 - 1 mL of 1 x PBS

solution and treated with antibodies in an analogous fashion was outlined in (Section 6.2.1.1). Following incubation, 1 mL of VersaLyse solution (1X) was added, vortexed immediately (1 sec) and incubated for 10 min at room temperature, protected from light. Post incubation, cells were centrifuged (150 x g for 5 min), supernatant aspirated and re-suspended in 3 mL of 1 X PBS solution. Due to mass cell lysis, great care was taken when discarding supernatant not to remove cells of interest. The sample was centrifuged, supernatant aspirated, treated with 1 mL of 0.1 % Retic Count diluted within PBS/BSA (2%) and allowed to incubate at room temperature for 1 hr protected from light. Post incubation, the sample was gently mixed, racked extensively and stored on ice for up to an hour prior to flow cytometric analysis. Instrument calibration standards (unstained) as well as single stained sample controls were also prepared for calibration and compensation respectively.

6.2.1.3 Human Granulocyte *PIG-A* Exposure Assay

6.2.1.3.1 Erythrocytic Depletion: Haemolysis Variant

Versalyse was stored as outlined within the manufacturer's guidelines at 18 – 25 °C and was used within a 90 day period starting the day of first use. Fluorescence aerolysin (FLAER) was purchased from VH Bio Ltd, Gates-head, UK and reconstituted within 1 mL of 1 x PBS solution, constructing a 50 µg/mL stock which was aliquotted and stored at -20 °C protected from light until further use. Blood was collected from a healthy control donor as outlined in (Section 6.2.1.1). 100 µL of heparinised un-diluted whole blood was transferred into a fresh 15 mL falcon tube, taking great care to expel the contents of the pipette directly into the base of the tube. The whole blood was treated with granulocyte specific antibodies, 20 µL of human anti-CD15 APC (IgM_k) (Cat No. 551376, BD Biosciences, Oxford, UK), pipetted up and down at least five times and incubated at room temperature for 30 min, protected from light. 15 min within to the incubation, the cells were treated with pre-warmed (37°C) 5 µL FLAER and incubated for the remaining 15 min from the previous

incubation. Post incubation, 1 mL of VersaLyse solution (1X) was added, vortex immediately (1 sec) and incubated at room temperature for 10 min, protected from light. Following this, the cells were centrifuged (150 x g for 5 min), supernatant carefully aspirated and washed a minimum of twice with 3-5 mL of (0.2% BSA/PBS) wash buffer. The cellular pellets were re-suspended in 1 mL of 1x PBS, treated with 5 µL of propidium iodide solution (1mg/mL) (Cat No. P-3566, Life ™ Technologies, Paisley, UK) and incubated on ice protected from light for a minimum of 5 min. Samples were stored once for up to an hour prior to flow cytometric analysis. Instrument calibration standards (unstained) as well as single stained sample controls were also prepared for calibration and compensation respectively.

6.2.1.3.2 Erythrocytic Depletion: Concentration Gradient Variant

Versalyse was stored as outlined within the manufacturer's guidelines at 18 – 25 °C and was used within a 90 day period starting the day of first use. Blood was collected from a healthy control donor as outlined in (6.2.1.1). However, 10 mL heparin coated vaccutainers (Cat No. 367 980, BD Biosciences, Oxford, UK) were used and loaded with 9 mL of venous blood. 5 mL of heparinised blood was transferred using a sterile 10 mL pipette in conjunction with a pipette controller onto 5 mL of histopaque ® 1077 (Cat No. 1077-100mL, Sigma Aldrich, Gillingham, UK) resting upon 5 mL histopaque ® 1113 (Cat No. 1113-100mL, Sigma Aldrich, Gillingham, UK) within a 15 mL Falcon tube. Samples were centrifuged (~300 x g for 30 min) at room temperature, forming a distinctly reproducible layered blood sample. Starting with the least dense, the plasma layer was removed, "buffy white coat" presumed lymphocytes, followed by the histopaque ® 1077, and very carefully the layer of polymorphonuclear white blood cells removed and aliquotted into a fresh 15 mL centrifuge tube (~100 µL volume). The erythrocyte dominated cellular pellet as well as the additional layers, excluding the granulocyte layer were discarded and disposed of according to health and safety protocol. Excess (~10 mL) of pre-warmed RPMI 1640 medium was added to the minimal volume of suspected reticulocytes and centrifuged at (~280 x g for 10 min) room temperature. Post centrifugation, supernatant was aspirated and the cell pellets initially re-suspended in a minimal

volume of RPMI 1640 medium, before additional excess was added. Cellular samples were centrifuged (~280 x g for 7 min), supernatant aspirated and discarded, and washed with excess RPMI medium – this step was repeated an additional two times. Cell pellets were re-suspended in 0.5 - 1 mL of 1 x PBS solution and treated with antibodies in an analogous fashion was outlined in (Section 6.2.1.1). Following incubation, 1 mL of VersaLyse solution (1X) was added, vortexed immediately (1 sec) and incubated for 10 min at room temperature, protected from light. Post incubation, cells were centrifuged (150 x g for 5 min), supernatant aspirated and re-suspended in 3 mL of 1 X PBS solution. The sample was centrifuged, supernatant aspirated, re-suspended in 1 mL of 1 x PBS solution and treated with 5 µL of propidium iodide solution (1 mg/mL) and incubated on ice protected from light for a minimum of 5 min. Samples were stored once for up to an hour prior to flow cytometric analysis. Instrument calibration standards (unstained) as well as single stained sample controls were also prepared for calibration and compensation respectively.

6.3 Results

All work carried out within this section was undertaken in direct collaboration with Dr Hasan Haboubi, who personally over saw the collection of the blood samples and contributed towards the undertaking of the optimisation/developmental experiments.

6.3.1 Human Erythrocyte (RBC) *PIG-A* Assay Platform Optimisation

In order to evaluate the potential of developing a sensitive and accurate bio-monitoring platform, initially an estimation of the spontaneous background frequency is required. In this specific context, the pre-existing frequency of phenotypic *PIG-A* mutants within "healthy" human patients is essential. Patients (healthy volunteers) were identified as "healthy" based on their own self-proclamation, adhering to a number of limited criteria, and the subsequently generated data would provide an estimation of the expected sensitivity, as well as any obvious pit falls within the current preliminary protocol. However, in addition to this, a number of additional experimental variables must be evaluated prior to generate confidence and primarily validate assay robustness. Preliminary investigations into antibody sensitivity, blood agglomeration status, viability and phenotypic marker selection were undertaken to assess the likelihood of establishing an assay platform with adequate robustness and reproducibility to facilitate long term bio-monitoring. If the platform was unable to establish a spontaneous mutant frequency, at the *PIG-A* gene locus, in-line with current publications, as well as showing some degree of reproducibility, there would be limited use within human health assessment. Future potential investigations should firstly; i) enable an extended validation of the test platforms and ii) correlate any measurable increases or decreases in patient phenotypic *PIG-A* mutant frequency with potential exposure acuteness or duration etc. The following body of work, all *PIG-A* mutant frequencies stated are phenotypic mutant frequencies; displaying a loss or partial loss of GPI-AP associated surface antigens, no sequencing validation has been undertaken to defined genotype.

6.3.1.1 Introductory Antibody Investigation

Due to the nature of fluorescent probes and the risks associated with photo bleaching, experimental incubation conditions were investigated to ensure optimum conditions were adhered to; promoting accuracy and validity within subsequent data.

Prior to detailed data analysis a crude gating strategy, based on size and granularity of presumed cellular events, was implemented. This enabled the subsequent investigation to comment on any observed generalised trends following experimentation. In addition, data was tested for normality utilising the Shapiro-Wilks Test to facilitate supplementary statistical analysis, if required. The experimental data was demonstrated to be normally distributed (P = 0.452), with direct protection from polarising light, minimised photo-bleaching, shown to result in a significantly (P = 0.048) higher average staining efficiency (99.96%) than parallel samples exposed to work bench light (99.91%). Furthermore, extending the incubation period was shown not to have a significant effect on the efficiency of sequential antibody staining, once optimal exposure had been reached (30 min incubation period (P>0.05)) (Figure 6.2).

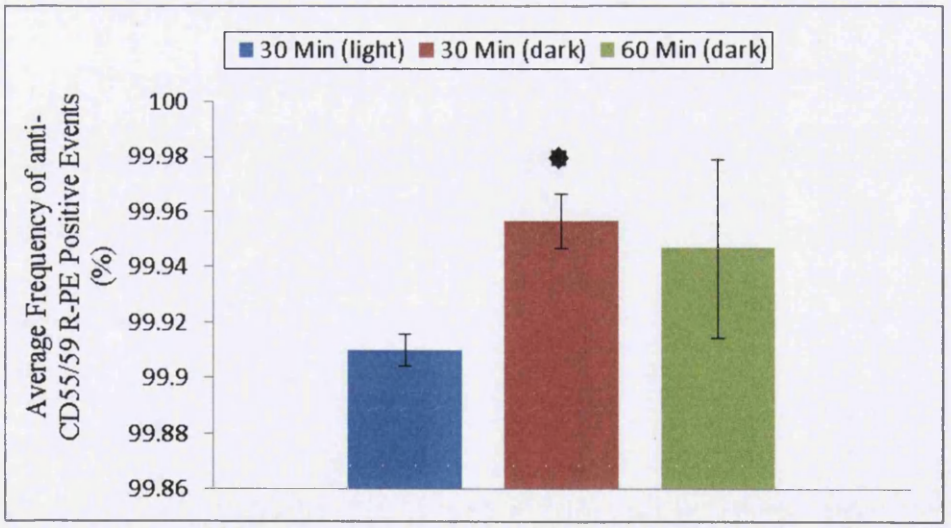

Figure 6.2. The frequency of defined single cell RBCs staining positive for the GPI-AP CD55 and/or CD59, following extended incubation and protection from direct polarising light, when compared to the generic incubation conditions. Data was demonstrated to be normally distributed, Shapiro Wilks, P = 0.452 (Dunnett's 2-sided T-test, P<0.05*, <0.01 **) (Error Bars ±SD) (N=3, from same donor)(10,000 cells scored).

Whole blood was used as the generic sample type with no prior sample separation implemented; therefore, cellular identity was based on crude FSC and SSC profiles generated during initial FCM analysis. In order to increase confidence within reported data, the practice of incorporating an erythrocyte sensitive antibody probe was employed; this provided further validity of the identity of presumptive RBC or RETs events scored on the flow cytometer. Anti-CD235a (Glycophorin A) was trialled for its use as a selective marker for erythrocytes, the smaller volumes of 5 and 10 µL (~99.5%) were shown to produce the most favourable results when compared to the larger 50 µL (97%) volume (Figure 6.3 A). 10 µL loading volumes generated the highest sequential staining efficiency and hence identification of an erythrocyte population (99.75%). As well as loading volume, the length of incubation was also assessed; little difference was shown between the analogous 30 min or 60 min incubation time's staining efficiency. However, 60 min on average generated the highest staining efficacy (99.75%) (Figure 6.4 A). Due to the presence of significant agglomeration following antibody treatment, sample racking was investigated to quantitate the effect "racking" had on agglomerations status. Two identical samples were constructed and a single sample vigorously physically agitated. The "un-racked "sample displayed a substantial presence of a second major population within the anti-CD235a fluorescence emission channel, indicative of doublets, or larger agglomerates (Figure 6.3 B). The "racked" sample was shown to exhibit a significantly smaller agglomerate population (Figure 6.4 C), and more highly resembled a mono-particle suspension of cultured cells.

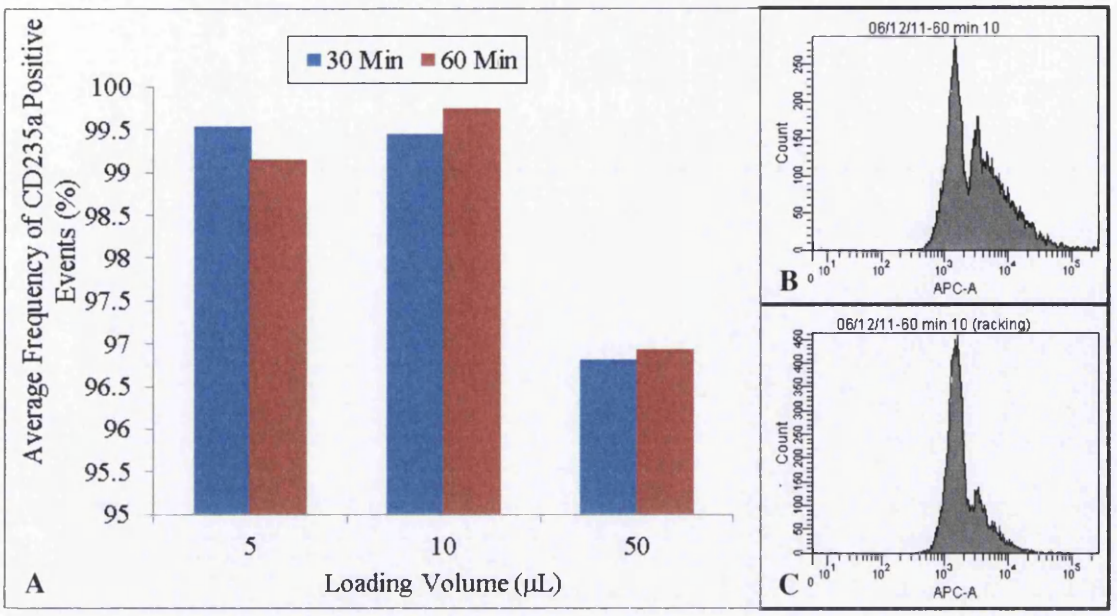

Figure 6.3. The frequency of defined single cell RBCs staining positive for the Glycophorin A sensitive CD235a primary antibody following variable incubation times and treatment concentrations (A). The effect that vigorous sample racking has on the distribution and frequency of RBC agglomerates (Pre-racking (B) and Post-racking (C)) (>10,000 cells analysed).

Finally, the effect of whole blood concentration and increased flow cytometry sample running rate were evaluated with respect to *PIG-A* mutant phenotype assessment. Typically a 1:20 blood dilution factor is used to generate RBC data, however, a second 1:10 dilution was set up to directly compare the effect a more concentrated sample could have on phenotypic mutant frequency. The results showed that the average background *PIG-A* mutant frequency was significantly lower (P = 0.0007) for the 1:20 sample (0.01%) when compared to the more concentrated 1:10 sample (0.08%). The background mutant frequency appeared to shown a positive correlation with sample concentration, i.e. as the concentration increased, so did the background mutant frequency (Figure 6.4).

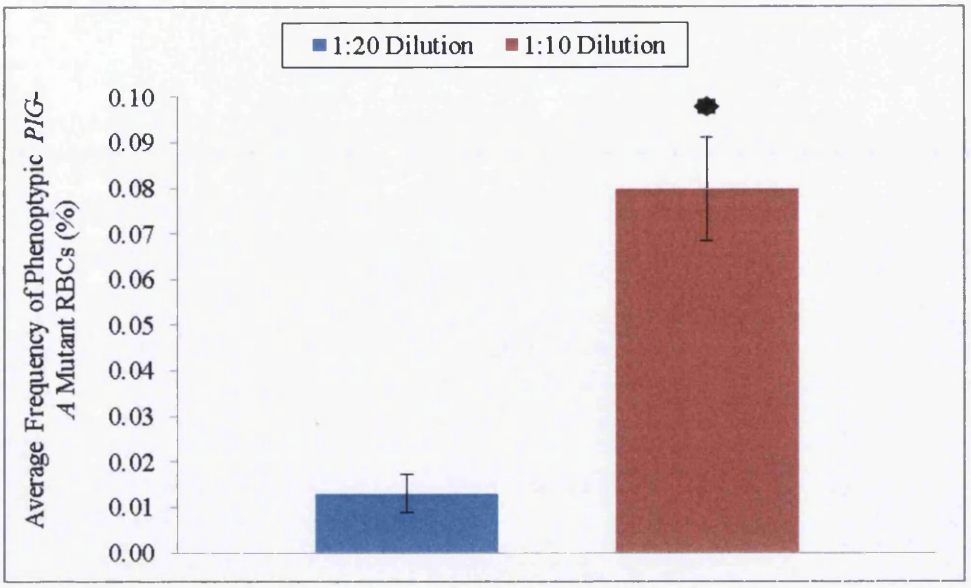

Figure 6.4. The average RBC *PIG-A* mutant phenotype frequency following anti-CD235a identification in conjunction with tandem *PIG-A* reporting, anti-CD55/59 R-PE antibody staining of whole blood. The effect of greater event capture through whole blood sample concentration and increased flow rate was investigated (~1x10^6 events scored) ((Dunnett's2 sided T-Test ($p < 0.05$*)(N=3, Error Bars ±1SD))

6.3.1.2 Human Erythrocyte (RBC) *PIG-A* Assessment – Spontaneous Mutant Frequency Derivation

Taking into account the initial antibody evaluation and optimisation, the crude assay platform was utilised to collect the data for the first "healthy" control patient, in order to assess enumeration of RBC and preliminary RET events, and their respective *PIG-A* status (Figure 6.5). The sample was run in triplicate and demonstrated an average spontaneous background mutant frequency as 0.013%, which correlated in the range of 100-200 *PIG-A* mutant phenotype cells per 1 x 10^6 events scored (Table 6.1); showing good correlation to published literature [280, 351]. The samples took on average 8-10 min to run, which facilitated the capture of >1 x 10^6 mature RBC and estimated >10,000 RET events; insufficient RET events would be able to be captured to provide sufficient statistical strength in mutation frequency estimation.

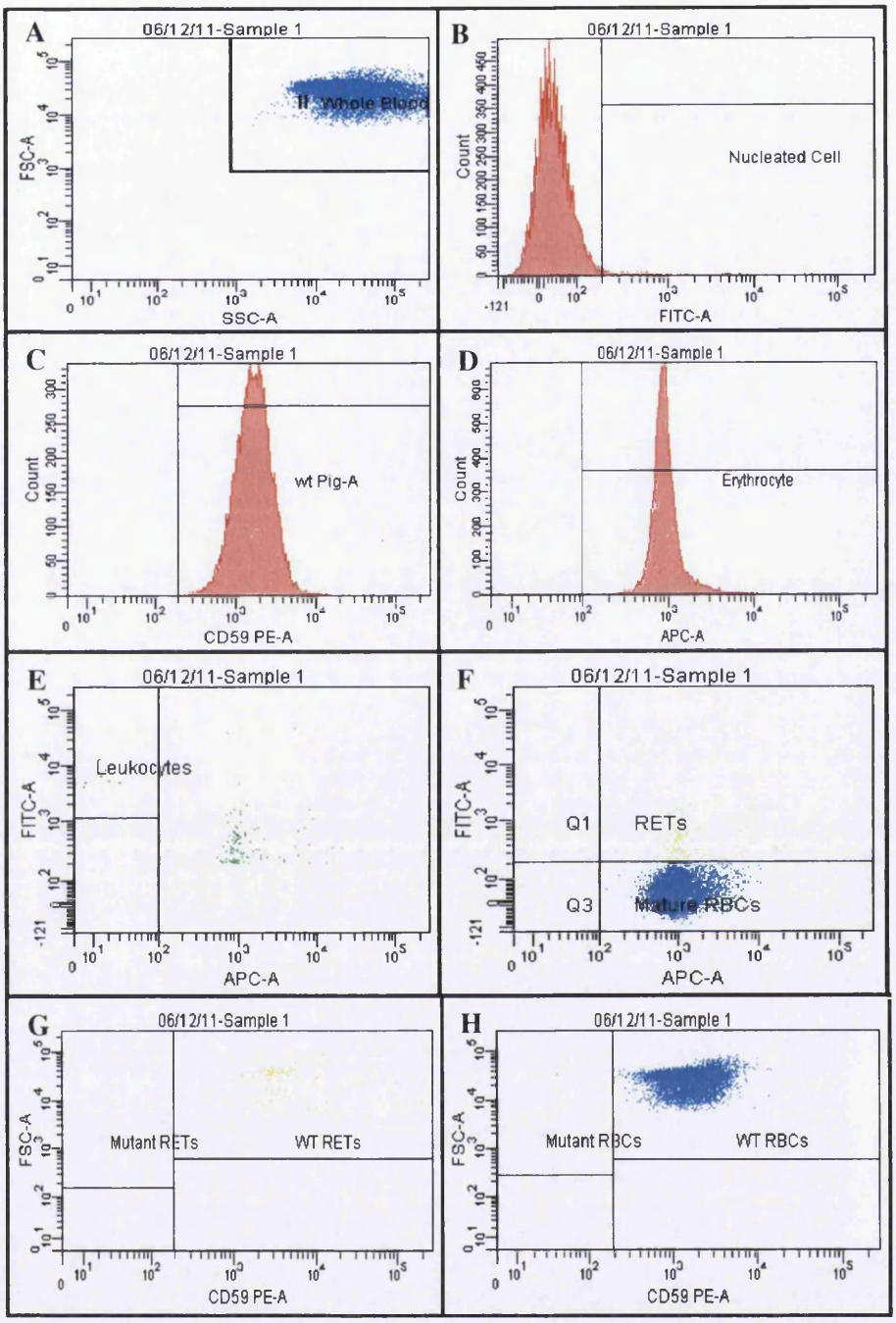

Figure 6.5. Flow cytometry analysis work flow, showing the progressive labelling, identification and sub-population derivation in order to obtain phenotypic *PIG-A* mutant frequency assessment. A) Crude FSC vs SSC dot plot indicative of morphology and cell size. B),C) and D) Relative fluorescence intensity for lineage specific markers; B) DNA content C), GPI-AP status and D) Glycophorin A presence. E) Leukocyte specific gating, F) RET and mature RBC identification and separation, G) GPI-AP assessment of RETs and H) GPI-AP assessment of RBCs (10,000 events shown for ease of visualisation from "healthy" patients).

Table 6.1. Summary of the initial PIG-A mutant phenotype Assessment within Mature RBCs (Limited Capture ~1,000,000 events scored)

Sample Identification	Total Number of Single Cell Events	Total Number of Defined Erythrocytes	Total Number of Defined RBCs	Number of Defined Mutant RBCs	Percentage *PIG-A* phenotypic Mutant RBCs
ICS	10000	3	3	3	100
Sample 1	1000000	999550	999468	82	0.008
Sample 2	1000000	999439	999282	157	0.016
Sample 3	1000000	998093	997942	151	0.015
Average	1000000	999027.3	990200	130	0.0130

6.3.2 Initial Human Erythrocyte (RET) and Granulocyte *PIG-A* Assay Platform Optimisation

6.3.2.1 Human Erythrocyte (RET) *PIG-A* Assay Platform

6.3.2.1.1 Preliminary Antibody Investigation – RETIC Count™

Based on the relative success of the preliminary RBC assay design, RET events were evaluated for their potential as a platform for *PIG-A* reporting. In order to capture, with confidence, sufficient RET events for phenotypic *PIG-A* assessment, to estimate background mutant frequency, specific antibody optimisation was required. The RETIC Count™ reagent was shown to be highly affected by the incubation temperature as well as the length, with 30 min on ice (~ 0-2 °C) generating the lowest identification of RET numbers within the whole blood sample. Both 30 and 60 min room temperature incubations displayed significantly higher numbers of RET identification ($P<0.01$), when directly compared to the 30 min ice incubated sample. 60 min RT generated the most reproducible, maximum identification of putative RET events within the whole blood sample and was selected for incorporation into the human erythrocyte RET assay design (Figure 6.6).

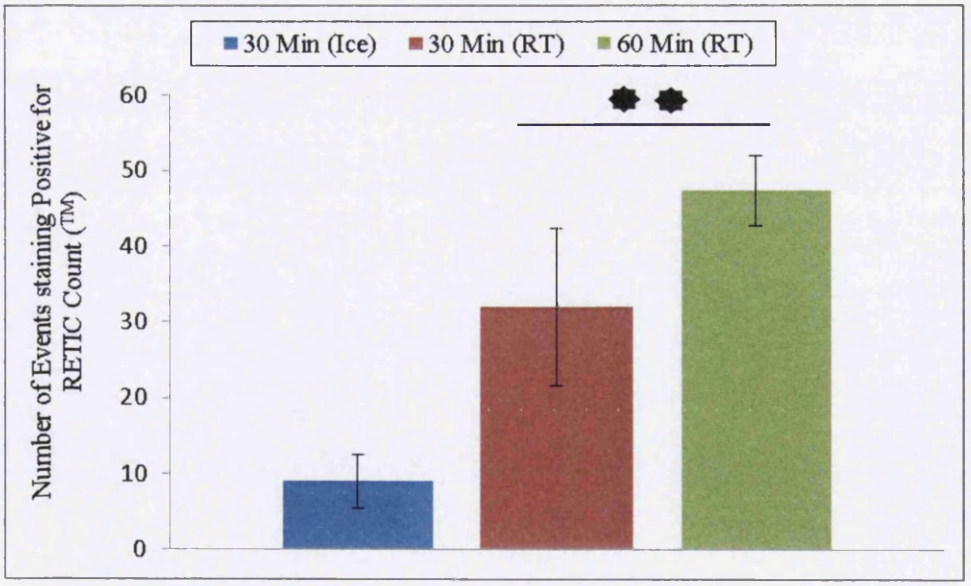

Figure 6.6. The average number of events displaying RETIC Count ™ positive staining, following varied incubation time and direct polarizing light exposure. Data was demonstrated to be normally distributed, Shapiro Wilks, $P = 0.384$ (Dunnett's 2-sided T-test, $P<0.05$*, <0.01 **)(Error Bars ±SD) (N=3) (RT - Room temperature, ICE- ~2°C).

6.3.2.1.2 Preliminary Human Erythrocyte (RET) *PIG-A* Assessment – Spontaneous Mutant Frequency Derivation

Following incorporation of the RETIC Count™ reagent into the erythrocyte RET assay design, preliminary phenotypic *PIG-A* assessment was undertaken in order to quantify the spontaneous background mutant frequency at the specific gene loci. The results were obtained from measuring the relative phenotypic *PIG-A* mutant frequency within whole blood taken from a "healthy" donor (Figure 6.7 and Table 6.2). Utilising a highly inclusive gating strategy, analogous to that within the initial developmental stages of the in vitro *PIG-A* assay design, approximately 10,000 defined RET events were able to be captured (staining positive for both RETIC Count™ and CD253a) in less than 20 minutes per sample. The average spontaneous *PIG-A* mutant frequency within the RET population was estimated to be 0.03% (Table 6.2), approximately 3 fold higher than the corresponding mutant *PIG-A* RBC frequency; this relationship is supported by the recently published literature [351, 358, 387]

Table 6.2. Summary of the preliminary relative phenotypic PIG-A mutant frequency within the RBC and RET population. Whole blood was exposed to anti-CD235a, tandem CD55/59 R-PE antibody exposure and REITC Count™; RETs were identified on their double positive nucleic acid staining and erythrocyte specific marker presence and assessed for GPI-associated PIG-A status. (~10,000 RET defined events were captured in 10-20 min sample running time).

Sample Identification	Total Number of Defined RBCs	Number of defined mutant RBCs	Percentage *PIG-A* phenotypic Mutant RBCs	Total Number of Defined RETs	Number of defined mutant RETs	Percentage *PIG-A* phenotypic Mutant RETs
Sample 1	702307	47	0.007	12475	0	0
Sample 2	654304	11	0.002	7626	2	0.026
Sample 3	778524	74	0.01	8544	6	0.07
Average	711712	44	0.01	9548.3	2.67	0.03

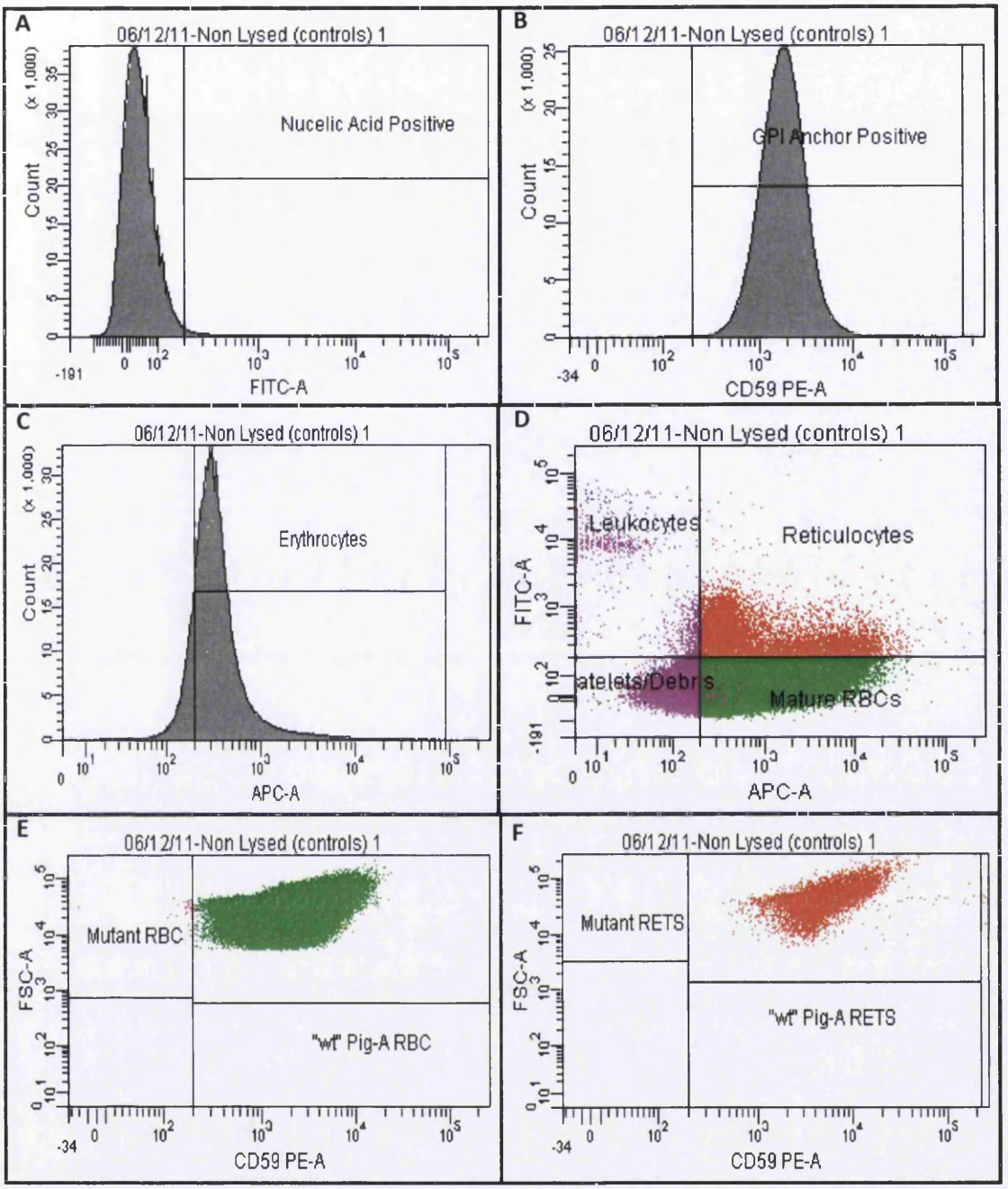

Figure 6.7. The preliminary RET *PIG-A* mutant frequency assessment within whole blood samples; A) Nucleic acid content, as defined by RETIC Count™ staining, B) GPI-AP status following anti CD55/59 R-PE tandem staining, C) Erythrocyte specific marker, anti-CD235a staining, D) Population distribution following advanced staining, E) Phenotypic *PIG-A* assessment within mature RBCs and F) Phenotypic *PIG-A* assessment within RETs (~10,000 RETs scored).

6.3.2.2 Human Granulocyte *PIG-A* Assay Platform Optimisation

6.3.2.2.1 Preliminary Enrichment Evaluation - Ammonium Chloride

Prior to the utilisation of enrichment methodology, the enumeration of sufficient granulocyte events had proven impossible within the tight experimental sample time constraints. The employment of an ammonium chloride solution was investigated to determine the possibility of FCM scoring >10,000 granulocyte events within an approximate 10-20 min analysis period; greater analysis periods could potentially elicit deleterious effects on the population viability. The results of lysis were demonstrated to have a distinct effect on the percentage constitution of different populations within the whole blood sample (Figure 6.8). Prior to lysis, 100,000 cells were captured without a single defined granulocyte event, CD15 positive, identified (Figure 6.8 A). However, following lysis, the granulocyte population was shown to increase to ~10% of the total sample constitution (Figure 6.8 B). During analysis it was shown to be possible to score 10,000 granulocyte events for sequential *PIG-A* phenotypic mutation status, within the allotted 10-20 min analysis time period. However, utilising this specific method of enrichment, there was little scope to increase the enumeration of events to the desire 1×10^6 within such limited time constraints.

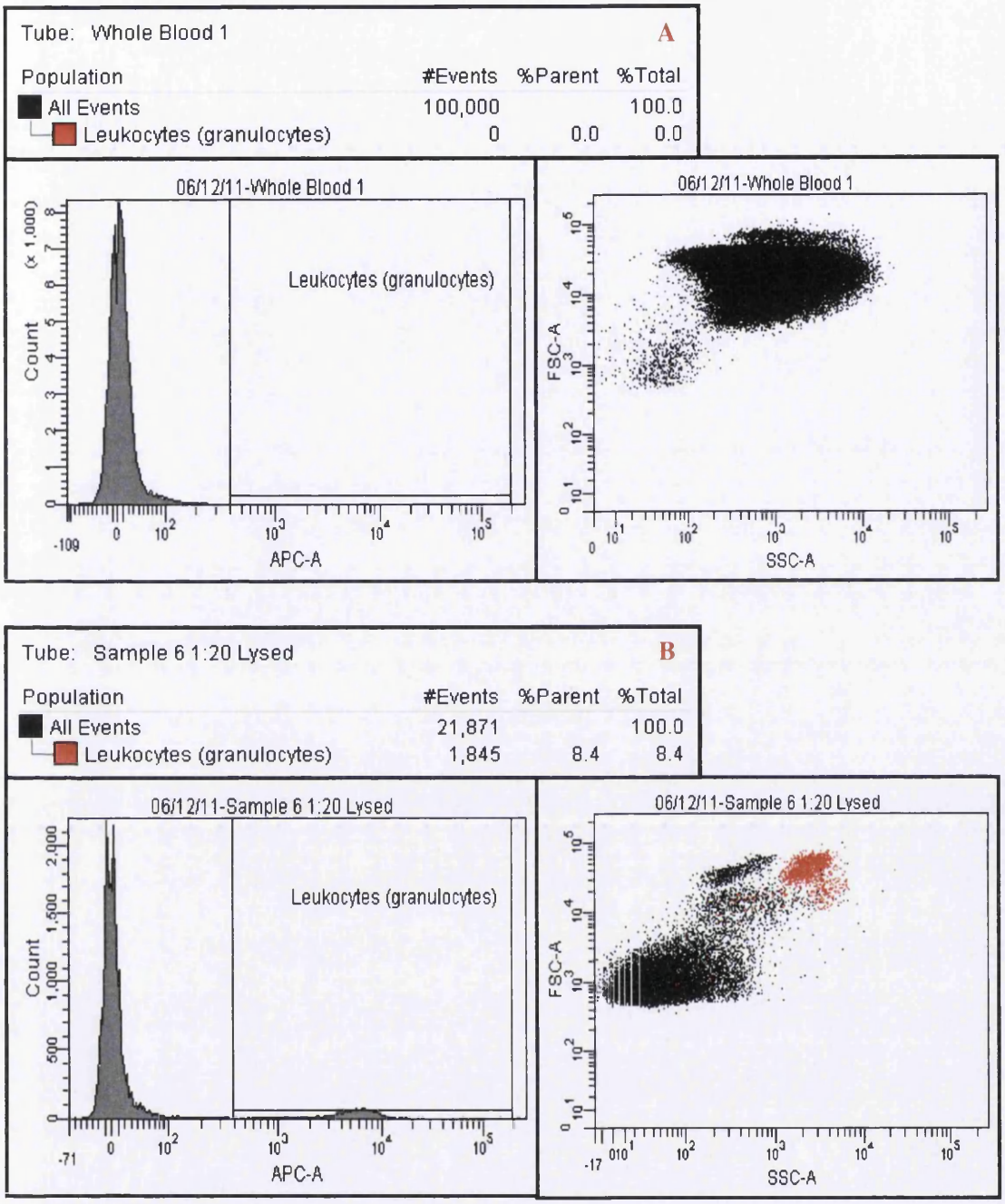

Figure 6.8. Overview of FCM data following capture of an un-treated, 1:10 diluted, whole blood sample (A) run in parallel with a ammonium chloride treated 1:10 diluted whole blood sample (B). An anti-CD15 APC-conjugated antibody was utilised as a granulocyte, activated neutrophil, specific antibody selective marker and was solely utilised to provide identity to the cells. FSC vs SSC dot plots (cytograms) were used to display the generic population data, CD-15 positive cells were painted Red for ease of visualisation retrospectively.

6.3.2.2.2 Preliminary Human Granulocyte *PIG-A* Assessment – Spontaneous Mutant Frequency Derivation

Following incorporation of a preliminary optimised ammonium chloride lysis step (Section 6.3.3.2.1), initial *PIG-A* mutant frequency assessment was undertaken in order to quantify the spontaneous background mutant frequency at the gene loci. The subsequent results initially mirrored the previous enrichment of the leukocyte population (Figure 6.8), as well as defined the spontaneous phenotypic *PIG-A* mutant frequency, within whole blood taken from a self-proclaimed "healthy" donor, utilising FLAER as the reporter mechanism (Figure 6.9). Applying an inclusive gating strategy, events were included based on their FSC vs SSC profiles in combination with CD15 positive staining, approximately 5,000-10,000 defined granulocyte events were able to be captured in less than 20 min per sample. The optimal average spontaneous phenotypic *PIG-A* mutant frequency within the granulocyte population was estimated to be 0.2% (Figure 6.9), utilising an undiluted FLAER treatment within an undiluted blood sample. An inversely proportional correlation was observed as decreasing concentrations of FLAER resulted in increasing background mutant frequencies. The current granulocyte assay platform is operating under a sensitivity levels approximately 20 fold lower than the corresponding mutant *PIG-A* RBC frequency, which in turn is 3 times more sensitive than the mutant RET platform. Insufficient numbers of defined granulocyte events could be scored to provide the assay with sufficient power to be a standalone assessment of *PIG-A* mutant frequency.

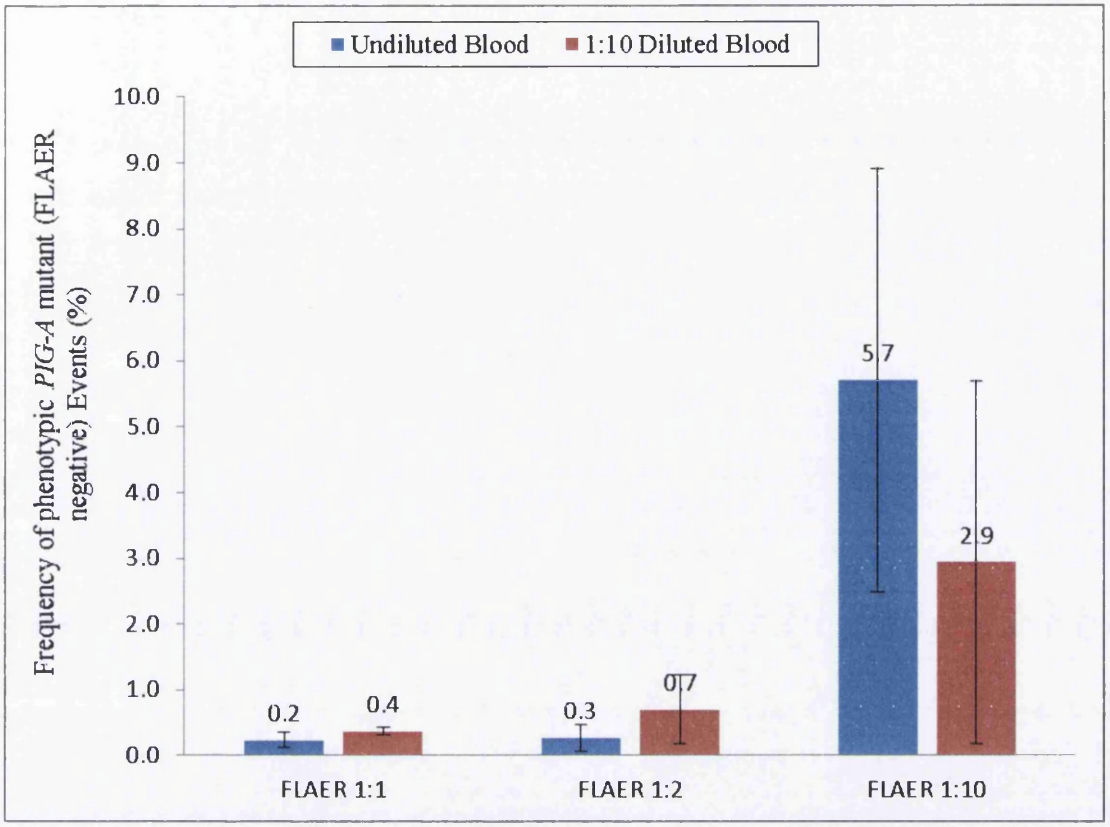

Figure 6.9. Average spontaneous background phenotypic mutant *PIG-A* frequency within CD15 labelled neutrophils (Granulocytes) utilising FLAER as the reporter for mutation; the effect of FLAER dilution as well as blood concentration was assessed within the content of *PIG-A* mutant frequency (Error Bars ±SD) (N=3).

6.3.3 Human *PIG-A* Assay Platform Supplementary Investigations

6.3.3.1 Lysis Buffer Evaluation

After completion of a retrospective compensation analysis (Section 2.8), the subsequent matrix was applied to the original lysis buffer optimisation FCM data and re-analysed thoroughly. The resultant populations were defined through simplistic FSC and SSC profiling with the combined usage of lineage specific markers (CD235a). It is apparent from the data that the concentration of the different buffer solutions did not have any significant influence on leukocyte enrichment. However, there were significant differences in leukocytes enrichment efficiency between the different types of buffer solutions; BD FACS lyse resulted in a significantly sub-optimal, approximately 20%, leukocyte composition. Easylyse and Versalyse were shown to produce very comparable results, ~80-90% relative enrichment, which appears to be independent of the concentration of the buffer used (Figure 6.10 A).

During reticulocyte enrichment, events defined as both RETIC Count™ and CD235a positive, both type of lysis buffer as well as relative concentration appeared to highly effect the consequential yield. Initally, both Easylyse and Versalyse solutions generated higher reticulocyte yields than the comprabale BD Facs lyse, across the concentration range investigated, with optimal yields being observed when using the most dilute (1/10 X) solution (~2.5-3.5%), for all buffers analysed. This appears to reinforce the intial observated relationship which separated BD FACS lyse from the comparable Easylyse and Versalyse solutions during leukocyte enrichment (Figure 6.9). Versalyse was shown to generate the optimum reticulocyte enrichment (3.867%) utilising the 1/10 X concentration, with the relative final reticulocyte consistuent frequency of the population being defined significantly smaller than the leukocyte population, following RBC lysis.

When analysing the data in terms of relative *PIG-A* mutant frequency; both Easylyse and Versalyse buffer solutions demonstrated analgous enrichment efficiency, superior to the BD FACS lyse data for leukocyte capture (concentration independent). However, their respective phenotypic *PIG-A* mutant status, post enrichment, were considerably different. Versalyse, using an undiluted or 1/10 X diluted sample, generated the most favourable data with respect

to the presence of GPI-AP on the cell surface (0.243% phenotypic *PIG-A* mutant frequency) (Figure 6.10 A and B). Subsequently, Versalyse was chosen to be implemented to enrich for leukocytes during the next stage of assay optimisation (FLAER analysis).

Reticulocyte *PIG-A* status was more complex in nature; Versalyse (1/10X) generated the optimal results in comparison to alternative buffer solutions in terms of RET enrichment. However, the phenotypic *PIG-A* mutant frequnecy was highly variable using either BD FACs or the Versalyse solution. Therefore, even though Easylyse was not the optimum buffer for enrichment, conforming to all additional needs of the platform, Easylyse was chosen as the buffer for reticulocyte enrichment. Using either undiluted or 1X concentrations favoured the populations with respect to *PIG-A* status (0.0 14-0.07%).

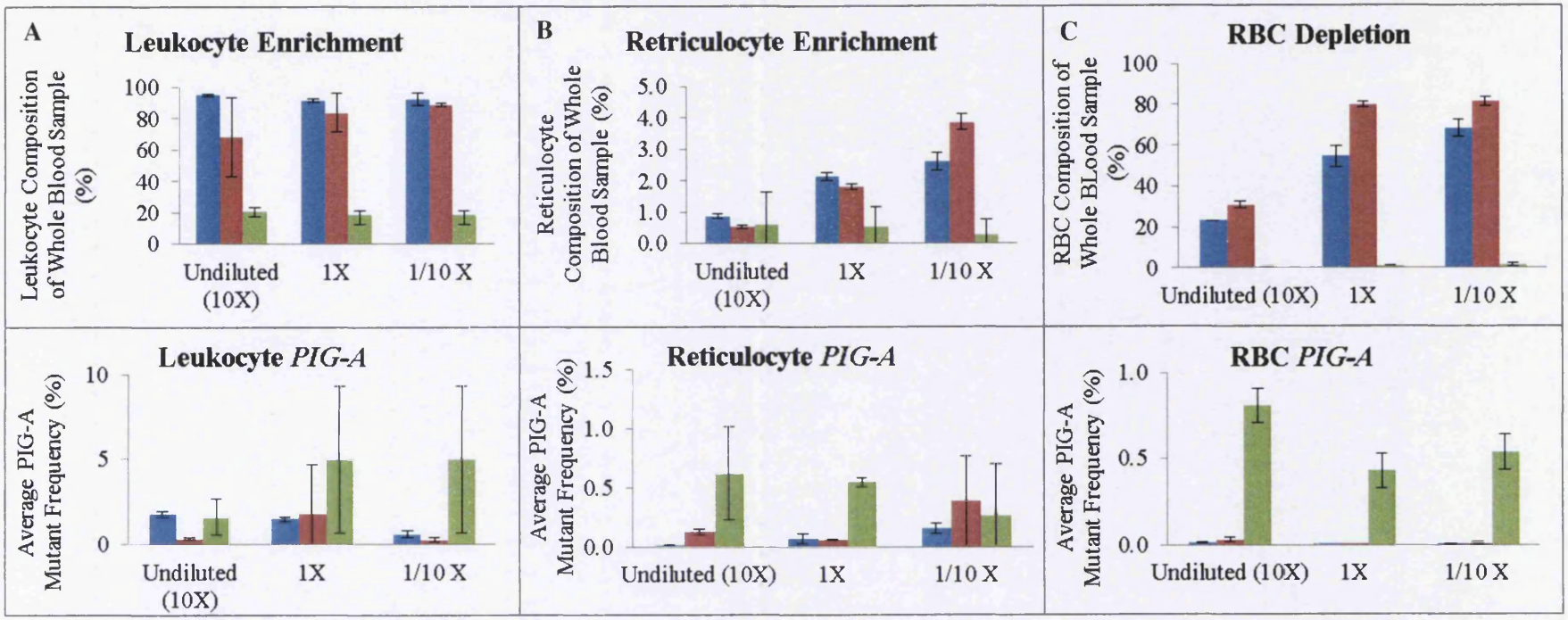

Figure 6.10. Percentage whole blood composition and relative cell type specific phenotypic *PIG-A* assessment (CD55/CD59) following variable RBC lysis buffer optimisation. Varying concentrations of three commercially available RBC lysis buffers were assessed for their incorporation into assay design and potential deleterious effects on *PIG-A* mutant frequency when facilitating leukocyte (A) and RET (B) enrichment and RBC depletion (C) - Easy Lyze ( ), Versa Lyze ( ) and BD FACS lyse ( ). (Approximately >100,000 RBC, 5,000 leukocytes and 5,000 RETs assessed) (Error Bars ± SD).

6.3.3.2 Cellular Viability during prolonged Human *PIG-A* Assessment

The results for the experiment were divided into the specific cell lineages present within peripheral human whole blood; when assessing the minor populations, RBC lysis was utilised in order to obtain sufficient sample cell number. Identification of the subgroups was mainly attributed to their unique FSC and SSC profiles, however, some lineage specific markers were also implemented during flow cytometry assessment. The results revealed that there was a significant presence of apoptotic cells within both the leukocyte (~10%) and reticulocyte (~0.5%) sub-populations (Figures 6.11 B and C respectively), when compared to unstained controls. However, the monitored levels of apoptosis, observed over the experimental time period, were surprisingly consistent within both populations. No significant variation in apoptosis was detected over the experimental time period when compared to con-current control samples (fresh whole blood sample). Apoptosis was not observed within the non-nucleated sub lineage (mature RBC) which supports the lack of intrinsic and extrinsic biological mechanisms (Figure 6.11 A).

Loss of membrane integrity (Cell Death) was apparent within all sub lineages across the whole blood sample (Figure 6.11). Within the erythrocytic cell lineages, the level of cell death remained consistently around the 5% figure, with no significant variations across the experimental time period. The percentage of dead cells present within the leukocyte sub-population was elevated (~20%) when compared to the comparable cell types, however, again it remained consistent across the extended experimental time (Figure 6.11 B). There was no obvious correlation between variance in cell death or apoptosis with respect to the experimental period; loss of cellular viability appeared independent of time.

Necrosis was defined as a morphological state in which the cells were presenting as annexin V positive as well as having a significant loss in membrane integrity, as depicted by propidium iodide positivity. Again, the results showed that necrosis was only observed within the nucleated sub-populations, and that relative levels remained consistent across the time course. Leukocytes again were shown to exhibit slightly elevated levels of necrosis than RETs, ~3% compared to 0.1%, similar to their relative levels of apoptosis. This result again appeared to show an analogous trend, the independence of cellular viability in regards to experimental time period. The

levels of apoptosis, necrosis and cell death were demonstrated to be cell lineage specific; however, they remained at a consistent level during the extended experiment with no significant variation detected.

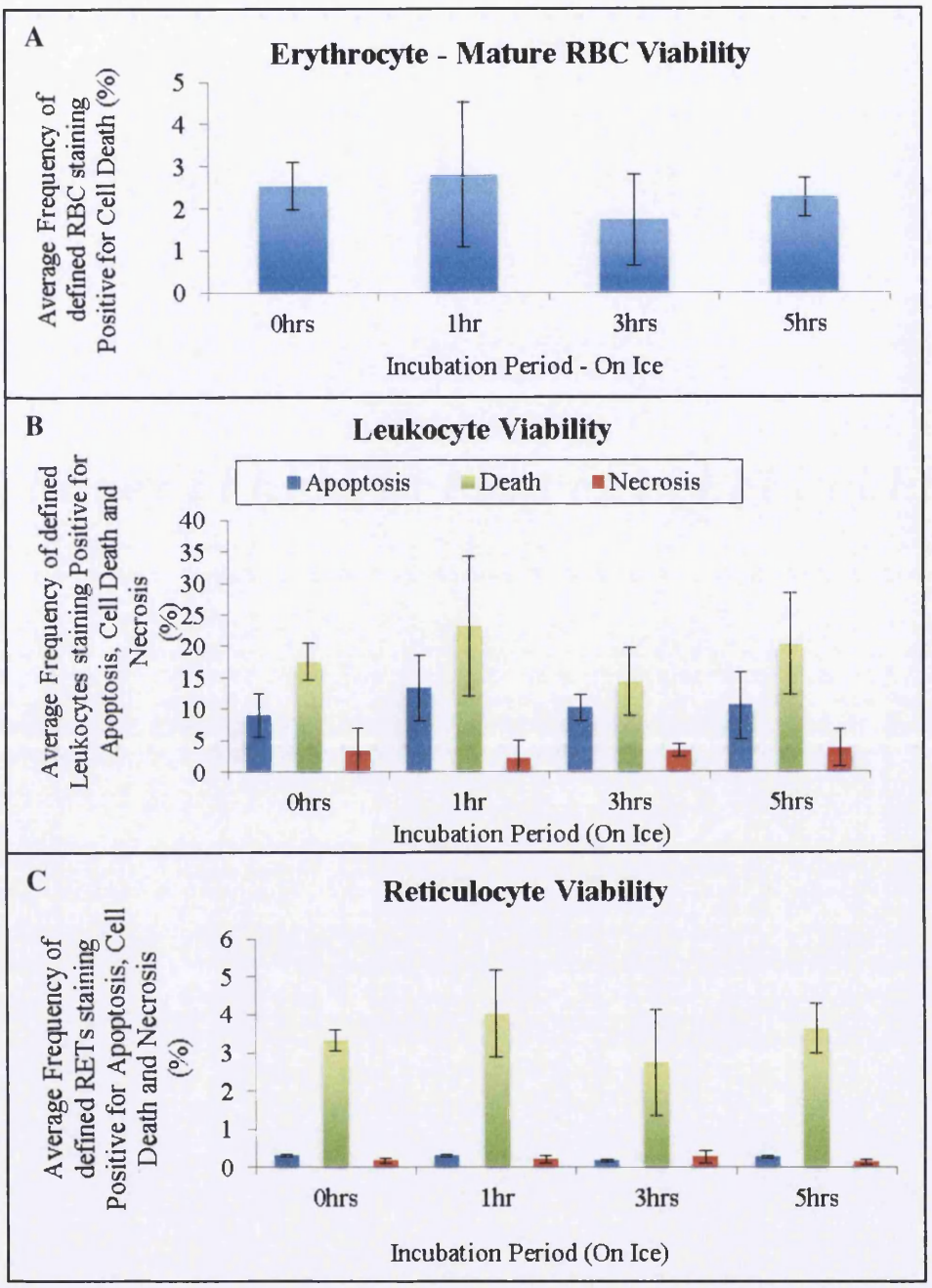

Figure 6.11. Summary of relative viability of the three sub-types of haemopoetic cells within human peripheral blood, over an extended experimental period (up to 6 hr). Cell death, i.e. membrane integrity, was assessed utilising Propidium Iodide nucleic acid dye presence; apoptosis was assessed using a phosphatidyl serine sensitive Alexa Fluor 488nm Annexin V conjugate antibody and finally, necrosis was monitored through combined assessment of membrane integrity and PS presence on the extracellular surface (>100,000 RBC (A) and >5,000 leukocyte (B) and RET (C) events scored.)

6.3.3.3 Cellular Enrichment Investigation

6.3.3.3.1 Centrifugation as the Sole Granulocyte Enrichment Tool and the effect FLAER Titration has on Spontaneous *PIG-A* background Mutant Frequency

Initially considering the population statistics following sole high speed centrifugation when compared to the more typical lysis method, approximately 7-10% of the resultant population post centrifugation were leukocyte in nature (based on FSC and/or SSC profiles). However, of the presumed leukocyte population, only ~10% were CD15 positive in nature (Table 6.3), highly dissimilar from the greater than 95% CD15 populations associated with RBC lysis optimisation (Section 6.3.3.1). Centrifugation demonstrated an apparent preferential enrichment for leukocytes in general, not specifically the CD15 activated neutrophil sub-population; this had a diluting general effect on granulocyte enrichment. FLAER titration generated results which were to be as expected, showing a general trend of increasing dilution leading to a greater spontaneous background frequency (Table 6.3). The optimum results were observed when using either un-diluted or a single 1:1 dilution within 2% BSA/PBS, resulting in an average 0.17 and 0.1% phenotypic *PIG-A* mutant frequency respectively. Larger dilution factors resulted in significantly higher spontaneous background mutant frequencies at the *PIG-A* locus, as demonstrated by the observed average 1.17% *PIG-A* mutant frequency following a 1:10 dilution.

Table 6.3. Summary of the affect centrifugation and FLAER titration have on preliminary PIG-A mutant frequency assessment.

Sample ID	Number of Defined Leukocytes	Leukocytes as a Percentage of Total Events Captured	Number of CD15 Positive Events	CD15 Positive Events as a Percentage of Leukocytes	Number of FLAER Positive Events	Percentage FLAER positive events as a Percentage of CD15 Positive Cells	Number of FLAER Negative Events	Percentage FLAER negative events as a Percentage of CD15 Positive Cells
ICS	3141	302	1	0	1	100	0	0
Neat A	5298	6.3	1187	22.4	1183	99.7	4	0.3
Neat B	155305	11.6	999	0.6	998	99.9	1	0.1
Neat C	131940	9.5	2757	2.1	2755	99.9	2	0.1
Average	97514.33	9.13	1647.67	8.37	1645.33	99.83	2.33	0.17
50% A	37669	7.8	2917	7.7	2915	99.9	2	0.1
50% B	29091		7702	26.5	7696	99.9	6	0.1
50% C	172519	9.3	8661	5	8652	99.9	9	0.1
Average	79759.67	7.50	6426.67	13.07	6421.00	99.90	5.67	0.10
10% A	16090	5.7	2957	18.4	2929	99.1	28	0.9
10% B	32942	6	5930	18	5786	97.6	144	2.4
10% C	197020	11.8	1614	0.8	1610	99.8	4	0.2
Average	82017.33	7.83	3500.33	12.40	3441.67	98.83	58.67	1.17

6.3.3.3.1.1 The Possible Effects on Cellular Viability as induced via High Speed Centrifugation

The potential effect on viability was assessed through the direct comparison of two analogous human peripheral blood samples, one exposed to high speed centrifugation separation and the second RBC lysis buffer (Versalyse) followed by viability dye staining. The resultant data demonstrated that lysis resulted in a significantly lower percentage of single cell events (~1% and 10% respectively), greater relative numbers of cells which have lost membrane integrity (~10% to 1%), and a greater population constitution of CD15 positive cells (~>95% to 25%) when compared to high speed centrifugation (Table 6.4). The only variable which remained constant between the two methods was the relative amount of apoptosis detected within the subsequent CD15 populations (~0.5%). As well as comparing the affect the separation/enrichment method had on the resultant viability of the population, extended experimental incubations were also evaluated for their effect on viability. The results demonstrated that apart from a marginal increase in the relative amount of loss of membrane integrity within the CD15 sub-population, all other measurable viability endpoints were consistent when compared to the immediate analysis and the pro-longed 6 hr delay period on ice and/or at room temperature (~22°C). Full experimental method can be found at (Appendix Section 6.2.3.3.2.1).

Table 6.4. Summary of the effect high speed centrifugation has on granulocyte viability and capture efficiency, when compared to lysed whole blood samples. (Sample ID 1a = Ice 6hr, 1b = Room Temperature 6hr and 2a = Room Temperature 0hr) ICS - Instrument Calibration Standard.

	Sample ID	Total Events	Number of Events Defined Single Cell	Single Cells as a Percentage of Total Events	Percentage of Single Cells Staining CD15 Positive	Number of Cells Defined Apoptotic	Percentage Apoptotic (%)	Number of Cells with Compromised Membrane Integrity	Percentage Membrane Compromised Cells (%)
Lysed	ICS 1a	115710	2562	2.2	0	12	0.5	59	2.3
	1a	495543	4336	0.9	99.7	4275	98.6	462	10.7
	ICS 1b	15268	2131	1.4	0.6	7	0.3	11	0.5
	1b	545443	9031	1.7	98.7	1239	13.7	779	8.6
	ICS 2a	1016223	7195	0.7	0.1	24	0.3	116	1.6
	2a	898123	9196	1	94.2	489	5.3	690	7.5
Centrifuged	ICS 1a	248716	35617	14.3	0.1	93	0.3	177	0.5
	1a	128136	19333	15.1	24.2	211	1.1	207	1.1
	ICS 1b	610675	45905	7.5	0	145	0.3	235	0.5
	1b	229035	23020	10.1	21.6	183	0.8	320	1.4
	ICS 2a	389160	47092	12.1	14	79	0.2	178	0.4
	2a	197021	22382	11.4	23	111	0.5	206	0.9

6.3.3.3.2 Investigations into Histopaque® Enrichment

Based on an average healthy adult's peripheral blood constituting 1-2% of immature red blood cells (RETs), the use of histopaque® was investigated to assess the feasibility of RET and Granulocyte sub-population enrichment in excess of previous methods and hence, subsequent FCM scoring in regards to *PIG-A* mutant frequency assessment. Following histopaque® enrichment, there were two obvious layers with characteristics corresponding to peripheral blood mononuclear cells (PBMCs) and poly-nuclear cells (PNCs) granulocytes with retrospective densities less than that of the mature RBC pellet. Each WBC layer was extracted, stained and FCM assessed for phenotypic *PIG-A* mutant status. In terms of enrichment, the results were not as comprehensive as previously described methods (RBC lysis buffer) only facilitating the enrichment of RETs to 2.9% of the total population when compared to between 5-10% with VersaLyse (Section 6.3.2). The distal layer, in terms of erythrocyte pellet, demonstrated highly minimal (<0.1%) CD235a staining, eluding at highly comprehensive separation of the differential cell lineages.

"Layer 1", the layer corresponding to the lower density, constituted of ~90% morphological leukocytes, which was significantly higher than "layer 2", the proximal layer to the erythrocyte pellet (<1%). However, even though defined leukocyte by their FSC/SSC profiles, approximately only 1.3% of the population were CD15 positive in nature, of which their respective *PIG-A* mutant frequency was on average 2% (Table 6.5). Although, "layer 2" generated a relatively small population of CD15 positive granulocytes (0.7%), the corresponding background mutant frequency at the *PIG-A* locus of an average 0.03%, which is the highest granulocyte sensitivity recorded within assay development. The lack of neutrophil enrichment in terms of fold change only facilitated the capture of approximately 2,000-5,000 granulocyte positive events and therefore, would require further optimisation in order to obtain the number of granulocytes required for strong statistical analysis.

The results in terms of population location within the histopaque ® centrifugation tube indicated that the granulocyte population was being split between the two layers flanking the histopaque ® layer and therefore, could be the reason for such poor

sample harvesting due to event loss within the histopaque ® removal. The number of CD15 positive events within a 3-7 mL whole blood sample should comfortably facilitate the capture of 1 - 10^6 events for subsequent *PIG-A* phenotype assessment.

Table. 6.5. Summary of the relative enrichment as well as phenotypic PIG-A status of the proposed "leukocyte" populations derived from either the first or second layer of removed cells following Histopaque® enrichment; Histopaque 1.077 g/mL utilised for concentration gradient centrifugation enrichment in combination with anti-CD15 APC for lineage specific identification.

	Total Number of Captured Events	Morphological "Leukocytes"	Percentage of Total Single Cells	Number of Leukocytes defined CD15 Positive	Percentage of Total Cells CD15 Positive	Phenotypic *PIG-A* Wild type Granulocytes	Percentage of *PIG-A* Positive Cells	Phenotypic *PIG-A* mutant Granulocytes	Percentage of *PIG-A* Negative Cells
Granulocyte Layer 1 S1	488400.0	428281.0	87.7	3796.0	0.8	3740.0	98.50	56.0	1.50
Granulocyte Layer 1 S2	260496.0	236359.0	90.7	2776.0	1.1	2757.0	99.30	19.0	0.70
Granulocyte Layer 1 S3	189240.0	180075.0	95.2	3594.0	1.9	3466.0	96.40	128.0	3.60
Average	**312712.0**	**281571.7**	**91.2**	**3388.7**	**1.3**	**3321.0**	**98.07**	**67.7**	**1.93**
Granulocyte Layer 2 S1	195288.0	2180.0	1.1	2092.0	1.1	2089.0	99.90	3.0	0.10
Granulocyte Layer 2 S2	418128.0	2523.0	0.6	2496.0	0.6	2495.0	100.00	1.0	0.00
Granulocyte Layer 2 S3	1117320.0	3195.0	0.3	3158.0	0.3	3157.0	100.00	1.0	0.00
Average	**576912.0**	**2632.7**	**0.7**	**2582.0**	**0.7**	**2580.3**	**99.97**	**1.7**	**0.03**

6.3.3.3.2.1 The Finalised Optimisation of Histopaque®

This experimental design was utilised to assess the potential robustness of the usage of two distinct histopaque ® layers to capture and isolate (PNC) granulocytes (Figure 6.12). The design of this experiment took into account the affect that temperature has on the enrichment protocol and also allowed the granulocytes and potentially reticulocytes layers to be isolated and harvested efficiently.

Within both samples the results generated were quite dissimilar, clear presumed granulocytes (PNC) layers were present and located above the erythrocytic pellet. The layers themselves were slightly pink in colour, eluding at the indication of potential RET isolation due to the spiking effect of erythrocyte presence; the colour change was more apparent as you proceeded down the layer. Both samples were subsequently stained for RET and granulocyte presence and were showed to generate significantly large granulocyte sub-populations. Following FCM analysis, the EDTA sample was observed to provide marginally better yields (granulocytes) however; the difference wasn't significant and did not affect the sample's ability to score granulocyte presence for an extended period of time (Table 6.6).

From averaging the running time for both EDTA and Heparin samples, to collect approximately 1 x 10^6 granulocyte events, the estimated acquisition time would approximately be 20-30 min per sample acquisition. The resultant phenotypic *PIG-A* mutant frequencies observed within both the EDTA (0.08%) and heparin (0.11%) samples were highly similar, approximately 0.1% spontaneous background mutant frequency (Table 6.6). The RET sub-population within both samples was demonstrated to comprise very few RET events and prevented full analysis; the subsequent data generated was not of particularly good quality and the spontaneous background phenotypic *PIG-A* mutant frequency was >10% *PIG-A* mutants. The exact reason for this discrepancy in data is not fully understood, however both temperature and technical ability highly influence the use of histopaque® solutions within assay protocols. EDTA generated the most appropriate results in terms of viability, phenotypic *PIG-A* mutant frequency as well as harvesting efficiency and will be utilised in the future as the granulocyte specific *PIG-A* assessment platform. Further investigations can been located within the appendix.

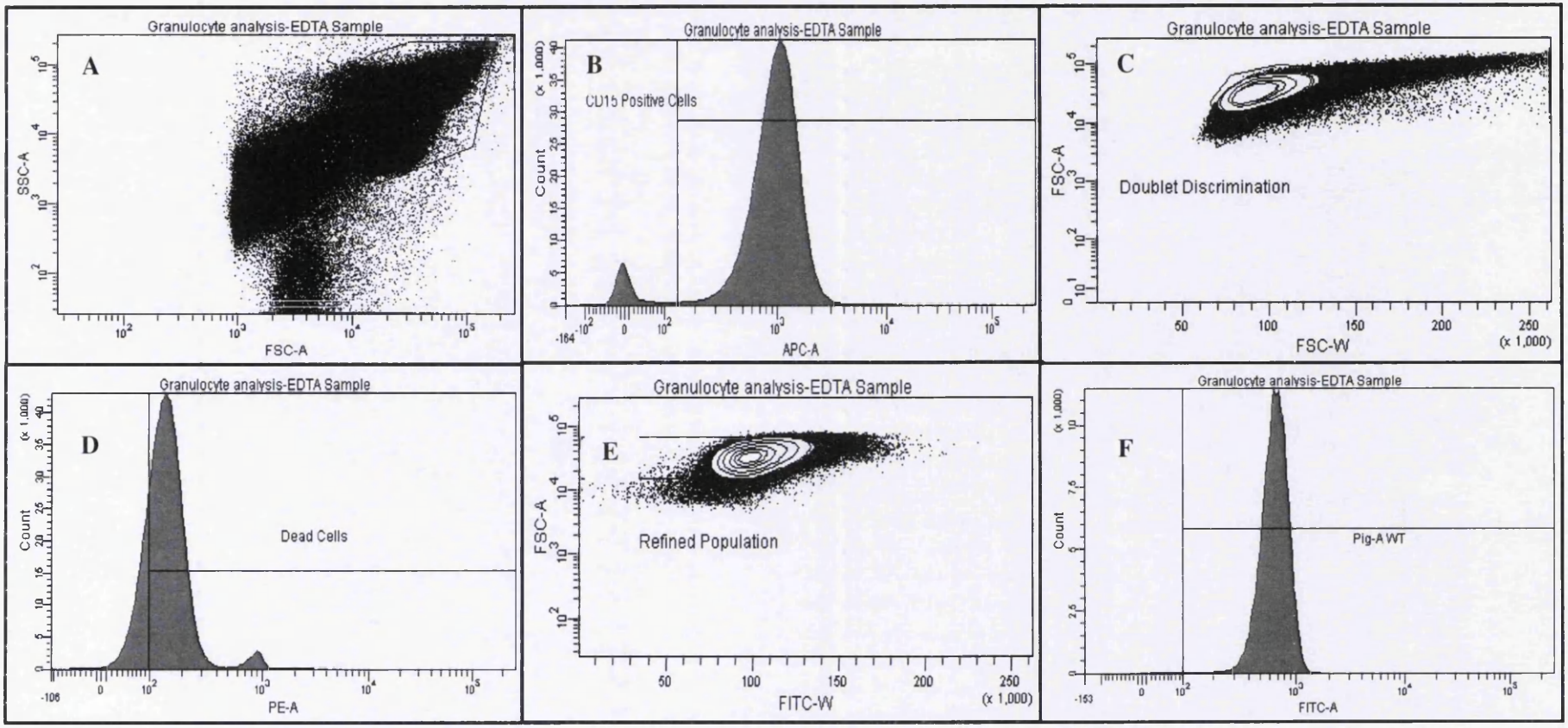

Figure 6.12. The progressive gating strategy devised for optimum Granulocyte *PIG-A* assessment sensitivity when used in combination with Histopaque® 1077 and 1113. A) Crude size and granularity assessment utilising FSC and SSC measurements, B) relative frequency of events staining positive for CD15 binding (lineage specific marker), C) FSC-W vs FSC-A doublet discrimination, D) Cellular Membrane Integrity Marker, E) refined population discriminant (FLAER-W as the variable) and F) relative PIG-A phenotypic status as defined by FLAER binding (>10,000 events scored for analysis).

Table 6.6. Summary of the average preliminary phenotypic PIG-A mutant frequency assessment following the optimisation of the combined use Histopaque ® 1077 and 1119 solutions.

Sample ID	Number of Events Defined CD15 Positive	Number of Single Cell Events	Number of Viable Cells	Number of Viable Cells which meet "refined" gating	Number of phenotypic *PIG-A* Wild type Cells	Number of phenotypic *PIG-A* Mutant Cells	Percentage phenotypic Mutant Cells of Refined Population
EDTA	112218	1049076	209063	197001	196836	165	0.08
Heparin	402576	385900	102729	97139	97035	104	0.11

6.3.4 Finalised Human Erythrocyte (RET) and Granulocyte *PIG-A* Assessment – Spontaneous Mutant Frequency Derivation

6.3.4.1 Human Erythrocyte (RET) *PIG-A* Assessment

Using analogous stains to the previously described protocol for mature red blood cell (RBC) capture (Section 6.2.1) in combination with VersaLyse RBC lysis and implementation of a more sophisticated gating strategy the finalised spontaneous background mutant frequency within RETs was investigated. Prior to this, utilising a updated compensation matrix it was apparent that the RETIC Count ™, FL1 fluorescence dye, used to measure residual RNA/DNA presence, was saturating the cells and causing additional spectral overlap into neighbouring fluorescent regions (data not shown).

Utilising a titration of RETIC Count™ reagent in combination with the protocol listed above the sub population of RETIC Count™ positive (RNA positive), CD235a positive (erythrocyte specific lineage) RETs were showed that irrespective of the concentration of RETIC Count ™ used, ranging from a 1:1 to 1:10 dilution, the channel compensation required was fixed at approximately 30% reduction. The resultant phenotypic *PIG-A* mutant frequencies observed across the concentration range were consistent at 0.05, 0.03 and 0.04% respectively (~5,000 events scored)(Figure 6.13). These background values are higher than the reported

corresponding mature RBC *PIG-A* mutant background frequencies (0.01%); however, the number of events scored and assessed is much fewer than the RBC platform and therefore, these figures provide robust estimates, but still remain under the 0.1% figure for sensitivity.

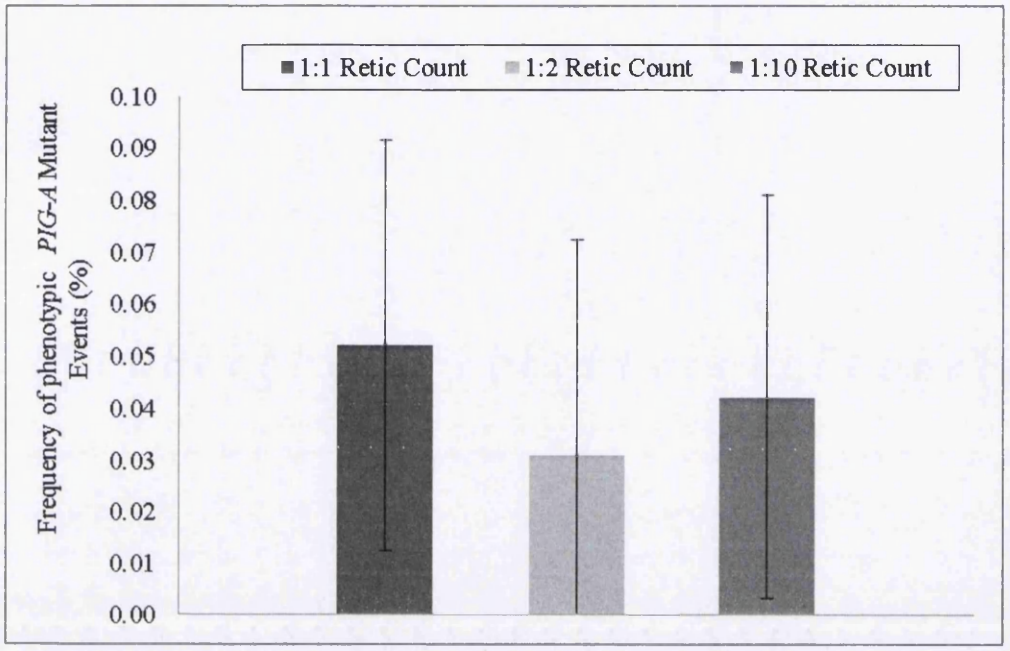

Figure 6.13. The average phenotypic PIG-A mutant frequency within the RET sub-population following titration of the RETIC Count ™ reagent. Tandem anti-CD55 and CD59 R-PE conjugates utilised as in-direct PIG-A reporters in conjunction with anti-CD235a - APC lineage specific marker (Error Bars ±SD) (N=3)(~5,000 events analysed).

6.3.4.2 Human Granulocyte *PIG-A* Assessment

FLAER staining was demonstrated to be superior to the analgous anti-CD59 R-PE antibody staining in terms of granulocyte reporter sensitivity. Following lysis, FLAER resulted in an approximate background spontaneous phenotypic *PIG-A* mutant frequency for a healthy control of 0.009%; significantly lower than the comparable 68% generated following anti-CD59 PE treatment (Figure 6.14). The results demonstrated comparable control metrics as previously defined in recent human *PIG-A* publications [175, 351, 358, 387].

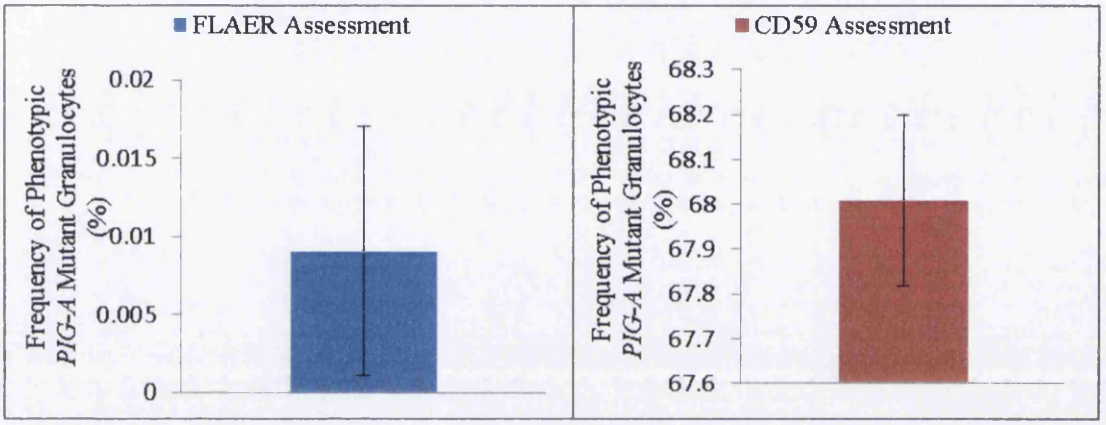

Figure 6.14. Average spontaneous background phenotypic mutant *PIG-A* frequency within CD15 labelled neutrophils (Granulocytes) utilising FLAER or anti-CD59 as the reporter for mutation; the effect of reporter sensitivity was assessed within the content of *PIG-A* mutant frequency analysis (Error Bars ±SD) (N=3).

6.4 Discussions and Conclusions

6.4.1 Human Erythrocyte (RBC) PIG-A Assay Platform - Preliminary Antibody Optimisation

The reporting system within the proposed human *PIG-A* gene mutation assay relies upon the principle usage of fluorescently conjugated antibodies. Therefore, this relatively simple reporter system must deliver on sensitivity and specificity to enable the accurate quantitative assessment of phenotypic mutant numbers. Therefore, there is a critical need to optimise the reagents utilised within the test system to enable their optimal performance to generate a holistic sensitive system. Fluorescently labelled antibodies are recommended to be kept protected from direct-light during the preparative stages prior to analysis, the results shown reflect the negative impact that polarising light has on the efficiency of antibody reporting during analysis (Section 6.3.1). The reason for this is due to the nature of fluorescence conjugates, once exposed to a suitable excitation source, the low energy electrons (ground state) within the system are promoted to a higher energy state, become unstable and release a quantum of energy at a detectable wavelength prior to falling to their original energy level [403]. This energy release has a specific wavelength which facilitates the capture of a signal. However, each dye has a unique number of emittable photos and therefore, a unique life span with regards to photo bleaching [404], the photochemical destruction of a dye by the light exposure necessary to stimulate them into fluorescing [405]. Therefore, if exposed to light prior to analysis, the resultant efficiency of a fluoresce dye to emit a detectable emission post FCM illumination can be severely reduced if not inhibited. The duration of antibody treatment, regardless of light exposure conditions, was demonstrated to have limited impact on the efficiency of staining; most likely as the minimal incubation time (30 min) is an approximate of the manufactures published optimised protocol. However, significantly extended incubation times can have a negative impact on the staining efficiency due to the formation of agglomerates within the cell sample.

Anti-CD235a is a commercially available antibody selectively raised against the glycophorin A protein on the surface of erythrocytes [406]. Glycophorin A is conservatively expressed across the red blood cell lineage and is highly expressed exclusively on the cell surface [254, 407]. Therefore, using a relatively small amount of antibody will suffice to produce a suitable signal to detect erythrocytes; however, over saturation of the blood sample, due to either excessive antibody exposure or incubation length can result in severe agglomeration. The antibody can cross link between the surfaces of neighbouring erythrocytes, acting like biological glue, forming large impenetrable agglomerates. This has the overall effect of causing mass agglomeration within the sample, reducing staining efficiency, inducing flow cytometry stream blockages and massively increasing the difficulty of re-suspending the cell pellet during preparations. The results demonstrated the optimum concentration of CD235a to use, within this setting, to provide adequate staining profiles whilst maintaining limited agglomeration. Incubation length did not appear to affect the staining efficiency, however, as expected a significant deleterious effect was observed when increasing the volume of anti-CD235a used (Section 6.3.1).

Therefore, to minimise any possible deleterious effects associated to C235a usage, racking was investigated. Racking is a physical force exerted onto the cells in order to dislodge loose agglomerates though mechanical shearing, which is less abrasive than sonication or vortexing based approaches [408]. The results demonstrated that the combined usage of the optimum amount of anti-CD235a with sufficient racking generated a sufficiently viable cellular population for FCM analysis, controlled racking had no deleterious effects on *PIG-A* mutant frequency within the assessed cell types.

Finally, in an effort to assess the estimated time taken to collect greater than 1 x 10^6 events in order to generate *PIG-A* assessment data with sufficient statistical strength, the initial concentration of the whole blood sample was investigated. Whole blood can be run directly through the FCM, when using the lowest possible flow rate; however, the resultant accuracy is reduced due to the sheer number of events analysed per second. Therefore, an appropriate dilution factor was investigated; the optimal results were obtained using the 1:20 dilution, with an observed negative correlation between more concentrated blood samples and relative *PIG-A* mutant frequency. The proposed reasons for this correlation are firstly, the finite amount of

antibody being exposed to the cellular sample. As the cell numbers increase, especially by factors of 10, in order to maintain antibody saturation to result in optimal sample signal, the resultant amount of antibody is also required to significantly increase. This regulates the number of events which are able to come into contact with the desired antibody molecules. Secondly, the slower the sample runs the higher the sensitivity and hence, the greater time within the laser light and subsequent detector regions; decreasing the software abort rate [409].

This human erythrocyte RBC assay platform has been demonstrated to perform at a sensitivity level comparable to current published studies [143, 351], and hence, suitable for both preliminary qualitative and quantitative assessment. Utilising the optimised protocol (Section 6.2.1.1) the spontaneous background mutant frequency at the *PIG-A* gene locus was estimated at 130 mutant RBCs per 1 x 10^6 total RBC events scored, enabling the undertaking of future HBM trials within peripheral blood haemopoetic cells. Work by Dr Haboubi, based on this preliminary protocol, has shown good initial progress into establishing a HBM platform [400-402].

6.4.2 Initial Human Erythrocyte (RET) and Granulocyte *PIG-A* Assay Platform Optimisation

6.4.2.1 Human Erythrocyte (RET) *PIG-A* Assay Platform

Reticulocytes are immature red blood cells, differentiated in the bone marrow from haemopoetic stem cells, which still have a relatively high RNA content when first exposed to the peripheral blood circulation [410]; during maturation (5-7 days) the cells eventually excrete their RNA content and adopt the characteristics of mature RBCs and continue to persist in the circulation for approximately 100 days [295, 411]. Reticulocytes are therefore, more functionally active, have limited exposure to complement protein activity [351] and are less differentiated than mature RBCs. As a result of this, RETs are more similar to the progenitor or stem cells, in which the original mutational event occurred, and are typically referred to as a more sensitive

reporter for this measurable end point [143, 167, 302]. Even though RET events are much more sparse within the peripheral circulatory system [410], when compared to mature RBCs, having an additional directly comparable analogous end point within homogenous samples provides increased strength and confidence within generated data, especially when a proposed known correlation should be apparent [160, 280, 351].

The RETIC Count™ reagent [412], a fluorescent SYTOX™ [413] like dye which intercalates nucleic acids and used to define residual RNA content was shown to be highly affected by the incubation temperature as well as the length (Section 6.3.2.1). RETIC Count™ highly analogous to the additional commercially available RET specific nucleic acid dye, thiazol orange, freely permeates the cells and intercalates between adjacent nucleotides within the DNA double helix structure. When excited by a suitable high energy light source, a corresponding measurable fluorescence emission is detected [412].

Utilising an elongated exposure time (60 min) as well as the highest assessed temperature (~22 °C), the most reproducible highest identification of putative RET events within the whole blood sample was generated; and subsequently selected for incorporation into the human erythrocyte RET assay design. Providing additional temperature during the fluorescence reagent incubation, as with any reaction, offers additional kinetic energy to the molecules which facilitates added collisions. Increasing the rate of collisions as well as the success by enabling the molecule to exceed the activation energy [414]. However, certain antibodies, under raised temperature conditions, often have reduced binding efficiencies due to the internalisation of the cellular surface receptors [415, 416], and hence, why antibody staining is generally undertaken at 2-4 degrees Celsius. Due to RETs being erythrocytes in nature and therefore, having limited gene expression; their sensitivity to environmental stimuli is decreased, which permits the use of a higher temperature to provide sufficient molecular interactions [295]. Similar to temperature, incubation length can be detrimental during elongated exposure due to the deleterious effects onto cellular gene expression, as well as photo bleaching of specific fluorophores [405]. However, adhering to good laboratory training [417], i.e. preventing the exposure of the fluorophore to plane polarising light permits the use of an extended

incubation period, in combination with the unique characteristics of RETs produces optimum results.

The results of the initial RET *PIG-A* assessment were encouraging in regards to the potential sensitivity of the RET assay platform, demonstrating a spontaneous back ground mutant frequency of 0.03% (Section 6.3.2.1.2), this is in-line with the stated RBC phenotypic *PIG-A* mutant frequency (Section 6.3.1.2). However, during the acquisition, 20 min, only 10,000 RET positive events were identified; insufficient numbers of RETs were able to be scored within a realistic time period to provide the assay with sufficient power to be a standalone assessment of *PIG-A* mutant frequency. Therefore, the current protocol will be used as a platform for additional optimisation, focussing on sub-population enrichment and statistical power calculations.

6.4.2.2 Human Granulocyte *PIG-A* Assay Platform Optimisation

Granulocytes, more specifically activated neutrophils were chosen as an additional parallel *PIG-A* assessment platform due to a number of distinct advantages they possess. Neutrophils are polymorphonuclear leukocytes (PMNs) [418], a critical component of the innate immune system, having an anti-infectious (phagocytosis) and a pro-inflammatory function (cytokine release) [419]. Neutrophils are amongst the first responders of the innate immune system to migrate towards the site of inflammation, penetrating tissues and removing microbial infection [420].

During activation, not only are extracellular pathogens affected but the surrounding cells and tissues of the host are also damaged. Therefore, neutrophils are quickly and efficiently removed from an inflammatory site by macrophage phagocytosis. However, they serve as a direct marker for environmental changes and hence, systemic damage. Neutrophils have a relatively limited lifespan, estimated between 5 hr – 5 days, and therefore, the bone marrow harbours a large constantly active granulopoiesis compartment [148, 418, 420]. Granulocytes are nucleated which permits direct sequencing to validate the presumed *PIG-A* deficient genotype, and

unlike analogous lymphocytes they are less morphogenic, and have a more stable cellular surface antigen expression throughout their lifespan [229].

Utilising fluorescent aerolysin (FLAER) as the generic marker for mutation at the *PIG-A* gene locus in combination with anti-CD15, an activated neutrophil marker [421, 422] and a crude RBC lysis through an ammonium chloride based mechanism preliminary *PIG-A* mutant frequency assessment was undertaken (Section 6.3.2.2). The results displayed demonstrate the relative enrichment of the leukocyte population (Figure 6.8) as well as the phenotypic *PIG-A* mutant frequency within whole blood taken from a self-proclaimed healthy donor; approximately 5,000-10,000 defined granulocyte events were able to be captured in less than 20 min per sample. The optimal average spontaneous *PIG-A* mutant frequency within the granulocyte population was estimated to be 0.2% (Figure 6.9), significantly higher than the comparable RET or RBC frequencies (Section 6.3.1.2 and 6.3.2.1). Theoretically, the granulocyte mutant frequency may be significantly higher due to its systemic role and close proximity to deleterious microenvironments, high concentrations of ROS contributing to potential deletion or abasic site formation [423]. Nevertheless, due to the lack of mutation fixation and hence, development of a null phenotype, granulocytes would only be microenvironment sensitive following direct exposure to limited sources of immediate DNA damage or epigenetic factors. Recent publications provide evidence to suggest that the current granulocyte assay platform is operating under a poor reporting sensitivity level [175], approximately 20 fold lower than the corresponding mutant *PIG-A* RBC frequency. Further optimisation of the enrichment protocol, especially to aid the capture of 1 x 10^6 events which is the pre-defined benchmark for statistical robustness [166, 175, 280, 301, 351], is required to facilitate routine patient granulocyte *PIG-A* assessment.

6.4.3 Human *PIG-A* Assay Platform Supplementary Investigations

6.4.3.1 Lysis Buffer Evaluation

RETs have a different intracellular environment than their comparable mature counterparts; due to the presence of differing quantities of residual RNA. Therefore,

the lysis protocols should not ultimately lyse the RET event but could have a deleterious effect (Section 6.3.3.1). Granulocytes, simialr to the RETs are nucleated and therefore, have limited suseptibility against changes in osmotic pressure and potential.

Following the completion of a retrospective compensation matrix, the results of the RBC lysis buffer evaluation were suitable for analysis and conclusions were drawn. The data demonstrated (Section 6.3.3.1), initially from a leukocyte enrichment point of view, that enrichment was independent of buffer concentration, and that no significance increases or decreases had particular impact on the subsequent enrichment figures (Figure 6.10). However, there were significant differences in the respective yield of leukocyte enrichment when compared between the different buffer solutions. This can primarily be attributed to the different constituents within the buffer solutions and therefore, their common or dissimilar mechanisms for lysis. BD FACS Lyse displayed dissimilar results to the previous optimisation work carried out utilising an ammonium chloride based solution [424, 425], the typical mechanism often exploited when depleting whole blood samples of RBCs [426]; this lysis buffer is believed to operate under a different mechanism, or alternatively an analogous mechanism utilising a difference salt solution [427]. BD FACS lyse was shown to result in suboptimum enrichment with some evidence suggesting leukocyte activation, which can potentially alter physical characteristics; however, the degree of alteration is somewhat unknown in the context of FSC vs SSC profiles [427-429]. Easylyse and Versalyse were similar in terms of results, showing robust comparisons and limited variability within the data sets; any effect lysis buffer concentration was to play, apart from speed of haemolysis, was mitigated by the exaggerated lysis incubation period.

The most concentrated whole blood samples would acquire more events per second during acqusitions and therefore, provide more robustness during statisical evaluation. With this in mind, Easylyse or Versalyse were put forward as potential candidates for granulocyte enrichment, the corresponding *PIG-A* assessment data demonstrated that Versalyse generated the most unaffected population with respect to the presence of GPI-AP on the cell surface (Figure 6.10). Therefore, Versalyse can be concluded as to have the least affect on the *PIG-A* status in the whole blood sample (leukocyte specific). Henceforth, Versalyse will be used to enrich for

granulocyte (CD15 positve) leukocytes during the next stage of assay optimisation (FLAER analysis).

RET enrichment data was shown to demonstrate that both lysis buffer concentration and buffer type, significantly affected the respective reticulocyte enriched population. Easylyse and Versalyse generated higher reticulocyte yields than BD FACS lyse, across the concentration range tested, providing additonal evidence to support the intial hypothesis that BD FACS lyse utilises a different method for lysis when compared to the two additonal buffer solutions. Versalyse generated the optimum results in terms of RET capture, but then again both concentration and incubation were demonstrated to be significant factors in the general health of this sub-population. Sensitivity of the *PIG-A* reporter, the most critical in terms of assay devlopment, was required to be assessed in conjunction with enrichment efficiency prior to drawing any permanent conclusions.

Providing a single protocol for reticlucyte enrichment was intricate, as the optimum buffer interms of enrichment generated highly variable effects on *PIG-A* mutant frquency (Figure 6.10). For that reason, even though Easylyse was not the optimum buffer for event enrichment, in general conforming to the specific needs of the assay secured the lysis buffer for future optimisation.

6.4.3.2 Cellular Viability during prolonged Human *PIG-A* Assessment

Apoptosis was a critical source of error within the in vitro *PIG-A* assay development, relatively regardless of methodology used [181, 301]. All versions of the *PIG-A* reporter system currently rely on the indirect measurement of the mutant frequency at the *PIG-A* gene locus via a physical measurement of a GPI-associated cell line specific epitope [77, 196]. However, many viability associated pathways and processes, such as apoptosis, membrane invaginations, blebbing and/or necrosis have been shown to influence cell membrane integrity (Sections 3.3.5, 4.3.3 and 5.3.4.2) and hence could potentially generate putative *PIG-A* mutant mimicking phenotypes which subsequently could be scored as false positive events [8, 274, 276].

Within future applications of this *PIG-A* assessment, blood is likely to be harvested off site and transported to the laboratory. In worse case scenarios, the blood may take as long as 6 hr or longer to be processed prior to FCM acquisition. Consequently, in order to better estimate the potential deleterious affect prolonged out of host blood incubation has on mutant *PIG-A* frequency, as well as to optimise the best storage method, cellular viability was investigated.

The results were subdivided into the specific cell lineages present within whole blood, based on their FSC vs SSC profiles. RBC lysis was utilised in order to enrich for the minor populations; RETs, leukocytes and nucleated cells. Apoptosis was recorded within the leukocyte and nucleated cell populations, the levels of apoptosis observed over the time course were highly consistent. Loss of membrane integrity (a characteristic of cell death) was apparent within all sub lineages across the whole blood spectra; the level of cell death (~5% within all samples) remained consistent across the experimental time period. Necrosis was characterised as late stage apoptosis in which cells were annexin V positive as well as having a significant loss in membrane integrity [274, 276, 353]. Necrosis was only observed within the nucleated sub lineages, and levels remained consistent across the time course (Figure 6.11).

The conclusions are as follows; i) viability appears to be independent of time within the context of sample storage, ii) each cell type has its own unique levels of viability, iii) viability appears to remain consistent across the prolonged incubation period (Figure 6.11). Temperature of storage equally does not seem to have any significant effect on the viability status of the blood (RBCs, RETs and generic leukocytes). Therefore, this evaluation provides further validity to the current experimental protocol and provides additional strength to the subsequently generated data.

A particular fear for the human ex vivo assay was the occurrence of FCM defined leukocyte positive cells undergoing apoptosis following prolonged storage; resultantly these events would generate potential false positive *PIG-A* assessments. However, viability was demonstrated to be independent of both storage time and temperature. Naturally, the concerns about erythrocytic lineages undergoing apoptosis were limited due to their apparent restricted functional RNA and hence, insensitivity to apoptosis [295, 411], GPI-AP deficient acquired insensitivity to

apoptosis [320] and the sheer quantity of published erythrocyte in vivo Pig-a data. However, leukocytes are highly different in terms of their sensitivity to external stimuli [230, 427], adaptiveness, GPI-AP expression profiles [229] and life span. The results showed no obvious decrease in viability, compared to base levels, over the time period. Conversely, a generic nucleated leukocyte population was monitored, based on FSC vs SSC profiles. A more specific identification of sub-populations, for example CD15 activated neutrophils, being required to provide more definitive conclusions.

6.4.3.3 Cellular Enrichment Investigation

6.4.3.3.1 Centrifugation as the Sole Granulocyte Enrichment Tool and the effect FLAER Titration has on Spontaneous *PIG-A* background Mutant Frequency

The aims of this project was to develop a combined system platform in which human bio-monitoring could be possible, however, within that scope assay robustness, reproducibility as well as cost were all influential sub-goals. Utilising FLAER as a generic marker for phenotypic GPI-AP absence is expensive, making large cohort studies problematic; only facilitating limited number of patients and therefore, potentially jeopardising data integrity. Additionally, subpopulation enrichment, utilising RBC lysis buffer, again potentially offers a source of error regarding phenotypic *PIG-A* mutant scoring, as well as an additional overhead cost. Consequently, in an aid to reduce assay costs whilst maintaining sensitivity and accuracy during *PIG-A* assessment, high speed centrifugation as well as FLAER titration were investigated for their potential enrichment and phenotypic reporting possibilities.

An issue with granulocytes is that they have relatively short life spans (5 hr to 5 days) [418, 419, 429], are moderately easily damaged, highly sensitive, communicative, especially in an in vivo environment, and demonstrate sensitivity to apoptosis. Combining these factors as well as the penetrance and systemic nature of exposure, granulocytes are likely to have a raised spontaneous *PIG-A* mutant

background frequency, either as a result from false positive inclusion or just greater exposure to potential sources of GPI-AP deficiency. Therefore, in order to account for the sensitive nature of the cell choice, removal of a potentially deleterious RBC lysis buffer exposure in favour for a less abrasive centrifugation may offer an alternative methodology for enrichment as well as reduce potential sources of error. However, centrifugation, especially at high speed is known to shear cellular surface antigens [430, 431], can alter cellular morphology [432] and potentially result in fewer captured cells post enrichment.

The enrichment yield following centrifugation was demonstrated to be encouraging, indicating an approximate 10% constitution of leukocytes within the sample; in which around 10% were CD15 positive (Section 6.3.3.3). This facilitated the collection of >10,000 CD15 positive events within a few minutes of relatively high speed FCM acquisition. The results were also shown to indicate the comprehensive presence of GPI-APs on the cellular surface within the CD15 positive granulocyte population; comprehensive FLAER binding (Figure 6.12) was observed within most of the concentrations trialled within the titration. The two highest concentrations of FLAER tested, undiluted and a single 1:1 dilution within PBS/BSA 0.2%, generated highly analogous results with respect to FLAER binding efficiency and therefore, produced an approximate 0.1% (0.1 and 0.17 % respectively) spontaneous *PIG-A* background mutant frequency. The lower dilution of 1:10 failed to generate such a background frequency compatible with a sensitive endpoint; however, the resultant mutant frequency was still < 5% (1.6%).

Therefore, with the achieved enrichment and subsequent phenotypic *PIG-A* background mutant frequencies falling in-line with previous reported RBC lysis optimisation experiments (Section 6.3.3.1), centrifugation appears to be a viable technique to incorporate within assay design. Further investigations into the potential effect on cellular viability, including GPI-AP loss as well as cell activation and apoptosis status is required to comprehensively assess the methodology. Currently, RBC lysis buffer appears to generate the most erythrocytic depleted population but also has specific subsequent unwanted effects on cellular viability which are not yet associated with centrifugation (Section 6.3.3.3).

6.4.3.3.1.1 The Possible Effects on Cellular Viability as induced via High Speed Centrifugation

With the intention of assessing the impact centrifugation has on cellular viability, the experimental design directly compared the subsequent effects to RBC lysis buffer exposure, as a benchmark for performance. As well as this, the samples were all collected simultaneously, with one being processed immediately, and the other two stored for 6 hours at room temperature and on ice respectively. The general aim was to come to a more conclusive decision with respect to the methodology for granulocyte enrichment, as well as re-assess the impact prolonged storage, under different conditions, can have on sample integrity.

For the RBC lysed samples, there was a distinct relationship observed between cellular viability and incubation time. As predicted, the most typical "normal" population of cells, in regards to viability, were observed within the immediately processed blood samples (5.3% apoptosis and 7.5% loss of cellular membrane integrity respectively). The two samples which were stored for 6 hr prior to acquisition displayed significantly higher levels of cytotoxity, especially prominent within the sample stored on ice with (98.6% apoptosis and 10.7% loss of cellular membrane integrity) (Table 6.4). Immediately, this was attributed to the limited life span of the specific cell lineage assessed; activated neutrophils are estimated to have a life span approximately between 5 hrs and 5 days [418, 419, 422] dependent upon their specific role at the time of activation. As the exposure period was in excess of the conservative estimate of life span, the expected loss of viability was assumed to be in the region of >50%. However, the sample stored for 6 hr at room temperature, which was expected to perform worse than the sample stored on ice considerably lower figures than those stored on ice (13.7% apoptosis and 8.6% loss of cellular membrane integrity) (Table 6.4). As a result of this, storage at temperatures below 5 ºC appeared to have a significant deleterious effect on the neutrophil population's vitality, an observed effect which was highly dissimilar from the prolonged viability assessment within the morphological "leukocyte" population (Section 6.3.3.2).

The same general relationship was observed within the centrifuged sample, however, the levels of cellular viability were much greater and minimal cytoxicity was

observed; the highest apoptosis and loss of cellular membrane percentages were observed when stored for 6 hr on ice but only reached 1.1 and 1.4% of the total population respectively (Table 6.4). Therefore, centrifugation appears to have a much more subtle effect on cellular viability and in terms of a proposed methodology for enrichment, looks favourable to the general aims of the assay development. Obviously, during either method, the entire activated neutrophil population may or may not have been captured, which could have a specific effect on the cytotoxity figures, with centrifugation having a much greater risk of event loss due to density alterations when compared to lysis buffer exposure. The general conclusions taken from this are; if possible blood samples should always be immediately processed and analysed to avoid any increases in loss of viability, however, if they are to be stored, within a breathable box, protected from light at ~22°C.

Centrifugation does appear to be a viable methodology with respect to sub-population enrichment with obvious advantages over comparable lysis methods [175]. However, the resultant sample post centrifugation was contaminated with a much greater percentage of erythrocytes (obvious within the "FSC vs. SSC" density plot). This was re-enforced by the observed decrease in percentage of CD15 positive cells within the total population of recorded events. Further optimisation will be required in order to reach optimum levels of cellular enrichment, in respect to the granulocyte population. In addition to enrichment optimisation, additional practice using this technique is required; the protocol is more technically challenging in order to separate whole blood in this manor, especially during the harvesting of the specific sub lineages without excessive contamination.

6.4.3.3.2 Investigations into Histopaque® Enrichment

The initial high speed centrifuge method relied purely on the separation of the cell types based on their densities within a whole blood sample; however, the combined use of high speed centrifugation within a density gradient to aid separation/resolution would potentially enable more accurate layer isolation and ease the technique for harvesting. The net results should enable a greater more specific enrichment with

again, minimal effects on the cellular viability. The chosen commercially available density gradient was histopaque® 1077, due to its relative density approximately in the range of that of a normal granulocyte, as well as published use in literature [175]. With the addition of a layer with a corresponding density highly similar to that of an average granulocyte, the population of interest should residue either within the layer or fractionally above to ease identification and harvesting.

The resultant centrifugation generated a distinctly separated whole blood sample, working from the top down; plasma layer, leukocyte (MNC), histopaque ® 1077 and then finally a red blood cell pellet. RETs were believed to residue within the surface layer of the RBC pellet, however, as the direct location of the granulocyte population was not defined; both the initial presumed MNC leukocytes as well as the minor fraction at the top of the RBC pellet were harvested. The results generated displayed a relatively poor enrichment; RETs were enriched to approximately 2.9% of the population when directly compared to previous lysis figures of 5-10% using Versalyse (Section 6.3.3.1). Equally CD15 positive granulocytes were demonstrated to constitute approximately 1% from either isolated layer, a poor yield. However, a positive outcome of this initial trial was the measurable spontaneous phenotypic *PIG-A* mutant frequency when assessed with FLAER exposure (in the region of 0.03%, layer 2, and 1.93%, layer 1) (Table 6.5). The conclusions able to be drawn from this are that from a purely enrichment point of view, the recovered yields of initially RET and granulocyte populations were significantly lower than expected, and what has been observed with alternative methods.

However, the fact that CD15 positive granulocytes are present within both presumptive layers does suggest that in-fact the specific density of the histopaque® solution utilised is within the expected density range of a normal granulocyte. There has been recent publications commenting on the differences between low and high density granulocytes [433, 434] and their distinctive roles within innate immunity, and therefore, to overcome this, further investigation utilising two specific flanking histopaque ® layers may provide more efficient sub type capture. Using a combination of two distinct histopaque ® solutions may permit the capture of the entire granulocyte population and drastically aid enrichment.

6.4.3.3.2.1 The Finalised Optimisation of Histopaque®

In an effort to generate a high throughput human granulocyte *PIG-A* assessment platform, tandem histopaque® enrichment was further investigated. The experimental design again utilised two discrete histopaque ® layers with densities 1.077 and 1.119 g/mL to evaluate any potential in the capture of the PNC cells within the confines of the flanking layers. The time, speed and temperature of the centrifugation separation were all adjusted to bring the protocol more in line with an analogous recent publications [175]; an additional inclusion of a loss of cellular membrane integrity dye was also implemented for viability monitoring.

The results of this experiment were dissimilar to the previous tandem histopaque ® solution trial, both samples (EDTA and Heparin) generated clearly defined presumptive granulocytes layers, located slightly above the erythrocyte pellet. Within the presumptive granulocyte layer, there was minor indication of potential RET presence due to a colour discrepancy as you travelled through the layer towards the RBC pellet. Both samples resulted in significant CD15 positive granulocyte populations; the consequential phenotypic *PIG-A* mutant frequencies observed within both the EDTA (0.08%) and heparin (0.11%) samples were comparable, approximately 0.1% spontaneous background mutant frequency respectively (Table 6.6). The RET sub-population within both samples was demonstrated to comprise very few RET events and prevented full analysis (data not shown).

EDTA generated the most favourable results in terms of viability, phenotypic *PIG-A* mutant frequency as well as harvesting efficiency and contrary to the current protocol should be considered as the anti-coagulant of choice for future bleeds (Appendix Section 6.3.3.3.2.2).

However, throughout the use of histopaque ® as an enrichment method to increase the numbers of CD15 positive events scored, the matching phenotypic *PIG-A* mutant frequencies have been elevated when compared to the previous RBC lysis protocols. The aim of assay development was reproducibility, a feature easily obtained through lysis, and robustness, fundamentally demonstrated by commercially bought lysis buffer and finally cost, which is again in favour of RBC lysis.

Therefore, even though through the use of histopaque® the numbers of cells scored for *PIG-A* assessment are increases, the resultant corresponding mutant frequency has yet to be shown to be competitive to either other published protocols [175] or alternatively analogous RBC lysis protocols. Therefore, due to the demonstrated stability of the cell types over time, this enables the combined use of RBC lysis and extended periods of sample acquisition (~45 mins) to generate patient data. In the confines of a minimalistic validatory study, running 2-3 parallel samples per session should not result in any significant assay complications. However, assay protocol could be further optimised to facilitate the use of this assay system as a popular screening system; with a favoured higher throughput methodology. Alternatively, wild type depletion can be undertaken with the use of either anti-FITC (granulocyte) or anti-PE (RET and RBC) para-magnetic beads in combination with an external magnetic field. A commercial set up utilising a pre-establish protocol such as Miltenyi [435] analogous to that used within the high throughput version of the erythrocyte in vivo Pig-a assay could also be used.

6.4.4 Finalised Human Erythrocyte (RET) and Granulocyte *PIG-A* Assessment – Spontaneous Mutant Frequency Derivation

6.4.4.1 Human Erythrocyte (RET) *PIG-A* Assessment

The aim of this final section was to come to a conclusion on a finalised protocol for a human RET *PIG-A* assay, in order to facilitate both high sensitivity and adequate samples size capture. Following the incorporation of the novel gating strategy (Section 5.3.4), and using an equivalent protocol as defined in (Section 6.3.2), the last variable to be assessed was the potential spectral overlap as a result of RETIC Count™ exposure. Spectral overlap can be a problem within any fluorescence application and therefore, it must be accounted for. Previously to this experiment, the compensation matrix was established utilising positively controlled spiked populations, however, the compensation required for the RETIC Count ™ reagent in

particular was very high. Generally any compensation >30% required a significant loss of signal and therefore, a corresponding sensitivity decrease. The previous level of compensation was ~80% signal reduction, and therefore, there was a noteworthy chance of a potential source of error within the subsequently generated data.

The subsequent results following RETIC count™ titration showed that irrespective of the concentration of RETIC Count ™ used, the compensation required was fixed at approximately 30% reduction in the FL1/FL2 overlap. This was lower than previously assessed, and resulted in corresponding phenotypic *PIG-A* mutant frequencies in the range of 0.03 - 0.05% (Figure 6.13). These background values are analogous to the previous values recorded (Section 6.3.2.1.2) and maintain the reported relationship between RET and RBC *PIG-A* mutant frequencies.

This human RET *PIG-A* assay platform was demonstrated to show a limited sample size capture, with a highly sensitive endpoint. This assay design can now be utilised to begin to gather human patient data, however, the limited sample size may be detrimental to the statistical significance of observed variation in mutant frequency. Apart from high content immunomagnetic bead separation to deplete wild type cells in combination with counting beads, no other immediate feasible options remain to continue protocol optimisation.

6.4.4.2 Human Granulocyte *PIG-A* Assessment

Utilising Versalyse, the erythrocyte population was heavily depleted, resulting in an enrichment of the leukocyte sub-population from ~0.0001 to between 2 and 3% (Section 6.3.3.1). This enrichment facilitated the capture of approximately 100,000 CD15 positive neutrophil events, within 10-20 min per sample acquisition. However, it was still unknown whether the more conventional anti-CD59/55 surface antigens [152, 229, 294, 387], commercially available and utilised heavily within the in vivo (Litron ™) [77, 143, 196] and in vitro *PIG-A* [181, 301] assay designs, were practical in this specific assay set up. FLAER [305] and CD59 staining were both utilised in parallel to produce comparative phenotypic marker scoring and scrutinised on sensitivity and accuracy of *PIG-A* mutant detection.

Based on the results generated from this experiment, CD59 was initially ruled out as a phenotypic granulocyte specific GPI-AP marker due to the varying expression demonstrated on the extra cellular surface membrane within the peripheral blood samples (Figure 6.14); neutrophils (CD15 positive) demonstrated an average, 30% expression of the CD59 antigen on the cellular membrane. The critical role played by CD59 in terms of complement protein mediation, via the preventing of the MAC or TTC formation, within erythrocyte was not shadowed by an analogous role within the neutrophil population [152, 153]. Due to the numbers of phenotypic *PIG-A* mutants constituting close to 70% of the total population, the marker was deemed insensitive as a reporter in this setting.

FLAER however, was demonstrated to be a highly sensitive marker for mutation as the *PIG-A* locus; the spontaneous background mutant frequency was shown to be in the region of 0.01%, and due to nature of FLAER binding, the accuracy of mutant calling is well validated [305] (Figure 6.14). By utilising Versalyse in combination with FLAER, an assay platform able to in-directly measure the *PIG-A* gene mutant frequency at an adequate sensitivity was developed. A cell surface GPI-AP specific marker could therefore, be implemented into the assay design instead of the more expensive FLAER, however, its use could be limited by the functional role such a marker would play within granulocyte specific lineages. For example, CD55 may generate a more comprehensive phenotypic wild type population due to an additional functional role within granulocytes [296] when compared to the analogous CD59 surface antigen.

The establishment of this preliminary protocol enables further investigation into the possible relationships between genomic instability and phenotypic *PIG-A* mutant frequency [175, 351].

Table 6.7. Summary of the data described within the chapter contents, the results and the conclusions drawn in relation to the advance of the in vitro PIG-A gene mutation assay standard operating procedure (SOP)

BD FACS Aria 1 – Flow Cytometry Assessment

Preliminary Human PIG-A Test System Development

Human Erythrocyte (RBC) *PIG-A* Assay Platform Optimisation

Introductory Antibody Investigation

Human Erythrocyte (RBC) *PIG-A* Assessment

– Spontaneous Mutant Frequency Derivation → **Antibody titre and exposure conditions optimised**

Racking implemented following agglomeration trial, assay protocol refined

Estimated spontaneous $100x10^{-6}$ background mutant frequency established, in line with recent publication

Initial Human Erythrocyte (RET) and Granulocyte *PIG-A* Assay Platform Optimisation

↓

Human Erythrocyte (RET) *PIG-A* Assay Platform

Preliminary Antibody Investigation – RETIC Count™

Preliminary Human Erythrocyte (RET) ***PIG-A*** Assessment

– Spontaneous Mutant Frequency Derivation → **RETIC Count ™ Reagent Optimised**

Estimated spontaneous $300x10^{-6}$ background mutant frequency established, in line with recent publication

Human Granulocyte *PIG-A* Assay Platform Optimisation

Preliminary Enrichment Evaluation - Ammonium Chloride

Preliminary Human Granulocyte *PIG-A* Assessment

– Spontaneous Mutant Frequency Derivation → **Lysis Buffer Preliminary Evaluated, 8.4% Leukocyte subpopulation enrichment**

Estimated spontaneous $2000x10^{-6}$ background mutant frequency established, significantly higher than current publications

↓

Human *PIG-A* Assay Platform Supplementary Investigations

Lysis Buffer Evaluation

Cellular Viability during prolonged
- Human *PIG-A* Assessment → **RET enrichment – Easylyse (Estimated $14x10^{-6}$ background mutant frequency)**
Leukocyte Enrichment – Versalyse (Estimated 6000x10-6 background mutant frequency)
Viability demonstrated to be independent of experimental time period, viability was shown to be cell lineage specific

↓

Cellular Enrichment Investigation

Centrifugation as the Sole Granulocyte Enrichment Tool
And the effect FLAER Titration has on Spontaneous *PIG-A* background Mutant Frequency

Investigations into Histopaque® Enrichment → **Centrifugation demonstrated to be an effective inoffensive enrichment strategy**
Histopaque® enrichment established a <100x10-6 background mutant frequency

Finalised Human Erythrocyte (RET) and Granulocyte *PIG-A* Assessment – Spontaneous Mutant Frequency Derivation

Human Erythrocyte (RET) *PIG-A* Assessment

Human Granulocyte *PIG-A* Assessment → **Utilising lysis based methodology and following further refinements**

Estimated RET ($30x10^{-6}$) and Estimated Granulocyte ($100x10^{-6}$) background phenotypic *PIG-A* mutant frequency, in line with current published data

Table 6.8. Summary of the additional supplementary data for this chapter, contained within the appendix, which details the validation and additional investigative experimentation surrounding the assay development.

Supplementary Data

BD FACS Aria 1 – Flow Cytometry Assessment

Gating Strategy Advancements

Gating Strategy: Pulse-Width Evaluation → **The use of non-reporting pulse-width measures can be used to significantly increase assay sensitivity. No obvious biasing during analysis following strict limitations on usage**

Estimated spontaneous background mutant frequency $20x10^{-6}$ mutant cells

Chapter 7: General Discussions and Conclusions

Throughout this thesis, the goal has been to develop an in vitro *PIG-A* assay. The assay was intended to share the endogenous reporter system as exploited within the in vivo rodent *Pig-a* gene mutation assay, and would hopefully enable the preliminary development of an additional human bio-monitoring assay. The reason for such an undertaking is primarily driven by the evolving regulatory guidance [219, 277] as well as the ethical and financial situation currently facing the cosmetics as well as the pharmaceutical industry. Modernising the current tiered battery of test systems, via the inclusion of high content, multiplex analysis within genetic toxicology safety assessment, will assist the future inclusion of an in vitro gene mutation assay within drug development. As well as securing future use, modernising reforms would potentially increase global effectiveness in terms of sensitivity, specificity and cost of hazard and risk assessment. Recent policy alterations, specifically targeting the field of scientific research, have seen ever increasing limitations placed on the use of animal models and in specific examples there has been a ban on animal testing; for example, the cosmetics industry [86, 203]. Consequently, with the new restrictions placed within the field, reforming and optimising the currently available in vivo [180, 219, 220, 277] and in vitro based test systems [112, 125, 208], as well as developing novel platforms, should result in advancing the ability of hazard and risk identification within genetic toxicology. Subsequently, the field of safety assessment, focussing on the manner in which data analysis and hazard identification is undertaken [63, 88, 103, 219, 263] will advance and hence, change the current regulatory decision making procedure.

Under the scope of the general aim, investigations were undertaken around the debated topic within the in vivo equivalent assay; the genotype to phenotype relationship [144, 161, 172, 173]. Incomplete validity with the identification of presumptive phenotypic *Pig-a* mutants, with no direct method of validation, has proven to be a potential drawback in the overall speed in advancements of the in vivo assay design and subsequent OECD guideline drafting. No conclusive evidence has been published to date demonstrating, within the actual assay platform and not an analogous system, complete proof of principle. As well as this, a broader thesis

aim was to investigate assay transferability; expansion of the in vitro *PIG-A* mechanism into additional tissues (Appendix Section 5.5.3.4) as well as investigating the potential of expanding the assay system into a human bio-monitoring context [175, 180, 351, 358, 387]. The former aim was specifically investigated to deliver more systemic genetic toxicology safety assessment data through the incorporation of point of contact and metabolism simulating tissue types [87, 89, 90, 92, 93, 310]. The latter was utilised to propose a preliminary assay design which could be used as a basis for future clinical trials [400-402]. Therefore, in addition to the developing and optimising of an in vitro assay design, multiple additional ex-vivo assay systems were to be analogously developed, in parallel, to potentially facilitate the undertaking of validatory human clinical trials. Each standalone assay platform adhered to a number of specific criteria; high precision, high content, high throughput and finally high sensitivity, in order to generate reproducible, robust standalone bio monitoring data.

The initial starting point of the thesis was to design an in vitro equivalent assay, retaining the reporter system as well as the haemopoetic and high throughput nature of the current in vivo rodent *pig-a* assay [160], whilst introducing a number of additional beneficial features, including nucleated properties of the cell platform and high content multiplexed analysis [208, 278]. Therefore, prior to the under taking of any additional goals, assay development was the fundamental pinnacle of the project. Initially the preconceived design went under a number of validatory/optimisation stages, prior to any real proof of principle experimentation; antibodies (Section 3.3.1), enrichment strategies (Section 3.3.2), cryopreservation enabling long term storage (Section 3.3.4), additional acquisition/analysis platform usage (Amnis Image Stream ™ or Laser Scanning Confocal) (Appendix Section 3.5.3), as well as many other additional topics covered within the first results chapter were investigated, with the overall aim to establish a central assay platform.

Antibody optimisation was of high priority, the basis of the reporter system fundamentally utilises fluorescently conjugated antibodies to report on the phenotype of the cellular population [160, 196], utilising such an in-direct mechanism has the potential of incorporating a number of sources of error. Therefore, any additional sources of error, or known error at such a critical early stage of analysis would have a significant impact on overall sensitivity and quantitative risk assessment [158,

263]. Both trialled antibody conjugates generated comparable low levels of error, (Section 3.3.1), however, the PE conjugate demonstrated a fluorescence profile much more suited to the assay design, in terms of phenotype separation as well as lower levels of Fc mediated un-specific binding. There was no scope for antibody titration, in terms of cost effectiveness, due to the observed loss of signal coverage as well as negatively correlated increases in difficulty to distinguish between phenotypic *PIG-A* wild type and putative mutant events. Due to the non-essential nature of the roles facilitated by the selected GPI-AP surface markers on the extracellular surface of the chosen lymphoblastoid cell lines [229], an additional enrichment or putative mutant depletion step was shown to be a necessity in order to deplete pre-existing mutants and subsequently lower the spontaneous background mutant frequency at the *PIG-A* gene locus. Mutant depletion or wild type enrichment steps are currently implemented within the validated HPRT/MLA assays [70, 75, 144, 183, 186]; HAT medium and 6-thioguannine (6-TG) or trifluorothymidine (TFT) are used respectively. OECD and similar regulatory acceptance would hinge on whether the assay could provide sufficient levels of sensitivity and robust detection of putative mutant events [73]. Even though clonal expansion was not the optimum method for mutant depletion; clonal expansion potentially introduces a source of error due to extending the assay period which in turn brings elevated passage number and genetic instability within the cell stock. No suitable alternative was able to be found, and therefore, was the most sensitive method for mutant depletion at the time (Section 3.3.2).

Providing the most sensitive assay system, would enable accurate, high precision, detection of putative *PIG-A* mutant events which in turn could enable the system to be used for quantitative dose response modelling [214, 226, 263, 277]. Quantitative modelling is an essential practice in toxicology [436], and is becoming more heavily utilised during hazard and risk assessment. An application which is now seeing further use within in-vitro potency assessment [88, 213, 227, 437], with approaches being investigated in the context of in vitro to in vivo, and in vitro to human extrapolation for risk assessment [88]. Therefore, by developing a system able to facilitate this, as well as function as a high throughput genetic toxicology assay, this could potentially greatly benefit the safety assessment field and genetic toxicology in general [100, 208, 226, 278]. In conjunction with such a system development, an

endeavour was made to establish a complete assay system that did not suffer from the current problems facing the genetic toxicology community; i) inter-laboratory variation, ii) lack of robustness between analogous cell lines and iii) discrepancies in analysis methodology. Providing a cellular platform, as well as an all in one analysis software package (Appendix Section 4.5.3.3), would enable a single method of data generation and again move the project in line with the global aims of harmonisation and standardisation across the field of scientific research [65, 73, 82].

Using the preliminary assay design, Ethyl Methane Sulfonate (EMS) was chosen as a model mutagen to initially evaluate the sensitivity of the assay system, as well as potentially provide some validation with the reporter system [181]. At the time, there was a plethora of published mutation spectra available for EMS, with a well characterised mode of action and significant additional published in vitro and in vivo genetic toxicology data [20, 39, 241-243, 350]. Within the proof of principle experiment, 24 hr acute dosing, extended assessment was implemented to enable phenotypic lag estimation as well as providing a sufficient mutational fixing period (Section 3.3.3); initially the data looked promising, it was apparently non-linear, most obvious at the day 4 (96 hr) time point and demonstrated the concept of a high throughput assay system. However, cytotoxicity issues were apparent from the start, potentially caused by overly sensitive toxicity measures, and the relatively high pre-existing numbers of putative phenotypic *PIG-A* mutant events resulted in higher dose response metrics than comparable HPRT data [350]. The assay demonstrated a correlation with respect to putative *PIG-A* mutants and cytotoxic events (Section 3.3.5), as expected to some degree; however, an additional insensitivity prevented quantitative dose response analysis, limiting the system to enable qualitative modelling.

Providing a high throughout, high content, human relevant in vitro assay system which enables qualitative dose response analysis provides very little benefit to the current field of drug development. Qualitative assessment lacks the refinement to ensure conservative, safe assessment, and can often result in a highly complex data set with evidence of cytotoxicity. Less critical safety assessment studies could make use of such an assay system, especially when regulatory decisions are made based on a whole host of data from in vitro and in vivo sources. However, to avoid adverse health effects, safety assessment without adequate sensitivity is fundamentally

floored. In vitro test systems have been criticised for being overly sensitive [105, 210]; high sensitivity enables highly accurate identification of the vast majority of human carcinogens, with increasing false positive rates as a direct consequence. Within this specific niche, airing on the side of caution has been historically accepted and has resulted in test systems (especially at the lower tiers) with very high sensitivity and specificity. However, as drug development becomes increasingly expensive, modem reforms have begun to trying to account for this potential problem [113-115]. Early stage drug attrition, based on a positive test result, within a known overly sensitive test system can retard or even inhibit drug development of a potential candidate due to misleading results; a practice which is finically uneconomical for pharmaceutical companies [217]. Exposure driven test systems could alleviate the potential of false positivity, current test systems often dose at non-therapeutic concentrations.

If this in vitro assay system cannot reach the basal level of sensitivity outlined by predecessor assays, then irrespective of the additional benefits the novel design may bring, the assay will have little scope in a hazard and risk assessment setting. Therefore, the aims of the second results chapter were slightly different, using the basic established assay design and initial data set collected; the chapter was intended to more accurately investigate the identity of putative *PIG-A* mutant events as well as investigate the most suitable cellular platform in terms of sensitivity and molecular benefits and further the assay design to facilitate assay distribution. The most logical place to start in respect to this particular assay would be the pre-existing (background) number of phenotypic *PIG-A* mutant events within the parental TK6 cell line; initially, additional TK6 cell lineages were to be assessed for potential inclusion within the in vitro *PIG-A* assay design.

There are problems faced by genetic toxicologists regarding the integrity and identity of the cell lines used within experimentation. Genetic drift cause through poor maintenance or inappropriate distribution leads to cell lines that do not conform to their pre-determined characteristics. Consequently, constructing a complete assay system able to be implemented into any laboratory primarily overcomes some of the problems associated to independent cell line maintenance and improper distribution. Therefore, the earliest "Low Passage" lineage of the TK6 cell line was obtained from the ILSI-HESI, NIHS (Masa Honma) and these cells were assessed for GPI-AP

expression as well as general morphological and physical characteristics (Section 4.3.1). The aim of this sub-study was to find a GPI-AP surface reporter marker candidate to be used in combination with the "Low Passage" cell line which facilitated highly sensitive mutation analysis without the need for a pre-enrichment step. However, prior to any *PIG-A* phenotypic assessment, obvious differences were detected between the normal and "Low Passage" cell lines; ranging from dissimilar morphology to unique responses following mutagen exposure.

Clonal expansion is a technique which has been utilised for decades within microbiology; however, in the context of genetic toxicology assays, it often has associated complications. Within current validated in vitro gene mutation assays, clonal expansion is utilised to provide sufficient cellular growth to enable visual identification of colonies post chemical exposure to enable scoring [70, 71, 112]. However, the cell lines used within testing contexts are often immortalised, some cancer, cell lines with abnormally high levels of genomic instability; this feature often provides increased sensitivity which again helps contribute to the overly sensitive stereotype [113-115, 210]. Therefore, extended experimental time periods can facilitate the accumulation of abnormal spontaneous mutation frequencies, often within non-human cell lines, which propagate additional genomic damage independent of chemical exposure. In order to move the field of in vitro genetic toxicology testing forward; human cell lineages, with representative functionality, as well as novel molecular techniques, which do not emphasise known technical issues, are required. Flow cytometry is a high throughput platform in which such an assay system can be developed, with potential to provide accuracy and sensitivity as well as additional high content features to enable multiplex analysis [235, 246]. Following the technological advances of the last decade, most bench top flow cytometers now have the ability to sort events of interest, using a technique known as FACS. This is a potential method to enable highly effective high–throughput mutant phenotype depletion prior to distribution and subsequent *PIG-A* assessment, eliminating the required need for a clonal expansion step. However, much like most modern technology, FACS is incredibly susceptible to loss of sensitivity, through poor event characterisation as well as machine error, following less than impeccable maintenance. Often the highly impressive numbers associated with potential FACS purity sorts can be obtained routinely by specialised FACS labs, but more general

laboratories would not be able to routinely reach the stated figures. Therefore, it comes at no great surprise that FACS was demonstrated to be highly effective; however, unable to obtain the required level of sensitivity to secure integration into the long term assay design (Section 4.3.2).

The assay system appeared to be subsiding below the required standards of sensitivity even prior to mutagenic exposure and therefore, the reporter system itself was fundamentally assessed for error. The preliminary experiments had quantified the sensitivity of the antibodies used in the assay; however, the additional proof of principle experiment had also highlighted the existence of a subset of putative *PIG-A* mutant events which were non-viable. This issue has been discussed previously, and is also an associated concern to the in vivo *Pig-a* assay due to the lack of the means to fully test and validate the genotype of the proposed mutant events. Having identified a relationship between cytotoxity and a corresponding increase in mutant frequency, as well as successfully identifying a sub population of non-viable putative in vitro *PIG-A* mutants (Section 3.3.5), alternative mechanisms were investigated for in vitro phenotypic mutant mimicking event induction. The "Low Passage" TK6 cells were assessed for viability pre-exposure to attempt to bring the system in-line with current validated levels of sensitivity, however, following only minor levels of detected apoptosis and cell death, the system still appeared to fundamentally lack the ability to differentiate induced from pre-existing phenotypic *PIG-A* mutant events (Section 4.3.3). This was mirrored within the preliminary EMS data utilising FACS enrichment, CD55 as the reporter for mutation and viability assessment within the *PIG-A* assay design. The resultant data again demonstrated a similar dose response with comparable defined metrics to the previous EMS exposure (Section 4.3.4). Highly varied GPI-AP expression, with seemingly no obvious correlation to surface distribution or expression was shown to be the critical sensitivity limiting factor in preventing the inclusion of the "Low Passage", apparently more stable, cell line within the assay design. Therefore, in order to fulfil the initial goals of constructing a standardised assay system, enabling mass reproducibility as well as data robustness, additional features as well as cellular platforms were to be assessed.

Cell lines utilised within genetic toxicology testing are generally quite similar in terms of physical characteristics and applicable uses, this is re-enforced by the common ancestry shared by a number of routine use cell lines [124, 126, 127, 182,

200]. However, genetic and phenotypic differences are often apparent and therefore, different cell lines are used for different genetic toxicology applications; for example, AHH-1 and MCL-5 cells have increased metabolic function than other analogous suspension cell lines and can be used when metabolic activation of the genotoxicant is required [28, 126, 182, 200, 306, 350]. However, in order to put forward a self-contained assay system with most, if not all, of the features currently desirable within the field, i.e. p53 functionality, apoptosis sensitivity and human relevance etc., assay optimisation as well as cell line characterisation is required [113]. To facilitate the automation and hence standardisation of the FCM in vitro *PIG-A* assessment, a number of different mathematical gating strategies were investigated to find a reproducible and accurate system for defining phenotypic status (Appendix Section 4.5.3.3). All gating strategies were shown to be robust and reproducible, and following further development of a graphical user interface (GUI) within a suitable programming environment, a simple automated statistical analysis package can be constructed. This would provide standardisation as well as a non-subjective method for analysing in vitro *PIG-A* mutation data; removing any potential inaccuracies as well as subjectivity and increasing data integrity.

Investigating alternative cell lines and GPI-AP combinations was shown to identify potential candidates for the in vitro assay design (Section 4.3.5), with the aim of identifying a cell line with a constituently expressed critical GPI-attached surface antigen, removing the need of any additional preparative stages (mutant depletion). In addition a brief validation of the candidate cell lines was undertaken to demonstrated potential p53 expression as well as functionality. All cell lines assessed demonstrated p53 presence, and some level of functionality which facilitated their inclusion in further experimentation and potential assay integration. MCL-5 cells were concluded as the most appropriate cellular platform for the assay for a number of reasons; their p53 competency, suspension growth dynamics, metabolism capability and general robustness were all suitable (Section 4.3.5).

By the end of the second results chapter the assay design had moved into the MCL-5 cell line, optimised the gating strategy, demonstrated feasible p53 competency and apoptosis capability, isolated a potential flaw in the current assay protocol with regards to non-viable putative *PIG-A* mutant mimicking events and identified a number of suitable GPI-AP to act as in-direct reporters for mutation. The assay was

beginning to coincide with the goals initially outlined by the project. However, the assay still lacked any real hard evidence for dose response data at a sensitivity level comparable to validated assay systems. A number of additional mechanistic problems were also investigated, FCM scoring bias as well as assay robustness (Appendix Section 4.5.3) and therefore, the ensuing chapter, was aimed to generate proof of principle data. As well as investigate in greater detail issues regarding GPI-AP coverage, imaging platform compatibility and potential sources of bias, including the cell cycle.

Conforming to the modernisation of the genetox field is critical to ensure the longevity of the assay test system. With ever increasing economic reforms applying increasing pressure on the restrictions with animal usage [86] and the desired application of the data [88], in vitro test systems are required to deliver on both cost efficiency and strength of subsequent data. No longer has it appeared to be sufficient to generate a test system with immense sensitivity, it also must ensure high content, toxicity assessment, high through put and often associated to a parental or analogous test system sharing a well validated mechanism. The pre-existing validated in vitro gene mutation assays have recently come under criticism for a number of reasons aforementioned [113-115], especially the test systems which offer little human relevance as well as limited strength. As a consequence of this, their future inclusion within safety assessment batteries, is not definite, especially with the development of novel high throughput analogous test systems [301]. Therefore, not only is there a current requirement for the development of novel test systems to meet demands of the evolving field, but also a strong supplementary feature which heavily favours this particular developing test system. The additional benefits the field would receive if an in vitro *PIG-A* platform could be validated not only could provide the high throughput, high precision nature of a gene mutation test system, but more importantly a stage for the further validation of the in vivo mechanism, a current limitation for OECD guideline drafting. By facilitating direct sequencing validation of the phenotypic *PIG-A* mutants, an in vitro *PIG-A* assay, meeting all the predefined criteria, guarantees inclusion within the near future of genetic toxicology. There are a number of currently published studies which have begun to investigate the relationship between phenotypic *Pig-a* mutant events and their respective genotypes, however, experimental design has prevented true representation. Experimental

designs are yet to truly reflect the reporter mechanism without any potential bias; however, data collected has shown some correlation between phenotype and genotype [144, 172, 438, 439]. This presumptive guarantee within the near future inclusion of toxicology research makes the assay unique, as well as additional quantitatively dose response modelling, providing human relevance, and a potential correlation to current in vivo data as well as human health potency assessments. The design and development of a suitable assay system exploiting the in vivo mechanism could provide a significant benefit to the genetic toxicology community and aid future regulatory decision making, human health risk assessment and field progression.

A complex relationship exists between toxicity and genotoxicity within the field of genetic toxicology. Following compound exposure and the saturation of homeostatic defence mechanisms, including DNA repair, induced lesions or mutational events are not repaired and subsequently, the cell begins to accumulate irreparable damage [8, 14, 118]. Each cell is unique in terms of the exact amount of tolerated damage, but once the threshold is met the cell either undergoes apoptosis, necrosis or has accumulated such genomic damage that it is unable to undergo a death pathway and results in the cancer phenotype. As a result of this, genotoxicity testing often does not exceed 40-50% cytotoxicity, to avoid falsely underestimating genotoxic potential of a compound. In addition and to further complicate the relationship, in vitro, toxicity can lead to genotoxicity through the release of ROS from dying cells [440]. However, minor physiological differences within either pathway progression are able to be exploited to define the subsequent results of genotoxic exposure. For example, cells undergoing genotoxic damage do not often have morphological alterations within the extracellular membrane; damage is often confined to the nucleus or other mechanism specific organelles [275, 276, 441].

Therefore, there is a great need for accurate viability assessment within safety assessment testing to ensure correct definition of damage and to prevent either grossly over or under exaggerating a compounds effect. Genetic toxicology has moved over the past decade into more high content multiplex analysis with specific focus placed on more accurate viability assessment. Previously, scoring viability has been based on the size of the cell, and traditionally RPD or RICC assessment has been the gold standard in cytotoxicity, cytostasis and mitotic arrest assessment [133,

357]. However, utilising the coulter principle and operating under the current standards, there is a high potential of cells being miss-incorporated into analysis as a result of poor viability assessment and subsequent definition. Molecular markers for apoptosis for example generally provide a much more accurate measure of the actual health of a cell however; such methods are more expensive and often have rate limiting associating properties. With the introduction of such platforms as FCM, the incorporation of viability dyes within the staining cocktail allows either monoclonal antibodies, or nucleic acid dyes to more accurately assess the health of the cellular population. The in vitro *PIG-A* assay designed to this point demonstrated some correlation between genotoxic potency and cytotoxicity, an unfortunate relationship adding to the complexities observed within such assay systems [65]. However, by utilising more modern methods along with additional viability assessment and a more complex gating strategy, this correlation should be removed. These efforts will provide help to establish a solid foundation from which to work on in the future developments, to allow this test system to be integrated in the in vitro test battery in future years.

The third results chapter focussed heavily on two separate aims; firstly to generate suitable qualitative MCL-5 dose response data, for proof of principle as well as showing potential applications of the assay (Section 5.3.1). Secondly, the undertaking of an apparent successful preliminary novel heterogeneous sequencing experiment, in which a direct assessment of phenotype to genotype relationship could be made, was investigated to potentially increase validation of the in vivo mechanism (Section 5.3.5). The novel approach utilised a metagenomics style in which heterogeneous populations were assessed for mutational spectra shift, following model mutagen induction, at multiple *PIG-A* related gene loci.

Initially, model mutagen exposure was utilised again to demonstrate proof of concept, with EMS, MNU and ENU being used as well characterised alkylating agents. However, the addition of a non-genotoxic 2,4 DNP compound as an assessment for false positivity and assay ability to detect mutagens and pro-mutagens from toxic, non-genotoxic compounds. In an attempt to demonstrate that the current reformed assay was free from cytotoxicity bias, 2-4 DNP was tested as well as a trans-membranous antigen marker, HLA-DR, included. HLA-DR inclusion, much like CD19 or equivalent antigens, is as an additional viability and phenotype validity

assessment. HLA-DR constituently present within the extracellular surface of lymphoblastoids, serves as a "self" marker for membrane integrity, which in turn increases phenotype validity by ensuring that cells with aberrant membranes are not scored as presumptive *PIG-A* mutant cells. The data generated looked promising, and all compounds exhibited non-linear dose responses, admittedly corresponding toxicity was often observed at the high doses, and were ranked in terms of potency by their respective fold increases in phenotypic *PIG-A* mutant frequencies (Section 5.3.1). Good specificity in identifying known model mutagenic compounds was apparent, in addition to this; the non-mutagenic compound was demonstrated not to increase phenotypic *PIG-A* mutant frequency. More importantly, the previous observed correlation between cytotoxicity and increase in mutant *PIG-A* frequencies was no longer apparent. This point in particular is of importance within the continued debate about the identity of putative *Pig-a* mutant events within the rodent *Pig-a* assay. However, the assay was unable to deliver on the sensitivity; the pre-existing background mutant frequency was elevated and hence, lacked the ability to detect minimal phenotypic *PIG-A* mutant induction. A feature required to bring the assay design in-line with the HPRT or MLA/TK assays and a continued problem requiring further optimisation prior to any chemical validation step. Flow cytometry gating improvements could be utilised (Section 5.3.4), especially in terms of false positivity refinement, tandem antibody GPI-AP marker stains can be used to increase validity of phenotype (Section 5.3.2), a technique recently exploited within the development of an analogous TK6 based in vitro *PIG-A* testing platform [301].

In addition to the lack of definitive sequencing evidence, which would provide comprehensive support for the in vivo *pig-a* mechanism, there also appears to be a data gap in regards to additional molecular derived supplementary data. The continued development of the in vivo *pig-a* assay, i.e. OECD guideline drafting, is currently being retarded by the lack of complete mechanistic validation. However, supplementary supporting molecular data could be used to strengthen the case of phenotype validity without excessive sequencing. For example, lipid raft associated sporadic cellular surface marker distribution, visualised following confocal imaging, is one of the reasons why tandem reporting surface markers should be incorporated into assay design. In addition to providing a physical image depicting a strong positive phenotype, the data also highlights potential flaws in the potential future

imaging platforms able to analyse the data correctly (Section 5.3.2). Utilising FCM based approaches would be appropriate as the diameter of the laser light used to excite the cellular events is greater than the average diameter of a MCL-5 cell, however, other platforms utilised alternative excitation approaches could induce significant bias within analysis. Identification of such technical issues provides insight into the future development of imaging technology as well as enables more accurate research. As well as this, exploiting more complex features within flow cytometry analysis could also provide additional sensitivity to the assay. Unlike the proposed in vitro assay designs, the rodent erythrocyte assay is pretty robust in terms of mutant identity. Erythrocytes lack the ability to apoptose and are heavily determined in terms of their fate and therefore, quite unresponsive post release into the circulatory system. However, although this cell type is idealistic for scoring purposes, they are less than ideal for validation. Moving the assay into a nucleated cell line for validatory reasons, splenocyte etc., potentially can introduce a number of associated cytoxicity problems. Utilising novel pulse width measurements, time of flight, as an additional in-direct method for phenotypic identification, could provide the assay with an increase in sensitivity, as well as enable the analyser to have increased confidence in the resultant data (Section 5.3.3). This modification improved the sensitivity through a decrease in spontaneous background mutant frequency that became in line with current validated test systems [301]. This preliminary data displayed within the chapter critically highlights the potential of this modified assay, as well as provides some level of confidence for future qualitative use, as sensitivity issues were mostly resolved.

The latter half of the chapter was focused on the investigations into the phenotype, genotype relationship. Flow cytometry defined putative phenotypic *PIG-A* mutant events were to be assessed through next generation sequencing approaches to validate their genomic identity (Section 5.3.5). The experimental design was free from biasing techniques and involved sequentially inducing phenotypic *PIG-A* mutant events, FACS isolating and capturing said events, and immediately sequencing the resultant heterogeneous pooled putative phenotypic mutant population. The genotype of the collected events were analysed at multiple gene loci, selected for their implicit relevance in assay design, which facilitated the calculation of the frequency of actual *PIG-A*$^{-}$ mutational events within the pooled population.

Contrary to current published data, all mutational events potentially resulting in a GPI-AP deficient phenotype were studied which enabled some comment on the validity of the *Pig-a* reporting mechanism. The main aim of this section was to potentially validate the proposed *Pig-a* mechanism and solidify the potential future use of the in vitro platform for future applications. The chapter showed good evidence to suggest that the current developmental process had reached a point to facilitate further advancement of the test system and to enable the potential fulfilment of larger more validatory goals.

Ethyl Methane Sulfonate (EMS) exposure appeared to result in an apparent correlation between presumptive mutant events and identified non-synonymous mutations within the coding region of the *PIG-A* gene. Exon 6 was preliminary identified as an area of high activity in terms of mutational events. However, mutational events were also preliminary defined within the CD59 and *PIG-T*, at a lesser frequency within the coding region than the comparable *PIG-A* data. Resultant proposed EMS induced mutants, across all the amplicons investigated, displayed higher frequencies of GC->AT transition mutations, when compared to any other form of mutational event. Therefore, the subsequent generated proposed mutation spectra were in-line with the published mechanism of the alkylating agent. However, the con-current control data failing within the DNA extraction stage of sample preparation prevented any conclusions being able to be associated with the data and therefore, the lack of direct sequencing data for the in vivo *Pig-a* mechanism is also still apparent. Recently, a number of additional *Pig-a* sequence papers have been published which show a mixture of findings. Data generated from the FDA laboratory utilising rodents (Rats) treated with both DMBA and ENU show strong correlation and evidence for *PIG-A* mutational events resulting in the GPI-AP deficiency. However, no additional genes were investigated other than the *PIG-A* gene loci, which is a potential limiting factor for OECD acceptance [438, 439]. Interestingly, two additional publications have put forward data demonstrating further *PIG* gene mutations inducing firstly, the PNH phenotype within human patients [146] as well as the GPI-AP deficient phenotype within human cell lines [442]. These publications provide some evidence for the validity of the mechanisms, as well as quite strong confounding evidence for additional, currently un-measured, genetic alterations resulting in the defined "PIG-A mutant" population. Therefore,

phenotypic scoring, data analysis and subsequent interpretation become more complex until future assay refinement. Without further investigation, and more direct sequencing data it is unclear whether these recent publications will further retard the development of the in vivo assay. However, their presence does generate further need for an in vitro test system utilising the mechanism to facilitate direct sequencing. The field requires the presence of conclusive data and therefore, further investigations are required. Potentially, within the upcoming IWGT work group specific data gaps will be focussed which should more readily move the community to a decision on the assay design.

As briefly discussed earlier, a test system is more likely to have a role in hazard and risk assessment if it is able to combine with a number of additional supplementary end points (multiplexing) or directly correlates to an in vivo genetox assay. The reason for this is the nature of the current regulatory decision making. Due to the holistic approach utilised when coming to a decision on safety assessment [226, 277]; often data is highly varied and can be quite unconnected and therefore, difficult to rank its potential strength. Consequently, if data can be directly compared to an analogous end point or partnering in vivo data set, and positive correlations observed, the strength of the data set is considerably increased. Accrediting more strength to an assay platform facilitates increases usage and longevity within safety assessment. Currently in vitro potency does not relate to human health assessment, and therefore, does not play a significant role in decision making. However, further developmental work within this specific field may demonstrate potency correlations which could enable more weight of evidence being placed on in vitro data sets. Due to the transferability derived from the comprehensive and conserved nature of the GPI-AP structure [163, 165, 174, 320, 352]; the potential scope for usage of the *PIG-A* mechanism is broader than a purely safety assessment role [180] (Appendix Section 5.5.3). Human biomarkers are rapidly being investigated in order to better characterise, diagnose and treat a number of human health conditions; however, many known disease phenotypes have no currently identified biomarkers associated with progression. Consequentially, miss-diagnosis or alternatively late stage diagnosis are more common which often complicate identification and can have life threatening complications and a more severe prognosis.

Rarely genetic toxicology end points have made the transition into the wider world of human bio monitoring; the micronucleus assay in its own right has been used in broader epidemiology studies for the past two decades [69, 382, 383]. However, the typical MN assay protocol is only sensitivity to environmental exposures which penetrate the bone marrow and result in subsequent DNA damage within peripheral blood cells; thus, having an un-invasive protocol, however, limiting the ability to detect acute exposures [46, 378, 379]. As well as this, few genetox end points are versatile enough to be used as a potential biomarker within HBM studies [144]. Additional MN assay platforms are available, for example buccal cells are targeted to investigate oral routes of exposure [382], however, these studies are less robust and often have additional costs (cheaper than current *pig-a* assessment) and invasive procedures associated. Therefore, development of a novel test system which equally enables high precision, highly sample volume and rapid sampling with a more systemic exposure metric as well as a specific tissue specific metric is highly attractive.

Over the past decade, the possibility to generate a robust human ex vivo *PIG-A* gene mutation assay has repeatedly been described [175, 351, 358, 387]; however, little correlation has ever been demonstrated between elevated *PIG-A* mutation frequencies and adverse phenotypes within such studies [175, 280]. The recent advances within the basic *Pig-A* assay design potentially now could be utilised to readdress the assay design and subsequently produce a more accurate reporting platform for human bio monitoring. The conserved GPI-AP structure enables the *PIG-A* mechanism to theoretically be undertaken within any cell type/tissue type as long as a suitable GPI-anchored surface protein can be identified to act as an in-direct reporter for mutagenesis. Similarly to the human MN studies, exposure would have to be systemic if haemopoetic cell lineages were to be utilised, similar to the traditional erythrocytic *pig-a* assay platform. However, utilising a more active cell lineage for example granulocytes or liver hepatocytes, would provide better models for comprehensive selective exposure to be measured, nevertheless, a number of confounding factors would also be introduced; including highly invasive biopsies, trypsinisation issues during sample homogenisation as well as metabolic instability and sample degradation.

A supplementary study was carried out in which an intracellular in vitro *PIG-A* assay design, with the ability to act as an organ/tissue specific platform, was put forward and investigated. Even though the data generated was purely proof of principle preliminary experimentation, the concept was demonstrated to be achievable (Appendix Section 5.5.3). The study was undertaken purely to demonstrate the transferability of the mechanism, an assay design which potentially could work for any X-linked gene which encoded a known constitutively expressed protein. Providing such a model is of great benefit to the genetic toxicology community as it offers the ability to measure genetox end point within any organ or tissue within the body. It also provides a slightly refined reporter mechanism, as it no longer introduces the potential complexities of the additional genes within the GPI-AP synthesis pathway, a recent contested point within the in vivo *Pig-a* development [442]. By directly measuring PIG-A protein presence, only a single gene locus is actively involved in the formation of the phenotype and hence, the genotype is more simply deduced. However additional investigations into the sample preparative procedure would be required prior to further validation, the current human cell line models provide little resistance in terms of sample preparation prior to high throughput analysis.

The results described in the fourth results chapter, outline the initial optimisation and development of a potential human RBC, RET and Granulocyte *PIG-A* assay, taking influence from a number of assay designs published over the past decade [175, 358, 387]. The finalised assay protocols were able to meet the desired sensitivity level to facilitate the further validation of a potential bio monitoring platform (Sections 6.2 – 6.4). The limitations still present within the use of erythrocytic cell lineages threatened the strength of the platform and again introduced scepticism into phenotypic classification. Therefore, granulocytes were chosen, because of existing fundamental protocols [175] as well as the potential for sequencing validation. Granulocytes were chosen over lymphocytes for a number of reasons, specifically their role in the innate immunity and hence, localisation to areas of chronic or acute exposure to deleterious micro environments throughout the body. This feature would be highly beneficial if localised blood sampling was to be undertaken, however utilising peripheral blood means that exposure should be bone marrow penetrating to enable response measuring. Granulocytes do not divide as such, and therefore have a

fixed lifespan ~5hr - 5days, similar to RBCs and should model bone marrow exposure accurately. However, they are also nucleated and are subjected to deleterious microenvironments following infection and/or inflammation [433, 434]. Both environments have been associated to cancer progression and are especially prominent in ROS, which can induce mutational events [148, 232, 443]. Due to lack of mutational fixing, neutrophils would theoretically have limited specificity to all mutational events, however, still could provide a more point of contact or systemic reflection of genomic health. Lymphocytes present a difficult situation as their characteristics make them both highly beneficial and inappropriate for drug screening. Their nucleated status, their un-invasive means of extraction make them an ideal cell lineage, however, their ability to alter surface antigen expression, especially at times of activation make them too heterogenous and subsequently errorous for routine assessment [198, 233, 292, 390].

Within traditional erythrocytic *Pig-a* research there is an abundance of red blood cells able to be phenotypically assessed. However, the nucleated leukocytes comprise a much smaller percentage constitution of blood and therefore, require extensive enrichment prior to assessment. The introduction of immunomagnetic [168] or differential gradients [175] as means of enrichment were key turning points in the relative development of their respective *Pig-a* protocols. The purpose of this study was to attempt to develop a platform able to be utilised in future validatory clinical trials associating the *PIG-A* deficient phenotype with genomic instability and specific disease phenotypes. Preliminary data, utilising this developing platform as a basis, has been presented demonstrating promise [400-402]. However, major limitations were also apparent during development; highly extended sample collection periods, frequently greater than an hour per sample in order to collect the number of events required to generate statistical significance. The problem stems back from the enumeration of the minor populations, RET and granulocytes, even following enrichment occupied less than 10% of the total blood population. Further optimisation into the proposed finalised protocols would have been preferential utilising immuno-enrichment approaches.

The potential benefits of developing such a bio monitoring platform, as a result of further assay platform refinement, could enable identification of exposure correlated mutation driven disease predisposition. During early stages, cancer is most treatable;

it is often contained and yet to metastasise and often responds well to chemo, radio therapy and/or novel treatments. Prognosis following early diagnosis is often very positive, especially within bowl cancer where the 5 year survival rate is >90% if detected early [444]. However, as the cancer phenotype progresses, the genetic as well as biological alterations begin to fester; subsequently allowing the cancer to develop further, switching off biological failsafe's and moving out of infancy [6, 66, 138, 205]. At this stage in progression cancer can become highly aggressive, completely self-sufficient and mobile, in which metastases are able to systemically attack other tissues within the host. Once the cancer has become well established its ability to respond to therapies is highly reduced and often becomes highly symptomatic [395, 443]. Therefore, deep tissue cancers once presenting symptoms are often untreatable and are highly associated to poor prognosis, Pancreatic cancers have a comparable 5 year survival rate of <10% [444]. One of the reasons for this is the dormant nature of the developing cancer which potentially been present asymptomatically for a number of years whilst it facilitates self-sufficiency and growth. Treatment in general is expensive, however, as the treatment becomes more novel and/or more critical the price tag escalated. Consequently, the associated costs of supplementing this treatment to the general public can be exorbitant, and therefore, as a financial model, treating cancer at an early stage is much more appealing; not only does it increase prognosis but is generally more effective. In addition to cancer, potentially obesity, diabetes, inflammatory diseases could all be monitored for progression, following the comprehensive refinement, validation of the test system platforms and the incorporation of localised blood harvesting/sampling, via this relatively un-invasive preliminary test system.

Identifying a novel approach of detecting a pre-disease phenotype, identified by an elevated level of genomic instability, through a cost effective, relatively un-invasive method would be highly financially and clinically beneficial. This supplementary project was able to generate three standalone preliminary assay protocols for high throughput, high precision human *PIG-A* assessment. However, apart from the RBC protocol, each assay fell short of the levels of sensitivity and robustness required to be highly comparative to currently published protocols or analogous in vivo assay designs [175, 351]. Further development is required to facilitate the complete usage of this preliminary test system as a standalone biomonitoring assay.

7.1 Thesis Summary and Proposed Future Work

Throughout the undertaking of this thesis project the in vitro *PIG-A* assay design has undergone a number of revisions, refinements and general modifications. The finalised assay protocol, within the time constraints of the thesis, was established within the metabolically active, genetically modified, human MCL-5 cell line. Using this assay design, proofs of principle experimentations were able to show the potential for future work, and that the general approach was promising. A number of assay refinements are still required, generally focussing on two separate areas, i) toxicity issues and ii) the genotype to phenotype relationship. Toxicity was demonstrated to be a continuous problem associated with the miss-identification of the putative *PIG-A* deficient phenotype; however, following much work, the problem was removed following the inclusion of membrane integrity markers such as HLA-DR or CD19 (highlighted by the 2,4-DNP case study)(Section 5.3.1). Interestingly, the previous versions of the assay design may also prove to be useful following a retrospective validation of the toxicity measures currently used within the assay design. RICC, RPD and RCC are all measures which were frequently used however, may be best suited with their initially intended usage within the MN assay. Shifting the toxicity measure more in-line with analogous test systems, such as HPRT and/or MLA, will potentially alleviate miss interpretation of phenotype, and more accurately report in-direct mutation status.

The genotype/phenotype relationship validation is still on-going, especially following the preliminary work presented (Section 5.3.5), as well as recent publications of additional confounding data [146, 442]. Potentially, due to the identification of additional genes active within the current phenotypic *PIG-A* scoring mechanism, challenging the current reporting with a more generic phenotypic for example, "GPI-AP deficiency" may provide a more accurate description of mutation. However, currently it looks promising that further investigation and refinement will lead to the establishment of a high content, high-throughput assay system with the potential to be used within a hazard and risk assessment environment.

The supplementary ex-vivo Human bio monitoring design development equally was shown to have a number of limitations (Section 6.3). However, the approach showed

good promise for actual future usage, especially within preliminary bio monitoring studies. Further refinement of the assay protocols is required to make use of the additional cell lineages within assessment, RETs and Granulocytes as currently they lack sensitivity and robustness. Making use of an analogous immunomagnetic column enrichment [168] may provide the increased enrichment required, and hence, enable the system to obtain the required level of sensitivity as well as specificity. However, if completed, the potential benefits the assay designs would offer to the field would be significant; an additional bio-monitoring platform with sufficient sensitivity to investigate the correlation between genomic instability and disease phenotype [175, 351, 358, 387]. This may be able to help early stage diagnosis and prevent un-necessity increased financial costs of treatment.

Table 7.1 – Summary of the thesis project major developments - described within the chapter contents, as well as the additional most important data presented within the appendix.

In vitro *PIG-A* gene mutation assay

- ✓ MCL-5 Cells (p53 Competent, Apoptosis sensitive, Metabolically active)
- ✓ Suspension Human Cell Line (No enrichment required, Biologically relevant)
- ✓ Novel FCM Gating Approach (Utilising FL-W measures)
- ✓ Viability and integrity markers (Apoptosis, cell death and membrane integrity)
- ✓ Tandem GPI-AP assessment (CD55 and CD59)
- ✓ Preliminary work demonstrated promising sensitivity and specificity

In vitro *PIG-A* platform Supplementary Investigations

- ✓ Cell line characterisation (TK6, AHH-1 and MCL-5)
- ✓ Proteomic validation (p53 status; p21, p-p53 and PIG-A protein)
- ✓ Cross platform validation (FCM, ImageStream ™ and laser scanning Confocal)
- ✓ Viability Assessment
- ✓ Preliminary Next Generation Sequencing analysis of phenotypic *PIG-A* mutants

Intracellular *PIG-A* gene mutation assay

- ✓ Standardised protocol for most tissue types
- ✓ Preliminary MCL-5 data to show intracellular localisation of PIG-A protein
- ✓ Proof of principle house keeper protein data
- ✓ Positive future for additional tissue validation

Development of ex vivo Human *PIG-A* bio monitoring assays

- ✓ Human RBC, RET and Granulocyte assay protocol development
- ✓ RBC assay in-line with currently published data
- ✓ RET and Granulocyte assay platforms show good promise, but require further work
- ✓ Assay protocols show great promise for potential future clinical trials

Bibliography

1. Young, R., Genetic Toxicology: Web Resources. 2002, Elsevier: Toxicology.
2. Lodish, H., A. Berk, and S. Zipursky, Molecular Cell Biology. 4th edition. 2000, New York: W. H. Freeman. Section 12.4.
3. Deoxyribonucleic Acid. 2014 15/06/2014]; Available from: http://superagatoide.altervista.org/DNA.html.
4. Le Fevre, A.C., et al., Characterization of DNA reactive and non-DNA reactive anticancer drugs by gene expression profiling. Mutat Res, 2007. 619(1-2): p. 16-29.
5. Preston, R.J. and G.M. Williams, DNA-reactive carcinogens: mode of action and human cancer hazard. Crit Rev Toxicol, 2005. 35(8-9): p. 673-83.
6. Yuspa, S.H., et al., Role of oncogenes and tumor suppressor genes in multistage carcinogenesis. J Invest Dermatol, 1994. 103(5 Suppl): p. 90s-95s.
7. Tonelli, A., et al., Seizures as the first manifestation of chromosome 22q11.2 deletion syndrome in a 40-year old man: a case report. Journal of Medical Case Reports, 2007. 1(1): p. 167.
8. Roos, W.P. and B. Kaina, DNA damage-induced cell death by apoptosis. Trends Mol Med, 2006. 12(9): p. 440-50.
9. Rutten, B.P., et al., The aging brain: accumulation of DNA damage or neuron loss? Neurobiol Aging, 2007. 28(1): p. 91-8.
10. Liu, Y., G. Fiskum, and D. Schubert, Generation of reactive oxygen species by the mitochondrial electron transport chain. J Neurochem, 2002. 80(5): p. 780-7.
11. Alam, S., et al., The cigarette smoke carcinogen benzo[a]pyrene enhances human papillomavirus synthesis. J Virol, 2008. 82(2): p. 1053-8.
12. Vanderkerken, K., et al., The mouse bone marrow micronucleus assay can be used to distinguish aneugens from clastogens. Mutagenesis, 1989. 4(1): p. 6-11.
13. Dertinger, S.D., et al., Efficient monitoring of in vivo pig-a gene mutation and chromosomal damage: summary of 7 published studies and results from 11 new reference compounds. Toxicol Sci, 2012. 130(2): p. 328-48.
14. Wiesm, et al., DNA Damage, Repair, and Diseases. Journal of Biomedicine and Biotechnology, 2002. 2(2): p. 45-45.
15. Lee, G.S., et al., Base alterations in yeast induced by alkylating agents with differing Swain-Scott substrate constants. J Mol Biol, 1992. 223(3): p. 617-26.
16. Beranek, D.T., Distribution of methyl and ethyl adducts following alkylation with monofunctional alkylating agents. Mutat Res, 1990. 231(1): p. 11-30.
17. Jansen, J.G., et al., Marked Differences in the Role of O6-Alkylguanine in hprt Mutagenesis in T-Lymphocytes of Rats Exposed in Vivo to Ethylmethanesulfonate, N-(2-Hydroxyethyl)-N-nitrosourea, or N-Ethyl-N-nitrosourea. Cancer Research, 1995. 55(9): p. 1875-1882.
18. Shahin, S., C. Cullinane, and P.J. Gray, Mitochondrial and nuclear DNA damage induced by sulphur mustard in keratinocytes. Chem Biol Interact, 2001. 138(3): p. 231-45.

19. Thiermann, H., F. Worek, and K. Kehe, Limitations and challenges in treatment of acute chemical warfare agent poisoning. Chem Biol Interact, 2013. 206(3): p. 435-43.
20. Klungland, A., et al., Spectrum of mutations induced by methyl and ethyl methanesulfonate at the hprt locus of normal and tag expressing Chinese hamster fibroblasts. Carcinogenesis, 1995. 16(6): p. 1281-5.
21. Swain, C.G. and C.B. Scott, Quantitative Correlation of Relative Rates. Comparison of Hydroxide Ion with Other Nucleophilic Reagents toward Alkyl Halides, Esters, Epoxides and Acyl Halides1. Journal of the American Chemical Society, 1953. 75(1): p. 141-147.
22. Jenkins, G.J.S., et al., Do dose response thresholds exist for genotoxic alkylating agents? Mutagenesis, 2005. 20(6): p. 389-398.
23. Chen, P. Alkylating. 2007 02/07/2014]; College of DuPage]. Available from: http://bio3400.nicerweb.com/Locked/media/ch15/alkylating.html.
24. Kumar, V., A. K. Abbas, and A. Jon, Robbins Basic Pathology: 9th Edition. 2013: Saunders (imprint).
25. Himes, R.H., et al., Action of the vinca alkaloids vincristine, vinblastine, and desacetyl vinblastine amide on microtubules in vitro. Cancer Res, 1976. 36(10): p. 3798-802.
26. Ohuchida, A., et al., Micronucleus test with vincristine administered by intraperitoneal injection and oral gavage. Mutat Res, 1989. 223(4): p. 395-8.
27. Santos, C.B., et al., Concurrence of fragile X and Klinefelter syndromes: report of a new case of paternal nondisjunction. Ann Genet, 2003. 46(1): p. 53-5.
28. Hernandez, L.G., J. van Benthem, and G.E. Johnson, A mode-of-action approach for the identification of genotoxic carcinogens. PLoS One, 2013. 8(5): p. e64532.
29. Alsina, L., et al., Novel and atypical splicing mutation in a compound heterozygous UNC13D defect presenting in Familial Hemophagocytic Lymphohistiocytosis triggered by EBV infection. Clin Immunol, 2014.
30. Clancy, S., Genetic Mutation - A single base change can create a devastating genetic disorder or a beneficial adaptation, or it might have no effect. How do mutations happen, and how do they influence the future of a species? Nature Education, 2008. 1(1): p. 187.
31. Sega, G.A., A review of the genetic effects of ethyl methanesulfonate. Mutat Res, 1984. 134(2-3): p. 113-42.
32. Eder, E., et al., The relationship between mutagenicity in His G46 Salmonella and the O(6)-guanine alkylation in bacterial DNA by monofunctional methanesulphonates. Toxicol In Vitro, 1990. 4(3): p. 167-74.
33. Waters, R., et al., DNA alkylations and mutation after exposure to ethyl methanesulphonate in mammalian cell lines routinely used in mutagenicity testing. Mutagenesis, 1990. 5 Suppl: p. 61-5.
34. Fenech, M., The in vitro micronucleus technique. Mutat Res, 2000. 455(1-2): p. 81-95.
35. Sega, G.A. and E.E. Generoso, Measurement of DNA breakage in specific germ-cell stages of male mice exposed to acrylamide, using an alkaline-elution procedure. Mutat Res, 1990. 242(1): p. 79-87.
36. Adler, I.D., et al., Clastogenic effects of acrylamide in mouse bone marrow cells. Mutat Res, 1988. 206(3): p. 379-85.

37. Pingarilho, M., et al., Induction of sister chromatid exchange by acrylamide and glycidamide in human lymphocytes: role of polymorphisms in detoxification and DNA-repair genes in the genotoxicity of glycidamide. Mutat Res, 2013. 752(1-2): p. 1-7.
38. Meuth, M. and J.E. Arrand, Alterations of gene structure in ethyl methane sulfonate-induced mutants of mammalian cells. Mol Cell Biol, 1982. 2(11): p. 1459-62.
39. Doak, S.H., et al., Mechanistic influences for mutation induction curves after exposure to DNA-reactive carcinogens. Cancer Res, 2007. 67(8): p. 3904-11.
40. Watzek, N., et al., N7-glycidamide-guanine DNA adduct formation by orally ingested acrylamide in rats: a dose-response study encompassing human diet-related exposure levels. Chem Res Toxicol, 2012. 25(2): p. 381-90.
41. Zair, Z.M., et al., N-methylpurine DNA glycosylase plays a pivotal role in the threshold response of ethyl methanesulfonate-induced chromosome damage. Toxicol Sci, 2011. 119(2): p. 346-58.
42. Gates, K.S., T. Nooner, and S. Dutta, Biologically relevant chemical reactions of N7-alkylguanine residues in DNA. Chem Res Toxicol, 2004. 17(7): p. 839-56.
43. Lee, C.Y., et al., Recognition and processing of a new repertoire of DNA substrates by human 3-methyladenine DNA glycosylase (AAG). Biochemistry, 2009. 48(9): p. 1850-61.
44. Parsons, J.L. and G.L. Dianov, Co-ordination of base excision repair and genome stability. DNA Repair (Amst), 2013. 12(5): p. 326-33.
45. New Research Directions in DNA Repair, ed. C. Chen. 2013: InTech.
46. Parry, E.M., et al., Detection and characterization of mechanisms of action of aneugenic chemicals. Mutagenesis, 2002. 17(6): p. 509-21.
47. Muller, F., et al., Parental origin of the extra chromosome in prenatally diagnosed fetal trisomy 21. Hum Genet, 2000. 106(3): p. 340-4.
48. Friedberg, E.C., L.D. McDaniel, and R.A. Schultz, The role of endogenous and exogenous DNA damage and mutagenesis. Curr Opin Genet Dev, 2004. 14(1): p. 5-10.
49. Douki, T., The variety of UV-induced pyrimidine dimeric photoproducts in DNA as shown by chromatographic quantification methods. Photochem Photobiol Sci, 2013. 12(8): p. 1286-302.
50. Wei, K., E. Wandl, and K.H. Karcher, X-ray induced DNA double-strand breakage and rejoining in a radiosensitive human renal carcinoma cell line estimated by CHEF electrophoresis. Strahlenther Onkol, 1993. 169(12): p. 740-4.
51. Li, X. and W.D. Heyer, Homologous recombination in DNA repair and DNA damage tolerance. Cell Res, 2008. 18(1): p. 99-113.
52. Wang, C.H., et al., Oxidative stress response elicited by mitochondrial dysfunction: implication in the pathophysiology of aging. Exp Biol Med (Maywood), 2013. 238(5): p. 450-60.
53. Government, U.K. Health and Safety Executive - What is REACH? 20/05/2014]; Available from: http://www.hse.gov.uk/reach/whatisreach.htm.
54. Authority, H.a.S. Hazard and Risk. 20/05/2014]; Available from: http://www.hsa.ie/eng/Topics/Hazards/.
55. Florida, U.o. 20/05/2014]; Available from: http://www.ehs.ufl.edu/programs/bio/toxins/toxin-table/.

56. Baird, S.J.S., et al., Noncancer risk assessment: a probabilistic alternative to current practice. Hum. Ecol. Risk Assess, 1996. 2: p. 79-102.
57. Dourson, M.L. and J.F. Stara, Regulatory history and experimental support of uncertainty (safety) factors. Regul Toxicol Pharmacol, 1983. 3(3): p. 224-38.
58. Lehman, A.J. and O.G. Fitzhugh, Comprehensive Toxicology, in Assoc. Food Drug Off. U. S. 1954, Elsevier. p. 33-35.
59. Research, C.f.D.E.a., F.a.D. Administration, and U.S.D.o.H.a.H. Services, 2011 Novel New Drugs. 2012.
60. life, A.B.m.t. Global pharmaceutical industry and market. 21/05/2014]; Available from: http://www.abpi.org.uk/industry-info/knowledge-hub/global-industry/Pages/industry-market-.aspx#fig2.
61. IMS. home - IMS Health. 2014 02/07/2014]; Available from: http://www.imshealth.com/portal/site/imshealth.
62. Limited, L. Derek-Nexus. 21/05/2014]; Available from: http://www.lhasalimited.org/.
63. Mombelli, E., An evaluation of the predictive ability of the QSAR software packages, DEREK, HAZARDEXPERT and TOPKAT, to describe chemically-induced skin irritation. Altern Lab Anim, 2008. 36(1): p. 15-24.
64. Harmonization, I.C.o. S2(R1). 20/05/2014]; Available from: http://www.ich.org/fileadmin/Public_Web_Site/ICH_Products/Guidelines/Safety/S2_R1/Step4/S2R1_Step4.pdf.
65. (FDA), F.a.D.A., Guidance for Industry: S2(R1) Genotoxicity Testing and Data Interpretation for Pharmaceuticals Intended for Human Use 2012.
66. Ames, B.N., et al., Carcinogens are mutagens: a simple test system combining liver homogenates for activation and bacteria for detection. Proc Natl Acad Sci U S A, 1973. 70(8): p. 2281-5.
67. Ames, B.N., F.D. Lee, and W.E. Durston, An Improved Bacterial Test System for the Detection and Classification of Mutagens and Carcinogens. Proceedings of the National Academy of Sciences, 1973. 70(3): p. 782-786.
68. McCann, J., et al., Detection of carcinogens as mutagens: bacterial tester strains with R factor plasmids. Proceedings of the National Academy of Sciences, 1975. 72(3): p. 979-983.
69. Fenech, M. and A.A. Morley, Measurement of micronuclei in lymphocytes. Mutat Res, 1985. 147(1-2): p. 29-36.
70. Lloyd, M. and D. Kidd, The mouse lymphoma assay. Methods Mol Biol, 2012. 817: p. 35-54.
71. Keohavong, P., L. Xi, and S.G. Grant, Molecular analysis of mutations in the human HPRT gene. Methods Mol Biol, 2014. 1105: p. 291-301.
72. OECD, OECD GUIDELINE FOR THE TESTING OF CHEMICALS - Test Guideline 487 - In Vitro Mammalian Cell Micronucleus Test 2012.
73. Library, O. Test No. 476: In vitro Mammalian Cell Gene Mutation Test. 1997 21/05/2014]; Available from: http://www.oecd-ilibrary.org/environment/test-no-476-in-vitro-mammalian-cell-gene-mutation-test_9789264071322-en.
74. Johnson, G.E., J.M. Parry, and E.M. Parry, Mammalian Cell Gene Mutation Assay: Test MethodsGenetic Toxicology. 2012, Springer New York. p. 55-67.
75. Meng, Q., et al., Molecular analysis of mutations at the HPRT and TK loci of human lymphoblastoid cells after combined treatments with 3'-azido-3'-

deoxythymidine and 2',3'-dideoxyinosinedagger. Environ Mol Mutagen, 2002. 39(4): p. 282-95.
76. Huerta, I., et al., Genotoxic evaluation of five Angiotesin II receptor blockers: In vivo and in vitro micronucleus assay. Mutat Res Genet Toxicol Environ Mutagen, 2014. 767c: p. 1-7.
77. Miura, D., et al., Development of an in vivo gene mutation assay using the endogenous Pig-A gene: I. Flow cytometric detection of CD59-negative peripheral red blood cells and CD48-negative spleen T-cells from the rat. Environmental and Molecular Mutagenesis, 2008. 49(8): p. 614-621.
78. Lambert, I.B., et al., Detailed review of transgenic rodent mutation assays. Mutat Res, 2005. 590(1-3): p. 1-280.
79. Collins, A., et al., The comet assay as a tool for human biomonitoring studies: the ComNet project. Mutat Res Rev Mutat Res, 2014. 759: p. 27-39.
80. Douglas, G., Transgenic Rodent Gene Mutation Assays: Current State of Validation 2010, OECD.
81. Administration, F.a.D. 2014 27/05/2014]; Available from: http://www.fda.gov/.
82. harminisation, I.C.o. ICH - Harmonising for better health. 2014 27/05/2014]; Available from: http://www.ich.org/.
83. Agency, E.E. 2014 27/05/2014]; Available from: http://www.eea.europa.eu/.
84. Health, N.I.o. National Institute of Health : Turning Discovery into Health. 2013 27/05/2014]; Available from: http://www.nih.gov/news/health/jun2013/nih-03.htm.
85. Initiative, R.s. National Centre for the Replacment,Refinement and Reduction of animal Testing. 27/05/2014]; Available from: http://www.nc3rs.org.uk/news.asp?id=246.
86. Union, E., 7th Amendment to the Cosmetics Directive. 2003.
87. dos Santos, G.G., et al., Progress on the development of human in vitro dendritic cell based assays for assessment of the sensitizing potential of a compound. Toxicol Appl Pharmacol, 2009. 236(3): p. 372-82.
88. Groothuis, F.A., et al., Dose metric considerations in in vitro assays to improve quantitative in vitro-in vivo dose extrapolations. Toxicology, 2013.
89. Costin, G.E., et al., Vaginal irritation models: the current status of available alternative and in vitro tests. Altern Lab Anim, 2011. 39(4): p. 317-37.
90. Elmore, S.A., et al., FutureTox II: Contemporary Concepts in Toxicology: "Pathways to Prediction: In Vitro and In Silico Models for Predictive Toxicology". Toxicol Pathol, 2014.
91. Gunther, W.C., et al., Evaluation of the Pig-a, micronucleus, and comet assay endpoints in a 28-day study with ethyl methanesulfonate. Environ Mol Mutagen, 2014.
92. Meng, X., et al., Stem cells in a three-dimensional scaffold environment, in Springerplus. 2014. p. 80.
93. Mathes, S.H., H. Ruffner, and U. Graf-Hausner, The use of skin models in drug development. Adv Drug Deliv Rev, 2014. 69-70c: p. 81-102.
94. Rothen-Rutishauser, B., et al., In vitro models of the human epithelial airway barrier to study the toxic potential of particulate matter. Expert Opin Drug Metab Toxicol, 2008. 4(8): p. 1075-89.
95. Kirsch-Volders, M., et al., In vitro genotoxicity testing using the micronucleus assay in cell lines, human lymphocytes and 3D human skin models. Mutagenesis, 2011. 26(1): p. 177-84.

96. Yu, J., et al., Three dimensional human small intestine models for ADME-Tox studies. Drug Discov Today, 2014.
97. Stebbins, N.D., M.A. Ouimet, and K.E. Uhrich, Antibiotic-containing polymers for localized, sustained drug delivery. Adv Drug Deliv Rev, 2014.
98. Wehling, M., [Paracetamol. Efficacious and safe for all ages]. Schmerz, 2013. 27(1): p. 20-5.
99. Jaga, K. and C. Dharmani, Global surveillance of DDT and DDE levels in human tissues. Int J Occup Med Environ Health, 2003. 16(1): p. 7-20.
100. Thomas, R.S., et al., Incorporating new technologies into toxicity testing and risk assessment: moving from 21st century vision to a data-driven framework. Toxicol Sci, 2013. 136(1): p. 4-18.
101. Gad, S.C., In vitro toxicology, second edition. 2000: Taylor and Francis.
102. Paschin, Y.V., V.I. Kozachenko, and L.E. Sal'nikova, Differential mutagenic response at the HGPRT locus in V79 and CHO Chinese hamster cells after treatment with chromate. Mutat Res, 1983. 122(3-4): p. 361-5.
103. MacGregor, J.T., et al., IWGT report on quantitative approaches to genotoxicity risk assessment II. Use of point-of-departure (PoD) metrics in defining acceptable exposure limits and assessing human risk. Mutation Research/Genetic Toxicology and Environmental Mutagenesis, (0).
104. Le Hegarat, L., et al., Performance of comet and micronucleus assays in metabolic competent HepaRG cells to predict in vivo genotoxicity. Toxicol Sci, 2014. 138(2): p. 300-9.
105. Walmsley, R.M. and N. Billinton, How accurate is in vitro prediction of carcinogenicity? Br J Pharmacol, 2011. 162(6): p. 1250-8.
106. Jia, L. and X. Liu, The conduct of drug metabolism studies considered good practice (II): in vitro experiments. Curr Drug Metab, 2007. 8(8): p. 822-9.
107. Walmsley, R.M., GADD45a-GFP GreenScreen HC genotoxicity screening assay. Expert Opin Drug Metab Toxicol, 2008. 4(6): p. 827-35.
108. Wang, C., et al., Three-dimensional in vitro cancer models: a short review. Biofabrication, 2014. 6(2): p. 022001.
109. Corporation, M. Skin Hydration. 2014 02/07/2014]; Available from: http://www.mattek.com/dermal/applications/skin-hydration.
110. Zeng, F., et al., Determination of the lowest concentrations of aldehyde fixatives for completely fixing various cellular structures by real-time imaging and quantification. Histochem Cell Biol, 2013. 139(5): p. 735-49.
111. Hoareau, L., et al., Effect of centrifugation and washing on adipose graft viability: a new method to improve graft efficiency. J Plast Reconstr Aesthet Surg, 2013. 66(5): p. 712-9.
112. Clarke, J.J., et al., Summary of in vitro genetic toxicology assay results: expected and unexpected effects of recent study design modifications. Environ Mol Mutagen, 2012. 53(8): p. 631-5.
113. Fowler, P., et al., Reduction of misleading ("false") positive results in mammalian cell genotoxicity assays. I. Choice of cell type. Mutat Res, 2012. 742(1-2): p. 11-25.
114. Fowler, P., et al., Reduction of misleading ("false") positive results in mammalian cell genotoxicity assays. II. Importance of accurate toxicity measurement. Mutat Res, 2012. 747(1): p. 104-17.
115. Fowler, P., et al., Reduction of misleading ("false") positive results in mammalian cell genotoxicity assays. III: Sensitivity of human cell types to known genotoxic agents. Mutat Res Genet Toxicol Environ Mutagen, 2014.

116. Rivlin, N., et al., Mutations in the p53 Tumor Suppressor Gene: Important Milestones at the Various Steps of Tumorigenesis. Genes Cancer, 2011. 2(4): p. 466-74.
117. Moll, U.M. and O. Petrenko, The MDM2-p53 interaction. Mol Cancer Res, 2003. 1(14): p. 1001-8.
118. Meek, D.W., The p53 response to DNA damage. DNA Repair (Amst), 2004. 3(8-9): p. 1049-56.
119. Agarwal, M.L., et al., p53 controls both the G2/M and the G1 cell cycle checkpoints and mediates reversible growth arrest in human fibroblasts. Proc Natl Acad Sci U S A, 1995. 92(18): p. 8493-7.
120. Bates, S. and K.H. Vousden, p53 in signaling checkpoint arrest or apoptosis. Curr Opin Genet Dev, 1996. 6(1): p. 12-8.
121. Molecular Genetics of Cancer Part 2. 2014 [cited 2014 07/07/2014]; Available from: http://what-when-how.com/acp-medicine/molecular-genetics-of-cancer-part-2/.
122. French, J.E., et al., Loss of heterozygosity frequency at the Trp53 locus in p53-deficient (+/-) mouse tumors is carcinogen-and tissue-dependent. Carcinogenesis, 2001. 22(1): p. 99-106.
123. Emamzadah, S., L. Tropia, and T.D. Halazonetis, Crystal structure of a multidomain human p53 tetramer bound to the natural CDKN1A (p21) p53-response element. Mol Cancer Res, 2011. 9(11): p. 1493-9.
124. Morris, S.M., et al., A mutation in the p53 tumor suppressor gene of AHH-1 tk+/- human lymphoblastoid cells. Mutat Res, 1996. 356(2): p. 129-34.
125. Bhattacharya, S., et al., Toxicity testing in the 21 century: defining new risk assessment approaches based on perturbation of intracellular toxicity pathways. PLoS One, 2011. 6(6): p. e20887.
126. Guest, R.D. and J.M. Parry, P53 integrity in the genetically engineered mammalian cell lines AHH-1 and MCL-5. Mutat Res, 1999. 423(1-2): p. 39-46.
127. Dobo, K.L., et al., Extensive loss of heterozygosity accounts for differential mutation rate on chromosome 17q in human lymphoblasts. Mutagenesis, 1995. 10(1): p. 53-8.
128. Hirsch, C., et al., Nanomaterial cell interactions: are current in vitro tests reliable? Nanomedicine (Lond), 2011. 6(5): p. 837-47.
129. Sui, M., W. Liu, and Y. Shen, Nuclear drug delivery for cancer chemotherapy. J Control Release, 2011. 155(2): p. 227-36.
130. Gonzalez, L., B.J. Sanderson, and M. Kirsch-Volders, Adaptations of the in vitro MN assay for the genotoxicity assessment of nanomaterials. Mutagenesis, 2011. 26(1): p. 185-91.
131. Izak-Nau, E., et al., Altered characteristics of silica nanoparticles in bovine and human serum: the importance of nanomaterial characterization prior to its toxicological evaluation. Part Fibre Toxicol, 2013. 10(1): p. 56.
132. Skuland, T., et al., Role of size and surface area for pro-inflammatory responses to silica nanoparticles in epithelial lung cells: importance of exposure conditions. Toxicol In Vitro, 2014. 28(2): p. 146-55.
133. Lee, Y.H., et al., Cytotoxicity, oxidative stress, apoptosis and the autophagic effects of silver nanoparticles in mouse embryonic fibroblasts. Biomaterials, 2014. 35(16): p. 4706-15.

134. Lanone, S., et al., Comparative toxicity of 24 manufactured nanoparticles in human alveolar epithelial and macrophage cell lines. Part Fibre Toxicol, 2009. 6: p. 14.
135. EPA, U., ToxCast(tm).
136. EPA, U., Tox 21.
137. Bryce, S.M., J.C. Bemis, and S.D. Dertinger, In vivo mutation assay based on the endogenous Pig-a locus. Environ Mol Mutagen, 2008. 49(4): p. 256-64.
138. Frank, S.A., Dynamics of Cancer: Incidence, Inheritance, and Evolution. 2007, Princeton University Press: Princeton (NJ).
139. Greer, J.P., et al., Wintrobe's Clinical Hematology, Volume 1. Vol. 1. 2009: Lippincott, Williams and Wiltkins.
140. Centre, T.S.K.C.C. John Hopkins Medicine. 03/06/2014]; Available from: http://www.hopkinsmedicine.org/kimmel_cancer_center/types_cancer/paroxysmal_nocturnal_hemoglobinuria_PNH.html.
141. Peffault de Latour, R., Z. Amoura, and G. Socie, [Paroxysmal nocturnal hemoglobinuria]. Rev Med Interne, 2010. 31(3): p. 200-7.
142. Medicine, U.N.L.o. Genetics Home Reference. 2007 03/06/2014]; Available from: http://ghr.nlm.nih.gov/gene/PIGA.
143. Dobrovolsky, V.N., et al., The in vivo pig-a gene mutation assay, a potential tool for regulatory safety assessment. Environmental and Molecular Mutagenesis, 2010. 51(8-9): p. 825-835.
144. Dobrovolsky, V.N., et al., Detection of in vivo mutation in the Hprt and Pig-a genes of rat lymphocytes. Methods Mol Biol, 2013. 1044: p. 79-95.
145. Moran, L. Estimating the Human Mutation Rate: Biochemical Method. 2013 03/06/2014]; Available from: http://sandwalk.blogspot.co.uk/2013/03/estimating-human-human-mutatin-rate.html.
146. Luzzatto, L., PNH from mutations of another PIG gene. Blood, 2013. 122(7): p. 1099-100.
147. Shichishima, T. and H. Noji, Heterogeneity in the molecular pathogenesis of paroxysmal nocturnal hemoglobinuria (PNH) syndromes and expansion mechanism of a PNH clone. Int J Hematol, 2006. 84(2): p. 97-103.
148. Futosi, K., S. Fodor, and A. Mocsai, Reprint of Neutrophil cell surface receptors and their intracellular signal transduction pathways. Int Immunopharmacol, 2013. 17(4): p. 1185-97.
149. Schofield, L., et al., CD1d-restricted immunoglobulin G formation to GPI-anchored antigens mediated by NKT cells. Science, 1999. 283(5399): p. 225-9.
150. Xi, J., et al., In Vitro Large Scale Production of Human Mature Red Blood Cells from Hematopoietic Stem Cells by Coculturing with Human Fetal Liver Stromal Cells. BioMed Research International, 2013. 2013: p. 12.
151. Zhu, Z. and D. Huangfu, Human pluripotent stem cells: an emerging model in developmental biology. Development, 2013. 140(4): p. 705-717.
152. Ruiz-Arguelles, A. and L. Llorente, The role of complement regulatory proteins (CD55 and CD59) in the pathogenesis of autoimmune hemocytopenias. Autoimmun Rev, 2007. 6(3): p. 155-61.
153. Information, N.C.f.B. CD59 (Complement Regulatory Protein). 2014 04/06/2014]; Available from: http://www.ncbi.nlm.nih.gov/gene/966.
154. Information, N.C.f.B. CD55 Decay Accelerating Factor (DAF). 2014 04/06/2014]; Available from: http://www.ncbi.nlm.nih.gov/gene/1604.

155. Franco, R.S., Measurement of red cell lifespan and aging. Transfus Med Hemother, 2012. 39(5): p. 302-7.
156. Qin, X., et al., Generation and phenotyping of mCd59a and mCd59b double-knockout mice. Am J Hematol, 2009. 84(2): p. 65-70.
157. Rushmere, N.K., S. Tomlinson, and B.P. Morgan, Expression of rat CD59: functional analysis confirms lack of species selectivity and reveals that glycosylation is not required for function. Immunology, 1997. 90(4): p. 640-6.
158. Dertinger, S.D., Quantitative analysis of in vivo mutation at the Pig-A locus. 2012, Google Patents.
159. Dertinger, S.D., Method for measuring in vivo mutation frequency at an endogenous gene locus. 2010, Google Patents.
160. Bryce, S.M. and S.D. Dertinger, Rapid in vivo gene mutation assay based on the pig-a gene. 2012, Google Patents.
161. Kimoto, T., et al., Manifestation of Pig-a mutant bone marrow erythroids and peripheral blood erythrocytes in mice treated with N-ethyl-N-nitrosourea: direct sequencing of Pig-a cDNA from bone marrow cells negative for GPI-anchored protein expression. Mutat Res, 2011. 723(1): p. 36-42.
162. Varki A, Cummings RD, and E.J.e. al., Essentials of Glycobiology. 2nd edition. 2009, Cold Spring Harbor (NY): Cold Spring Harbor Laboratory Press.
163. Mayor, S. and H. Riezman, Sorting GPI-anchored proteins. Nat Rev Mol Cell Biol, 2004. 5(2): p. 110-20.
164. (CRL), I.C.R.L., Genetics and gene transfer in oncology. 2014.
165. Kulkarni, S. and M. Bessler, The effect of GPI-anchor deficiency on apoptosis in mice carrying a Piga gene mutation in hematopoietic cells. J Leukoc Biol, 2002. 72(6): p. 1228-33.
166. Dertinger, S.D., et al., International Pig-a gene mutation assay trial: evaluation of transferability across 14 laboratories. Environ Mol Mutagen, 2011. 52(9): p. 690-8.
167. Lynch, A.M., et al., International Pig-a gene mutation assay trial (stage III): results with N-methyl-N-nitrosourea. Environ Mol Mutagen, 2011. 52(9): p. 699-710.
168. Dertinger, S.D., et al., When pigs fly: immunomagnetic separation facilitates rapid determination of Pig-a mutant frequency by flow cytometric analysis. Mutat Res, 2011. 721(2): p. 163-70.
169. Bhalli, J.A., et al., Report on stage III Pig-a mutation assays using benzo[a]pyrene. Environ Mol Mutagen, 2011. 52(9): p. 731-7.
170. Torous, D.K., et al., In vivo flow cytometric Pig-a and micronucleus assays: highly sensitive discrimination of the carcinogen/noncarcinogen pair benzo(a)pyrene and pyrene using acute and repeated-dose designs. Environ Mol Mutagen, 2012. 53(6): p. 420-8.
171. Dobrovolsky, V.N., et al., The in vivo Pig-a gene mutation assay, a potential tool for regulatory safety assessment. Environ Mol Mutagen, 2010. 51(8-9): p. 825-35.
172. Yoon, J.H., et al., Mutation analysis of the PIG-A gene in Korean patients with paroxysmal nocturnal haemoglobinuria. J Clin Pathol, 2002. 55(6): p. 410-3.

173. Savoia, A., et al., Identification of three novel mutations in the PIG-A gene in paroxysmal nocturnal haemoglobinuria (PNH) patients. Hum Genet, 1996. 97(1): p. 45-8.
174. Kinoshita, T., Biosynthesis and deficiencies of glycosylphosphatidylinositol. Proc Jpn Acad Ser B Phys Biol Sci, 2014. 90(4): p. 130-43.
175. Rondelli, T., et al., The Frequency of Granulocytes with Spontaneous Somatic Mutations: A Wide Distribution in a Normal Human Population. PLoS ONE, 2013. 8(1): p. e54046.
176. Cammerer, Z., et al., Report on stage III Pig-a mutation assays using N-ethyl-N-nitrosourea-comparison with other in vivo genotoxicity endpoints. Environ Mol Mutagen, 2011. 52(9): p. 721-30.
177. Phonethepswath, S., et al., Erythrocyte-based Pig-a gene mutation assay: demonstration of cross-species potential. Mutat Res, 2008. 657(2): p. 122-6.
178. Nakamura, J., et al., Detection of <italic>PIGO</italic>-Deficient Cells Using Proaerolysin: A Valuable Tool to Investigate Mechanisms of Mutagenesis in the DT40 Cell System. PLoS ONE, 2012. 7(3): p. e33563.
179. Caldwell, J., Perspective on the usefulness of the mouse lymphoma assay as an indicator of a genotoxic carcinogen: ten compounds which are positive in the mouse lymphoma assay but are not genotoxic carcinogens. Teratog Carcinog Mutagen, 1993. 13(4): p. 185-90.
180. Schuler, M., et al., Need and potential value of the Pig-ain vivo mutation assay-a HESI perspective. Environ Mol Mutagen, 2011. 52(9): p. 685-9.
181. Rees, B.J., et al., Development of the in vitro Pig-A mutation assay; exploring the low dose response region for known alkylating agents MNU and EMS., in UKEMS. 2012. p. 116.
182. Dobo, K.L., D.A. Eastmond, and A.J. Grosovsky, The influence of cellular apoptotic capacity on N-nitrosodimethylamine-induced loss of heterozygosity mutations in human cells. Carcinogenesis, 1997. 18(9): p. 1701-7.
183. Storer, R.D., et al., The mouse lymphoma L5178Y Tk+/- cell line is heterozygous for a codon 170 mutation in the p53 tumor suppressor gene. Mutat Res, 1997. 373(2): p. 157-65.
184. Tennant, R.W., et al., Prediction of chemical carcinogenicity in rodents from in vitro genetic toxicity assays. Science, 1987. 236(4804): p. 933-41.
185. Clive, D., et al., A mutational assay system using the thymidine kinase locus in mouse lymphoma cells. Mutation Research/Fundamental and Molecular Mechanisms of Mutagenesis, 1972. 16(1): p. 77-87.
186. Clive, D., et al., Validation and characterization of the L5178Y/TK< sup>+/- </sup> mouse lymphoma mutagen assay system. Mutation Research/Fundamental and Molecular Mechanisms of Mutagenesis, 1979. 59(1): p. 61-108.
187. Toxicity Testing in the 21st Century: A Vision and a Strategy. 2007: The National Academies Press.
188. Fluckiger-Isler, S., et al., Assessment of the performance of the Ames II assay: a collaborative study with 19 coded compounds, in Mutat Res. 2004: Netherlands. p. 181-97.
189. Tanaka, T., et al., ATM activation and histone H2AX phosphorylation as indicators of DNA damage by DNA topoisomerase I inhibitor topotecan and during apoptosis. Cell Prolif, 2006. 39(1): p. 49-60.

190. Kuo, L.J. and L.X. Yang, Gamma-H2AX - a novel biomarker for DNA double-strand breaks. In Vivo, 2008. 22(3): p. 305-9.
191. Simpson, K., et al., The BlueScreen-384 assay as an indicator of genotoxic hazard potential in early-stage drug discovery, in J Biomol Screen. 2013: United States. p. 441-52.
192. Biosciences, B., Introduction to flow cytometry: a learning guide. 2000.
193. Zeiss. Laser Scanning Microscopes Confocal scanning, spectral imaging and topography. 2014 01/07/2014]; Available from: http://www.zeiss.co.uk/microscopy/en_gb/products/confocal-microscopes.html.
194. Amnis. Integrating flow cytometry and microscopy to advanced discovery. 2014 01/07/2014]; Available from: https://www.amnis.com/.
195. U, M. Confocal Microscopy: Basic Concepts. 2014 07/07/2014]; Available from: http://www.microscopyu.com/articles/confocal/confocalintrobasics.html.
196. Bryce, S.M., J.C. Bemis, and S.D. Dertinger, In vivo mutation assay based on the endogenous Pig-a locus. Environmental and Molecular Mutagenesis, 2008. 49(4): p. 256-264.
197. Skopek, T.R., et al., Isolation of a human lymphoblastoid line heterozygous at the thymidine kinase locus: possibility for a rapid human cell mutation assay. Biochem Biophys Res Commun, 1978. 84(2): p. 411-6.
198. Levy, J.A., M. Virolainen, and V. Defendi, Human lymphoblastoid lines from lymph node and spleen. Cancer, 1968. 22(3): p. 517-24.
199. Crespi, C.L. and W.G. Thilly, Mutation assays involving blood cells that metabolize toxic substances. 1999, Google Patents.
200. Crespi, C.L., et al., A metabolically competent human cell line expressing five cDNAs encoding procarcinogen-activating enzymes: application to mutagenicity testing. Chem Res Toxicol, 1991. 4(5): p. 566-72.
201. Xia, J.F., et al., Flavonoids as potential anti-hepatocellular carcinoma agents: recent approaches using HepG2 cell line. Drug Discov Ther, 2013. 7(1): p. 1-8.
202. Hsie, A.W., et al., Multiple-endpoint mutagenesis with Chinese hamster ovary (CHO) cells: evaluation with eight carcinogenic and non-carcinogenic compounds. Mol Toxicol, 1987. 1(2-3): p. 217-34.
203. Daniela, M., et al., Establishment of timetables for the phasing out of animal experiments for cosmetics. 2004: European Commision.
204. Strauss, G.H. and R.J. Albertini, Enumeration of 6-thioguanine-resistant peripheral blood lymphocytes in man as a potential test for somatic cell mutations arising in vivo. Mutat Res, 1979. 61(2): p. 353-79.
205. Knudson, A.G., Jr., Mutation and cancer: statistical study of retinoblastoma. Proc Natl Acad Sci U S A, 1971. 68(4): p. 820-3.
206. Wang, L., et al., Somatic single hits inactivate the X-linked tumor suppressor FOXP3 in the prostate. Cancer Cell, 2009. 16(4): p. 336-46.
207. Eastmond, D.A., et al., Mutagenicity testing for chemical risk assessment: update of the WHO/IPCS Harmonized Scheme. Mutagenesis, 2009. 24(4): p. 341-349.
208. Elespuru, R.K., et al., Current and future application of genetic toxicity assays: the role and value of in vitro mammalian assays. Toxicol Sci, 2009. 109(2): p. 172-9.

209. Agency, G.F.E. Human Biomonitoring. 2015 12/02/2015]; Available from: http://www.umweltbundesamt.de/en/topics/health/commissions-working-groups/human-biomonitoring-commission.
210. Kirkland, D., Improvements in the reliability of in vitro genotoxicity testing. Expert Opin Drug Metab Toxicol, 2011. 7(12): p. 1513-20.
211. Cao, X., et al., Quantitative dose-response analysis of ethyl methanesulfonate genotoxicity in adult gpt-delta transgenic mice. Environ Mol Mutagen, 2014. 55(5): p. 385-99.
212. Johnson, G.E., et al., Derivation of point of departure (PoD) estimates in genetic toxicology studies and their potential applications in risk assessment.
213. Slob, W., Benchmark dose and the three Rs. Part I. Getting more information from the same number of animals. Crit Rev Toxicol, 2014. 44(7): p. 557-67.
214. Project, C.-R., Dose-Response Modeling with Smoothing Splines. 2014.
215. Li, L.X., et al., Development of A Reference Dose for BDE-47, 99, and 209 Using Benchmark Dose Methods. Biomed Environ Sci, 2014. 27(9): p. 733-9.
216. Crump, K.S., A new method for determining allowable daily intakes. Fundam Appl Toxicol, 1984. 4(5): p. 854-71.
217. Dykens, J.A., L.D. Marroquin, and Y. Will, Strategies to reduce late-stage drug attrition due to mitochondrial toxicity. Expert Rev Mol Diagn, 2007. 7(2): p. 161-75.
218. Kenyon, M.O., et al., An evaluation of the sensitivity of the Ames assay to discern low-level mutagenic impurities. Regul Toxicol Pharmacol, 2007. 48(1): p. 75-86.
219. Cimino, M.C., Comparative overview of current international strategies and guidelines for genetic toxicology testing for regulatory purposes. Environ Mol Mutagen, 2006. 47(5): p. 362-90.
220. Brusick, D., Genetic Risk Estimation, in Principles of Genetic Toxicology. 1987, Plenum Publishing Corporation: New York.
221. Biosciences, B. CD59 Antibody Reagent Price List. 2014 07/10/2014]; Available from: http://www.bdbiosciences.com/eu/search?text=cd59&x=0&y=0.
222. Hu, R., et al., PIG-A mutations in normal hematopoiesis. Blood, 2005. 105(10): p. 3848-54.
223. Pickles, S., N. Arbour, and C. Vande Velde, Immunodetection of Outer Membrane Proteins by Flow Cytometry of Isolated Mitochondria. J Vis Exp, 2014(91).
224. Nelson, A.L., Antibody fragments: hope and hype. MAbs, 2010. 2(1): p. 77-83.
225. Pu, J.J., et al., The small population of PIG-A mutant cells in myelodysplastic syndromes do not arise from multipotent hematopoietic stem cells. Haematologica, 2012. 97(8): p. 1225-33.
226. Dourson, M., et al., Advancing human health risk assessment: integrating recent advisory committee recommendations. Crit Rev Toxicol, 2013. 43(6): p. 467-92.
227. Hernández, L.G., et al., Can carcinogenic potency be predicted from in vivo genotoxicity data? a meta-analysis of historical data.
228. Pegg, D.E., Principles of cryopreservation. Methods Mol Biol, 2007. 368: p. 39-57.

229. Hernandez-Campo, P.M., et al., Normal patterns of expression of glycosylphosphatidylinositol-anchored proteins on different subsets of peripheral blood cells: a frame of reference for the diagnosis of paroxysmal nocturnal hemoglobinuria. Cytometry B Clin Cytom, 2006. 70(2): p. 71-81.
230. Lin, M.W., et al., An antibody-based leukocyte-capture microarray for the diagnosis of systemic lupus erythematosus. PLoS One, 2013. 8(3): p. e58199.
231. Bizzaro, N., et al., Are anti-nucleosome antibodies a better diagnostic marker than anti-dsDNA antibodies for systemic lupus erythematosus? A systematic review and a study of metanalysis. Autoimmun Rev, 2012. 12(2): p. 97-106.
232. Nielsen, C.T., Circulating microparticles in systemic Lupus Erythematosus. Dan Med J, 2012. 59(11): p. B4548.
233. Ho, J.W., et al., Inferring differential leukocyte activity from antibody microarrays using a latent variable model. Genome Inform, 2008. 21: p. 126-37.
234. Herkel, J., et al., MHC class II-expressing hepatocytes function as antigen-presenting cells and activate specific CD4 T lymphocyutes. Hepatology, 2003. 37(5): p. 1079-85.
235. Alvarez-Barrientos, A., et al., Applications of flow cytometry to clinical microbiology. Clin Microbiol Rev, 2000. 13(2): p. 167-95.
236. Kitano, H., Systems biology: a brief overview. Science, 2002. 295(5560): p. 1662-4.
237. Le Meur, N., et al., Data quality assessment of ungated flow cytometry data in high throughput experiments. Cytometry A, 2007. 71(6): p. 393-403.
238. Tiersch, T.R. and S.S. Wachtel, Sources of error in screening by flow cytometry for the effects of environmental mutagens.
239. Biosciences, B. BD FACS Aria. 26/09/2014]; Available from: http://www.bdbiosciences.com/instruments/facsaria/.
240. Zuba-Surma, E.K., et al., The ImageStream System: a key step to a new era in imaging. Folia Histochem Cytobiol, 2007. 45(4): p. 279-90.
241. Gocke, E. and M. Wall, In vivo genotoxicity of EMS: statistical assessment of the dose response curves. Toxicol Lett, 2009. 190(3): p. 298-302.
242. Lutz, W.K., The Viracept (nelfinavir)--ethyl methanesulfonate case: a threshold risk assessment for human exposure to a genotoxic drug contamination?, in Toxicol Lett. 2009: Netherlands. p. 239-42.
243. Muller, L. and T. Singer, EMS in Viracept--the course of events in 2007 and 2008 from the non-clinical safety point of view. Toxicol Lett, 2009. 190(3): p. 243-7.
244. Martin-Ruiz, C.M., et al., Reproducibility of telomere length assessment: an international collaborative study. Int J Epidemiol, 2014.
245. Stephens, A.D., et al., ICSH recommendations for the measurement of haemoglobin F. Int J Lab Hematol, 2012. 34(1): p. 14-20.
246. Porwit, A., et al., Revisiting guidelines for integration of flow cytometry results in the WHO classification of myelodysplastic syndromes-proposal from the International/European LeukemiaNet Working Group for Flow Cytometry in MDS. Leukemia, 2014. 28(9): p. 1793-8.
247. Takacs, B.J., Characterization of functional Fc receptor material from human lymphoblastoid cell lines--I. Large scale purification and biochemical analysis. Mol Immunol, 1980. 17(10): p. 1293-314.

248. James, L.C. and D.S. Tawfik, The specificity of cross-reactivity: promiscuous antibody binding involves specific hydrogen bonds rather than nonspecific hydrophobic stickiness. Protein Sci, 2003. 12(10): p. 2183-93.
249. Buchwalow, I., et al., Non-specific binding of antibodies in immunohistochemistry: fallacies and facts. Sci Rep, 2011. 1: p. 28.
250. Biosciences, B. Fc Block Reagent. 2014 07/10/2014].
251. Technology, L. Fundamentals of Fluorescence. 2014 04/10/2014]; Available from: http://www.lifetechnologies.com/uk/en/home/references/molecular-probes-the-handbook/introduction-to-fluorescence-techniques.html.
252. Dobrovolsky, V.N., et al., Flow cytometric detection of Pig-A mutant red blood cells using an erythroid-specific antibody: application of the method for evaluating the in vivo genotoxicity of methylphenidate in adolescent rats. Environ Mol Mutagen, 2010. 51(2): p. 138-45.
253. Pfitzenmaier, J., et al., The detection and isolation of viable prostate-specific antigen positive epithelial cells by enrichment: a comparison to standard prostate-specific antigen reverse transcriptase polymerase chain reaction and its clinical relevance in prostate cancer. Urol Oncol, 2007. 25(3): p. 214-20.
254. Jaatinen, T. and J. Laine, Isolation of hematopoietic stem cells from human cord blood. Curr Protoc Stem Cell Biol, 2007. Chapter 2: p. Unit 2A.2.
255. Guez-Barber, D., et al., FACS purification of immunolabeled cell types from adult rat brain. J Neurosci Methods, 2012. 203(1): p. 10-8.
256. Maguire, O., et al., Flow Cytometry and Solid Organ Transplantation: A Perfect Match. Immunol Invest, 2014. 43(8): p. 756-774.
257. Ben-Porath, I. and R.A. Weinberg, When cells get stressed: an integrative view of cellular senescence. J Clin Invest, 2004. 113(1): p. 8-13.
258. Park, C.M., et al., Induction of p53-mediated apoptosis and recovery of chemosensitivity through p53 transduction in human glioblastoma cells by cisplatin. Int J Oncol, 2006. 28(1): p. 119-25.
259. Thilly, W.G., Assay for mutagenesis in diploid human lymphoblasts. 1976, Massachusetts Institute Of Technology: USA.
260. Simson, E., Wallace Coulter's life and his impact on the world. Int J Lab Hematol, 2013. 35(3): p. 230-6.
261. Technologies, L. Flow Cytometry Counting Beads. 2014 15/10/14]; Available from: https://www.lifetechnologies.com/uk/en/home/life-science/cell-analysis/flow-cytometry/flow-cytometry-calibration/flow-cytometer-cell-counting-beads.html.
262. Sarkar, S., Molecular Models of Life: Philosophical Papers on Molecular Biology. 2005: Massachusetts Institute of Technology.
263. Gollapudi, B.B., et al., Quantitative approaches for assessing dose-response relationships in genetic toxicology studies. Environ Mol Mutagen, 2013. 54(1): p. 8-18.
264. Thomas, A.D., et al., Influence of DNA repair on nonlinear dose-responses for mutation. Toxicol Sci, 2013. 132(1): p. 87-95.
265. Genomes, K.K.E.o.G.a. Glycosylphosphatidylinositol(GPI)-anchor biosynthesis - Homo sapiens (human). 15/10/2014]; Available from: http://www.genome.jp/kegg-bin/show_pathway?hsa00563.
266. Collection, A.T.C. Long term storage of cultures. 2011 15/10/2014]; Available from: http://atcc.custhelp.com/app/answers/detail/a_id/976/~/long-term-storage-of-cultures.

267. Nonami, H. and E.D. Schulze, Cell water potential, osmotic potential, and turgor in the epidermis and mesophyll of transpiring leaves. Planta, 1989. 177(1): p. 35-46.
268. Reuter, M., et al., Mechanosensitive channels and bacterial cell wall integrity: does life end with a bang or a whimper? Journal of The Royal Society Interface, 2014. 11(91).
269. Moeckel, G.W., Hypertonic stress and cell death. Focus on "Multiple cell death pathways are independently activated by lethal hypertonicity in renal epithelial cells", in Am J Physiol Cell Physiol. 2013: United States. p. C1009-10.
270. Ghosh, A., P.C. Keng, and P.A. Knauf, Hypertonicity induced apoptosis in HL-60 cells in the presence of intracellular potassium. Apoptosis, 2007. 12(7): p. 1281-8.
271. Morris, G.J., et al., Effect of osmotic stress on the ultrastructure and viability of the yeast Saccharomyces cerevisiae. J Gen Microbiol, 1986. 132(7): p. 2023-34.
272. Technologies, L. 7-Aminoactinomycin D. 2014 17/10/2014]; Available from: http://www.lifetechnologies.com/order/catalog/product/A1310.
273. Technologies, L. Annexin V Alexa Fluor 488. 2014 17/10/2014]; Available from: http://www.lifetechnologies.com/uk/en/home/references/protocols/cell-and-tissue-analysis/flow-cytometry-protocol/apoptosis/alexa-fluor-488-annexin-v-dead-cell-apoptosis-kit.html.
274. Allen, R.T., W.J. Hunter, 3rd, and D.K. Agrawal, Morphological and biochemical characterization and analysis of apoptosis. J Pharmacol Toxicol Methods, 1997. 37(4): p. 215-28.
275. Fadok, V.A., et al., Exposure of phosphatidylserine on the surface of apoptotic lymphocytes triggers specific recognition and removal by macrophages. J Immunol, 1992. 148(7): p. 2207-16.
276. Elmore, S., Apoptosis: a review of programmed cell death. Toxicol Pathol, 2007. 35(4): p. 495-516.
277. Dearfield, K.L. and M.M. Moore, Use of genetic toxicology information for risk assessment. Environ Mol Mutagen, 2005. 46(4): p. 236-45.
278. Mahadevan, B., et al., Genetic toxicology in the 21st century: reflections and future directions. Environ Mol Mutagen, 2011. 52(5): p. 339-54.
279. Mauthe, R.J., et al., The syrian hamster embryo (SHE) cell transformation assay: review of the methods and results. Toxicol Pathol, 2001. 29 Suppl: p. 138-46.
280. Dobrovolsky, V.N., et al., Monitoring humans for somatic mutation in the endogenous PIG-a gene using red blood cells. Environ Mol Mutagen, 2011. 52(9): p. 784-94.
281. Bagamery, K., et al., Are platelets activated after a rapid, one-step density gradient centrifugation? Evidence from flow cytometric analysis. Clin Lab Haematol, 2005. 27(1): p. 75-7.
282. Jenkins, G.J., et al., Genotoxic thresholds, DNA repair, and susceptibility in human populations. Toxicology, 2010. 278(3): p. 305-10.
283. Negishi, K., D. Loakes, and R.M. Schaaper, Saturation of DNA mismatch repair and error catastrophe by a base analogue in Escherichia coli. Genetics, 2002. 161(4): p. 1363-71.

284. Ahluwalia, D. and R.M. Schaaper, Hypermutability and error catastrophe due to defects in ribonucleotide reductase. Proc Natl Acad Sci U S A, 2013. 110(46): p. 18596-601.
285. Weng, M.-w., et al., Repair of mitomycin C mono- and interstrand cross-linked DNA adducts by UvrABC: a new model. Nucleic Acids Research, 2010. 38(20): p. 6976-6984.
286. Okamoto, S., et al., Impact of DNA repair pathways on the cytotoxicity of piperlongumine in chicken DT40 cell-lines. Genes Cancer, 2014. 5(7-8): p. 285-92.
287. Brusehafer, K., et al., Chromosome breakage induced by the genotoxic agents mitomycin C and cytosine arabinoside is concentration and p53 dependent. Toxicol Sci, 2014. 140(1): p. 94-102.
288. Mahmood, T. and P.C. Yang, Western blot: technique, theory, and trouble shooting. N Am J Med Sci, 2012. 4(9): p. 429-34.
289. Goldring, J.P., Protein quantification methods to determine protein concentration prior to electrophoresis. Methods Mol Biol, 2012. 869: p. 29-35.
290. Heid, C.A., et al., Real time quantitative PCR. Genome Res, 1996. 6(10): p. 986-94.
291. Technologies, L. TaqMan® Chemistry vs. SYBR® Chemistry for Real-Time PCR. 2014 24/10/2014].
292. Schwartz, J.L., et al., Baseline levels of chromosome instability in the human lymphoblastoid cell TK6. Mutagenesis, 2004. 19(6): p. 477-82.
293. Geraghty, R.J., et al., Guidelines for the use of cell lines in biomedical research. Br J Cancer, 2014. 111(6): p. 1021-46.
294. Ruiz-Delgado, G.J., et al., Abnormalities in the expression of CD55 and CD59 surface molecules on peripheral blood cells are not specific to paroxysmal nocturnal hemoglobinuria. Hematology, 2009. 14(1): p. 33-7.
295. Baldini, M. and I. Pannacciulli, The maturation rate of reticulocytes. Blood, 1960. 15: p. 614-29.
296. Veninga, H., et al., A novel role for CD55 in granulocyte homeostasis and anti-bacterial host defense. PLoS One, 2011. 6(10): p. e24431.
297. Wang, Y., et al., Long-term cultured mesenchymal stem cells frequently develop genomic mutations but do not undergo malignant transformation. Cell Death Dis, 2013. 4: p. e950.
298. Yentsch, C.M.a.C.L.a.P.D.A., Flow Cytometry and Cell Sorting : Problems and Promises for Biological Ocean Science Research. 2013: p. 141--155.
299. Macey, M.G., Flow Cytometry Principles and Applications. 2007, Totowa, NJ, USA: Humana Press Inc.
300. Hawley, T.S. and R.G. Hawley, Flow Cytometry Protocols. 2011, NJ, USA: Humana Press.
301. Kruger, C.T., M. Hofmann, and A. Hartwig, The in vitro PIG-A gene mutation assay: mutagenicity testing via flow cytometry based on the glycosylphosphatidylinositol (GPI) status of TK6 cells. Arch Toxicol, 2014.
302. Kimoto, T., et al., Further development of the rat Pig-a mutation assay: measuring rat Pig-a mutant bone marrow erythroids and a high throughput assay for mutant peripheral blood reticulocytes. Environ Mol Mutagen, 2011. 52(9): p. 774-83.

303. Peghini, P.E. and J. Fehr, Clinical evaluation of an aerolysin-based screening test for paroxysmal nocturnal haemoglobinuria. Cytometry B Clin Cytom, 2005. 67(1): p. 13-8.
304. Howard, S.P., et al., Nucleotide sequence of the gene for the hole-forming toxin aerolysin of Aeromonas hydrophila. J Bacteriol, 1987. 169(6): p. 2869-71.
305. Brodsky, R.A., et al., Improved Detection and Characterization of Paroxysmal Nocturnal Hemoglobinuria Using Fluorescent Aerolysin. Am J Clin Pathol, 2000. 114(3): p. 459-66.
306. Davies, R.L., et al., Development of a human cell line by selection and drug-metabolizing gene transfection with increased capacity to activate promutagens. Carcinogenesis, 1989. 10(5): p. 885-91.
307. Commission, E. EURL-ECVAM. 2014 27/11/2014]; Available from: https://eurl-ecvam.jrc.ec.europa.eu/.
308. (WHO), W.H.O. IARC. 2014 27/11/2014]; Available from: http://www.iarc.fr/.
309. Zhan, D.J., et al., Characterization of DNA adducts in Chinese hamster ovary cells treated with mutagenic doses of 1- and 3-nitrosobenzo[a]pyrene and the trans-7,8-diol-anti-9,10-epoxides of 1- and 3-nitrobenzo[a]pyrene. Mutat Res, 1997. 379(1): p. 43-52.
310. Hakura, A., et al., Use of human liver S9 in the Ames test: assay of three procarcinogens using human S9 derived from multiple donors. Regul Toxicol Pharmacol, 2003. 37(1): p. 20-7.
311. Hull, A.W., H.E. F., and F.R. Elder, The Dynatron Detector -a new heterodyne receiver for continuous and modulated waves, P.o.t.I.o.R. Engineers, Editor. 1922. p. 320-343.
312. authors, Handbook of Biological Confocal Microscopy 2006, Berlin: Springer.
313. Janesick, J.R., Scientific Charged Coupled Devices. 2001, Washington: SPIE - The International Society for Optical Engineering.
314. Amnis, Amnis and the ImageStream® System - Frequently Asked Questions 2009.
315. Cytometry, A., Electronics. 2010.
316. Kang, K., et al., Flow cytometric fluorescence pulse width analysis of etoposide-induced nuclear enlargement in HCT116 cells. Biotechnol Lett, 2010. 32(8): p. 1045-52.
317. Wersto, R.P., et al., Doublet discrimination in DNA cell-cycle analysis. Cytometry, 2001. 46(5): p. 296-306.
318. Bohmer, R.M., E. Bandala-Sanchez, and L.C. Harrison, Forward light scatter is a simple measure of T-cell activation and proliferation but is not universally suited for doublet discrimination. Cytometry A, 2011. 79(8): p. 646-52.
319. Lang, F. and E.K. Hoffmann, Role of ion transport in control of apoptotic cell death. Compr Physiol, 2012. 2(3): p. 2037-61.
320. Savage, W.J., et al., Glycosylphosphatidylinositol-anchored protein deficiency confers resistance to apoptosis in PNH. Exp Hematol, 2009. 37(1): p. 42-51.
321. Bouillon, M., et al., Lipid raft-dependent and -independent signaling through HLA-DR molecules. J Biol Chem, 2003. 278(9): p. 7099-107.

322. Trowsdale, J., et al., Sequences related to HLA-DR alpha chain on human chromosome 6: restriction enzyme polymorphism detected with DC alpha chain probes. Proc Natl Acad Sci U S A, 1983. 80(7): p. 1972-6.
323. Mangalam, A.K., V. Taneja, and C.S. David, HLA class II molecules influence susceptibility versus protection in inflammatory diseases by determining the cytokine profile. J Immunol, 2013. 190(2): p. 513-8.
324. Yamazaki, F., et al., Successful treatment of metastatic rhabdomyosarcoma with radiochemotherapy and allogeneic hematopoietic stem cell transplantation. Jpn J Clin Oncol, 2014.
325. Taneja, V. and C.S. David, HLA class II transgenic mice as models of human diseases. Immunol Rev, 1999. 169: p. 67-79.
326. Franca, L.T., E. Carrilho, and T.B. Kist, A review of DNA sequencing techniques. Q Rev Biophys, 2002. 35(2): p. 169-200.
327. Quinones-Mateu, M.E., et al., Deep sequencing: becoming a critical tool in clinical virology. J Clin Virol, 2014. 61(1): p. 9-19.
328. Yadav, N.K., et al., Next generation sequencing: potential and application in drug discovery. ScientificWorldJournal, 2014. 2014: p. 802437.
329. Nature. $1,000 Genome. 2015 20/05/2015]; Available from: http://www.nature.com/news/is-the-1-000-genome-for-real-1.14530.
330. Bromberg, Y., Building a genome analysis pipeline to predict disease risk and prevent disease. J Mol Biol, 2013. 425(21): p. 3993-4005.
331. Wang, S. and J. Xing, A Primer for Disease Gene Prioritization Using Next-Generation Sequencing Data. Genomics & Informatics, 2013. 11(4): p. 191-199.
332. Alkan, C., et al., Personalized copy number and segmental duplication maps using next-generation sequencing, in Nat Genet. 2009: United States. p. 1061-7.
333. Li, H. and R. Durbin, Fast and accurate short read alignment with Burrows-Wheeler transform, in Bioinformatics. 2009: England. p. 1754-60.
334. Ng, S.B., et al., Targeted capture and massively parallel sequencing of 12 human exomes, in Nature. 2009: England. p. 272-6.
335. McKenna, A., et al., The Genome Analysis Toolkit: a MapReduce framework for analyzing next-generation DNA sequencing data, in Genome Res. 2010: United States. p. 1297-303.
336. Oulas, A., et al., Metagenomics: tools and insights for analyzing next-generation sequencing data derived from biodiversity studies, in Bioinform Biol Insights. 2015: New Zealand. p. 75-88.
337. Altmann, A., et al., A beginners guide to SNP calling from high-throughput DNA-sequencing data. Hum Genet, 2012. 131(10): p. 1541-54.
338. Pabinger, S., et al., A survey of tools for variant analysis of next-generation genome sequencing data, in Brief Bioinform. 2014: England. p. 256-78.
339. Berkeley Drosophila Genome Project. 28/07/2014]; Available from: http://www.fruitfly.org/seq_tools/promoter.html.
340. Denmark, C.f.b.s.a.-T.U.o. Promoter 2.0 Prediction Server. 2014 28/07/2014]; Available from: http://www.cbs.dtu.dk/services/Promoter/.
341. Berry, S. 2014 28/07/2014]; Available from: http://www.softberry.com/.
342. Technologies, A. 2014 28/07/2014]; Available from: https://earray.chem.agilent.com/suredesign/.
343. Burrows Wheeler A.igner (BWA). 02/03/2015]; Available from: http://bio-bwa.sourceforge.net/.

344. SAMTools. 02/03/2015]; Available from: http://samtools.sourceforge.net/.
345. VarScan. 02/03/2015]; Available from: http://varscan.sourceforge.net/.
346. Rieger, A.M., et al., Modified Annexin V/Propidium Iodide Apoptosis Assay For Accurate Assessment of Cell Death, in J Vis Exp. 2011.
347. Fu, D., J.A. Calvo, and L.D. Samson, SERIES: Genomic instability in cancer Balancing repair and tolerance of DNA damage caused by alkylating agents. Nat Rev Cancer. 12(2): p. 104-20.
348. Antonenko, Y.N., et al., Penetrating Cations Enhance Uncoupling Activity of Anionic Protonophores in Mitochondria, in PLoS One, H.W. van Veen, Editor. 2013: San Francisco, USA.
349. Grundlingh, J., et al., 2,4-Dinitrophenol (DNP): A Weight Loss Agent with Significant Acute Toxicity and Risk of Death, in J Med Toxicol. 2011: New York. p. 205-12.
350. Johnson, G.E., et al., Non-linear dose-response of DNA-reactive genotoxins: recommendations for data analysis. Mutat Res, 2009. 678(2): p. 95-100.
351. Dertinger, S.D., et al., Human erythrocyte PIG-A assay: An easily monitored index of gene mutation requiring low volume blood samples. Environ Mol Mutagen, 2014.
352. van Zanten, T.S., et al., Hotspots of GPI-anchored proteins and integrin nanoclusters function as nucleation sites for cell adhesion. Proc Natl Acad Sci U S A, 2009. 106(44): p. 18557-62.
353. Rixe, O. and T. Fojo, Is cell death a critical end point for anticancer therapies or is cytostasis sufficient? Clin Cancer Res, 2007. 13(24): p. 7280-7.
354. Maecker, H.T. and J. Trotter, Flow cytometry controls, instrument setup, and the determination of positivity. Cytometry A, 2006. 69(9): p. 1037-42.
355. Carey, J.L., P.J. McCoy, and D.F. Keren, Flow Cytometry in Clinical Diagnosis (4th edition). 2007: American Society for Clinical Pathology.
356. Kinnunen, M., et al., Effect of the size and shape of a red blood cell on elastic light scattering properties at the single-cell level. Biomed Opt Express, 2011. 2(7): p. 1803-14.
357. Garcia-Belinchon, M., et al., An Early and Robust Activation of Caspases Heads Cells for a Regulated Form of Necrotic-like Cell Death. J Biol Chem, 2015.
358. Peruzzi, B., et al., The use of PIG-A as a sentinel gene for the study of the somatic mutation rate and of mutagenic agents in vivo. Mutat Res, 2010. 705(1): p. 3-10.
359. Fredriksson, N.J., et al., Systematic analysis of noncoding somatic mutations and gene expression alterations across 14 tumor types. Nat Genet, 2014. 46(12): p. 1258-1263.
360. INC, D. Scientific Notes/Human Genome. 2013 20/05/2015]; Available from: https://wiki.dnanexus.com/Scientific-Notes/human-genome#The-%22hg19%22-conventions-(by-UCSC).
361. (UCSC), U.o.S.C. UCSC genome bioinformatics browser 2014 28/07/2014]; Available from: https://genome.ucsc.edu/.
362. Burrows Wheeler Aligner (BWA). 02/03/2015]; Available from: http://bio-bwa.sourceforge.net/.
363. Lundberg, D.S., et al., Practical innovations for high-throughput amplicon sequencing. Nat Meth, 2013. 10(10): p. 999-1002.
364. Scale, C.T.P.H.B.m.o.a.E. Human Biomonitoring. 12/02/2015]; Available from: http://www.eu-hbm.info/cophes/human-biomonitoring.

365. Organisation, W.H., Biomarkers and Human Biomonitoring. 2011.
366. REACH-ECHA. REACH. [cited 2015 21/07/2015]; Available from: http://echa.europa.eu/regulations/reach.
367. Association, E.P.S. EPSA. [cited 2015 21/07/2015]; Available from: http://www.epsa-online.org/index.php.
368. Porta, M., A Dictionary of Epidemiology. 2014: Oxford University Press.
369. Doll, R. and A.B. Hill, The mortality of doctors in relation to their smoking habits: a preliminary report: (Reprinted from Br Med J 1954:ii;1451-5), in Bmj. 2004. p. 1529-33.
370. Doll, R. and A.B. Hill, Lung Cancer and Other Causes of Death in Relation to Smoking. Br Med J, 1956. 2(5001): p. 1071-81.
371. Pfeifer, G.P. and P. Hainaut, On the origin of G --> T transversions in lung cancer. Mutat Res, 2003. 526(1-2): p. 39-43.
372. Pfeifer, G.P., et al., Tobacco smoke carcinogens, DNA damage and p53 mutations in smoking-associated cancers. Oncogene, 2002. 21(48): p. 7435-51.
373. Brusick, D., Principles of Genetic Toxicology. 1987: Springer Science & Business Media.
374. Sen, D., Working with asbestos and the possible health risks, in Occup Med (Lond). 2015, (c) Crown copyright 2015. p. 6-14.
375. Lutz, W.K. and R.W. Lutz, Statistical model to estimate a threshold dose and its confidence limits for the analysis of sublinear dose-response relationships, exemplified for mutagenicity data. Mutat Res, 2009. 678(2): p. 118-22.
376. Agency, U.S.E.P. US-EPA PBTs. [cited 2015 21/07/2015]; Available from: http://www.epa.gov/pbt/.
377. Lovreglio, P., et al., Evaluation of chromosome aberration and micronucleus frequencies in blood lymphocytes of workers exposed to low concentrations of benzene. Mutat Res Genet Toxicol Environ Mutagen, 2014. 770: p. 55-60.
378. Bolognesi, C., et al., Clinical application of micronucleus test: a case-control study on the prediction of breast cancer risk/susceptibility. PLoS One, 2014. 9(11): p. e112354.
379. Speit, G., J. Zeller, and S. Neuss, The in vivo or ex vivo origin of micronuclei measured in human biomonitoring studies. Mutagenesis, 2011. 26(1): p. 107-110.
380. Society, E.M.a.G. 2015 EMGS - US. 2015 [cited 2015 21/07/2015]; Theme for a session - Mutagenicity as an apical end point within carcinogenesis]. Available from: http://www.emgs-us.org/AM2015/agendamon.asp.
381. Speit, G. and O. Schmid, Local genotoxic effects of formaldehyde in humans measured by the micronucleus test with exfoliated epithelial cells. Mutat Res, 2006. 613(1): p. 1-9.
382. Holland, N., et al., The micronucleus assay in human buccal cells as a tool for biomonitoring DNA damage: the HUMN project perspective on current status and knowledge gaps. Mutat Res, 2008. 659(1-2): p. 93-108.
383. Stopper, H., et al., Pilot study for comparison of reticulocyte-micronulei with lymphocyte-micronuclei in human biomonitoring. Toxicol Lett, 2005. 156(3): p. 351-60.
384. Dertinger, S.D., et al., Micronucleated CD71-positive reticulocytes: a blood-based endpoint of cytogenetic damage in humans. Mutat Res, 2003. 542(1-2): p. 77-87.

385. Flanagan, J.M., et al., Assessment of genotoxicity associated with hydroxyurea therapy in children with sickle cell anemia. Mutat Res, 2010. 698(1-2): p. 38-42.
386. Simpson, A.J., The natural somatic mutation frequency and human carcinogenesis. Adv Cancer Res, 1997. 71: p. 209-40.
387. Araten, D.J., et al., A quantitative measurement of the human somatic mutation rate. Cancer Res, 2005. 65(18): p. 8111-7.
388. Brar, J.E. and R.J. Quigg, Complement activation in the tubulointerstitium: AKI, CKD, and in between. Kidney Int, 2014. 86(4): p. 663-666.
389. Janeway, C.A.J., et al., Immunobiology, 5th editionThe Immune System in Health and Disease. 2001, New York: Garland Science.
390. Joshua, D., et al., Peripheral blood lymphocyte surface antigen expression and prognosis in myeloma: Australian Leukaemia Study Group Study. Leuk Lymphoma, 1994. 14(3-4): p. 303-9.
391. Institute, N.C. Blood Cell Lineages. [cited 2015 21/07/2015]; Available from: http://training.seer.cancer.gov/leukemia/anatomy/lineage.html.
392. Collins, A.R., et al., The comet assay: topical issues. Mutagenesis, 2008. 23(3): p. 143-151.
393. Law, P.S.-A.a. Genetic Data: The Future of Toxic Tort Litigation. 2013 12/02/2015].
394. Marchant, G.E. Genetic Data in Toxic Tort Litigation. ~2014 12/02/2015]; Available from: http://www.americanbar.org/content/dam/aba/administrative/litigation/materials/2014_sac/2014_sac/genetic_data_in_toxic_tort_litigation.authcheckdam.pdf.
395. Hanahan, D. and R.A. Weinberg, The hallmarks of cancer. Cell, 2000. 100(1): p. 57-70.
396. Kodack, D.P., et al., Emerging Strategies for Treating Brain Metastases from Breast Cancer. Cancer Cell, 2015. 27(2): p. 163-175.
397. (NHS), N.H.S. Rheumatoid Arthritis Treatment. 19/08/2015]; Available from: http://www.nhs.uk/Conditions/Rheumatoid-arthritis/Pages/Treatment.aspx.
398. Mittal, M., et al., Reactive oxygen species in inflammation and tissue injury. Antioxid Redox Signal, 2014. 20(7): p. 1126-67.
399. Ruiz-Laguna, J. and C. Pueyo, Hydrogen peroxide and coffee induce G:C-->T:A transversions in the lacI gene of catalase-defective Escherichia coli. Mutagenesis, 1999. 14(1): p. 95-102.
400. Haboubi, H., et al. 50 Shades of Pig-A: Investigating the Issues in Validating the Ex Vivo Pig-A Assay. in ENVIRONMENTAL AND MOLECULAR MUTAGENESIS. 2014. WILEY-BLACKWELL 111 RIVER ST, HOBOKEN 07030-5774, NJ USA.
401. Haboubi, H., et al. Can the Pig-A gene mutation assay be used as a biomarker to predict the risk of developing Oesophageal Adenocarcinoma? in MUTAGENESIS. 2014. OXFORD UNIV PRESS GREAT CLARENDON ST, OXFORD OX2 6DP, ENGLAND.
402. Haboubi, H., et al. Investigating the Pig-A Gene Mutation Assay As a Potential Biomarker in Patients with Esophageal Cancer: A Pilot Study. in ENVIRONMENTAL AND MOLECULAR MUTAGENESIS. 2014. WILEY-BLACKWELL 111 RIVER ST, HOBOKEN 07030-5774, NJ USA.
403. Lakowicz, J.R., Principles of Fluorescence Spectroscopy. 2006: Springer.

404. Technologies, L. Fluorescence Fundamentals. 2015 12/02/2015]; Available from: http://www.lifetechnologies.com/uk/en/home/references/molecular-probes-the-handbook/introduction-to-fluorescence-techniques.html.
405. Ghauharali, R.I. and G.J. Brakenhoff, Fluorescence photobleaching-based image standardization for fluorescence microscopy. J Microsc, 2000. 198 (Pt 2): p. 88-100.
406. Biolegend. FITC anti-human CD235a (Glycophorin A) Antibody. 2010 12/02/2015]; Available from: http://www.biolegend.com/fitc-anti-human-cd235a-glycophorin-a-antibody-6701.html.
407. Fujimi, A., et al., Anti-erythropoietin receptor antibody-associated pure red cell aplasia accompanied by Coombs-negative autoimmune hemolytic anemia in a patient with T cell/histiocyte-rich large B cell lymphoma. Int J Hematol, 2014. 100(5): p. 490-3.
408. Portillo, M.E., et al., Sonication versus vortexing of implants for diagnosis of prosthetic joint infection. J Clin Microbiol, 2013. 51(2): p. 591-4.
409. Abcam. Ten tips for successful flow cytometry results. 2011 16/02/2015]; Available from: http://www.abcam.com/blog/print.cfm?id=68C85067-5056-9C00-30B85B57B15E7F72.
410. Clinical Methods: The History, Physical, and Laboratory Examinations. 3rd edition. 1990, Boston: Butterworths.
411. Ney, P.A., Normal and disordered reticulocyte maturation. Curr Opin Hematol, 2011. 18(3): p. 152-7.
412. Biosciences, B. RETIC Count(tm). 2014 16/02/2015].
413. Technologies, L. Nonfixable Viability Dyes for Flow Cytometry. 16/02/2015]; Available from: http://www.lifetechnologies.com/uk/en/home/life-science/cell-analysis/flow-cytometry/cell-health-and-viability-assays-for-flow-cytometry/cell-viability-assays-for-flow-cytometry/flow-nonfixable-viability-dyes.html?s_kwcid=AL!3652!3!59699571744!b!!g!!+sytox&ef_id=VLkucAAAAVG1JCgV:20150216154547:s.
414. Clark, J. The effect of temperature on reaction rates. 16/02/2015]; Available from: http://www.chemguide.co.uk/physical/basicrates/temperature.html.
415. Abcam. TROUBLE SHOOTING TIPS - FLOW CYTOMETRY. 16/02/2015]; Available from: http://www.abcam.com/ps/pdf/protocols/flow_troubleshooting.pdf.
416. School, Y.M. Flow cytometry (FACS) staining protocol (Cell surface staining). 2011 16/02/2015]; Available from: http://medicine.yale.edu/labmed/cellsorter/protocols/analystain.aspx.
417. Agency, M.a.H.P.R. Good laboratory practice (GLP) for safety tests on chemicals. 2014 16/02/2015]; Available from: https://www.gov.uk/good-laboratory-practice-glp-for-safety-tests-on-chemicals.
418. Nauseef, W.M., How human neutrophils kill and degrade microbes: an integrated view. Immunol Rev, 2007. 219: p. 88-102.
419. Allen, L.A. and R.L. McCaffrey, To activate or not to activate: distinct strategies used by Helicobacter pylori and Francisella tularensis to modulate the NADPH oxidase and survive in human neutrophils. Immunol Rev, 2007. 219: p. 103-17.
420. Ssemaganda, A., et al., Characterization of neutrophil subsets in healthy human pregnancies. PLoS One, 2014. 9(2): p. e85696.

421. Stocks, S.C. and M.A. Kerr, Stimulation of neutrophil adhesion by antibodies recognizing CD15 (Le(X)) and CD15-expressing carcinoembryonic antigen-related glycoprotein NCA-160. Biochem J, 1992. 288(Pt 1): p. 23-7.
422. Albrechtsen, M. and M.A. Kerr, Characterization of human neutrophil glycoproteins expressing the CD15 differentiation antigen (3-fucosyl-N-acetyllactosamine). Br J Haematol, 1989. 72(3): p. 312-20.
423. Chastain, P.D., et al., Abasic sites preferentially form at regions undergoing DNA replication. The FASEB Journal, 2010. 24(10): p. 3674-3680.
424. eBiosciences. 1X RBC Lysis Buffer. 16/02/2015]; Available from: http://www.ebioscience.com/media/pdf/tds/00/00-4333.pdf.
425. Education, W. RBC Lysing Solutions and Cell Lysing Procedure. 16/02/2015]; Available from: https://depts.washington.edu/flowlab/Cell%20Analysis%20Facility/RBC%20Lysing%20Solutions%20and%20Cell%20Lysing%20Procedure.pdf.
426. Chernyshev, A.V., et al., Erythrocyte lysis in isotonic solution of ammonium chloride: theoretical modeling and experimental verification. J Theor Biol, 2008. 251(1): p. 93-107.
427. Pan, Q., et al., Effects of red blood cell lysing solutions on the detection of peripheral basophils of healthy normals and SLE patients by flow cytometry. J Immunoassay Immunochem, 2014. 35(4): p. 368-77.
428. Matsumura, T., et al., Neutral endopeptidase 24.11 in neutrophils modulates protective effects of natriuretic peptides against neutrophils-induced endothelial cytotoxity. Journal of Clinical Investigation, 1996. 97(10): p. 2192-2203.
429. Albertine, K.H., et al., Morphological analysis of the activation of adherent neutrophils in vitro. Tissue Cell, 1988. 20(4): p. 519-30.
430. Lee, D. and M.R. King, Shear-Induced Capping of L-Selectin on the Neutrophil Surface During Centrifugation. J Immunol Methods, 2007. 328(1-2): p. 97-105.
431. Peterson, B.W., et al., Bacterial Cell Surface Damage Due to Centrifugal Compaction. Appl Environ Microbiol, 2012. 78(1): p. 120-5.
432. Pembrey, R.S., K.C. Marshall, and P. Schneider Ré, Cell Surface Analysis Techniques: What Do Cell Preparation Protocols Do to Cell Surface Properties? Appl Environ Microbiol, 1999. 65(7): p. 2877-94.
433. Carmona-Rivera, C. and M.J. Kaplan, Low density granulocytes: a distinct class of neutrophils in systemic autoimmunity. Semin Immunopathol, 2013. 35(4): p. 455-63.
434. Fu, J., M.C. Tobin, and L.L. Thomas, Neutrophil-like low-density granulocytes are elevated in patients with moderate to severe persistent asthma. Ann Allergy Asthma Immunol, 2014. 113(6): p. 635-640 e2.
435. Miltenyi. QuadroMACS Separator and Starting Kit. 2015 06/03/2015]; Available from: http://www.miltenyibiotec.com/en/products-and-services/macs-cell-separation/manual-cell-separation/separators/quadromacs-separator-and-starting-kits.aspx.
436. Quantitative Modeling in Toxicology. 2010: Wiley.
437. Teubner, W., et al., Computer models versus reality: how well do in silico models currently predict the sensitization potential of a substance. Regul Toxicol Pharmacol, 2013. 67(3): p. 468-85.

438. Dobrovolsky, V.N., et al., CD48-deficient T-lymphocytes from DMBA-treated rats have de novo mutations in the endogenous Pig-a gene. Environ Mol Mutagen, 2015.
439. Revollo, J., et al., Confirmation of Pig-a mutation in flow cytometry-identified CD48-deficient T-lymphocytes from F344 rats. Mutagenesis, 2015. 30(3): p. 315-24.
440. Satoh, T., et al., Production of reactive oxygen species and release of L-glutamate during superoxide anion-induced cell death of cerebellar granule neurons. J Neurochem, 1998. 70(1): p. 316-24.
441. Zamai, L., et al., Optimal detection of apoptosis by flow cytometry depends on cell morphology. Cytometry, 1993. 14(8): p. 891-7.
442. Nicklas, J.A., E.W. Carter, and R.J. Albertini, Both PIGA and PIGL mutations cause GPI-a deficient isolates in the Tk6 cell line. Environ Mol Mutagen, 2015.
443. Rakoff-Nahoum, S., Why Cancer and Inflammation? The Yale Journal of Biology and Medicine, 2006. 79(3-4): p. 123-130.
444. UK, C.R. Why is early diagnosis important. 2015 [cited 2015 17/07/2015].

Contents

Appendix

All cellular cultures utilised during the undertaking of this Ph.D. were established and subsequent work undertaken in an aseptic manor; fluorescence staining was carried out in the absence of direct light, all antibody incubations were undertaken in a temperature controlled environment, preventing internalisation of cellular receptors, and thorough decontamination protocols were in place to prevent contamination. Unless otherwise stated, all culture work was carried out within a class 2 safety cabinet and all necessary safety precautions were taken with regards to the work embodied within this chapter. Initially, antibody optimisation was undertaken to increase confidence in the ensuring data generated utilising the in vitro *PIG-A* assay platform, enrichment methodologies were investigated to improve assay sensitivity, and model mutagen exposure followed for preliminary assay assessment. Following establishment of a functioning assay design, validation of putative *PIG-A* mutant events ensued in which additional high throughput techniques such as Amnis Image Stream ™ were implored to facilitate investigation.

Chapter 3: The Concept and Development of an early stage in vitro *PIG-A* gene mutation assay

3.2 Materials and Methods

3.2.2 Enrichment Strategies to Optimise CD59 Expression with the Human Lymphoblastoid TK6 Cell Line

3.2.2.1 Dynabead ® Enrichment and Subsequent Magnetic Bead Retrieval of the TK6 cells Expressing the CD59 Cellular Surface Antigen

DSB-X™ Biotin Protein Labelling Kit (Cat No. D-20655, Molecular Probes, Life™ Technologies, Paisley, UK) was utilised in order to fully biotinylate an anti-human anti-GPI-AP fluorescently labelled antibody. Prior to biotinylation, kit contents were stored at 2-4°C as well as fresh PBS pH 7.2 as well as 1M sodium bicarbonate were prepared as follows. PBS; 0.36 g of $NaH_2PO_4*H_20$, 1.02 g of Na_2HPO_4 and 8.77 g of NaCl were dissolved in 750 mL of deionized water. pH was initially measured and adjusted to 7.2 using 1M NaOH and/or 1M HCL stock solutions, final volume adjusted to 1 L with dH_20. 1M sodium bicarbonate; 8.4 g of $NaHCO_3$ (molecular mass 84 g) was dissolved in 100 mL of dH_20.

200 µL of a 0.5mg/mL antibody solution along with 20 µL of freshly prepared 1M sodium bicarbonate were added to a 2 mL reaction tube containing a small metallic stir bar (Component C). Simultaneously 40 µL of DMSO (Component B) was added to a vial of DSB-X biotin succinimidyl ester (Component A), critically completely dissolving the contents of the vial. 2 µL of the DSB-X biotin solution was then added to the anti-human purified CD59, clone P282 (H19) Mouse IgG2a $_k$ antibodies purchased from BD Biosciences (Cat No. 555761, BD Pharmingen™, San Jose CA, USA), whilst being stirred, mixed thoroughly, ensuring that 3-8 DSB-X molecules covalently bound per antibody molecule and incubated for 1-1.5 hr at room temperature. A spin column (Component E) was then placed within a glass tube and

subsequently a 1 mL volume of purification resin (Component D) was added and allowed to settle. Additional suspension was added until the volume was approximately 1.5 mL, the column was allowed to drain by gravity initially and then centrifuged for 3 min at 1100 x g. Post incubation, the antibody-DSB-X conjugate (~220 µL) was added to the centre of the prepared spin column, allowed to absorb into the gel and centrifuged for a further 5 min within a new collection tube. Post centrifugation the newly conjugated DSB-X biotinylated antibody was eluted within the collection tube, retaining the excess free DSB-X biotin within the spin column. Using the following equation, extracted from Life ™ guidance documentation [1], concentration of the newly synthesised conjugate was calculated, due to a potential loss of 15% recovery.

Equation 1

$$\textbf{mg/mL DSB-X biotin-labelled protein} = \frac{\text{Initial mg of protein} \times 0.85}{\text{mL in collection tube}}$$

As the final concentration of the purified antibody conjugate was less than 1 mg/mL, bovine serum albumin (BSA) was added to a concentration of 1-10 mg/mL, the conjugate was stored at 2-4°C for future usage.

Dynabeads ® Flow Comp™ Flexi Kit (Cat No. 11061D, Molecular Probes, Life™ Technologies, Paisley, UK) was utilised to purify the phenotypic PIG-A wild type cells. 10 mL of isolation buffer was initially prepared (Ca^{2+},Mg^{2+} free PBS, supplemented with 2% Foetal Bovine Serum (FBS) and 2 mM Ethylenediaminetetraacetic acid (EDTA)). Cell cultures were established as outlined in (Section 2.2), centrifuged and re-suspended in 500 µL of pre-cooled (2-8°C) isolation buffer. 25 µL of DSB-X ™ biotin labelled antibody was added to the solution, mixed well, incubated at 2-8°C (protected from light) for 30 min. 2 mL of

cold isolation buffer was added, cells were collected by centrifugation (8 min at 350 x g), supernatants carefully aspirated and re-suspended in 1 mL of cold isolation buffer. 75 µL of vortexed Flow Comp ™ Dynabeads ® were added mixed thoroughly and incubated for 15 min (2-8°C rolling and tilting). The tube contents were then transferred into a 2 mL micro centrifuge tube (MCT), placed within the 12-tube magnetic rack (Cat No. 36912, Qiagen, Manchester, UK) for 2 min, prior to removing (and discarding) the supernatant. Prior to re-suspension in 1 mL cold isolation buffer, the tube was removed from the magnet, this step was repeated once. 1 mL of Flow Comp ™ release buffer was added to the bead bound cells, mixed thoroughly and incubated for 10 min (25°C under rolling and tilting). Post incubation, the suspension was mixed thoroughly, via inversion, and the tube placed into the magnet rack for 2 min. The supernatant, containing the bead free cells, was transferred into a new MCT, placed back into the rack for an additional 2 min, ensuring removal of residual Dynabeads ®. The suspension was transferred into a new centrifuge tube and centrifuged (350 x g) for 8 min, supernatant aspired and placed within a 25 cm^2 cell culture flask.

Following magnetic enrichment, quality assurance (QA) FCM based *PIG-A* phenotype assessment was carried out following enrichment, the recovered TK6 cells were centrifuged (~250 x g for 7 min) and re-suspended in long term storage media, as outlined within (Section 2.3) and cryo-preserved within liquid nitrogen for future use in conjunction with model genotoxin exposure and the in vitro *PIG-A* gene mutation assay.

3.3 Results

3.3.3 Proof of Principle Evaluation Utilising CD59 as a Phenotypic Reporter for Mutation at the *PIG-A* Locus within the TK6 cell line following EMS Exposure

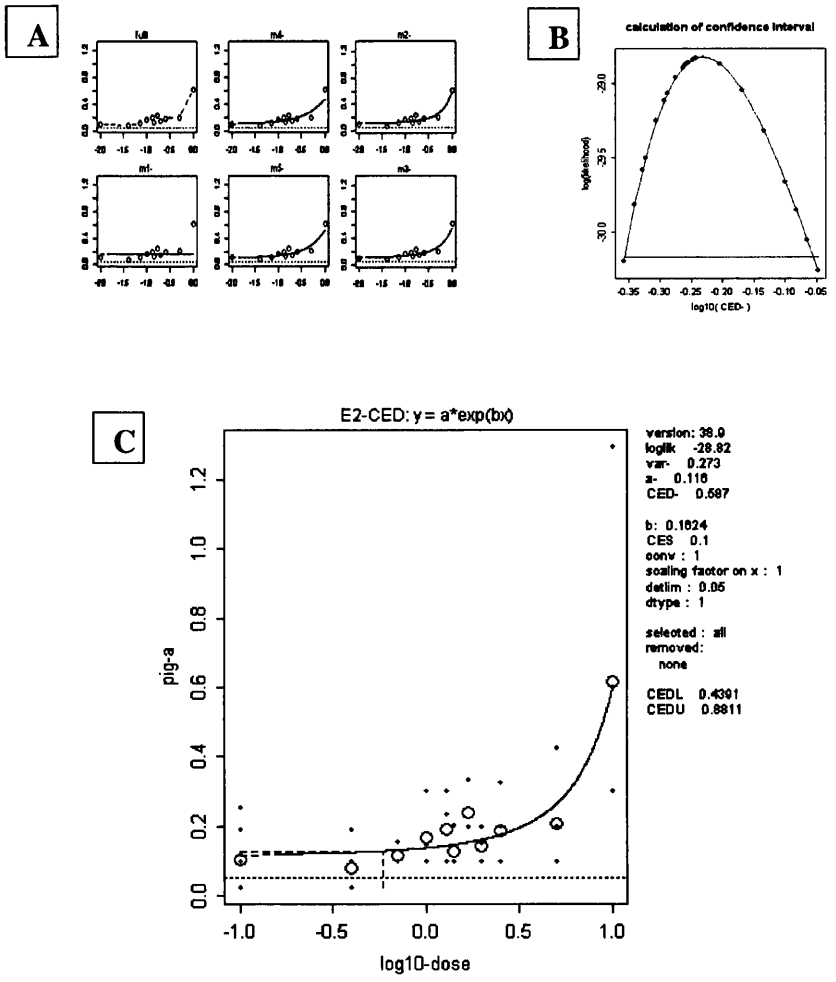

Figure 3.1 Human lymphoblastoid cells (TK6) Day 4 *PIG-A* mutation frequency data following 24 hr. low dose EMS exposure, CD59 antigen utilised. Day 4 frequencies of *PIG-A* mutant TK6 cells (Clonally selected) following 24 hr low dose EMS exposure. (n=3) *PIG-A* mutants displayed as percentage of total single cellular events (0.1% *PIG-A* Mutants = 1 mutant x 10^{-3} cells). A) Graphical output of the Nested set of models utilised to derive the CED_{10} (BMD_{10}) value, B) PROAST modelling; CED, CEDL and CEDU represent the BMD_{10}, $BMDL_{10}$ (Lower confidence limit) and $BMDU_{10}$ (Upper Confidence Limit) respectively and C) Calculation of Confidence Intervals (CEDL10 and CEDU10) based on likelihood function (in this case log-likelihood).

3.3.4 Long-term Cryo-preservation Assessment on CD59 Phenotype Stability

Table 3.1. Summary of CD59 cellular surface antigen expression of human lymphoblastoid TK6 cells, prior to long term liquid nitrogen cryo-preservation. Data generated for the human TK6 population following clonal expansion enrichment for the CD59 cellular surface antigen (Section 3.2.2.2). All expression data was defined utilising an un-stained ICS to gauge auto fluorescence, within the R-PE specified detector, as well as to identify a population free of aggregates and cellular debris (Single Cell Population). Intra-experimental biological replicate data is shown within the table below.

Day 0 - Control Data						
Sample ID	**Total Number of Events**	**Single Cells as a Percentage of Parent**	**Number of CD59 negative Cells**	**Number of CD59 Negative Cells as a percentage of Single Cells**	**Number of CD59 positive Cells**	**Number of CD59 Positive Cells as a percentage of Single Cells**
ICS	10826	90.5	10826	100.0	0	0.0
Sample 1	9938	83.2	12	0.1	9926	99.9
Sample 2	9452	81.1	21	0.2	9431	99.8
Sample 3	9329	80.0	10	0.1	9319	99.9
Average	**9573.00**	**81.43**	**14.33**	**0.15**	**9558.67**	**99.85**

Table 3.2. Summary of Human TK6 cellular viability following 72 hr recovery period post liquid nitrogen cryo-preservation. The viability data below are relative to the growth of DMSO M human TK6 cells following 72 hr recovery post awakening, cell counts were undertaken on a Z1 Coulter Counter (Beckman Coulter) with 5-17μm size classifier.

	Relative Cell Counts (RCC) Following 72 hr Culture (%)		
Medium Constituents	**Month 1**	**Month 3**	**Month 6**
DMSO M	100.00	100.00	100.00
DMSO S	131.71	125.87	102.82
DMSO HiS	145.42	124.56	91.28
Gly M	38.40	63.99	63.31
Gly S	41.70	34.12	0.06
Gly HiS	44.84	85.29	67.27
Suc M	2.15	1.60	0.78
Suc S	1.16	4.94	0.32
Suc HiS	0.41	6.75	0.42

The data recorded, 72 hr post cryo-preservation awakening, showed that the samples within DMSO or Glycerol generally appeared to remain stable and consistent in terms of viability over the experimental period. However, in the specific example of Glycerol supplemented with serum, the recovery potential of the culture appeared to decrease periodically over the experimental period, 41.7, 34.12 and 0.06%, highly apparent at the 6 month awakening time period. This data potentially was as a result of human error and therefore, cannot be attributed excessive weight as evidence for this observed relationship.

Each major constituent was demonstrated to produce reproducible viability data irrespective of the minor constituent within the storage cocktail. Taking DMSO as an example, the 1 month RCC following 72 hr incubation/recovery was 100, 131.71 and 145.42 % for M, S and HiS samples respectively. DMSO was shown to generate

increased yields in terms of cell numbers post awakening when directly compared to the other two major constituents.

Sucrose (10%) was demonstrated to be highly deleterious to the cells in terms of recovery potential post cryopreservation. All samples containing sucrose as a major constitutive demonstrated insufficient numbers of single cells remaining post awakening to extract a $1x10^6$ cell sample for ensuing immunofluorescence staining and flow cytometric analysis.

3.5 Supplementary Work

3.5.1 Introduction

In an endeavour to identify the most appropriate novel high content, high throughput and highly sensitive platform for the recording of the phenotypic identification of putative *PIG-A* mutant events, as well as further *PIG-A* mechanisms evaluation, a number of additional technologies other than FCM we also deliberated. FCM provides the majority of the features required for the development of the assay however, it does not provide any insight into the validity of identity of the presumptive *PIG-A* mutant events. Therefore, in an endeavour to provide significantly more confidence and thus attributing a greater weight of evidence to the subsequently generated data, additional microscopic based platforms were investigated for use. Traditional confocal or fluorescent microscope based applications were tested, however, the preparation work associated and highly exaggerated analysis times were proven detrimental to the scoring of phenotypic *PIG-A* mutations, especially when using live cells. Therefore, the more recent establishment of the Amnis Image Stream ™ range of high throughput, imaging, flow cytometers potentially brought a solution to the assessment of the presumptive mutant events whilst maintaining all the associated benefits of flow cytometry. The following section of work comments on the versatility of the Amnis Image Stream ™ platform and its potential use in conjunction with the in vitro *PIG-A* reporter system.

3.5.2 Materials and Methods

3.5.2.1 Preliminary Evaluation of the Amnis ImageStream ™ as a Potential Qualitative Platform for the in vitro *PIG-A* Gene Mutation Assay

A vial of pre-enriched TK6 cells, clonally expanded for the CD59 antigen, were awoken (Section 2.2) and RPD monitored (Section 2.2.1) prior to treatment with an anti-CD59 human R-PE conjugated antibody in an analogous method as outlined in (Section 2.8.1).

Following antibody treatment, all samples were washed twice with 1 X PBS pH 7.4 solution and either; re-suspended in 1 mL of BD Cell Fix or 4% paraformaldehyde solution (Section 2.7), incubated for 1 hr at 4°C or alternatively re-suspended in 50 µL of sterile PBS solution and transferred into a 750 µL micro centrifuge eppendorf tube for immediate flow cytometric analysis on the Amnis platform.

The cells which were fixed, post incubation were centrifuged (250 x g for 7 mins), supernatant aspirated carefully, and re-suspended in 50 µL of 1 x PBS in the identical manner as above. Fixed samples were able to be stored in a temperature controlled environment, 2-4°C, protected from light for a period of up to 7 days prior to analysis. Immediately before analysis, samples were re-suspended by thorough flicking, preventing blockages during sample input.

3.5.2.2 Amnis Image Stream ™ Assessment on Physical Agitation and Corresponding Antibody-Antigen Shearing

Pre-enriched TK6 cells were treated with an anti-CD59 human R-PE conjugated antibody in an analogous method as outlined in the previous (Section 2.8.1).

Following antibody treatment, all samples were washed and either fixed in BD Cell Fix ™ or 4% paraformaldehyde (Section 2.7) or re-suspended in PBS, as described in section (Appendix 3.5.2.1) and stored on ice, protected from light, until ready to be analysed. Each sample was prepared in duplicate to facilitate one sample being vigorously flicked prior to analysis, and one sample being minimally re-suspended to prevent blockages. Immediately before analysis, both samples were re-suspended by moderate flicking, preventing blockages during sample input.

3.5.2.3 Critical Amnis Image Stream ™ Assessment on Cellular Characteristics of High Resolution Imaging and Incorporation within the in vitro *PIG-A* assay

Pre-enriched TK6 cells were treated with antibodies in an analogous manner as described in detail (Section 2.8.1).

Following antibody treatment samples were either re-suspended in 1 mL of BD Cell Fix™, 4% Paraformaldehyde (Gibco ® PBS base), Dulbecco's 4% paraformaldehyde solution (with Mg^{2+} and Ca^{2+} ions) or Dulbecco's 4% paraformaldehyde solution (without Mg^{2+} or Ca^{2+} ions). Each culture was incubated, protected from light, for 1 hr at 2-4°C. Additionally, a single sample was not fixed, and therefore, immediately processed and analysed on the Amnis Image Stream™ platform within 1 hr post antibody treatment. Post incubation, samples were centrifuged (250 x g for 7 mins), supernatant aspirated and washed twice with 1 x PBS solution.

Following the wash steps the samples were re-suspended in 50 µL of 1 x PBS in an analogous protocol as outlined in the previous sections. Fixed samples are much more stable and can be re-fridgerated (2-4°C) for up to and including 7 days prior to

analysis. Once intended to be analysed, all samples were gently re-suspended to prevent blockages within the sample inlet system.

3.5.3 Results

3.5.3.1 Preliminary Evaluation of the Amnis ImageStream ™ as a Potential Qualitative Platform for the in vitro *PIG-A* Gene Mutation Assay

The Amnis Image Stream ™ is a highly sophisticated imaging flow cytometer, combining the high-content, high-throughput, high precision and fluorescence sensitivity of a conventional flow cytometer with the functionality of high resolution light microscopy. Incorporation of Image Stream ™ technology into the *PIG-A* assay design potentially could provide insight into the true identity of putative *PIG-A* mutant events; visual descriptors could be applied to each event allowing validation of generated data. High content analysis could also provide the ability to add further fluorescence detection of noteworthy characteristics, including cellular viability as well as cell cycle information, facilitating a more holistic approach to measuring mutagenesis.

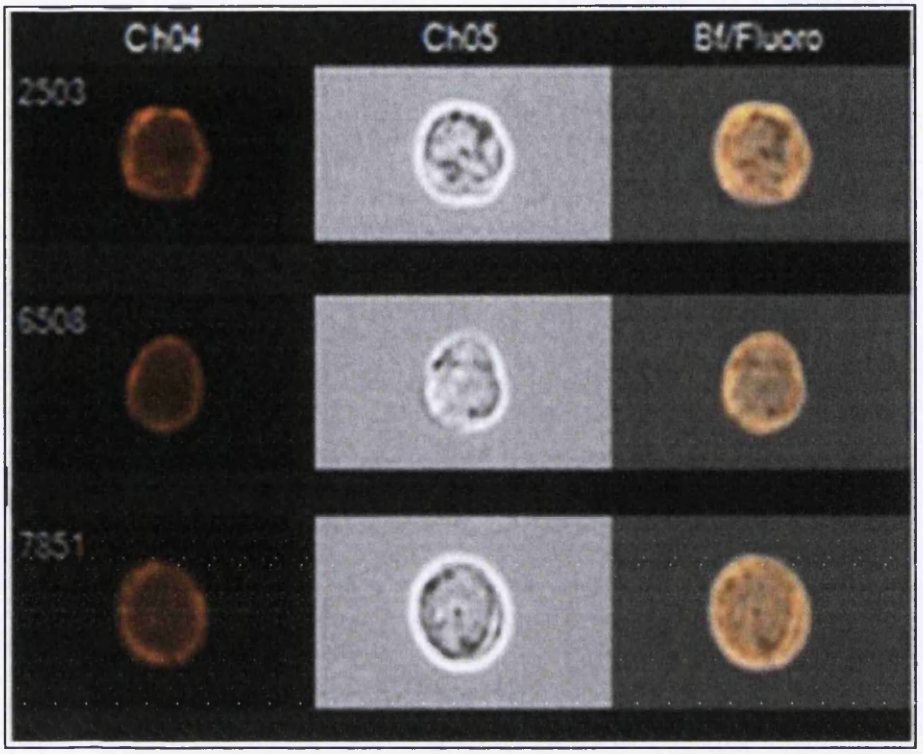

Figure 3.5.1. Image Stream ™ generated images of live TK6 cells treated with anti-CD59 PE Ab. A single cell population was defined, aspect ratio ≥0.75 and an area of 100-500, each single cell was evaluated for focus, gradient RMS (Root mean square of the rate of change of the image intensity profile) score ≥40-60 prior to still capture of high resolution images displaying anti-CD59 PE binding on the extracellular surface membrane. "Ch04" detected anti-CD59 PE fluorescence, "Ch05" brightfield images and "Bf/Fluoro" composite combined images.

The results of the initial live cell capture images, as well as the additional fixed cell images showed the extracellular location of the bound anti-CD59 R-PE antibody (Appendix Figure 3.5.1); binding was sporadic in nature and appeared solely confined to the extracellular surface. The multiple fixatives utilised within this section of work were shown to have no effect on the location of antibody binding.

Table 3.5.1. Summary of Image Stream ™ dose response data following EMS treatment of TK6 cells, the CD59 surface antigen was used as a reporter for mutant frequency. Data displayed in the table below was collected using a standardised approach (Appendix Section 3.5.2); A single cell population was defined, aspect ratio ≥0.75 and an area of 100-500, each single cell was evaluated for focus, gradient RMS (Root mean square of the rate of change of the image intensity profile) score ≥40-60 prior to fluorescence intensity data acquisition. ≥10,000 focussed, single cellular events were collected for each sample analysed (PFA = Paraformaldehyde).

	Dose of EMS (µg/mL)	Average Cellular Area	Average Cellular Area Range	Average Fluorescence Intensity
Un-fixed	0	205.43	104 - 452.25	29732.39
Un-fixed	10	208.96	104 - 455	29322.52
PFA (4%)	0	233.04	108.5 - 455	30915.30
PFA (4%)	10	245.59	104 - 456.75	29521.72
BD Cell Fix ™	0	257.15	106.5 - 455.5	33335.63
BD Cell Fix ™	10	264.51	105 - 457	32323.99

A

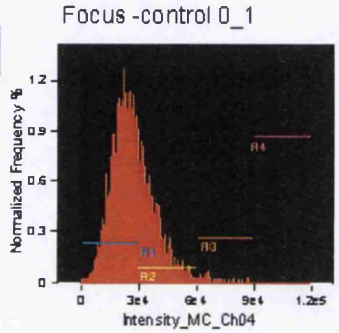

Intensity_MC_Ch04

Population	Count	%Gated	%Plotted	Mean	Median	Minimum	Maximum
Focus & Single Cells	5825	100	100	26771.92	25355.71	20.82	86623.36
R1 & Focus & Single Cells	3854	66.2	100	20631.21	21203.88	473.58	29576.51
R2 & Focus & Single Cells	1905	32.7	100	37803.49	36076.95	29587.83	59218.21
R3 & Focus & Single Cells	62	1.06	100	68362.67	65475.41	60138.19	86623.36
R4 & Focus & Single Cells	0	0	0	NaN	NaN	NaN	NaN

B

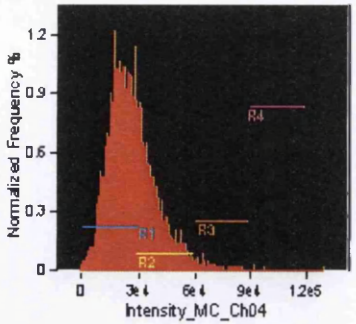

Intensity_MC_Ch04

Population	Count	%Gated	%Plotted	Mean	Median	Minimum	Maximum
Focus & Single Cells	5856	100	100	26153.41	24489.5	226.15	128973.57
R1 & Focus & Single Cells	3899	66.6	100	19381.53	19784.5	259.08	29570.41
R2 & Focus & Single Cells	1872	32	100	38325.86	36464.66	29588.17	59439.08
R3 & Focus & Single Cells	74	1.26	100	68526.85	66518.33	60690.27	85097.11
R4 & Focus & Single Cells	3	0.05	100	93528.95	91705.05	91635.06	97246.75

Figure 3.5.2.A Image Stream ™ data following EMS treatment of un-fixed TK6 cells, CD59 surface antigen utilised as the reporter for mutation. Relative fluorescence intensity values for human TK6 cells (Clonally selected) cultures following 24 hr low dose EMS exposure. A) Un-treated control B) 10 µg/mL EMS (~10,000 focussed single cellular events divided into four regions of increasing relative fluorescence intensity, R1, R2, R3 and R4)

A

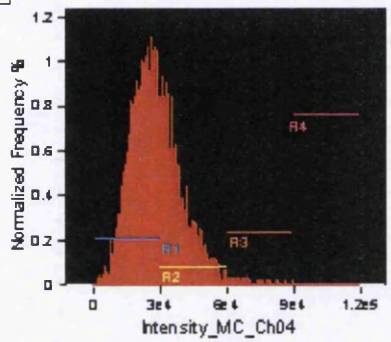

Intensity_MC_Ch04

Population	Count	%Gated	%Plotted	Mean	Median	Minimum	Maximum
Focus & Single Cells	6564	100	100	27745.2	26432.31	2003.13	89508.11
R1 & Focus & Single Cells	4038	61.5	100	21010.74	21632.25	2003.13	29575.37
R2 & Focus & Single Cells	2469	37.6	100	37850.7	36052.34	29581.8	59340.56
R3 & Focus & Single Cells	56	0.85	100	66700.33	64592.8	60249.27	85539.38
R4 & Focus & Single Cells	1	0.02	100	89508.11	89508.11	89508.11	89508.11

B

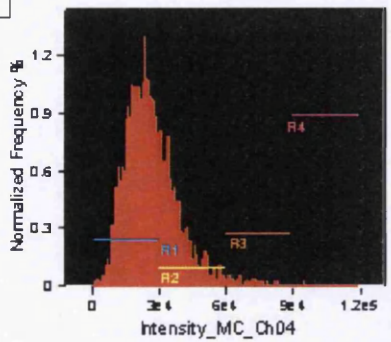

Intensity_MC_Ch04

Population	Count	% Gated	% Plotted	Mean	Median	Minimum	Maximum
Focus & Single Cells	5684	100	100	25834.56	24228.15	1378.14	94991.2
R1 & Focus & Single Cells	3940	69.3	100	20175.45	20587.76	1378.14	29579.08
R2 & Focus & Single Cells	1684	29.6	100	37615.8	35780.13	29588.92	59179.9
R3 & Focus & Single Cells	56	0.99	100	66667.52	65149.1	60236.25	82892.61
R4 & Focus & Single Cells	1	0.02	100	94991.2	94991.2	94991.2	94991.2

Figure 3.5.2.B - Image Stream ™ data following EMS treatment of paraformaldehyde (4%) TK6 cells, CD59 surface antigen utilised as the reporter for mutation. Relative fluorescence intensity values for paraformaldehyde (4%) human TK6 cells (Clonally selected) cultures following 24 hr low dose EMS exposure. A) Un-treated control B) 10 µg/mL EMS (~10,000 focussed single cellular events divided into four regions of increasing relative fluorescence intensity, R1, R2, R3 and R4)

A

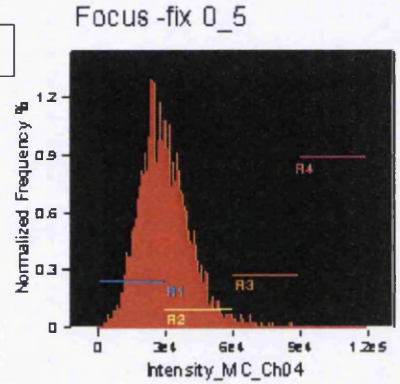

Intensity_MC_Ch04

Population	Count	%Gated	%Plotted	Mean	Median	Minimum	Maximum
Focus & Single Cells	4917	100	100	29266.03	28429.89	2320.86	85399.82
R1 & Focus & Single Cells	2693	54.8	100	21882.48	22771.03	2320.86	29577.37
R2 & Focus & Single Cells	2189	44.5	100	37765.47	36273.5	29587.38	59236.18
R3 & Focus & Single Cells	32	0.65	100	66367.57	64736.91	60232	85399.82
R4 & Focus & Single Cells	0	0	0	NaN	NaN	NaN	NaN

B

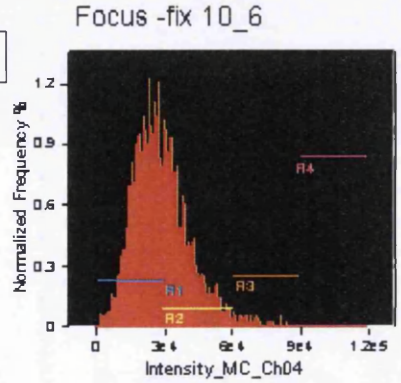

Intensity_MC_Ch04

Population	Count	%Gated	%Plotted	Mean	Median	Minimum	Maximum
Focus & Single Cells	4311	100	100	27891.84	26544.65	1369.18	84031.4
R1 & Focus & Single Cells	2580	59.8	100	20634.59	21227.96	1369.18	29578.56
R2 & Focus & Single Cells	1679	38.9	100	37830.11	36153.81	29580.58	59492.63
R3 & Focus & Single Cells	50	1.16	100	67357.54	65336.27	60236.03	84031.4
R4 & Focus & Single Cells	0	0	0	NaN	NaN	NaN	NaN

Figure 3.5.2.C Image Stream ™ data following EMS treatment of BD Cell Fix™ TK6 cells, CD59 surface antigen utilised as the reporter for mutation. Relative fluorescence intensity values for BD Cell Fix ™ human TK6 cells (Clonally selected) cultures following 24 hr low dose EMS exposure. A) Un-treated control B) 10µg/mL EMS (~10,000 focussed single cellular events divided into four regions of increasing relative fluorescence intensity, R1, R2, R3 and R4)

Initially, each fixation method was run in duplicate with a single replicate being exposed to a high dose of EMS (10 µg/mL) and the other un-treated. All three methodologies investigated were demonstrated to have an apparent decrease in their respective relative fluorescence intensity values recorded within the corresponding channel to the PE signal, when comparing acute high dose EMS treatment with untreated samples. Live cells demonstrated the lowest difference in fluorescence intensity values, with paraformaldehyde (4%) and BD Cell Fix ™ having significantly larger intensity differences, 1393.58 and 1011.64 units respectively. The data appeared to correlate an increased average decrease in fluorescence intensity post EMS treatment with the method of sample fixation; difference was significantly higher in fixed samples when compared to un-fixed analogous control samples (Appendix Figure 3.5.2).

Following compartmentalisation of the x-axis, relative fluorescence intensity within channel 4, and all EMS treated samples showed an increase in the percentage of the total population of focussed single cells residing within the lowest fluorescence compartment, R1, when compared to their un-treated control samples. This relationship was observed within all test samples un-fixed (Figure 3.5.2.A), paraformaldehyde (4%) (Figure 3.5.2.B) and BD Cell Fix ™ (Figure 3.5.2.C), however, population statistics within the higher fluorescence compartments appeared to stay relatively stable in comparison.

3.5.3.2 Amnis Image Stream ™ Assessment on Physical Agitation and Corresponding Antibody-Antigen Shearing

Table 3.5.2. Image Stream ™ evaluation of the impact physical agitation (flicking of prepared sample) has on anti-CD59 R-PE antibody binding to the CD59 antigen on the cellular surface of TK6 cells. Data displayed in the below above was collected using a standardised approach (Appendix Section 3.5.2.1); A single cell population was defined, aspect ratio ≥0.75 and an area of 100-500, each single cell was evaluated for focus, gradient RMS score ≥40-60 prior to fluorescence intensity data acquisition. ≥10,000 focussed, single cellular events were collected for each sample analysed.

	"No-Flicking"			"Flicking"		
	Average Cellular Area	**Average Cellular Area Range**	**Average Intensity**	**Average Cellular Area**	**Average Cellular Area Range**	**Average Intensity**
No Fix	202.46	104 - 351.5	32246.85	209.55	106.25 - 330.25	26057.98
Paraformaldehyde (4%)	244.79	104 - 455.75	39916.43	240.53	104.25 - 457	36894.54
BD Cell Fix ™	270.57	109.5 - 456.75	34442.32	278.33	104.25 - 456.75	35210.67

A

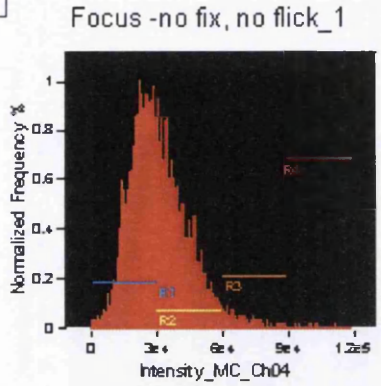

Intensity_MC_Ch04

Population	Count	%Gated	%Plotted	Mean	Median	Minimum	Maximum
Focus & Single Cells	6367	100	100	30135.23	28360.48	424.9	111673.68
R1 & Focus & Single Cells	3453	54.2	100	21204.73	22004.56	424.9	29578.12
R2 & Focus & Single Cells	2768	43.5	100	39227.51	37701.1	29586.49	59452.98
R3 & Focus & Single Cells	136	2.14	100	68141.62	66035.06	60127.47	88481.66
R4 & Focus & Single Cells	5	0.08	100	100517.29	100243.59	93227.6	111673.68

B

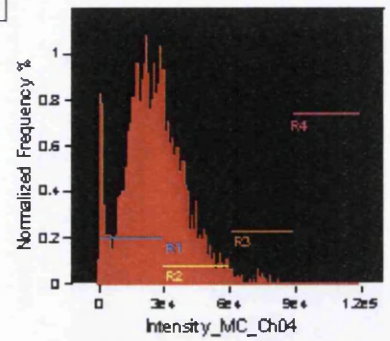

Intensity_MC_Ch04

Population	Count	%Gated	%Plotted	Mean	Median	Minimum	Maximum
Focus & Single Cells	4722	100	100	24874.7	24105.59	-199.96	82337.03
R1 & Focus & Single Cells	3169	67.1	100	18358.47	19579.31	237.13	29576.75
R2 & Focus & Single Cells	1492	31.6	100	38065.03	36377.19	29598.05	59369.67
R3 & Focus & Single Cells	34	0.72	100	67813.85	65281.76	60278.64	82337.03
R4 & Focus & Single Cells	0	0	0	NaN	NaN	NaN	NaN

Figure 3.5.3.A Image Stream ™ antibody-antigen integrity analysis data for un-treated TK6 cells, anti-CD59 R-PE antibody assessed. Relative fluorescence intensity values for untreated human TK6 cells (Clonally selected) cultures following selective physical agitation. A) Un-treated control B) Vigorously flicked samples (~10,000 focussed single cellular events divided into four regions of increasing relative fluorescence intensity, R1, R2, R3 and R4)

A

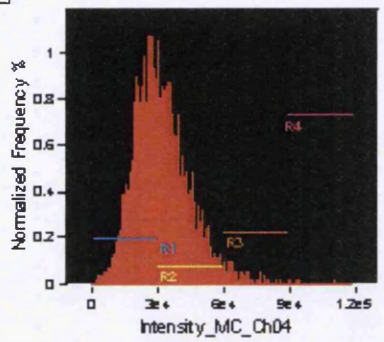

Intensity_MC_Ch04

Population	Count	%Gated	%Plotted	Mean	Median	Minimum	Maximum
Focus & Single Cells	5957	100	100	31680.35	30339.42	1690.49	111081.37
R1 & Focus & Single Cells	2809	47.2	100	22065.87	22903.29	1690.49	29566.79
R2 & Focus & Single Cells	3017	50.6	100	39093.86	37509.3	29580.19	59484.3
R3 & Focus & Single Cells	119	2	100	66325	64149.51	60105.13	85620.9
R4 & Focus & Single Cells	5	0.08	100	95734.41	93462.19	89774.72	111081.37

B

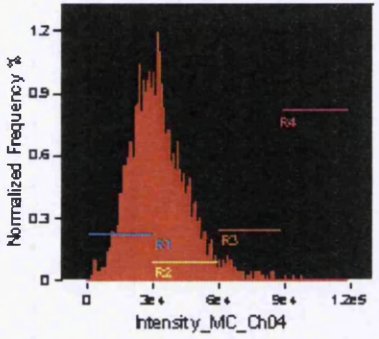

Intensity_MC_Ch04

Population	Count	%Gated	%Plotted	Mean	Median	Minimum	Maximum
Focus & Single Cells	5094	100	100	32051.25	30716.5	1208.1	97682.71
R1 & Focus & Single Cells	2337	45.9	100	22065.82	23063.87	1208.1	29577.38
R2 & Focus & Single Cells	2633	51.7	100	39250.66	37639.98	29611.4	59487.96
R3 & Focus & Single Cells	114	2.24	100	67141.96	65330.1	60114.87	84249.58
R4 & Focus & Single Cells	3	0.06	100	93922.02	93724.46	90358.89	97682.71

Figure 3.5.3.B Image Stream ™ antibody-antigen integrity analysis data for BD Cell Fix™ TK6 cells, anti-CD59 R-PE antibody assessed. Relative fluorescence intensity values for BD Cell Fix ™ human TK6 cells (Clonally selected) cultures following selective physical agitation. A) Un-treated control B) Vigorously flicked samples (~10,000 focussed single cellular events divided into four regions of increasing relative fluorescence intensity, R1, R2, R3 and R4)

A

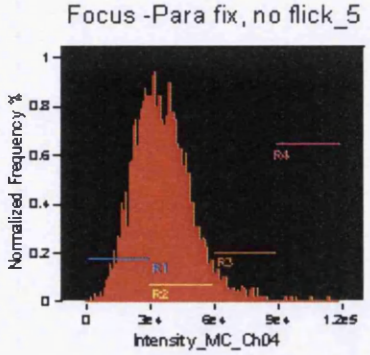

Intensity_MC_Ch04

Population	Count	%Gated	%Plotted	Mean	Median	Minimum	Maximum
Focus & Single Cells	5914	100	100	35018.09	33821.58	1640.77	113893.37
R1 & Focus & Single Cells	2110	35.7	100	22699	23669.09	1640.77	29577.46
R2 & Focus & Single Cells	3594	60.8	100	40307.7	39167.7	29585.62	59458.09
R3 & Focus & Single Cells	193	3.26	100	67742.78	65113.24	60088.31	85143.57
R4 & Focus & Single Cells	6	0.1	100	100645.36	97584.05	93452.3	113893.37

B

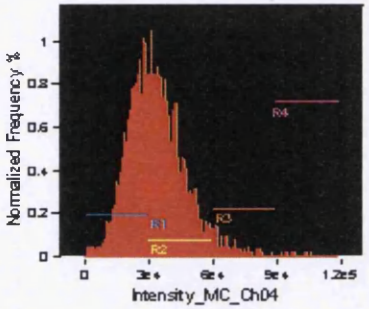

Intensity_MC_Ch04

Population	Count	%Gated	%Plotted	Mean	Median	Minimum	Maximum
Focus & Single Cells	6359	100	100	33067.7	31696.1	941.94	105927.13
R1 & Focus & Single Cells	2719	42.8	100	22204.2	23097.03	941.94	29575.07
R2 & Focus & Single Cells	3441	54.1	100	39660.67	38227.06	29581.86	59489.21
R3 & Focus & Single Cells	177	2.78	100	66942.46	65552.19	60089.76	87579.36
R4 & Focus & Single Cells	7	0.11	100	97940.99	96769.69	91856.48	105927.13

Figure 3.5.3.C Image Stream ™ antibody-antigen integrity analysis data for paraformaldehyde (4%) TK6 cells, anti-CD59 R-PE antibody assessed. Relative fluorescence intensity values for paraformaldehyde (4%) human TK6 cells (Clonally selected) cultures following selective physical agitation. A) Un-treated control B) Vigorously flicked samples (~10,000 focussed single cellular events divided into four regions of increasing relative fluorescence intensity, R1, R2, R3 and R4)

Fixation methods were demonstrated to elicit a distinct effect on the integrity of the antibody-antigen conjugate; this affect was observed within the average fluorescence intensities of the samples post vigorous physical agitation (flicking) when compared to their relative controls. Un-fixed samples were shown to have a substantial decrease, 6189 arbitrary units, in fluorescence value (26057), post flicking when compared to their con-current control sample, (32246.85) (Appendix Table 3.5.2). This relationship was mirrored in the 4% paraformaldehyde samples, however, the decrease was less apparent, 3021.89 arbitrary units. Alternatively, BD Cell Fix™ was demonstrated to increase the average fluorescence intensity of the sample following flicking, 768.35 arbitrary units.

Un-fixed samples were observed to have a significant increase in the percentage of single focussed events falling within the R1 compartment, following physical agitation when compared to control values 54.2, to 67.1% respectively (Appendix Figure 3.5.3.A). This increase was visualised within the adjacent histogram via the presence of a sharp peak within the R1 compartment within the agitated sample which was not mirrored within the un-fixed control. Fixed samples, 4% paraformaldehyde and BD Cell Fix ™ were shown to be less affected by physical agitation and therefore, displayed lower corresponding increases in the percentage R1 population, and no novel observed peak was present within the R1 region within the gated histograms (Appendix Figure 3.5.3.B and C).

The results appear to suggest that fixation can prevent the loss of signal differentiation associated with physical agitation, and even in specific examples improve the efficiency of fluorescence conjugate antigen tagging during such agitation. The affect physical agitation had on the samples was again more easily envisaged within corresponding 2-D fluorescence intensity histograms (Appendix Figures 3.5.3.A, B and C).

3.5.3.3 Critical Amnis Image Stream ™ Assessment on Cellular Characteristics of High Resolution Imaging and Incorporation within the in vitro PIG-A assay

Table 3.5.3. Summary of Unstained cellular morphology data following Image Stream ™ analysis of TK6 cells, unstained sample inclusion for definition of maximum auto-florescence within the relevant channel. Data displayed in the tables below were collected using a standardised approach (Sections 2.7 - 2.8); A single cell population was defined, aspect ratio ≥0.75 and an area of 100-500, each single cell was evaluated for focus, gradient RMS score ≥40-60 prior to fluorescence intensity data acquisition. ≥7000 focussed, single cellular events were collected for each sample analysed.

	Unstained Samples (ICS) - A		
	Average Cellular Area	**Area Cellular Range**	**Fluorescence Maxima (Arbitrary Units)**
Un-fixed	188.25	104 - 332.25	32707.49
Paraformaldehyde (4%) pH controlled	223.04	115.5 - 456.25	35450.34
D-Para 4 (Mg^{2+} and Cl^- Negative)	229.63	107.75 - 456.75	34442.59
D-Para 4 (Mg^{2+} and Cl^- Positive)	217.87	106.25 - 440.5	22551.74
BD Cell Fix ™	239.89	104.75 - 455.75	26617.47

Table 3.5.4 Summary of presumptive PIG-A mutant cellular morphology data following Image Stream ™ analysis of TK6 cells, unstained sample inclusion for definition of maximum auto-florescence within the relevant channel. Data displayed in the tables below were collected using a standardised approach (Sections 2.7 – 2.8); A single cell population was defined, aspect ratio ≥0.75 and an area of 100-500, each single cell was evaluated for focus, gradient RMS score ≥40-60 prior to fluorescence intensity data acquisition. ≥7000 focussed, single cellular events were collected for each sample analysed.

	Stained Samples (Presumptive Mutant Analysis) - B				
	Number of Single Cells	**Number of CD59 Positive Cells**	**Number of CD59 Negative Cells**	**Percentage CD59 Positive Cells**	**Percentage CD59 Negative Cells**
Un-fixed	7594	776	6818	10.22	89.78
Paraformaldehyde (4%) pH controlled	7570	2478	5092	32.73	67.27
D-Para 4 (Mg^{2+} and Cl^- Negative)	7654	2231	5423	29.15	70.85
D-Para 4 (Mg^{2+} and Cl^- Positive)	7340	304	430	41.42	58.58
BD Cell Fix ™	7654	4332	3322	56.60	43.40

The results indicate that fixation in general was demonstrated to increase the average area of the samples when compared to their un-fixed negative controls (Appendix Table 3.5.3); un-fixed samples had an average area of 188.25 units, which was lower when compared to all fixation methodologies, 4% paraformaldehyde 223.04, D-Para 4 (Ion +ve) 229.63, D-Para 4 (Ion –ve) 217.87 and BD Cell Fix ™ 239.89. The fluorescence maxima values, corresponding to auto-fluorescence within the channel, were observed to decrease within fixed samples; un-fixed 32707.49 compared to D-Para 4 (Ion –ve) 22551.74 arbitrary units.

Within all experimental samples, including the un-fixed treated control, the number of CD59 negative events, as defined by any event scoring a value greater than the fluorescence maxima of the ICS, was meaningfully higher than comparable flow cytometric data (Appendix Section 3.3.3). CD59 negative frequencies were observed at a maxima value of 89.7% of the total, focused, single cell population within un-treated controls (Appendix Table 3.5.4).

The result appear to reflect the lack of signal separation and hence, indirect sensitivity observed within the technology when compared to an equivalent flow cytometer as a result of insufficient signal filtering technology within the Amnis ™ Image Stream Platform.

3.5.4 Discussions and Conclusions

3.5.4.1 Amnis® Image Stream ™ Evaluation

Incorporating high-content, high-throughput and high–precision technology is an assured way to advance the field of genetic toxicology. Undertaking a more holistic approach to data acquisition, analogous to systems biology [2], has the ability to provide a greater degree of relevance as well as context. Providing such data at earlier stages within drug discovery/development should facilitate a more precise and cost effective safety assessment [3, 4]. The Amnis Image Stream ™ is a platform which enables the combination of high resolution imaging in combination with flow cytometric analysis [5]. In the context of the in vitro *PIG-A* gene mutation assay, the Image Stream ™ potentially can more dependably confirm the identity of currently debated putative mutants events however, had a higher than expected background mutant frequency (Appendix Table 3.5.4). Currently, presumptive *PIG-A* mutant events are thought to possible include non-viable cells, cells within G_0/G_1, cells stripped of the surface antigen marker or GPI anchor and additional inaccuracies associated with flow cytometry sample preparation including aggregation or cellular debris.

GPI anchors are attached to the membrane in clusters associated with areas of dense lipid concentration, known as lipid rafts, to monitor functionality, and therefore, have highly limited and cholesterol sensitive expression on the outer surface of the cellular membrane [6]. Unfortunately, this association does not lend itself well to laser illuminating assays with single image capture due to the precise path of illumination. Laser light must transverse the cell in the correct orientation to correctly detect stained GPI-AP clusters. Initial antibody location assessment (Figure 3.5.1), in which the extracellular membrane was experimentally demonstrated to be sporadically covered with comprehensive CD59 expression, confirmed this initial concern. However, the extent in which this limitation would impact the subsequent data analysis was unknown and therefore, the Image Stream ™ was assessed for the

ability to detect significant differences following model mutagenic exposure within the TK6 population.

Average fluorescence intensity, area and basic morphology were evaluated, the results indicated that even though there were defined differences between the concurrent negative control and the EMS treated samples, in terms of area and morphology, the differences, were in-sufficient to be utilised as potential markers for exposure. However, the number of cells falling within the lowest fluorescence value region was confirmed to increase following EMS exposure (Figure 3.5.2.A, B and C); potentially this reflects the induction of novel putative *PIG-A* mutant events following mutagenesis. Acute mutagenic exposure, at the doses tested, would potentially only induce an additional few hundred mutant events within the allotted experimental time period [7-9] and therefore supports the generated data. However, due to the high level of auto-fluorescence detected within the un-stained control sample, a potential weakness associated with the Image Stream's ™ lack of band pass filters and mirrors as well as imaging system, this method is currently limited to basic qualitative dose response analysis.

Following EMS exposure, fixation did appear to increase the difference in average fluorescence between the top dose and the untreated samples (Table 3.5.1). The reason for this was thought to be the increased stability of the antibody-antigen binding complex following protein-aldehyde crosslinking [10] and hence, subsequent more precise identification of wild type and *PIG-A* mutant events. The GPI anchor structure within white blood cells (WBC) is known to be less comprehensive than the erythroid counterpart [11-13]; WBC have two fatty acid chains/tails protruding into the membrane, compared to three within RBC and therefore, could be susceptible to dislodgement or shearing following physical agitation

To further investigate the effect of physical agitation on *PIG-A* mutant frequencies, within flow prepared samples, a variety of aldehyde based fixatives were assessed. The results confirmed that heavily "flicking" the tubes prior to analysis induced a significant decrease in average fluorescence within the R-PE channel (Appendix Table 3.5.2); re-enforcing that the current spontaneous background mutant frequency at the *PIG-A* locus may constitute additional mimicking events not solely *PIG-A*

mutants. This observation was in the best way observed with the generation of a novel sub population of GPI-AP deficient cells within the R1 gated region of the un-fixed control (Appendix Figure 3.5.3.A, B and C).

However, fixation was observed to greatly limit the decrease in average fluorescence value and therefore, could potentially be a viable inclusion into the assay design to prevent the induction of novel *PIG-A* mutant mimicking events through sample processing. Fixation was also demonstrated to have a beneficial effect on the physical morphology of cells, with the average area observed to increase substantially when compared to un-fixed negative control samples (Appendix Table 3.5.3). This observation was attributed to the variance in pH value between the buffered fixatives, and hence the corresponding change in osmotic pressures applied onto the cells following submergence. Increasing or decreasing the pH can have a distinct effect on the solubility of previously bound reactive groups, generally located within protein macro-molecules, resulting in an increase or decrease in osmotic potential [14, 15]. Creating a uniform population in terms of area would be valuable in several ways; initially the cells would be easier to image due to a common focal plane and secondly, more accurate size descriptors could be implemented into assay design to further precisely define the critical sub population under assessment.

Within this section of work the Image Stream ™ platform was assessed for the ability to accurately define *PIG-A* mutant events post mutagenic exposure. Although the ImageStream ™ has distinctive features which potentially could enhancement the basic *PIG-A* assay design; for example, generation of high resolution images, providing validation of antibody binding specificity as well as *PIG-A* phenotype (Appendix Figure 3.5.1), high content analysis, providing insights into cell cycle and a highly intuitive analysis software package. The technique was considered inappropriate for assay incorporation due to the overwhelming number of associated limitations, but would be utilised in a supplementary role for high content validatory mechanistic image analysis.

In brief, the spontaneous background *PIG-A* mutant frequency, following antibody treatment, was approximately 80%. Elucidating that 800,000 cells were presumptive *PIG-A* mutants per 1 x 10^6 cells scored. This was directly compared to the more

realistic presumed 0.1-0.2% *PIG-A* mutant population using the flow cytometer [7]. Fluorescent outliers within the instrument calibration standard, generated as a result of "focal smearing" were the reason for this spiked the maximum auto-fluorescence value, resulting in inconsistent gating strategies. "Focal smearing" describes the occurrence of an artificially saturated pixel, and hence false positive resultant signal as a direct result of a fluorescing event passing the camera out of focus. Unlike the flow cytometer the ImageStream™ utilising 8-bit image capture, not PMT photon capture, and relative intensity is measured through pixel saturation. This problem can be potentially over come via the use of extended depth of field capture, a 3-D render of the cellular events, more accurately displaying the location of the bound anti-CD59 R-PE conjugate antibody. However, accounting for the potential focussing issues, the Image Stream ™ platform is inferior to the FACS Aria 1 in terms of precision and sample throughput and therefore, was not included in future quantitative *PIG-A* assessment.

Chapter 4: Consideration of Cell Lines in the Further Development of an in vitro *PIG-A* Gene Mutation Assay

4.2 Materials and Methods

4.2.5 Normal TK6, AHH-1 and MCL-5 Cell Line Characterisation

"Low Passage" TK6 and Normal TK6 cell cultures were established and maintained as outlined in (Sections 2.1 - 2.2). Cultures were washed, counted (Section 2.2.1) and equivalent volumes containing $1x10^6$ cells aliquotted into sterile 15 mL BD Falcon tubes. Samples were prepared in triplicate in order to generate comparable metrics for direct comparison between both cell lines; FLAER, CD48 and CD55/59 tandem treatment were all assessed for their relative receptor presence. Each cell line had a unique ICS to facilitate accurate flow cytometric analysis.

Fluorescent Aerolysin (FLAER) Staining Protocol

Prior to use, 1 mL of 1 X PBS was added to 25 µg of powdered (lyophilised) FLAER in order to construct a stock solution. The stock solution was diluted 1 in 10 within dH_20 and aliquotted into 50 µL volumes within 0.5 mL eppendorf tubes to facilitate long term storage. Each individual tube or vial was wrapped in aluminium foil and stored at -20°C, protected from direct light.

Twelve samples for each cell line, containing $1x10^6$ cells, were transferred into sterile 15 mL falcon tubes, centrifuged (250 x g for 7 min), supernatant aspirated and re-suspended in 100 µL of fresh pre-warmed culture medium. Cell pellets were carefully re-dispersed, minimalizing cellular agitation, and treated with 5 µL of various concentrations, in triplicate, of FLAER; FLAER (1X) – undiluted FLAER taken directly from the pre-aliquotted vials, FLAER (0.5X) requiring a single 1 in 2 dilution using 2% BSA/PBS and finally FLAER (0.1x) requiring a 1 in 10 dilution using 2% BSA/PBS. Each tube was incubated for 15 min at room temperature, protected from direct light. Post incubation, samples were centrifuged, supernatant aspirated, and re-suspended within 10 mL of 1 X PBS. Samples were returned to the

centrifuge, spun down, supernatant aspirated carefully and re-suspended within 1 mL of 1x PBS. All samples were placed on ice, protected from light; to maintain the stability of the suspensions and the fluorophores used, prior to flow cytometer analysis.

CD48 - β-Lymphocyte Activation Marker 1 (BLAST-1) Staining Protocol

Four $1x10^6$ cellular samples were transferred into separate sterile 15 mL BD falcon tubes, centrifuged (250 x g for 7 min), supernatant aspirated and re-suspended in 100 µL of fresh pre-warmed culture medium. Cell pellets were carefully re-dispersed, minimalizing cellular agitation, and treated with 20 µL of mouse anti-human anti-CD48 R-PE antibody (Cat No. 552855, BD Biosciences, Hertfordshire, UK) and incubated at room temperature, protected from direct light, for 30 min. Post incubation, samples were centrifuged, supernatant aspirated, and re-suspended within 10 mL of 1 X PBS. Samples were returned to the centrifuge, spun down, supernatant aspirated carefully and re-suspended within 1 mL of 1x PBS. All samples were placed on ice, protected from light; to maintain the stability of the suspensions and the fluorophores used, prior to flow cytometer analysis.

CD55 and CD59 Tandem Staining Protocol

Four $1x10^6$ cellular samples were transferred into separate sterile 15 mL BD falcon tubes, centrifuged (250 x g for 7 min), supernatant aspirated and re-suspended in 100 µL of fresh pre-warmed culture medium. Cell pellets were carefully re-dispersed, minimalizing cellular agitation, and treated with 20 µL of mouse anti-human anti-CD55 R-PE antibody and 20 µL of mouse-anti-human anti-CD59 R-PE antibody, and incubated at room temperature, protected from direct light, for 30 min. Post incubation, samples were centrifuged, supernatant aspirated, and re-suspended within 10 mL of 1 X PBS. Samples were returned to the centrifuge, spun down, supernatant aspirated carefully and re-suspended within 1 mL of 1x PBS. All

samples were placed on ice, protected from light; to maintain the stability of the suspensions and the fluorophores used, prior to flow cytometer analysis.

4.2.5.1 Western Blotting –Sodium Dodecyl Sulphate – Poly-Acrylamide Gel Electrophoresis (SDS-PAGE)

4.2.5.1.2 Activ Motif Nuclear and Cytoplasmic Protein Extraction

Refined protein extraction was undertaken with the use of the Active Motif Nuclear Extract Kit (Cat. No. 40010, Active Motif, La Hulpe, Belgium) all kit components were stored at 2-4°C upon arrival and protected from direct light. Cell cultures were establish as outlined in (Section 2.2), counted and washed (Sections 2.2) prior to protein extraction protocol. Additionally, the following solutions were also required to be constructed prior to lysis.

4.2.5.1.2.1 Quick Chart for Preparing Buffers

All buffers containing biological components were made fresh at the start of the protein extraction protocol, stored on ice, and protected from direct light. Phosphatase and protease inhibitor cocktails progressively lose activity, approximately 2 hr post thawing, and therefore, cannot be stored long term as ready-made solutions. Following construction and subsequent short term storage, 2-4 °C, of the PBS/Phosphatase inhibitor solution, if precipitation occurs and the solution becomes turbid, heat at 50 °C for 10 min to dissolve precipitate. The DTT solution provided within the kit comes supplied as a 1M solution, prior to buffer construction the solution is required to be diluted with filter prepared dH_20 to a 10 mM solution; this solution can be stored at -20 °C for up to a year.

Table 4.1. Buffer components and their respective quantities in respect to the volume of starting material.

	Size of Plate or Equivalent Number of Cells (Starting material)		
	60 mm plate (or 3.2x10^6 cells)	**100 mm plate (or 8.8 x 10^6 cells)**	**150 mm plate (or 2 x 10^7 cells)**
PBS/Phosphatase Inhibitors(mL)			
10X PBS	0.4	0.8	1.6
Distilled water	3.4	6.8	13.6
20X Phosphatase Inhibitors	0.2	0.4	0.8
TOTAL REQUIRED	**4**	**8**	**16**
1X Hypotonic Buffer (µL)			
10X Hypotonic Buffer	25	50	100
Distilled water	225	450	900
TOTAL REQUIRED	**250**	**500**	**1000**
Complete Lysis Buffer 10 mM (µL)			
DTT (10mM)	2.5	5	10
Lysis Buffer AM1 22.	25	44.5	89
Protease Inhibitor Cocktail	0.25	0.5	1
TOTAL REQUIRED	**27.25**	**50**	**100**

4.2.5.1.2.2 Cellular Lysis and Protein Extraction

The following method is based on the manufacturers supplied protocol for 3.2 x 10^6 cells, which accompanies purchase of the protein extraction kit. Cellular pellets were re-suspended and subsequently washed with 3 mL of pre-cooled, ice-cold, PBS/Phosphatase inhibitor solution, centrifuged (~250 x g for 7 min) and the supernatant discarded. Following centrifugation, an additional 1 mL volume of ice-cold PBS/phosphatase inhibitors was added, ensuring complete re-suspension, centrifuged and then the resultant supernatant aspirated. Cell pellets were stored immediately on ice throughout the entire protocol. Cellular pellets were re-suspended in 250 µL 1X hypotonic buffer solution, ensuring that the pellets were re-suspended thoroughly via pipetting the mixture several times. Post mixing, the cells were transferred to pre-chilled micro-centrifuge tubes (1.5 mL Eppendorf's), and incubated for 15 min on ice. Post incubation, 12.5 µL of detergent was added, the samples vortexed for 10 seconds at high speed and subsequently centrifuged (14,000 x g for 30 sec). The supernatant, containing the cytoplasmic protein fraction, was transferred into pre-chilled 1.5 mL micro centrifuge tubes as well as three 5 µL aliquots were removed for protein quantification. The cytoplasmic protein fractions were stored at -80°C ready for future use.

The residual cellular pellet was re-suspended in 25 µL complete lysis buffer (10 mM), via pipette agitation/mixing. Immediately, the samples were vortexed for 10 sec at high speed prior to 30 min incubation on ice within a rocking platform (150 rpm). Post incubation, samples were vortexed for an additional 30 sec at high speed, centrifuged (14,000 x g for 10 min) and the resultant supernatant, nuclear protein fraction, transferred into additional pre-cooled micro centrifuge tubes. Analogous to the cytoplasmic fraction, three 5 µL aliquots were removed for protein quantification and the larger volume stored at -80°C.

4.2.5.1.3 Protein Quantification

All protein quantification within this body of work was carried out using the DC ™ Protein Assay Kit 1 (Cat No. 500-01111, Bio-Rad, Hertfordshire, UK) as outlined within the supplied manufactures protocol. Prior to protein quantification, bovine serum albumin (BSA) (Cat No. A9418, Sigma Aldrich, Gillingham, UK) powder was purchased and dissolved in dH_20 in order to construct excess 2.5 mg/mL solution, the solution was aliquotted into 0.75 mL eppendorf tubes and immediately frozen within a -20°C freezer for long term storage. A single aliquot of (2.5 mg/mL) BSA was removed from the freezer and thawed over ice; the following BSA standards were constructed.

4.2.5.1.3.1 Bovine Serum Albumin (BSA) Protein Standards

For each protein quantification plate, five protein (BSA) standards, with known concentration, were constructed, facilitating the use of the stand curve approach to estimate unknown protein quantification. BSA was either diluted in AM1 lysis buffer or 1x hypotonic buffer solution for use with nuclear and cytoplasmic refined, Active Motif ™, protein extraction respectively or alternatively RIPA buffer for use with crude protein extraction methodology.

Table 4.2. BSA standard construction.

Concentration of BSA Standard (mg/mL)	Volume of BSA component (µL)	Volume of Buffer component (µL)
0	0	20
0.5	4	16
1	8	12
1.5	12	8
2	16	4
2.5	20	0

4.2.5.1.3.2 Protein Quantification - Microplate Reader

30 µL of reagent S was added to 1.5 mL of reagent A, in the ratio of 1:50, this amount is adequate for approximately 60 wells, thoroughly mixed via a pipette and placed on ice. Each experimental sample was loaded in triplicate within a 96-well microtiter plate (96-Well Standard Microplate, Thermo Scientific, Hampshire, UK) as well as corresponding protein standards, using the correct diluent for optimum results.

Each 96-well plate was constructed as outlined below; note that the number of samples under assay is highly variable between experiments.

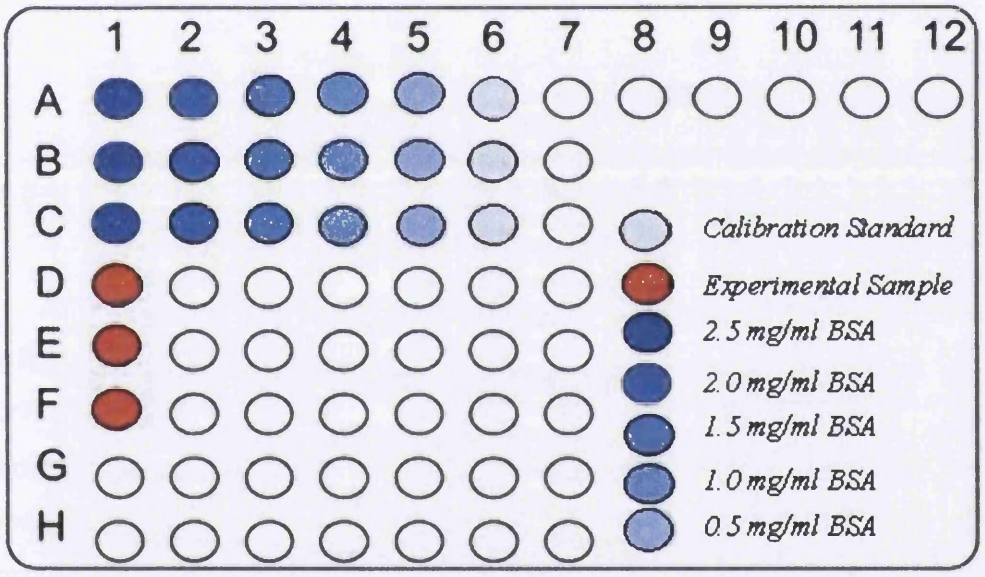

Figure 4.1. Overview of the 96 well plates used for protein quantification prior to incubation pre-plate reader analysis. Colour coding included, highlighting the decrease in protein standard concentrations as one moves horizontally across the plate.

5 µL of each protein (BSA) standard solution was pipetted directly into a clean, dry, 96-well microtiter plate, repeated in triplicate, enabling sequential protein quantification. Nuclear and cytoplasmic protein fractions were analysed separately using different standard solutions on separate plates. Following experimental and standard plating, 25 µL of working reagent A was pipetted directly into each well, 200 µL of reagent B, supplied within the purchased kit, was added sequentially and each plate was incubated for 15 min at room temperature under rolling (150 rpm) conditions. During the incubation, the reagents were able to mix thoroughly; in the event of bubble formation within the well, using a needle (21G) each bubble was individually dispersed. Post incubation, each well was examined for the characteristic colour change as well as assessed for the absence of bubbles. The plates were transferred and read on the FLUOstar Omega spectrophotometer (BMG Labtech, Ortenberg, Germany) at 750 nm, and their respective protein quantities estimated. If plates were unable to be read immediately, they were placed on ice and protected from direct light for a maximum of an hour prior to analysis.

4.2.5.1.3.3 FLUOstar Omega Protein Quantification Data Analysis

All retrospective data analysis carried out, post protein extraction, was undertaken utilising the FLUOstar plate reader and corresponding MARS Data Analysis Software (BMG Labtech, Ortenberg, Germany). The instrument was directed to measure the absorbance at 750 nm of the well contents in turn and utilising the protein standards, of known concentration construct, a standard/calibration curve was calculated. Utilising a common approach to data analysis, a linear regression fit function was chosen and the model was assessed for "Goodness of fit". Spurious results were omitted in order to achieve an r^2 value of >0.99, however, only a maximum of a single data point was removed within each triplicate to retain statistical integrity. Each run took approximately 1-30 mins depending upon the number of empty wells on each plate, omitted from data analysis. Using the derived standard curve, the concentration of the unknown experimental protein samples was estimated. Plates were discarded post analysis and disposed of according to health and safety regulations.

4.2.5.1.4 Western Blotting Buffer Solution Preparations

Prior to the undertaking of any Western Blott analysis, a combination of long term (up to one month storage) and short term buffer solutions (maximum of one week storage) were required to be constructed. Short term buffer solutions were made up fresh on the day of experimentation, and used immediately.

4.2.5.1.4.1 Preparation of Long Term Buffer Solutions

10% (w/v) Ammonium Persulphate (APS) – 1 g of Ammonium Persulphate (Cat No. GE17-1311-01, Sigma Aldrich, Gillingham, UK), weighed accurately on a Sartorius LA120S Analytical Balance, was transferred into a fresh 250 mL glass McCartney bottle. 5 mL of filter prepared dH_20 was added to dissolve the solute, prior to the final volume being adjusted to a 10 mL total volume, the solution was stored at 2-4°C protected from direct light.

Laemmli Buffer (2X concentrate) was purchased from Bio-Rad (Cat No. 161-0737, Bio-Rad, Hertfordshire, UK), stored at room temperature on the bench top, protected from direct light. Prior to use the buffer was activated via the addition of B-mercaptoethanol (BME) (Cat. No 161-0710, Bio-Rad, Hertfordshire, UK); 50 µL (BME) was added to 950 µL of (2X) Laemmli buffer within the AFA1000 fume cupboard, mixed thoroughly and stored on ice prior to immediate use.

Alternatively Laemmli buffer could have been constructed using the following recipe (62.5 mM Tris (pH 6.8), 2% (w/v) Sodium Dodecyl sulphate (SDS), 10% (v/v) Glycerol, 0.02% (w/v) Bromophenol blue (store at -80°C as 245µL aliquots). Add 5µL (2% v/v) B-mercaptoethanol before use.

10% (w/v) Sodium Dodecyl Sulphate (SDS) – 25 g of SDS (Cat No. 151-21-3, Sigma Aldrich, Gillingham, UK) was weighed accurately and transferred into a 500 mL glass McCartney bottle. 100 mL of double distilled filter prepared H_20 was initially added to dissolve the solute, with an additional volume of H_20 added in order to construct a final volume of 250 mL. Solution was stored on the bench top at room temperature protected from direct light.

1.5M Tris (pH 8.8) – 45.4 g of Tris Base (Cat No. 77-86-2, Sigma Aldrich, Gillingham, UK) was weighed accurately and transferred into a 1 L glass McCartney bottle. 250 mL ddH20 was added, mixed thoroughly and the solute dissolved. Using a Jenway 3510 pH meter, the pH was initially measured and adjusted to 8.8 via the drop wise addition of Hydrochloric Acid (1M). Excess dH_20 was added in order to construct a total volume of 1 L (molecular weight of Tris is 121.14g/Mol). Solution was stored on the bench top at room temperature protected from direct light.

1M Tris (pH 6.8) - 30.3 g of Tris Base, weighed out accurately, was added to 250 mL of ddH_20 within a glass McCartney bottle. Using a pH meter, the pH was adjusted via the drop wise addition of 1M HCL solution and total volume adjusted to 1 L via the addition of excess dH_20. Solution was stored on the bench top at room temperature protected from direct light.

Tris/Glycine/SDS 10X – 30.3g of Tris Base was weighed accurately and transferred into a glass McCartney bottle containing 500 mL of ddH_20, mixed thoroughly and dissolved. 144.1g of glycine (Cat No. G8898, Sigma Aldrich, Gillingham, UK) and 100 mL of 10% (w/v) SDS were also added sequentially, and excess ddH_20 was used to adjust the total volume to 1 L. Solution was stored on the bench top at room temperature protected from direct light. (250nM Tris (pH 8.3), 1.92 M Glycine and 1% (w/v) SDS).

TBS 10 X – 24.2 g of Tris Base and 80.1g of Sodium Chloride (NaCl) (Cat No. S7653, Sigma Aldrich, Gillingham, UK) were weighed separately and accurately prior to being transferred into a 1l glass McCartney bottle. 800 mL of ddH_20 was added, mixed thoroughly and solutes diluted, pH measured and adjusted to prevent acidic properties, and the final volume was adjusted to 1 L via the addition of excess dH_20. (200mM Tris (pH 7.6) and 1.37 M NaCl). Solution was stored on the bench top at room temperature protected from direct light.

4.2.5.1.4.2 Preparation of Short Term Buffer Solutions

Running Buffer – 100 mL of Tris/Glycine/SDS 10X (Appendix 4.2.5.1.4.1) solution was transferred into a fresh 1 L McCartney bottle, 900 mL of ddH_20 was added, the bottle inverted several times and labelled according to GLP. Once suitably mixed, the bottle was placed on the bench top, protected from direct light and used with 24-48 h. (25mM Tris (pH 8.3), 192 mM Glycine, 0.1% (w/v) SDS)

TBS/T Wash Buffer – 100 mL of TBS 10X (Appendix 4.2.5.1.4.1) was measured out and transferred into glass 1 L McCartney bottle, to this 10 mL of 10% (v/v) Tween 20 (Cat No. P9416-50 mL, Sigma Aldrich, Gillingham, UK) was added and the contents of the bottle inverted several times. Prior to refrigeration, the final volume of the solution was adjusted to 1 L via the addition of ddH_20. (20mM Tris (pH 7.6), 125 mM NaCl, 0.1% (v/v) Tween20)

Bovine Serum Albumin (BSA) blocking buffer – 12.5 g of BSA powder was weighed accurately and transferred into a 500 mL glass McCartney bottle. To this, TBS/T was added to achieve a final volume of 250 mL, flee added and the solution mixed thoroughly at room temperature until the BSA had dissolved producing a distinct colour change. (20mM Tris (pH 7.6), 137 mM NaCl, 5% (w/v) BSA) 0.1% (v/v) Tween20)

Stripping Buffer – 3.8g of glycine was weighed, transferred into a 500mL glass McCartney bottle followed by the sequential addition of 2.5 mL 10% (w/v) SDS (Appendix 4.2.5.1.4.1) and 2.5 mL 10% (v/v) Tween20. Prior to addition of ddH_20, the pH was measured and adjusted via drop wise addition of HCL (1m) solution and the final volume adjusted to 250 mL. (200mM Glycine (pH 2.2), 0.1% (w/v) SDS, 1% (v/v) Tween 20). Alternatively, Restore Western Blott Stripping Buffer (Cat No. 21059, Thermo Scientific, Hampshire, UK)

Transfer Buffer – 200 mL of absolute methanol (34860 – 2L, Sigma Aldrich, Gillingham, UK) was measured out within an AFA1000 fume cupboard, and decanted into a 1 L glass McCartney bottle. 100 mL Tris/Glycine, SDS 10X (Appendix 4.2.5.1.4.1) was added and the total volume adjusted to 1 L via the addition of ddH_20. (20mM Tris (pH 8.3), 192 mM Glycine, 20% (v/v) Methanol, 0.1% (w/v) SDS)

4.2.5.1.5 Polyacrylamide Gel Preparation

All western blot analysis was carried out following the procedures outlined in (Appendix 4.2.5.1), the gels constructed for this body of work were polyacrylamide based and the constituent components of each gel were purchased and stored according to manufactures guidance; 30% Acrylamide/Bis solution, 19:1 dilution ratio (Cat No. 161-0154, Bio-Rad, Hertfordshire, UK) and TEMED (Cat No. T-9281-50 mL, Sigma Aldrich, Gillingham, UK) were stored at 2-4°C protected from light and further information about the buffers used can be found in (Appendix 4.2.5.1.4.1 – 4.2.5.1.4.2). The addition of TEMED in combination with Polyacrylamide forms a gels matrix suitable for the resolution of macromolecules; percentage composition polyacrylamide governs the lattice structure, in conjunction with detergent treatment facilitates a 2-dimensional linear separation of proteins. The percentage composition of resolving gel was based directly upon the molecular

weight of the protein under assay; large proteins required lower acrylamide composition. Preparation of gels was undertaken in an AFA1000 fume hood due to the environmental pollutant nature of the chemicals used.

Table 4.3.Gel constituents.

	Stacking Gel		**Resolving Gels**							
	4%		**6%**		**8%**		**10%**		**12%**	
	2 Gels	4 Gels	2 Gels	4 Gels	2 Gels	4 Gels	2 Gels	4 Gels	2 Gels	4Gels
30% Acryl	0.65	1.3	3	6	4	8	5	10	6	12
dd$H_2$0	3	6	8	16	7	14	6	12	5	10
1.5M Tris (pH 8.8)			3.75	7.5	3.75	7 .5	3.75	7.5	3.75	7.5
1M Tris (pH 6.8)	1.25	2.5								
10% SDS (µL)	50	100	150	300	150	300	150	300	150	300
10% APS	25	50	75	150	75	150	75	150	75	150
TEMED (µL)	5	10	15	30	15	30	15	30	15	30

4.2.5.1.6 Gel Casting and Electrode Assembly

All western blott apparatus used within this project was purchased from Bio-Rad; however, many of the Kits have been discontinued in recent years, therefore, where appropriate the currently available kit will be referenced. Be aware that the current kit may contain newer versions of the apparatus used; however, their basic design and features are analogous to the apparatus used when casting and running the Western Blott gels and subsequent analysis.

Prior to casting, all plates, spacers, combs and casting stands (Mini-PROTEAN Tetra Cell #165-8007, Bio-Rad, Hertfordshire, UK) were washed thoroughly with 70% ethanol and allowed to air dry, facilitating correct set up alignment. 1.5 mm glass plate assemblies were fitted together, the larger plate at the rear, assembled into the casting stand and the whole set up was checked for integrity. .

The desired resolving gel recipe was prepared and then applied directly to the cast via 5 mL pipette and pipette gun (MACROMAN ™ Pipette Controller, Gilson, Middleton, USA), leaving approximately 2-3 cm for the stacking gel. Isopropanol, (Cat No. 190764, Sigma Aldrich, Gillingham, UK) minimal volume, was applied across the top of the gel and incubated at room temperature for 30-60 minutes. Post incubation, the gel was assessed for hardening and the entire rack inverted and isopropanol discarded. The stacking gel was applied directly onto of the resolving gel, in an analogous method, and the corresponding (1.5mm) 10 well comb was inserted evenly into the resolving gel. Following a final assessment for alignment and potential retarding bubble formation, the set up was incubated for a further 30-60 min at room temperature.

Post hardening and gel melding the plate assembly was removed from the casting stand, comb removed and transferred into central chamber of the 2-gel vertical electrophoresis system. 20-40 µg of protein sample was added to equal volumes of activated (addition of BME) Laemmli buffer (1:1), vortexed for 30 sec at high power and heated at 95-100°C for 5 min. Dual colour (Precision Plus Protein ™ Dual colour standards #161-0374, Bio-Rad, Hertfordshire, UK) and biotinylated

molecular weight ladder (Cat No. B2487, Sigma Aldrich, Gillingham, UK) were thawed during the incubation.

Post incubation, the central chamber was placed within the 2-gel electrophoresis system and partially filled with running buffer (Appendix 4.2.5.1.4.2). Running buffer was poured directly into the wells to facilitate loading as well as covering the electrode at the base of the chamber sufficiently. 10 µL of the protein standards, Dual colour and biotinylated were pipetted into the first two wells respectively followed by the protein-Laemmli samples into the corresponding remaining wells. When pipetting samples the pipette tip was placed firmly within the centre of the well and removed prior to full discharge preventing bubble formation. The lid of the electrophoresis system was placed onto the chamber, connected via colour coded leads to the power pack (PowerPack Basic Power Supply, Cat No. 164-5050, Bio-Rad, Hertfordshire, UK) and the whole assembly was run at 120 V for approximately 60 min. When the dye front had migrated to within an inch of the base of the gel, the power pack was disconnected and the running buffer removed and discarded.

Each assembly was run at 120 v until the dye front had reached the bottom of the gel which took approximately 60 mins.

4.2.5.1.7 Protein Transfer

Protein transfer during this thesis project was carried out using the Mini Trans-Blot® Electrophoretic Transfer Cell kit contents (Cat. No. 170-3930, Bi-Rad, Hertfordshire, UK), operated according to manufacturer's supplied guidance. Unless otherwise stated, all apparatus was supplied within the kit and used in conjunction with buffers prepared according to (Appendix 4.2.5.1.4.1 – 4.2.5.1.4.2).

Immuno-Blot PVDF membranes (Bio-Rad, Hertfordshire, UK), one per protein gel, were submerged in 100% methanol, performed within an AF1000 fume hood, until the membrane became translucent (~10-30 sec). Simultaneously to this, two fibre pads, extra thick blott papers (cat No. 170-3965, Bio-Rad, Hertfordshire, UK) were incubated in pre-cooled 4°C transfer buffer (Appendix 4.2.5.1.4.2). Post incubation,

transfer cassettes were constructed ready to house the freshly ran protein gels. Transfer cassettes were opened, placed flat on a drainable work surface and loaded with a single fibre pad and filter paper. Protein gels were removed from their glass-ware, washed in transfer buffer, and placed faced down (standard on the right hand side) onto the filter paper. A re-hydrated PVDF membrane was positioned on top of the gel, ensuring full coverage, and the cassette was completed via the addition of an additional filter paper and fibre pad. Before the cassettes were finalised, a small rolling pin was used to flatten the membrane against the gel to ensure an effective protein transfer. The cassette was lock and placed within a Transfer cell, prior to the sequential addition of cooling unit (containing frozen transfer buffer) and filled with cold transfer buffer. The whole apparatus was placed within a polystyrene container filled with ice and moved into the cold room to maintain a constant 2-4°C environment. A power pack was attached to the transfer cell and ran at 400 mA for 1.5 hr.

Post transfer, the cassette was removed from the transfer cell and unlocked; all contents except for the membranes were discarded according to laboratory health and safety protocols. The membrane was submerged in pre-cooled (2-4°C) TBS/T wash buffer (Appendix 4.2.5.1.4.2), agitated and cut via a scalpel to ensure separation of the protein samples and the biotinylated ladder, preventing any potential contamination issues. A small notch was cut in the lower left corner of each membrane piece to facilitate correct orientation during Western Blott analysis.

4.2.5.1.8 Membrane Blocking and Antibody Incubation

Membrane/s were incubated overnight (approximately 8-12 hr) in approximately 5-10 mL of pre-cooled blocking buffer (Appendix 4.2.5.1.4.2) at 2-4°C. The membrane/s was placed on a rocking/shaking platform (~200 rpm) for the duration. As a precaution, to minimise detection of endogenous biotin carrier proteins, approximately 50 µg/mL of avidin was added to the biotinylated protein standards blocking buffer/solution. Post incubation, blocking buffer was removed and the membranes washed; wash steps were achieved via the addition of 5-10 mL of TBS/T

buffer (Appendix 4.2.5.1.4.1) and placed on a rotating platform (~1500 rpm) for 5-7 min.

Generally, primary antibodies raised against the protein of interest within that specific blott were rabbit monoclonal antibodies and diluted within 10 mL of blocking buffer. Post dilution, membrane/s were treated with the primary antibody solution (10 µL primary antibody solution diluted 1:1000 within BSA blocking buffer) for 1 hr at room temperature under shaking conditions (~200 rpm), washed several times (a minimum of 4) and sequentially incubated in corresponding horse radish peroxidase (HRP)-conjugated secondary antibody solution (10 µL HRP-antibody diluted 1:1000 within BSA blocking buffer) for an additional 1 hr. The biotinylated protein standards were incubated in the Streptavidin HRP-conjugate (Bio-Rad, Hertfordshire, UK) BSA blocking buffer (1:1000) solution for an analogous incubation period. Post incubation, membranes were washed five times and during this period of time the ChemiDoc ™ XRS (Bio-Rad, Hertfordshire, UK) was switched on and the supplied Quantity One (Bio-Rad, Hertfordshire, UK) software loaded.

4.2.5.1.9 Protein Detection – ChemiDoc ™ XRS

4.2.5.1.9.1 Protein of Interest Detection

Protein detection was under taken using the Clarity Western ECL substrate (Cat No. 170-5060, Bio-Rad, Hertfordshire, UK) chemilluminescence kit, stored and operated as per manufacturers supplied instructions. Prior to visualisation, the "luminol" enhancer and peroxide buffer solutions were mixed, 1:1 and stored protected from light until ready for use. Post washing, the membranes were removed and placed onto the pre-cleaned ChemiDoc™ surface.70% ethanol and professional care tissues were used to clean the surface thoroughly without causing damage. Using stainless steel straight forceps the membrane was moved into position and aligned with its corresponding biotinylated standards under epi-white light. Once in position, the

white light was switched off, and the pre-made visualising agents was applied liberally to the membrane, concentrating on regions of interest, the ChemiDoc™ was closed and the membrane incubated for 5 min. Post incubation the camera was adjusted within the Quantity One software to a high focus and the membranes were exposed to trans-UV light for a minimum of 10-30 sec, exposure length was highly variable depending upon abundance and the protein bands visualised and captured via the incorporated digital camera.

4.2.5.1.9.2 Stripping Membranes and House Keeper Detection

Post probing for the protein of interest, the membranes were removed, washed (Appendix 4.2.5.1.8) and treated with Restore Western Blott Stripping Buffer. Membranes were exposed twice to 5-10 mL of striping buffer for a period of 10-15 min, washed extensively and re-hydrated in 100% methanol. Following re-hydration, membranes were washed and treated with the anti-house keeper antibody as outlined in (Appendix 4.2.5.1.8). Succeeding secondary conjugation, washing and placement in the ChemiDoc ™, the membrane was aligned and treated with the illuminator/enhancer solution (Appendix 4.2.5.1.9.1) and incubated prior to protein band detection (Appendix 4.2.5.1.9.1).

4.2.5.1.10 Protein Quantification – Quantity One Software

All protein band detection and estimated quantification were retrospectively undertaken using the Quantity One – Advanced software purchased from Bio-Rad, Hertfordshire, UK. During protein band visualisation the Quantity One software was loaded, save directory chosen and used initially to capture a still image of the western blott membrane post UV exposure (Appendix 4.2.5.1.9). The image was cropped, aligned correctly and each band was distinctly classified, including an additional band for background. The relative band intensities were initially standardised against the background, following this, each sample band was

normalised against the corresponding house keeper band, averaged against experimental replicates and divided against the con-current negative control generating the average relative fold increase in band intensity when compared to un-treated controls. Western Blott analysis for proof of principle experimentation was carried out in experimental replicates, Standard error of the Mean (SEM) error bars included, however, within experiments requiring a greater level of confidence, biological replicates from individual cell cultures were utilised.

4.2.5.2 Qualitative Real Time – Polymerase Chain Reaction Protocol

4.2.5.2.1 Ribonucleic Acid (RNA) Extraction

Total RNA was extracted from the human lymphoblastoid cell lines using the Qiagen RNeasy Mini Kit (Qiagen, Sussex, UK) and followed according to the manufacturers` instructions. Cell cultures were established as outlined in (Section 2.2), counted and washed prior to the extraction. The volume of cells equivalent to 8 x 10^6 cells was extracted from the cultures, transferred into 50 mL centrifuge tubes, centrifuged (250 x g for 7 min) and supernatant was aspirated. Cellular pellets were re-suspended in 600 µL of RLT buffer, homogenized (passing the lysate through a needle (21G) a minimum of 3 times) and then diluted in 600 µL of 70% ethanol. Following ethanol addition, solutions were mixed thoroughly using a 1000 µL pipette and the contents (~700 µL) was applied to the supplied columns within the kit. The column was then placed within a 5424 24 Place Eppendorf Micro centrifuge (Eppendorf, Hamburg, Germany), centrifuged (>8000g for 15 sec) and diluent discarded. This step was repeated in order to load the total ~1200 µL volume of starting solution into the column. Post centrifugation, DNase digestion followed; DNase I stock solution was added to 70 µL RDD buffer - RNase-Free DNase Set (Qiagen, Sussex, UK) – 350 µL RW1 buffer was added to the column and centrifuged (as above). Post centrifugation, the DNase I incubation mix (80 µL) was directly applied to the centre of the column membrane and incubated at room temperature for 15 min. Following incubation, the column was washed with 350 µL

RW1 buffer, centrifuged (as above) and washed again with a 500 µL volume of RPE buffer. Following centrifugation (as above) another 500 µL of RPE buffer was added to the column and centrifuged (≥8000 x g for 2 min). The column was carefully removed, and then transferred to a fresh collection tube and centrifuged at full speed for 1 min to ensure complete dryness. The column was transferred to a fresh collection tube, 33 µL Nuclease-free water was added to the column membrane and incubated for 3 min at room temperature, prior to being centrifuged (≥8000 x g for 1 min). The contents of the collection tube was labelled according to GLP protocol, 3 µL aliquot removed for purity assessment and placed within a -80°C freezer for short term storage.

4.2.5.2.2 RNA purity Assessment - Nanodrop

Following the RNA extraction (Appendix 4.2.5.2.1) the RNA yield was measured and the purity assessed (260:280 ratio) using a NanoDrop ND-1000 Spectrophotometer (Labtech International, Uckfield, UK). The NanoDrop was switched on and the supplied software loaded, prior to being directed to assess "Nucleic Acids", in which "RNA" was selected, for purity and content. 1 µL of sterile, nuclease-free, dH_20 was pipetted directly onto the detector plate, the machine was calibrated and the water wiped off using professional care wipes (Kimberly Clark ®, Kent, UK).1 µL volumes of the extracted RNA were pipetted sequentially onto the detector, a wash step using nuclease-free water was implemented between each assessment, (260:280), (260:230) and content were recorded for each sample; excess RNA was stored at -80 °C until further use.

4.2.5.2.3 Double Stranded Copy DNA (cDNA) Synthesis

Double stranded cDNA synthesis was carried out for all the human lymphoblastoid cell lines using the QuantiTect Reverse Transcriptase Kit (Cat No. 2053111, Qiagen, Sussex, UK) and followed according to the manufacturers` instructions. The protocol is for use with 10 pg to 1 µg RNA, therefore, reaction volumes can be scaled up to enable > 1 µg RNA starting material. All stages of cDNA synthesis were carried out

within the PCR hoods, thorough 70% ethanol cleaning followed by RNase decontamination (RNase ZAP™, Life Technologies ™, Paisley, UK) and extensive UV sanitization were under taken prior to any work. Previous to thawing the total RNA, all precipitates within the gDNA Wipe-out buffer were dissolved by vortexing, no precipitates required warming (37°C) to dissolve. Template RNA, Quantiscript reverse transcriptase, RT primer Mix, gDNA Wipe-out buffer, Quantiscript RT buffer and nuclease-free H_20 were all thawed over ice for 30 min, flicked to enable mixing and centrifuged briefly to collect the liquid from the sides of the tubes. For the duration of the protocol all solutions were kept on ice and protected from direct light. The initial stage within the protocol was to establish a genomic DNA elimination reaction as follows; 2 µL of gDNA Wipe-out Buffer (7x) was added to a variable volume of RNA template, equivalent to 1 µg within a 0.75 mL eppendorf, and RNase-free water was added to create a final reaction volume of 14 µL. Each sample was incubated at 42°C for 2 min within a T100 PCR Thermal Cycler (BioRad, Hertfordshire, UK) and immediately placed on ice post incubation. The second stage of the protocol was to enable first strand synthesis and subsequent amplification of the newly formed genomic cDNA. 1 µL of Quantiscript Reverse Transcriptase, 1 µL RT Primer mix and 4 µL of Quantiscript RT buffer (5X) were aliquotted into a fresh 0.75 mL eppendorf, these components when mixed made up the reverse-transcriptase master mix. To the master mix, 14 µL of newly prepared template RNA was added and placed on ice prior to incubation. Each sample was transferred back into the heating block of theT100 PCR thermal cycler and incubated at 42 °C for 15 min. Incubation time can be increased to a maximum of 30 min, if the RT-PCR product is longer than 200 bp, in order to maximise yields. Post incubation, each sample was in-activated for 3 min at 95°C, within the thermal cycler, and immediately labelled according to GLP prior to short term storage within a -80 °C freezer.

4.2.5.2.4 Quantitative Real-Time Polymerase Chain Reaction (qRT-PCR)

Real-time PCR experiments were undertaken using the QuantiFast™ SYBR® Green PCR Kit (Qiagen, Sussex, UK) in combination with synthesised cDNA following the

protocols outlined in (Appendix 4.2.5.2.3). The reactions were set up in the PCR hood using sterile equipment, as described in (Appendix 4.2.5.2.3) and all stock solutions kept on ice protected from light. Master mixes, prepared in triplicate, were initially constructed consisting of the following; 50 µL (2X) QuantiFast SYBR Green PCR Mast Mix, 1 µL Primer A, 1 µL Primer B, 6 µL of template cDNA (genomic DNA can be used) and 42 µL of RNase-free water, constructing a total reaction volume of 100 µL (4 x 25 µL). All solutions were made in excess within 0.75 mL Eppendorf's, as each sample was run in triplicate and thawed over ice, protected from light prior to experimentation. 25 µL of each resultant master mix was aliquotted separate adjacent wells of a sterile 96-well 0.2 mL PCR plate (Sarstedt, Nuembrecht, Germany). Experimental samples, standard serial dilutions as well as non-template negative controls were also included for each primer pair. Within the negative controls, cDNA was replaced with RNase-free water and the inclusion of standard wells allowed post analysis PCR efficiency to be calculated. Post plating, each individual 96 well-plate was sealed with an Absolute QPCR Seal sheet (Thermo Scientific, Surrey, UK), any air pockets disrupted and centrifuged briefly before being transferred into the iCycler iQ5 thermal Cycler (BioRad, Hertfordshire, UK). The thermal cycler was then programmed with the following schedule which took approximately 1.5 hr per plate.

4.2.5.2.4.1 iCycler iQ5 thermal Cycler Programme Breakdown

Step 1 - 95°C for 5min

Step 2 - 95°C for 10sec ┐
Step 3 - 60°C for 30sec ┘ X 40

Step 4 - 95°C for 1min

Step 5 - 55°C for 1min

Step 6 - 0.5°C increments in temperature starting from 55°C to 95°C - melt curve analysis

Step 1 is included to activate the HotStarTaq Plus DNA polymerase, with subsequent steps 2 and 3 representing the PCR reaction (denaturation and annealing/elongation). Steps 4, 5 and 6 are included in order for the software to generate an accurate melt curve. Data was collected at step 3 as well as step 6 for PCR amplification and melt curve respectively and analysed in real time. Retrospective analysis was carried out following the completion of the entire plates, cross plate comparisons were also under taken utilising the on-board software to create a "gene study".

4.2.5.2.4.2 iCycler iQ5 Data Analysis

All retrospective analysis was carried out using the manufacturer supplied iCycler iQ5 software version 2.1 (BioRad, Hertfordshire, UK). Melt curve analysis was undertaken; specificity of PCR products as well as the efficiency of the plate was defined. Any discrepancies found within the melting temperature (Tm) of the PCR product, or the PCR efficiency, resulted in that specific wellbeing omitted from analysis. Relative quantitation of gene expression was achieved using the standard curve method [16]. Standard samples, non-template controls as well experimental samples were all defined within the "sample setup" view. Stock cDNA samples were constructed (10-fold serial dilutions with the dilution values: 1, 10, 100 and 1000). The standard wells were utilised to construct a standard curve, omitting errorous wells non-conforming to an r^2 figure of 0.99 or greater, i.e. the data fell outside of the acceptable criteria for a "good fit". The threshold points or crossing points (C_Ts) were plotted against the log of the template amount, resulting in a straight line. Threshold cycle (C_T) values for the experimental samples were then used with the standard curve to estimate the amount of starting template in each well. All samples were normalised by their respective endogenous control genes selected with homogenous high expression across all tissue or cell lines under assay, and the resultant normalised target value used to calculate the fold-difference in target when compared to con-current negative or un-treated samples.

4.2.5.2.4.3 Equations Used During iCycler iQ5 Data Analysis

4.2.5.2.4.3.1 Normalised Target (Well Specific)

Normalized target = Target/Endogenous control

The normalized target values were then divided by one another (concurrent or un-treated sample) to calculate the fold-difference in target quantity.

4.2.5.2.4.3.2 Fold Difference (Treatment Specific)

Fold difference = Normalized target (treated sample)/ Normalized target (un-treated sample)

4.2.5.3 P53 Functionality Assessment Following MMC Treatment

Mitomycin C (MMC) (Cat No. M4287-2MG, Sigma Aldrich, Gillingham, UK) came supplied as a 2 mg powder, stabilised within 48 mg of NaCl to enable minimum effort dissolving and distribution. 4 mL of dH_20 was added to the powder and re-constituted at the final concentration of 0.5 mg/mL (0.5g/L). The solution was aliquotted into 0.5 m L eppendorf tubes and stored, sealed in a separate box, and placed within a -20 ºC freezer. Prior to usage within the experiment, a serial dilution was undertaken, utilising dH_20 as the diluent generating a 0.05 mg/mL stock defined as "A" and a further 0.005 mg/mL stock "B".

4.3 Results

4.3.5 Normal TK6, AHH-1 and MCL-5 Cell Line Characterisation

In order to evaluate the potential variability between the low passage and normal TK6 cell cultures, in terms of surface antigen expression, immunofluorescence staining was employed to assess the expression of well characterised cellular surface antigens as well as their diverse nature of functionality within the cell line. CD55 and CD59 are typical cellular surface antigens found within haemopoetic lineages, FLAER is a bacterial toxin able to bind to the GPI anchor moiety which attaches a whole plethora of cellular surface markers to the membrane and CD48 is a cell line specific marker for activation. Evaluation of the generated results would be an indication of how comparable the cell lines are outside of the context of dose sensitivity and recovery to genotoxic exposure.

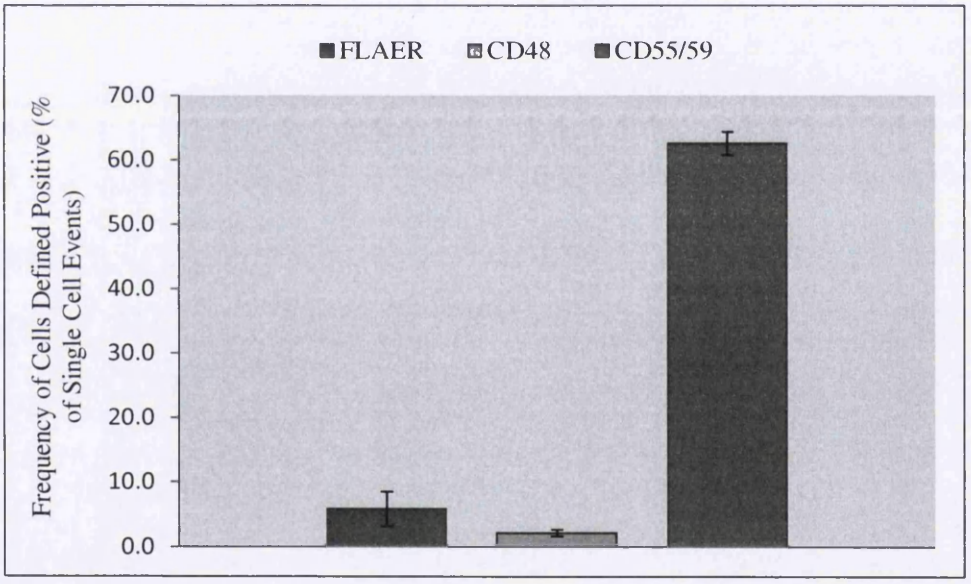

Figure 4.2. Relative average cell surface marker expression, with respect to parental control parental population, within "Low Passage" TK6 cells. FLAER (stock conc) – Alexa Fluor 488 ™ conjugate, CD48 phycoerythrin conjugate and CD55/59 phycoerythrin conjugate fluorescent dyes utilised and data captured within their respective detectors. (~10,000 single cellular events) (N=3, Error Bars ±1SD).

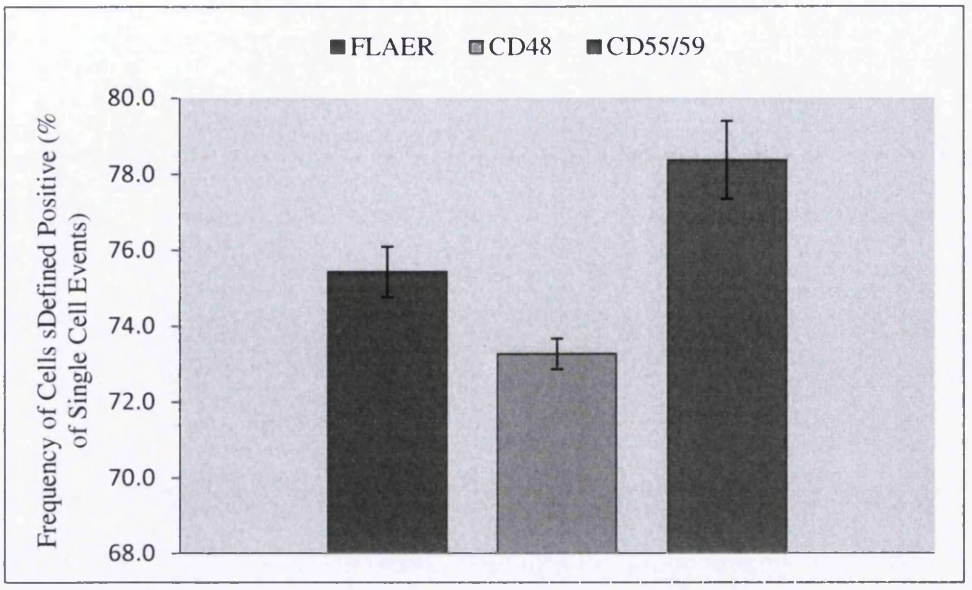

Figure 4.3. Relative average cell surface marker expression, with respect to parental control parental population, within "Normal" TK6 cells. FLAER (stock conc) – Alexa Fluor 488 ™ conjugate, CD48 phycoerythrin conjugate and CD55/59 phycoerythrin conjugate fluorescent dyes utilised and data captured within their respective detectors. (~10,000 single cellular events) (N=3, Error Bars ±1SD).

The "Low Passage" TK6 cells were shown to have minimal FLAER staining (5.9%), even at the top concentration tested (top concentration (2.5 µg/mL), negligible CD48 staining (2.2%) and marginal CD55/59 expression (62.6%) (Appendix Figure 4.2). Relatively little variation was observed within the culture and cells were microscopically assessed for signs of distress prior to assessment. The "Normal" TK6 cells demonstrated comprehensive staining, approximately 75% for all markers challenged within the scope of this experiment; CD48 (73.3%), CD55/59 (78.4%) and finally top concentration FLAER (75.4%) (Appendix Figure 4.3). The "Normal" TK6 population demonstrated extensively greater average expression values when compared to the "Low Passage" cell stock.

4.4.2 CD55 Antigen Optimisation using Fluorescence Activated Cell Sorting (FACS)

As a particle passes through the nozzle the fluorescence illumination data is acquired, following excitation and subsequent emission and said particle is assigned an identity. The user is able to directly charge the nozzle and apply a unique voltage to a cell or sub population of interest. As the stream reaches its break off point and forms successive droplets of sheath fluid, each potentially containing a single or multiple events, it passes through two charged deflector plates. The droplets fall through said plates, and the pre-determined carried charge facilitates repulsion and hence, re-direction from the parental stream, into a side stream which is able to be captured for further passage and analysis [17]. Immunofluorescence staining is often utilised in tandem with FACS to identify and isolate sub populations of cells from heterogenous parental populations; applications within clinical medicine [18], disease diagnosis as well as scientific research [19] are common.

The initial rounds of sorting took approximately 2-5 hrs, the various set up stages were time consuming and often required minor alterations which were highly tedious and prolonged set up. The side-stream intensity, as measured by diode laser intersection, and hence stability was the major perturbing factor, especially prominent during the accudrop drop delay calibration and hence directly affected sorting efficiency. Following, the initial sorting methodology (Section 2.8.3), the cell population was visually separated into viable and non-viable fragmented cells. The viable population, the right quadrant on a bi-modal distribution, had a fluorescence profile matching the 50% upper percentile of the pre-enriched sample. However, severe viability problems immediately post sort predestined that the recovered cells often displayed expression profiles consistent with debris or fragmented cells and following further propagation cultures displayed noteworthy *PIG-A* mutant populations (Figure 4.5). Additional rounds of investigation and protocol amendment were utilised to assess the impact collection vessel size, constituency in terms of

density and collection liquid viscosity had on viability and hence sort efficiency (Section 4.3.2).

Apart from the physical properties of the flow cytometer set up an additional software level of regulation is built in, referring to the stringency of the sort process. This in turn can be broken down into two separate issues, i) drop count (yield and purity masking) and ii) phase masking which both have a similar effect of the efficiency. Drop count refers to the stringency of the sort process to determine how many drops the system will deflect when a target particle is detected (sort event). When a particle is expected to be close to the edge of a drop it is beneficial to sort the adjacent drop, depending upon stringency, one or two drops can be sorted. Purity masks prevent the drop from being deflected if no particle of interest is actually present within the droplet. Finally, phase masking, only applicable with purity masks, govern the effects the presence of additional particles within a close proximity to the droplet of interest, and defines the conditions in-which software aborts occur. The more stringent the control of the sort process the more frequent the cytometer will abort the sort to prevent potential contamination (software aborts), and therefore, increase sort purity, not yield [20].

Cell viability pre and post sorting, particularly prominent in this instance due to the potential of non-viable single cell events mimicking presumptive *PIG-A* mutants, is critical in aiding recovery as well as yield. Cell lines are highly sensitive to changes in pH and buffer constituency and often as a result fail to recover post sorting [15, 21], intense attention to detail in terms of cell wellbeing is essential for optimum results; the time in which the process occurs to prevent apoptotic triggers [22], the aseptic nature of the entire process, the respiration rate and maintained temperature post sort all impact the purity results.

4.4.5 Normal TK6, AHH-1 and MCL-5 Cell Line Characterisation

In order to come to a final decision whether to incorporate "Low Passage" TK6 cells into the in vitro *PIG-A* assay design, an additional comparison of potential GPI-AP reporter markers was investigated. The "Low Passage" TK6 cells were shown to have consistently reduced GPI-AP or FLAER staining (Appendix Figure 4.2) when

compared to the normal TK6 cell lineage (Appendix Figure 4.3). As FLAER is a generalised marker for a plethora of GPI anchored protein ligands, the resultant percentage expression was uncharacteristically low and therefore, in conjunction with no obvious potential future surface anchor candidate to select as an in-direct reporter the decision was made to cease usage of the cell line. Without more detailed genomic information, there are no further conclusive remarks to be made about the discrepancies observed during staining.

Prior to the selection of a new cell line platform for the current in vitro *PIG-A* assay design, the functionality as well as constitutive TP53 gene status within the current cell line candidates must be evaluated. P53 is a nuclear transcription factor, which when inactive is often bound to MDM2 and shuttled into the cytoplasm distal to any potential nuclear targets. In response to oxidative stress, DNA damage, hypoxia etc., p53 is returned to the nucleus, activated through a conformational change via a phosphorylation at the n-terminal (serine 15) and dissociated from MDM2 (dramatic half-life increase). Once active, p53 has a prominent role in cell cycle regulation, more specifically the up-regulation of p21 (WAF1/CIP1) and the inhibition of CDk2 activity, resulting in a maintained $G_1/_2$ arrest (cell cycle check point). At this point DNA damage can either be repaired or alternatively, the cell is directed towards programmed cell death (apoptosis) if repair is deemed inefficient [23-26].

Tentatively, the conclusions which can be drawn from this section are that each cell line demonstrates some level of p53 activity and hence, functionality via the measurement of p21 induction, however, currently, no definitive conclusion can be made on the actual tp53 mutational status of the cell lines assessed. Further molecular analysis and potential sequencing is required to reveal the actual stats of the tp53 gene within the tested cell lines. Due to the unsurpassable GPI-AP presence and subsequent comparable p53 assessment, the MCL-5 cell line was chosen as the novel cell line to facilitate in vitro *PIG-A* assay development.

4.5 Supplementary Work

4.5.1 Introduction

The work embodied within chapter 4, explores the prospect of optimising the sensitivity of the current in vitro *PIG-A* gene mutation assay by incorporating a number of modifications; a novel in-direct reporter of mutation, CD55 GPI-AP, as well as the use of a proclaimed superior cell line, "Low Passage" TK6, viability dyes, Annexin V and 7-AAD and an optimised phenotypic wild type enrichment methodology, FACS. Following the evaluation of the protocol modifications, additional human cell lines were assessed in terms of molecular characterisation i.e. p53 status and functionality, as novel candidates for the assay platform.

However, in addition to the work described within the results chapter a number of further investigative directions were also taken to provide additional validation as well as look into specific topics which were fundamental to the future development of the in vitro *PIG-A* assay system. Therefore, the following work describes the subtle molecular and physiological differences between the "Low Passage" TK6 cells and the pre-existing normal TK6 cell stocks, utilised here at Swansea University, in terms of their strengths and weaknesses within the content of the in vitro *PIG-A* assay system. The work also focusses heavily on FCM, in specific, the novel gating strategies devised and trialled to increase assay sensitivity, as well as explore the potential bias induced through analysis. In addition to this statistically derived FCM analysis protocols, which could help to greatly remove bias within subjective flow cytometry scoring, were also devised and assessed for their potential future inclusion as a supplied standalone test system.

4.5.2 Materials and Methods

4.5.2.1 "Low Passage" TK6 Cell Line Stability and Viability, Following Genotoxic Exposure

A vial of Low Passage TK6 cells as well as Normal TK6 cells were established and maintained as outlined within (Section 2.2) and assessed for cytotoxicity profile following EMS exposure. Following sufficient growth to certify population fitness cells were counted using a Haemocytometer as well as a Coulter Counter (Section 2.2.1) and the equivalent volume housing $1x10^6$ cells were transferred into sterile 25 cm^2 pre-labelled culture flasks (9 per TK6 culture). The final volume of each culture flask was adjusted to 10 mL via the addition of fresh culture media (Section 2.4) constructing a final concentration of $1x10^5$ cells/mL. Prior to genotoxic handling, suitable PPE was collected, worn and appropriate disposal vessels collected. Ethyl methanesulfonate was collected from storage and diluted within an apt vehicle, to enable dissolving under minimal effort and stock concentration establishment (Section 2.4). Serial dilutions within DMSO were utilised to construct the required stock solutions and subsequent doses (0, vehicle, 0.1, 0.2, 0.4, 1, 2, 5 and 10 µg/µL). Cellular cultures were treated with 100 µL volume doses of EMS and incubated, under controlled environment, for 24 hr. Following treatment, cultures were washed (excess 1 X PBS) and re-suspended in 10 mL fresh culture media and counted (Section 2.2.1). Cultures were incubated for an additional 24 hr and counted to provide population statistics for a total of 48 hr post chemical treatment. Relative population doubling (RPD), relative cell counts (RCC) and estimated mean generation time (EMGT) were calculated from the produced cell counts in order to facilitate direct cell line comparisons in terms of stability and sensitivity post genotoxicant exposure.

4.5.2.1.1 Compensation Matrix and General Viability (Positive Control Samples)

A vial of CD55 enriched Low Passage TK6 cells were established and maintained as outlined within (Section 2.2). Following sufficient growth to certify population fitness cells were counted using a Haemocytometer as well as a Coulter Counter (Section 2.2.1) and the equivalent volume housing $1x10^6$ cells were transferred into four sterile 25 cm^2 pre-labelled culture flasks. Each flask was diluted with fresh culture media to a final volume of 10 mL and received a different treatment: i) 4 hr 10 µm Ionomycin, ii) 30 min 10µm Staurosporine, iii) Combined 10µm Staurosporine (30 min) and 4 hr Ionomycin and iv) no treatment. Following treatment, cultures were transferred into 15 mL BD Falcon tubes and washed with 1X PBS (Section 2.8.1). Cellular pellets were re-suspended in 50 µL of pre-warmed fresh medium and exposed to antibody treatment; however, ICS samples remained untreated throughout. 20 µL of anti-CD55 PE antibody solution was added in an analogous manner to the protocol defined in (Section 2.8.1). Post incubation, cultures were washed in excess 1 X PBS and re-suspended in 1 mL of 1 X annexin-binding buffer. Binding buffer was supplied at 10X concentration and therefore, required a simple 1 in 10 dilution in dH_20 prior to usage. Cultures were centrifuged (1100 rpm for 7 min), supernatant aspirated and re-suspended in an additional 100 µL of 1 X annexin binding buffer. 5 µL of Alexa Fluor® 488 annexin V was added to each culture, excluding the ICS and incubated in an equivalent manner to the protocol defined in (Section 4.2.3.1). Post incubation, excess 1 X annexin binding buffer was added, cultures centrifuged, supernatant aspirated and re-suspended in 200 µL of annexin binding buffer. 5 µl (0.25 µg) per test (per million cells) of 7-AAD was added, mixed thoroughly and incubated for 5 minutes, protected from light, on ice. Samples were maintained on ice protected from light for a maximum of 4 hr prior to flow cytometric analysis.

Based on the staining method above, seven samples were created in order to construct a comprehensive compensation matrix:

Single Stained ("FITC-A" positive) – 30 min Staurosporine treatment culture

Single Stained ("PE-A" positive) – Untreated ICS culture

Single Stained ("APC-A" positive) – 4 hr Ionomycin treatment culture

Double Stained ("PE-A" and "APC-A" positive) – 4 hr Ionomycin treatment culture

Double Stained ("FITC-A" and "APC-A" positive) – 4 hr Ionomycin and 30 min Staurosporine treatment culture

Double Stained ("PE-A" and "FITC-A" positive) – 30 min Staurosporine treatment culture

Combined Staining ("PE-A", "FITC-A" and "APC-A" positive) – 4 hr Ionomycin and 30 min Staurosporine treatment culture

Each sample was assessed on the flow cytometer in which the respective signal intensities of the specific fluorophore were reduced in order to prevent signal detection in neighbouring channels. Following this, the dual stained samples were analysed in order to evaluate the effect the proposed matrix had on resultant signal detection. Finally, the combined signal was assessed for signal detection, solidifying the utility of the compensation matrix.

4.5.2.2 Preliminery Linear Dose Response Capture Utilsing both Fluorescence-Area and Fluoresence-Height as Potential Descriptors

Low passage TK6 cell cultures were established and maintained as outlined in (Section 2.2) and exposed to EMS for 24 hr under standard chemical treatment as described within (Section 2.4). Post chemical exposure, cultures were washed, counted and seeded ready for initial flow cytometric analysis using anti-human CD55 PE conjugate, Alexa Fluor 488® Annexin V and 7-AAD (Section 3.2.5). Flow cytometric analysis as defined in (Section 2.8.2) was undertaken within an hour of sample preparation, samples were stored on ice, protect from direct light, until analysed.

After gating for single cells on a SSC/FSC dot plot and/or counter map, a minimum of 10,000 events were analysed for the surface expression of the CD55 surface antigen. *PIG-A* phenotype was assessed utilising an instrument calibration standard (ICS), an unstained sample used to set voltages and mutant gating. During ICS analysis, the mutant mimicking sample is utilised to detect auto fluorescence within the channel of collection in order to distinguish between a positive event and background noise at the channel's photon multiplier tube (PMT).

EMS dose response data were produced using a FACSAria I cell-sorter ™ (BD Biosciences, Hertfordshire, UK) equipped with the standard three, 405 nm ultraviolet, 488 nm blue and 635 nm red lasers and the default filter wheel set-up. All analyses within this section of work were performed using a standard 70 µm nozzle at the manufactures suggested 70 psi pressure. FACS Diva 6.0 software (BD Biosciences) was used for operating the cytometer and for data analysis. All fluorescence measurements on the FACSAria were recorded using the "FL-Area" as well as the "FL-H" parameter; R-PE was assessed within the pre-specified "PE" detector, 556 LP combined with a 585/42 band pass filter. PE was excited off the 488nm laser line, best matching its excitation maxima.
Following flow cytometric analysis, parental cell cultures were removed from incubation every 24 hr for repeated *PIG-A* mutagenesis assessment as described at length in (Section 2.10).

4.5.2.3 Gating Strategy Assessment – Statistical Approach

A number of unstained ICS samples as well as untreated control samples were acquired on the flow cytometer and Amnis Image Stream ™ over a period of 14 days. Untreated samples were stained with anti-CD59 PE antibody and subsequent PE emission data was captured following typical 488 nm laser light excitation. During flow cytometry acquisition of the ICS, a number of additional data was collected including emission data for forward (FSC) and side scatter (SSC), Green light emission (FITC) and Orange Light emission (PE) following 488 nm laser excitation, Red light emission (APC) post 635 nm laser light excitation and Blue light emission (eFluor450) corresponding to 405 nm laser light excitation. Auto

fluorescence signals within a number of widely distributed detectors were collected to facilitate automated robust gating strategy evaluation. Flow cytometry data was exported from the BD FACS Aria I in the typical FCS 2.0 or 3.0 (flow cytometry standard) format and into tabulated data able to be read by excel using the "FCSExtract.app" [27]. A number of statistical approaches were employed within the R-software (R-3.0.2, Free Software Foundation's GNU project) to initially evaluate the inter sample variance on the FACS Aria flow cytometer (day 0, 7 and 14) as well as to generate a number of potential automated gating strategies which could be implemented into the in vitro assay design to produce the most reliable, reproducible *PIG-A* mutation data. The graphical outputs were coded by Sion Bayliss.

4.5.2.3.1 Methods for Deriving Threshold Values during Reproducible Gating Strategy Assessment

Method 1 : Mean and Standard Deviation

The threshold value is set at 2* the standard deviation (SD) of the mean for the ICS sample, assumes threshold to be 97.5 % of the distribution.

SD = Square root of the average of the squared differences of the values from their average value.

Method 2 : Outlier Exclusion

The threshold is set at the maximum value which is determined not to be an outlier, as defined by the equation below.

Threshold Value = Quartile 3 + (Interquartile Range * 1.5)

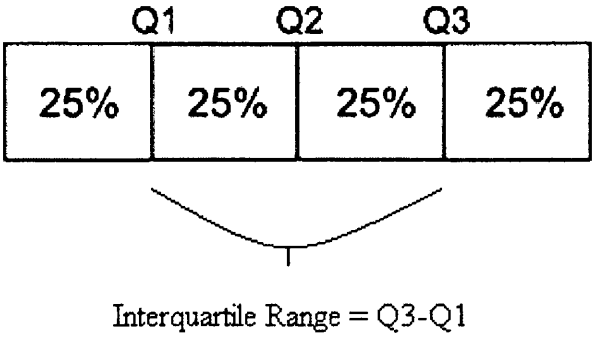

Figure 4.5.1. A summary of the quartiles and where they sit in relation to the defined data set, figure adapted from [28]

Method 3 : Upper Quartile

The threshold value is set at the 95 % upper quartile of the ICS sample.

4.5.3 Results

4.5.3.1 "Low Passage" TK6 Cell Line Stability post Genotoxic Exposure and General Viability

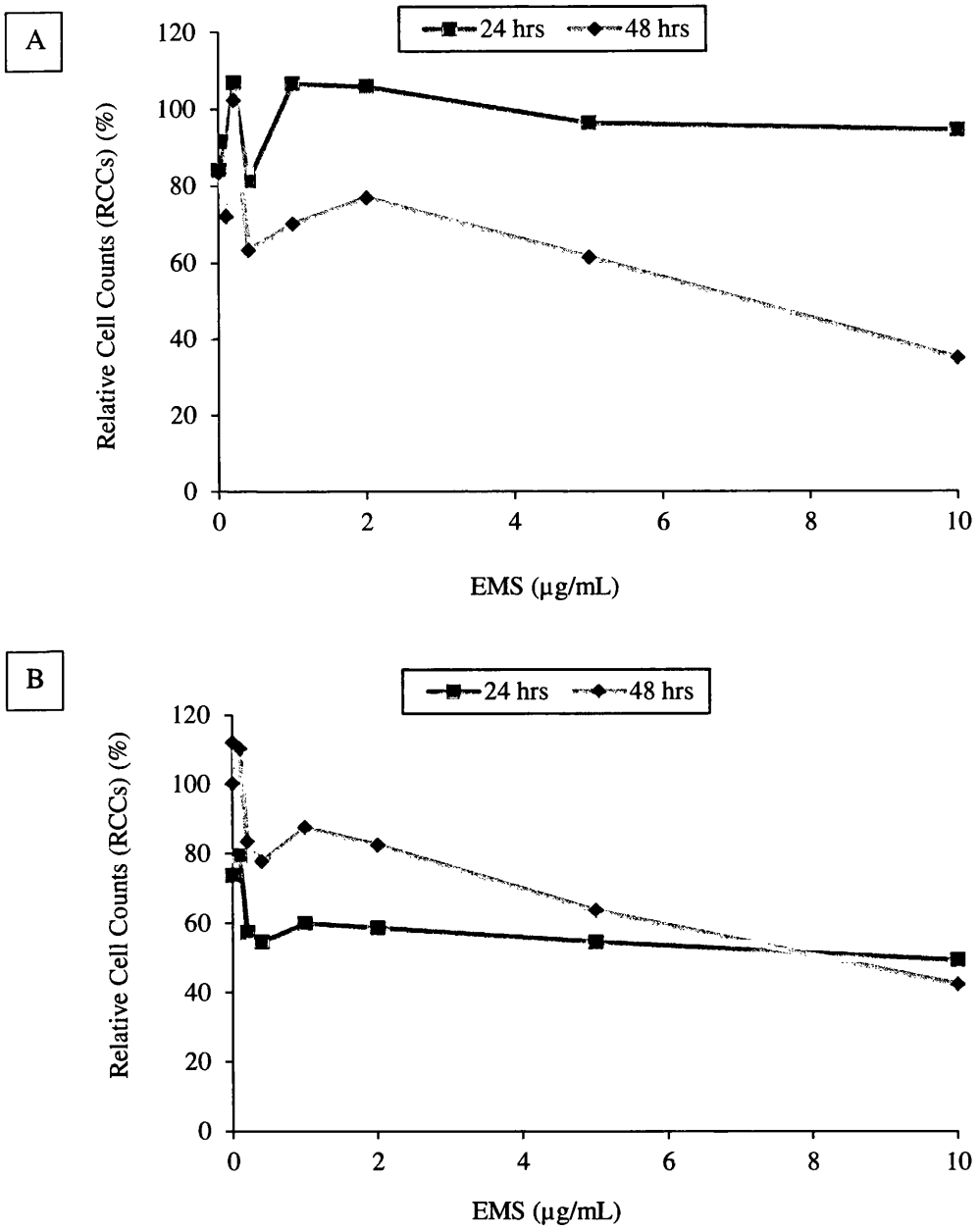

Figure 4.5.2 Relative Cell Counts (RCC) for Normal (A) and Low Passage (B) TK6 cellular cultures following 24 hr acute EMS treatment. Vehicle control data (DMSO) labelled as "0", and true untreated controls omitted from graph (N=1).

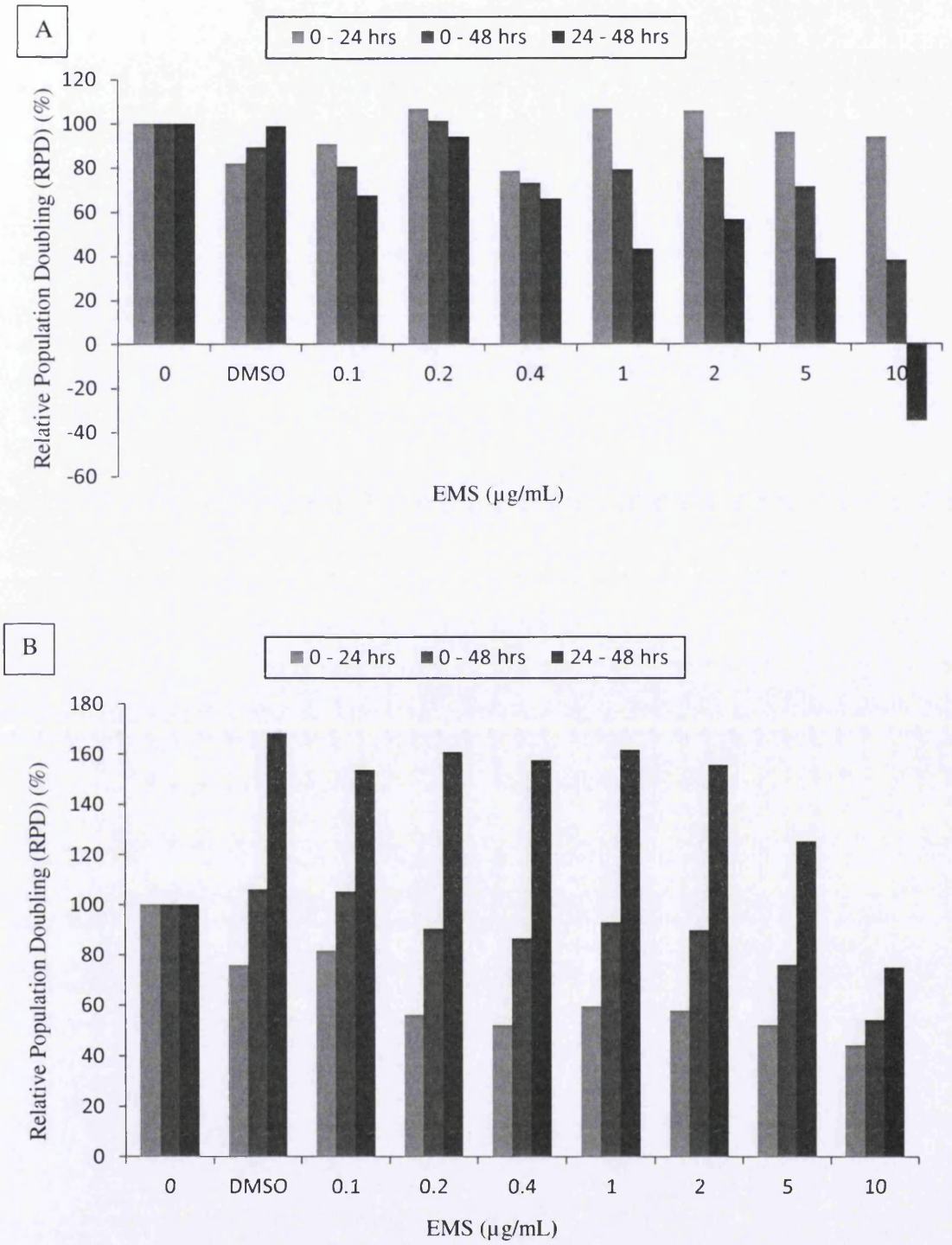

Figure 4.5.3. Relative Population Doubling (RPD) for Normal (A) and Low Passage (B) TK6 cellular cultures following 24 hr acute EMS treatment. Data displayed as a bar chart to emphasize the variations or similarities between recovery periods (N=1).

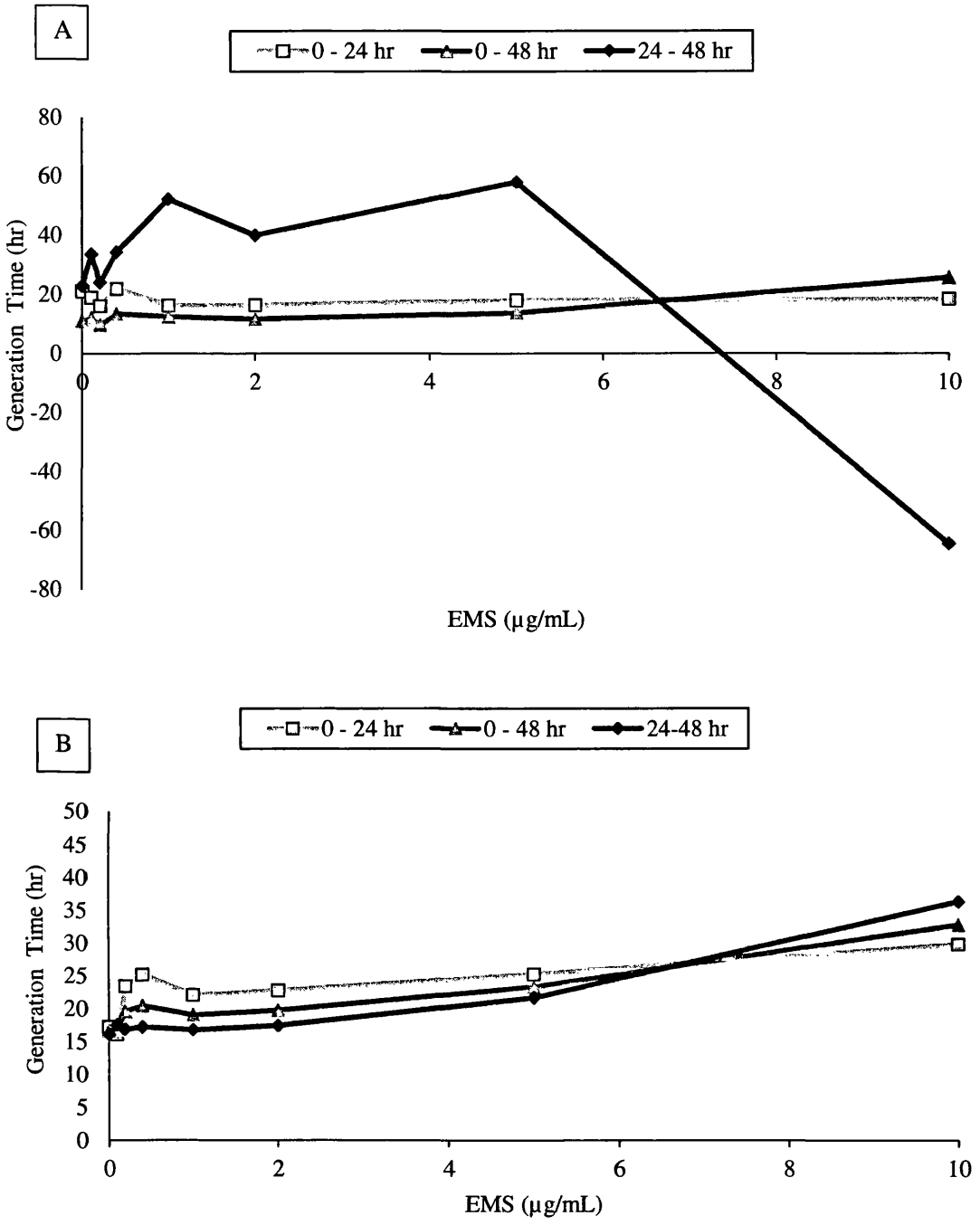

Figure 4.5.4. Relative Estimated Generation Time (EGT) for Normal (A) and Low Passage (B) TK6 cellular cultures following 24 hr acute EMS treatment. Vehicle control data (DMSO) labelled as "0", and true untreated controls omitted from graph (N=1).

"Low Passage" Epstein-Barr viral transformed TK6 human B-lymphoblastoid cells, were further investigated to assess the likelihood of potential beneficial qualities including insensitivity to apoptosis when compared to the original "normal" TK6 stock culture. Initially, simultaneously, parental cultures of both TK6 cell types were exposed to acute model mutagen treatment and monitored in terms of cell recovery and cell doubling time over the following experimental time period. Particular attention was placed on reproducibility and robustness of dose response, both intra and inter sample comparable, with a finalised aim to come to a preliminary conclusion about potential usage of low passage TK6 cells within the developing in vitro *PIG-A* assay design. However, the variation observed both intra and inter sample would be subtle and therefore, limited conclusions can be drawn from the data outside of the context of *PIG-A* assay incorporation.

Initially considering the data from a holistic point of view the generalised trend mutually observed within both TK6 cell cultures was a dose dependent decrease in cellular viability across the EMS dose range (Appendix 4.5.3.1). The relative cell counts (RCC) data demonstrates the overall trend observed within both cultures; nevertheless, there is a discrepancy with regards to the cell line recovery from the genotoxic treatment. The "Low passage" TK6 culture appear to be more sensitive and responded faster than the normal TK6 cultures (Appendix Figures 4.5.2 – 4.5.4) as represented by the low dose effect on cytotoxicity and the exaggerated early observation of viability concerns, observed at the 24 hr time period, respectively. The "Low Passage" TK6 cells display sparse evidence for a lag period immediately following genotoxic exposure, compared to the normal TK6 cultures which appear unaffected until 48 hr post treatment. An analogous dose response was observed within the normal TK6 cultures at the 48 hr time period (Appendix Figure 4.5.2), the 24 hr sample time appeared to reflect an extended lag period associated with genotoxic exposure as illustrated by limited effect on cytotoxicity values. Lower doses of EMS appeared to illicit an effect within the "Low Passage" TK6 cells when compared to their normal TK6 counterparts, minimal effect was observed with doses less than 0.4 µg/mL within the normal TK6 cells.

The relative population doubling (RPD) data again displayed a generalised association between data sets and mimicking the overall trend of the data. However, the Low passage TK6 data appeared to be more consistent between dose in terms of

reproducibility as well as overall trend. The data reflects the early significant decrease in cellular doubling times over the initial 24 hr time point, followed by an accelerated doubling time, as demonstrated with the rapid increase in population doublings between the 24 and 48 hrs (Appendix Figure 4.5.3). Re-establishing the typical doubling time of the cell line appears to exceed two cell cycles and additional extended time points would be required for more precise definition. The normal TK6 data is less reproducible in terms of intra dose trends, though still mimics the generalised decrease in population doublings across the dose range. The top doses appear to be more highly affected that the low passage TK6 cells, with the top dose observed to display negative growth figures for the 24- 48 hr period. Similarly to the RCC data, the normal TK6 cells population doubling reflects the observed trend in which they appear relatively unaffected over the initial 24 hr period, where as a dose dependent decrease in doubling is observed within the low passage TK6 cells. Doses greater than 0.4 µg/mL appeared to decrease population doubling within the normal TK6 cultures, as apparent within the 24 – 48 hr experimental period (Appendix Figure 4.5.3). However, lower doses appeared to illicit an adverse effect on doubling times within the low passage cultures.

The estimated generation time data demonstrated that the top dose (10 µg/mL) illicit a significant effect on the normal TK6 population in which the cell culture did not double over the 24-48 hr period, this is also apparent within the RPD data. As previously reported, the low passage TK6 data is more reproducible across the dose range, as well as the experimental time period, and clearly demonstrates a correlation between extended generation time and increase dose of genotoxin. The normal TK6 data again reflects this general trend, as apparent within both RCC and RPD data sets; however, the data is more variable between experimental time points (Appendix Figure 4.5.4).

4.5.3.1.1 Compensation Matrix and General Viability (Positive Control Samples)

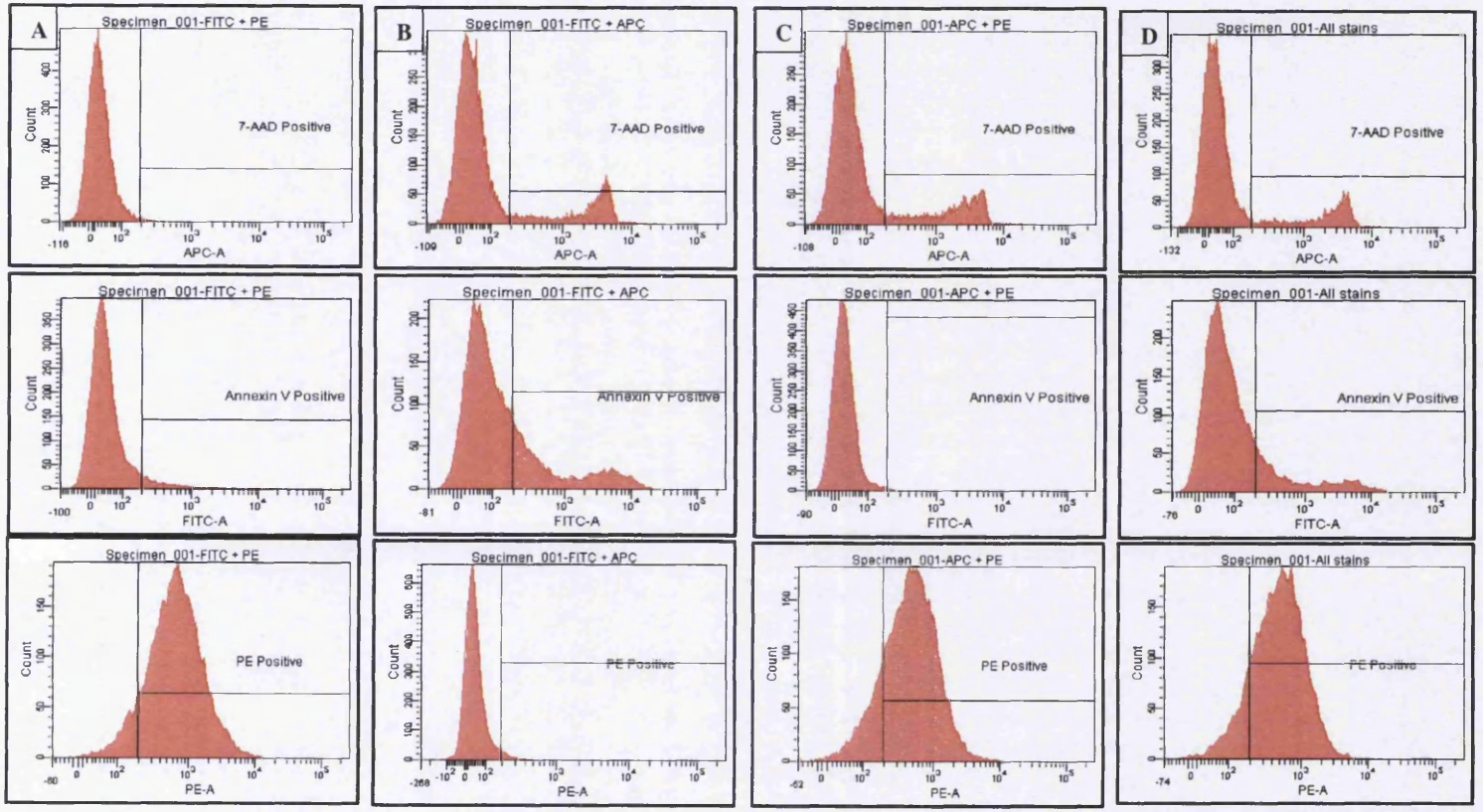

Figure 4.5.5. Construction of a compensation matrix for multi-fluorescence assessment, within the common excitation line utilising neighbouring fluorescence detectors. A) Annexin V and CD55 R-PE Positive, B) Annexin V and 7-AAD Positive, C) CD55 R-PE and 7-AAD Positive and D) Annexin V, CD55 R-PE and 7-AAD Positive (~10,000 Single Cellular Events based on FSC-A vs SSC-A scatter plots).

Fluorophore emission spectra were assessed for potential spectral overlap to prevent ambiguity within the subsequent results. Spectral overlap is the phenomenon in which fluorophores, regardless of their excitation frequency, emit subsequent light of varying wavelengths which may happen to be of an analogous nature and therefore, detected within a single detector. As a result of this, the PMT is unable to clarify the origins of the detected photons and the resultant signals become merged within the detector as an ambiguous trace. In order to assess the basal viability of low passage TK6 cells, viability dyes will be incorporated into the staining protocol to better characterise the cells, as previously described in chapter (Section 3.3.5).

The preceding data displays the flow cytometry outputs following the construction of a compensation matrix based on single stained cell populations. The use of the dual stained sample was to evaluate the successful nature of the matrix, preventing over compensation and loss of induced signal detection.

Specimen A displays the flow cytometry data following CD55 R-PE in combination with Alexa Fluor 488 ™ Annexin V exposure. The data suggests that limited apoptosis was detected within the" FITC" detector and a significant "PE" signal was identified reflecting the majority *PIG-A* wild type population status. Specimen B resultant output shows an apparent signal detected within both the "7-AAD" as well as "FITC" detectors, corresponding to the dual Staurosporine and ionomycin treatments. Specimen C displays positivity within the "7-AAD" and "PE" detectors, and defines the limited amount of cell death observed within the nearly exclusively *PIG-A* wild type population. Finally, specimen D was observed to display positivity within all three assessed detectors. The compensation matrix generated from the single stained experimental samples; PE/FITC 47.5%, FITC/PE 0.4%, APC/PE 0.1% and PE/APC 11.7% was evaluated within these results and deemed acceptable for use within cell line viability assessment (Appendix Figure 4.5.5).

The establishment of a typical calibration matrix, which fundamentally was utilised in the initial preliminary viability assessment (Section 4.3.2), was implemented from this point on within the project due to the simultaneous use of similar fluorophores.

4.5.3.2 Preliminery Linear Dose Response Capture Utilsing both Fluorescence-Area and Fluoresence-Height as Potential Descriptors

Simplistic dose response experiments were carried out in order to investigate the potential effect logarithmic capture as well as fluorescence area (FL-A) as the descriptor for emitted signal has on *PIG-A* mutant frequencies. Low passage TK6 cells were treated with EMS and assessed daily for *PIG-A* mutant frequency utilising both the FL-A as well as fluorescence height (FL-H) descriptors. The flow cytometry data was initially captured in a linear amplification manner, and descriptors directly compared for variance. "*PIG-A* mutants" are events phenotypic of CD55 absence and therefore, are presumptive *PIG-A* mutants. Experimental design permitted the initial capture of 10,000 cellular events, and utilised the FLW measure as an additional size descriptor.

A)

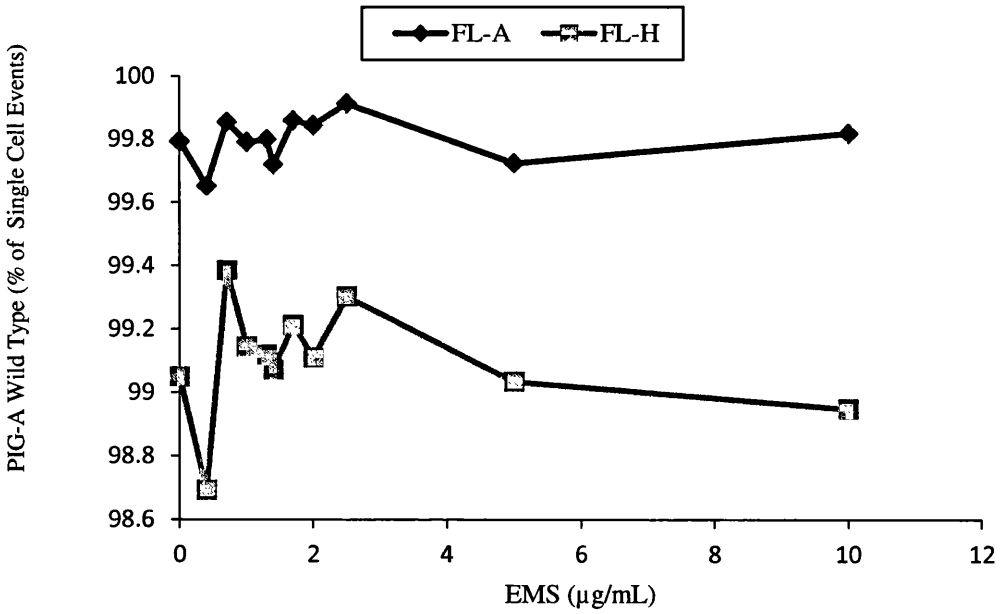

B)

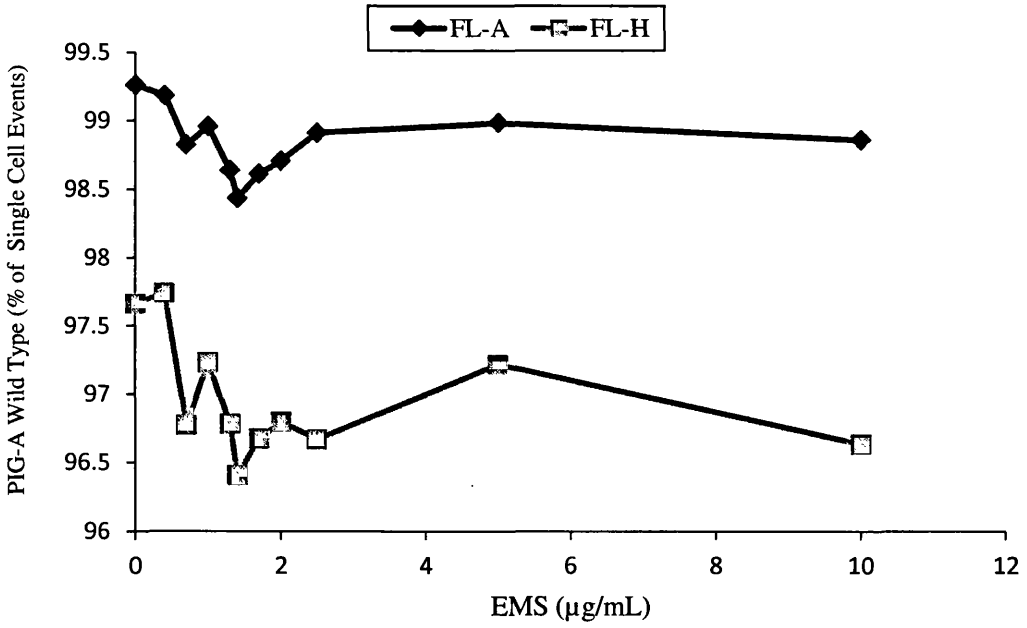
FL-A
FL-H
PIG-A Wild Type (% of Single Cell Events)
99.5
99
98.5
98
97.5
97
96.5
96
0
2
4
6
8
10
12
EMS (µg/mL)

C)

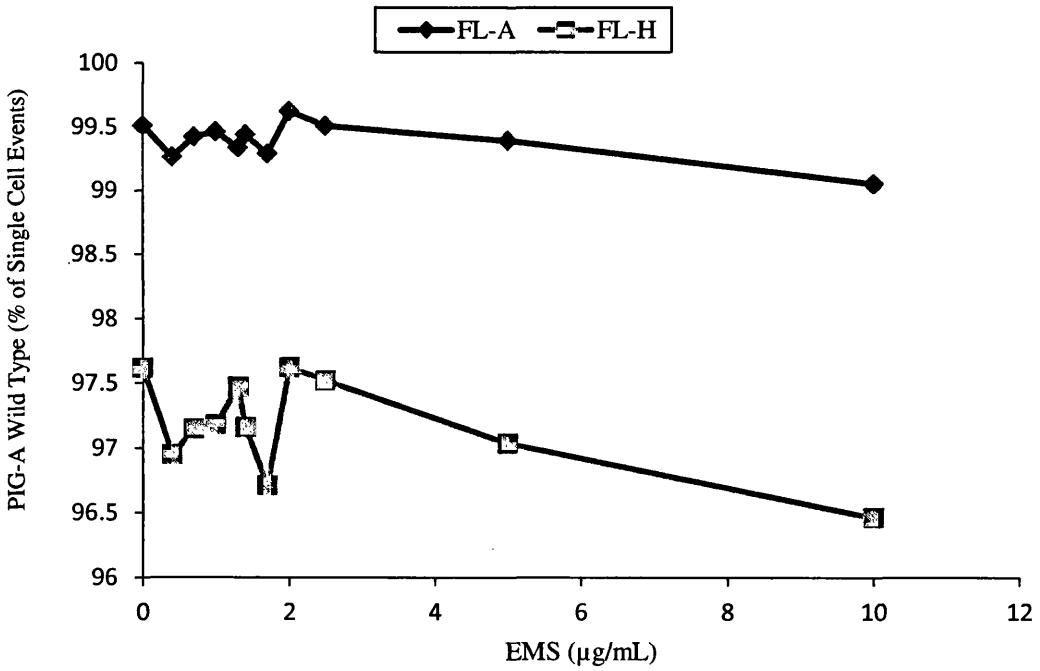
FL-A
FL-H
PIG-A Wild Type (% of Single Cell Events)
100
99.5
99
98.5
98
97.5
97
96.5
96
0
2
4
6
8
10
12
EMS (µg/mL)

D)

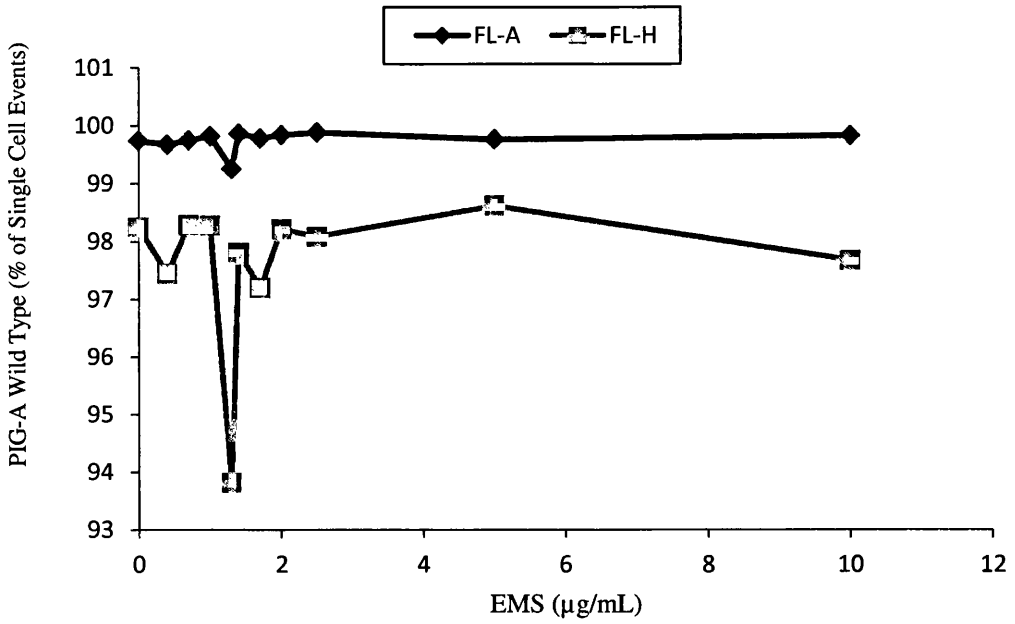

E)

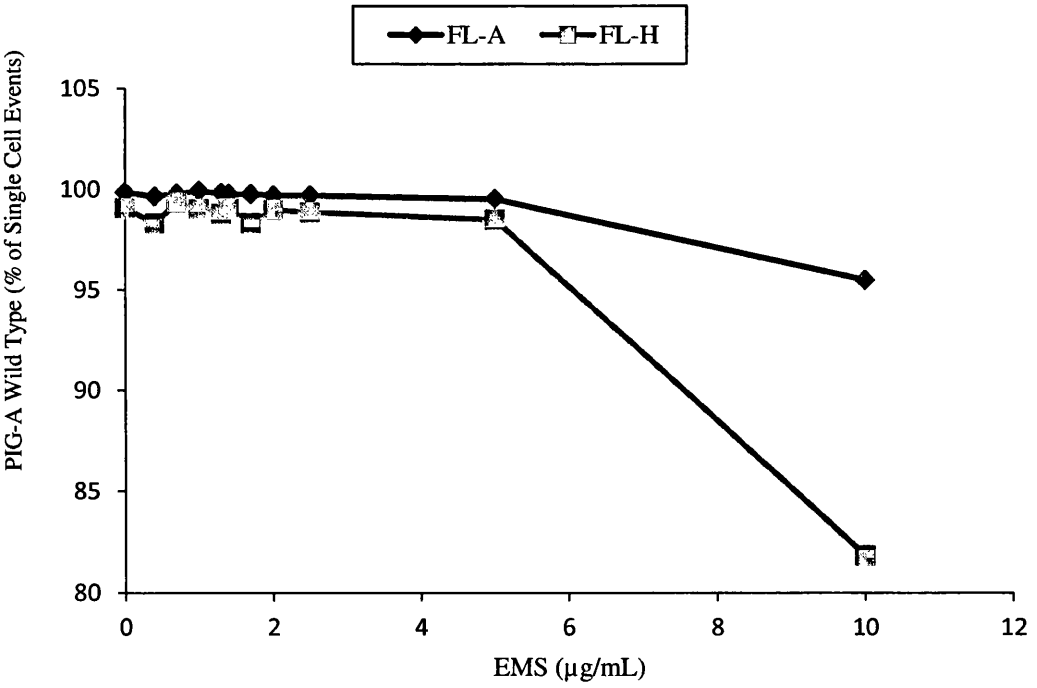

Figure 4.5.6. A,B,C,D and E – Days 0-4, low passage human lymphoblastoid cells (TK6) *PIG-A* wild type frequency following 24 hr low dose EMS exposure, CD55 antigen utilised as reporter for mutation. Fluorescence data amplified linearly, integration of additional size parameter (FL-W) and a direct comparison between FL-A and FL-H sensitivity. (N=1) *PIG-A* wild type displayed as percentage of total single cellular events (99.9% *PIG-A* wild type = 1 mutant x 10^{-3} cells).

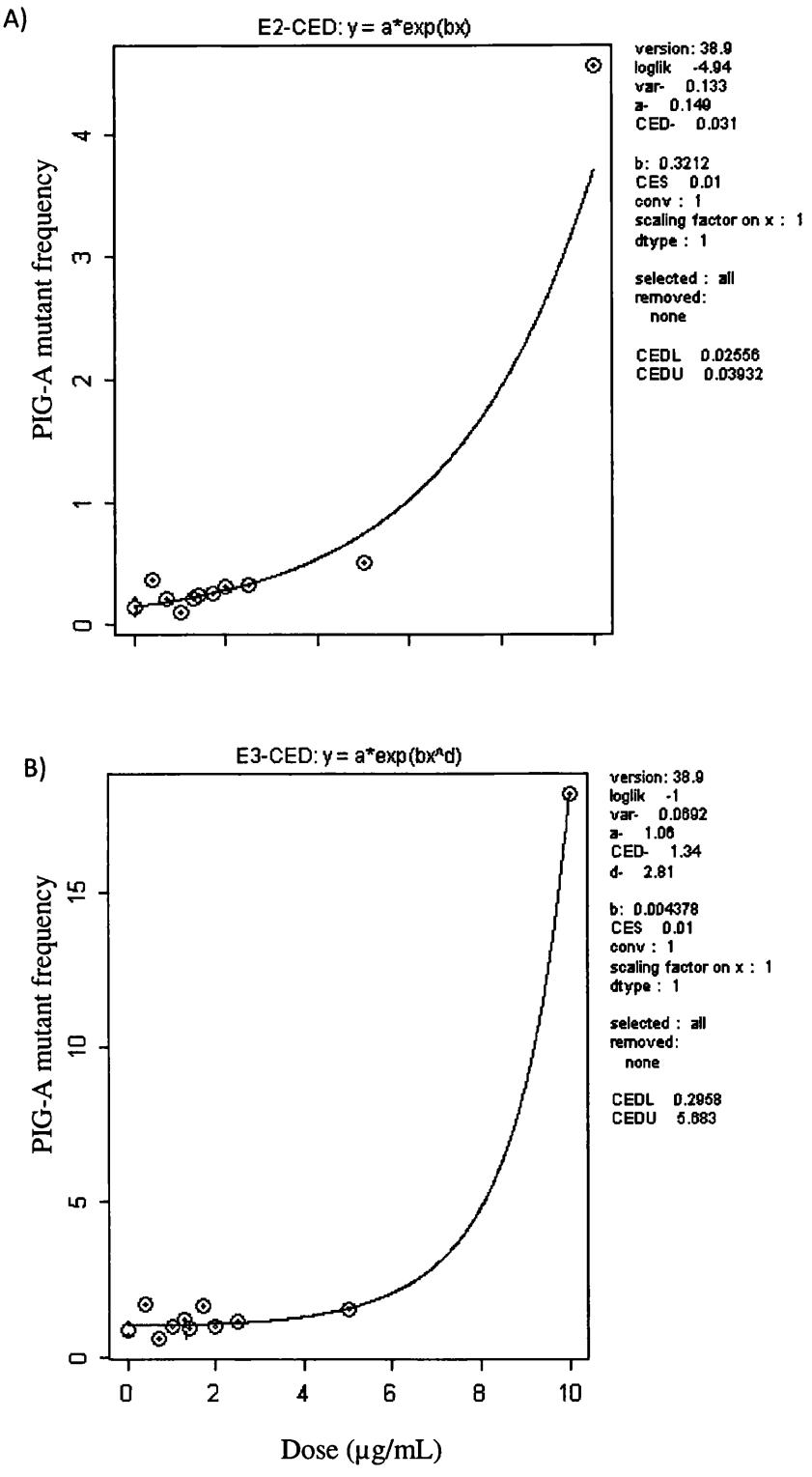

Figure 4.5.7 Day 4 FL-A (A) and FL-H (B) PROAST 38.9 modelled low passage human lymphoblastoid cells (TK6) *PIG-A* mutant frequency following 24 hr low dose EMS exposure, CD55 antigen utilised as reporter for mutation. Data amplified linearly, integration of additional size parameter (FL-W). (N=1) *PIG-A* mutant displayed as percentage of total single cellular events (0.1% *PIG-A* mutant = 1 mutant x 10^{-3} cells).

Considering the day 0 data, both descriptors (FL-A and FL-H) generate a distinctly comparable relationship between the two dose responses. There are no apparent significant increases or decreases in the percentage *PIG-A* wild type with respect to dose of EMS, although there is a definite discrepancy between the background *PIG-A* mutant frequencies utilising both methods. FL-A as a descriptor generated an approximate spontaneous *PIG-A* mutant frequency of 0.2%, however, FL-H defined a much greater background of approximately 1%, which translates into an 8,000 difference in number of defined *PIG-A* mutant events (Appendix Figure 4.5.6). Linear amplification capture appears to have little impact on the subsequent flow cytometry data as background appears in line with the previously generated data utilising CD59 as the reporter for *PIG-A* mutation (Section 3.3.3).

The day 1 data shows no apparent dose dependent relationship in terms of viable *PIG-A* mutants, however, does mimic the overall trend of FL-H data being more variable and having a much greater spontaneous background mutant frequency than the comparable FL-A data. The background mutant frequency in general was higher than the previous day of analysis and the FL-H background mutant *PIG-A* frequency approached 2.5% with respect to the total single cell population (Appendix Figure 4.5.6). Day 2 and Day 3 data both display analogous dose responses for both descriptors. FL-A is very consistent with respect to the percentage of viable *PIG-A* mutant phenotype cells across the entire dose range, whereas FL-H data is more variable and has an increased background mutant frequency (approaching 2.5 and 2% respectively for days 2 and 3).

Day 4 data is dissimilar in terms of both dose response relationships displayed and the background mutant frequency utilising the comparable detectors. FL-A again as demonstrated to have a seemingly low background mutant frequency within the region of 0.1-0.5%, comparable to the previous preliminary experiments (Section 3.3.3), however, FL-H also was demonstrated to produce an analogous background mutant frequency. FL-A displayed again a consistent non-dose dependent relationship in terms of viable *PIG-A* mutants, but the FL-H data displayed a significant increase in the frequency of viable *PIG-A* mutant phenotype cells at the top dose. 10 µg/mL was demonstrated to increase mutant *PIG-A* frequency by approximately x19 with respect to con-current control values. Significant differences

were observed between the data generated as a result of descriptor choice, in terms of dose response as well as variability.

A direct comparison was made following PROAST 38.9 modelling of both the final day's analysis data. Even though the data was in singlet and thus the data set highly limited, the results reflect the potential variation in subsequent generated BMD value due to variance within the background of the collection method. The FL-A descriptor generated a lower background mutant frequency and therefore, a lower BMD_{10} value (Appendix Figure 4.5.7).

4.5.3.3 Gating Strategy Assessment – Statistical Approach

During flow cytometry analysis, the maximal auto-fluorescence, or back ground noise, is estimated in the detector of interest via the use of an unstained ICS, and is subsequently utilised as the limit or definition of positivity. Any signal with a fluorescence emission value greater than the maximum observed ICS value for that specific detector is defined as positive. However, due to the variable nature of biological data, specific outlying presumed cellular events often have an emission value significantly higher than the mean value for the analysed population and therefore, result in a skewed non Poisson distributed data set. In order to assess potential machine variability, both same day acquisition as well as time course assessment was carried out, and evaluate the potential limitations in current gating strategy; more specifically its impact on reproducibility, initial preliminary statistical investigation was undertaken. All data sets unless otherwise describes consisted of >10,000 events presumed single cell in nature.

A)

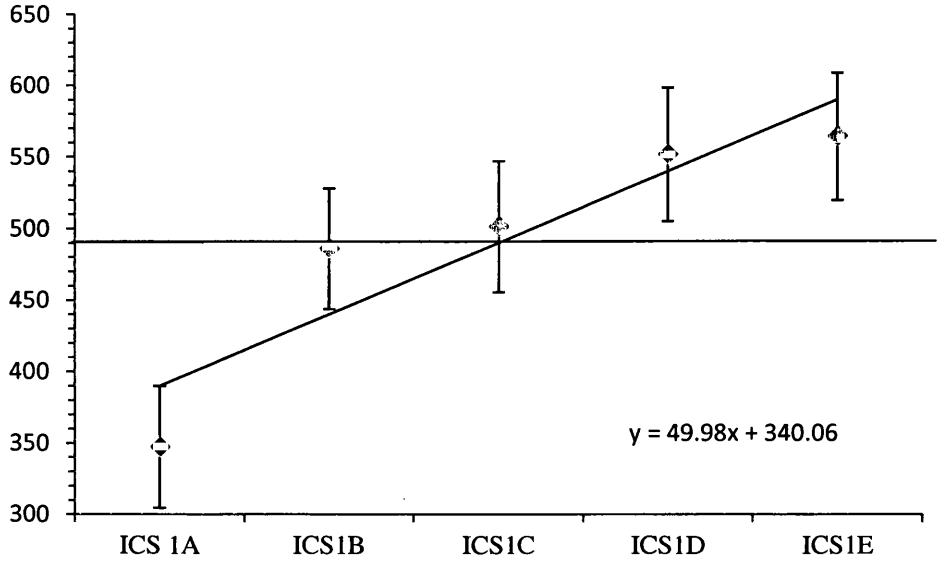

Figure 4.5.8.A Average maximum fluorescence emission signal recorded within the Phycoerythrin specific detector during unstained, normal TK6, instrument calibration standard flow cytometry acquisition at the same time point (Day 0) (>10,000 single cellular events) (Error Bars ±1SD, (-) Average Maximum Fluorescence value recorded across all samples) Trend line and equation of the line include on graph.

B)

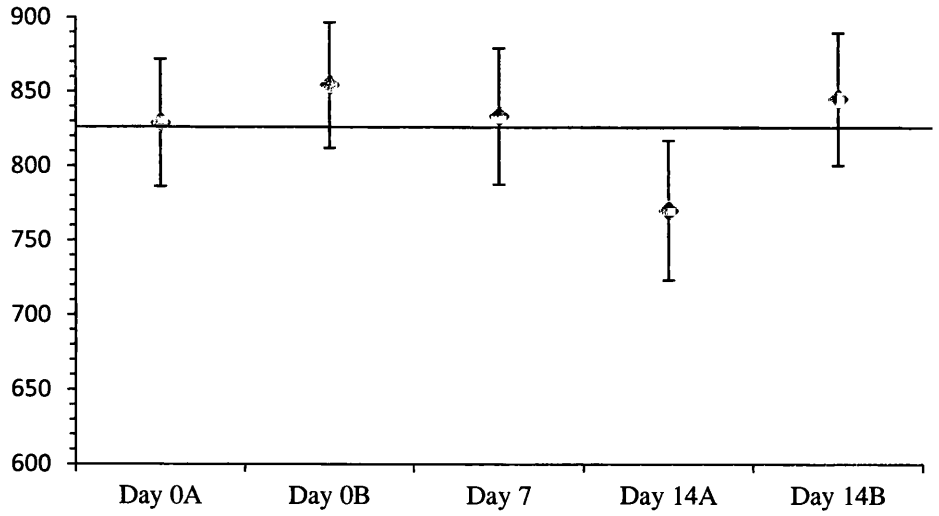

Figure 4.5.8.B Average maximum fluorescence emission signal recorded within the Phycoerythrin specific detector during unstained, normal TK6, instrument calibration standard flow cytometry acquisition at multiple different time points (day 0,7 and 14) (>10,000 single cellular events) (Error Bars ±1SD, (-) Average Maximum Fluorescence value recorded across all samples).

Same day acquisition data demonstrated that the variance observed within each sample was minimal as illustrated by the relative small standard deviation around the means, although the variance between each of the five samples was larger than expected. The lowest mean maximum fluorescence value recorded was 347.2, and the largest 564.2 with a range of 217 arbitrary units. The average mean fluorescence maxima value for this sample set was 490 arbitrary units. A correlation was observed between time and arbitrary maximum fluorescence value, as sequential samples average value was demonstrated to rise (Appendix Figure 4.5.8.A). Each sample was acquired using the identical protocol as well as BD FACS Aria I configurations, therefore, preventing unwanted bias within the data.

Time course assessment generated data re-enforced the results taken from the previous experiment (Appendix Figure 4.5.8.A). There was a reduced range of average mean maximum fluorescence values 84.4 in comparison to 217 arbitrary units, and comparable variance between samples collected on different experimental days (Appendix Figure 4.5.8.B). Although there was less variance observed between data acquired on different days than consecutive acquisition, there was no definite consistency to the data. The fluorescence values for the consecutive collection of data were much lower when compared to the time course acquisition and the previously mentioned increase in average fluorescence value with time appeared to be apparent within these data.

4.5.3.3.1 Methods for Deriving Threshold Values during Reproducible Gating Strategy Assessment

A)

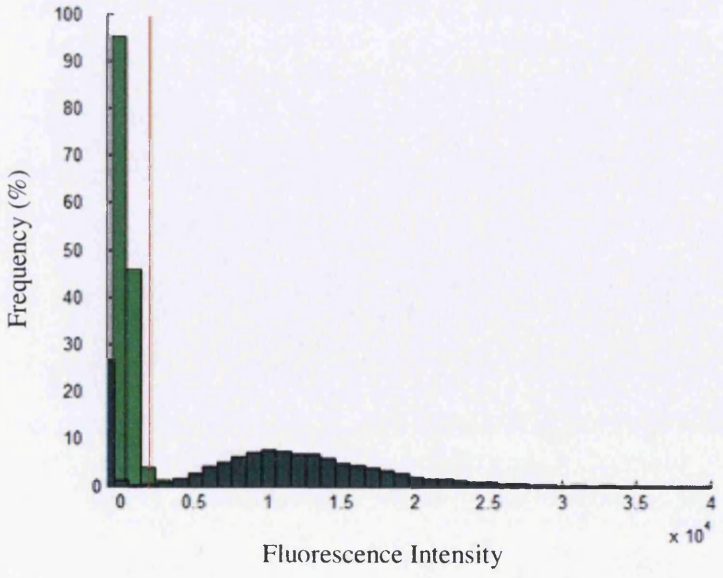

B)

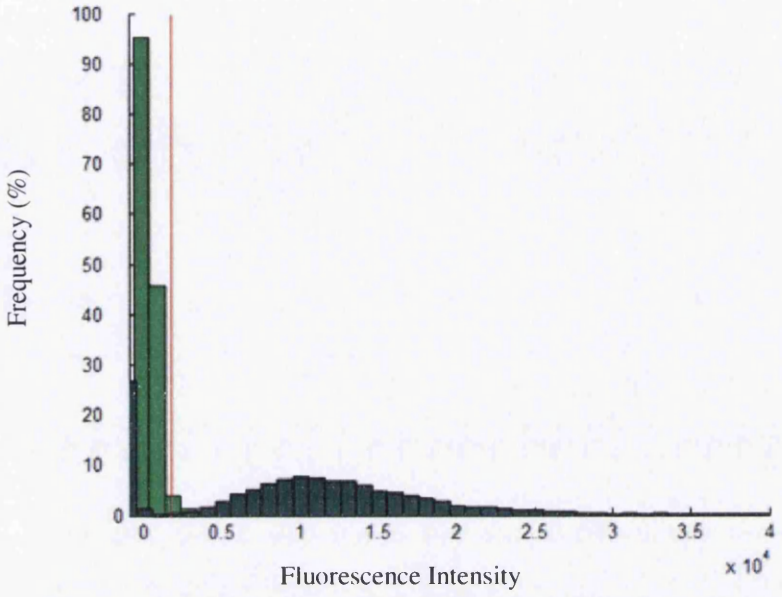

C)

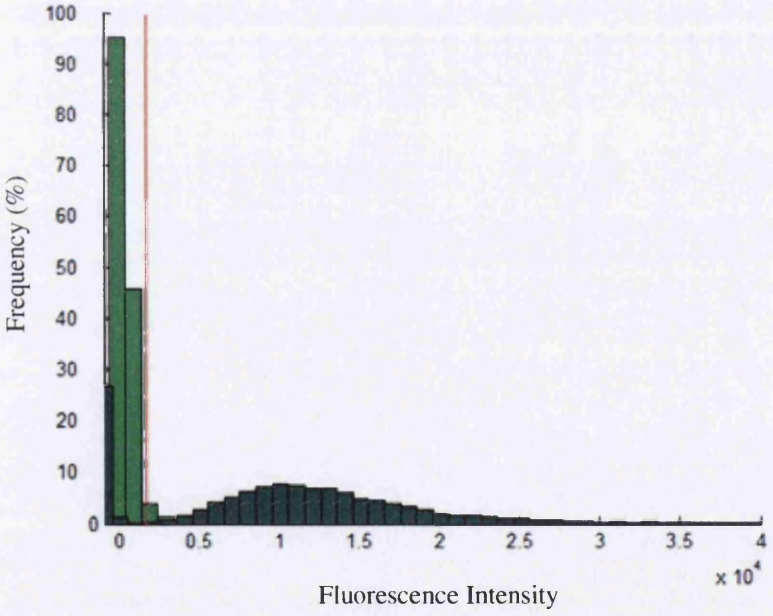

Figure 4.5.9. Mean and Standard Deviation (Mean + (2* STD)) (A) Statistical Outlier Exclusion (B) and Upper quartile (95%) (C) approaches for evaluating a reproducible gating strategy. Data generated using normal untreated TK6 cells; ICS sample ([ ]) and stained, anti CD59 PE antibody, sample ([ ]) (>10,000 cells analysed)(Red vertical line represents the derived threshold value).

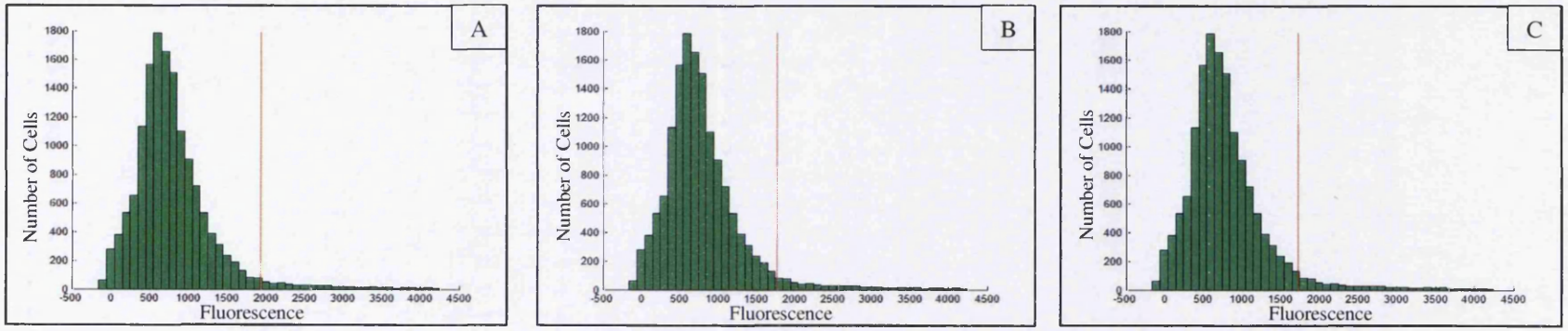

Figure 4.5.10. Normal TK6 cells fluorescence emission data for an unstained ICS, collected within the "PE" detector and analysed in triplicate using the proposed automated gating strategies. A) Mean and standard deviation, B) Outlier exclusion and C) Upper quartile (95%). >10,000 cells acquired and ~10,000 single cell events analysed (Red vertical line represents the derived threshold value).

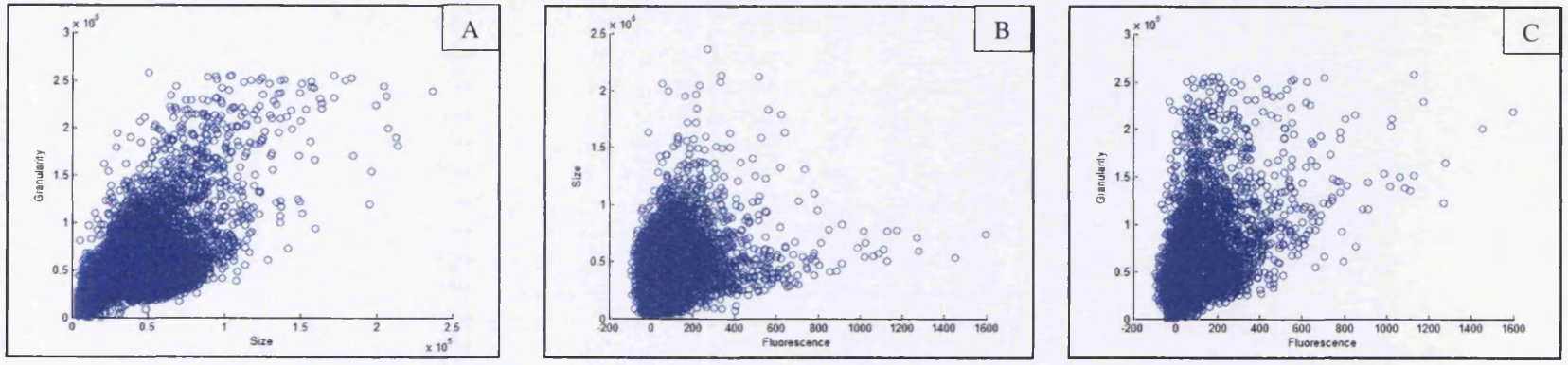

Figure 4.5.11. Normal TK6 unstained ICS data collected within the "PE" detector for the arbitrary fluorescence values given. A) Forward scatter (FSC) vs Side scatter (SSC), B) FSC vs Relative Fluorescence and C) SSC vs Relative fluorescence. >10,000 cells acquired and ~10,000 single cell events analysed.

A)

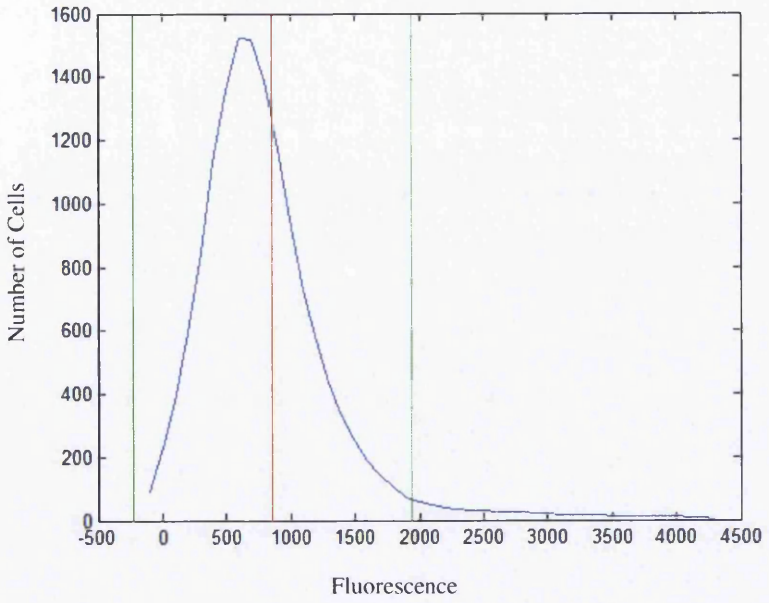

Figure 4.5.12.A Normal TK6 unstained ICS data collected within the "PE" detector for the arbitrary fluorescence values given. >10,000 cells acquired and ~10,000 single cell events analysed ((--) Mean and (--) 2 Standard Deviations)

B)

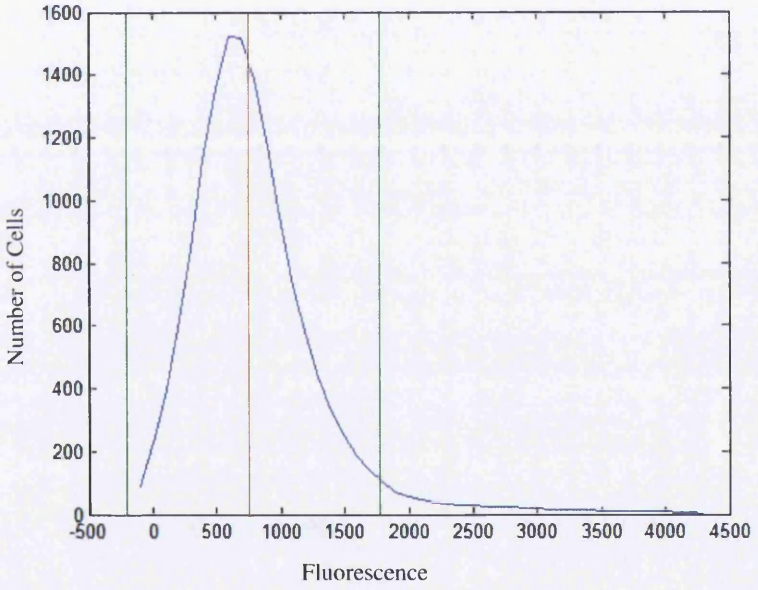

Figure 4.5.12.B Normal TK6 unstained ICS data collected within the "PE" detector for the arbitrary fluorescence values given. >10,000 cells acquired and ~10,000 single cell events analysed ((--) Median and (--) Outliers (0.75 + (1.5 * IQR))

The results generated for the mean and standard deviation approach, which assumes the threshold value at 97.5 % of the distribution, for defining a threshold value indicated that the population of data which were being modelled did not conform to a Poisson or Gaussian distribution. Within a normal distribution, 2*standard deviation should encompass 97.5 % of the population, however, the skewed data resulted in 3.7 % of the ICS population being defined as a positive result within the channel of interest, i.e. greater than the expected 2.5 %. When this threshold value was taken forward onto a stained, untreated sample, 77.5 % of the population was deemed positive (Appendix Figure 4.5.9.A and 4.5.10.A), which corresponding well to the expected ratio of surface antigen negative cells within the heterogeneous parental TK6 population. The stated threshold value derived for this approach was 1.9351 x 10^3. The outlier approach, which assumes the threshold value to be the maximum value not considered an outlier, was demonstrated to produce an analogous threshold value to the standard deviation method when modelling an identical data set. The value defined was 1.7808 x10^3, and resulted in 4.5827 % of the ICS samples being defined as positive as well as 77.457 % of the subsequent untreated stained sample to be assigned as surface antigen positive (Appendix Figure 4.5.9.B and 4.5.10.B). The outlier approach appeared to result in a lower threshold value which subsequently resulted in no effect on the overall threshold for positivity within the subsequent population analysis. The final approach considered was upper quartile, assuming that the value equivalent to the 95 % upper quartile was defined as the threshold, again generated highly comparable results. The threshold was defined as 1.7272 x 10^3 arbitrary units, which resulted in 4.9986 % of the ICS population being defined as positive and 77.4810 % of the subsequent population being defined as positive or presumed *PIG-A* wild type (Appendix Figure 4.5.9.C and 4.5.10.C). The results were highly comparable across the three proposed methods, indicating that potentially any of these methods could be incorporated into an assay design; however, each method did have subtle differences in the final population data.

When considering the location of the defined threshold with respect to the distribution of the population, all three methods generated slightly different results. As the population data was demonstrated not to be normal and hence, did not fit a normal distribution well, the subsequent data set had a positive skew, quite apparent within the distribution histograms (Appendix Figure 4.5.10). As a direct result of this

apparent skew, the approaches which favoured population statistics descriptive of normal data, i.e. standard deviation, generated the most poorly fitting threshold value. The outlier and upper quartile approach both generated threshold values more fitting to the data set provided and subsequently, defined values less than the standard deviation approach. As a direct result of this, less of the skewed tail was included within threshold derivation and therefore, fitted the data more appropriately. The upper 95% quartile approach produced the most favourable threshold in terms of data distribution; however, the outlier approach generated a highly comparable fit to the data set. The standard deviation method was further visually clarified to not be the best fit to the data when the deriving variables, i.e. mean and standard deviation were directly compared to the median and outlier calculation for the outlier approach (Appendix Figure 4.5.12). The mean is visually skewed towards the positive on the x-axis and therefore, the resultant threshold value obtained is more inclusive of skew data, as previously stated. The median value appears to be much more appropriate for these data set, and the resultant threshold value utilising the approaches which incorporate the median value over the mean are more robust in terms of potential bias exerted on the population following increase or decrease within skewed data.

As well as investigating the reproducibility and fit of a preliminary defined threshold value, the fundamentals of flow cytometry, i.e. variance, correlations etc. were also evaluated for potential biasing effect on the generated data which potentially could influence threshold derivation and robustness. Initially, a preliminary positive correlation between sampling time and fluorescence appeared to be apparent within the inter/intra machine variability data (Appendix Figure 4.5.8.A). However, when a much larger sample set was evaluated, fluorescence value was demonstrated to be independent of time, in terms of both correlation and probability (Rho = 0.008, p = 0.3312), similarly particle size was also demonstrated to be independent of the time (Rho = -0.0137, p = 0.0988). Conversely, even though a negative correlation was observed when time and granularity were assessed (Rho = -0.0183) a significant amount of variance within the data set was attributed to this relationship (p = 0.0267) (Appendix Figure 4.5.11). In order to address the potential bias in which the size of cells have on fluorescence arbitrary units, a particular worry in the context of cellular variability and the effect the cell cycle has on potential *PIG-A* data, correlation was

investigated. Initially size (defined by FSC value) and granularity (defined by SSC value) were demonstrated to be significantly correlated (Rho = 0.418, p = <0.01), about 17.5 % of variation between the samples was explained by this. However, when both size and granularity were assessed for correlation against fluorescence independently, even though both were defined as significantly correlated (p = <0.01), only 0.384% of sample variance was a result of size in comparison to 19.14% as a result of granularity (Appendix Figure 4.5.11), alluding to the fact that granularity or SSC value was more of a potential biasing variable in terms of inaccuracies during *PIG-A* analysis.

4.5.4 Discussions and Conclusions

4.5.4.1 "Low Passage" TK6 Cell Line Stability post Genotoxic Exposure and General Viability

"Low passage" TK6 cells were directly compared against the normal TK6 cell stock in terms of their cytotoxic response to the known genotoxicant compound EMS. The data was initially utilised as a dose finding study for the subsequent preliminary *PIG-A* analysis however, additional discrepancies between the two cell lines were identified which could offer some explanation for the variance in data obtained utilising homologous genotoxic end points. In general terms, the RCC and RPD data generated for both cell lines reflected the overall trend which was to be expected, i.e. a dose dependent decrease in cellular viability. However, even though analogous in response, subtle variations occurred between like cell stock.

The "Low Passage" TK6 cells were demonstrated to be more sensitive in terms of the dose of genotoxic which induced some level of cytotoxic effect, as well as more consistent in their response to the dose over a 48 hr time period. There was no apparent observation of a lag period following the dose which has become routine when using the TK6 cell line [29]. Following the observed discrepancies between the low passage and normal TK6 cells in terms of CD59 surface antigen expression, their genomic levels of variance is currently unknown, however, they are presumed genomically identical. Following typical chemical exposure, in this case EMS, the normal TK6 cells were observed to undergo a period of time in which no apparent decrease in cytotoxicity is observed. This lag is apparent across the entire dose range until a period of approximately 24-48 hr has passed, leading to a dose dependent decrease in cell viability, compound specific.

However, the "Low Passage" TK6 cells not only provide different physical and morphological growth dynamics, when compared to their "older" counterparts, but also demonstrate no lag phase (Appendix 4.5.3.1). This increase in sensitivity, in regards to the time period of effect as well as the dose which induced an adverse effect on viability is quite different between the two cultures. Potentially, variance in one of a number of genes integral within cell cycle regulation, p53 DNA damage

mediated responses etc. could be the cause of these discrepancies. However, the cell line is very consistent in terms of how the cells behave over an extended time period following exposure, unlike the previously utilised normal TK6 batch, possibly suggesting at a greater level of genomic stability and hence, more effective recovery post exposure. More definitive conclusions, apart from stating that on a certain level of investigation these cell lines appear different, cannot be drawn without more extensive pair-wise genomic analysis.

Establishment of compensation matrices is a fundamental procedure when utilising multiple fluorescence dyes with similar emission profiles on a machine capable of detecting multiple fluorescence emission signals [30]. The resultant compensation matrix generated following induced positivity, within control samples, was heavily focussed on the "FITC" and "PE" detector channel fluorophores. Due to the nature of fluorescence emission, the emission spectra is greater, in terms of wavelength, due to the occurrence of a stokes sift and consequently, the subsequent emission may partially be located within the neighbouring [31]. In this specific example, the Alexa Fluor® 488 dye following excitation falls partially within the band pass filter set up utilised to capture "PE" channel data, and therefore, when in combined use with a "PE" based fluorophore the Alexa Fluor® 488 signal data was negatively biased to reduce/remove any potential cross talk between the fluorophore and the neighbouring detector. This method was repeated and a finalised matrix was constructed and when applied, the previously demonstrating significant presence of the "FITC" signal within the "PE" channel, marginal presence of the PE signal within the "APC" channel and negligible presence of the "PE" single within the "FITC" channel were all removed. However, two potential inaccuracies were identified, firstly, the use of a different laser light to excite the 7-AAD dye, recorded within the "APC" detector, should have prevented any noise between the two additional detectors due to the physical difference in fibre optic collection, however, a noticeable signal overlap was detected (~10%) and secondly, due to the excessive induction of signal within the positive controls (Section 4.5.3.1) the resultant matrix was quite severe in nature (up to 40% reduction in Alexa Fluor® 488 signal was utilised). As a direct result of this, minor signals detected within the FITC channel may be indistinguishable from noise due to the bias on the subsequent detector sensitivity. However, if a lesser matrix was not to be used, there would be significant

potential for erroneous false positivity within the "PE" channel signal (Appendix 4.5.3.1.1).

4.5.4.2 Preliminery Linear Dose Response Capture Utilsing both Fluorescence-Area and Fluoresence-Height as Potential Descriptors

Current *PIG-A* mutant frequnecy assessment is undertaken through immunofluorensence staining and subsequent flow cytometry anaylsis. Up to date, all the data generated during acquisition has been collected and displayed through a logarithmic function [32]. However, there are alternative methods of acquiring the data within flow cytomery; traditonally, the majority of fluoresnece data is captured via a logarythmic amplifciation and displayed on a log-log or log-linear axis. The reason for this is the excessive variability and extensive range in arbitrary fluoresence units often observed within a specific sample, therefore a qualitative assessment is made. Linear amplification capture is utilised when recording and displaying data inwhich a more quantitaitive approach is required. Cell cycle data is the most prominent example of such data; the G_2/M peak contains twice the nucleic acid composition of the G_0/G_1 peak and therefore, even though arbitrary in nature there is a linear relationship which defines distinct values for DNA content [33, 34].

Fluorescence signal emission, post fluorophore excitation, is generally highly reproducible, and generates a distinctive bell-shaped curve, analagous to a poisson or gaussian distribution. However, following more intrinisic investigation, especially prevelent within biological control data, the data is actually not normally distributed (shapiro Wilks, $P<0.05$). The reason for this is a presence of finite outlier events, which spike the average fluorescence values, and hence, influence the standard deviation providing a poor fit to the data set (Appendix igure 4.5.12). Due to variability in outlier fluorescence and number, the definition of positivity, i.e. the threshold value is often highly varied between samples. In an attempt to simplify the current predicament, and provide increased resolution at the lower region of the x-axis, the *PIG-A* data was assessed using linear acquisition and the possible effect this conceivably had on the sensitivity of the overal test system (Appendix 4.5.3.2). In

additon to this, the actual descriptor of fluorescence was also investigated for potential increments in sensitivity. Fluorescence height was trialled as an alternative to the typical fluoresence area measure generally used within analysis [12, 35-38]. Fluoresence height can be thought of as the maximum amplitude of a fluorescence wave signal, and therefore, potentially could provide more definitive separation between wild type and presumed *PIG-A* mutant events, increasing the resolution between the two sub populations, which is especially usefull when specific events fall at the threshold value for positivity [39].

The resultant data was very intriguing, using the typical FL-A measure, the background mutant frequnecy was within the predicted range (0-0.5%); within a cell line not enriched for wild type, or alternatively depleted for pre-existing mutants, prior to assessment. However, utilsing the FL-H measure, the background was significantly higher, and reached a maxima of ~2.5% of the total viable population (Appendix Figure 4.5.6). As well as appearing to have a distinct effect on the presumptive mutant frequency statistics, the final day of analysis demonstrated a substantial increase in the number of presuptive *PIG-A* mutant events (~20%). This exaggerated figure was most likely influenced by a limited sample size, but still was immesnly variable when compared to the FL-A measure which remained consistent (Appendix Figure 4.5.6). Fluorescence area as a measure or descriptor of fluorescence signal takes into account the ampltude of the signal as well as duration of the signal to be recorded (time of flight). However, fluoresence height, solely reflects the maximum amplitude of said fluorescence signal and disregards the time taken; hence, is not decriptive of the total properties of the wave. Due to this difference in descriptor, FL-H measurements are much more susceptible to increase variance within heterogenous populations with no fixed particle shape. The plane of the particle at the time of laser illumiunation and subsequent data acquisition is highly variable and consequently has a direct effect on the fluorescence signal generated.

Consider two cells, one cell is long and thin along the verticle axis and the other, identicle however, rotated 90°. The two events have the same fluoresence probe intensity and coverage. As each event passes through the path of the laser, during excitation, the resultant fluoresence signal appears distinctly different, as the

orientation of the plane signifcantly affects the amplitude of said signal as well as the time of flight measurement. Therefore, the FL-H measurement and the FL-W measure are highly variable between the two different cells; however, they have the identicle area and therefore, their FL-A values are consitent. Aspect ratio is consequently, critical when using FL-H measures to generate comparable data. Fluorescence area providers an average signal collected over the entire signal duration, FL-H simply measures the maximum amplitude. The conclusion that can be drawn for this data is that when utilsing heterogeneous populations of cells with no fixed shape or aspect ratio, especially following cytotoxic exposure which may induce debris, fluorescence area is a more accurate descriptor; providing more robust data, taking into account size and shape desripencies. However, on the contrary FL-H and FL-W are therefore, more useful in terms of separation of cells purely based on physical orientation and morphology and hence, are utilised extensively to remove the presence of debris. Linear capture appeared to have no significant affect on the sensitivty and consequential dose respone data following assessment.

4.5.4.3 Gating Strategy Assessment – Statistical Approach

Currently, one of the major caveats associated with flow cytometry is the potential subjectivity implied within analysis gating; numerous control samples are required for correct instrument set up however, their use is highly specific to the fluorophore and hence, detector under assay. For example, generally PMT voltages are set through the use of an unstained sample and corresponding first quartile signal presence. However, when using fluorophores with longer emission wavelength, they have correspond less auto-fluorescence, and therefore, their corresponding negative signal should fall practically at the zero origin of the scale [39].

Utilising a standard approach of detecting auto-fluorescence within the channel of interest, via the use of an unstained calibration standard (ICS), and then using this maximum arbitrary value as the threshold for defined positivity; has generated the data to this point. However, this approach is subjective in specific cases when outlier events with fluorescence arbitrary values corresponding to extremely positive signals are observed within the unstained control. Following this method, the threshold is set to a corresponding value equivalent to a definitive positive signal and therefore, the subsequent *PIG-A* assessment data is highly obtuse. As well as the potential errorous results due to the inclusion of outlier events, due to the physical drawing of the threshold gate, retrospective analysis would potentially always result in minor variation between the *PIG-A* data; especially when multiple operators were to analyse the same data set.

In an attempt to refine the current threshold gating strategy, as well as identify any additional caveats with respect to the use of flow cytometry, three distinct methods of statistically deriving a method for defining a reproducible and robust threshold were assessed, utilising a shared data set.

Initially, consecutive same day assessment highlighted the variability as to be expected within biological samples, however, an additional apparent relationship of a correlation between sample time and fluorescence became apparent (Appendix Figure 4.5.8.A). This correlation was re-enforced within the time course assessment on machine variability, which again reflected biological variability (Appendix Figure

4.5.8.B). Due to the highly limited sample size, in terms of independent samples (N=5), a sample was run over an extended period of time in which >10,000 events were plotted with respect to their acquisition time; the resultant data was shown to disprove the hypothesised correlation between acquisition time and fluorescence. The apparent relationship can be explained by the necessity to warm the lasers fully prior to assessment, as a laser warms the voltage required to generate the same signal intensity is reduced, hence if the signal voltage is fixed, the resultant fluorescence emissions signal will increase until optimum temperature is reached and remain consistent.

The three statistical methods were shown to individually generate analogous threshold values, when provided with an identical data set (Appendix 4.5.3.3.1). However, subtle differences within the values and the effects said differences had on the assay design were observed. The initial method of utilising the mean and hence, 2*standard deviation in order to exclude the upper 2.5% (technically the 97.5 percentile) was demonstrated to define the highest value in terms of arbitrary fluorescence units. However, when assessed for goodness of fit to the data, the model was shown to be substandard when compared to the alternative approaches. The reason for this is due to the nature of the data, flow cytometry data of this type is non-normally distributed and hence, skewed; parametric metrics will poorly fit the data. Therefore, even though the alternative approaches utilising the 95% upper percentile and outlier exclusion method provided slightly lower threshold values, their derivation was based on the median and 95% quartiles and therefore, more accurately model the data (Appendix Figure 4.5.12).

Additional relationships were also investigated for correlation via spearman's Rho analysis; size (FSC) and granularity (SSC) were demonstrated to be positively correlated, and were also defined to be independently positivity correlated to fluorescence (Appendix Figure 4.5.11). Although, only 0.384% of sample variance was a result of size in comparison to 19.14% as a result of granularity, alluding to the fact that granularity or SSC value was more of a potential biasing variable in terms of inaccuracies during *PIG-A* analysis. Therefore, as a result of this potentially smaller (FSC), less granular (SSC) events, such as debris have a large implication as presumptive *PIG-A* mutant mimicking events during data analysis.

In order to establish a gating system which generates the expected number of presumptive *PIG-A* mutant phenotype cells, as biology dictates, a number of different factors must be addressed. Initially a cellular platform with a background low enough to be comparable to currently validated in vitro assay systems is required, in addition a reproducible, non-subjective gating strategy which solely includes single cell events, excluding non-viable as well as debris needs to be implemented. When the currently assessed gating strategies were applied to control untreated data, ~75% of the populations were deemed *PIG-A* phenotypic wild type, however, no additional gating was implemented to remove cells based on size from analysis. Therefore, either utilising the outlier or upper 95% upper quartile approach to threshold gating in conjunction with a novel gating system to remove cells not conforming to the correct FSC and SSC metric should offer an unbiased, robust approach to *PIG-A* analysis.

Chapter 5: MCL-5 Optimisation, Preliminary Next Generation Sequencing and Continued Investigation into the in vitro *PIG-A* gene mutation assay platform

5.1 Introduction

Throughout confocal laser scanning, a laser beam, generally argon ion, passes through a light source aperture and then is focused by an objective lens onto the surface of a specimen. In most biological applications the specimen, usually a tissue, has some fluorescence properties, generally from the addition of fluorescence probes, and subsequent scattered and reflected laser light as well as any fluorescent light from the illuminated spot is then re-collected by the objective lens. The collected light is separated by a beam splitter, and is passed through one or a number of fluorescence filters to allow selective emitted fluorescence light to pass, blocking transmitted light, and subsequently be detected. At this stage, the light passes through a pinhole, which removes any un-focused light, and provides the confocal with its high resolution nature and the light intensity is detected by a photo detection device (usually a photomultiplier tube (PMT)) [40].

5.2 Materials and Methods

5.2.5 Next Generation Sequencing

5.2.5.1 Identification of Target Sequences

Gene of interest target sequences were initially explored using the University of Santa Cruz (UCSC) genome bioinformatics browser [41], gene direction, exon number and generalised structural features were established. Utilising the promoter prediction tool supplied within the UCSC browser, investigating ~1000 bp upstream of the start codon, guanine and cytosine residues were identified and their respective frequencies measured. Combining this information with additional classifiers and generalised contextual information for the specific area the browser was able to provide a sequence in which it believed encompassed the entire gene of interest and upstream promoter region, this was generated using the sequence retrieval tool. The generated sequence was cross referenced against a number of different browser based programmes, utilising the reference sequence as starting material, in order to quality assure the original prediction. Berkley Drosophila Genome Project –Neural Network Promoter Prediction [42], Promoter 2.0 Prediction Server [43] and SoftBerry – FPROM [44] assessed the reference sequence and the promoter sequences generated were assessed for homogeneity. As an additional quality assurance check, Ensembl [45] references were used to confirm exon number and gene structure.

5.2.5.2 Sure Select Primer Design for Target Sequences

Following the establishment of a consensus decision about the structure and location of a gene of interest target sequence, the subsequent stage was the design of Agilent SureSelect oligonucleotide primers corresponding to the region. Primer design would be required to span the entire region with sufficient coverage to provide confidence and integrity with subsequent next generation sequencing results.

SureDesign [46] was used to produce a mixture of oligonucleotides which would span the gene of interest based on a set of classifiers or parameters fed into the browser based application. Initially the species of interest was defined, consensus target sequences of the genes of interest bulk inputted and the parameters describing the coverage and stringency of the primer location and overlap edited. The browser based programme was able to produce primer mixtures for each gene of interest with an estimated coverage of ≥90% and a primer synthesis every 24 bp; all regions not claimed to be covered by SureSelect primers were assessed for their location within their respective gene of interest using UCSC genome browser [46]. All regions not covered by the design process were demonstrated to be intrinsic sequences believed to have less impact on protein function and folding than corresponding exonic regions.

5.2.5.3 DNA Extraction Pilot of Human Kidney Cells

Following FACS (Section 2.8.3), the purification and extraction of DNA within this section of work was carried out using a QIAamp DNA Micro Kit (50) (Cat No. 56304, Qiagen, Manchester, UK) with a user-adapted protocol supplied by Qiagen. Buffers AL, ATL, AW1 and AW2 were prepared according to the instructions given in the QIAamp DNA Micro Handbook (page 14) supplied with the corresponding kit outlined above, following this, carrier RNA was prepared in buffers AE and AL according to the instructions given in the QIAamp DNA Micro Handbook (page 15). Carrier RNA (310 µg) was dissolved in 310 µL of Buffer AE and mixed thoroughly via pipetting (minimum of 10 times). The dissolved RNA was sequentially diluted 1 in 99 in Buffer AL and inverted ten times to mix. 1-100 µL of media containing the cells under assay were transferred into a 1.5 mL eppendorf, 100 µL of ATL buffer was added constructing a final volume of 100 µL. Following this, 10 µL of proteinase K and 100 µL of AL buffer were added, eppendorf closed and pulse-vortexed at high speed briefly for 15 seconds. Post vortexing, the samples were incubated at 56 °C for 10 min – shaken moderately during incubation – and briefly centrifuged, 50 µL of ethanol (absolute) was added to the eppendorf, mixed thoroughly by pulse-vortexing for 15 sec, incubated for 3 min at room temperature

and centrifuged briefly. The contents of the eppendorf were carefully transferred into a QIAamp MinElute ® column, centrifuged (6000 x g for 1 min) and washed with 500 µL AW1 buffer. The column was centrifuged (6000 x g for 1 min) and washed with 500 µL of buffer AW2, followed by an additional homologous centrifugation. Pot washing in AW buffers, the column was centrifuged (20,000 x g for 3 min) to dry the membrane and 20-100 µL of AE buffer or distilled water was added. The columns were incubated at room temperature for 1 min, centrifuged (20,000 x g for 1 min) and flow through collected within a clean sterile collection tube. The resultant isolated DNA was quantified using the NanoDrop ND-1000 Spectrophotometer (Section 4.2.5.2.2) and Qubit ® 2.0 Fluorometer (Life ™ Technologies, Paisley, UK) apparatus.

5.2.5.4 Qubit ® 2.0 Fluorometer Protocol

RNA and DNA yield estimation and integrity analyses were carried out using a NanoDrop (Appendix Section 5.2.5.3) and Qubit ® 2.0 Fluorometer apparatus. The Qubit ® 2.0 fluorometer was used in line with supplied manufacture's standards and protocol; briefly, standards (#1, 2 and 3) were loaded into the machine, read sequentially, and were used to construct a calibration curve (concentration vs. fluorescence). Working solution, supplied within the Qubit ™ HS assay kit (Cat. No. Q32851, Life ™ technologies, Paisley, UK), was added, allowed to incubate for 2 min, at room temperature, to the extracted DNA samples. Post incubation, samples were inserted into the machine, sequentially, and their corresponding fluorescence read in order to determine DNA yield. Original concentration of DNA (pg/µL) was back calculated via the known amount of Qubit ™ working solution added to each sample.

5.2.5.5 Next Generation Sequencing Overview

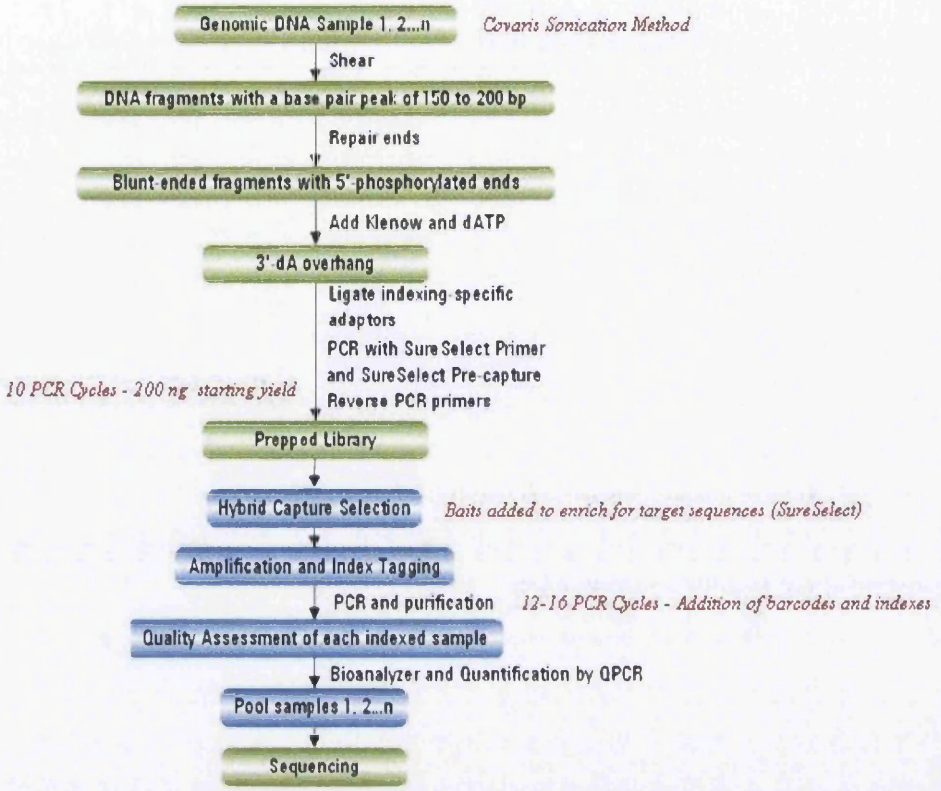

Figure 5.1. Overall schematic of SureSelect Target Enrichment and subsequent Illumina Paired-End MiSeq sequencing of target specific regions. Amended protocol adapted from the supplied SureSelect Protol.pdf (Agilent Technologies, Wokingham, UK). Deviation from the hybrid capture system utilising SureSelect capture library and magnetic bead enrichment, major work flow amendments, key stages highlighted in red.

5.2.5.6 Covaris Sonication Method

The Qubit ® 2.0 fluorometer was used as outlined in (Section 5.2.5.4) to determine the concentration of the gDNA samples extracted from the FACS MCL-5 cells (260/280 absorbance ratios monitored for integrity). 200 ng of starting DNA was diluted with 1 X TE buffer in a 1.5 mL LoBind Tube (Cat No. 022431021, Eppendorf, Hamburg, Germany) to a total volume of 50 µL. The contents of the LoBind tube was transferred into a Covaris microTube, placed within the loading station and the Covaris M220 Focused-ultrasonicator ™ (Covaris, Massachusetts,

USA), recently serviced and refilled, set to 360 sec of treatment time, 200 cycles per burst and bathing temperature of 4-8 °C. Post sonication, a pipette was inserted through the pre-split septa and the sheared DNA removed and subsequently transferred into a sterile 1.5 mL LoBind Tube. Optional quality assurance performed on a 2100 Bioanalyzer (Agilent Technologies, Wokingham, UK) can be carried out at this stage to ensure effective DNA shearing has occurred, a single maximum peak between 120-150 bp in length should be observed.

5.2.5.7 End Repair – Blunt Ended dsDNA Construction

Using the SureSelect Library Prep Kit (ILM) a master mix was prepared containing the following (Nuclease free water 35.2 µL, 10x End Repair Buffer 10 µL, dNTP Mix 1.6 µL, T4 DNA Polymerase 1 µL, Klenow DNA Polymerase 2 µL and T4 Polynucleotide Kinase 2.2 µL). 48 µL of the DNA sample was aliquotted into a fresh tube, 52 µL of master mix was added, mixed thoroughly (vortexing) and incubated for 30 min at 20 °C – constructing blunt ended double stranded DNA molecules.

5.2.5.8 5' Adenine Overhang Construction

Continuing with the use of the SureSelect Library Prep Kit (ILM) a second master mix was constructed for the 5' addition of adenine for subsequent paired end adapter ligation. The master mix contained, Nuclease free water 11 µL, 10X Klenow Polymerase Buffer 5 µL, dATP 1 µL and Exo(-) Klenow 3 µL and was added to 30 µL of DNA blunt-ended sample and consequently, incubated for 30 min at 37°C.

5.2.5.9 Adapter Ligase and Amplification

Next SureSelect Adapter Oligo Mix was diluted 1:10 in nuclease free water, and used to construct a master mix containing (nuclease free water 15.5 µL, 5X T4 DNA Ligase Buffer 10 µL, Diluted SureSelect Adaptor Oligo Mix 10 µL and T4 DNA ligase 1.5 µL. 37 µL of master mix was added to 13 µL of DNA, mixed thoroughly,

and incubated at 20 °C for 15 min. During the incubation, the adaptor was ligated to the newly formed dsDNA, with 5' adenine over hangs, prior to amplification, the following kits and reagents were used; SureSelect Library Prep Kit (ILM), SureSelect Target Enrichment Kit (ILM) indexing Hyb Module Box #2 and Herculase II Fusion DNA Polymerase (Agilent Technologies, Wokingham, UK). The first master mix to be constructed contained, nuclease free water 6 µL, SureSelect Primer 1.25 µL, SureSelect ILM Indexing Pre Capture PCR reverse primer 1.25 µL, 5X Herculase II Rxn Buffer 10 µL, 100 mM dNTP mix 0.5 µL and finally, Herculase II Fusion DNA polymerase 1 µL. 20 µL of master mix was added to 30 µL of the sample DNA, mixed by pipetting placed within the T100 thermal cycler (Bio-Rad, Hertfordshire, UK) and run.

5.2.5.10 Thermal Cycler Amplification Programme

Step 1 98°C 2 min
Step 2 98 °C for 30 sec
Step 3 65 °C for 30 sec
Step 4 72 °C for 1 min
Step 5 – Repeat Step 2 through step 4 for a total of 16-20 times
Step 6 72 °C for 10 min
Step 7 4 °C hold.

5.2.5.11 Sample Purification using Agencourt AMPure XP Beads

AMPure XP beads (Cat No. A63882, Beckman Coulter, High Wycombe, UK) were warmed to room temperature, mixed until homogenous in nature, 90 µL of the beads were added to a 1.5 mL LoBind tube containing ~50 µL of the previously amplified library. The contents of the tube were mixed well, via vortexing and incubated at room temperature for 5 min. The tube was then transferred into a magnetic stand, solution was allowed to clear (3-5 min) and clear supernatant discarded. 500 µL of 70% ethanol (Sigma Aldrich, Gillingham, UK) was added to the tube, incubated for 1 min and then removed – this wash step was repeated an additional time. The tube

was then transferred into a centrifuge, spun briefly and returned to the magnetic stand for 30 seconds, any residual ethanol was removed at this point via a pipette. The samples were then transferred to a heating block and dried (37°C) for 5 min until all residual ethanol completely evaporated. 30 µL of nuclease-free water was added, mixed well via vortexing and incubated at room temperature for 2 min. The tube was replaced back into the magnetic stand, incubated for 2-3 min until supernatant turned clear and then the supernatant was transferred into a fresh sterile LoBind 1.5mL tube (~30 µL). At this point an additional quality assurance step utilising a 2100 Bioanalyzer System and DNA 1000 Assay (Agilent Technologies, Wokingham, UK) can be undertaken, a single peak of approximately 225-275 bp should be observed.

5.2.5.12 Hybridisation

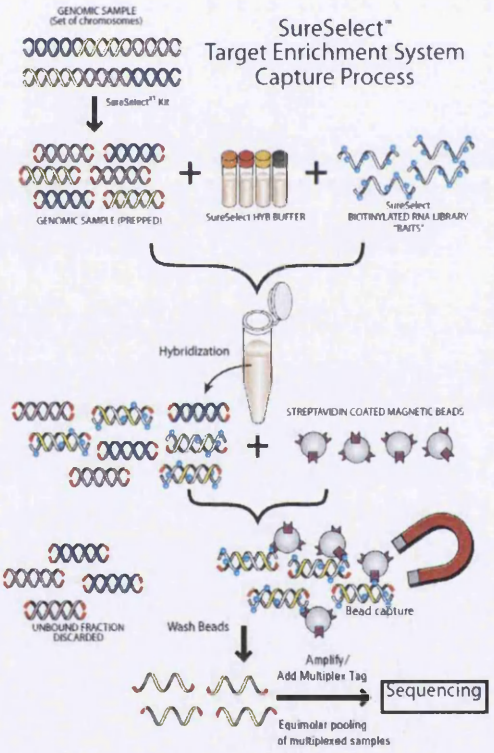

Figure 5.2. SureSelect Target Enrichment System Capture Process. Post amplification, prepped library becomes integrated with SureSelect biotinylated baits (capture library), which sequentially can be enriched for by the external presence of a magnetic field following the addition of streptavidin coated magnetic beads. Beads can be eluted and the resultant enriched target sequences sequenced.

The hybridisation reaction required 750 ng of DNA in a maximum volume of 3.4 µL, if the concentration of the prepped sample was too low then the use of a vacuum concentrator was permitted. Hybridisation buffer was constructed via the addition of the following components; SureSelect Hyb#1 25µL, SureSelect Hyb#2 1 µL, SureSelect Hyb#3 10 µL and SureSelect Hyb#4 13 µL – if precipitation formed the buffer was warmed to 65°C for 5 min.

Within a PCR plate (Greiner-Bio One, Gloucestershire, UK) the SureSelect capture Library mix was prepared for target enrichment; for each sample 2-5 µL of SureSelect Library was pipetted into a well, 5-2 µL of pre-diluted SureSelect RNase Block was added, mixed thoroughly in order to construct a final volume of 7 µL.

SureSelect Block mix was then constructed, consisting of SureSelect Indexing Block #1 2.5 µL, SureSelect Block #2 2.5 µL and SureSelect Indexing Block #3 0.6 µL. 3.4 µL of 221 ng/ µL of prepped library was added to row B of a fresh 96 well PCR plate, 5.6 µL of SureSelect Block Mix was added to each well within row B, and mixed thoroughly. Row B wells were sealed with caps and the plate transferred into a T100 thermal cycler, heated for 5 min at 95°C and held at 65°C. The plate was held at 65°C whilst 40 µL of hybridization buffer was added to each well of row A, the row was sealed with strip caps and kept at 65°C for 5 min. The capture library mix (7 µL) was then added to the row C of the same PCR plate, the row was sealed with strip caps and incubated at 65°C for 2 min.

The plate was maintained at 65°C, whsilst 13 µL of hybridisation buffer from row A was added to the capture library mix in row C and mixed thorughly. The contents of row B (prepped library) was then transferred into the hydridisation solution within row C and mixed well by pipetting up and down a minimum of ten times (~27-29 µL total volume). Wells were sealed with new strip cap to maintain intregirty of the seals and incubated for 16-24 hr at 65 °C.

5.2.5.13 Magnetic Bead Enrichment of Target Sequence

Dynabead MyOne Streptavidin T1 solution was vigorously re-suspended on a vortex, at high speed, to prevent bead settling. 50 µL of Dynabeads were added to a 1.5 mL LoBind tube for reach hybridisation. 200 µL of pre-warmed (65°C) SureSelect Binding Buffer was added to the magnetic beads, mixed on a vortexer for 5 seconds and the tubes transferred into a Dynal magnetic separator (Life ™ technologies, Paisley, UK). The tubes were allowed to stay within the magnet for a number of minutes, and the supernatant removed and discarded – this step was repeated for a total of 3-4 washes, with a final re-suspension of the beads within 200 µL of SureSelect Binding Buffer. Following the volume of hybridization solution being measured, excess evaporation can result in sub optimal capture conditions; the hybridisation solution was transferred directly into the bead solution mixed thoroughly via tube inversion. The mixture was incubated for 30 min at room temperature under rolling conditions, centrifuged briefly and placed within a magnetic separator. The supernatant as removed following a 3 minute incubation period within the magnet, and the beads re-suspended in 500 µL of SureSelect Wash 1. The samples were vortexed, and incubated for 15 min at room temperature, before being centrifuged and replaced within the magnetic separator to remove the supernatant. Post supernatant aspiration the beads were re-suspended in 500 µL of pre-warded (65°C) SureSelect Wash 2, vortex mixed for 5 sec and incubated for 10 min at 65°C within a temperature controlled water bath. Post incubation, the samples were briefly centrifuged, supernatant aspirated following magnetic separation and washed an additional 3 times with SureSelect Wash 2 solution. Following washing, the beads were re-suspended in 30 µL of nuclease-free water on a vortex mixer.

5.2.5.14 Addition of Index Tags by Post Hybridisation Amplification

The reaction mix was prepared as follows, mixed thoroughly and stored on ice ready for future use, 5x Herculase II Rxn Buffer 10 µL, 100 mM dNTP Mix 0.5 µL, Herculase II fusion DNA polymerase 1 µL and SureSelect ILM indexing Post

capture forward PCR primer 1 µL. 35 µL of the reaction mix was transferred into a fresh tube or well within a 96 well plate, 1 µL of the appropriate PCR Primer Index 1-16 was also added and the contents mixed thoroughly. 14 µL of the DNA, post magnetic bead enrichment, was added to each well or tube and placed within a T100 thermal cycler.

5.2.5.15 PCR programme for Amplification Post Capture

Step 1 98°C 2 min
Step 2 98 °C 30 sec
Step 3 57 °C 30 sec
Step 4 72 °C 1 min
Step 5 Repeat steps 2 – 4 for a total of 12-16 times
Step 6 72 °C 10 min
Step 7 4 °C Hold

*The number of cycles depends upon the capture size of the target sequences, 1kb – 0.5 MB (16 cycles), 0.5 Mb – 1.49 Mb (14 cycles), >1.5 MB (12 cycles) and All exon (10-12 cycles).

5.2.5.16 Sample Purification using Agencourt AMPure XP Beads

AMPure XP beads were warmed to room temperature, mixed until homogenous in nature, 90 µL of the beads were added to a 1.5 mL LoBind tube containing ~50 µL of the previously amplified post capture library. The contents of the tube were mixed well, via vortexing and incubated at room temperature for 5 min. The tube was then transferred into a magnetic stand, solution was allowed to clear (3-5 min) and clear supernatant discarded. 500 µL of 70% ethanol (Sigma Aldrich, Gillingham, UK) was added to the tube, incubated for 1 min and then removed – this wash step was repeated an additional time. The tube was then transferred into a centrifuge, spun briefly and returned to the magnetic stand for 30 seconds, any residual ethanol was removed at this point via a pipette. The samples were then transferred to a heating

block and dried (37°C) for 5 min until all residual ethanol completely evaporated. 30 µL of nuclease-free water was added, mixed well via vortexing and incubated at room temperature for 2 min. The tube was replaced back into the magnetic stand, incubated for 2-3 min until supernatant turned clear and then the supernatant was transferred into a fresh sterile LoBind 1.5mL tube (~30 µL). At this point an additional quality assurance step utilising a 2100 Bioanalyzer System and DNA 1000 Assay (Agilent Technologies, Wokingham, UK) can be undertaken, a single peak of approximately 250-350 bp should be observed.

5.2.5.17 QPCR – Quantity Assessment of Index Tagged Amplified Library

QPCR NGS Library Quantification Kit (Illumina) (Cat No. G4880A, Agilent Technologies, Wokingham, UK) was used to determine the concentration of the concentration of each index-tagged captured library. A calibration or standard curve was prepared via the use of the supplied quantification standards included in the kit, according to the instruction provided in the user guide. The index-tagged captured library were subsequently diluted in nuclease free water in order to fall within the standard curve range, this generally I in the range g a 1:1000 – 1:10,000 dilution of the captured DNA. The master mix was prepared, including the Illumina adaptor specific PCR primers, and added to the template DNA. Using a QPCR system, for example iCycler IQ5 (BioRad, Hertfordshire, UK), the thermal profile outlined within the instruction manual supplied was run in combination with the SYBR green instrument settings, in order to facilitate the quantification of each unknown index-tagged library.

5.2.5.18 Sample Pooling for Multiplex Sequencing

5.2.5.18.1 Volume of Index Equation

$$\text{Volume of Index} = \frac{V(f) \times C(f)}{\# \times C(i)}$$

Where,

V(f) is the final desired volume of pool

C(f) is the desired final concentration of the entire DNA in the pool, for example 10 nM for Illumina.

is the number of index

C(i) is the initial concentration of each index sample.

Each library was combined such that each index-tagged sample is present in equimolar amounts within the pool, 1 X Low TE buffer was added to each pool in order to standardise the final volume.

5.2.5.19 Sequencing on the MiSeq ™

5.2.5.19.1 Illumina Reagent Preparation and MiSeq™ Set Up

The flow cell was initially inspected and cleaned thoroughly before use as outlined in detail within the MiSeq System User Guide, the cartridge was removed from -20°C storage and placed within a temperature controlled water bath filled with deionised water (~25°C). The cartridge thawed for approximately 60-90 min, was tapped dry onto tissue paper and inverted ten times to thoroughly mix the components. The cartridge was placed on the bench and tapped to reduce air bubbles within the reagent and stored on ice until ready for future use.

5.2.5.19.2 Illumina MiSeq ™ Reagent Cartridge

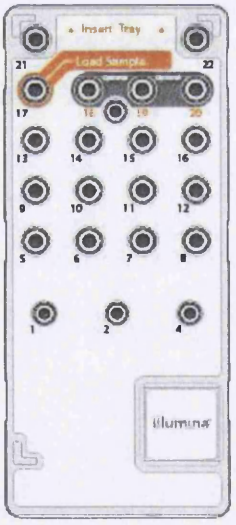

Figure 5.3. The illumina MiSeq ™ Reagent Cartridge. The Cartridge is supplied prefilled with each well labelled with the corresponding well contents. Well 17 is the well designated to accept the pooled prepared denatured DNA sample for high resolution sequencing.

5.2.5.19.3 Denaturation and Dilution for MiSeq ™ Sequencing

Fresh NaOH was prepared in the following manor in advance of the denaturation process , 200 µL of 1M NaOH was added to 800 µL of laboratory grade dH_20 – it is important to maintain the concentration of NaOH equal to 0.2 M in the denaturation solution and not more than 1 mM in the final solution post diluting with HT1 buffer. 4 nM of DNA, within a total volume of 5 µL, was added to 5 µL of 0.2 M NaOH, vortexed briefly and centrifuged (280 x g for 1 min). Post centrifugation, the solution was incubated for 5 min at room temperature to denature the DNA into single strands. 990 µL of pre-chilled HT1 buffer was added to the denatured DNA solution and placed on ice ready for future use. Additional HT1 buffer was added at this point in order to dilute the 20 pM denatured DNA into appropriate concentrations, inverted briefly and then loaded directly within the MiSeq reagent cartridge (PhiX controls were simultaneously constructed in an analogous manor).

5.2.5.19.4 MiSeq ® Next Generation Sequencing (NGS)

The Illumina MiSeq® was loaded, set up and cleaned according to the Illumina MiSeq® system user guide, the MiSeq control software (MCS) was launched simultaneously and from the on screen user guided interface Sequence" selected. Following the sequence selection, the machine begins the run setup steps and prompts the user through the next generation sequencing process. Real time analysis of run efficiency and progress was carried out on an adjacent personal computer running Sequence Analysis Viewer (SAV) software (Illumina, San Diego, UK), a post run-wash using laboratory grade dH_20 mixed with Tween20 was carried out following the successful run.

5.3 Results

5.3.1 Trialled usage of HLA-DR staining to validate single marker *PIG-A* dose response data within MCL-5 cells

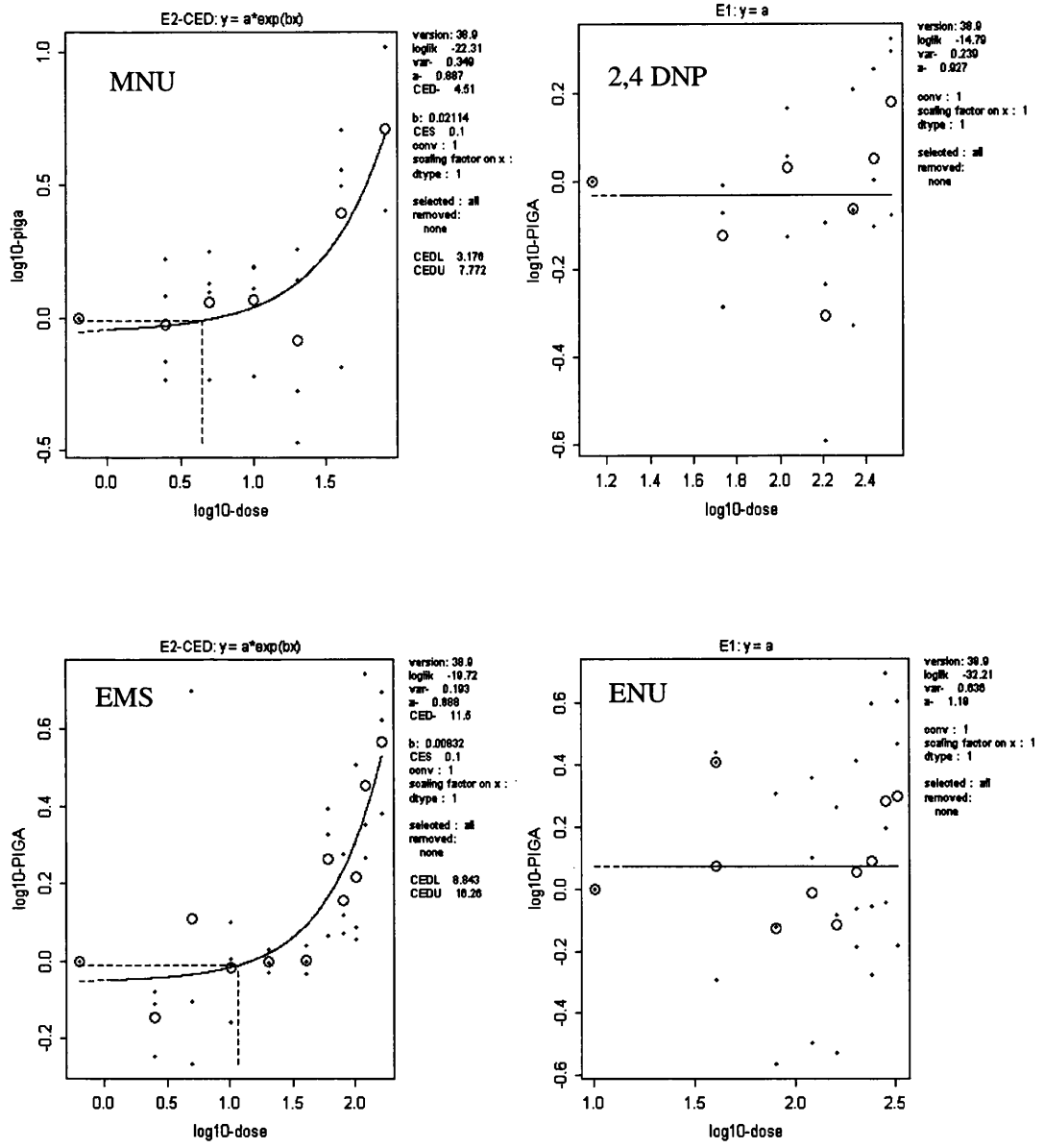

Figure 5.4 Day 4, low passage human lymphoblastoid cells (MCL-5) average relative phenotypic *PIG-A* mutant frequency following 24 hr MNU, 2,4 DNP, EMS and ENU exposure PROAST data, CD59 antigen utilised as reporter for mutation. BMD_{10} (CED_{10}) and confidence intervals ($CEDL_{10}$ and $CEDU_{10}$) derived following statistical modelling

5.3.5 Next Generation Sequencing

Initially, considering the *PIG-A* gene inclusive amplicon, there appears to be a basal level of coverage, the total number of reads covering a single nucleotide, across the majority of the amplicon (Figure 5.5 AI, AII). The basal read depth is approximately 5-10,000 reads per nucleotide, however, there are also areas across the amplicon with significantly higher read depth, >200,000 reads. Single nucleotide polymorphisms (SNP) variants were called across the entire sequence (5287) (Appendix Section 5.3.5.1), with evidence indicative of specific clustering (Figure 5.5 and 5.6). An apparent relationship between SNP variant frequency and the total number of reads at a specific nucleotide was observed, when grossly exceeding the threshold of basal coverage. Therefore, maximum read depth was capped to ensure standardisation and alignment integrity during graphical analysis; 45 insertion and deletion mutations (indels) were also identified across the amplicon.

When focussing on the specific *PIG-A* gene region, it was apparent that the majority of called SNPs were located outside of exonic coding regions (4972), however, the SNPs which did fall within the exons (315, 5.95%) displayed corresponding high variant frequencies, particularly in exon 6. All exonic regions demonstrated some level of mutational activity, except exon 1, which is the smallest of all the coding regions within the gene (Appendix Section 5.3.5.1). SNPs were demonstrated to be both synonymous and non-synonymous in nature, with few proving to result in a nonsense mutation (Figure 5.6). The most frequent mutational variant identified within the *PIG-A* inclusive amplicon was supportive of the primary mutagenic mode of action induced by the EMS treatment, a GC-AT transition mutation, encompassing 27% of the total SNPs (Appendix Section 5.3.5.1).

The *PIG-T* inclusive amplicon was demonstrated to exhibit SNPs variants (16,141) and indels (132) across the entire sequence, with significant evidence indicative of specific clustering outside of the coding exonic regions (Figure 5.7). When focussing on the *PIG-T* gene region, it was apparent that the majority of called SNPs were located outside of exonic coding regions (16,137); only 0.02% of the SNPs fell within the exons (4). The majority of the exonic regions demonstrated no level of mutational activity, except exon 10 and 12 (Appendix Section 5.3.5.2) SNPs again were demonstrated to be both synonymous and non-synonymous in nature, with none proving to result in a nonsense mutation. The most frequent

mutational variant identified within the *PIG-T* inclusive amplicon was again the GC-AT transition mutation, encompassing 25.9% of the total SNPs.

The *CD59* inclusive amplicon was demonstrated to display SNPs variants across the entire sequence (14,071), with again significant evidence indicative of SNP clustering outside of the coding exonic regions; 121 indels were also identified (Figure 5.8). When focussing on the *CD59* gene region, the majority of called SNPs were located outside of exonic coding regions (13,618). Exons 1, 2 and 6 displayed some evidence of mutational activity (3.2% of total SNPs (Appendix Section 5.3.5.3) in which SNPs again were demonstrated to be both synonymous and non-synonymous in nature, with few proving to result in a nonsense mutation. Similar to both the previously assessed genes regions, the most common mutational variant identified within the *CD59* inclusive amplicon was again the GC-AT transition mutation, encompassing 23.7% of the total SNPs.

Finally, the *CD55* inclusive amplicon displayed an analogous pattern to all the comparative amplicons assessed in terms of SNP (13,166) and indels (106) identification. However, not a single SNP was located within the coding exonic regions (0, 0% (Appendix Section 5.3.5.4)). When focussing on the *CD55* gene region, the entirety of called SNPs were located outside of exonic coding regions, falling within the introns (Figure 5.9). However, again, similar to all the previously assessed genes regions, the most common mutational variant identified within the *CD55* inclusive amplicon was again the GC-AT transition mutation, encompassing 23.9% of the total SNPs.

The *PIG-A* gene inclusive amplicon demonstrated the highest level of exonic mutational activity, 5.95%, when directly compared to all of the other amplicons. Even though the *PIG-A* gene didn't display the greatest total number of called variants, it's significantly smaller length (~16 kb) than the CD59 (33 kb) gene for example can account for this. All genes assessed resulted in the GC-AT transition mutation as the consensus for most common variant, which matches the mechanism of the treatment chemical (Appendix Section 5.3.5).

5.3.5.1 *PIG-A* Gene

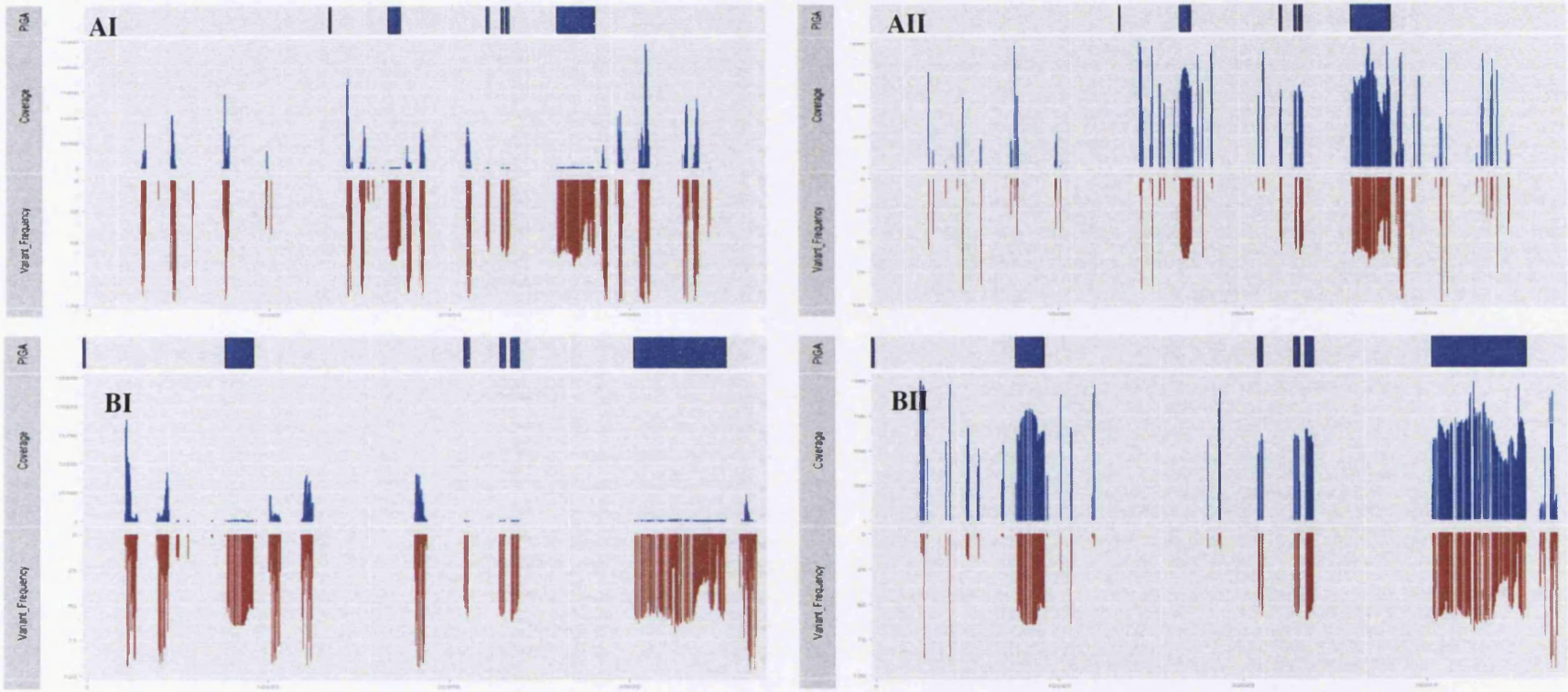

Figure 5.5. Next Generation Sequence of the entire *PIG-A* amplicon (A) or specific *PIG-A* gene (B), scaled and shaded blue to define exonic coding regions, following *PIG-A* reference amplicon alignment and variant calling of an EMS induced heterogeneous phenotypic *PIG-A* mutant population. Total coverage (I) and thresholded coverage ≤10,000 reads (II), Variant frequency represented in (-) and Coverage in (-).

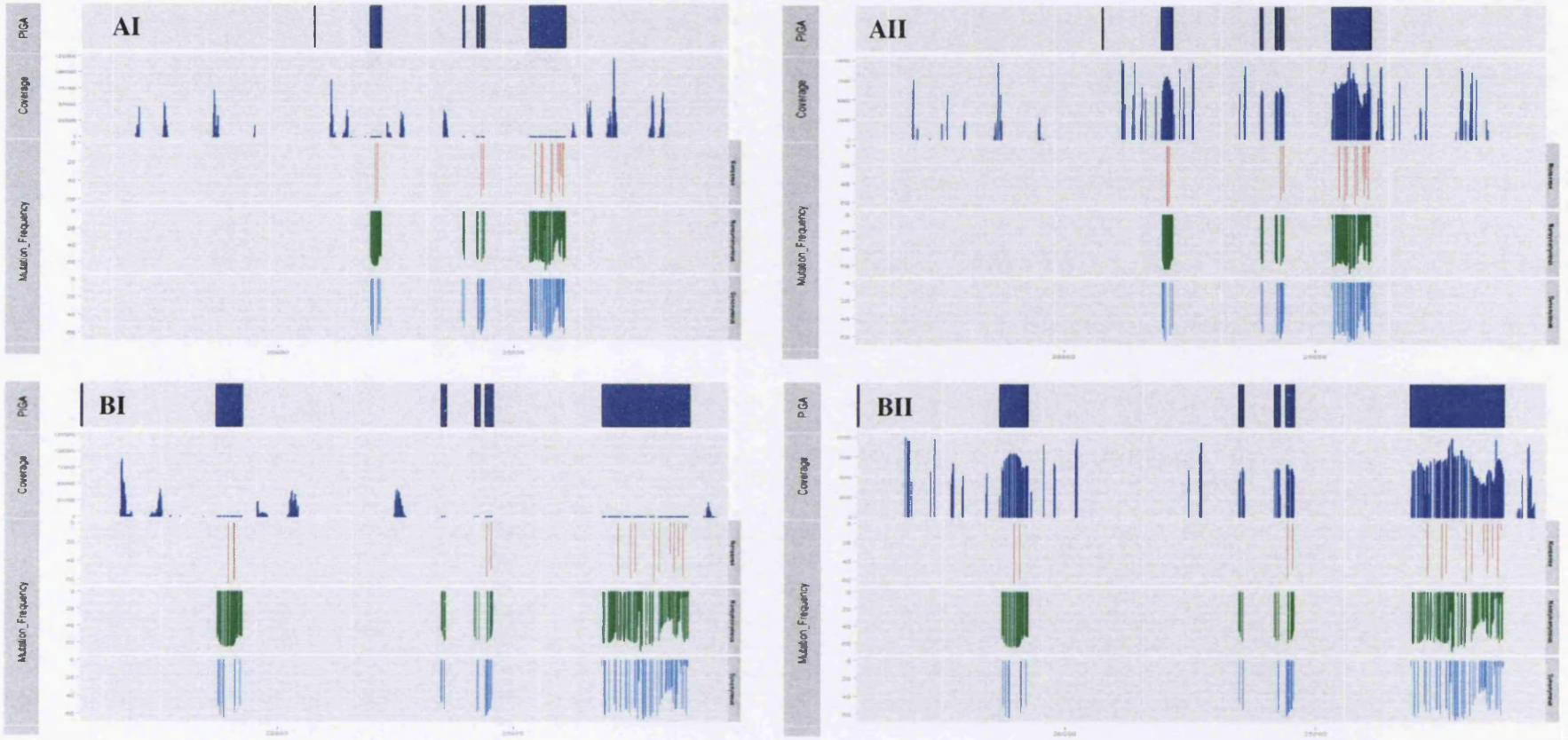

Figure 5.6. Next Generation Sequence of the entire *PIG-A* amplicon (A) or specific *PIG-A* gene (B), scaled and shaded blue to define exonic coding regions, following *PIG-A* reference amplicon alignment and variant calling of an EMS induced heterogeneous phenotypic *PIG-A* mutant population. Total coverage (I) and thresholded coverage ≤10,000 reads (II). Coverage represented in (-), additional annotation undertaken to provide preliminary identity of mutation frequency; nonsense (-), nonsynonymous (-) and synonymous (-).

Table 5.1 - Summary of the SNP data generated for the entire PIG-A gene inclusive amplicon.

		Percentage of Total Variants
A Allele Variants	2078	39.30395309
C Allele Variants	937	17.7227161
G Allele Variants	968	18.30905996
T Allele Variants	1304	24.66427085
Total Number of SNPS	5287	100

	Number of SNPs	Percentage of Total Homologous Allele SNPs	Percentage of Total SNPs
AT-CG	199	20.41025641	3.76394931
AT-GC	694	71.17948718	13.12653679
AT-TA	82	8.41025641	1.550974087
Total	975	100	18.44146019
CG-AT	375	23.11960543	7.092869302
CG-GC	160	9.864364982	3.026290902
CG-TA	1087	67.01602959	20.55986382
Total	1622	100	30.67902402
GC-AT	1438	87.15151515	27.19878948
GC-CG	77	4.666666667	1.456402497
GC-TA	135	8.181818182	2.553432949
Total	1650	100	31.20862493
TA-AT	265	25.48076923	5.012294307
TA-CG	661	63.55769231	12.50236429
TA-GC	114	10.96153846	2.156232268
Total	1040	100	19.67089086
Total	**5287**	**Total**	**100**

Indels	**45**

Table 5.2 - Summary of the SNP data generated for Exon 2 of the PIG-A gene region.

		Percentage of Total Variants
A Allele Variants	9	14.0625
C Allele Variants	21	32.8125
G Allele Variants	20	31.25
T Allele Variants	14	21.875
Total Number of SNPS	64	100

	Number of SNPs	Percentage of Total Homologous Allele SNPs	Percentage of Total SNPs
AT-CG	3	33.33333333	4.6875
AT-GC	5	55.55555556	7.8125
AT-TA	1	11.11111111	1.5625
Total	9	100	14.0625

CG-AT	2	9.523809524	3.125
CG-GC	5	23.80952381	7.8125
CG-TA	14	66.66666667	21.875
Total	21	100	32.8125

GC-AT	17	85	26.5625
GC-CG	2	10	3.125
GC-TA	1	5	1.5625
Total	20	100	31.25

TA-AT	1	7.142857143	1.5625
TA-CG	12	85.71428571	18.75
TA-GC	1	7.142857143	1.5625
Total	14	100	21.875

Total	**64**	**Total**	**100**

Table 5.3 - Summary of the SNP data generated for Exon 3 of the PIG-A gene region

		Percentage of Total Variants
A Allele Variants	1	11.11111111
C Allele Variants	4	44.44444444
G Allele Variants	3	33.33333333
T Allele Variants	1	11.11111111
Total Number of SNPS	9	100

	Number of SNPs	Percentage of Total Homologous Allele SNPs	Percentage of Total SNPs
AT-CG	0	0	0
AT-GC	0	0	0
AT-TA	1	100	11.1111111
Total	1	100	11.1111111
CG-AT	1	25	11.1111111
CG-GC	1	25	11.1111111
CG-TA	2	50	22.2222222
Total	4	100	44.4444444
GC-AT	1	33.33333333	11.1111111
GC-CG	2	66.66666667	22.2222222
GC-TA	0	0	0
Total	3	100	33.3333333
TA-AT	0	0	0
TA-CG	1	100	11.1111111
TA-GC	0	0	0
Total	1	100	11.1111111
Total	**9**	**Total**	**100**

Table 5.4 - Summary of the SNP data generated for Exon 4 of the PIG-A gene region

		Percentage of Total Variants
A Allele Variants	0	0
C Allele Variants	0	0
G Allele Variants	4	80
T Allele Variants	1	20
Total Number of SNPS	5	100

	Number of SNPs	Percentage of Total Homologous Allele SNPs	Percentage of Total SNPs
AT-CG	0	0	0
AT-GC	0	0	0
AT-TA	0	0	0
Total	0	0	0
CG-AT	0	0	0
CG-GC	0	0	0
CG-TA	0	0	0
Total	0	0	0
GC-AT	3	75	60
GC-CG	0	0	0
GC-TA	1	25	20
Total	4	100	80
TA-AT	0	0	0
TA-CG	1	100	20
TA-GC	0	0	0
Total	1	100	20
Total	**5**	**Total**	**100**

Table 5.5 - Summary of the SNP data generated for Exon 5 of the PIG-A gene region

		Percentage of Total Variants
A Allele Variants	8	42.10526316
C Allele Variants	5	26.31578947
G Allele Variants	3	15.78947368
T Allele Variants	3	15.78947368
Total Number of SNPS	19	100

	Number of SNPs	Percentage of Total Homologous Allele SNPs	Percentage of Total SNPs
AT-CG	0	0	0
AT-GC	8	100	42.10526316
AT-TA	0	0	0
Total	8	100	42.10526316
CG-AT	1	20	5.263157895
CG-GC	0	0	0
CG-TA	4	80	21.05263158
Total	5	100	26.31578947
GC-AT	3	100	15.78947368
GC-CG	0	0	0
GC-TA	0	0	0
Total	3	100	15.78947368
TA-AT	1	33.33333333	5.263157895
TA-CG	2	66.66666667	10.52631579
TA-GC	0	0	0
Total	3	100	15.78947368
Total	**19**	**Total**	**100**

Table 5.6 - Summary of the SNP data generated for Exon 6 of the PIG-A gene region

		Percentage of Total Variants
A Allele Variants	49	22.47706422
C Allele Variants	55	25.2293578
G Allele Variants	69	31.65137615
T Allele Variants	45	20.64220183
Total Number of SNPS	218	100

	Number of SNPs	Percentage of Total Homologous Allele SNPs	Percentage of Total SNPs
AT-CG	5	10.20408163	2.293577982
AT-GC	33	67.34693878	15.13761468
AT-TA	11	22.44897959	5.04587156
Total	49	100	22.47706422

CG-AT	16	29.09090909	7.339449541
CG-GC	5	9.090909091	2.293577982
CG-TA	34	61.81818182	15.59633028
Total	55	100	25.2293578

GC-AT	51	73.91304348	23.39449541
GC-CG	7	10.14492754	3.211009174
GC-TA	11	15.94202899	5.04587156
Total	69	100	31.65137615

TA-AT	13	28.88888889	5.963302752
TA-CG	23	51.11111111	10.55045872
TA-GC	9	20	4.128440367
Total	45	100	20.64220183

Total	**218**	**Total**	**100**

5.3.5.2 *PIG-T* Gene

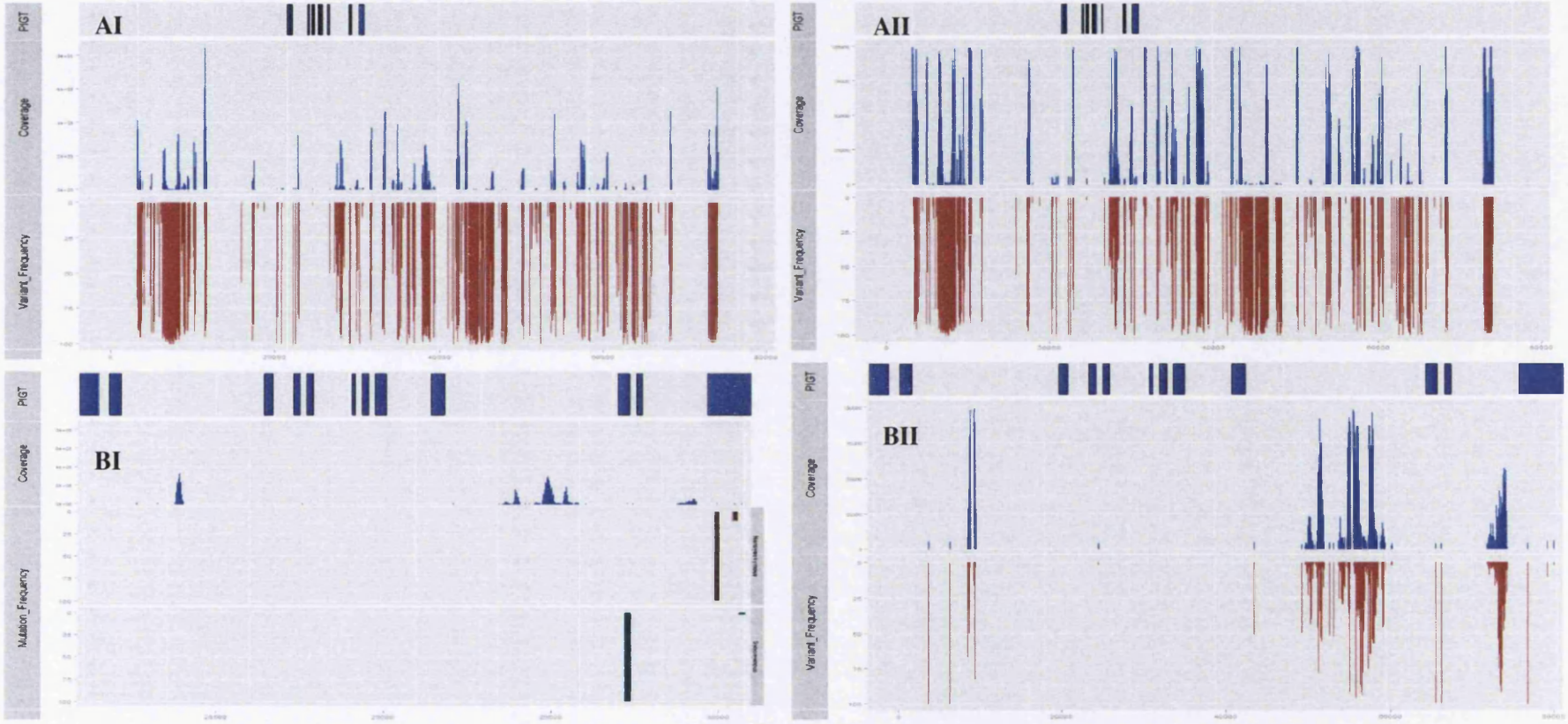

Figure 5.7. Next Generation Sequence of the entire *PIG-T* amplicon (A) or specific *PIG-T* gene (B), scaled and shaded blue to define exonic coding regions, following *PIG-T* reference amplicon alignment and variant calling of an EMS induced heterogeneous phenotypic *PIG-A* mutant population. Total coverage (I) and thresholded coverage ≤10,000 reads (II). Variant frequency represented in (-), coverage in (-), additional annotation undertaken to provide preliminary identity of mutation frequency - synonymous ( ) and non ( ).

Table 5.7- Summary of the SNP data generated for the entire PIG-T amplicon.

		Percentage of Total Variants
A Allele Variants	6286	38.94430333
C Allele Variants	3350	20.75460009
G Allele Variants	3007	18.62957685
T Allele Variants	3498	21.67151973
Total Number of SNPS	16141	100

	Number of SNPs	Percentage of Total Homologous Allele SNPs	Percentage of Total SNPs
AT-CG	678	21.51697874	4.200483241
AT-GC	2160	68.54966677	13.3820705
AT-TA	313	9.933354491	1.939161142
Total	3151	100	19.52171489
CG-AT	1106	24.51784527	6.85211573
CG-GC	533	11.81556196	3.302149805
CG-TA	2872	63.66659277	17.79319745
Total	4511	100	27.94746298
GC-AT	4180	87.61265982	25.89678459
GC-CG	278	5.826870677	1.722322037
GC-TA	313	6.560469503	1.939161142
Total	4771	100	29.55826777
TA-AT	1000	26.96871629	6.195403011
TA-CG	2394	64.5631068	14.83179481
TA-GC	314	8.468176915	1.945356545
Total	3708	100	22.97255436
Total	**16141**	**Total**	**100**

Indels	**132**

Table 5.8 - Summary of the SNP data generated for Exon 10 of the PIG-T gene region.

		Percentage of Total Variants
A Allele Variants	1	0
C Allele Variants	0	0
G Allele Variants	0	0
T Allele Variants	0	0
Total Number of SNPS	1	0

	Number of SNPs	Percentage of Total Homologous Allele SNPs	Percentage of Total SNPs
AT-CG	0	0	0
AT-GC	0	0	0
AT-TA	0	0	0
Total	0	0	0
CG-AT	0	0	0
CG-GC	0	0	0
CG-TA	0	0	0
Total	0	0	0
GC-AT	1	100	100
GC-CG	0	0	0
GC-TA	0	0	0
Total	1	100	100
TA-AT	0	0	0
TA-CG	0	0	0
TA-GC	0	0	0
Total	0	0	0
Total	**1**	**Total**	**100**

Table 5.9 - Summary of the SNP data generated for Exon 12 of the PIG-T gene region.

		Percentage of Total Variants
A Allele Variants	1	0
C Allele Variants	2	0
G Allele Variants	0	0
T Allele Variants	0	0
Total Number of SNPS	3	0

	Number of SNPs	Percentage of Total Homologous Allele SNPs	Percentage of Total SNPs
AT-CG	1	100	33.33333333
AT-GC	0	0	0
AT-TA	0	0	0
Total	1	100	33.33333333
CG-AT	0	0	0
CG-GC	0	0	0
CG-TA	0	0	0
Total	0	0	0
GC-AT	1	100	33.33333333
GC-CG	0	0	0
GC-TA	0	0	0
Total	1	100	33.33333333
TA-AT	0	0	0
TA-CG	1	100	33.33333333
TA-GC	0	0	0
Total	1	100	33.33333333
Total	**3**	**Total**	**100**

5.3.5.3 CD59 Gene

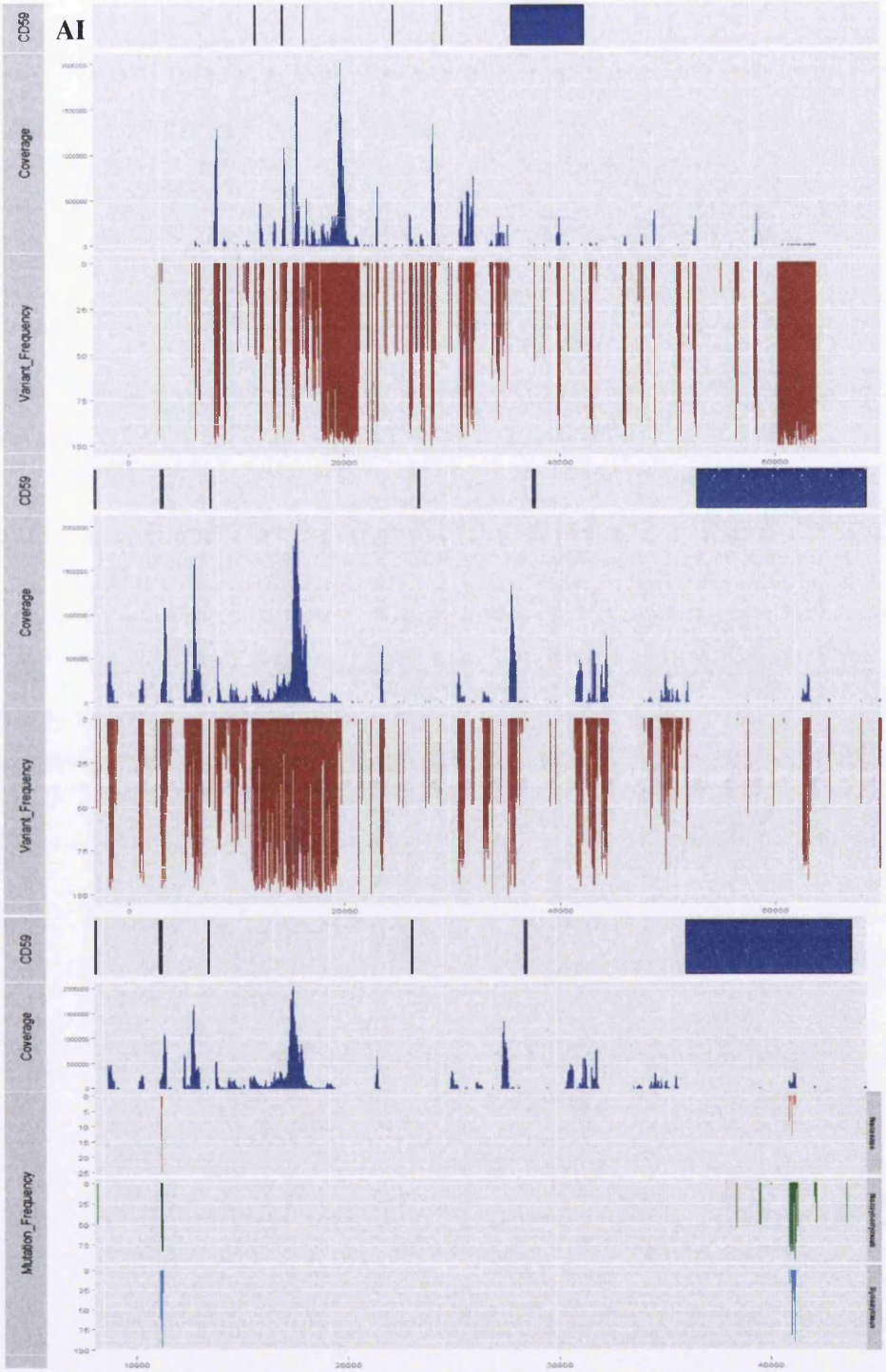

Figure 5.8. Next Generation Sequence of the entire *CD59* amplicon (A) or specific *CD59* gene (B), scaled and shaded blue to define exonic coding regions, following CD59 reference amplicon alignment and variant calling of an EMS induced heterogeneous phenotypic *PIG-A* mutant population. Total coverage (I) and thresholded coverage ≤10,000 reads (II). Variant frequency represented in (-), coverage (-), additional annotation undertaken to provide preliminary identity of mutation frequency; nonsense (-), nonsynonymous (-) and synonymous (-).

Table 5.10 - Summary of the SNP data generated for the entire CD59 amplicon.

		Percentage of Total Variants
A Allele Variants	5222	37.11179021
C Allele Variants	3022	21.47679625
G Allele Variants	2906	20.65240566
T Allele Variants	2921	20.75900789
Total Number of SNPS	14071	100

	Number of SNPs	Percentage of Total Homologous Allele SNPs	Percentage of Total SNPs
AT-CG	646	20.37212236	4.591002772
AT-GC	2164	68.24345632	15.3791486
AT-TA	361	11.38442132	2.565560372
Total	3171	100	22.53571175
CG-AT	964	26.4326844	6.85097008
CG-GC	450	12.33890869	3.198066946
CG-TA	2233	61.22840691	15.86951887
Total	3647	100	25.9185559
GC-AT	3328	85.48677113	23.65148177
GC-CG	238	6.113537118	1.691422074
GC-TA	327	8.399691754	2.323928648
Total	3893	100	27.66683249
TA-AT	930	27.67857143	6.609338355
TA-CG	2138	63.63095238	15.1943714
TA-GC	292	8.69047619	2.075190107
Total	3360	100	23.87889986
Total	**14071**	**Total**	**100**

Indels	**121**

Table 5.11 - Summary of the SNP data generated for Exon 1 of the CD59gene region.

		Percentage of Total Variants
A Allele Variants	0	0
C Allele Variants	1	100
G Allele Variants	0	0
T Allele Variants	0	0
Total Number of SNPS	1	100

	Number of SNPs	Percentage of Total Homologous Allele SNPs	Percentage of Total SNPs
AT-CG	0	0	0
AT-GC	0	0	0
AT-TA	0	0	0
Total	0	0	0
CG-AT	0	0	0
CG-GC	0	0	0
CG-TA	0	0	0
Total	0	0	0
GC-AT	0	0	0
GC-CG	0	0	0
GC-TA	0	0	0
Total	0	0	0
TA-AT	0	0	0
TA-CG	1	0	100
TA-GC	0	0	0
Total	1	0	100
Total	**1**	**Total**	**100**

Table 5.12 - Summary of the SNP data generated for Exon 2 of the CD59gene region.

		Percentage of Total Variants
A Allele Variants	49	35.25179856
C Allele Variants	28	20.14388489
G Allele Variants	25	17.98561151
T Allele Variants	37	26.61870504
Total Number of SNPS	139	100

	Number of SNPs	Percentage of Total Homologous Allele SNPs	Percentage of Total SNPs
AT-CG	5	19.23076923	3.5971223
AT-GC	21	80.76923077	15.1079137
AT-TA	0	0	0
Total	26	100	18.705036
CG-AT	3	0	2.15827338
CG-GC	3	0	2.15827338
CG-TA	35	0	25.1798561
Total	41	0	29.4964029
GC-AT	38	88.37209302	27.3381295
GC-CG	3	6.976744186	2.15827338
GC-TA	2	4.651162791	1.43884892
Total	43	100	30.9352518
TA-AT	8	27.5862069	5.75539568
TA-CG	20	68.96551724	14.3884892
TA-GC	1	3.448275862	0.71942446
Total	29	100	20.8633094
Total	**139**	**Total**	**100**

Table 5.13 - Summary of the SNP data generated for Exon 6 of the CD59gene region.

		Percentage of Total Variants
A Allele Variants	135	43.13099042
C Allele Variants	55	17.57188498
G Allele Variants	66	21.08626198
T Allele Variants	57	18.21086262
Total Number of SNPS	313	100

	Number of SNPs	Percentage of Total Homologous Allele SNPs	Percentage of Total SNPs
AT-CG	14	20.28985507	4.47284345
AT-GC	49	71.01449275	15.6549521
AT-TA	6	8.695652174	1.91693291
Total	69	100	22.0447284
CG-AT	21	0	6.70926518
CG-GC	10	0	3.19488818
CG-TA	45	0	14.3769968
Total	76	0	24.2811502
GC-AT	90	87.37864078	28.7539936
GC-CG	7	6.796116505	2.23642173
GC-TA	6	5.825242718	1.91693291
Total	103	100	32.9073482
TA-AT	24	36.92307692	7.66773163
TA-CG	34	52.30769231	10.8626198
TA-GC	7	10.76923077	2.23642173
Total	65	100	20.7667732
Total	**313**	**Total**	**100**

5.3.5.4 CD55 Gene

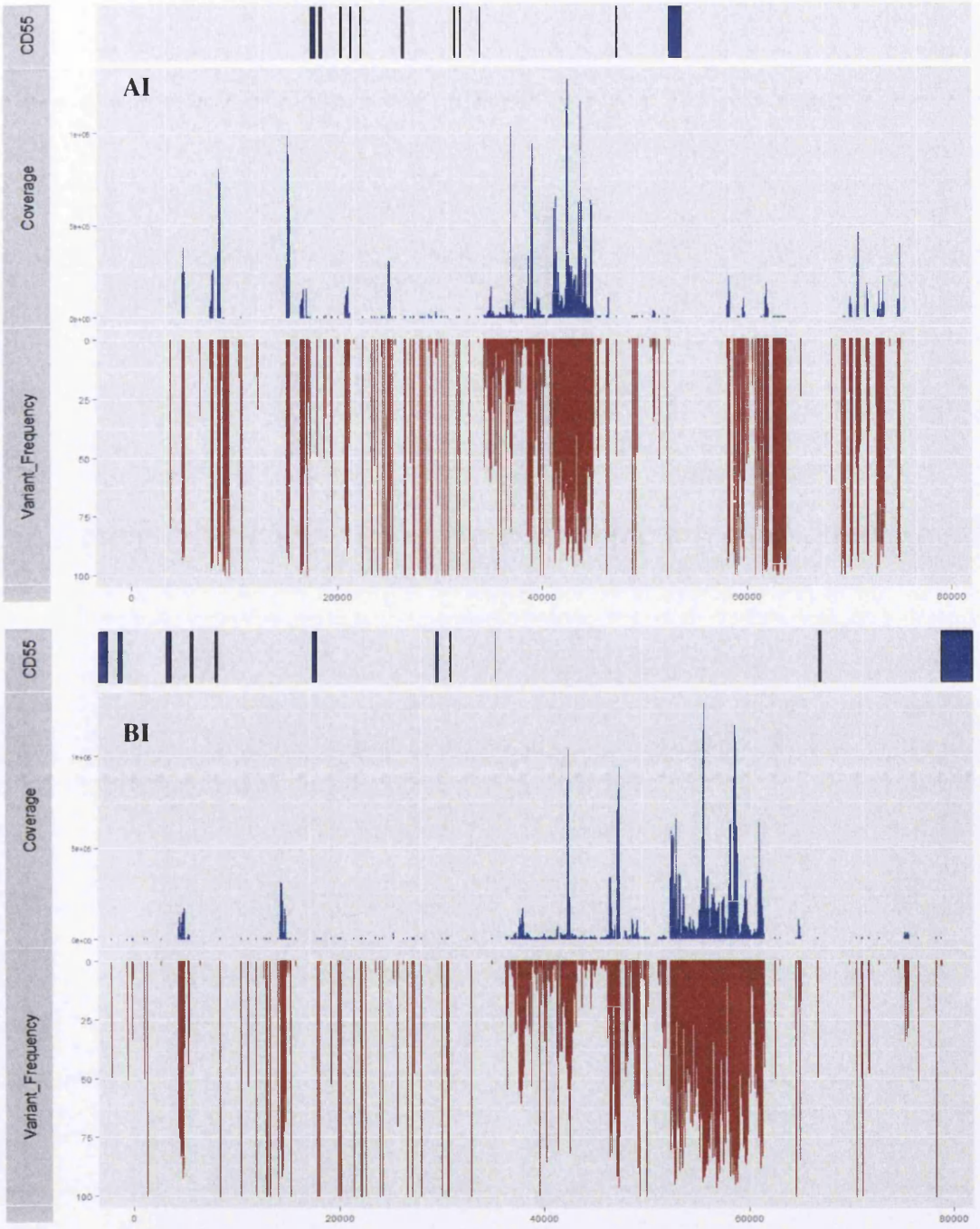

Figure 5.9. Next Generation Sequence of the entire *CD55* amplicon (A) or specific *CD55* gene (B), scaled and shaded blue to define exonic coding regions, following CD55 reference amplicon alignment and variant calling of an EMS induced heterogeneous phenotypic *PIG-A* mutant population. Total coverage (I) and thresholded coverage ≤10,000 reads (II). Variant frequency represented in (-), coverage (-).

Table 5.14 - Summary of the SNP data generated for the entire CD55 amplicon

		Percentage of Total Variants
A Allele Variants	4939	37.51329181
C Allele Variants	2899	22.0188364
G Allele Variants	2594	19.70226341
T Allele Variants	2734	20.76560839
Total Number of SNPS	13166	100

	Number of SNPs	Percentage of Total Homologous Allele SNPs	Percentage of Total SNPs
AT-CG	574	20.90313183	4.359714416
AT-GC	1852	67.44355426	14.06653501
AT-TA	320	11.65331391	2.43050281
Total	2746	100	20.85675224
CG-AT	793	23.89993972	6.023089777
CG-GC	379	11.4225437	2.878626766
CG-TA	2146	64.67751658	16.29955947
Total	3318	100	25.20127601
GC-AT	3147	86.8137931	23.90247607
GC-CG	210	5.793103448	1.595017469
GC-TA	268	7.393103448	2.035546104
Total	3625	100	27.53303965
TA-AT	999	28.73166523	7.587725961
TA-CG	2115	60.82830026	16.06410451
TA-GC	363	10.44003451	2.757101625
Total	3477	100	26.4089321
Total	**13166**	**Total**	**100**

Indels	**106**

5.4 Discussions and Conclusions

5.4.1 Trialled usage of HLA-DR staining to validate single marker *PIG-A* dose response data within MCL-5 cells

2,4 DNP has an essential function as a proton ionophore, an agent that can shuttle protons (electron acceptors or hydrogen cations) across biological membranes [47]. It therefore, defeats the proton gradient across established across the mitochondria and chloroplast membranes, and collapses the proton motive force that the cell uses to produce most of its ATP chemical energy [48]. The overall effect is to reduce the efficiency of the electron transport chain, limit oxidative phosphorylation and the subsequent production of ATP and therefore, increases metabolism to compensate for the loss of energy production; the energy of the proton gradient is extensively lost as heat. For this purpose 2,4 DNP was extensively used in diet pills within the early 20th century until recalled due to onset of dangerous side effects; i.e. increase of internal temperature, highly variable administered dose and rapid development of cataracts were observed [49].

5.4.4 Assay Refinement - Gating Strategy Comparison and Apoptotic Morphology Investigation.

5.4.4.1 Gating Strategy Direct Comparison

Using FL-W and the reporting fluorophore of *PIG-A* mutant phenotype' FL-A scatter plots as a tertiary level of single cell identification induces a significant bias into the gating strategy; in this case R-PE FL-A is the definitive factor in discriminating between wild type and mutant phenotype, and therefore, cannot be

used to further subdivide the population regardless of the corresponding incorporated FL-W measures.

Typically, FSC/SSC and then FSC-A/FSC-W (or H) will provide you enough information to accurately gate an intact and single cell population. However, using fluorescence width of a fluorophore not directly associated with *PIG-A* mutant phenotype definition as a supplementary factor providing additional data for doublet discrimination, excluding cells with a pulse width measure not linear to the FSC-A, appears to provide additional accuracy and sensitivity in terms of event exclusion, and has been observed more frequently within current literature [50]. Therefore, utilising this novel approach within the contest of in vitro *PIG-A* analysis appears to establish a platform which has a perceived sensitivity comparable to analogous validated genetox assays measuring the equivalent end point.

5.4.4.2 Apoptotic Morphology Investigation

Due to the debated TP53, or p53 functionality within MCL-5 cells, [51, 52] it is not definitely known whether or not the cell line is sensitive to apoptosis; this is highly beneficial from an in-direct reporter mechanistic sensitivity point of view but equally the platform will receive scrutiny for the potential effect lack of p53 functionality will have on the subsequent dose response data (Section 5.3.1). Following initial investigation, MCL-5 cells were shown to be able to undergo both apoptosis and necrosis following acute Staurosporine exposure (Section 5.3.4.2); dose dependent increase in relative numbers of apoptosis and necrosis with respect to length of Staurosporine exposure was apparent, with analogous positive correlation being defined. Therefore, the use of viability dyes, excluding apoptotic or necrotic event based on Annexin V sensitivity as well as loss of membrane integrity are deemed essential within the in vitro *PIG-A* assay design.

5.4.5 Next Generation Sequencing

The results generated appeared to show a whole plethora of SNP variants called along the coding and non-coding regions of all the genes assessed (Appendix Section 5.3.5). However, interestingly the *PIG-A* amplicon displayed the highest percentage of SNP variants within the coding region (exons) when compared to any of the other amplicons 5.95%, PIG-T 0.02%, CD59 3.2% and CD55 0%. Typically, assuming that variants within the coding region have a potential larger impact on phenotype, the *PIG-A* gene inclusive amplicon appears to be the most affected by mutational events. In addition to this, the *PIG-A* amplicon is the only hemizygotic sequence, and therefore, dramatically increases the likelihood that each mutational event detected could result in a null-phenotype, when compared to the homozygous *PIG-T*, *CD55* and *CD59*.

Focussing on the *PIG-A* inclusive amplicon, the range of variant frequency observed by any specific SNP was 1-98.5%, reflecting the occurrence of SNPs within the mixed heterogeneous population. Assuming the DNA extraction and amplification steps were effective and without bias, specific common SNPs were observed across the entire heterogeneous population. Loosely exon 6 can be classified as a "hot spot" of mutational activity within the *PIG-A* gene, as 69.2% of the total coding mutations occurred within this region. Similarly exon 6 within the CD59 gene saw an apparent 69% of the total SNPs fall within the region when compared to the total SNPs over the entire amplicon. The other two genes of interest failed to generate any obvious areas of intense mutational activity.

Data analysis was undertaken in a blind manner to prevent the unnecessary biasing of the data, i.e. the alignment, pileup and SNP calling were carried out by an appointed bioinformatician. Therefore, the subsequent data analysis, i.e. SNP identification, localisation and mutational finger printing were carried out independently of potential bias. Interestingly, each amplicon was analysed separately and all mutational fingerprinting results showed the sample pattern. GC-AT transition mutations were the most common mutational occurrence across all amplicons, more interestingly; they were also the most common SNP within the coding regions of the *PIG-A* gene. The main mutagenic mode of action which EMS operates is the 0^6ethyl guanine lesion which results in the miss alignment of a

thymine residue opposite the adducted-lesion resulting in an eventual GC-AT mutation following replication [53-57]. Therefore, the mutational fingerprint observed across all the amplicons was supportive of the EMS mode of action and potentially indicative of EMS treatment.

However, prior to taking any conclusions from this data the con-current negative control sequencing data must first be re-run and analysed prior to removing any common SNPs from the treated data sets. This will generate a SNP background across the amplicons, as a result of spontaneous mutations, and will allow the identification of novel SNPs as a direct result of treatment. Therefore, until this has occurred, even though the data looks promising and indicative of EMS treatment, the data could be as a result of spontaneous mutational events independent of the treatments undertaken.

In addition to the control data, a second compound Benzo[a]pyrene (B[a]P) which operates under a different primary mechanism to EMS was also used to induce phenotypic *PIG-A* mutant cellular populations. B[a]P is a known mutagen present as a bi-product of incomplete combustion and is found within cigarette smoke and cooked meats. However, unlike EMS, which induces mainly abasic sites and specific GC-AT transition mutations, induces a large bulky adduct which results in a high proportion of GC-TA transversion mutations [58-60]. B[a]P requires metabolic activation, into the highly mutagenic epoxide, which is provided sufficiently through the upregulated p450 activity of the MCL-5 cell line [51, 61]. Theoretically, as the mutation spectra for the two chemicals are distinctly different, with minor overlap, the NGS data following FACS isolation should demonstrate the ability for the *PIG-A* mechanism to identify mutations with enough integrity to observe a shift in mutation spectra and hence, subsequently providing additional validation to the reporting system. However, similarly to the EMS control data, the samples failed to be run successfully.

5.5 Supplementary Work

5.5.1 Introduction

5.5.1.1 Antibody Specificity

In general, across all scientific disciplines, specificity and sensitivity are two words which are highly common. Both terms are of the upmost importance and are routinely the features which result in the sale of new technology. But aside from the development and sale of novel technology sensitivity and specificity are often used to describe the functionality of many aspects of molecular biology. As previously discussed antibodies or in this specific case immunoglobulin G (IgG), consist of four identical chains; two heavy chains and two light chains [62, 63]. Within the IgG structure, the chains orientate themselves in a typically "Y" shape, resulting in the formation of two protein binding sites. Thus these protein molecules once assembled can bind selectively to their desired antigen target through the active site or antigen binding site. However, alterative mechanisms of non-specific antibody binding are prevalent including Fc region mediated interactions, hydrogen bonds as well as non-specific hydrophobic interactions [62, 64, 65]. Most commercial companies' now selling antibodies have comprehensive research and development departments angled at product development and validation, however, antibodies are always assigned a disclaimer, suggesting that the operator utilise their own evaluation prior to usage. Therefore, as a result of this, even though most comparable antibodies, i.e. monoclonal etc. raised against analogous proteins are similar there is often specific differences and alterations with activity. As a direct result of this, different antibodies suit different molecular applications, are often best suited to a single application, and require through testing and titration prior to usage to optimise the desired product.

In the specific example of the in vitro *PIG-A* gene mutation assay, or any in-direct protein reporter system, antibody sensitivity is of the upmost importance [66-69]. The assay's overall sensitivity and hence ability is defined by its quantification of finite numbers of phenotypic antigen negative cells, often comprising <1% of the total population. Therefore, prior to assay development it is critical to deconstruct the protocol and validate each and every component of such protocol to assess

functionality and weaknesses, as often such minor details have an exaggerated and deleterious result on the finalised properties of the test system. In the in vitro *PIG-A* test system the single or tandem use of antibody markers for GPI-associated surface antigens must be scrutinised for effectiveness prior to usage as the false identification or miss-identification of phenotypic mutants in order to understand the limitation of the system and provide confidence in the results generated. A failure at this stage to enable accurate quantitation limits if not prevents usage of a test system within specific applications; in the case of drug screening and safety assessment, unless the test has unparalleled sensitivity, its usage is highly limited and more often completely restricted [69, 70].

5.5.1.2 Subtle Cell Line Differences and their effect on Chemical Exposure

During the development of a gene mutation test system, typically the initial compounds which are assessed and used to preliminary validate the reporting mechanism. These compounds are the "well-known" chemicals; they have highly validated mechanisms of actions as well as sufficient pier reviewed publications to warrant confidence. As such, these chemicals have easily predicted response metrics, which are directly able to be recognised and facilitate system critique. Limitations can be identified and solutions carried out leading to system reform. Continued optimisation of the test system will eventually result in re-testing and further validation with progressively less model chemicals. Eventually the system will develop to the point in which the designer will want to fully test the capabilities of the system, in order to define specificity and sensitivity in order to allow a more inclusive peer review of the system to warrant distribution and commercial usage.

However, one aspect of chemical selection which is often overlooked is the lack of predictive response without pre-existing data for an analogous assay design. For example, chemical exposure and subsequent response metrics can easily be predicted assuming that there is previously published data within an analogous set up. Obviously depending upon the variants between the two assay designs specific caveats must be taken into account and the resultant data may be subtly different.

The problem faced within the genetic toxicology word is the vast differences in generated data observed when using analogous test platforms. Similar cell lineages for example, even derived from a common ancestor can be significantly different on a proteomic level and therefore, the subsequent response metrics can be dissimilar. Therefore, prior to utilising reviewed chemicals as model compounds for exposure, one must generate data on the expected response of such chemical within the test system preceding actually running the chemical in the test system; this often requires fundamentally deconstructing the assay design. As often is the case within microbiology, the most subtle differences, especially at a fundamental level, have colossal ramifications on phenotype.

Currently within the field of genetic toxicology, debate about p53 status and hence, biological relevance is often at the forefront of regulatory and safety assessment reform [68, 71-74]. The reason for this is not only the limitations such confounding factors as p53 deficiency and rodent origins have on strength of data within a weight of evidence decision making strategy [75, 76] but also the lack of standardisation within genetic toxicology data. Subsequently, due to variation within assay designs the consequential generated data is often highly dissimilar when generated by analogous assay systems utilising the same chemical. As a result of this, data loses strength and the test systems themselves come under increasing criticism. In order to resolve this problem, the initial stage of harmonisation is comprehensive cell line assessment; in which all aspects of the cell line are evaluated, including responses to known model chemicals prior to distribution. Following cell line distribution, assay protocols can be harmonised and then fully validated to ensure similarity in subsequently generated data. Following this, data can be attributed strength and enables a more simplistic approach to regulatory decision making when data can be attributed a value or rank in respect to comparable biological data.

5.5.1.3 The Cell Cycle as a biasing factor within the in vitro *PIG-A* gene mutation assay

The cell cycle is the highly characterised, critically maintained, mechanisms in which the cell progresses prior to replication in order to facilitate genetic inheritance [26, 34, 77, 78]. During mitosis the cell under goes initial duplication, synthesis, of genomic material, which eventually resides within two identical daughter cells following cytokinesis [79]. The daughter cells are exact replicates with regards to nuclear material and organelles; however, their area is significantly reduced to maintain homeostasis within the cell. As cells grow, their increase in intracellular complexity requires an exponential increase in fuel uptake; membrane transportation constitutes the major intake of fuel within the cell and therefore, division is necessary to prevent the finite membrane surface area from initiating cell death [80].

Therefore, the resultant cells immediately following cytosolic cleavage are under sized, with regards to their potential maximum intra cellular surface area, and are highly active to facilitate new growth and expansion. During cleavage, even though the concentrations of cytosolic proteins as well as mRNA and additional protein structures would remain consistent, the number of such macromolecules would be significantly diminished. Consequently, within this potential period, interphase, in which the cell is rapidly growing in terms of intracellular surface area, intracellular components such as macromolecules are being replenished. GPI-AP proteins are highly associated to lipid dense, lipid rafts, regions of the cellular membrane which are diverse in nature. For that reason, there is an increased chance that due to diminished protein products laser bisection within fluorescence based applications could suffer a negative bias, when compared to more well established cells, within latter stages of the cell cycle with higher densities of GPI-AP on the cell surface.

5.5.1.4 The versatility of the *PIG-A* reporter system, could intracellular *PIG-A* staining offer a conservative design to facilitate point of contact screening?

The effects of compound exposure are highly unique to the tissue in which said compound was exposed. Let's consider an acute exposure of a compound which requires metabolism in order to generate toxic metabolites, for example Paracetamol [81]. Paracetamol overdoses typically result in acute liver toxicity, due to the liver being the most metabolically active organ and hence, the resultant accumulation of toxic metabolites [82]. However, if paracetamol did not require metabolism and was toxic, then the initial point of contact associated to the mechanism of drug delivery would most likely be the most severe tissue presenting toxicity post exposure [83]. Therefore, due to this complex relationship, relying on a single test system, within a specific tissue type, could potentially under or overestimate adverse drug reactions; due to the uniqueness and complexity of drug pharmacodynamics and kinetics [29, 84]. A potential resolution to this problem would be the use of a systemic tissue model, for example peripheral circulating blood, which potentially gives a more holistic approach to drug exposure [7, 85, 86]. Nonetheless, inaccuracies in evaluating adverse drug reactions, especially within acute exposures, are possible.

The most appropriate solution to this problem would be a collective tiered approach to drug screening, with a variety of tissues, including metabolically active and primary sites of exposure, included to provide a more comprehensive screen [3]. However, due to the unique qualities each sub set of tissue provide, which facilitate the usage of particular test systems, finding a highly conservative fundamental mechanism which can be exploited as a test system potentially would offer a large benefit. Having a single, comparable genetic toxicology end point, able to be undertaken within a large variety of tissue could increase the robustness of generated data and provide a more rounded assessment of potential adverse drug reactions. Within this results chapter we begin to explore a more fundamental *PIG-A* mechanism which potentially will facilitate a wider range of tissues to be utilised as a platform for the assay design.

5.5.2 Materials and Methods

5.5.2.1 Antibody Specificity Assessment

Low passage MCL-5 cell cultures were established and maintained as outlined in (Section 2.2) and counted. The equivalent volume containing $1x10^6$ cells was transferred into fresh 15 mL centrifuge tubes (10 samples in total), centrifuged (250 x g for 7 min) and supernatant removed. 50-100 µL of pre-warmed media was added to re-suspend the cell pellets; 5 µL of Fc blocker was added to three samples and incubated for 20 mins at room temperature, samples not receiving Fc blocker (seven samples) were kept at room temperature for 20 min (protected from light), a single sample was treated as an ICS and received no staining. Post incubation all samples, excluding the ICS, were treated with either 20 µL of their respective isotype for the anti-human, anti-CD55/59 R-PE antibodies (Cat No. 555574 BD Biosciences, Hertfordshire, UK) (three samples in total) or 20 µL anti-human, anti-CD55/59 R-PE antibodies and incubated for 30 min at room temperature, protected from light. Following incubation, samples were centrifuged (250 x g for 7 min), supernatant aspirated and discarded and washed in 5 mL of 1 x PBS solution. Samples were returned to the centrifuge, spun (250 x g for 7 min), supernatant aspirated and re-suspended in 100 µL 1 x PBS; the three experimental samples which received 20 µL anti-human anti-CD55/59 R-PE antibody treatment also were treated with 10 µL 7-AAD to facilitate dead cell exclusion within the gating assessment. All samples were kept on ice for a maximum of 1 hr prior to analysis and were diluted prior to running the samples with excess 1 x PBS solution.

5.5.2.2 Dose Finding Study, EMS and MNU Exposure

A vial of Low Passage MCL-5 cells were established and maintained as outlined within (Section 2.2). Following sufficient growth to certify population fitness, cells were counted using a Haemocytometer as well as a Coulter Counter (Section 2.2.1)

and the equivalent volume housing $1x10^6$ cells were transferred into sterile 25 cm^2 pre-labelled culture flasks. The final volume of each culture flask was adjusted to 10 mL via the addition of fresh culture media constructing a final concentration of $1x10^5$ cells/mL. Prior to genotoxic handling, suitable PPE was collected, worn and appropriate disposal vessels collected. Ethyl methanesulfonate and N-nitroso-methyl-urea were collected from storage and diluted within an apt vehicle, to enable dissolving under minimal effort and stock concentration establishment (Section 2.4). Serial dilutions within DMSO were utilised to construct the required stock solutions and subsequent doses. Cellular cultures were treated with 100 µL volume doses of EMS or MNU independently and incubated, under controlled environment, for 24 hr. Following treatment, cultures were washed (excess 1 X PBS) and re-suspended in 10 mL fresh culture media and counted. Cultures were incubated for an additional 24 hr and counted to provide population statistics for a total of 48 hr post chemical treatment. Relative population doubling (RPD), relative cell counts (RCC) and estimated mean generation time (EMGT) were calculated from the produced cell counts in order to facilitate direct cell line comparisons in terms of stability and sensitivity post genotoxin exposure.

5.5.2.3 Preliminary Investigations into Cell Cycle and GPI-AP Expression Correlation

5.5.2.3.1 Amnis Image Stream™ Investigation

MCL-5 cells were established as outlined in (Section 2.2), counted and the equivalent volume of culture corresponding to 1 x 10^6 cells was aliquotted into a sterile 15 ml centrifuge tube, this was repeated six times in total to generate the following samples; an ICS, a single anti-CD55/CD59 R-PE, a single Hoescht 33342, and three Hoechst 33342 and anti-CD55/59 R-PE. Samples were centrifuged (250 x g for 7 min), supernatant aspirated and re-suspended in 5 mL of PBS. The samples were centrifuged again, supernatant aspirated and re-suspended in 100 µL of pre-warmed medium. The required samples were treated with 20 µL of both anti-CD55

and anti-CD59 R-PE antibodies and incubated at room temperature for 30 min, protected from light. Following the incubation, samples were centrifuged, supernatant aspirated and discarded and re-suspended in 10 mL of 1 X PBS. Post washing, samples were again centrifuged and re-suspended in 1 mL of pre-warmed 4% PFA solution and incubated for 15 min at 37°C. Following incubation, the cellular samples were centrifuged (~350 x g for 7 min), supernatant aspirated and re-suspended in 10 mL of 1 x PBS solution. The samples were returned to the centrifuge, spun and re-suspended in 250 µL of 1 x PBS and treated with 5 µL of 10 mg/mL RNase A solution, prior to being incubated at 37 °C for 1 hr. Following the incubation, the intended samples were treated with 10 µL of the working solution of Hoechst 33342 (Cat No. H3570, Life ™ Technologies, Paisley, UK) (1 in 100 dilution within dH_20) and incubated for 10 min, protected from light. Samples were centrifuged, and re-suspended in a final volume of 50 µL of 1 x PBS, prior to Image Stream ™ analysis.

5.5.2.3.2 BD FACS Aria 1 Investigation

MCL-5 cells were established as outlined in (Section 2.2), counted and the equivalent volume of culture corresponding to 1 x 10^6 cells was aliquotted into a sterile 15 ml centrifuge tube, this was repeated four times in total to generate the following samples; an ICS, and three Hoechst 33342 and anti-CD55/59 R-PE. Samples were centrifuged (250 x g for 7 min), supernatant aspirated and re-suspended in 5 mL of PBS. The samples were centrifuged again, supernatant aspirated and re-suspended in 100 µL of pre-warmed medium. The required samples were treated with 20 µL of both anti-CD55 and anti-CD59 R-PE antibodies and incubated at room temperature for 30 min, protected from light. Following the incubation, samples were centrifuged, supernatant aspirated and discarded and re-suspended in 10 mL of 1 X PBS. Post washing, samples were again centrifuged and re-suspended in 1 mL of pre-warmed 4% PFA solution and incubated for 15 min at 37°C. Following incubation, the cellular samples were centrifuged (~350 x g for 7 min), supernatant aspirated and re-suspended in 10 mL of 1 x PBS solution. The samples were returned to the centrifuge, spun and re-suspended in 1 mL of 1 x PBS

and treated 10 μL of the working solution of Hoechst 33342 (Cat No. H3570, Life ™ Technologies, Paisley, UK) (1 in 100 dilution within dH_20) and incubated for 10 min, protected from light. Samples were centrifuged, and re-suspended in a final volume of 1 mL of 1 x PBS, prior to flow cytometry analysis.

5.5.2.4 Preliminary Intracellular PIG-A Investigation

5.5.2.4.1 Proof of principle *PIG-A* monoclonal antibody binding, Western Blott Analysis

Western blott analysis was undertaken utilising primary PIG-A antibody solutions (Abcam and Sigma) under an analogous method as outlined in (Section 4.2.5.1). When utilised in conjunction with corresponding HRP-conjugated secondary antibodies, UV stimulated images are able to be detected using a ChemiDoc™ and corresponding band densities estimated.

5.5.2.4.2 Initial Flow Cytometry Fix and Perm® Intracellular Signal Presence within MCL-5 Cells and Confocal Imaging Evaluation

Intracellular staining was under taken with the usage of a Fix and Perm ® cell fixation and permeabilisation kit (Cat No. GAS-003, Life ™ Technologies, Paisley, UK), anti-human IgG (gamma-chain specific)-R-Phycoerythrin antibody produced in goat (cat No. p9170-5mL, Sigma Aldrich, Gillingham, UK) and anti-PIG-A antibody produced in rabbit (Cat No. SAB2105628-50UG, Sigma Aldrich, Gillingham, UK). Primary antibody was reconstituted within dH_20 generating a 1 mg/mL final concentration, aliquotted to prevent freeze thaw cycles and stored at -20°C until ready for use. Additional buffers not provided within the kit were also constructed including Blocking Buffer solution 5% (v/v) FBS and 2% (w/v) BSA in DPBS.

Low passage MCL-5 cell cultures were established and maintained as outlined in (Section 2.2), counted and the equivalent volume of culture medium containing 1 x 10^6 cells transferred into a sterile 15 mL centrifuge tube; this step was repeated in order to establish the required number of samples. Samples were centrifuged (~250 x g for 7 min) and re-suspended by flicking or gently vortexing the tube, prior to the addition of 4 mL of 1 x PBS solution. Samples were centrifuged, supernatant aspirated and re-suspended in 100 µL of Reagent A (fixation Medium) and incubated for 15 mins at room temperature. Following incubation, cells were centrifuged (400 x g for 5 mins), supernatant aspirated and washed twice through the addition of 3-5 mL of PBS/5% FBS solution. Following washing, samples were centrifuged, supernatant aspirated and re-suspended in blocking buffer (5% (v/v) FBS and 2% (w/v) BSA in DPBS) at room temperature for 1 hr. Post incubation, samples were centrifuged, supernatant decanted and re-suspended in 100 µL of Reagent B (Permeabilisation Medium) and treated with 0.2 mL of 1 µg/mL of primary antibody (Cat No. ab69768, Abcam, Cambridge, UK) within blocking buffer. Each sample was vortexed briefly (1-2 sec) and incubated at room temperature for 20-30 min or alternatively, the tubes were sealed with parafilm, and incubated for 16 to 18 hours (overnight) at 4°C (fridge). Following staining, cells were washed twice in blocking buffer post staining. Subsequently, the cells were treated with 10 µL of 0.5 mg/mL secondary antibody (Cat No. P92870.25ML, Sigma Aldrich, Gillingham, UK) within 0.2 mL of Blocking buffer and incubated at room temperature for 1 hour, protected from light. Samples were centrifuged (350 x g for 5 min), supernatant aspirated, and washed twice in blocking buffer. Finally, the samples were re-suspended in 1 mL PBS/Blocking buffer for immediate flow cytometry analysis.

Following flow cytometry analysis, remaining samples were centrifuged, supernatant discarded and re-suspended in minimal volume (~100 µL) of 1 x PBS. The pre-existing FCM sample was divided into three experimental samples, as well as the ICS being divided into two further samples; one intended to act as an additional ICS for the confocal experiment as well as a sample intended to be exposed to both phalloidin (Alexa Fluor 594) and Hoechst but excluding the R-PE stain to enable removal of background auto fluorescence. A staining solution was established comprising of 1480 µL of PBS, 10 µL Hoechst 33342 (1 in 100 dilution with dH_20) and 10 µL Phalloidin (Cat No. A12381, Life Technologies ™, Hertfordshire, UK),

500 µL was added directly to the re-suspended cell pellets within minimal PBS. Samples were incubated at room temperature, protected from light, for 15 min. Parallel to this, 300 µL of poly-L-lysine solution (1 in 10 dilution within dH_20) was pipetted applied directly into the bottom of a 4 well chamber slides (Nunc® Lab Tek®, MA, USA) and incubated for 15 min at room temperature. Following the incubation, cellular samples were centrifuged (~350 x g for 7 min), supernatant aspirated and re-suspended in 10 mL of PBS, washed and re-suspended in 300 µL of PBS. The 4-well chamber plate was washed thoroughly with dH20, and the relevant experimental samples transferred into each separate well and incubated for 15 min at room temperature. Post incubation, chambers were kept submerged in minimal PBS, covered with foil and stored on ice until ready to image.

5.5.2.4.3 Intracellular Method Optimisation; Methanol Fixation

Low passage MCL-5 cell cultures were established and maintained as outlined in (Section 2.2), counted and the equivalent volume of culture medium containing 1 x 10^6 cells transferred into a sterile 15 mL centrifuge tube. Centrifuged (250-300 x g for 7 min), supernatant aspirated and washed in pre-cooled (4°C) 1 x PBS (5 mL), three times in total. The cellular samples were re-suspended within 100 µL of 1 x PBS solution; simultaneously, a 50 mL aliquot of 100% methanol was placed within the -80 °C freezer and incubated to ensure a temperature of ~ -20°C. 900 µL of pre-cooled absolute methanol was added to the cell suspension and re-suspended thoroughly and incubated for 5 min at room temperature. Post methanol fixation, 10 mL ice-cold 1 x PBS was added, centrifuged (~650 x g for 7 min) and supernatant aspirated. Washing was repeated two more times, to remove any excess fixative.

Goat serum (Cat No. G9023-5ML, Sigma Aldrich, Gillingham, UK) was forced through a (0.2 µm) filter (Nalgene Syringe Filters, Thermo Scientific, MA, USA) via the use of a 5 mL syringe (Thermo Scientific, MA, USA) and three subsequent solutions were prepared; 15 mL of 10% goat serum/PBS, 5mL of 1% goat serum/PBS and 10 mL of 1% BSA/PBS. 2 mL of 10% goat serum/PBS solution was added to the washed, fixed cells and incubated for 30 min at room temperature. The

blocking incubation must be undertaken using serum from the species of the secondary antibody intended on being used. Following incubation, the cells were centrifuged, washed thoroughly within ice cold 1 x PBS and re-suspended within 100 µL of primary antibody solution; either (1 in 3000) anti-histone H3 rabbit mab (Cat No. Ab1220, Cambridge, UK) or an (1 in 40) anti-PIG-A rabbit mab within 1% goat serum/PBS solution. The cells were exposed for 30 min at room temperature; all incubations were undertaken protected from light under rolling and tilting conditions. Following incubation, cells were washed within 1 x PBS three times and re-suspended within 100 µL of secondary antibody solution; 10 µL of phalloidin Alexa Fluor 594, 1.25 µL of (1 in 800) anti-rabbit Alexa Fluor 488 ™ goat secondary (Cat No. A11008, Life Technologies ™, Hertfordshire, UK) within 1%BSA/PBS. The cells were exposed to the secondary antibody within 1% BSA/PBS for 30 min at room temperature, following incubation, cells were washed within 10 mL PBS and re-suspended in 50 µL PBS. 25 x 25 mm cover slips were placed on blue roll, and a 10 µL aliquot of DAPI within Vector Shield (Cat No. H1200, Vecta Laboratories, Peterborough, UK) was pipetted into the centre. 10 µL of stained MCL-5 cells were directly added to the pre-existing mountant and very carefully a polished glass microscope slide was dropped onto the cover slip at a 45° angle. A layer of nail varnish was applied around the periphery of the cover slips to prevent motion, and hence prevent cell shearing. Samples were stored at 2-4 °C either as a constructed microscope slide or alternatively, within a 15 ml BD Falcon centrifuge tube as a cell suspension. All samples were stored protected from light, i.e. wrapped in foil.

5.5.2.4.5 Fluorescence Microscopy Imaging

Fluorescence microscopy was carried out using an Axio Imager M1 microscope with attached AxioCam MRm and supplied Axiovision software in conjunction with either a 40x or 63x oil immersion DIC objective (Carl Zeiss, Cambridge, UK). All fluorochromes/fluorophores were excited using the 405, 488, 594 or 633 nm lines. Objectives, laser excitation intensity and laser gain settings remained consistent to provide comparable data sets, however, proof of principle experiments were mainly

undertaken to validate flow cytometric data. Retrospective image analysis was carried out using the ZEN software, as described within the manufacturers supplied information.

5.5.3 Results

5.5.3.1 Antibody Specificity Assessment

Table 5.5.1. Summary of the control isotype antibody relative binding efficiency data, in the presence and absence of Fc Block reagent, within untreated MCL-5 cells. Isotype IgG 2_K utilised, homologous to the human anti-CD55 R-PE conjugate utilising within current in vitro PIG-A mutation analysis binding (~10,000 defined single cellular events were assessed).

Sample Identification	Total Number of Recorded Events	Number of Events Defined "Single Cell"	Percentage "Single Cell" Events of Total Events	Number of Events Defined CD55 Positive	Percentage CD55 Positive of "Single Cell" Events
Fc Block -ve 1	20246.000	9681.000	47.817	1.000	0.010
Fc Block -ve 2	65881.000	31414.000	47.683	4.000	0.013
Fc Block -ve 3	41210.000	20130.000	48.847	1.000	0.005
Average Fc Block -ve	42445.667	20408.333	48.116	2.000	0.009
Fc Block +ve 1	24099.000	10192.000	42.292	1.000	0.010
Fc Block +ve 2	19883.000	10146.000	51.029	0.000	0.000
Fc Block +ve 1	21125.000	10211.000	48.336	0.000	0.000
Average Fc Block +ve	21702.333	10183.000	47.219	0.333	0.003

In order to maintain accuracy within the in vitro *PIG-A* mutant assessment method, following the relative successful trial data for the novel refined gating system, antibody specificity, potential gating bias and further investigations into the morphological alterations observed during apoptosis were explored. Even though all antibodies utilised were monoclonal in nature, antibodies are able to bind unspecifically through Fc mediated interactions (Appendix Section 5.5.3.1), especially prominent within leukocytes [64].

The specificity assessment data (Appendix Table 5.5.1) showed that the average percentage of MCL-5 single cellular events shown to bind to the isotype control antibody was 0.009%, samples size exceeded 10,000 single cellular events. The unspecific binding efficiency, a result of Fc mediated interactions, was subsequently estimated at 0.006%; following the acquisition of the Fc block regent data (0.003% resultant antibody binding). The additional 0.003% of isotype control binding, in the presence of Fc block regent, was defined to not be the result of Fc region mediated interactions and was subsequently a result of an alternative unspecific mechanism.

The results generated were comparable to the analogous CD59 R-PE conjugate antibody data (Section 3.3.1); however, the CD55 antibody was shown to be the most specific in terms of Fc mediated interactions and generated the most optimum results.

5.5.3.2 Dose Finding Study, EMS and MNU Exposure

In order to assess the MCL-5 cell line's ability to be incorporated into the in vitro *PIG-A* assay design, initially a dose finding assessment was carried out to estimate an approximate LD_{50} value to be utilised as a descriptor for cytotoxicity within subsequent assessment. The LD_{50} or lethal dose 50 is the estimated dose in which cytotoxity is observed to reach 50% of the total population assessed; at the equivalent dose and above; any observed genotoxic results cannot be accurately distinguished from cytotoxity induced effects. Ethyl methane sulfonate (EMS) and n-methyl-n-nitrosourea (MNU) were selected as the initial chemicals to investigate due to their highly potent mutagenic characteristics, abundance of published literature and well defined mutation spectra, able to be utilised in forthcoming validatory sequencing analysis.

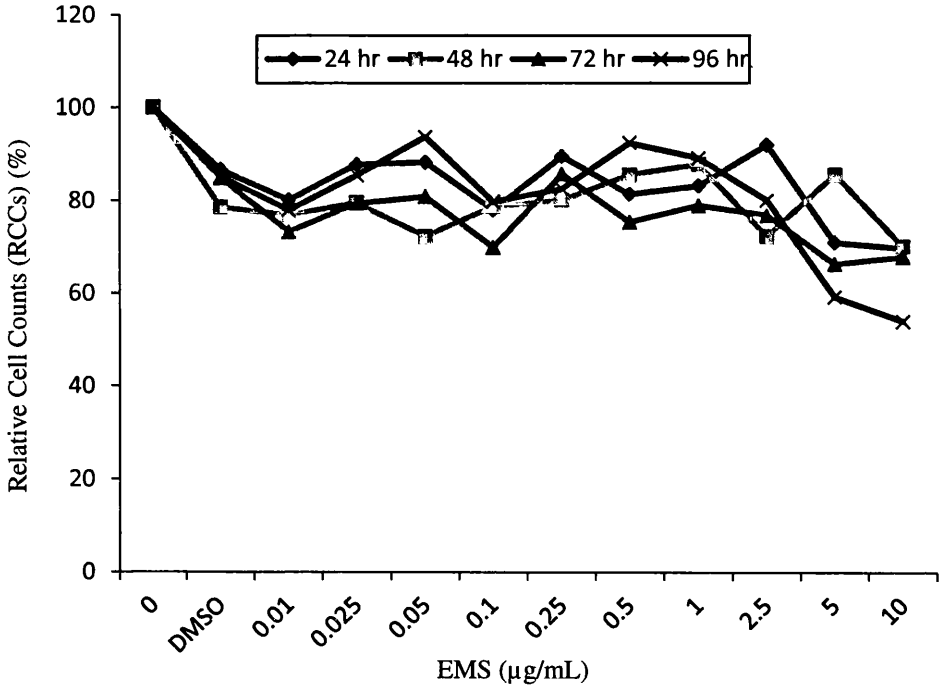

Figure 5.5.1.A - Relative Cell Counts (RCC) for MCL-5 cell cultures, following 24 hr acute EMS treatment (N=1).

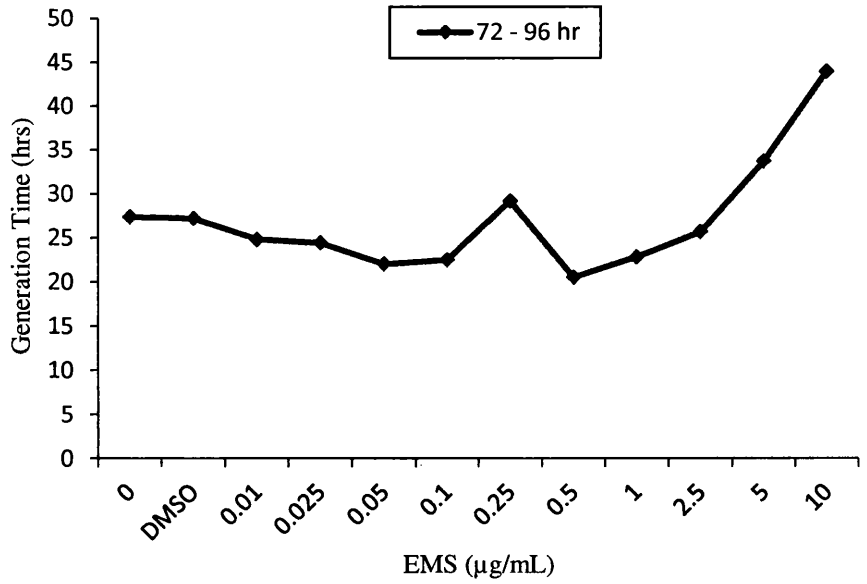

Figure 5.5.1.B Estimated Generation Time for MCL-5 cell cultures, following 24 hr acute EMS treatment (N=1).

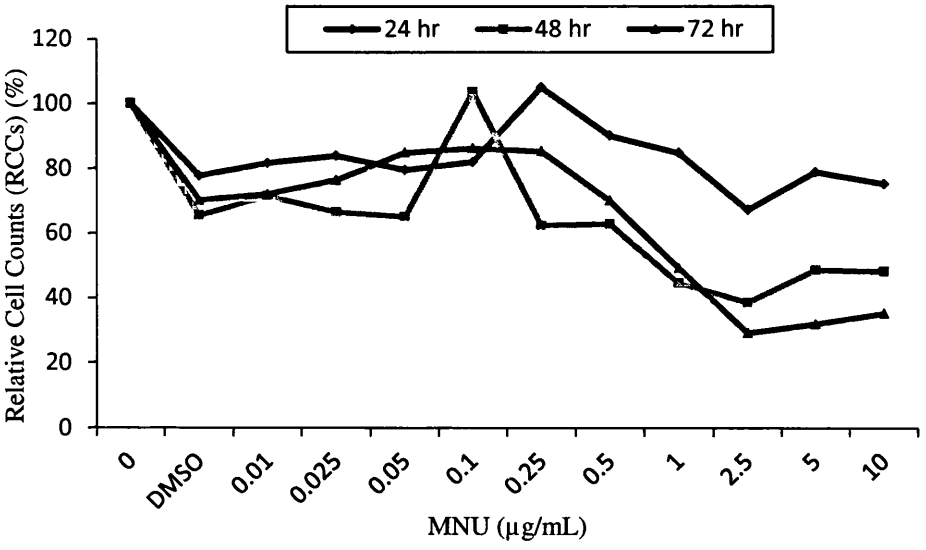

Figure 5.5.2.A - Relative Cell Counts (RCC) for MCL-5 cell cultures, following 24 hr acute MNU treatment (N=1).

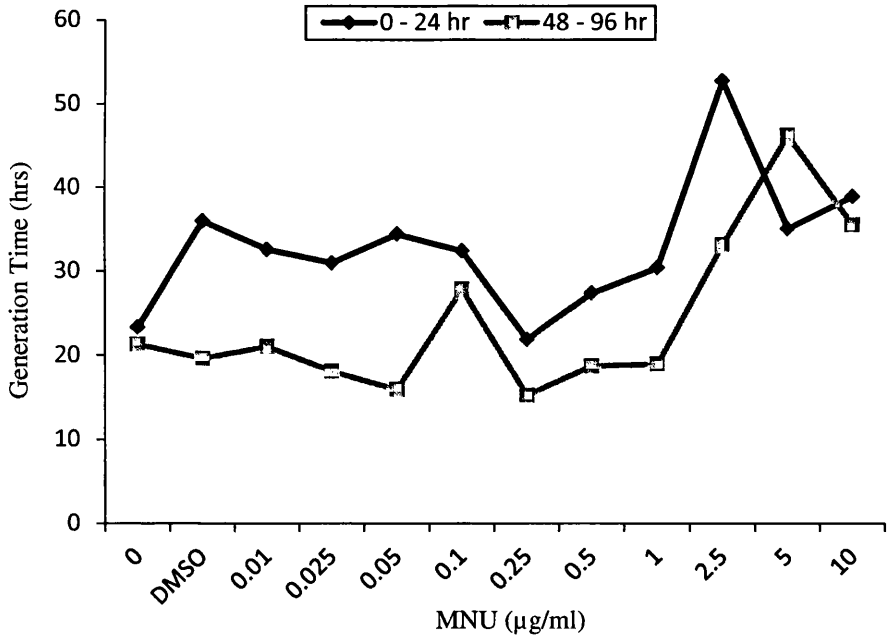

Figure 5.5.2.B - Estimated Generation Time for MCL-5 cell cultures, following 24 hr acute MNU treatment (N=1).

The results following the 24 hr acute EMS, within MCL-5 cells, appear to demonstrate that little or no measurable variation in growth occurred within the first 24 hr post mutagenic exposure. The cell cultures continued to show no obvious signs of growth until 24-48 hr post treatment, however allowing the full 1.5-2 cell cycles of recovery showed the desired toxic effects post recovery and generated an apparent dose dependent increase in cytotoxicity; as the dose increases, there is a corresponding increase in cytotoxity which results in the RCC values decreases across the dose range. This relationship is more apparent on the fourth day of the experiment (96 hr) in which the top two doses of 5 and 10 µg/mL induce a 41 and 46.3% decrease in RCC values when compared to the con-current negative controls (Appendix Figure 5.5.1.A). The relationship is less clear on prior experimental days (0-72 hr) in which minor discrepancies can be observed throughout the dose range without any substantial decreases in RCC values being observed. The estimated generation time was shown to mimic the correlation as defined by the RCC data, and a noteworthy increase in the generation time was observed to steady increase in a

linear manner for doses greater than 2.5 µg/mL (Appendix Figure 5.5.1.B). Untreated, established MCL-5 cell cultures, generally take approximately 22-24 hr to divide successfully [61, 87], this value is in accordance within the generation time data acquired. The estimated LD_{50} value for acute EMS exposure, within MCL-5 cells, was able to be defined as marginally higher than 10 µg/mL, a comparable metric when compared to the previously utilised TK6 cells (Section 5.3.1).

The results following acute MNU exposure showed a similar relationship with regards to increase in cytotoxity at the top doses when compared to the previous EMS exposure, however, the data does appear to show minimal lag following mutagenic exposure, prior to cellular growth. Following the completion of the initial 24 hr recovery period immediately following dosing, an additional single cell cycle was adequate in order to assess dose dependent cytotoxicity; both 48 and 72 h data demonstrated a dose dependent increase in cytotoxicity. RCC values were observed to approximately fall to 50% at the 1 µg/mL dose, further decreases in cellular viability were apparent at the three addition higher doses (Appendix Figure 5.5.2.A). Doses greater than and including 1 µg/mL elicited significant cytotoxicity affects onto the treated MCL-5 cultures and resulted in a maximal 72% decrease in cellular viability, when compared to the concurrent controls, at the 72 hr - 2.5 µg/mL dose. The LD_{50} value can be estimated in the region of 1 µg/mL for MNU within MCL-5 cultures and therefore, can be used as the top dose for future routine screening.

5.5.3.3 Preliminary Investigations into Cell Cycle and GPI-AP Expression Correlation

5.5.3.3.1 Amnis Image Stream™ Investigation

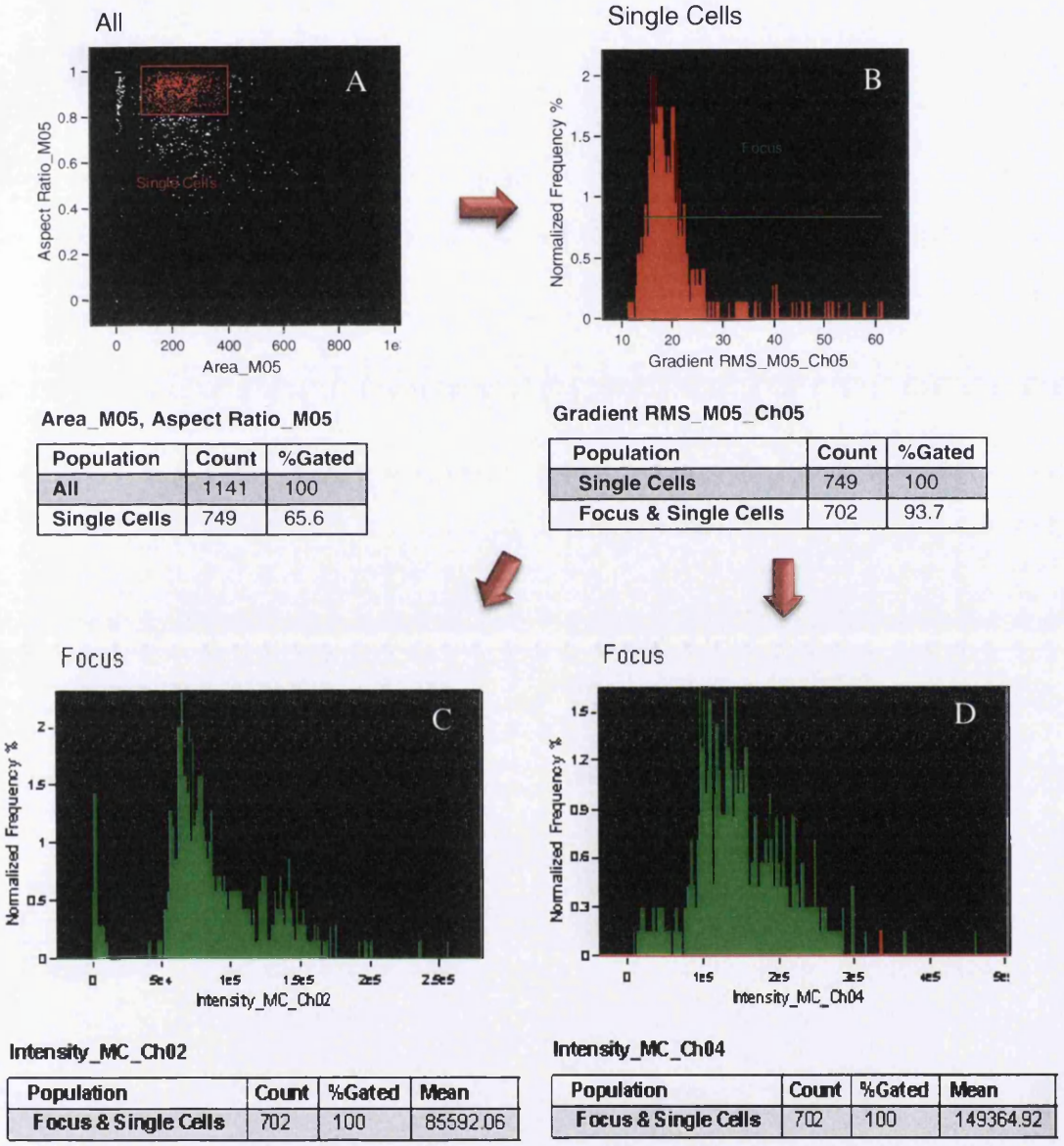

Area_M05, Aspect Ratio_M05

Population	Count	%Gated
All	1141	100
Single Cells	749	65.6

Gradient RMS_M05_Ch05

Population	Count	%Gated
Single Cells	749	100
Focus & Single Cells	702	93.7

Intensity_MC_Ch02

Population	Count	%Gated	Mean
Focus & Single Cells	702	100	85592.06

Intensity_MC_Ch04

Population	Count	%Gated	Mean
Focus & Single Cells	702	100	149364.92

Figure 5.5.3. Preliminary Cell Cycle and GPI-AP expression correlation analysis within untreated 4% PFA fixed MCL-5 cells, stained with Hoechst 33342 and anti-CD55/59 R-PE antibodies. A) Aspect ratio defined single cell gate, B) Focal smear gate, C) relative fluorescence intensity for the nucleic acid stain and D) relative fluorescence intensity of the GPI-AP markers (~1,000 Events Captured).

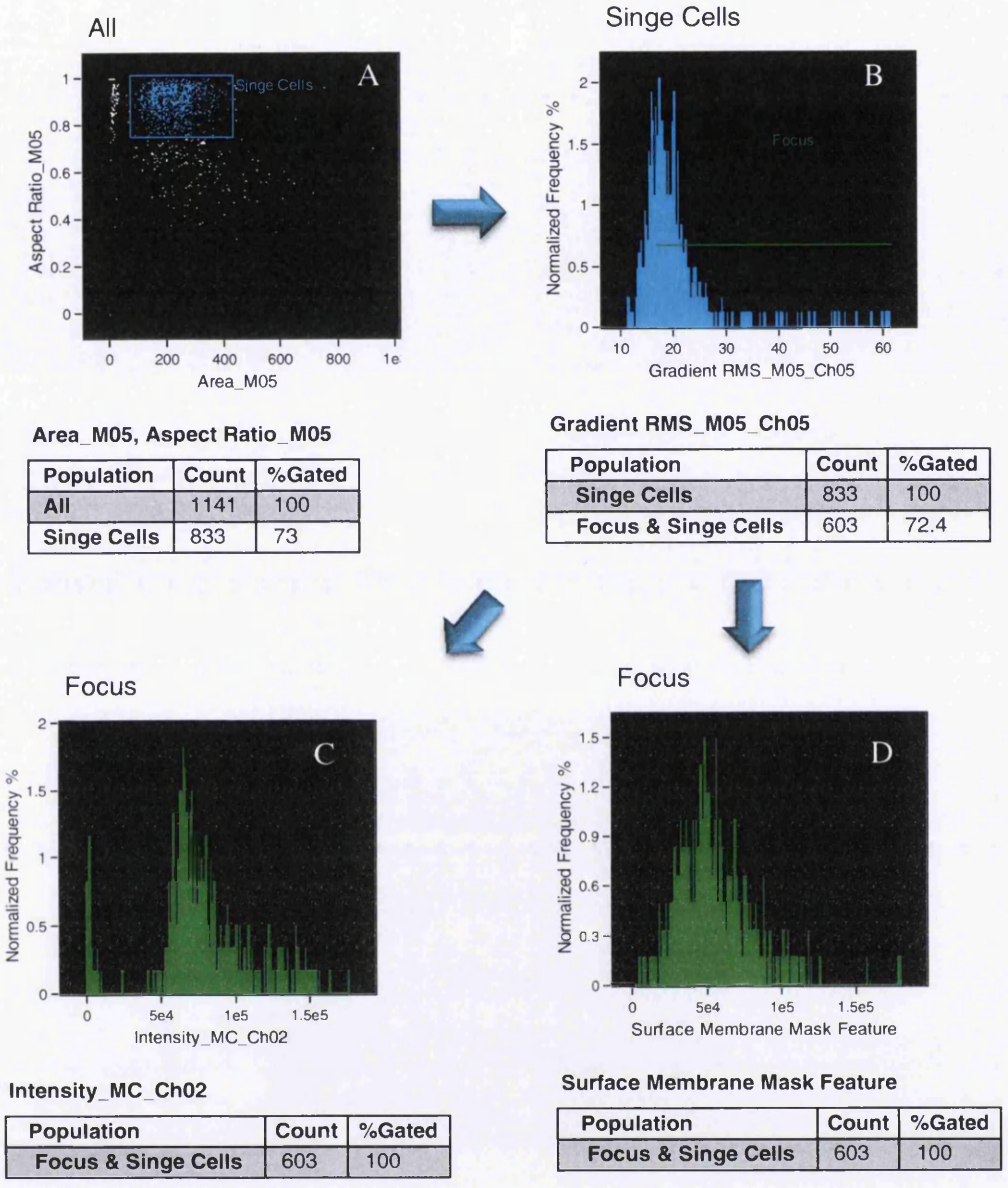

Area_M05, Aspect Ratio_M05

Population	Count	%Gated
All	1141	100
Singe Cells	833	73

Gradient RMS_M05_Ch05

Population	Count	%Gated
Singe Cells	833	100
Focus & Singe Cells	603	72.4

Intensity_MC_Ch02

Population	Count	%Gated
Focus & Singe Cells	603	100

Surface Membrane Mask Feature

Population	Count	%Gated
Focus & Singe Cells	603	100

Figure 5.5.4. Preliminary Cell Cycle and GPI-AP expression correlation analysis within untreated 4% PFA fixed MCL-5 cells, stained with Hoechst 33342 and anti-CD55/59 R-PE antibodies and implemented mask feature to prevent spectral overlap. A) Aspect ratio defined single cell gate, B) Focal smear gate, C) relative fluorescence intensity for the nucleic acid stain and D) relative fluorescence intensity of the GPI-AP markers (~1,000 Events Captured)

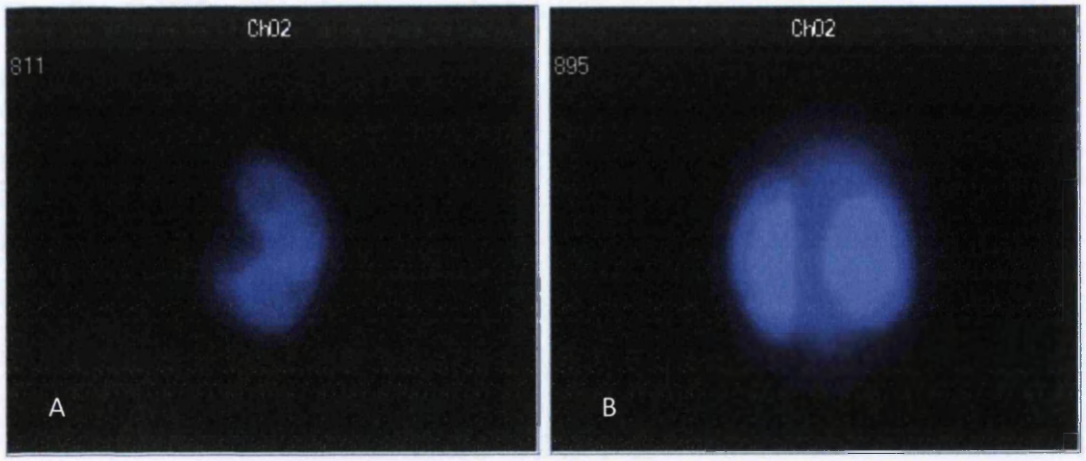

Figure 5.5.5. Bi-nucleate images derived from a selected bin within the estimated G2/M population within untreated 4% PFA fixed MCL-5 cells, stained with Hoechst 33342 and anti-CD55/59 R-PE antibodies. A) Bi-nucleate derived independently of the mask feature and B) Bi-nucleate derived within the mask feature, compensating for potential spectral overlap of the nucleic acid dye (~1,000 Events Captured)

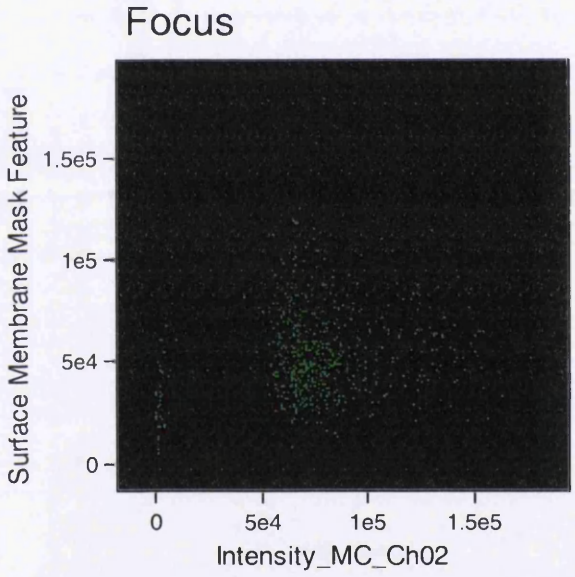

Intensity_MC_Ch02, Surface Membrane Mask Feature

Population	Count	%Gated
Focus & Singe Cells	603	100

Figure 5.5.6. Preliminary estimation at the relative GPI-AP marker fluorescence with respect to the nucleic acid dye intensity; hence, the correlation between GPI-AP expression and cell cycle progression within untreated MCL-5 cells. Samples were RNase treated, fixed in 4% PFA and stained with Hoechst 33342 and tandem anti CD59/55 RPE antibodies (<1,000 events captured).

In order to evaluate the possible relationship between GPI-AP expression and nucleic acid quantity, immediately following cytokinesis a potential time period in which surface antigen expression is reduced when compared to a more established cell, the Image Stream™ platform in conjunction with Hoechst 33342 and anti-CD55/59 R-PE tandem exposure was utilised. Initially, cells were visualised and characterised through their relative aspect ratio and particle size, and non-focussed events were excluded from data analysis due to their potential effect on subsequent interpretation.

At first, in the absence of any retrospective masking or features applied, the single cell population with the stained MCL-5 population, were demonstrated to exhibit a typically normal cell cycle profile; the majority of cells within the population having nucleic acid dye content analogous to G0/G1 phase, the minor population had significantly larger quantities of DNA and therefore, were labelled as cells post DNA replication i.e. G2/M (Appendix Figure 5.5.3). Cells binned within the G2/M phase were visually inspected for their nucleic acid dye content, and the resultant images were clearly bi-nucleate in nature with distinctive hemispheres of content (Appendix Figure 5.5.5.A).

The corresponding GPI-AP data demonstrated a typical Gaussian like distribution; with the inclusion of outlier events and an apparent visual skew (Appendix Figure 5.5.3). DNA content, i.e. cell cycle progression was shown to apparently not be correlated to GPI-AP expression, as the resultant graphical interpretation of the data was not clearly linear in nature and displayed limited evidence for any positive correlation (Appendix Figure 5.5.6).

The identical data set was retrospectively assessed utilising an applied mask and feature, in which potential spectral overlap was compensated for by the inclusion of a nuclear acid dye mask within the extra-cellular surface space. The masked data demonstrated analogous results to the previously reported data, there was a highly similar DNA content profile for the cellular population (Appendix Figure 5.5.4), a typical GPI-AP expression and no clear correlation between GPI-AP expression and relative DNA content; the gating system was again evaluated by the binning of selected specific DNA content events and visually inspected to ensure concordance. The only potential difference in the two distinctly different analysis methods was the

clarity of DNA nuclear content, visually within the selected binned images, the mask feature appeared to slightly increase focus (Appendix Figure 5.5.5.B), when directly comparing images

5.5.3.3.2 BD FACS Aria 1 Investigation

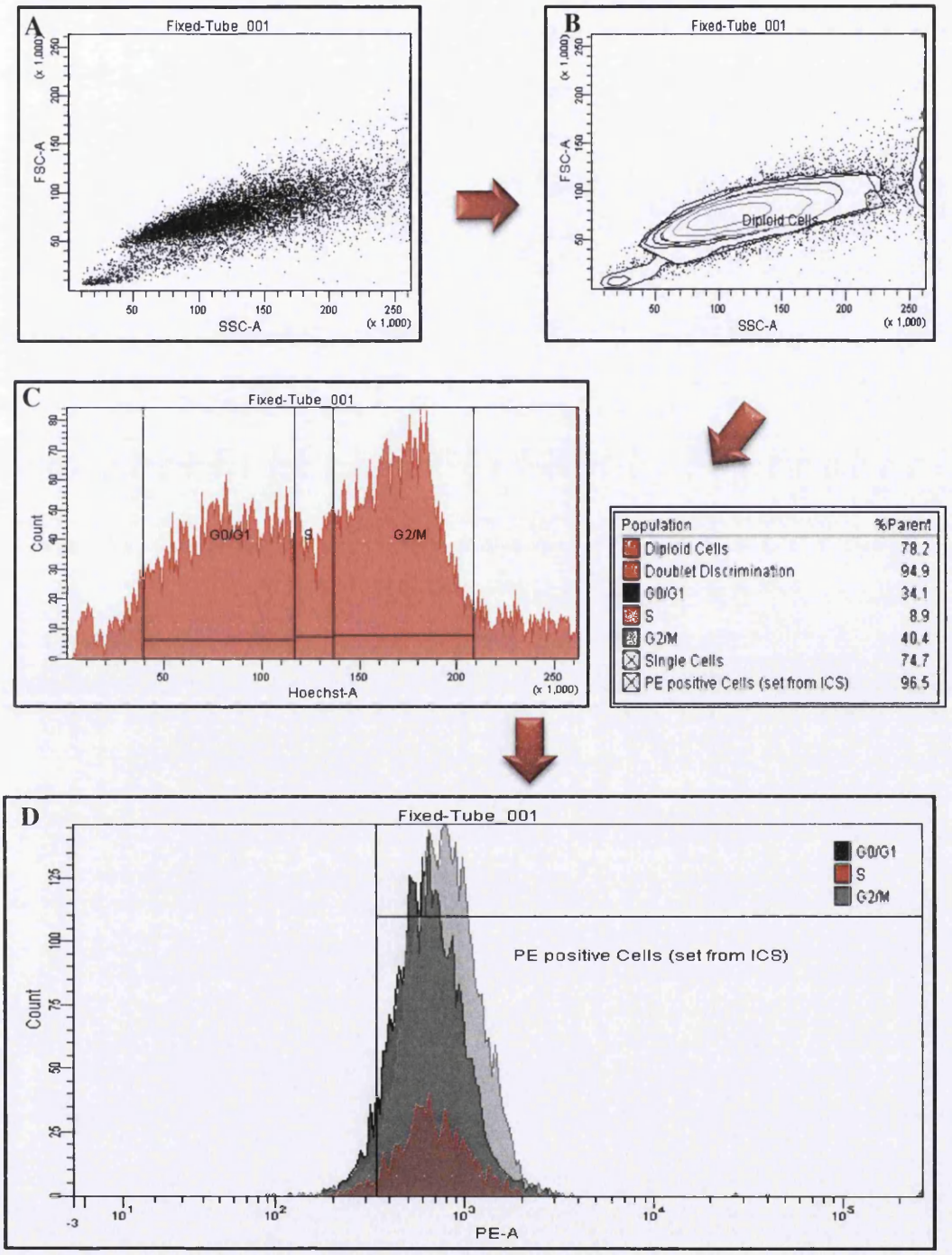

Figure 5.5.7. Cell cycle and GPI-AP correlation re-evaluation utilising the BD FACS aria Platform within untreated MCL-5 cells. Cells were un-treated, fixed in 4% PFA and stained with Hoechst 33342 nucleic acid dye in conjunction with tandem anti-CD55/59 R-PE antibodies; A) FSC-A vs SSC-A scatter plot, B) Doublet Discriminant gate, C) Cell cycle analysis and D) GPI-AP expression, correlated to Cell cycle progression (>12,000 events scored, ~10,000 single cell events scored analysed).

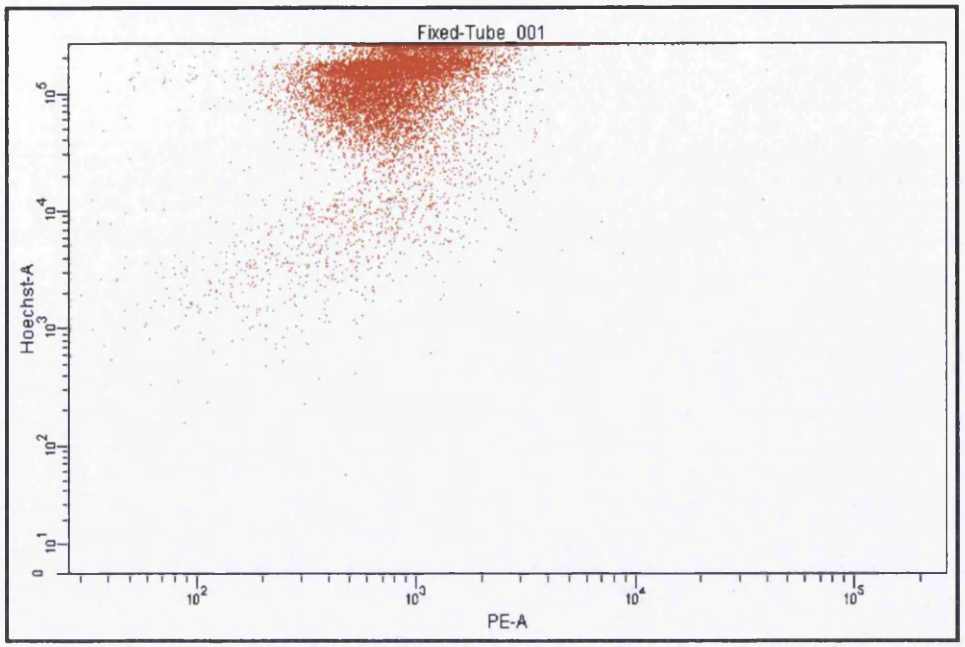

Figure 5.5.8. Cell cycle and GPI-AP correlation assessment utilising the BD FACS aria Platform within untreated MCL-5 cells. Cells were un-treated, fixed in 4% PFA and stained with Hoechst 33342 nucleic acid dye in conjunction with tandem anti-CD55/59 R-PE antibodies (>12,000 events scored, ~10,000 single cell events scored analysed).

To provide additional weight of evidence for no significant correlation between GPI-AP expression and relative nucleic acid content, flow cytometry was implemented in conjunction with Hoechst 33342 and tandem CD55/59 R-PE staining. Initially, cells were assessed for their respective light scatter profiles and a crude single cell population was defined, this in turn was further refined by the inclusion of doublet discrimination (Appendix Figure 5.5.7 B).

The single cell population, were demonstrated to exhibit a cell cycle profile consistent with an increase in the latter G2/M phase and a subsequent minor population presence within the earlier stages of the cell cycle; the majority of cells within the population having a relatively high nucleic acid dye content analogous to G2/M phase, a phenotype consistent with direct pre-division (Appendix Figure 5.5.7.C). The corresponding GPI-AP data demonstrated a typical Gaussian like distribution, with the inclusion of outlier events and no apparent visual skew.

DNA content, i.e. cell cycle progression was again demonstrated to not be significantly correlated to GPI-AP expression, as the resultant graphical interpretation of the data only demonstrated minor evidence for a minimal increase in average florescence emission for cells within G2/M when compared to early stages of the cell cycle (Appendix Figure 5.5.7.D). This relationship was investigated further via the addition of a supplementary figure describing the direct relationship between GPI-AP expression and nucleic acid content (Appendix Figure 5.5.8); again no direct relationship was distinctly apparent, with minor evidence for a positive correlation.

5.5.3.4 Preliminary Intracellular *PIG-A* Investigation

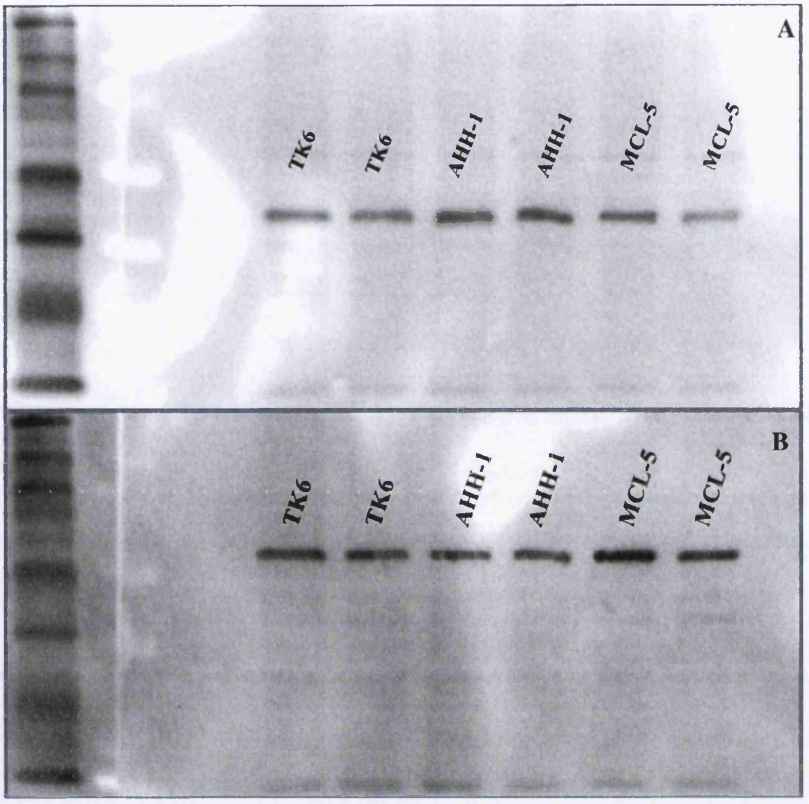

Figure 5.5.9. Discreet proteins bands following secondary-HRP conjugated antibody probing, within total protein extracted from human lymphoblastoid cell lines, and visualised following UV exposure; A) anti-B-actin primary antibody and B) anti-*PIG-A* primary antibody (Abcam). 20 µg of total protein loaded into each well along in conjunction with the use of known molecular weight precision plus protein standard.

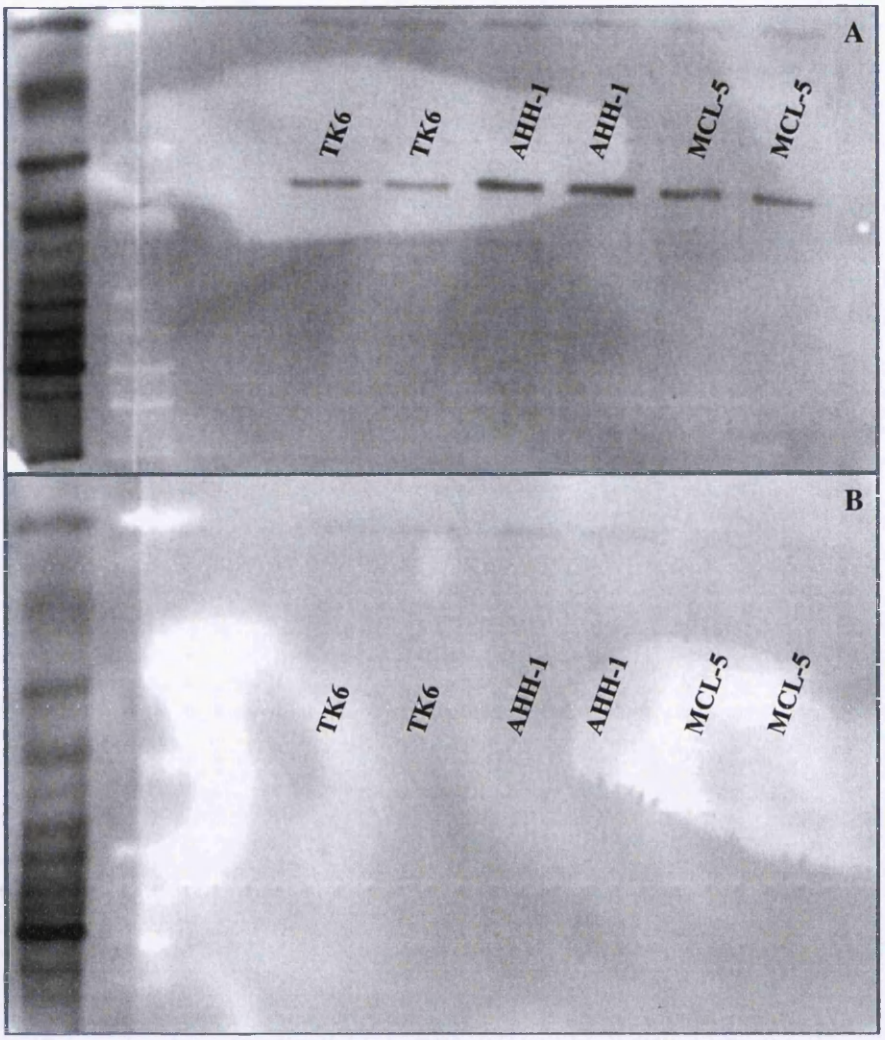

Figure 5.5.10. Discreet proteins bands following secondary-HRP conjugated antibody probing, within total protein extracted from human lymphoblastoid cell lines, and visualised following UV exposure; A) anti-B-actin primary antibody and B) anti-PIG-A primary antibody (Sigma Aldrich). 20 µg of total protein loaded into each well along in conjunction with the use of known molecular weight precision plus protein standard.

Table 5.5.2 - Summary of intracellular PIG-A data following Fix and Perm® treated MCL-5 lymphoblastoid cells, exposed to anti-PIG-A (Abcam) primary and corresponding anti-rabbit R-PE secondary antibody treatment (~10,000 events flow cytometry analysed for intracellular R-PE conjugate signal).

Sample Identification	Total Number of Events	Number of Single Cell Events	Percentage Single Cell of Total Population	Number of Single Cell Events which stain Positive for *PIG-A* (Conservative)	Percentage *PIG-A* Positive of Single Cell Events	Number of Single Cell Events which stain Positive for *PIG-A* (Inclusive)	Percentage *PIG-A* Positive of Single Cell Events
ICS	14038	10746	76.5	1	0.009305788	-	-
30 min P, 1 hr S - A	15585	10344	66.4	43	0.415699923	-	-
30 min P, 1 hr S - B	15974	10604	66.4	53	0.499811392	-	-
30 min P, 1 hr S - C	15516	10276	66.2	60	0.58388478	-	-
Average	15691.67	10408	66.33	52	0.499798698	-	-
ICS	14284	10831	75.8	3	0.027698273	-	-
12 hr P, 1 hr S - A	14298	10397	72.7	35	0.336635568	-	-
12 hr P, 1 hr S - B	14740	10603	71.9	60	0.565877582	-	-
12 hr P, 1 hr S - C	14682	10700	72.9	65	0.607476636	-	-
Average	14573.33	10566.67	72.5	53.33	0.503329928	-	-
ICS	15446	10417	67.4	1	0.009599693		0
12 hr P, 72 hr S - A	15769	10430	66.1	5891	56.48130393	10208	97.87152445
12 hr P, 72 hr S - B	15303	10247	67	7295	71.19156826	10025	97.83351225
12 hr P, 72 hr S - C	15097	10334	68.5	7265	70.30191601	10104	97.77433714
Average	15389.67	10337	67.2	6817	65.99159607	10112.33333	97.82645795

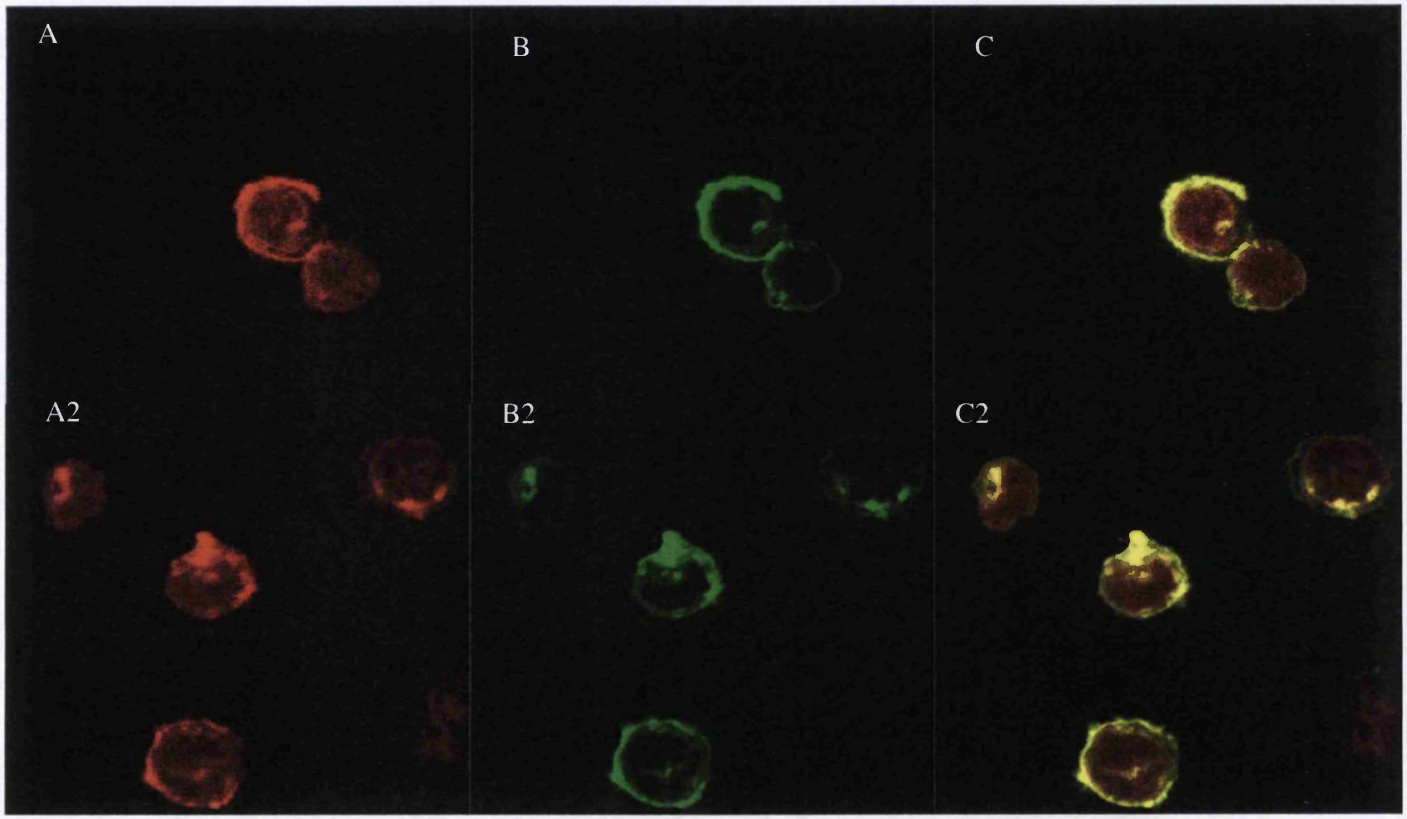

Figure 5.5.11 - Intracellular PIG-A data following Fix and Perm® treated MCL-5 lymphoblastoid cells, exposed to anti-PIG-A (Abcam) primary and corresponding anti-rabbit R-PE secondary antibody treatment; with retrospective Phalloidin (596 nm) staining, captured on the x 63 oil immersion objective using laser confocal imaging. 1) Single stained Phalloidin control sample, 2) Multi-stained Phalloidin and anti-PIG-A experimental sample; A) anti-PIG-A intracellular signal (Red), B) Phalloidin Signal (Green) and C) Composite image, dual signal (Yellow)

Figure 5.5.12 - Intracellular IHC staining and sequential fluorescence microscopy imaging of extended 100% methanol fixed MCL-5 cells; exposed to anti-histone H3 primary and corresponding anti-rabbit R-PE secondary antibody treatment (Green), with retrospective Phalloidin (596 nm) (Red) and DAPI nuclear staining (Blue), captured on the x 63 oil emersion objective. A) Channel 1 (Phalloidin), B) Channel 2 (Histone H3), C) Channel 3 (DAPI) and D) Composite Image.

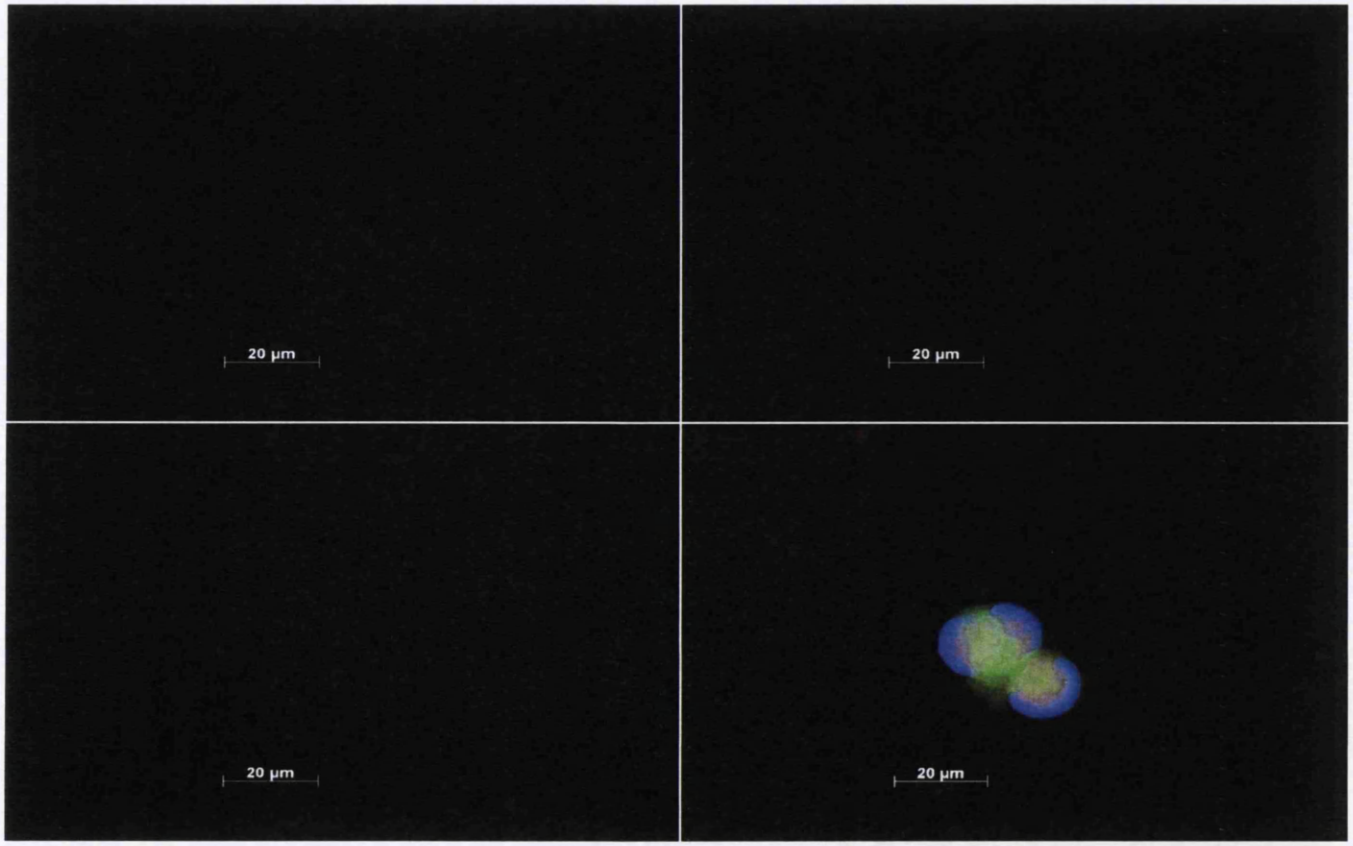

Figure 5.5.13 - Intracellular IHC staining and sequential fluorescence microscopy imaging of extended 100% methanol fixed MCL-5 cells; exposed to anti-PIG-A primary and corresponding anti-rabbit R-PE secondary antibody treatment (Green), with retrospective Phalloidin (596 nm) (Red) and DAPI nuclear staining (Blue), captured on the x 63 oil emersion objective. A) Channel 1 (Phalloidin), B) Channel 2 (PIG-A), C) Channel 3 (DAPI) and D) Composite Image.

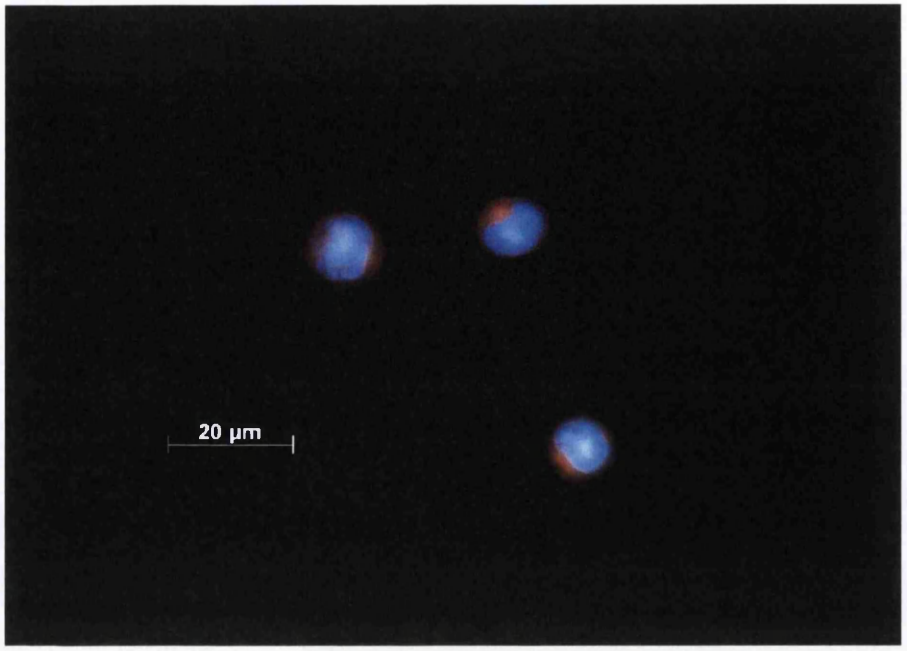

Figure 5.5.14 - Intracellular IHC staining and sequential fluorescent microscopy imaging of minimal 100% methanol fixed MCL-5 cells; Isotype Control - exposed to no primary antibody, anti-rabbit R-PE secondary antibody treatment (Green), with retrospective Phalloidin (596 nm) (Red) and DAPI nuclear staining (Blue), captured on the x 63 oil immersion objective

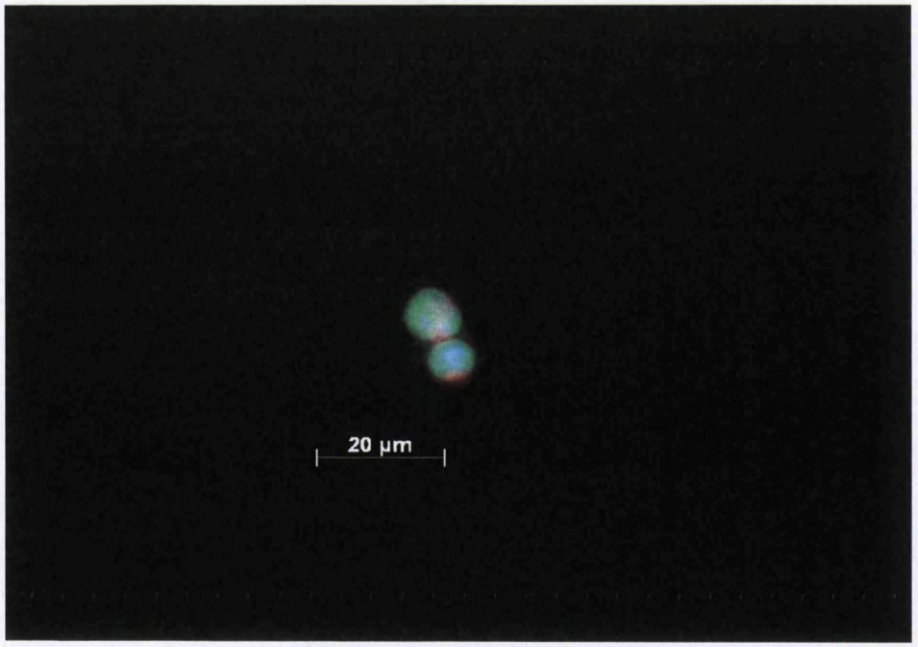

Figure 5.5.15 - Intracellular IHC staining and sequential fluorescent microscopy imaging of minimal 100% methanol fixed MCL-5 cells; exposed to anti Histone-H3 primary and corresponding anti-rabbit R-PE secondary antibody treatment (Green), with retrospective Phalloidin (596 nm) (Red) and DAPI nuclear staining (Blue), captured on the x 63 oil immersion objective

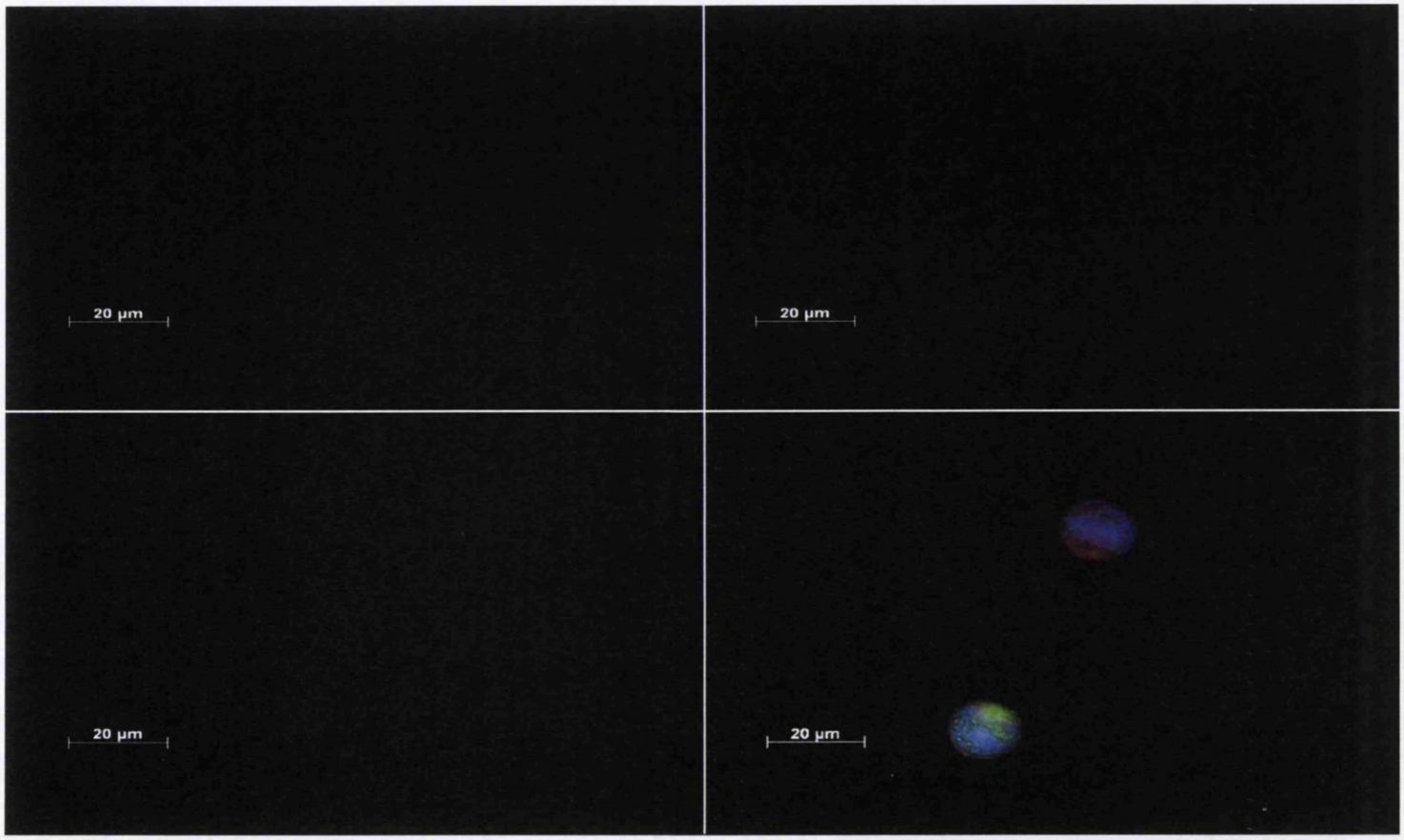

Figure 5.5.16 - Intracellular IHC staining and sequential fluorescence microscopy imaging of minimal 100% methanol fixed MCL-5 cells; exposed to anti-PIG-A primary and corresponding anti-rabbit R-PE secondary antibody treatment (Green), with retrospective Phalloidin (596 nm) (Red) and DAPI nuclear staining (Blue), captured on the x 63 oil emersion objective. A) Channel 1 (Phalloidin), B) Channel 2 (PIG-A), C) Channel 3 (DAPI) and D) Composite Image.

Following the initial failure of the high throughput flow cytometry assessment of the intracellular in vitro *PIG-A* background frequency (data not shown), initially western blott analysis was implemented to assessed the efficacy of the purchased novel anti PIG-A primary antibodies. The abcam purchased anti-PIG-A primary antibody was shown to generate distinct comprehensive protein bands for both the house keeper (B-actin) and the anti-PIG-A primary following 20 µg total protein extraction within the MCL-5 cell line; the distinct dense protein bands were approximately 40 and 50 KDa in size respectively (Appendix Figure 5.5.9). The sigma antibody, which was previously utilised for the background frequency assessment, demonstrated a clear protein band for the housekeeper (b-actin) at approximately 40 KDa; no visible bands were detected when exposed to the anti-PIG-A primary (Appendix Figure 5.5.10). The identical raw protein fraction was utilised in both cases to allow a directly comparable assessment to be undertaken.

Following selection of the abcam manufactured primary antibody, in combination with the pre-purchased Fix and Perm ™ (Life Technologies ™, Hertfordshire, UK), a second assessment of the potential intracellular PIG-A background mutant frequency likely to be observed within MCL-5 cells was undertaken by flow cytometry acquisition and subsequent analysis. The data demonstrated highly limited evidence for any significant PIG-A protein presence within the MCL-5 parental population when utilising both the 30 min room temperature and 12 hr cold room primary incubations, both in combination with corresponding 1 hr room temperature secondary exposure; irrespective of gating strategy utilised, maximum PIG-A protein presence was recorded as 0.4997 and 0.5033% respectively (Table 5.5.2). When utilising a highly extended IHC staining protocol, 12 hr primary (cold room) in conjunction with a 72 hr secondary (cold room) exposure, 65.9 and 97.83% of the parental MCL-5 population were demonstrated to express the PIG-A protein when utilising the conservative and highly inclusive gating strategies respectively (Table 5.5.2).

The extended IHC staining protocol sample was retrospectively stained with an additional cytoskeletal phalloidin (596 nm) dye and then assessed in tandem with a single stained phalloidin sample to assess the internalisation and origin of the PIG-A signal on the confocal microscope. The resultant data for the tandem stain sample displayed a significant presence of a phalloidin signal around the periphery of the

cell, with extensive staining apparent associated just under the extracellular membrane (Appendix Figure 5.5.11). In addition to this, the sample displayed a similar signal for the PIG-A antibody, with a distinct extracellular localisation, with some evidence for a more internalised presence. The single stained phalloidin sample was also analysed and displayed a highly similar staining profile in both PIG-A and phalloidin signal channels; a reduced analogous PIG-A staining signal was presence, in the absence of the PIG-A primary antibody within the staining protocol. The PIG-A stained sample was shown to have an increased signal strength, demonstrated by heat map analysis (data not shown) when compared to the unstained phalloidin control, with the additional signal strength being solely located to the extracellular surface of the antibody.

Methanol fixation was assessed for its ability to both fix and permeabilise the MCL-5 extracellular membrane to facilitate complete intracellular access for antibody binding applications. The extended methanol fixation protocol was assessed within two fluorescence microscope samples utilising different primary antibodies, one specific to histone H3 and one for PIG-A; subsequent data were collected and displayed within separate channel and composite images. The initial histone H3 sample displayed three apparently mono nucleated MCL-5 cells each comprising of a highly reduced cytoplasmic fraction volume, with some evidence to suggest of cellular membrane rapture and subsequent cytoplasmic projected into the surrounding area. The histone H3 signal was strong across all three cells and highly comprehensive across the entire DAPI stained nuclear area with no distinct localisation (Appendix Figure 5.5.12). The subsequent PIG-A stained specimen demonstrated two neighbouring MCL-5 cells, one mono-nucleated and the other apparently bi-nucleated in nature in terms of selective DAPI staining. Again the cells showed extensive cytoplasmic shrinkage, with the cytoskeletal marker barely protruding the nuclear boundaries. There was some evidence for a strong PIG-A signal presence within the intracellular region of the cells, no distinctive localisation of the stain (Appendix Figure 5.5.13).

The effects in terms of penetrance and cellular morphology of reducing the methanol fixation exposure was assessed within three subsequent samples, an isotype control, a histone H3 and PIG-A primary antibody specimen. Within the isotype control sample, three single mono-nucleated cells were detected, again displaying similar

cytoplasmic shrinkage, however, slightly less in terms of nuclear association when compared to the extended protocol. The DAPI staining resulted in distinctive nuclear boundary establishment, with a more granulated appearance, as expected with the leukocyte nature of the cell line; little evidence was present to infer a significant antibody signal within the captured images (Appendix Figure 5.5.14). The histone H3 specimen sample displayed two distinct mono-nucleate cells, with some evidence for a cytoplasmic fraction outside the clear nuclear membrane boundaries. The DAPI signal provided evidence for large intact nuclei with a corresponding comprehensive histone H3 signal present across the entire nuclear area, no data to suggest potential histone H3 presence within the cytoplasm (Appendix Figure 5.5.15). Finally, the PIG-A stained specimen demonstrated two mono-nucleated MCL-5 cells, with strong granular nuclei, as defined by DAPI staining, with a fair cytoplasmic fraction present. The PIG-A signal itself was strong and highly localised within definitive positions within the nucleus, with a more comprehensive less specific presence within the cytoplasm, inferring a strong intracellular presence (Appendix Figure 5.5.16).

5.5.4 Discussions and Conclusions

5.5.4.1 Antibody Specificity Assessment

Prior to the continued development of the in vitro *PIG-A* assay protocol, antibody specificity must be challenged again following the incorporation of novel tandem markers. Even though the antibody raised against the novel surface antigen (CD55) is the same isotype as the previously utilised anti-CD55 RPE (igG 2 K) it is critical that integrity of the assay design is maintained. As described previously, the MCL-5 cell line resides within the lymphoblastoid lineage and therefore, has a constitutively high expression of Fc receptors on the cell surface; their activity stimulates phagocytic or cytotoxic cells to destroy microbes, or infected cells by antibody-mediated phagocytosis [88, 89]. Due to this existence, there is a potential for un-specific Fc receptor mediated antibody binding indiscriminately to *PIG-A* mutant cells generating a false positive signal during flow cytometry analysis. The subsequent results of the experiment demonstrated that the isotype control (IgG k molecule lacking the variable region sensitive to the CD55/59 epitope) did not bind at any notable frequency to the surface within the chosen MCL-5 cell line (0.009%). Due to the accuracy involved in low dose quantitative screening, even an unspecific 0.009% binding frequency potentially contributes 90 falsely phenotypic wild type cells for every 1 million cells scored; this is especially protuberant when a statistically significant increase in mutant frequency can be an equivalent number of events. However, as this minimal error is carried through to all experimental samples, the conclusion is that primarily the antibody is operating under the correct specific mechanism to facilitate qualitative and potential future quantitative dose response modelling.

5.5.4.2 Dose Finding Study, EMS and MNU Exposure

Limitations and caveats associated with routine drug screening data are apparent within pharmaceutical drug testing, however, recognising such limitations and providing a comprehensive strength of evidence based approach to a decision, enables more accurate hazard and risk assessment. Within genetic toxicology screening, confidence within data interpretation is critical, and therefore, indistinguishability and additional sources of potential error must be standardised in order to enable accurate decision making. Cytotoxicity and genotoxicity even though distinctly different mechanisms resultant from potentially independent events, often share a number of common inducers, phenotypic alterations or morphological changes during progression. Due to this, when cytotoxicity is elevated within a sample, the end point assessment data can no longer be assumed to be as a direct consequence of solely genotoxicity derived mode of actions and therefore, the data consequentially loses strength. In order to maintain data integrity, protocols have undergone standardisation, in which test compounds are assessed up to a pre-determined dose resulting in a set level of cytotoxicity, in an effort to prevent ambiguity within the subsequent data [90, 91].

Following the selection of MCL-5 as the potential future platform for the in vitro *PIG-A* assay, prior to preliminary compound assessment, cytotoxicity screening was undertaken. For the purpose of assay protocol development, compounds are to be assessed up to the lethal dose 50 percent (LD_{50}), a dose in which 50% of cells undergo cell death as a result of exposure or treatment. As mentioned previously, subtle variation within highly similar cell lines can result in dramatically different dose response kinetics, and therefore, in order to make a well informed decision on a chosen screening platform, sufficient dose response data requires to be generated. Cell lines known for homozygous p53 functionality, such as TK6, are relatively sensitive to chemical exposure, not overly sensitive, readily undergo apoptosis and have unique characterised recovery periods post exposure [92]. MCL-5 cells, even though are highly similar to TK6, have a less well defined TP53 genotype and therefore, are potentially more sensitive, exhibit delayed apoptosis and increasingly prone to acquire genotoxic damage [52, 93, 94]. The MCL-5 population currently

utilised have been experimentally demonstrated to undergo apoptosis, through PS inversions, and therefore, appear to have some basal level of p53 functionality (Section 5.3.4.2).

MCL-5 cells were shown to take on average 22-26 hr to divide, and therefore, would require a longer recovery period to truly gauge the effects of the toxic treatment, when compared to similar AHH-1 or TK6 cell lines. Following acute EMS treatment the cell cultures displayed limited immediate growth, potentially reflecting the presence of the G1/S checkpoint following p21 induction [77], until 24-48 hr post treatment. However, incorporating the OECD advised, 1.5-2 cell cycles of recovery allowed the desired toxic effects to be apparent [95]. 94 hr post exposure, an apparent dose dependent increase in toxicity was observed; the RPD value for the top dose tested had dropped to approximately 50% (Appendix 5.5.3.2). MNU data were slightly different; the cells began to grow immediately following seeding and treatment, no obvious lag was observed. Allowing the full 1.5-2 cell cycles of recovery again showed the desired toxic effects and generated an obvious dose response (Appendix 5.5.3.2). LD_{50} values were estimated for both compounds, ~10 and 1 μg/mL respectively, to be utilised as the respective top doses tested within future assay design.

Some preliminary conclusions can be taken from the data; initially MCL-5 cells appear to have functional p53 due to the presence of a potential checkpoint arrest following genotoxin exposure, as well as observed physical signs of apoptosis. MNU a known more potent alkylating agent when compared to EMS resulted in more severe cytotoxity, in line with published data, providing additional authentication to the data sets [55].

5.5.4.3 Preliminary Investigations into Cell Cycle and GPI-AP Expression Correlation

Due to the limitations in intracellular area imposed on the cell via a fixed maximum expansion of the cellular surface membrane, all cells must undergo cleavage to enable continued metabolic activity, at a relatively fixed rate [96, 97]. Therefore, cells are continuously progressing through the cell cycle, resulting in cytokinesis and cellular division creating two identical daughter cells; this process facilitates the direct replacement of dead, dying or damaged cells [80]. The cell cycle is a higher regulation of cellular progression and function, which can be exploited by homeostatic mechanisms to prevent excessive uncontrolled growth; p53 mediated checkpoint arrest, DNA damage repair or induced apoptosis [26, 77]. However, as often observed within many cancer cases, patient present novel mutations within critical genes controlling such vital stages within cellular progression. As a direct result of such mutations, uncontrollable increase in growth rate, elevated angiogenesis, to overcome hypoxia, and down regulation of know tumour suppressor genes are common; facilitating the cancer phenotype [77, 78, 98, 99]. The cell cycle may however, also play a potential biasing role within the constraints of the in vitro *PIG-A* gene mutation assay design, as an analysis biasing factor; especially within the image stream ™ platform.

Theoretically, when a cell progresses through the final stage of the cell cycle, and is for want of a better term, split into two genetically identical daughter cells, the precise details in terms of mRNA division and regulation as well as surface membrane morphology and topography is vague. Therefore, presumably, due to cytoplasmic cleavage through a vesicle mediated furrow [100], the mRNA as well as pre-existing protein levels are fundamentally divided, potentially somewhat unevenly, resulting in differential proteomic concentration, as well as surface profiling within the daughter cells. From a genetic point of view, this has little impact on the assay design; however, as the assay utilises an in-direct reporting mechanism, reliant upon protein expression, un-uniform or distribution within such a fundamental cellular process could induce bias within analysis. Especially prominent within CCD reliant imaging, un-even surface distribution as a result of mitosis would

heavily impact the scoring of positive or negative events, in regards to their GPI-AP surface protein expression.

Newly synthesis daughter cells therefore, are theoretically more likely to have underestimated GPI-AP presence and score as false negative events, during the immediate period following cytokinesis. Within this potential lag period newly synthesis cells are discriminated against in terms of analysis, and the extent in which this potential bias prevails within latter stages of the cell cycle is unknown; presumably expansive intracellular metabolism will rapidly return a more normal extracellular phenotype. As well as this, this potential lag period could be cell line dependent; within erythrocytic cells the presence of GPI-AP expression is vital for cellular survival through complemented inhibition. However, within leukocyte cell lineages often GPI-AP expression is reduced and their respective function less critical in terms of cell survival [101], and therefore, theoretically could have a much more exaggerated lag period post cytokinesis.

Initially, the potential biasing effect of the cell cycle in terms of relative GPI-AP expression was assessed on the Image Stream ™ platform, and then further investigated on the BC FACS Aria flow cytometer. The Image Stream displayed the PFA fixed MCL-5 cells within a typical cell cycle distribution, in terms of DNA content, with the majority of the population appearing to be within the initial stages of the cell cycle (G0/G1/S) (Appendix 5.5.3.3). Due to the limitations associated with the lack of filter wheel presence; there was a significant chance of spectral overlap and hence, the DNA content signal being present within the respective GPI-AP signal channel. In order to counteract this, a complex mask and subsequent feature was established; in which the intracellular fluorescence signals were omitted from analysis during GPI-AP expression profiling, via the removal of the pixels containing a light emission with an intracellular origin. Both data sets were analysed and resulted in highly comparable outputs in terms of DNA content distribution and subsequent GPI-AP expression. When the data set were modelled for correlation between GPI-AP surface signal intensity against DNA content, the resultant data displayed limited evidence to suggest any potential positive correlation. DNA content appeared to be independent of GPI-AP expression.

In order to re-assess these preliminary finding, the BD FACS Aria was utilised to repeat this protocol and generate a comparable distribution within the same cell type. The subsequent generated data resulted in a DNA content distribution typical of a population with a potential G2/M checkpoint arrest; with the majority of cells being present within the latter stages of the cell cycle. This is common quite commonly observed within immortalised cell lines following compound exposure [102, 103], particularly common following p53 mediated genotoxin exposure [77]. However, additional external environmental stimuli may also account for such a distribution; cellular stress as a result of hypoxia, within the sealed preparative centrifuge tubes, can result in up regulation of HIF-1 and hence, contribute to G2/M arrest [104].

However, when the BD Aria data was assessed for positive correlation between DNA content as well as GPI-AP expression, or relative intensity, there again was little strong evidence to suggest such a relationship. Within this data one could say that there was some evidence to suggest that larger cells, in terms of surface area and DNA content, had higher relative GPI-AP signals; G2/M population data displayed GPI-AP fluorescence intensity greater than both G0/G1 and S phase phenotypic populations (Appendix 5.5.3.3). However, in the context of this assay platform, the variance observed was minimal and should not play any critical role in biasing subsequent analysis data.

The data within this section, displayed strong evidence to suggest that utilising multiple flow cytometric platforms, DNA content and GPI-AP expression profiling was both practical and achievable. The subsequent collected data, across both platforms, suggested that there was little evidence to confirm a strong positive correlation between GPI-AP expression and cellular DNA content. Therefore, smaller cells in terms of cellular surface area, as well as lower DNA content, did not appear to exhibit a significantly lower GPI-AP expression signal to any other cellular phenotype which could induce bias within the ensuing in vitro PIG-A analysis.

5.5.4.4 Preliminary Intracellular *PIG-A* Investigation

The unique characteristic of in-direct mutation reporting, as exploited by both the in vivo and in vitro *PIG-A* gene mutation assays, is a significant advantage as well as a point of contention. The simplicity of the reporting system lends itself well to the nature and robustness of erythrocytic cell lineages; however, it also is a major weakness for cell lineages with differential or sporadic GPI-AP expression and limited attachment [6, 11, 105, 106]. Some degree of ambiguity within the corresponding data analysis can be directly associated to the in-direct reporting system, as the likelihood of inaccurate reporting is potential; unless a number of mitigating factors have been implemented. If however, a high throughput analogous PIG-A mutation assay can be developed with a more direct reporter system, utilising the current conserved mechanism [12], there is a potential for extensive diverse tissue usage as well as interspecies expansion.

In brief, the current reporter system describes a phenotypic *PIG-A* negative event based on the statistically most prominent cause of the GPI-AP deficient phenotype; as the *PIG-A* gene is the only sex linked and hence hemizygous gene statistically it is the most common genotypic alteration resulting in the null phenotype. However, as mentioned previously, recently the human PNH condition has been observed within patients presenting an intact *PIG-A* gene, a double recessive mutations within the *PIG-T* alleles [107]. In addition to *PIG-T* there are upwards of 20 additional genes critically involved with the direct synthesis of the GPI-AP structure as well as the intracellular modification and transporting [106]. However, if a direct reporter system quantitatively measuring a sex linked gene product could be established within a commonly used tissue type and made accessible to high throughput scoring, the foundations of a potentially highly sensitive gene mutation assay are established [3, 4, 108, 109].

Initially, intracellular *PIG-A* reporting was investigated within MCL-5 cells; to enable a direct comparison if low dose modelling data were to be undertaken, with the ideology of mimicking the developed in vivo method, initially utilising primary haemopoetic cell lineages and then expanding the technique to comprise primary hepatic tissue. The initially collected data, data not shown, reported an extensive lack

of signal following untreated wild type intracellular *PIG-A* assessment, utilising the Fix and Perm® Life Technologies ™ kit. However, this was further investigated and attributed to a defective primary antibody; western blott analysis was utilised on total protein extracts to evaluate the specificity and efficacy of novel primary antibody binding. The resultant data demonstrated that the Sigma Aldrich antibody was unable to bind to the PIG-A protein presence within the extractions (Appendix Figure 5.5.10), whereas the independently obtained Abcam antibody displayed comprehensive binding within the extracted samples. The establishment of a generic immunohistochemical staining protocol comprised of a number of different primary and secondary incubations, under different conditions, was established to enable conceptual assay development. The standard, more typical IHC protocols utilising the analogous Fix and Perm® kit demonstrated minimal or absence of corresponding PIG-A protein signal within the parental populations (Appendix Table 5.5.2), however, the significantly elongated protocol resulted in comprehensive binding. When assessed for signal validity via confocal microscopy, the data was demonstrated to be as a result of unspecific binding, heavily associated to the extracellular surface of the cell membrane as well as spectral overlap from the phalloidin signal, utilised for cellular morphology visualisation purposes. An immediate conclusion of lack of cellular permeability was recognized, due to the successful nature of the analogous western blott data, and a more abrasive pemeabilising agent was investigated for use, when compared to the 2% formaldehyde and pemeabilising agent combination within the pre-purchased kit.

Methanol fixation was demonstrated to be a more comprehensive fixative and pemeabilising agent, not requiring the use of individual solutions. Precipitating (or denaturing) fixatives, such as methanol, act by reducing the solubility of protein molecules, through disruption of hydrophobic interactions and hence, compromising tertiary structure [62]. However, the fixation period when utilising 100% methanol is highly variable depending upon the tissue type, and as such the initial incubation must be assessed individually for chosen cell type. The extended methanol fixation protocol demonstrated extensive cell damage, with highly apparent morphological disruption of the typical cell phenotype (Appendix Figures 5.5.11 – 5.5.13). The cytoplasmic composition of the cell was highly reduced, with cytoplasmic shrinkage an obvious adverse effect of fixation, subsequently distinguishing between the

origins of the phalloidin cytoskeletal dye and the intracellular PIG-A signal was highly complex and potentially misleading. Therefore, utilising a reduced fixation, the resultant high resolution fluorescence microscopy images demonstrated an apparent intra-cellular PIG-A signal with stronger weight of evidence to suggest a more valid localisation and origin, following known location house keeper protein visualisation (histone H3).

The conclusion which can be taken from this initial work is that it does appear distinctly possible to undertake an intracellular PIG-A gene mutation assay, in potentially any primary tissue type, utilising methanol fixation and subsequent permeabilisation. However, the sensitivity of such a system is unknown, and therefore, flow cytometry based validatory assessment will be required to estimate the apparent background or pre-existing number of phenotypic *PIG-A* mutants prior to any low dose response modelling, this ideally supported by sequencing analysis. The use of a more direct reporting system could remove the ambiguity of the identity of presumptive phenotypic *PIG-A* mutant events within the sequential flow cytometry based analysis. However, the establishment of this generic protocol with the apparent successful IHC validation images puts forward a strong foundation for a high throughput assay development, with little need for high content screening; the current need for the addition of such specific morphological markers is due to the distinct impact morphological alterations can have on subsequent GPI-AP expression. Utilising a direct reporter system removes the potential for the additional genes involved in GPI-AP synthesis, protein shuttling and extracellular expression (*PIG* genes) genes to have a significant impact on reporting *PIG-A* phenotype.

6.2 Materials and Methods

6.2.3.3.2.2 The Possible Effect Anticoagulant has on Spontaneous *PIG-A* background Mutant Frequency

Blood was collected from a healthy control donor via a venous puncture into the median cubital vein. Venous blood was removed directly into a heparinised 5 ml vaccutainer as well as a 5ml EDTA coated vaccutainer. From the first vaccutainer, 5 mL of heparinised blood was transferred using a sterile 10 ml pipette onto a 10 mL mixture of histopaque ® 1077 as well as histopaque ® 1113 within a 15 ml Falcon tube. This was repeated from the second vaccutainer containing EDTA treated blood.

Both samples were centrifuged at 2000 RPM for 30 min at room temperature, plasma layer carefully removed and very precisely the layer of MNC (mononuclear Cells) isolated and transferred into fresh falcon tubes. As well as this, carefully the next layer of cells (100 µL suspected granulocytes and RETs) were also isolated and collected. Excess RPMI media/PBS 10 mL was added, centrifuged at 1600 RPM, at room temperature, for 10 mins.

Following centrifugation, very accurately the supernatant was removed, and the cell pellet re-suspended in RPMI media (0.5 mL) initially, and then continued to add excess until the tube was full (~10 mL). The samples were centrifuged, 1600 RPM 7-10 mins, supernatant aspirated. This wash step was repeated 2-3 times in order to remove any residual histopaque® from the solutions. Post washing, the cells were re-suspended in 0.5-1 mL of 1XPBS solution.

20 µL of anti-CD15 APC was added samples incubated in the dark, at room temperature, for 30 minutes (both WBC and suspected RET layer were stained for granulocyte presence). Following 15 min of the incubation, samples were treated with FLAER; a previously constructed aliquot of FLAER was removed from the cold room and allowed to warm to room temperature. 5µl of FLAER (1x stock as

made up previously) was added to the samples and allowed to incubate for a further 15 min at room temperature protect from light.

1 mL of VersaLyse solution (1X) was added and vortexed immediately (1 sec) and allowed to incubate for 10 min at room temperature, protected from light. Immediately following incubation, each sample was centrifuged, (150 x g for 5 min), supernatant aspirated and re-suspended in 3 mL of Wash buffer (0.2% BSA/PBS). The samples were centrifuged, re-suspended in 1 mL of Wash Buffer and treated with 5 µL of Propidium Iodide, and allowed to incubate for 5 min on ice, protected from light on ice, prior to acquisition on the flow cytometer.

6.3 Results

6.3.3.3.2.2 The Possible Effect Anticoagulant has on Spontaneous *PIG-A* background Mutant Frequency

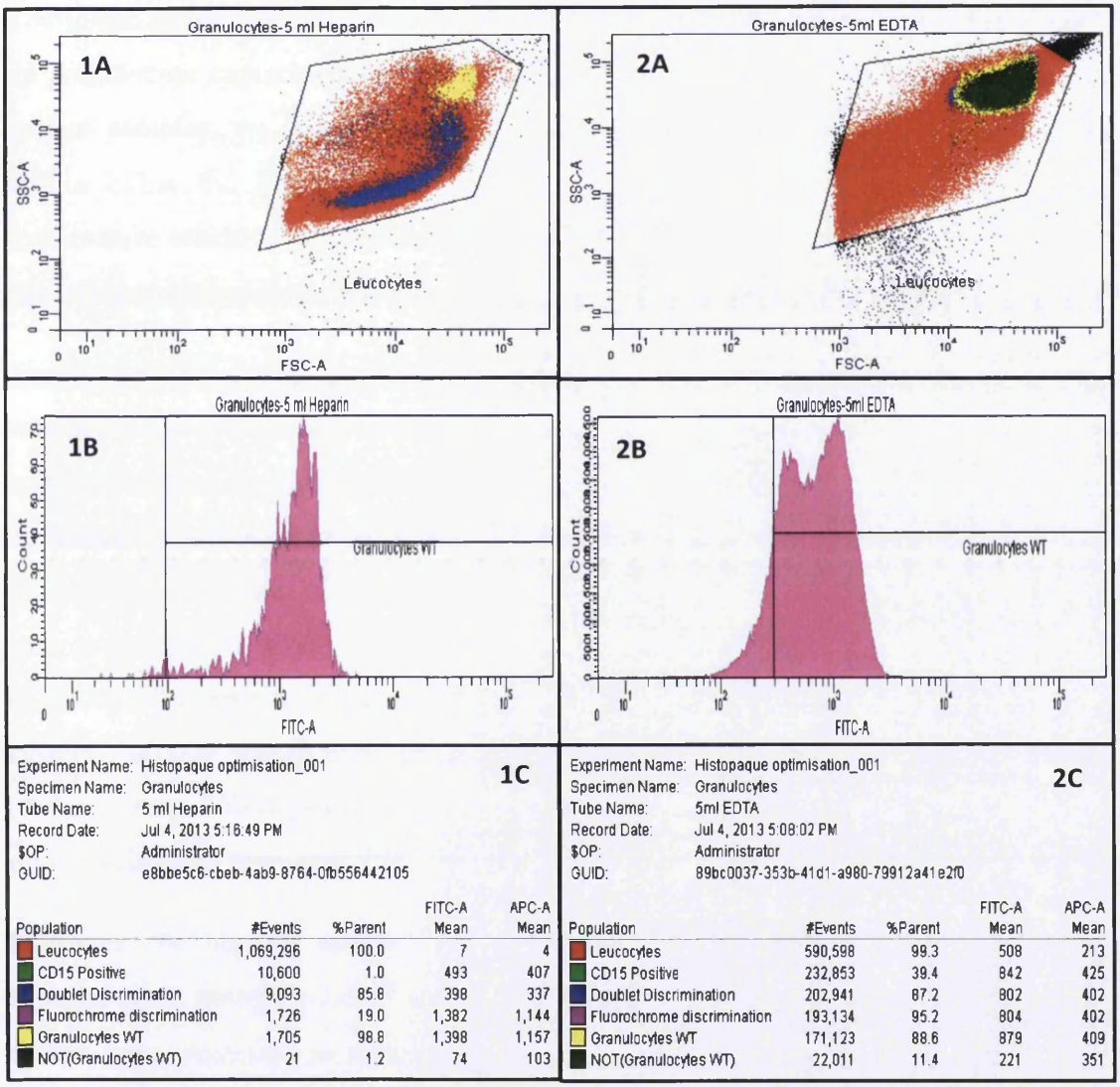

1C

Experiment Name: Histopaque optimisation_001
Specimen Name: Granulocytes
Tube Name: 5 ml Heparin
Record Date: Jul 4, 2013 5:16:49 PM
$OP: Administrator
GUID: e8bbe5c6-cbeb-4ab9-8764-0fb556442105

Population	#Events	%Parent	FITC-A Mean	APC-A Mean
Leucocytes	1,069,296	100.0	7	4
CD15 Positive	10,600	1.0	493	407
Doublet Discrimination	9,093	85.8	398	337
Fluorochrome discrimination	1,726	19.0	1,382	1,144
Granulocytes WT	1,705	98.8	1,398	1,157
NOT(Granulocytes WT)	21	1.2	74	103

2C

Experiment Name: Histopaque optimisation_001
Specimen Name: Granulocytes
Tube Name: 5ml EDTA
Record Date: Jul 4, 2013 5:08:02 PM
$OP: Administrator
GUID: 89bc0037-353b-41d1-a980-79912a41e2f0

Population	#Events	%Parent	FITC-A Mean	APC-A Mean
Leucocytes	590,598	99.3	508	213
CD15 Positive	232,853	39.4	842	425
Doublet Discrimination	202,941	87.2	802	402
Fluorochrome discrimination	193,134	95.2	804	402
Granulocytes WT	171,123	88.6	879	409
NOT(Granulocytes WT)	22,011	11.4	221	351

Figure 6.1. Direct comparison between the population statistics derived from variable direct anticoagulant capture; EDTA (1) and Heparin (2) utilised as trialled anticoagulants. A) Crude size and granularity assessment utilising FSC and SSC measurements, B) relative frequency of events staining positive for FLAER binding (phenotypic PIG-A wild types) and C) comparable results table displaying the subsequent population statistics, detailing the hierarchical approach.

The experimental design was to aid investigation into the initial combined use of histopaque ® 1077 and 1119 as well as assess the potential effects different anticoagulants had on cell isolation and phenotype stability. The PNC layer theoretically was to be trapped between the two specific density histopaque ® solutions utilised in order to facilitate effective and robust granulocyte capture.

The initial results we generated were very poor in terms of layer separation as well as granulocyte capture (data not shown) quite different; within the two different patient samples, we were unable to see any potential granulocyte layer (PNCs) within either the histopaque® or on top of the erythrocyte pellet. Following temperature sensitive adjustments, as well as an increase in centrifugation intensity, the results captured were able to compare and contrast anti-coagulant effects.

The subsequent results generated showed a distinctive granulocyte (PNC) layer within the EDTA sample, however, it was located on top of the erythrocyte pellet and not between the two different histopaque ® solutions. The heparin sample gave no distinct granulocyte layer at all, and therefore, for the purpose of this experiment the equivalent section of the sample was removed and FCM assessed. The EDTA sample generated a 40% CD15 positive leukocyte population, allowing the collection of >500,000 events within a suitable time frame. Implementing the revised gating system, 200,000 granulocytes positive events were scored and approximately 88.6% of these were *PIG-A* positive; a significant increase in event enrichment, however, poor results with respect to *PIG-A* phenotype assessment.

However, the heparin sample only yielded an approximate 1% CD15 positive sample; even though $>1x10^6$ events were scored, following gating, only a 1,726 events were classified as neutrophils with a corresponding *PIG-A* phenotypic wild type frequency of 98.8%. Typically heparin is used within clinical applications in terms of sample collection as well as storage, however, the results demonstrate that EDTA generate significantly higher CD15 capture, and only marginal loss of *PIG-A* phenotype. Both methods generated in-efficient CD15 populations in terms of *PIG-A* mutant sensitivity and therefore, would require further optimisation prior to routine use for *PIG-A* assessment within human granulocytes (Appendix Figure 6.1).

6.4.3.3.2.2 The Possible Effect Anticoagulant has on Spontaneous *PIG-A* background Mutant Frequency

Throughout the optimisation of the human *PIG-A* assay platforms we have operated under the assumption that the blood collection within heparin coated vaccutainers is not biasing or influencing the data acquisition in any way. Heparin is a sulphated glycosaminoglycan and is widely used as an injectable anticoagulant [110]. It has a highly negative charge density [111] and its commercially utilised heavily within the medical industry to form an inner anticoagulant surface on various experimental and medical devices. It operates under the premise of binding to the enzyme inhibitor anti-thrombin III (AT), causing a conformational change that results in its activation through an increase in the flexibility of its reactive site loop. Activated AT, inactivates thrombin and other proteases involved in blood clotting, most notably factor Xa. Heparin has the ability of increasing the rate of inactivation of such proteases by up to 1,000 – fold [112]. Heparin's excessive negative charge has the effect of dramatically increasing its ability to interact within the AT enzyme as well as providing an excessively favourable environment for inhibition following Ca^{2+} ions interaction [113]. However, heparin is also associated with heparin-induced thrombocytopenia (HIT), caused by an immunological reaction that makes platelets a target of immunological response [114], the potential impact of this as well as the charged nature of heparin may have deleterious effects on the cells within the blood sample and negatively influence their *PIG-A* assessment.

Therefore, in order to generate some comparable data a second anti-coagulant was also trialled, ethylenediaminetetraacetic acid (EDTA) is an aminopolycarboxylic acid. Its usefulness within the field of biology directly relates to its ability to act as a chelating agent [115]; EDTA binds metal ions such as Ca^{2+} and $Fe^{3+,}$ following binding metal ions remain in solution but exhibit diminished reactivity [116]. Therefore, it activity inhibits the Calcium induced clotting cascade and readily is utilise as an anti-coagulant [117]. However, its uses remain more commercial,

especially prominent within specific scientific buffers, but yet to be highly associated to clinical applications.

As well as trialling the effects specific anticoagulants have on the spontaneous *PIG-A* mutant frequency, this experiment was also designed to incorporate a second distinct histopaque® solution within the method in an attempt to aid enrichment. Histopaque ® 1077 and 1119 g/mL will be utilised to potentially capture and isolate the PNC (poly nuclear cells) layer. The initial results were very poor (data not shown), the centrifugation failed to result in any separation of the whole blood samples, however after a detailed literature search, a single paper [118] providing sufficient details within their analogous method to enable potential solution. The centrifugation speed was increased to be in line with the publication and the subsequent results showed a distinctive "granulocyte" layer within the EDTA sample; although, the localisation of the layer was highly proximal to the top of the RBC pellet and not the between the histopaque® solutions as expected. The heparin sample gave no distinct granulocyte layer at all; however, for the purpose of this experiment the equivalent section of the sample was removed and assessed.

The EDTA sample generated a subsequent 40% CD15 positive population following centrifugation, the capture of 500,000 morphological leukocytes events within the pre-allotted time for analysis. Combining this method with the trialled novel gating system, 200,000 defined granulocytes were scored with a respective phenotypic mutant *PIG-A* frequency of 11.4%. The heparin sample yielded a 1% CD15 positive constitution within the blood sample, and therefore, resulted in a highly limited (~2,000) granulocyte population to be scored. Although, within this population on 1.2% were phenotypic *PIG-A* mutants, a significant increase in sensitivity when compared to the EDTA sample.

The results of this experiment in terms of enrichment were highly promising, especially for the EDTA sample, facilitating ~$5x10^5$ cells scored easily within the acquisition time. However, both heparin and EDTA generated unacceptably high spontaneous background *PIG-A* mutant frequencies, preventing any potential quantitative data modelling for the HBM (Appendix Figure 6.1). The reason why heparin resulted in a much lower granulocyte enrichment from a biological standpoint are unknown, however, the observed results are most likely due to some

element of user error as the construction of the sample pre-centrifugation, as well as cell harvesting are particular advanced. Therefore, limited conclusions can be drawn from this experiment except that yet again, additional factors introduced within the experimental design can have a significant impact on the sensitive of the measurable endpoint and deleteriously affect the overall assay platform performance.

6.5 Supplementary Work

6.5.1 Introduction

Flow cytometry gating is still a prominent potential source of experimental error within scientific research. Until relatively recently, few publications on analysis standardisation have impacted the field and resultantly, analysis is often highly varied and subjective [39, 50, 119-123]. This has a direct effect on robustness, data integrity and transferability. However, recent movements within the field have resulted in an attempt to harmonize approaches and have significantly refined the publication procedure; consequently standards have greatly improved [124]. As the field develops, increasing properties of the fluorescence signal are being utilised within analysis to provide additional features to enable more detailed and comprehensive population assessment [50, 125, 126]. However, as the technical level of analysis increases, so does the knowledge base required to interpret the data. Therefore, as often is the case within scientific research, the technology advances beyond the understanding required to fully comprehend the intellectual need. Consequently, incorrect usage of the novel features can potentially have deleterious effects on the integrity of the generated data; noticeably bias can be introduced which fundamentally significantly reduces the weight of evidence attributed to the data.

In an endeavour to increase flow cytometry resolution within data analysis and fundamentally increase the sensitivity of the assay, the ability of incorporating novel pulse-width measures within the test system were investigated. Pulse width can provide increased refinement of sub population identification and significantly provide additional information in terms of morphological size and form, to enable more accurate phenotypic scoring. Therefore, more accurately identifying and removing doublets, debris and any cell type which does not resemble normality should increase reporting accuracy and reduce the risk of false negative/positive results. Nevertheless, the benefit from introducing significantly more complex gating strategies can be heavily outweighed by the deleterious consequences if the gating is

not true and remains critical to unbiased reporting. Introducing ever increasing limiting strategies to remove outlier events also runs the risk of excluding actual viable events from analysis.

6.5.2 Materials and Methods

6.5.2.1 Gating Strategy Advancements: Investigations into Potential Analysis Bias

A single patients under went venepuncture, bled from the Median Cubital Vein located on the ventral surface of the forearm, into a 5 mL heparin coated Vaccutainer. The tubes receiving antibody treatment, pre-lysis, were treated with 20 µL of anti-CD15 APC and incubated in the dark, at room temperature, for 30 minutes. Following 15 minutes, the samples were treated with FLAER. A previously constructed aliquot of FLAER was removed from the cold room and allowed to warm to room temperature. 5 µL of FLAER (1x stock as made up previously) was added to the samples and allowed to incubate for a further 15 min at room temperature protect from light.

1 mL of VersaLyse solution (1X) was added, vortexed immediately (1 sec) and allowed to incubate for 10 min at room temperature, protected from light. Immediately following incubation, the samples were centrifuged, 150 x g for 5 min, supernatant aspirated and washed, via the addition of 3 mL of wash buffer (0.2% BSA/PBS). The samples were centrifuged as above, and re-suspended in 1 mL of Wash Buffer, samples were treated with 5µL of Propidium Iodide, allowed to incubate for 5 mins, protected from light, on ice. Samples were analysed immediately on the flow cytometer.

6.5.3 Results

6.5.3.1 Gating Strategy Advancements: Investigations into Potential Analysis Bias

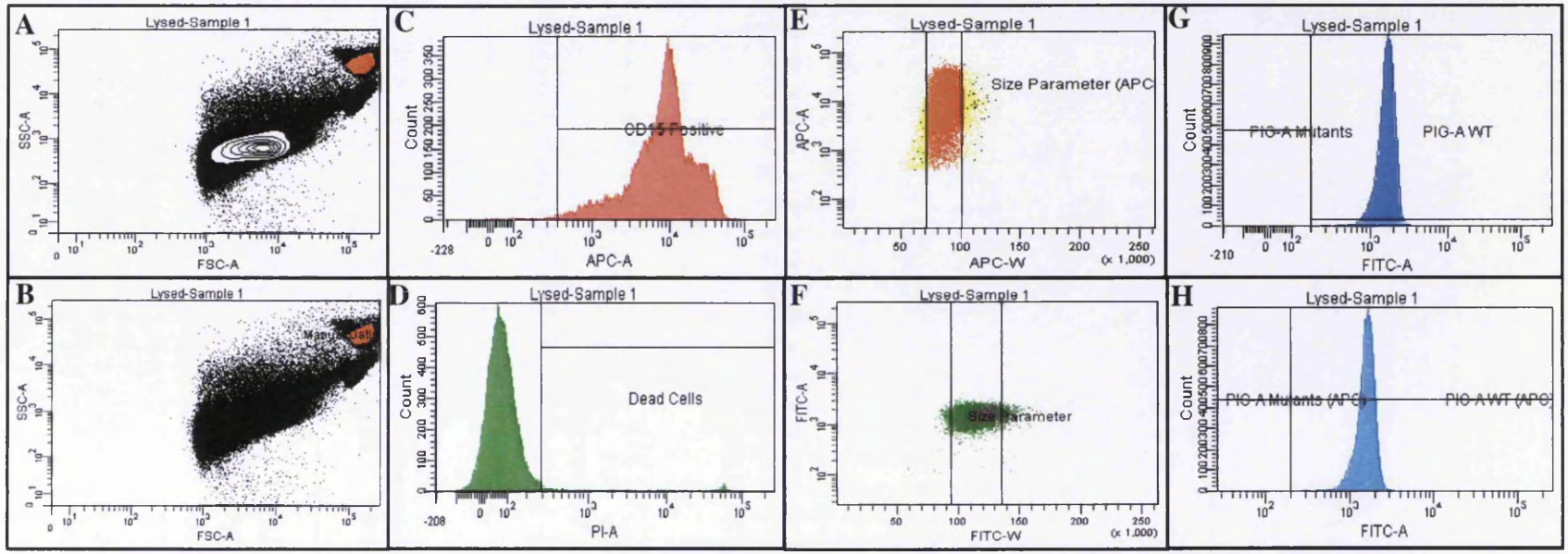

Figure 6.5.1. A flow cytometry analysis work flow, showing the progressive labelling, identification and sub-population derivation in order to obtain *PIG-A* mutant frequency assessment within human granulocyte cells utilising both potential novel gating strategies. A) and B) Crude FSC vs SSC contour/dot plot indicative of morphology and cell size. C) Relative fluorescence intensity for lineage specific marker CD15, D) Relative fluorescence intensity for cellular viability marker (Propidium Iodide), E) Experimental lineage marker specific width measure , F) Experimental GPI-AP status marker width measure, G) Resultant *PIG-A* mutant frequency assessment following and D) Glycophorin A presence. E) Leukocyte specific gating, F) RET and mature RBC identification and separation, G) GPI-AP assessment of RETS and H) GPI-AP assessment of RBCs (10,000 events shown for ease of visualisation).

Table 6.5.1.A) Summary of the preliminary population statistics derived from a lysed healthy control patient donor; stained with anti-CD15 APC neutrophil marker in conjunction with PI.

Sample ID	All Events	Leukocytes	CD15 Positive	Percentage of Parent (%)	Viable Cells	Percentage of Parent (%)
Sample 1	2024878	14270	14145	99.1	13802	97.6
Sample 2	1086108	10736	10539	98.2	10303	97.8
Sample 3	4700000	31075	30875	99.4	30044	97.3
Average	2603662	18693.67	18519.67	98.9	18049.67	97.57

Table. 6.5.1.B) Summary of the population statistics derived from a lysed healthy control patient donor; stained with anti-CD15 APC neutrophil marker in conjunction with FLAER, utilising the FLAER FL-W gating strategy.

FITC - Pulse Width (Time of Flight Measurement)

Sample ID	Doublets and Debris exclusion	Percentage of Parent (%)	*PIG-A* WT	Percentage of Parent (%)	*PIG-A* Mutants	Percentage of Parent (%)
Sample 1	13180	95.5	13180	100	0	0
Sample 2	10000	97.1	10000	100	0	0
Sample 3	28949	96.4	28949	100	0	0
Average	17376.33	96.33	17376.33	100	0	0

Table. 6.5.1.C) Summary of the population statistics derived from a lysed healthy control patient donor; stained with anti-CD15 APC neutrophil marker in conjunction with FLAER, utilising the CD15 FL-W gating strategy.

	APC - Pulse Width (time of flight measurement)				
Sample ID	Doublets and Debris exclusion	*PIG-A* WT	Percentage of Parent (%)	*PIG-A* Mutants	Percentage of Parent (%)
Sample 1	12391	12390	100	1	0
Sample 2	9246	9246	100	0	0
Sample 3	27273	27273	100	0	0
Average	16303.33333	16303	100	0.333333	0.002%

In order to assess the feasibility of increasing assay sensitivity, initially at low sample number, without lysis enrichment, and then scaling up for larger enumerations of phenotypic mutant event, two novel gating strategies were trialled. Analogous to previous optimisation work within the in vitro *PIG-A* gene mutation assay, a generic "healthy" human patent sample was initially analysed in order to construct a baseline of mutant frequency. Following this, the inclusion of novel highly sensitive gating strategies utilising pulse width measures were included to evaluate the potential of induced assay bias. The resultant initial data generated an average capture of ~$2.6x10^6$ single cell events, of which 18,000 were identified as leukocytes due to their crude unique FSC vs SSC profiles. Following this, 98.9% of the parental leukocyte population were demonstrated to be positive for the CD15 lineage specific antigen and less than 2.5% of the population showed loss of cellular membrane integrity, the latter was omitted from analysis (Appendix Table 6.5.1.A).

The two trialled gating strategies delivered similar but distinctive results, utilising the FITC-A vs FITC-W measures, approximately 17,000 leukocytes were identified of which 96.3% were defined CD15 positive, activated neutrophils, and 0 average cellular events were scored as phenotypic *PIG-A* mutants (Appendix Table 6.5.1.B). APC-A vs APC-W generated analogous population statistics with approximately 16,000 leukocytes, however, the average phenotypic mutant frequency was defined

as 0.002% (Appendix Table 6.5.1.C). Utilising the FL-W measure of the *PIG-A* phenotypic reporter marker in conjunction with the FL-A data, resulted in a strong correlation to an absence of phenotypic *PIG-A* mutant events. The FITC-A vs FITC-W pulse data showed some evidence for a biasing effect on sequential *PIG-A* scoring.

6.5.4 Discussions and Conclusions

6.5.4.1 Gating Strategy Advancements: Investigations into Potential Analysis Bias

Granulocytes when compared to the other cell type within whole blood have elevated levels of cytotoxicity within their culture, specifically demonstrating high levels of cellular death and apoptosis (Section 6.3.3.2). This is due to their nucleated status, permitting them to undergo apoptosis as well as their unique role within innate immunity within the human body [127]; systemic exposure to micro-environments inducive of pro-inflammation and DNA damage [127-130].These factors have the potential effect of generating putative *PIG-A* deficient phenotype events within the heterogenous population, resulting in false positive FCM data. *PIG-A* mutants are isolated on the flow cytometer via their lack of phenotypic marker associated fluorescence, homologous to the in vivo erythrocyte *Pig-a* assay [131], therefore, putative non-viable cells which have the "correct FSC vs SSC profile" (recently undergoing apoptosis for example) could lose their phenotypic *PIG-A* marker on the cell surface via localised membrane inversion/integrity or associated gene expression with apoptotic death pathways [132]; apoptosis progression in general provides increased difficulties for accurate cell identification [123].

Initially to account for potential false positive events, a complex compensation matrix utilising single stained positive control samples to account for any potential spectral overlap from introducing three different coloured fluorochromes within the assay design was presented (data not shown). In combination with the compensation matrix a gating system similar to the novel strategy introduced within the in vitro assay (Section 5.3.4) was trialled in combination with the use of propidium iodide, a generic intercalating fluorescent dye to measure membrane integrity [126, 133]. The results indicated that not only did this version of the assay platform surpass the previous lowest spontaneous background mutant frequency (0.01%), but significantly increased assay sensitivity (0.002% putative *PIG-A* mutant frequency). Apparently the combination of improvements generated a highly accurate method for

putative false positive *PIG-A* mutant detection and exclusion via a combination of viability dye incorporation and pulse width measurement. However, limited solid conclusions can be taken from the data due to the limited sample size, approximately 15,000 events, as well as the potential bias within the resultant data.

Utilising the APC-W measure the assay sensitivity was significantly shown to increase, as the APC detector was measuring the CD15 specific fluorescent signal. However, when the FLAER associated FITC-W signal was utilised the background mutant frequency was unable to be estimated as not a single phenotypic *PIG-A* mutant event was scored. The nature of the FL-W measure utilised as an additional size discriminator has a massive impact on the resultant *PIG-A* data. Therefore, within future applications, and FL-W measure directly associated to mutant phenotype scoring within FCM analysis will not be able to be utilised as an additional discriminate. The reason for this is the events which have a smaller FL-W (even utilising FITC-W in this case) are not necessarily biased against when scored, however, in combination with the FL-A measure and a limited specific population gate their ability to be incorporated into further analysis stages is highly biased against. Therefore, using the FL-W of an un-associated fluorescence signal from the phenotypic scoring is apparently appropriate.

The main conclusions which can be taken from this is that the assay platform design can be directly transferred, replacing propidium iodide with 7-AAD, in its current form into the human RET *PIG-A* assay design in order to potentially increase assay sensitivity. Additional larger sample sizes will be required to be captured prior to further conclusive remarks.

7. Bibliography

1. Technology, L. DSB-X™ Biotin Protein Labeling Kit (D-20655). 2001 26/09/2014]; Available from: http://tools.lifetechnologies.com/content/sfs/manuals/D-20655_DSB-X_biotinylation_for_Flexi_protocol_(101001).pdf.
2. Kitano, H., Systems biology: a brief overview. Science, 2002. 295(5560): p. 1662-4.
3. Mahadevan, B., et al., Genetic toxicology in the 21st century: reflections and future directions. Environ Mol Mutagen, 2011. 52(5): p. 339-54.
4. Toxicity Testing in the 21st Century: A Vision and a Strategy. 2007: The National Academies Press.
5. Amnis. Integrating flow cytometry and microscopy to advanced discovery. 2014 01/07/2014]; Available from: https://www.amnis.com/.
6. van Zanten, T.S., et al., Hotspots of GPI-anchored proteins and integrin nanoclusters function as nucleation sites for cell adhesion. Proc Natl Acad Sci U S A, 2009. 106(44): p. 18557-62.
7. Miura, D., et al., Development of an in vivo gene mutation assay using the endogenous Pig-A gene: I. Flow cytometric detection of CD59-negative peripheral red blood cells and CD48-negative spleen T-cells from the rat. Environmental and Molecular Mutagenesis, 2008. 49(8): p. 614-621.
8. Gunther, W.C., et al., Evaluation of the Pig-a, micronucleus, and comet assay endpoints in a 28-day study with ethyl methanesulfonate. Environ Mol Mutagen, 2014.
9. Lynch, A.M., et al., International Pig-a gene mutation assay trial (stage III): results with N-methyl-N-nitrosourea. Environ Mol Mutagen, 2011. 52(9): p. 699-710.
10. Sutherland, B.W., J. Toews, and J. Kast, Utility of formaldehyde cross-linking and mass spectrometry in the study of protein-protein interactions. J Mass Spectrom, 2008. 43(6): p. 699-715.
11. Kinoshita, T., Biosynthesis and deficiencies of glycosylphosphatidylinositol. Proc Jpn Acad Ser B Phys Biol Sci, 2014. 90(4): p. 130-43.
12. Dobrovolsky, V.N., et al., The in vivo pig-a gene mutation assay, a potential tool for regulatory safety assessment. Environmental and Molecular Mutagenesis, 2010. 51(8-9): p. 825-835.
13. Kimoto, T., et al., Manifestation of Pig-a mutant bone marrow erythroids and peripheral blood erythrocytes in mice treated with N-ethyl-N-nitrosourea: direct sequencing of Pig-a cDNA from bone marrow cells negative for GPI-anchored protein expression. Mutat Res, 2011. 723(1): p. 36-42.
14. Nonami, H. and E.D. Schulze, Cell water potential, osmotic potential, and turgor in the epidermis and mesophyll of transpiring leaves. Planta, 1989. 177(1): p. 35-46.
15. Will, B.R. and R.A. Brace, Physiological effects of pH changes on colloid osmotic pressures. Am J Physiol, 1985. 248(6 Pt 2): p. H890-3.
16. University of Illinois, C. Real Time PCR Handbook. 2003 17/07/2014].
17. Biosciences, B. BD FACS Aria. 26/09/2014]; Available from: http://www.bdbiosciences.com/instruments/facsaria/.
18. Carey, J.L., P.J. McCoy, and D.F. Keren, Flow Cytometry in Clinical Diagnosis (4th edition). 2007: American Society for Clinical Pathology.

19. Guez-Barber, D., et al., FACS purification of immunolabeled cell types from adult rat brain. J Neurosci Methods, 2012. 203(1): p. 10-8.
20. Biosciences, B., BD FACSDiVa Option. 2002.
21. Mackenzie, C.G., J.B. Mackenzie, and P. Beck, THE EFFECT OF pH ON GROWTH, PROTEIN SYNTHESIS, AND LIPID-RICH PARTICLES OF CULTURED MAMMALIAN CELLS. J Biophys Biochem Cytol, 1961. 9(1): p. 141-56.
22. Alberts, B.J., A,Lewis, J et al., Molecular Biology of the Cell. 4th edition. 2002, New York: Garland Science.
23. Muller, P.A. and K.H. Vousden, Mutant p53 in cancer: new functions and therapeutic opportunities. Cancer Cell, 2014. 25(3): p. 304-17.
24. Meek, D.W., The p53 response to DNA damage. DNA Repair (Amst), 2004. 3(8-9): p. 1049-56.
25. Moll, U.M. and O. Petrenko, The MDM2-p53 interaction. Mol Cancer Res, 2003. 1(14): p. 1001-8.
26. Bates, S. and K.H. Vousden, p53 in signaling checkpoint arrest or apoptosis. Curr Opin Genet Dev, 1996. 6(1): p. 12-8.
27. Glynn, E.F., FCSExtract Utility. 2005: Stowers Institute for Medical Research. p. Software for converting FCS format data into tabulated results.
28. Mathsisfun.com. Quartiles. 2014 07/01/2015]; Available from: http://www.mathsisfun.com/data/quartiles.html.
29. Eliaz, R.E., et al., Determination and modeling of kinetics of cancer cell killing by doxorubicin and doxorubicin encapsulated in targeted liposomes. Cancer Res, 2004. 64(2): p. 711-8.
30. Roederer, M., Compensation in flow cytometry. Curr Protoc Cytom, 2002. Chapter 1: p. Unit 1.14.
31. Piatkevich, K.D., et al., Photoswitchable red fluorescent protein with a large stokes shift. Chem Biol, 2014. 21(10): p. 1402-14.
32. Rees, B.J., et al., Development of the in vitro Pig-A mutation assay; exploring the low dose response region for known alkylating agents MNU and EMS., in UKEMS. 2012. p. 116.
33. Brusehafer, K., et al., Chromosome breakage induced by the genotoxic agents mitomycin C and cytosine arabinoside is concentration and p53 dependent. Toxicol Sci, 2014. 140(1): p. 94-102.
34. Marie, D., et al., Enumeration and Cell Cycle Analysis of Natural Populations of Marine Picoplankton by Flow Cytometry Using the Nucleic Acid Stain SYBR Green I. Appl Environ Microbiol, 1997. 63(1): p. 186-93.
35. Kruger, C.T., M. Hofmann, and A. Hartwig, The in vitro PIG-A gene mutation assay: mutagenicity testing via flow cytometry based on the glycosylphosphatidylinositol (GPI) status of TK6 cells. Arch Toxicol, 2014.
36. Pu, J.J., et al., The small population of PIG-A mutant cells in myelodysplastic syndromes do not arise from multipotent hematopoietic stem cells. Haematologica, 2012. 97(8): p. 1225-33.
37. Torous, D.K., et al., In vivo flow cytometric Pig-a and micronucleus assays: highly sensitive discrimination of the carcinogen/noncarcinogen pair benzo(a)pyrene and pyrene using acute and repeated-dose designs. Environ Mol Mutagen, 2012. 53(6): p. 420-8.
38. Kimoto, T., et al., Further development of the rat Pig-a mutation assay: measuring rat Pig-a mutant bone marrow erythroids and a high throughput

assay for mutant peripheral blood reticulocytes. Environ Mol Mutagen, 2011. 52(9): p. 774-83.
39. Maecker, H.T. and J. Trotter, Flow cytometry controls, instrument setup, and the determination of positivity. Cytometry A, 2006. 69(9): p. 1037-42.
40. Fellers, T.J. and M.W. Davidson. Introduction to Confocal Microscopy. 2004 - 2009; Available from: http://www.olympusconfocal.com/theory/confocalintro.html.
41. (UCSC), U.o.S.C. UCSC genome bioinformatics browser 2014 28/07/2014]; Available from: https://genome.ucsc.edu/.
42. Berkeley Drosophila Genome Project. 28/07/2014]; Available from: http://www.fruitfly.org/seq_tools/promoter.html.
43. Denmark, C.f.b.s.a.-T.U.o. Promoter 2.0 Prediction Server. 2014 28/07/2014]; Available from: http://www.cbs.dtu.dk/services/Promoter/.
44. Berry, S. 2014 28/07/2014]; Available from: http://www.softberry.com/.
45. Ensembl. 2014 28/07/2014]; Available from: http://www.ensembl.org/index.html.
46. Technologies, A. 2014 28/07/2014]; Available from: https://earray.chem.agilent.com/suredesign/.
47. Grundlingh, J., et al., 2,4-Dinitrophenol (DNP): A Weight Loss Agent with Significant Acute Toxicity and Risk of Death, in J Med Toxicol. 2011: New York. p. 205-12.
48. Antonenko, Y.N., et al., Penetrating Cations Enhance Uncoupling Activity of Anionic Protonophores in Mitochondria, in PLoS One, H.W. van Veen, Editor. 2013: San Francisco, USA.
49. (FSA), F.S.A. Food Standards Agency issues urgent advice on consumption of 'fat burner' capsules containing DNP. 2003 06/01/2015].
50. Hickerson, D.H., et al., Development of a flow cytometry-based pulse-width assay for detection of aggregates in cellular therapeutics to be infused by catheter. Cytotherapy, 2014. 16(11): p. 1545-57.
51. Guest, R.D. and J.M. Parry, P53 integrity in the genetically engineered mammalian cell lines AHH-1 and MCL-5. Mutat Res, 1999. 423(1-2): p. 39-46.
52. Morris, S.M., et al., A mutation in the p53 tumor suppressor gene of AHH-1 tk+/- human lymphoblastoid cells. Mutat Res, 1996. 356(2): p. 129-34.
53. Cao, X., et al., Quantitative dose-response analysis of ethyl methanesulfonate genotoxicity in adult gpt-delta transgenic mice. Environ Mol Mutagen, 2014. 55(5): p. 385-99.
54. Gocke, E. and M. Wall, In vivo genotoxicity of EMS: statistical assessment of the dose response curves. Toxicol Lett, 2009. 190(3): p. 298-302.
55. Johnson, G.E., et al., Non-linear dose-response of DNA-reactive genotoxins: recommendations for data analysis. Mutat Res, 2009. 678(2): p. 95-100.
56. Muller, L. and T. Singer, EMS in Viracept--the course of events in 2007 and 2008 from the non-clinical safety point of view. Toxicol Lett, 2009. 190(3): p. 243-7.
57. Sega, G.A., A review of the genetic effects of ethyl methanesulfonate. Mutat Res, 1984. 134(2-3): p. 113-42.
58. Alam, S., et al., The cigarette smoke carcinogen benzo[a]pyrene enhances human papillomavirus synthesis. J Virol, 2008. 82(2): p. 1053-8.
59. Bhalli, J.A., et al., Report on stage III Pig-a mutation assays using benzo[a]pyrene. Environ Mol Mutagen, 2011. 52(9): p. 731-7.

60. Zhan, D.J., et al., Characterization of DNA adducts in Chinese hamster ovary cells treated with mutagenic doses of 1- and 3-nitrosobenzo[a]pyrene and the trans-7,8-diol-anti-9,10-epoxides of 1- and 3-nitrobenzo[a]pyrene. Mutat Res, 1997. 379(1): p. 43-52.
61. Crespi, C.L., et al., A metabolically competent human cell line expressing five cDNAs encoding procarcinogen-activating enzymes: application to mutagenicity testing. Chem Res Toxicol, 1991. 4(5): p. 566-72.
62. Daneshtalab, N., J.J. Dore, and J.S. Smeda, Troubleshooting tissue specificity and antibody selection: Procedures in immunohistochemical studies. J Pharmacol Toxicol Methods, 2010. 61(2): p. 127-35.
63. Feige, M.J. and J. Buchner, Principles and engineering of antibody folding and assembly. Biochim Biophys Acta, 2014. 1844(11): p. 2024-2031.
64. Buchwalow, I., et al., Non-specific binding of antibodies in immunohistochemistry: fallacies and facts. Sci Rep, 2011. 1: p. 28.
65. James, L.C. and D.S. Tawfik, The specificity of cross-reactivity: promiscuous antibody binding involves specific hydrogen bonds rather than nonspecific hydrophobic stickiness. Protein Sci, 2003. 12(10): p. 2183-93.
66. Alvarez-Barrientos, A., et al., Applications of flow cytometry to clinical microbiology. Clin Microbiol Rev, 2000. 13(2): p. 167-95.
67. Dobrovolsky, V.N., et al., Flow cytometric detection of Pig-A mutant red blood cells using an erythroid-specific antibody: application of the method for evaluating the in vivo genotoxicity of methylphenidate in adolescent rats. Environ Mol Mutagen, 2010. 51(2): p. 138-45.
68. Fowler, P., et al., Reduction of misleading ("false") positive results in mammalian cell genotoxicity assays. III: Sensitivity of human cell types to known genotoxic agents. Mutat Res Genet Toxicol Environ Mutagen, 2014.
69. Kenyon, M.O., et al., An evaluation of the sensitivity of the Ames assay to discern low-level mutagenic impurities. Regul Toxicol Pharmacol, 2007. 48(1): p. 75-86.
70. Walmsley, R.M. and N. Billinton, How accurate is in vitro prediction of carcinogenicity? Br J Pharmacol, 2011. 162(6): p. 1250-8.
71. Clarke, J.J., et al., Summary of in vitro genetic toxicology assay results: expected and unexpected effects of recent study design modifications. Environ Mol Mutagen, 2012. 53(8): p. 631-5.
72. Fowler, P., et al., Reduction of misleading ("false") positive results in mammalian cell genotoxicity assays. I. Choice of cell type. Mutat Res, 2012. 742(1-2): p. 11-25.
73. Fowler, P., et al., Reduction of misleading ("false") positive results in mammalian cell genotoxicity assays. II. Importance of accurate toxicity measurement. Mutat Res, 2012. 747(1): p. 104-17.
74. Kirkland, D., Improvements in the reliability of in vitro genotoxicity testing. Expert Opin Drug Metab Toxicol, 2011. 7(12): p. 1513-20.
75. Cimino, M.C., Comparative overview of current international strategies and guidelines for genetic toxicology testing for regulatory purposes. Environ Mol Mutagen, 2006. 47(5): p. 362-90.
76. Dearfield, K.L. and M.M. Moore, Use of genetic toxicology information for risk assessment. Environ Mol Mutagen, 2005. 46(4): p. 236-45.
77. Agarwal, M.L., et al., p53 controls both the G2/M and the G1 cell cycle checkpoints and mediates reversible growth arrest in human fibroblasts. Proc Natl Acad Sci U S A, 1995. 92(18): p. 8493-7.

78. Sheppard, K.E. and G.A. McArthur, The cell-cycle regulator CDK4: an emerging therapeutic target in melanoma. Clin Cancer Res, 2013. 19(19): p. 5320-8.
79. Lodsh, H.e.a., Molecular Cell Biology - Sixth Edition. 2007: W.H. Freeman.
80. Morgan, D., The Cell Cycle: Principles of Control. 2006: OUP Oxford.
81. Wehling, M., [Paracetamol. Efficacious and safe for all ages]. Schmerz, 2013. 27(1): p. 20-5.
82. Soliman, M.M., M.A. Nassan, and T.A. Ismail, Immunohistochemical and molecular study on the protective effect of curcumin against hepatic toxicity induced by paracetamol in Wistar rats. BMC Complement Altern Med, 2014. 14(1): p. 457.
83. Sass, N., Humane endpoints and acute toxicity testing. Ilar j, 2000. 41(2): p. 114-23.
84. Jia, L. and X. Liu, The conduct of drug metabolism studies considered good practice (II): in vitro experiments. Curr Drug Metab, 2007. 8(8): p. 822-9.
85. Pfitzenmaier, J., et al., The detection and isolation of viable prostate-specific antigen positive epithelial cells by enrichment: a comparison to standard prostate-specific antigen reverse transcriptase polymerase chain reaction and its clinical relevance in prostate cancer. Urol Oncol, 2007. 25(3): p. 214-20.
86. Dobrovolsky, V.N., et al., Detection of in vivo mutation in the Hprt and Pig-a genes of rat lymphocytes. Methods Mol Biol, 2013. 1044: p. 79-95.
87. Crespi, C.L. and W.G. Thilly, Mutation assays involving blood cells that metabolize toxic substances. 1999, Google Patents.
88. Indik, Z.K., et al., The molecular dissection of Fc gamma receptor mediated phagocytosis. Blood, 1995. 86(12): p. 4389-99.
89. Garcia-Garcia, E. and C. Rosales, Signal transduction during Fc receptor-mediated phagocytosis. J Leukoc Biol, 2002. 72(6): p. 1092-108.
90. Kirsch-Volders, M., et al., In vitro genotoxicity testing using the micronucleus assay in cell lines, human lymphocytes and 3D human skin models. Mutagenesis, 2011. 26(1): p. 177-84.
91. Library, O. Test No. 476: In vitro Mammalian Cell Gene Mutation Test. 1997 21/05/2014]; Available from: http://www.oecd-ilibrary.org/environment/test-no-476-in-vitro-mammalian-cell-gene-mutation-test_9789264071322-en.
92. Schwartz, J.L., et al., Baseline levels of chromosome instability in the human lymphoblastoid cell TK6. Mutagenesis, 2004. 19(6): p. 477-82.
93. Park, C.M., et al., Induction of p53-mediated apoptosis and recovery of chemosensitivity through p53 transduction in human glioblastoma cells by cisplatin. Int J Oncol, 2006. 28(1): p. 119-25.
94. Roos, W.P. and B. Kaina, DNA damage-induced cell death by apoptosis. Trends Mol Med, 2006. 12(9): p. 440-50.
95. OECD, OECD GUIDELINE FOR THE TESTING OF CHEMICALS - Test Guideline 487 - In Vitro Mammalian Cell Micronucleus Test 2012.
96. Thomasova, D. and H. Anders, Cell cycle control in the kidney. Nephrol Dial Transplant, 2014.
97. Ben-Porath, I. and R.A. Weinberg, When cells get stressed: an integrative view of cellular senescence. J Clin Invest, 2004. 113(1): p. 8-13.
98. Brenner, A.K., et al., Therapeutic targeting the cell division cycle 25 (CDC25) phosphatases in human acute myeloid leukemia--the possibility to

target several kinases through inhibition of the various CDC25 isoforms. Molecules, 2014. 19(11): p. 18414-47.
99. Hao, Q. and W.C. Cho, Battle Against Cancer: An Everlasting Saga of p53, in Int J Mol Sci. 2014. p. 22109-22127.
100. Prekeris, R. and G.W. Gould, Breaking up is hard to do - membrane traffic in cytokinesis. J Cell Sci, 2008. 121(Pt 10): p. 1569-76.
101. Veninga, H., et al., A novel role for CD55 in granulocyte homeostasis and anti-bacterial host defense. PLoS One, 2011. 6(10): p. e24431.
102. Kong, Y., et al., Cucurbitacin E induces cell cycle G2/M phase arrest and apoptosis in triple negative breast cancer. PLoS One, 2014. 9(7): p. e103760.
103. Yin, F., et al., Apigenin inhibits growth and induces G2/M arrest by modulating cyclin-CDK regulators and ERK MAP kinase activation in breast carcinoma cells. Anticancer Res, 2001. 21(1a): p. 413-20.
104. Goda, N., et al., Hypoxia-Inducible Factor 1α Is Essential for Cell Cycle Arrest during Hypoxia, in Mol Cell Biol. 2003. p. 359-69.
105. Hernandez-Campo, P.M., et al., Normal patterns of expression of glycosylphosphatidylinositol-anchored proteins on different subsets of peripheral blood cells: a frame of reference for the diagnosis of paroxysmal nocturnal hemoglobinuria. Cytometry B Clin Cytom, 2006. 70(2): p. 71-81.
106. Genomes, K.K.E.o.G.a. Glycosylphosphatidylinositol(GPI)-anchor biosynthesis - Homo sapiens (human). 15/10/2014]; Available from: http://www.genome.jp/kegg-bin/show_pathway?hsa00563.
107. Luzzatto, L., PNH from mutations of another PIG gene. Blood, 2013. 122(7): p. 1099-100.
108. Thomas, R.S., et al., Incorporating new technologies into toxicity testing and risk assessment: moving from 21st century vision to a data-driven framework. Toxicol Sci, 2013. 136(1): p. 4-18.
109. Elespuru, R.K., et al., Current and future application of genetic toxicity assays: the role and value of in vitro mammalian assays. Toxicol Sci, 2009. 109(2): p. 172-9.
110. Salzman, E.W., et al., Effect of Heparin and Heparin Fractions on Platelet Aggregation. J Clin Invest, 1980. 65(1): p. 64-73.
111. Muhl, L., et al., High negative charge-to-size ratio in polyphosphates and heparin regulates factor VII-activating protease. (1742-4658 (Electronic)).
112. Gray, E., J. Hogwood, and B. Mulloy, The anticoagulant and antithrombotic mechanisms of heparin. Handb Exp Pharmacol, 2012(207): p. 43-61.
113. Bedsted, T., et al., Heparin and calcium ions dramatically enhance antithrombin reactivity with factor IXa by generating new interaction exosites. Biochemistry, 2003. 42(27): p. 8143-52.
114. Al-Eidan, F.A., Pharmacotherapy of heparin-induced thrombocytopenia: Therapeutic options and challenges in the clinical practices. J Vasc Nurs, 2015. 33(1): p. 10-20.
115. Aoki, M. and S. Koike, EDTA chelating agent. 1995, Google Patents.
116. Soldatovic, D., et al., Compared effects of high oral Mg supplements and of EDTA chelating agent on chronic lead intoxication in rabbits. Magnes Res, 1997. 10(2): p. 127-33.
117. Banfi, G., G.L. Salvagno, and G. Lippi, The role of ethylenediamine tetraacetic acid (EDTA) as in vitro anticoagulant for diagnostic purposes. Clin Chem Lab Med, 2007. 45(5): p. 565-76.

118. Rondelli, T., et al., The Frequency of Granulocytes with Spontaneous Somatic Mutations: A Wide Distribution in a Normal Human Population. PLoS ONE, 2013. 8(1): p. e54046.
119. Hawley, T.S. and R.G. Hawley, Flow Cytometry Protocols. 2011, NJ, USA: Humana Press.
120. Macey, M.G., Flow Cytometry Principles and Applications. 2007, Totowa, NJ, USA: Humana Press Inc.
121. Porwit, A., et al., Revisiting guidelines for integration of flow cytometry results in the WHO classification of myelodysplastic syndromes-proposal from the International/European LeukemiaNet Working Group for Flow Cytometry in MDS. Leukemia, 2014. 28(9): p. 1793-8.
122. Yentsch, C.M.a.C.L.a.P.D.A., Flow Cytometry and Cell Sorting : Problems and Promises for Biological Ocean Science Research. 2013: p. 141--155.
123. Zamai, L., et al., Optimal detection of apoptosis by flow cytometry depends on cell morphology. Cytometry, 1993. 14(8): p. 891-7.
124. Lee, J.A., et al., MIFlowCyt: the minimum information about a Flow Cytometry Experiment. Cytometry A, 2008. 73(10): p. 926-30.
125. Kang, K., et al., Flow cytometric fluorescence pulse width analysis of etoposide-induced nuclear enlargement in HCT116 cells. Biotechnol Lett, 2010. 32(8): p. 1045-52.
126. Wersto, R.P., et al., Doublet discrimination in DNA cell-cycle analysis. Cytometry, 2001. 46(5): p. 296-306.
127. Nauseef, W.M., How human neutrophils kill and degrade microbes: an integrated view. Immunol Rev, 2007. 219: p. 88-102.
128. Albertine, K.H., et al., Morphological analysis of the activation of adherent neutrophils in vitro. Tissue Cell, 1988. 20(4): p. 519-30.
129. Dorward, D.A., et al., Technical advance: autofluorescence-based sorting: rapid and nonperturbing isolation of ultrapure neutrophils to determine cytokine production. J Leukoc Biol, 2013. 94(1): p. 193-202.
130. Futosi, K., S. Fodor, and A. Mocsai, Reprint of Neutrophil cell surface receptors and their intracellular signal transduction pathways. Int Immunopharmacol, 2013. 17(4): p. 1185-97.
131. Bryce, S.M., J.C. Bemis, and S.D. Dertinger, In vivo mutation assay based on the endogenous Pig-a locus. Environmental and Molecular Mutagenesis, 2008. 49(4): p. 256-264.
132. Elmore, S., Apoptosis: a review of programmed cell death. Toxicol Pathol, 2007. 35(4): p. 495-516.
133. Rieger, A.M., et al., Modified Annexin V/Propidium Iodide Apoptosis Assay For Accurate Assessment of Cell Death, in J Vis Exp. 2011.